SOLVENTS AND SOLUTIONS

SOLVENTS AND SOLUTIONS
STRUCTURE AND PROPERTIES

KESHRA SANGWAL
Emeritus Professor, Department of Applied Physics
Lublin University of Technology, Poland

Paragon Publishing, 4 North Street, Rothersthorpe,
Northamptonshire NN7 3JB, UK

Library of Congress Cataloging-in-Publication Data

Names: Sangwal, Keshra, author.
Title: Solvents and Solutions: Structure and Properties / by Keshra Sangwal
Description: First edition. | Paragon Publishing, Northamptonshire, UK, 2021 |
Subjects: 1. Solvents. 2. Solutions.

ISBN 978-1-78222-847-9 (paperback)
ISBN 978-1-78222-990-2 (e-book)

Book design, layout and production management by Into Print
www.intoprint.net
01604 832149

In memory
of those
who are no more with me

Knowledge acquired by an individual
is indivisible wealth;
distribution of this wealth
enriches each of its recipient.

Proverb

CONTENTS

PREFACE

The properties of solvents and solutions are associated with the structure of particles (i.e. atoms, molecules or ions) composing them and may broadly be grouped into three categories: (a) static properties, (b) transport properties, and (c) thermal properties. Density, refractive index, dielectric constant, and surface tension are essentially static properties and are connected with the statistical distribution of particles composing a liquid. Viscosity and electrical conductivity belong to transport properties and are associated with the motion of particles in the bulk liquid. In contrast to the viscosity of a liquid which is determined by the relative motion of all particles in the liquid, electrical conductivity is associated with the transport of charged particles. Thermal conductivity, thermal expansivity, freezing and evaporation of liquids fall in the category of thermal properties and are determined by the thermal motion of particles composing them. In fact, it is the structure of particles which ultimately interact with each other and decide their arrangement and instantaneous distribution in the liquid state and determine the properties of liquids.

Solvents used on both laboratory and industrial scale are liquids existing in the liquid state at ordinary temperature and pressure conditions. These liquids are inorganic compound like water and many organic compounds composed of molecules (molecular liquids) and a diverse group of salts composed of large organic structures as cations and organic or inorganic-based relatively small anions (low-temperature ionic liquids). Molecular solvents are widely used as a reaction medium, for sample extraction and preparation, for various industrial cleaning applications, and for recrystallization to purify compounds and growth of their single crystals suitable for applications. In comparison with conventional organic solvents, enormous interest in low-temperature ionic liquids (ILs) during the last three decades is due to a unique combination of their properties. At normal temperature and pressure conditions ILs have negligible vapor pressure, larger temperature range for the liquid state, high viscosity, high electrical conductivity, density higher than that of water, and moderate polarity. Consequently, ILs are miscible with different substances having a wide range of polarities and can dissolve both organic and inorganic substances. High viscosities are favorable for their application as lubricants.

Interest in the physical properties of electrolyte and nonelectrolyte solutions is due to various diverse reasons. They give information about interactions taking place between the ions/molecules in the mixtures and solutions, and are used for the determination of the concentration of a solute in the solution, for the monitoring of supersaturation in a crystallization run and for the calculations of establishing material balances and equipment volumes for crystallization processes. For example, refractive index measurements are usually employed to determine sugar content from aqueous sugar solutions. Refractive index measurements are also used to control supersaturation of systems during industrial crystallization and to study nucleation processes during crystallization from solutions. Similarly, viscosity data are indispensable for the verification and development of theoretical models of the liquid structure, and for the control and planning of fluid flow, and mass and heat transfer processes in various industries.

My interest in solutions goes back to the late nineteen sixties during my initial research activities concentrated on devising suitable etching solutions for revealing dislocations on the surfaces of ionic crystals. The main problems at that time were to explain why some solutions of specific compositions in certain temperature intervals revealed well-defined etch pits at the emergence points of dislocations on the surfaces of natural and artificial single crystals and why the shapes of etch pits produced even on the surfaces of the same crystallographic indices of the crystals were different. The narrative description of modification of growth habit, usually known as the final shape or morphology, of ionic crystals from aqueous solutions by different impurities (Buckley, 1951) did draw my attention to the possible role of solution structure, but my concepts of the connection between change in the shapes of dislocation etch pits on the surfaces of ionic crystals and their habit modification remained uncrystallized.

Irrespective of the solvent involved in the preparation of a solution at a given temperature by dissolving an electrolyte or a nonelectrolyte having a positive temperature coefficient of solubility, supersaturated solutions at high temperatures, as a rule, approach the structure of electrolyte melts. These solutions are composed of relatively high concentration of the solute such that the solute constituents are poorly solvated. Under these circumstances, it is difficult to believe that the solute is present in the solution as isolated ions or molecules. In contrast to the structure of real solutions, the theories of growth and morphology of crystals are based on the concept of integration of isolated ions or molecules on the growing surfaces of the crystals. This situation resulted in the concept of growth units of crystals in the beginning of nineteen eighties (Sunagawa, 1985), when I became involved in the investigation of growth of single crystals of electrolytes and nonelectrolytes from solutions under different experimental conditions. The findings that drew our attention were poor quality of crystals growing from highly supersaturated solutions at a constant temperature and growth of large good-quality single crystals at elevated temperatures of solutions, such as boiling solutions. Another related problem identified at that time was the variation of the final shape or morphology of the crystals growing under different experimental conditions.

Later we worked out a long review on the theoretical, technical and scientific aspects of the growth of crystals from boiling solutions with particular emphasis on the investigations of the nature of solutions, the range of applicability of the method, and the merits of the method over low-temperature solution growth. The original draft of this manuscript also comprised a survey of the macroscopic properties and structure of solvents and electrolyte solutions. In view of the length of the manuscript and somewhat auxiliary nature of the structure and properties of solutions, the finally published version of the review was restricted merely to the growth and characterization of single crystals from boiling solutions (Rodriquez-Clemente et al., 1988). Unfortunately, the seventy-page machine-written part of the original manuscript of the review devoted to the structure and properties of solutions surveying the literature published up through 1985 remained unpublished and later practically forgotten due to changes in my affiliation and other academic commitments.

During a check-up of the original drafts of different manuscripts published during the last three decades, I found the forgotten manuscript some three years ago. After going through the contents of this manuscript, I gathered an impression that, instead of the old version of this short review, an updated work comprising reviews of different topics with latest developments in the field of solvents and solutions would be of interest to a wider section of readership. The present monograph is an attempt in this direction.

There is huge literature on the structure and properties of electrolyte solutions. Important developments in the field were comprehensively reviewed six decades ago by Robinson and Stokes (1959). These authors also discussed different aspects of viscosity and electrical conductivity of solutions. Bockris and Reddy (1970) describe processes involved in the dismantling of ionic solids (e.g. ion–solvent and ion–ion interactions) and in the transport of molecules and ions in the liquid phase (viscosity and electrical conductivity). An introductory level textbook on electrolyte solutions was published recently by Wright (2007). There are also two works exclusively devoted to the viscosities of liquids (Stokes and Mills, 1965; Viswanath et al., 2007). While Stokes and Mills (1965) reviewed in their monograph measurement techniques and different viscosity equations for electrolyte solutions covering the literature published up to 1963, Viswanath et al. (2007) described developments in the theories of viscosities of liquids and commonly used methods for the estimation and correlation of viscosities of liquids and solutions. A systematic and comprehensive collection of advances made in estimating and correlating different properties of aqueous electrolyte solutions with emphasis on basic understanding of the properties and behavior of aqueous electrolyte solutions was published more than three decades ago by Horvath (1985). This monograph surveys mathematical expressions used to describe the dependence of data of physical and transport properties of aqueous electrolyte solutions on the experimental parameters like electrolyte concentration and solution temperature and presents various trends and regularities existing among selected physical, thermodynamic and transport properties of aqueous electrolyte solutions.

The literature on the properties of solvents and solutions has grown enormously during the last four decades, and is scattered in different specialized journals such as: Fluid Phase Equilibria, Journal of Chemical and Engineering Data, Journal of Chemical Thermodynamics, Journal of Molecular Liquids, Journal of Physical Chemistry, Journal of Solution Chemistry, Zeitschrift für Physikalische Chemie, and Zhurnal Fizicheskoi Khimii. This period has also witnessed the emergence of the new class of solvents known as low-temperature ionic liquids for their applications in diverse fields. Most researchers usually have insufficient time to scan the increasingly large number of articles covering a broad spectrum of problems in their scientific field and require a comprehensive review for reference and guidance. Since the available monograph by Horvath (1985) on the physical properties of aqueous electrolyte solutions was published more than three decades ago and ionic liquids and their mixtures with other commonly used solvents have drawn considerable interest during this period, a systematic compilation reviewing the present status of important problems related to the properties of solvents and solutions is desired. The present monograph is to fill this gap.

There is huge literature devoted to different aspects of solvents and solutions under usual temperature and pressure conditions. Therefore, the choice of topics and their coverage during the writing of this academic book from the published literature is based on my interest in the field. I have placed emphasis on explaining the basic concepts involved in understanding the properties and behavior of solutions of electrolytes and nonelectolytes in a consistent manner. My aim here has been to make the book not only self-contained but also to make the contents of different chapters practically independent of each other.

The contents of the monograph may be divided into three parts. The first part describes the general characteristics of structure of solvents and solutions (Chapter 1) and the solubility of electrolytes and nonelectrolytes under normal temperature and pressure conditions (Chapter 2). The second part deals with the static properties of solvents and solutions. This part, comprising Chapters 3 and 4, describes and discusses different aspects of the density and the refractive index of solvents and dilute as well as concentrated solutions. The last part is devoted to transport and thermal properties of solvents and solutions. The topics described are their viscosity (Chapter 5), electrical conductivity (Chapter 6) and thermal expansivity (Chapter 7). The organization of contents of the first six chapters is broadly based on the old, unpublished manuscript dealing with aqueous solutions, but they are practically rewritten to reflect developments in the investigation of solvents and solutions during the last three decades. In the present form these chapters have a much wider scope than the modest contents of the old manuscript and give overviews of the present status of the literature. In some recent publications I came across discussion of the thermal expansivity of solutions. Since this is a derived property from volumetric measurements and is usually not discussed, I believe that a chapter devoted to the thermal expansivity of solvents, solutions and solutes will be a useful addition to the contents of the monograph.

The book is primarily addressed to researchers who are looking for an uptodate overview of the physical and transport properties of solvents and solutions. It can equally serve as a reference source for workers in chemical industries and related fields and for graduate students of chemical engineering and physical chemistry.

It is practically impossible to write an academic book like the present one without referring to the works published before by other authors. The present book is not an exception. In fact, I have depended strongly on the concepts and ideas on different topics from the available literature and have used experimental data and figures published by different authors in various journals and books. I express my gratitude to the authors and the publishers of the works I have used in the book. The relevant sources of such works are duly cited whenever they appear in the text.

I am indebted to my former collaborators with whom I had the previledge of investigating different aspects of solutions used in the crystallization of inorganic and organic compounds. I am especially grateful to Dr Sabino Veintemillas-Verdaguer, Professor Rafael Rodriguez-Clemente, and Professor Fernando Ruiz-Perez for their stimulating discussions on the structure and properties of solution during my several visits to Instituto de Materiales de Barcelona (CSIC) in the nineteen eighties. I also express my gratitude to Professor Ewa Mielniczek-Brzóska and Dr Krystyna Giełzak-Koćwin for going through the first draft of the chapters of the manuscript and for their suggestions to improve their contents, to Dr Jarosław Borc and Mr Krzysztof Zabielski for their generous assistance with the preparation of figures, and to Professor Grzegorz Gładyszewski for his constant interest in the progress of the manuscript. Finally, I thank my wife, Marta, for her unending support and patience.

Lublin, March 2021.

References

Bockris, J.O’M., and A.K.N. Reddy (1970). *Modern Electrochemistry*, Vol. 1. Plenum, New York.

Buckley, H.E. (1951). *Crystal Growth*. Wiley, New York.

Horvath, A.L. (1985). *Handbook of Aqueous Electrolyte Solutions: Physical Properties, Estimation and Correlation Methods*. Ellis Horwood, Chichester.

Robinson, R.A., and R.H. Stokes (1959). *Electrolyte Solutions*, 2nd edition, Butterworths, London.

Rodriquez-Clemente, R., S. Veintemillas-Verdaguer, F. Rull-Perez, and K. Sangwal (1988). Crystal growth from boiling solutions, *Prog. Cryst. Growth Charact. Mater*. 17, 1-40.

Stokes, R.H., and R. Mills (1965). *Viscosity of Electrolytes and Related Properies*. Pergamon Press, Oxford.

Sunagawa, I. (Editor) (1985). *Morphology of Cry*stals, Parts A-C. Terrapub, Tokyo / Kluwer, Dordrecht.

Viswanath, D.S., T.K. Ghosh, D.H.L. Prasad, N.V.K. Dutt, and K.Y. Rani (2007). *Viscosity of Liquids: Theory, Estimation, Experiment, and Data*. Springer, Dordrecht.

Wright, M.R. (2007). *An Introduction to Electrolyte Solutions*. Wiley, Chichester.

FREQUENTLY USED SYMBOLS

a	activity; constant; distance of closest approach for ions; number of ions
$a_1, a_2, \ldots$	constants
$a_i, a_j, \ldots$	regression constants
A	constant; Madelung number; surface area
$A_1, A_2, \ldots$	constants
b	constant; number of ions
$b_1, b_2, \ldots$	constants
b_i	regression constants
b_{v}'s	empirical constants
B	constant; viscosity coefficient ($\text{kg}\cdot\text{mol}^{-1}$)
c	concentration in molarity (moles of solute per liter of solvent); constant; velocity of light
C	constant; fitting parameter
C_i	regression constant
C_p	heat capacity
d	density ($\text{g}\cdot\text{cm}^{-3}$ or $\text{kg}\cdot\text{m}^{-3}$)
D	fitting parameter; function; proportionality constant; self-diffusion constant
e	electric charge
E	dimensionless activation free energy of holes in binary mixture; electric field strength; energy; fitting parameter; total energy of system
E_{D}	activation energy for diffusion
E_{p}	potential energy
E_{η}	activation energy for viscous flow
f	force constant; fraction; frequency
F	fitting parameter; force
G	Gibbs free energy of system; thermodynamic quantity
h	parameter related to solution enthalpy
h_{P}	Planck constant ($6.626\cdot10^{-34}$ J·s)
H	enthalpy (heat) of system
I	current intensity
J	fitting parameter
k	conductivity cell constant; constant
k_{B}	Boltzmann constant ($1.38\cdot10^{-23}\ \text{J}\cdot\text{K}^{-1}$)
K	constant; dissociation constant; interaction parameter; packing coefficient of liquid/solution
l	azimuthal quantum number; length

m	concentration in molality (moles of solute per kg solvent), exponent
m_l	magnetic quantum number
M	molar mass (g·mol^{-1})
M_i	regression parameter
n	concentration of charge carriers defined as number of charges per unit volume; exponent; integer; main quantum number; number of moles of a component; refractive index
n_{H1}	coordination number of first solvation shells of ions
N	integer; normality; number; number of $-CH_2$ groups
N_{A}	Avogadro number ($6.02 \cdot 10^{23}$ mol^{-1})
p	exponent; pressure; probability
P	molar polarization
q	dimensionless parameter; elementary charge ($1.602 \cdot 10^{-19}$ C)
Q	constant; function
r	radius
r_0	equilibrium distance between atoms
R	resistance
R_{G}	gas constant (8.3145 J·mol^{-1}·K^{-1})
R_{M}	molar refraction (cm^3·mol^{-1})
S	entropy of system; fitting parameter
S_i	regression parameter
S_{v}	constant in Masson's equation
T	temperature
T_{b}	boiling temperature
T_{f}	freezing temperature
T_{g}	glass transition temperature
T_{m}	melting temperature
u	flow velocity of liquid; mobility of ions
U	potential difference; potential energy
v	velocity
V	dimensionless molar volume of holes in binary mixture; volume
V_{M}	molar volume (cm^3·mol^{-1})
w	concentration in weight percent (wt%; gram solute/100 gram solvent); interaction energy; bond energy; weight; weight fraction
W	interaction energy density of solute and solute–solvent mixture; number of ways
x	concentration in mole fraction (moles of solute divided by sum of moles of solute and solvent)
Y	parameter; quantity
z	valency of an ion
Z	atomic number; coordination number; impedance; integer

Greek symbols

α	constant; degree of dissociation; polarizability of molecules
α_V	volumetric thermal expansion coefficient or expansivity (K^{-1})
β	compressibility; constant
δ	parameter; solubility parameter
ε	dielectric constant
ϕ	angle; fluidity; volume fraction
γ	surface tension
η	viscosity (mPa·s)
κ	parameter
λ	ionic conductivity; parameter; parameter related to solution activity coefficient; wavelength of light
μ	dipole moment of molecule
ν	frequency of vibration; kinematic viscosity (η/d)
θ	angle, constant
ρ	specific resistance
σ	proportionality constant; specific conductivity ($S\cdot m^{-1}$)
ξ	normalized concentration
ζ	parameter equal to about unity; Trouton constant
Δ	change in a quantity
Φ_V	apparent molar volume
Φ_V^o	apparent molar volume at infinite dilution ($= V_{M2}^o$)
Λ	molar or equilvalent conductivity ($mS\cdot m^2\cdot mol^{-1}$ or $mS\cdot m^2\cdot eq\text{-}mol^{-1}$)
Ω	constant
Ψ	strength parameter of liquid; wave function

Subscripts

a	anion
A	association
b	boiling
R	Boltzmann constant
c	cation, critical
eq	equilibrium; equivalent
G	gas constant
h	hole; hydration
HB	hydrogen bonds
i	component *i*
lim	limiting
L	liquid
m	melting
max	maximum

min	minimum
mix	mixing
M	molar
p	isobaric
rel	relative value
s	saturation; solute; solution; solvent
sol	dissolution; solution
S	isoentropic; solid
T	isothermal
V	volume
w	water

Superscripts

E	excess quantity
id	ideal
m	mixture

CONCENTRATION UNITS AND THEIR CONVERSION

Commonly used units to denote the concentration of a solute dissolved in a solvent are weight percent (wt%; gram solute/100 gram solvent), molality *m* (moles of solute per kg solvent), molarity *c* (moles of solute per liter of solvent), and mole fraction *x* (moles of solute divided by sum of moles of solute and solvent) whereas that of a solvent in a its mixture with another miscible solvent are wt%, volume percent (vol%; ml of added solvent/100 ml of main solvent) and mole fractions. In the published literature one frequently encounters different units for concentration to denote experimentally obtained data of various physical quantities even for the same or for similar systems. However, for a comparison of these data for practical purposes and for their analysis using the available theoretical concepts and equations, conversion from one concentration unit to another is desired. These conversions are given in Table 1.

Table 1. Conversion from one solute concentration unit to another[a,b]

Desired unit	wt%	Molality *m*	Molarity *c*	Mole fraction *x*
wt%	--	$\frac{100mM_2}{1000+mM_2}$	$\frac{cM_2}{10d}$	$\frac{100xM_2}{xM_2+(1-x)M_1}$
Molality *m*	$\frac{100\text{wt\%}}{M_2(100-\text{wt\%})}$	--	$\frac{1000c}{1000d-cM_2}$	$\frac{1000x}{M_1-xM_1}$
Molarity *c*	$\frac{10d\,\text{wt\%}}{M_2}$	$\frac{1000dm}{1000-mM_2}$	--	$\frac{1000dx}{xM_2+(1-x)M_1}$
Mole fraction *x*	$\frac{\text{wt\%}/M_2}{\frac{\text{wt\%}}{M_2}+\frac{(100-\text{wt\%})}{M_1}}$	$\frac{mM_2}{mM_1+1000}$	$\frac{cM_1}{c(M_1-M2)+1000d}$	--

[a] Adapted from Engineering Tool Box (web: https://www.engineeringtoolbox.com; [b] M_1 denotes molar mass of solvent (g mol^{-1}), and M_2 molar mass of solute (g mol^{-1}).

1

STRUCTURE OF LIQUIDS

Solvent is defined as a chemical substance (usually a liquid) that dissolves other substances, which may be gaseous, liquid or solid, without chemically changing them. A homogeneous mixture of physically combined two or more substances is known as solution. A solvent as well as a solution exhibit the same properties throughout its volume. The component which is present in excess is usually referred to as the solvent whereas the other component combining with the former in different proportions is termed the solute.

Solvents used on both laboratory and industrial scale exist in the liquid state at ordinary temperature and pressure conditions. They are inorganic compound like water and many organic compounds composed of molecules (molecular liquids) as well as a diverse group of salts composed of large organic structures as cations and organic or inorganic-based relatively small anions (low-temperature ionic liquids). Molecular solvents are widely used as a reaction medium for sample extraction and preparation, for various industrial cleaning applications, and for recrystallization to purify compounds and growth of their single crystals suitable for applications. Organic solvents are also commonly used for dissolving paint, oil and grease, mixing or thinning pigments, pesticides, glues, epoxy resins and paints, and cleaning automotive parts, tools and electronics. Partitioning between an organic phase and an aqueous phase is an effective way of extracting products.

During the last three decades, low-temperature ionic liquids (ILs) have drawn enormous interest as new solvents for the synthesis and extraction of materials (Handy, 2011; Marsh et al., 2004; Sindt et al., 2011; Zhang et al., 2006; Zhao, 2017). This increasing interest in ILs is due to a unique combination of their properties. In comparison with conventional organic solvents, at normal temperature and pressure conditions ILs have negligible vapor pressure, larger temperature range for the liquid state, high viscosity, relatively high electrical conductivity, density higher than that of water, and moderate polarity. Consequently, ILs are miscible with different substances having a wide range of polarities and can dissolve both organic and inorganic substances. High viscosities are favorable for their application as lubricants.

This chapter describes some general features of structure and properties of solvents and solutions. After a brief description of the structure of atoms and molecules composing solvents, different types of bonds in the building units in condensed states and characteristics of solidification and evaporation of alkanes and alcohols (Section 1.1), properties of molecular and low-temperature ionic-liquid solvents (Section 1.2), structure of solvents (Section 1.3), and models of liquid structure (Section 1.4) are presented. Finally, typical processes involved during the formation of aqueous and nonaqueous solutions of different solutes and the structure of solutions are described in Sections 1.5 and 1.6. The reader is referred to the literature for more information on the following topics: general topics (for example, see: Atkins, 1998; Barrow, 1973; Eggers et al., 1964; Mortimore, 2008), electrolyte solutions (Bockris and Reddy, 1970; Horvath, 1985; Marcus, 2009; Stokes and Mills, 1965; Wright, 2007), and ionic liquids (Handy, 2011; Zhang et al., 2014).

1.1. Different states of matter

The aim of this section is to discuss what holds different atoms in molecules and the molecules in different phases. We start from the structure of atoms and the distribution of electrons around the atomic nucleus, the packing of atoms/molecules in condenced phases (i.e. liquid and solid), and then describe characteristic features of transformation of different phases.

1.1.1. Electronic structure of atom

Hydrogen is the simplest atomic system which plays a key role in understanding atomic structure. According to Bohr's model, a hydrogen-like atom consists of an immobile nucleus ($+Ze$ charge, with the number of unit charges on the nucleus $Z \geq 1$) and an electron ($-e$ charge) moving around it in specific orbits at distance r, held together by attractive electrostatic force between them. The potential energy U of the electron for this system is

$$U = -\frac{1}{4\pi\varepsilon_0}\frac{(Ze)e}{r}, \tag{1.1}$$

where ε_0 is the dielectric constant of vacuum and $Z = 1$ for hydrogen. Since the hydrogen-like atom is a trap for the electron restricting its motion to specific orbits in space, the movement of the electron in an orbit around the nucleus can be treated as electron density distribution (i.e. probabilty of locating its position around the nucleus) using the wave function ψ, described by Schrödinger equation

$$\nabla^2\psi + \frac{8\pi^2 m_\mathrm{e}}{h_\mathrm{P}^2}(E - U)\psi = 0\,, \tag{1.2}$$

where E is the energy of the system, m_e is the mass of the electron, and h_P is the Planck constant. Eq. (1.2) has a solution when $E < 0$ (i.e. the electron is bound in the atom) and has discrete energy values. Since the field in which an electron moves around the nucleus has spherically symmetry, it is convenient to use polar coordinates (r, and two angles θ and ϕ), as shown in Figure 1.1, to solve Eq. (1.2). Since the potential energy U of the electron depends only on the distance r and is independent of the angles, the quantized values of the energy E of the electron in the atom are given by

$$E_n = -\frac{m_e e^4}{32\varepsilon_0^2 h_P^2}\frac{Z^2}{n^2}, \qquad \text{with } n = 1, 2, 3, \ldots. \tag{1.3}$$

The integer n is known as the *main quantum number* and refers to the orbital in which the electron of energy E_n can be localized. According to the Bohr model, the difference ΔE in the energies of two successive energy levels E_{n+1} and E_n of orbitals $n+1$ and n is a constant energy quantum equal to $h_P\nu$, where ν is the frequency of radiation absorbed by the electron moving from an orbital of higher energy E_{n+1} to one of lower energy E_n.

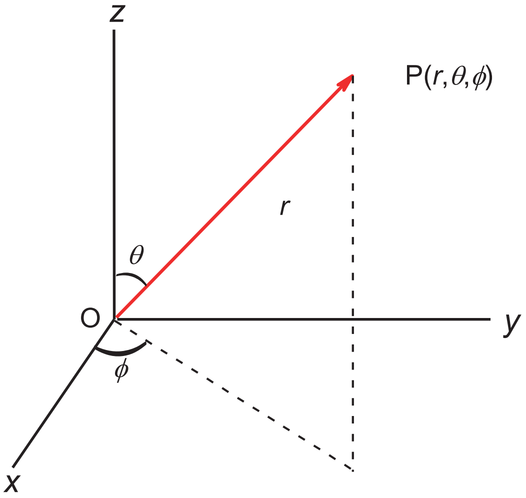

Figure 1.1. Definitions of angles θ and ϕ for the solution of the Schrödinger equation, Eq. (1.2). Nucleus has coordinates 0,0,0 whereas the electron is at a distance r from the nucleus.

It should be mentioned that the term *orbital* for an electron surrounding the nucleus of an atom sounds similar to that of the *orbit* for the movement of a planet around the Sun, but they differ in their meanings. The movement of a planet occurs in its definite path, called an orbit, which can be defined by the exact location and trajectory of the planet. The model of a hydrogen-like atom looks similar because of the motion of the electrons around the nucleus in its orbit. However, in reality it impossible to define the orbit for an electron around a nucleus because the Heisenberg Uncertainty Principle states that both the position and the momentum of an electron cannot be defined with absolute precision at the same time. Instead, the electrons can be located anywhere in regions of space known as orbitals and have an energy E_n, if they are in their orbitals of a principal quantum number n.

The wave function ψ of Eq. (1.3) has three parameters n, l and m_l, expressed by

$$\psi = \psi_{n,l,m_l}(r,\theta,\phi). \tag{1.4}$$

The parameters l and m_l are *azimuthal* and *magnetic quantum numbers*, respectively. The maximum value of $l = (n-1)$, such that, for a given n, the azimuthal quantum number l can take n different values, i.e.

$$l = 0, 1, 2, \ldots, (n-1). \tag{1.5}$$

For a given l, the quantum number m_l can take $2l+1$ different values, i.e.

$$m_l = \pm l, \tag{1.6}$$

with l given by Eq. (1.5).

According to Eq. (1.3) the energy of the electron depends only on the main quantum number n. Consequently, for $n \geq 2$, each value of E_n corresponds to several different functions ψ_{n,l,m_l} differing in the values of the quantum numbers l and m_l. In other words, the hydrogen-like atom can have one and the same value of energy existing in many different states. Quantum states of the same values of energies are called degenerate states, whereas the number of states of the same values is called the degeneracy of the given energy level. Taking into account the possible values of l and m_l one can easily calculate the degeneracy in these energy levels. Since each of the orbital n of azimuthal quantum number l correspond to $2l+1$ values of the magnetic quantum number m_l, the number of different states corresponding to a given n may be given by

$$\sum_{l=0}^{n-1}(2l+1) = n^2 . \tag{1.7}$$

Obviously, the degeneracy of the energy levels of a hydrogen-like atom is n^2 and is summarized in Table 1.1 for the first three energy levels.

With reference to the nucleus of an atom, the energy levels of the main quantum number n are denoted as 1, 2, 3, …, with increasing distance from the atomic nucleus. These numbers correspond to the lines K, L, M, …, of the optical spectrum of hydrogen. All energy states with different azimuthal quantum number l also have their notations. An electron existing in the state $l = 0$ is known as *s electron* (i.e. *s* state), in $l = 1$ as *p electron*, in $l = 2$ as *d electron*, in $l = 3$ as *f electron*, and in the subsequent states as *g*, *h* and so on according to the letters in the English alphabet. The notations *s*, *p*, *d* and *f* have their origin in the English names used to denote the lines of the spectra of atoms: *sharp*, *principal*, *diffuse* and *fundamendal*. The orbitals of the energy level E_n are denoted by the main quantum number n given before the azimuthal quantum number l, as listed in Table 1.1.

According to the above convention, the *s* orbitals are spherically symmetric around the nucleus. The 2*s* orbital is similar to a 1*s* orbital, with the difference that it is at the second energy level and the region where there is the greatest probability of finding the electron is farther from the nucleus. The likelihood of finding an electron at a particular place in some region is described by the electron density as shown in Figure 1.2a for the 1*s* and 2*s* orbitals.

Table 1.1. Degeneracy of energy levels of a hydrogen-like atom

Energy level E_n	Wave function ψ_{n,l,m_l}	Values of quantum numbers			Notation
		n	l	m_l	
E_1	ψ_{100}	1	0	0	1*s*
E_2	ψ_{200}	2	0	0	2*s*
	ψ_{21-1}	2	1	−1	2*p*
	ψ_{210}	2	1	0	2*p*
	ψ_{21+1}	2	1	+1	2*p*
E_3	ψ_{300}	3	0	0	3*s*
	ψ_{31-1}	3	1	−1	3*p*
	ψ_{310}	3	1	0	3*p*
	ψ_{31+1}	3	1	+1	3*p*
	ψ_{32-2}	3	2	−2	3*d*
	ψ_{32-1}	3	2	−1	3*d*
	ψ_{320}	3	2	0	3*d*
	ψ_{32+1}	3	2	+1	3*d*
	ψ_{32+2}	3	2	+2	3*d*

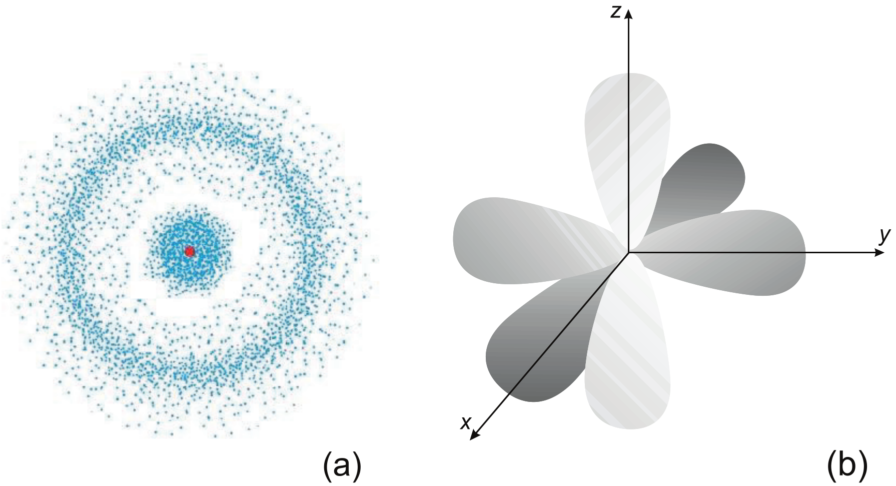

Figure 1.2. (a) 2*s* and (b) 2*p* orbitals of hydrogen electron. Orbitals 2*s* of (a) from Halliday et al. (2001).

Apart from the 2*s* orbital at the second energy level, there are 2*p* orbitals. The 2*p* orbitals have the shape of two identical balloons tied together at the nucleus and pointing mutually at right angles to each other in the *x*, *y*, and *z* directions. The three *p* orbitals are equivalent and are arbitrarily denoted as p_x, p_y and p_z (Figure 1.2b). The *p* orbitals at the second energy level are called $2p_x$, $2p_y$ and $2p_z$. Similarly, there are orbitals, like $3p_x$, $3p_y$, $3p_z$, $4p_x$, $4p_y$, $4p_z$ and so on, at subsequent energy levels. Since the s orbitals are closer to the nucleus than the p orbitals, the energy levels of s orbitals lie somewhat lower than those of the $2p$ orbitals.

The above wave mechanical model of hydrogen-like atom may be extended to describe the type of orbitals occupied by the various electrons in a complex atom using the Pauli exclusive principle which states that no two electrons in an atom can have the same quantum numbers. This is described by the selection rule for the azimuthal quantum number, i.e. $\Delta l = \pm 1$. This rule implies that only those transitions are possible in which l changes by 1. This is associated with the fact that a foton representing the electron has its intrinsic angular momentum which can have only two values: $+\frac{1}{2}(h/2\pi)$ and $-\frac{1}{2}(h/2\pi)$. This gives a fourth quantum number, the spin quantum number s, which can have two possible values: $+\frac{1}{2}$ and $-\frac{1}{2}$. Therefore, to define the state of an electron, one gives the three quantum number n, l and m_l, and the spin quantum number s. When the spin s of an electron is taken into account, the total number of energy levels becomes $2n^2$ (see Table 1.1, and Eq. (1.7)). The electron spins are indicated by arrows arbitrarily taking the arrow (↑) directed upward and the arrow (↓) directed downward to denote opposite spins of the two.

A $1s$ orbital holding 2 electrons is written as $1s^2$, $2s$ orbital having 2 electrons as $2s^2$, $2p$ orbital with 2 electrons as $2p^2$, and so on. Note that the index 2 here denotes the number of electrons and has nothing to do with the energy level. According to this notation the lone electron of a hydrogen atom may be written as $1s^1$, which implies that filling of this orbital by another electrons gives it the energy level of neutral He atom.

Following the above procedure of filling an extra electron into the next available orbital by moving from one atom to the next in the periodic table, the electronic structure of the next atom can be determined. As a first approximation such atoms can be considered to be consisting of two parts: (1) a core made up of the nucleus and all electrons belonging to filled orbitals, and (2) the electron(s) of interest. Electrons fill low energy orbitals closer to the nucleus before filling orbitals of higher energies. We consider the example of lithium atom containing three protons in its nucleus and three electrons distributed about the nucleus. The first two of these electrons will occupy the lowest energy level ($n = 1$), leaving the third electron to occupy the second level ($n = 2$) in the available s or p orbitals. Since an electron in a $2s$ orbital ($l = 0$) has a much higher probability of penetrating into this core than does an electron in the $2p$ orbital ($l = 1$), this third electron will occupy the $2s$ orbital. This results in the electron configration of Li as $1s^2$, $2s^1$.

The electron configuration for Be is $1s^2$, $2s^2$, for B is $1s^2$, $2s^2$, $2p^1$, and for C is $1s^2$, $2s^2$, $2p^2$. However, in the case of C, the two p electrons occupy two different p orbitals because the parallel arrangement of spins of the two electrons ensures a lower energy state than that in which the spins are antiparallel as in the same p orbital. In other words, if there is a choice between orbitals of equal energy, they fill the orbitals singly as far as possible before pairing up. States in which two electrons have the same spin are known as triple states because they are triply degenerate. This is due to the fact that the resulting spins are +1, −1 and possibly 0. The filling of orbitals singly whenever possible is known as *Hund's rule*. It applies to orbitals with exactly the same energies.

In the elements N through Ne the other 2*p* orbitals are occupied. In Na the 3*s* orbital is occupied, and the elements thereafter follow a pattern similar to the first row elements of the periodic table ending with Ar with the configuration: $1s^2$, $2s^2$, $2p^2$, $2p^6$, $3s^2$, $3p^6$. In K and Ca the 4s orbitals are filled. However, with the next element scandium (Sc), the 3*d* orbitals begin to be filled. Thus, we enter the first group of transition elements, which are characterized by multiple valency and colored compounds. These properties are due to the fact that 3*d* and 4*s* energy levels are close to each other. Figure 1.3 schematically shows the energies of the orbitals up to the 4*d* level.

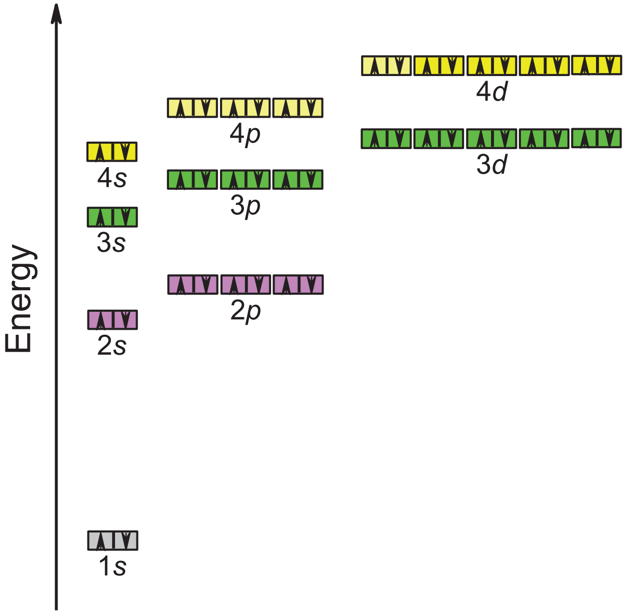

Figure 1.3. Schematically presentation of energies of orbitals up to the 4*p* level. Opposite spins of electrons occupying a given orbital are shown by arrows ↑ and ↓.

It should be emphasized that the *s* orbital always has a slightly lower energy than the *p* orbitals at the same energy level. Therefore, the *s* orbitals are filled with electrons before the corresponding *p* orbitals. The position of the 3*d* orbitals is unusual because they are at a slightly higher level than the 4*s*. Consequently, the 4*s* orbital is filled first, followed by all the 3*d* orbitals and finally the 4*p* orbitals.

The physical and chemical properties of atoms are intimately connected with the most weakly bound electrons with their nuclei. The trends of these properties may be understood from the arrangement of elements in six horizontal columns of the periodic table. With the exception of the first row containing H and He containing $1s^1$ and $1s^2$ orbitals, the elements in the periodic table are arranged in such a manner that each of the elements begins from the left with the chemically very active alkali metal (Li, Na, K, Rb, etc.) and ends up on the right with chemically inert nobel gas (Ne, Ar, Kr, etc.). For example, if one considers the energy of ionization of the elements, its value for the elements in a row is the lowest for the very reactive alkali metals and is the highest for the nobel gas elements, and for the elements in a column decreases with the atomic number Z. These trends are associated with the amount of energy absorbed by the atoms of the lower energy state to attain a higher energy state and the value of this energy shows a general tendency to increase with the number of electrons in the outermost orbitals of atoms.

As mentioned above, the charge distribution around an atom is not restricted into a rigid spherical space. Therefore, the size of an atom depends on whether it is free, or in a metal, or in an ionic crystal. For example, the radius of a sodium atom in metallic sodium is taken as 0.186 nm but that of a sodium ion is 0.124 nm. However, in general, the sizes of atoms and ions of various elements increase relatively insignificantly with their atomic number Z because of increasingly stronger coulombian attraction between the $Ze+$ charge of the nucleus and the surrounding electrons.

1.1.2. Binding of atoms and molecules

Molecules are composed of similar or different atoms held together by interatomic interactions called *chemical bonds*. Molecules are stable systems that exist in different states of matter at usual temperature and pressure conditions. Existence of molecules is an evidence of the presence of forces acting between atoms. Dissociation of a molecule into its atoms composing it is possible only when certain amount of work is done. This means that the formation of a molecule from its atoms is always accompanied with the release of a certain amount of energy (e.g. as heat). The energy released in the formation of a molecule is a measure of the value of these forces.

Depending on the distance r between two atoms, there are two types of interactions: (1) attractive, and (2) repulsive interactions (see Figure 1.4a). Here the distance r is taken between the centers of the nuclei of atoms. The attractive interaction forces occur over long distances, but the repulsive forces become pronounced at short distances. These forces are usually known as *long-* and *short-range forces*, respectively. There is no interaction between atoms separated from each other at sufficiently large distance r, but a decrease in the distance r between the atoms results in increasing interaction forces F_1 of mutual attraction with r. At small distances r, short-range repulsive forces F_2 begin to operate. At still smaller distances these repulsive forces are so large that they do not allow the atoms approach more closer. In other words, there is an equilibrium distance r_0 between the atoms when the resulting force is zero and the system of two atoms is stable. Without paying attention to the physical origin of the forces between the two atoms, the resulting force as a function of r may be given by

$$F = F_1 + F_2 = -\frac{A}{r^{a'}} + \frac{B}{r^{b'}}, \tag{1.8}$$

where A and B are constants, the exponent $a' \ll b'$, and A, B, a' and b' are chracteristics for the molecule. Note that attractive force $F_1 < 0$, repulsive force $F_2 > 0$, and the curvatures of $F_1(r)$ and $F_2(r)$ depend on the values of a' and b'. From Eq. (1.8) the potential energy $E_p(r)$ of one of the atoms in the presence of the second may be given as

$$E_p(r) = -\int_0^r F dr = -\frac{A}{ar^a} + \frac{B}{br^b}, \tag{1.9}$$

where $a = (a'-1)$ and $b = (b'-1)$. The force F and the energy E_p between the two atoms of the molecule are shown schematically in Figure 1.4a and b, respectively. In the stable configuration when $r = r_0$, $F_1+F_2 = 0$ and there is a minimum in the $E_p(r)$ curve and the corresponding energy is negative. This energy, taken as $-E_p(r_0)$, is the dissociation energy of the molecule. Dissociation may occur when the molecule absorbs energy supplied externally.

From Eq. (1.9) the equilibrium distance r_0 and the corresponding binding energy $E_p(r_0)$ may be obtained in terms of the constants A, B, a and b in the form:

$$r_0 = \left(\frac{B}{A}\right)^{\frac{1}{b-a}}, \tag{1.10}$$

and

$$E_p(r_0) = -\frac{A}{ar_0^a}\left(1 - \frac{a}{b}\right). \tag{1.11}$$

It should be noted that although the attractive and repulsive forces are equal in the equilibrium position of the two atoms at $r_0 = 0$, these two forces are not equal because $a \neq b$ and both a and b are positive quantities. In fact, when $b \gg a$, the binding $E_p(r_0)$ is essentially determined by the energy of attraction $-A/ar_0{}^a$, with $a \geq 1$.

As seen from Figure 1.4, a minimum in the $E_p(r)$ curve is possible only when $b > a$. Physically, this condition means that the repulsive forces F_2 are of short range in comparison with the attractive forces F_1 which are of long range. In Eq. (1.9) the contributions to the total potential energy E_p due to these two forces are represented by power-law functions with the constants b and a. The value of the repulsive exponent b between two ions is related to the distribution of electronic charges in the outer orbitals, which correspond to the closed-shell electronic configurations of inert gas atoms. This value of b is expected to increase with the charges Z_Ae^- and Z_Ce^- associated with the interacting anion and cation of atomic numbers Z_A and Z_C, respectively. The values of b, suggested by Pauling, are 5, 7, 9, 10 and 12 for He(Li^+), Ne(Na^+, F^-), Ar(Cu^+, K^+, Cl^-), Kr(Ag^+, Rb^+, Br^-) and Xe(Au^+, Cs^+, I^-), respectively; for example, see Dekker (1964). Therefore, the average value of b is 6 for LiF, 8 for NaCl, 9 for KCl, and 12 for CsI. With these values of the repulsive exponent b and the value of the attractive exponent a in the molecules of different types, the binding energy $E_p(r_0)$ in the molecules may be calculated. For example, in the case of molecules composed of oppositely-charged ions involving electrostatic interactions, the attractive exponent $a = 1$ in Eq. (1.9) and, depending on the dimensions of the ions, the repulsive exponent b lies between 6 and 12. Then this $E_p(r)$ equation is known to represent *electrostatic* or *Coulomb potential*. When the attractive interactions between the atoms of the molecule are weak as in intert gas atoms, it is considered that $a = 6$ and $b = 12$ in Eq. (1.9). Then this equation is known to represent *Lennard–Jones potential*, with $A = 4\varepsilon\sigma^6$, and $B = 4\varepsilon\sigma^{12}$, where ε and σ are new parameters related to the properties of inert gas crystals.

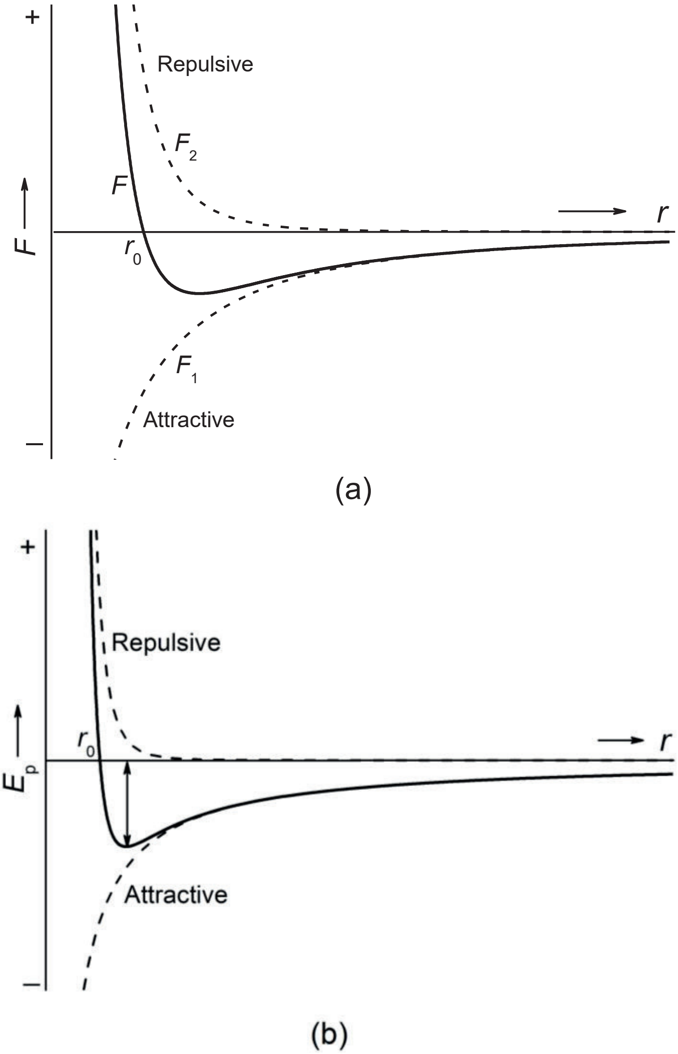

Figure 1.4. Schematic representation of (a) forces F and (b) energies E_p between two atoms as a function of their separation r. Dashed curves show attractive and repulsive components whereas solid curves represent the sums of these attractive and repulsive components.

From the above discussion it may be concluded that the power-law relations are useful in understanding general features of different types of chemical bonds. However, it is found that power-law functions do not represent the repulsive interaction accurately, as in the case of strong bonding by electrostatic interaction where an exponential function is used. For more details on this subject, the reader is referred to the literature (for example, see Kittel, 1976).

Interactions between atoms may be understood keeping in mind that: (1) an atom as a whole is an electrically neutral entity, and (2) electrons occupying the outermost orbitals, usually known as valence electrons, of the atomic structure are responsible for the interatomic interactions. The latter requirement is consistent with the fact that the ionization potentials of valence electrons are much lower than those of the electrons lying in deeper completely filled orbitals. We consider first the binding in a biatomic molecule according to the sharing of electrons by them.

The chemical bond between atoms in molecules may be considered to be of two extreme types. In the first type of bonds, known as *heteropolar* or *ionic bond*, an electron from the outermost *occupied* orbital of one of the atoms is transferred to the outermost *unoccupied* orbital of the other atom such that the occupied orbitals of the two atoms attain the electron structure of inert gas atoms. Conseqently, the electrons surrounding the nuclei are rearranged in such a way that an excess of electrons is created around the nucleus of one of the atoms and a deficiency of electrons around the nucleus of the other. The electron structure surrounding individual nuclei of the atoms is considered to belong entirely to each of them. Charged entities containing the number of electrons less and more than the number of electrons in the corresponding atoms are known as *cations* and *anions*, respectively. Example of ionic bonds are: Na^+Cl^-, K^+Cl^-, and H^+Cl^-.

The second type of bonds, known as *homeopolar bond* (or *covalent* or *atomic bond*), occurs in molecules in which part of the valence electrons moves around both nuclei. This bond is formed by electrons of antiparallel spins involved during similar attraction of two nuclei of atoms for electrons, with the result that the bonding electrons may be considered to be shared equally between them. Examples are diatomic molecules like H_2, N_2 and O_2 composed of similar nuclei and molecules like CN composed of different nuclei. The electrons in the first type of molecules are arranged symmetrically whereas they are arranged somewhat asymmetrically in the second type of molecules, with the result that these molecules have an electrical dipole moment.

There are only two bonding 1*s* electrons of two H atoms in H_2 molecule to form a single bond, whereas there are six bonding electrons in N_2, one pair occupying a σ orbital and the other two occupying π orbitals, to constitute a triple bond, and four net bonding electrons, two σ and two π, to constitute a double bond in O_2 (about σ and π bonds; see below). In contrast to the above symmetrical molecules, the asymmetrical molecule CN is formed by four and three bonding electrons of C and N atoms, constituting a triple bond and leaving an unbonded electron with C. It should be mentioned here that the energy associated with the formation of a bond in a molecule depends on the distance r between the atoms and the orientaion of the spins of the valence electrons, as shown schematically in Figure 1.5. Homeopolar bond in a molecule is formed only when the electrons of the approaching atoms have antiparallel spins. Parallel spins of the electrons result in increasing repulsion between the atoms and are not favorable for bond formation.

It should be mentioned here that an essentially covalent bond is always accompanied by a certain degree of ionic character which is determined by the electronegativity of the atoms involved, i.e. the relative electron-attracting ability of the nuclei of two atoms. The electron affinities and ionization potentials of atoms are used to define the electronegativity of atoms. The electron affinity is a measure of the energy evolved on addition of an atom to the neutral atom, while the ionization potential is a measure of the energy required to remove an electron from the neutral atom.

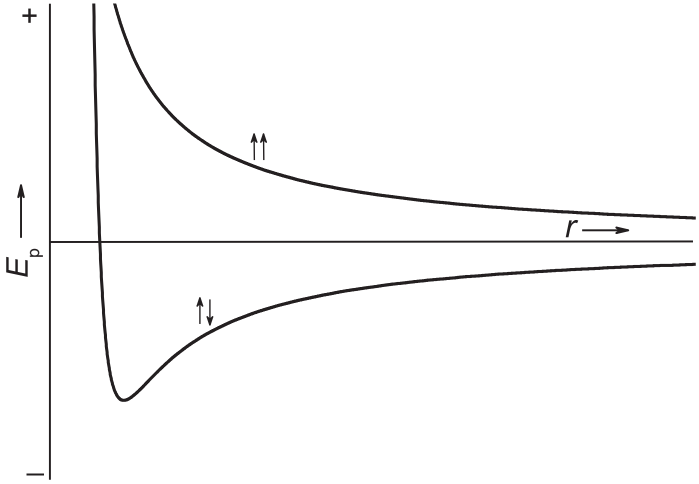

Figure 1.5. Schematically illustration of dependence of interaction energy $E_p(r)$ on the distance r between atoms for parallel (↑↑) and antiparallel (↑↓) spins of their valence electrons.

The geometrical arrangement of atoms in polyatomic molecules is determined by the number of electron pairs about their central atoms, and may be predicted from the simple principle that electron pairs show coulombian repulsion and even stronger Pauli repulsion for other electron pairs at short range. Thus, a preferred spatial arrangement is one which places electron pairs as far as possible from each other. For example, when there are two electron pairs about a central atom, the resulting molecule is linear. When there are three electron pairs about a central atom, the favored arrangement is triangular (for example, BF_3 molecule). However, for four electron pairs, the structure is tetrahedral (CH_4); for six electron pairs, the arrangement is octahedral (SF_6 molecule).

Electronic orbitals in the central atoms in the molecules are frequently of different types. In the case of CH_4 molecule for example, the four orbitals of the central C atom to form covalent bonds with the $1s^1$ orbitals of H atoms are $2s^2$ and $2p^2$. Therefore, one may anticipate the formation of different classes of bonds with the four $1s^1$ orbitals of H atoms by the $2s^2$ and $2p^2$ orbitals. Since the four C–H bonds about the central C atom are the same and are represented by a regular tetrahedral arrangement (Figure 1.6a), the above unsatisfactory description is reconciled in terms of four equivalent *hybrid orbitals*, each of which is constructed from one *s* and three *p* atomic orbitals, written as sp^3 orbitals. However, hybrid orbitals can also be constructed by combining atomic orbitals other than sp^3. Some hybrid orbitals and the resulting atomic configurations are listed in Table 1.2.

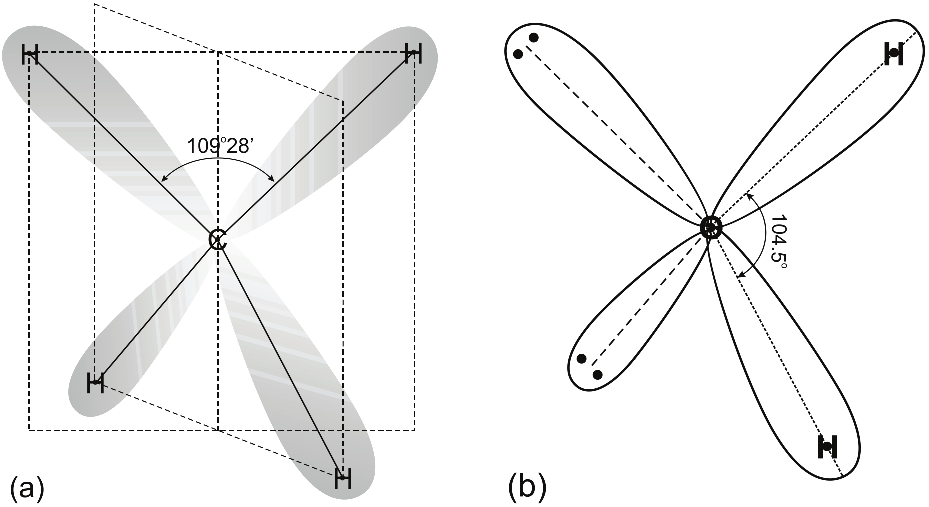

Figure 1.6. Arrangement of bonding orbitals in molecules of (a) CH_4 and (b) H_2O. Carbon and oxygen atoms are situated at the center of the tetrahedron.

Table 1.2. Some examples of hybrid orbitals and atomic confurations

Orbital	Configuration	Bond angle
sp^2	Triangular (plane)	120°
sp^3	Tetrahedral	109°28'
dsp^2	Square (plane)	90°
d^2sp^3	Octahedral	90°

The arrangements of atoms in NH_3 and H_2O molecules can also be described in terms of four sp^3 orbitals formed along the direction joining the central N and O atoms to the corners of a tetrahedron such that their H atoms are placed at its corners and tetrahedral angle is 109°. The atomic arrangement in a H_2O molecule is shown, as an example, in Figure 1.6b. Of the four electron orbitals in four equivalent directions in space, two are used in the O–H bonds, and the remaining two remain as free orbitals for the lone pair of electrons. In the water molecule the H–O–H angle is about 104.5° and the O–H distance lies between 0.096 and 0.102 nm. This deviation from the tetrahedral angle is associated with the fact that the lone pairs of electrons exhibit stronger repulsion on the other electron pairs than do the electrons involved in O−H bonds. A similar interpretation holds in the observed deviation in the H−N−H angle in the NH_3 molecule.

From the viewpoint of charge distribution, a water molecule can be represented as an assembly of four charges (quadrupole) of equal magnitude q, a charge of $+q$ near each hydrogen atom and two charges each of value $-q$ near the oxygen atom. However, although a water molecule is neutral electrically, the centers of its negative and positive charges do not coincide, leading to excess (positive) charge $+\delta$ concentrated on each H^+ atom bonded to O^{2-} atom, with excess (negative) charge -2δ concentrated on the O^{2-} atom. Thus, a water molecule may be considered as an electric dipole.

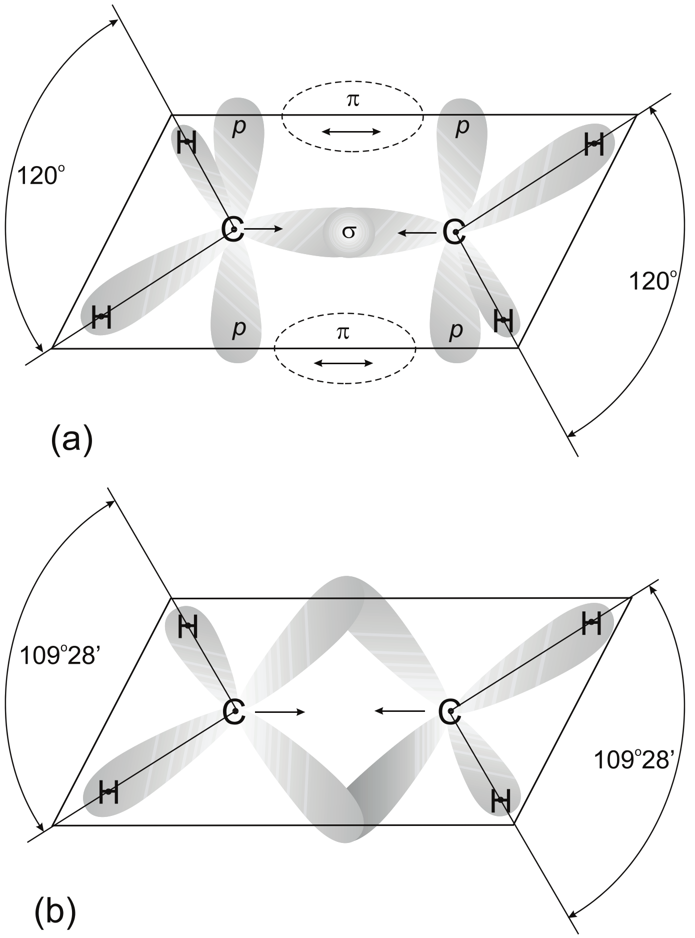

Figure 1.7. Formation of bonds in ethylene (C_2H_4) by (a) sp^2 and (b) sp^3 orbitals. See text for details.

In contrast to the above single bonds due to single bonding orbitals, two and more bonding orbitals result in double and more bonds. To describe such bonds we consider an ethylene molecule (C_2H_4) in which two different hybrid orbitals between the two C atoms can bind the $-CH_2$ groups of the molecule, as shown in Figure 1.7. If one considers the sp^2 hybrid orbitals between the two C atoms (i.e. triangular configuration, with an angle 120° between the bonds), the arrangement of Figure 1.7a is possible. This orbital has σ symmetry, and is therefore known as a σ bond. However, this arrangement leaves a *p* orbital projecting at right angles to the plane of the hybridized orbitals. Therefore, the two atomic *p* orbitals give a second bond of π symmetry. This type of bonding is known as the σ–π double bond. Another type of double bond involves the formation of two equivalent orbitals between the carbon atoms by two sp^3 hybridized orbitals from each atom, as presented in Figure 1.7b. In this arrangement the possible angle between the C–H bonds is 109°28'.

The above description may be used to understand the arrangement of different types of multiple bonds in complex molecules and molecular groups (called ligands) about a central ion as well as single and double bonds in various radicals such as OH^- and $H–O=O^-$. The nature of bonds in the molecules of simple alkanes and alcohols may also be described in a similar way. The linear structure of alkanes C_nH_{2n+2} (written as n-C_6H_{14} for hexane for example), composed of an orbital bonding between two successive C atoms, may be constructed by inserting a CH_2 group between the central C atom of tetrahedral arrangement of a CH_4 molecule and one of its H atoms. The additional bond between the two C atoms is obtained by combining one sp^3 orbitals from each C atom. This orbital has σ symmetry. A two-dimensional presentation of the arrangement of atoms in a *n*-hexane molecule is shown below:

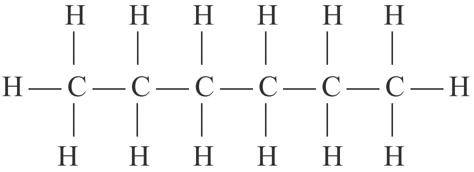

$$\begin{array}{ccccccccccccc} & & H & & H & & H & & H & & H & & H & & \\ & & | & & | & & | & & | & & | & & | & & \\ H & — & C & — & C & — & C & — & C & — & C & — & C & — & H \\ & & | & & | & & | & & | & & | & & | & & \\ & & H & & H & & H & & H & & H & & H & & \end{array}$$

However, it may be noted that insertion of a $-CH_2$ group is also possible in one of the branched positions in alkanes with carbon number $n \geq 4$, i.e. butane (C_4H_{10}) onwards.

The arrangement of atoms in an alcohol molecule containing *n* number of C atoms differs from the molecule of its alkane counterpart in the substitution of one of the C–H bond by a C–O–H bond. In the case an *n*-alcohol (n-$C_nH_{2n+1}OH$) molecule the C–O–H bond occurs with one of the two terminal C atoms. However, this substitution can also take place with carbon atoms in the branched positions.

As in the case of an atom, the change in the energy of a molecule occurs as a result of a change in the electronic configuration of the outer part of the molecule. However, for a given electronic configuration, the nuclei of the molecule can oscillate and rotate about the common center of mass. There are particular values of energies associated with these oscillations and rotations. The total energy E of the molecule may, therefore, be expressed as a sum of different type of movements as

$$E = E_{\text{elec}} + E_{\text{osc}} + E_{\text{rot}}\,, \tag{1.12}$$

where E_{elec} is the energy resulting from the electronic configuration (electronic energy), E_{osc} is the energy corresponding to the vibrations in the molecule (oscillation energy), and E_{rot} is the energy associated with the rotation of the molecule (rotational energy). Since each component of the energy E has a series of distinct quantized energy levels, variations in its value are possible only in quanta, leading to the formation of molecular spectra.

Here no attempt is made to discuss the origin of energy spectra of molecules. A curious reader can find appropriate information on the subject in the specialized literature. However, the idea of quantization of energy levels in the $E_{\text{p}}(r)$ curve of Figure 1.4 due to vibrations of nuclei in a molecule may be had by considering them as those by a linear harmonic oscillator. According to quantum mechanics, the possible energy levels of a harmonic oscillator are given by

$$E_{\text{osc}} = \left(n_{\text{osc}} + \frac{1}{2}\right)h_{\text{P}}\nu\,, \qquad n_{\text{osc}} = 0,\ 1,\ 2,\ \ldots, \tag{1.13}$$

where n_{osc} is the oscillation quantum number, and ν is frequency of vibration of the oscillator. The term $h_{\text{P}}\nu/2$ is the zero-point energy of the oscillator. This value corresponds to oscillation quantum number $h_{\text{P}}\nu/2 = 0$ and indicates the occurrence of vibrations of nuclei in the molecule at $T = 0$ K. For a transition between the possible energy levels of the oscillator the following selection rule holds:

$$\Delta n_{\text{osc}} = \pm 1. \tag{1.14}$$

This means that absorption of photon energy $h_{\text{P}}\nu$ results in a transition with $\Delta n_{\text{osc}} = +1$, but emission of $h_{\text{P}}\nu$ leads to a transition with $\Delta n_{\text{osc}} = -1$. The wave-numbers ν^* corresponding to these transitions may be calculated from the relation: $\nu^* = 1/\lambda = \nu/c$, where c is the velocity of light in vacuum and λ is the wavelength of light.

1.1.3. Binding of building units in condensed states

Under appropriate temperature and pressure conditions all elements and compounds can exist in the vapor, liquid and solid states. The basic structural units that are present in different states of matter are atoms, monatomic ions, and molecular or ionic groups which may be recognized in different phases.

The different states of matter are characterized by the mean distance between the atoms and molecules composing them, and the ratio of the average potential energy of atoms/molecules to their kinetic energy is a characteristic parameter of the state. In the vapor state the atoms/molecules move randomly undergoing elastic collisions among themselves in the entire space available to them and the average distance between them is much larger than their size. The attractive forces between the atoms/molecules are too small to keep them close to each other. In the liquid state the average distance between the atoms/molecules is decreased to the extent that mutual attractive forces hold them close to each other. In other words, there is short-range order between nearest neighbors and both the number and the positions of nearest neighbors are, on an average, the same for all. However, atoms/molecules in the liquid have sufficient kinetic energy to jump from one position to the next. In the solid state the distance between the neighboring atoms/molecules in the entire volume is similar to the average distance between them in the liquid state. In this case the attractive forces are strong enough to keep them in their equilibrium positions despite their thermal motion and are of long-range order.

1.1.3.1. The crystalline state

We consider crystalline solids in which the atoms/molecules are arranged in a regular manner, forming a periodic three-dimensional structure known as lattice. Here we are not concerned with such solids as glass, rubber or wood, in which the atoms/molecules are not arranged peridically in the three dimensions. As examples of three-dimensional periodicity in the arrangement of building units the crystal structures of sodium chloride, copper and diamond crystals are illustrated in Figure 1.8. The common feature of these structures is that a building point occupies each of the eight corners of the unit cube of edge length *a*, and, if the smaller building units (Na^+ ions here) are not taken into consideration, another building unit occupies the center of each of the six side faces. These types of crystal structures are known as *face-centered cubic* (fcc) lattices.

It may be seen that the NaCl lattice may be considered to be composed of two face-centered cubic lattices of Na^+ and Cl^- ions displaced relative each other by $a/2$, and the unit cube of Figure 1.8a contains four NaCl molecules in contrast to four atoms of Cu in the unit cube of Figure 1.8b. Each Cu atom has six nearest neighbors and 12 next nearest neighbors in the Cu lattice (Figure 1.8b), whereas each ion has six ions of opposite kind as its nearest neighbors and 12 similar ions as its next nearest neighbors holding them together in the lattice (Figure 1.8a). The nearest neighbors reproducing the periodicity in a structure are used to define its unit cell containing the lowest number of atoms in it. Therefore, the elementary cell is of unit cube of edge length *a* for the Cu structure and of a one-half unit cube of length $a/2$ for the NaCl-type structure. In contrast to the NaCl and Cu lattices, one cannot choose a unit cell for the diamond lattice on the basis of two idential C atoms associated with each lattice point such that there is only one atom per unit cell. This is due to the tetrahedral bonding of the diamond structure in which each atom has four nearest neighbors and 12 next nearest neighbors (Figure 1.8c). The diamond structure may be viewed as two fcc structures displaced from each other by one-quarter of the unit cube diagonal. The unit cube of diamond lattice contains eight atoms.

It is well known that in the solid state NaCl is an insulator, Cu is a good conductor, whereas diamond is a poor conductor of electricity. If the elemental solids are compared, diamond is the hardest material and melts at about 2000 ^{o}C, but Cu metal is relatively soft and melts at 300 ^{o}C. The differences in the properties of crystalline solids are associated with the nature of chemical bonding in them, which may be classified as follows: (i) ionic crystals (NaCl, CsI), (ii) covalent crystals (diamond, Si, SiC), (iii) metals (Cu, Ag, Mg), and (iv) van der Waals and hydrogen-bonded crystals.

(i) Ionic crystals. In ionic crystals one or more electrons from the outermost orbital (i.e. valence electrons) of one type of atoms are transferred to the outmost orbital of another type of atoms, resulting in the formation of cations and anions. For example, NaCl crystal may be considered to result from the stacking of Na^+ and Cl^- ions alternately in the three directions. The cohesive energy of these crystals is mainly determined by electrostatic interactions between the oppositely charged ions. The internuclear distance between the neighboring ions in these crystals is equal to the sum of their radii considered to be spherical. Because of the spherical geometry of the ions, the crystal structure acquired by their arrangement in the available space is densely packed and is determined by the ratio of the radii r_C of cation C and r_A of anion A in the three-dimensional aggregation of ions.

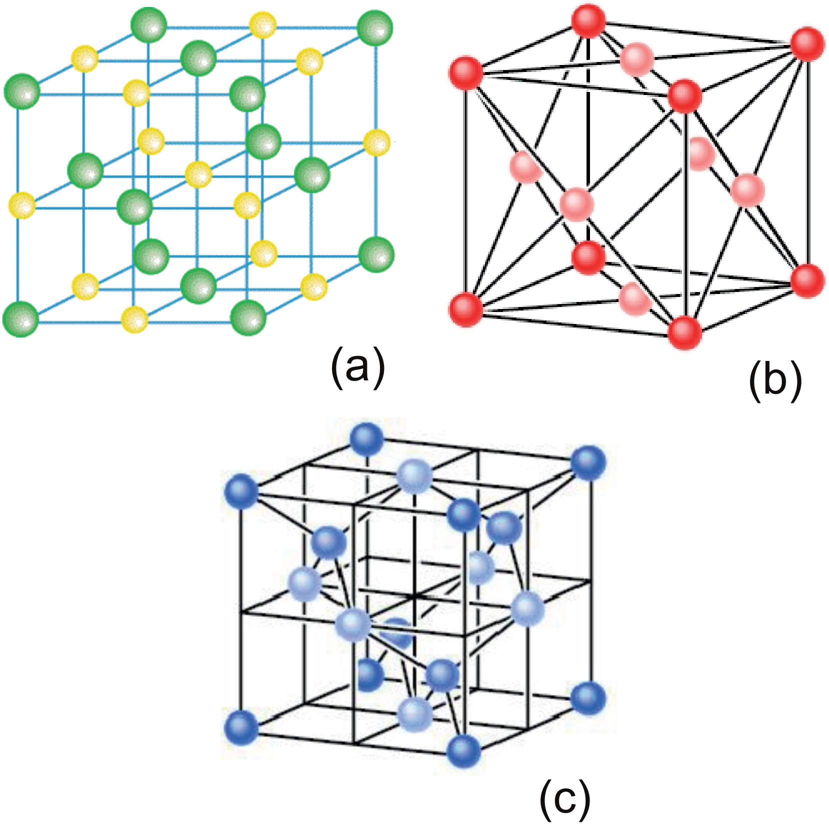

Figure 1.8. Crystal structures of (a) sodium chloride, (b) copper and (c) diamond crystals. In (a) small, grey balls denote Na^+ ions and large, dark balls denote Cl^- ions. Adapted from (a) internet source centros.edu.xunta.es accessed 11 October 2019, and (b,c) Halliday et al. (2001).

When the ratio r_C/r_A exceeds 0.732, the ions form a CsCl-type lattice, known as *body-centered cubic* (bcc) lattice, in which an ion of one type is situated in the center of a unit cube of edge length a and eight ions of the other type are situated at the corners of the cube, ensuring a coordination number of eight (Figure 1.9a). There is one CsCl molecule in a unit cube. With decreasing ionic ratio, the ions first form an NaCl-type lattice ($0.732 > r_C/r_A > 0.414$), and finally a cubic ZnS-type (zinc blende) lattice ($0.414 > r_C/r_A > 0.225$). Thus, with a decrease in the ratio r_C/r_A of the radii, the coordination number (i.e. the number of nearest neigh bors) of an ion decreases from eight for the CsCl-type lattice to six for the NaCl-type lattice and four for the ZnS-type lattice. The cubic ZnS-type structure results when Zn atoms are displaced on one face lattice and S atoms on the other fcc lattice, as shown in Figure 1.9b. About each atom there are four equally distant atoms of the opposite kind arranged at the corners of a regular tetrahedron, and there are four ZnS molecules in the unit cube.

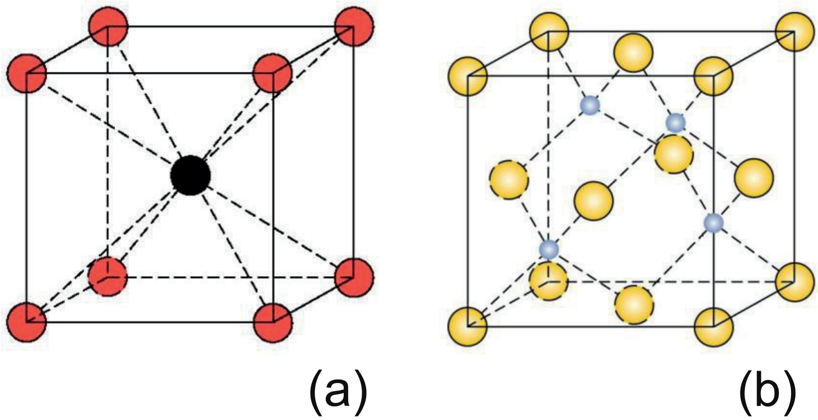

Figure 1.9. Arrangement of (1) CsCl-type and (b) ZnS-type lattice. In (a) central Cs^+ ion has octahedral coordination with Cl^- ions, and in (b) small and large circles denote Zn^{2+} and S^{2-} ions, respectively. Adapted from internet sources: (a) slideshare.com, and (b) chegg.com accessed 11 October 2019.

The long-range interaction between ions with charge $\pm e$ is the electrostatic interaction $\pm e^2/r$ attractive between ions of opposite charge and repulsive between ions of the same charge. The ions arrange in a particular crystal structure that gives the strongest attractive interaction compatible with the repulsive interaction at short distances between the ionic nuclei. The total lattice energy E_{total} of a crystal of N_A pairs of ions at the equilibrium separation r_0 is given by

$$E_{\text{total}} = -\frac{N_A A e^2}{r_0}\left(1-\frac{1}{b}\right), \tag{1.14}$$

where the term $-N_A A e^2/r_0$ is called the Madelung energy, and the contribution of repulsive interactions is about 10% because the repulsive exponent b lies between 6 and 12. In Eq. (1.14) N_A is the Avogadro constant and the constant A is known as the Madelung constant which is the sum of contributions of attractive and repulsive interactions between a reference ion and ions of successive nearest-neighbor charges of opposite and same types. Typical values of Madelung constant are: 1.7627 for the CsCl-type lattice, 1.7476 for the NaCl-type lattice, and 1.6381 for the cubic ZnS-type lattice. Thus, it may be concluded that: (1) the main contribution to the binding energy of ionic crystals is electrostatic, (2) the Madelung contribution to the cohesive energy decreases with decreasing number of nearest-neighbor ions of opposite charges, and (3) the purely ionic chemical bond of the CsCl-type and NaCl-type lattices becomes partly covalent in the cubic ZnS-type lattice.

The lattice energy E_{total} of ionic crystals strongly depends on the interionic distance r_0, and lies between 1014 kJ·mol^{-1} for LiF crystals ($r_0 = 0.201$ nm) and 567 kJ·mol^{-1} for CsI crystals ($r_0 = 0.395$ nm). For alkaline-earth oxide crystals composed of bivalent ions, E_{total} is about four-times higher than those for the alkali halides.

(ii) Covalent crystals. Covalent crystals are characterized by strong covalent bonds formed by the sharing of electron pairs from neighboring atoms. Diamond is a typical example of covalent crystals, where the formation of a covalent bond is described in terms of hybridal sp^3 orbitals of carbon with the usual tetrahedral orientation of the four bonds about a carbon (see Figure 1.7b). The carbon–carbon distance in the lattice is 0.154 nm. Silicon and germanium elemental crystals and ZnS crystals are other examples of covalent crystals. Each atom has four nearest neighbors. Another example of covalent bonds is graphite, which is a stable form of carbon at ordinary temperatures. Graphite crystal structure has successive sheets of carbon atoms lying in planes. Each sheet is composed of a skeleton of a polynuclear aromatic compound (i.e. a connected series of benzene rings) such that the bonds in the plane may be described as hybridal sp^2 bonds. The carbon–carbon distance in the planes of graphite lattice is 0.134 nm. Bonds between the carbon atoms of successive sheets are much weaker than those within the sheets and are attributed to the nonlocalized π orbitals. Since the π orbital electrons are delocalized over all atoms of the crystal, graphite is a conductor in contrast to diamond which is essentially an insulator. The situation in the case of graphite crystals is similar to that in metals which are conductors.

Purely covalent bonds are nonpolar and are formed between identical atoms as in diamond, silicon and germanium. Any other covalent crystal containing different kinds of atoms is to some extent ionic. The crystal lattice of cubic ZnS is an example of atoms in which the bonding is partially ionic. In this case, if bond formation between Zn and S atoms is described in terms of overlapping of hybridal sp^3 orbitals, one expects the participation of Zn^{2+} and S^{2-} ions in bond formation between them. However, since S atom is more electronegative than Zn, the bond is polar and has a contribution from the ionic form of Zn^{2+} and S^{2-}.

The main feature of covalent crystals is the formation of directional bond. The covalent bonds are strong and are comparable with the bonds in ionic crystals, although they are formed between neutral atoms by mutual sharing of their outer orbital electrons.

(iii) Metal crystals. Metals are characterized by high electrical conductivity and a tendency to crystallize in packing arrangements of high coordination number. In a face-centered cubic (fcc) or a hexagonal close-packed (hcp) crystal, the coordination number is twelve. In a body-centered cubic (bcc) crystal, the coordination number is eight. The first characteristic suggests that there is a large number of *conduction electrons* which are loosely bound to any particular atom and are relatively free to move throughout the crystals. The second characteristic suggests that the formation of twelve or more well-defined (i.e. *localized*) bonds in terms of paired electrons (known as *delocalized electrons* from neighboring atoms) as in ionic or covalent crystals is unlikely.

The origin of metallic bonds in crystals is associated with the fact that the inner electrons in the orbitals of individual atom are essentially localized and are tightly bonded to the nuclei whereas the outer, valence, electrons in their orbitals are delocalized (weakly bonded) and behave as if each valence electron from the metal atoms belong to the assembly of positively-charged ions. Thus, a metal crystal may be considered as an array of positive ions immersed in a uniformly distributed cloud of negative charge coming from all valence electrons. Therefore, the cohesive energy in metals is essentially due to coulombian interaction between the positive ions and the electronic cloud charge. Because of this smeared out electronic charge, the dimensions of "positive ions" of atoms, spherical in shape, involved in the formation of metallic crystals are relative large in comparison with those in the ionic crystals of these atoms, and the cohesive energies of metallic crystals are much lower than those of ionic crystals. For example, in Li crystals, the Li–Li distance $r_0 = 0.346$ nm and $E_{\text{latt}} = 163$ kJ·mol^{-1}.

The low cohesive energy of metallic lattices and the spherical shape of their building units enable metals to crystallize in more than one structure, each structure being stable over a certain temperature interval. The structures are: bcc, fcc and hcp. The number of next-neighbors is 8 in bcc and 12 in fcc and hcp structures. The latter two structures are closely related, but they differ from each other in the stacking of atoms in successive layers.

The difference in the fcc and hcp structure in metals may be illustrated with reference to Figure 1.10, which shows a closely packed layer of spheres, each sphere surrounded by six neighbors in the layer. This type of atomic layer, say A, can be the (0001) plane of the hcp structure or the (111) plane of the fcc structure. A second layer may be obtained by placing each sphere in contact with three spheres of the A layer. Two families of geometrically equivalent interstices, denoted in the figure by normal B and inverted triangles C, are available for the arrangement of spheres in the second layer. Assume that the second layer is obtained by the stacking of spheres in the interstitial positions of normal triangles such that this is layer B. The third layer may be added either directly over the spheres in the first layer (i.e. layer A) or over the interstices in the first layer not occupied by the second layer (i.e. interstices denoted by inverted triangles). In the former case the sequence of arrangement of successive layers is ABABAB…, and the structure is hcp with hexagonal primitive cell. However, in the second case the packing sequence is ABCABCABC…, and the structure is fcc.

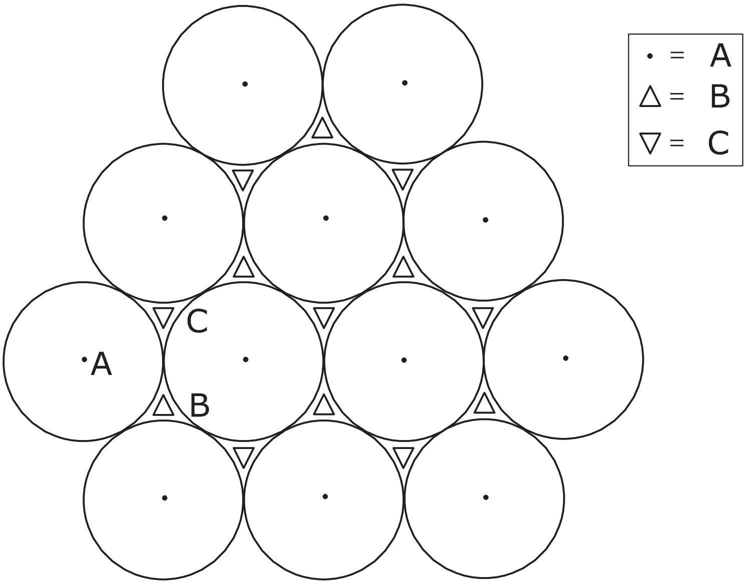

Figure 1.10. Illustration of closely packed layer of spheres in the (0001) plane of the hcp structure or the (111) plane of the fcc structure, and possibility of stacking of different succesive layers. See text for details.

Following a procedure similar to that for the arrangement of atoms in the hcp and fcc of metallic lattices, the sequence of arrangement of successive layers in bcc and simple cubic (sc) lattice structures of metals may be obtained taking the stacking of four atoms about a given atom in the (100) plane as the reference A layer (see Figure 1.8b). In the bcc structure of Figure 1.8b, the stacking of atoms in the next layer is similar to that in the reference layer A with the difference that the atoms in this new layer, say B, are displaced by a distance equal to $3^{1/2}/2$ times the unit cube edge length a (i.e. the interatomic distance a). Thus, the sequence of arrangement of successive atoms in the bcc structure is ABABAB. In contrast to the bcc structure, the successive layers in the sc crystal structure are identical with the A layer. Therefore, in this case the sequence of layers is AAAAA.

A simple consequence of the different kinds of stacking of atomic spheres in successive layers in different lattice structures is that their total volume filled by the spheres is 0.74 for both the fcc and hcp structures, 0.68 for the bcc structure and 0.523 for the sc structure. These different filled volumes of the crystal structures are directly related to the coordination numbers of their atoms (i.e. twelve for the hcp, eight for the bcc and four for the sc structure).

(iv) Van der Waals and hydrogen-bonded crystals. Van der Waals and hydrogen-bonded crystals differ from ionic, covalent and metallic crystals in the nature of their building units and the binding interactions between them in their lattices. The former are composed of various types of molecules which are not capable

of forming a crystalline lattice by electron-pair bonds, but are held together by weak van der Waals and hydrogen bonds between the molecules. Although van der Waals crystals are usually called molecular crystals, both van der Waals and hydrogen-bonded crystals may equally be considered true molecular crystals.

The van der Waals attractive interactions between the molecules are of three types. The first is associated with the mutual *dipole–dipole attraction* between polar molecules of permanent dipole moment μ (i.e. $E_1 \propto \mu^4/r^6$). The second is due to the *induced attraction* caused by the presence of a polar molecule on the polarization of electrons in the second molecule. This induced attraction depends on the dipole moment μ and polarization α of the two interacting molecules (i.e. $E_2 \propto \alpha\mu^2/r^6$). The last attractive interaction is due to *dispersion forces*, also known as *London forces*, in all types of polar and nonpolar molecules as well as in atoms. These dispersion forces arise due to the interaction between the neighboring atoms, each considered as a system of fluctuating dipoles. A fluctuating atomic dipole is formed by a combination of moving negative electrons and the nucleus of the atom. The dispersion attraction energy $E_3 \propto \alpha^2/r^6$. The crystals involving the above three types of interactions are called van der Waals crystals.

It is found that the contribution of dispersive attraction potential E_3 usually dominates over dipole–dipole and induced attraction potentials E_1 and E_2 in different types of molecular crystals, but the dipole–dipole potential E_1 becomes dominant over, or comparable with, the dispersive potential E_3 in larger hydrogen-bonded molecular solids such as ice (for example, see Barrow, 1973). It should be noted that dispersion interaction appears between atoms and molecules both in the liquid and solid states.

Hydrogen-bonded crystals form a special type of molecular crystals. Crystalline water (ice) is an example of hydrogen-bonded crystal. A hydrogen bond is formed when the hydrogen atom bonded to an atom of high electronegativity (e.g. oxygen, nitrogen and fluorine) of a molecule interacts with the atom of high electronegativity of another molecule. In the case of crystalline water, hydrogen bonds are formed between each terminal hydrogen atom of the O–H bond and the oxygen atoms of other water molecules. In other words, each hydrogen atom of water molecules is attached to oxygen atoms by an electron pair bond to another by hydrogen bond, the interaction essentially being electrostatic in nature. The hydrogen bond, about 0.175 nm long and bond energy of the order of 20 $\text{kJ}\cdot\text{mol}^{-1}$, between the terminal hydrogen atom of an O–H bond of one water molecule with the O atom of the other water molecule is traditionally represented by dotted line as O–H·····O. Therefore, the ice crystal structure is such that each oxygen atom has disposed about it four other oxygen atoms at the corners of a tetrahedron, with hydrogen atoms lying on the line joining each pair of oxygen atoms, as shown in Figure 1.11. Since each oxygen atom (large circles) forms octahedral hydrogen bonds (small circles) with another oxygen atom, the number of nearest neighbors in ice is four. In the figure solid lines represent covalent bonds whereas dotted line represent hydrogen bonds. Dark, gray and open oxygen atoms represent first, second and third levels of water molecules parallel to the plane of the paper. Oxygen atoms lie in layers perpendicular to the plane of the paper in a direction parallel to the shorter edge (i.e. the *x* direction), with each layer forming a network structure of open hexagonal rings composed of water molecules joined by hydrogen bonds.

Van der Waals bonds in molecular crystals are weak and are usually less than about 15 kJ·mol^{-1}. Consequently, molecular crystals are relatively soft and have low melting point. Moreover, the structure of these crystals has a tendency to efficient packing of individual molecules. In contrast to the van der Waals crystals, hydrogen-bonded crystals are comparatively hard and have relatively high melting points because of relatively strong hydrogen bonds involved in their crystal structure. In view of the directional bonds in these hydrogen-bonded crystals, they have open network structure with large empty space in their volume.

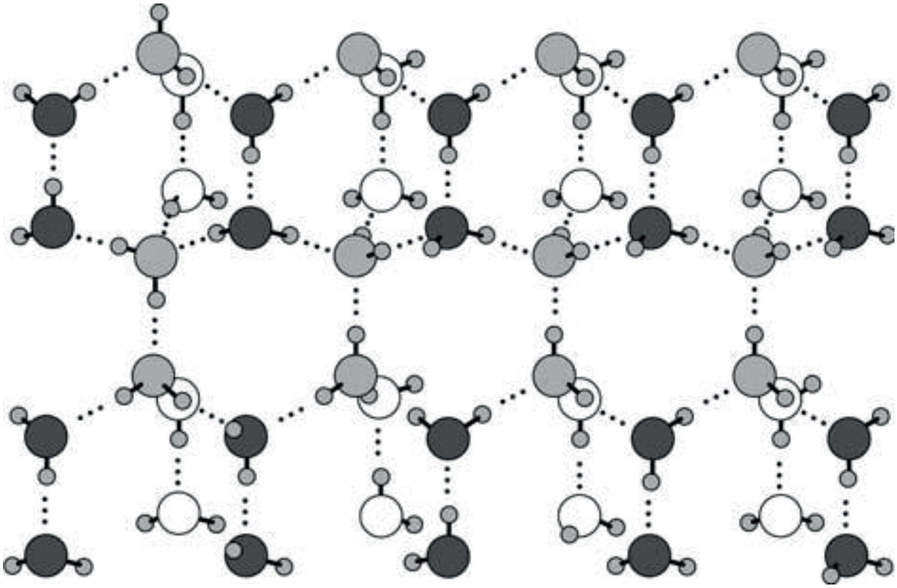

Figure 1.11. Network structure of ice with large interstitial spaces. Large and small circles denote oxygen and hydrogen atoms, respectively. Solid lines represent covalent bonds whereas dotted line represent hydrogen bonds. Structure of a free water molecule is also shown. Note that free, unassociated water molecules can be accomodated in the large interstitial voids. Internet source of image file is unknown.

1.1.3.2. Close-packed and random-packed arrangements

It was mentioned above that the filling of the total volume in different lattice structures depends on the number of nearest neighbors in the stacking of spheres in successive layers. The arrangements of atoms or molecules filling the available volume of a crystal structure are known as close-packed or dense-packed structures. Among the hcp (or fcc), bcc and sc structures, the first is the closest-packed structure, and the last the least close-packed structure. A measure of close-packing of a lattice structure is its packing or filling factor, which is the fraction of the volume of a crystal lattice filled by atoms/molecules composing it. The closet-packed arrangement of filling factor 0.74 is achieved in the hcp crystal lattice involving a coordination number of 12, but the lowest packed arrangement of packing coefficient 0.523 is attained in the sc crystal lattice involving a coordination number of four.

Close-packed arrangements of atoms/molecules, considered as spheres, occurs in the hcp, fcc, bcc and sc structures of crystals composed of atoms/molecules bonded together by ionic, metallic and van der Waals interactions which are nondirectional. In covalent and hydrogen-bonded crystals involving directional tetrahedral bonding of diamond structure and octahedral hydrogen bonds of open network structure of ice structure, their lattices are relatively emply. For example, in the diamond structure in which a carbon also has four nearest neighbors, this filling factor is only 0.34, which is about 65 percent of the filling factor for the least close-packed sc structure.

The value of the filling factor for a given structure is an indicator of the average distance between its atoms/molecules (building units) and its density d. For example, depending on the temperature and pressure conditions, several metals are known to have different structures. This means that a rearrangement of atoms/molecules involved in these transformations leads to a change in the average distance between them and the density of the crystalline phases. Similar changes are also expected to occur during the melting of a substance from the crystalline phase into its molten phase as well as during its crystallization from the liquid phase. In the former case the process may be considered to involve the dismantling of the long-range order existing between the building units in the crystalline phase. In other words, short-range attractive forces alone are present between the atoms/molecules of the substance in the liquid phase. In the absence of long-range attractive forces, an ideally close-packed arrangement of atoms/molecules is not expected to be present in the liquid phase. This type of arrangement of atoms/molecules in the liquid phase may be considered as randomly packed. The filling factor in randomly-packed structures is about 0.64, which is always lower than that in the closest-packed crystal structures by about 13.5 percent.

1.1.4. Characteristics of transformation in the states of matter

At a given pressure p, with an increase in temperature T every solidified material first transforms to the liquid form at a temperature T_m and this liquid thereafter begins to boil at temperature T_b and transforms to the vapor phase. Conversely, with a slow decrease in temperature a material initially existing in the vapor phase condenses into the liquid phase at the temperature T_b, and the cooling of the liquid later solidifies at the temperature T_m and remains in this phase. Figure 1.12 illustrates schematically the change in the volume V of a hypothetical solidified material of close-packed structure during its transforma-tion to liquid and vapor phases with a change in temperature T at a given pressure p. As indicated by the directions of arrows in the figure, there are two ways to observe these transformations: (a) the material originally present in the vapor phase is cooled at a constant rate, and (b) the material initially present in the solid form is heated at a constant rate.

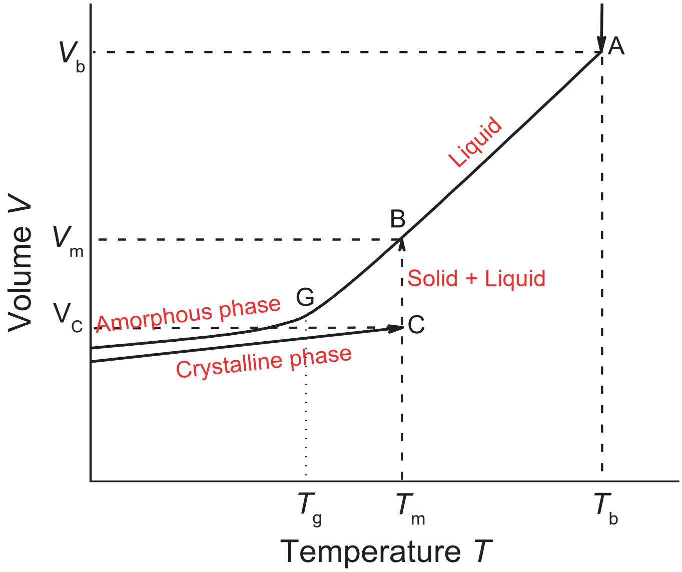

Figure 1.12. Schematic illustration of change in the volume *V* of a hypothetical solidified material during its transformation to liquid and vapor phases with temperature *T*. Directions of transformation of phases during heating of solidified material and cooling of vapor of the material are indicated.

First we consider the situation when heat is supplied to the solid at a constant rate at a constant pressure p. With the supply of heat, the temperature of the solid increases initially with a simultaneous increase in the volume V. When the temperature of the solid reaches T_m, it begins to melt (point C). The corresponding volume of the solid at this point is V_c. With further supply of heat, the temperature remains unchanged at T_m and an increasing amount of the solid transforms into the liquid state until the entire mass of the solid is melted, leading to the volume V_m of the liquid phase (point B). With more supply of heat, the temperature of the liquid increases with simultaneous increase in its volume until T_b when the liquid begins toevaporate (point A, liquid volume V_b). With increasing supply of heat, evaporation of the liquid continues until it is entirely evaporated and occupies a volume V_∞ when the atoms/molecules composing the solid no longer interact with each other. Obviously, the entire process of transformation of the solid into the vapor phase is associated with the supply of two specific amounts, ΔH_m and ΔH_b, of heat energy responsible for the increases (V_m–V_c) and (V_∞–V_b) in the volume V_c and V_b at temperatures T_m and T_b, respectively. The magnitude of ΔH_m with reference to the temperatures T_m of a solid is determined by the difference in the energies associated with the transfer of molecules in the solid state to the liquid state and involves, among others, changes in their energies associated with the vibrations and rotation of the molecules in the two states (see Eq. (1.12)). Similarly, the magnitude of ΔH_b with reference to T_b represents the difference in the energies involved in the transfer of molecules from the liquid to the vapor state.

Instead of heating a solid substance to transform it into the vapor phase via its liquid (molten) phase involving two specific amounts, ΔH_m and ΔH_b, of heat energy, the reverse process of transformation of the substance to the solid phase from the vapor phase via the liquid phase is also possible by cooling it. This process is accomplished when solid nuclei, initially formed in the liquid phase as soon as it becomes undercooled (i.e. $T < T_m$), grow three-dimensionally until the entire liquid is crystallized. Since the process of crystallization of a substance is associated with the reorganization of its atoms/molecules during cooling, this process is possible only at low cooling rates. Ideally, this occurs when the liquid volume is V_m and the temperature is T_m. This temperature is known as the freezing temperature T_f because it is attained during the freezing/cooling of the liquid. Although both these temperatures have the same value for a liquid, physically they are distinguished from each other by the volumes corresponding to them. When cooling of the liquid is fast, instead of undergoing crystallization, it attains a bulky rigid state, known as glassy state, at temperature T_g as a result of freezing of the liquid atoms/molecules. Unlike the values of the melting (or freezing) points T_m of solids, the temperature T_g, known as glass transition temperature, of a substance depends on the applied rate of cooling of the liquid, higher cooling rates leading to lower T_g. Because of relatively disordered arrangement of atoms/molecules in the glassy state, they are formed at a volume higher than V_c. It is observed, as a rule, that $T_g < T_m$.

The thermal energy of atoms/molecules of solid and liquid phases increases with increasing temperature, leading to an increase in their volume with temperature such that this increase in the volume is more in the liquid than in the solid. If it is assumed that the number of nearest neighbors in the liquid phase is the same as in the crystalline phase, one expects that: (1) the volume V occupied by atoms/molecules of a substance of mass m in the liquid phase is higher that that in the crystalline phase, and that (2) the increase in V with temperature is more in the liquid than that in the solid phase. This implies that, at a given pressure p, the density d of a solid at T_m is higher than that of the molten liquid at T_m, and the densities d of the solid and liquid phases decrease with increasing temperature T, the decrease being higher in the liquid state than in the solid state.

It should be emphasized here that the above inferences hold only in the case of crystalline solids involving nondirectional bonds such as metallic and van der Waals-type interactions. Although atoms/molecules in the liquid state may be treated as randomly packed with a high filling factor to result in its relatively high density d, whether the solid density is lower or higher than that in the liquid density is related to the type of solid structures.

Figure 1.13 shows, as an example, the dependence of density d of ice and water on temperature T. It may be seen that: (1) the density d of ice is about 10 percent lower than that of liquid water at T_m, (2) the densities of both ice and liquid water decrease with increasing temperature but this decrease is enormous in liquid water (about 0.04 $g \cdot cm^{-3}$) in comparison with that in ice (about 0.01 $g \cdot cm^{-3}$) for temperature difference of 100 °C, and (3) in the region close to T_m, the density d of ice decreases practically linearly with increasing temperature T but that of liquid water appears to follow a binomial relation. The first observation of high density of water is associated with the closed hexagonal structure of ice. During the melting of ice, water molecules are dissociated from it and these dissociated water molecule are trapped in the hexagonal ice structure, decreasing thereby the volume of the liquid water. The latter two observations are associated with the fact that the amplitudes of vibrations of water molecules in the ice lattice are smaller than those in the liquid water. The difference in the trends of the temperature dependence of *d* of ice and liquid water is associated with their structures.

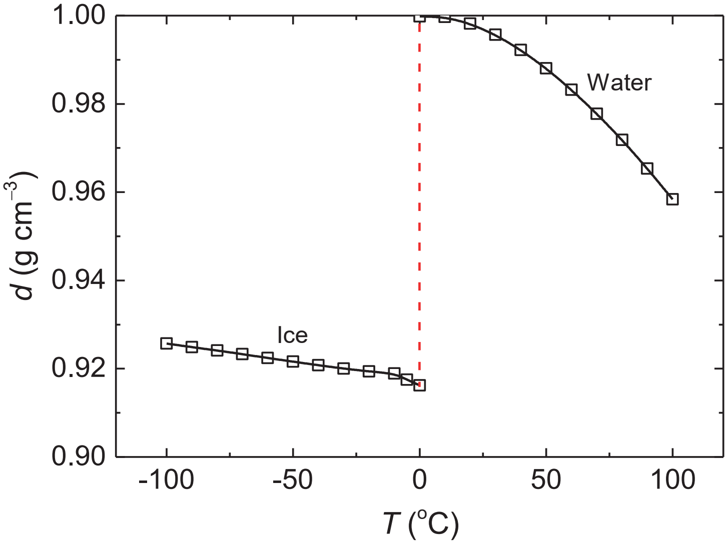

Figure 1.13. Dependence of density *d* of water and ice on temperature *T*. Data of density *d* for ice from www.EngineeringToolBox.com accessed 12 January 2017, and for water from Lide (1996/1997).

1.1.5. Characteristics of solidification and evaporation of alkanes and alcohols

A system is in thermodynamic equilibrium during its phase transformation like melting and evaporation at a given pressure. Then the change ΔG in the Gibbs free energy G of the system is zero, i.e.

$$\Delta G_{\mathrm{m,b}} = \Delta H_{\mathrm{m,b}} - T_{\mathrm{m,b}} \Delta S_{\mathrm{m,b}} = 0\,, \tag{1.15}$$

where $\Delta H_{\mathrm{m,b}}$ and $\Delta S_{\mathrm{m,b}}$ are changes in the enthalpies and entropies of melting or boiling of the system and correspond to the melting or boiling temperature $T_{\mathrm{m,b}}$. Obviously, these temperatures are related to $\Delta H_{\mathrm{m,b}}$ and $\Delta S_{\mathrm{m,b}}$ by

$$T_{\mathrm{m,b}} = \frac{\Delta H_{\mathrm{m,b}}}{\Delta S_{\mathrm{m,b}}}\,. \tag{1.16}$$

Solidification and evaporation of liquids occur at their standard melting point T_{m} and boiling point T_{b} with corresponding changes in the heat energies ΔH_{m} and ΔH_{b}, respectively, under atmospheric pressure, and there are the entropy changes $\Delta S_m = \Delta H_m/T_m$ and $\Delta S_b = \Delta H_b/T_b$ associated with these processes. At equal pressures the entropy of the phase stable at higher temperatures is always higher than that at lower temperatures. Therefore, melting and vaporization of different liquids lead to an increase in their entropy at their normal melting and boiling points.

Some features of vaporation of various type of liquids are known (for example, see Barrow, 1976). For many organic liquids referred to as normal liquids, the vaporization entropy $\Delta S_b = \Delta H_b/T_b \approx 10.5R_G \approx 88$ J·mol^{-1}·K^{-1} and this relationship is called *Trouton's rule*. Here the gas constant $R_G = k_BN_A$, where k_B is the Boltzmann constant and N_A is the Avogadro number. However, this vaporization entropy ΔS_b is about $5R_G$ for simple monoatomic liquids, $7.5R_G$ for acetic acid and up to about $15R_G$ for water, alcohols and other hydrogen-bonded liquids, and several bivalent chlorides such as $PbCl_2$ and $ZnCl_2$, which behave as associated liquids.

The associated liquids are also known as structured liquids. where their "structuredness" is related to the subtle interactions characterizing bulk properties of the liquids (Marcus, 1992; 2009), which are described in terms of "stiffness", "openness", and "order" of a liquid. A measure of stiffness of a liquid is the work done to create a cavity in it, the openness of a liquid, related to its free volume, is the difference between the bulk molar volume V_M and the intrinsic molar volume V_M^{in}, whereas the order existing in a liquid is the deficit of its molar entropy with respect to the same substance in the ideal gas phase (Marcus, 2009). According to this concept, an ordered liquid is one for which the Trouton constant $\Delta S_b/R_G = \Delta H_b/R_GT_b > 12$, implying that water is an ordered (or associated) liquid.

The trends of melting entropy $\Delta H_m/T_m$ of different substances are also somewhat similar to those of the vaporization entropy $\Delta H_b/T_b$, but their values are lower than those of $\Delta H_b/T_b$ for a given substance. For substances which behave as normal liquids $\Delta H_m/T_m$ lies between about R_G and $2R_G$, but for associated liquids like water and bivalent chlorides its value is up to $5R_G$. In the case of alkali halides and many organic compounds $\Delta H_m/T_m$ is about $3R_G$ and $6R_G$, respectively (Sangwal, 1989; see Section 2.5).

Some general features of the dependence of T_m and T_b of some simple alcohols and the entropies $\Delta H_m/T_m$ and $\Delta H_b/T_b$ of their melting and evaporation are described below and compared with those of normal alkanes up to decane. The alcohols were chosen in view of the fact they are the commonly used solvents and reliable data on their physical properties are available. The *n*-alkanes were chosen in view of similarity of their chemical structure with that of alcohols.

Figure 1.14 compares the data of T_m and T_b of some 1- and 2- alcohols with those of *n*-alkanes as a function of the number N of carbon atoms in their chemical formula. The data are taken from Lide (1996/1997). Except for the $T_b(N)$ data for the alkanes, which were observed to follow the second-order equation:

$$T_{b,m}(N) = a_0 + a_1N + a_2N^2\,, \tag{1.17}$$

a_0, a_1 and a_2 are fitting parameters, all other $T_b(N)$ data for the alcohols and the $T_m(N)$ data for the alcohols as well as the alkanes could be described by a linear relation (i.e.

$a_2 = 0$ in Eq. (1.17)). The intercepts of the $T_b(N)$ and $T_m(N)$ plots, equal to a_0 in Eq. (1.17), are denoted hereafter as T_b^0 and T_m^0, respectively, and represent a hypothetical compound of $N = 0$. The boiling points T_b of the 1- and 2-alcohols increase linearly with the number N of carbon atoms. While analyzing the $T_m(N)$ data for both types of alcohols as well as alkanes the data for methanol and methane were excluded. The constants of Eq. (1.17) for these data are listed in Table 1.3, where the values of the parameters are given in K instead of °C in Figure 1.14.

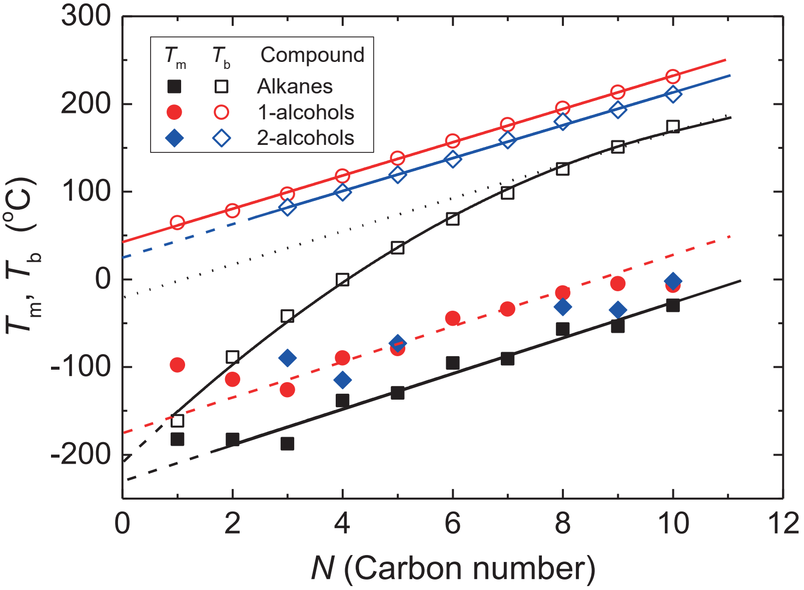

Figure 1.14. Dependence of T_m and T_b of some simple alcohols and alkanes on the number N of carbon atoms in their chemical formula. Plots are drawn according to Eq. (1.17), with values of its parameters given in Table 1.3.

It may be noted from Figure 1.14 and Table 1.3 that the slopes a_1 of the linear $T_b(N)$ plots for the alcohols are practically constant equal to about 19 K per $-CH_2$ group, but the extrapolated value of T_b^0 is lower for 2-alcohols than that for 1-alcohols. The value of T_b for different alkanes is always lower than that of the corresponding alcohols of the same carbon number N. However, the difference between their T_b's decreases with increasing N such that the $T_b(N)$ plot for octane onwards may be considered to follow a linear dependence with intercept $T_b^0 \approx 254.2$ K and slope $a_1 \approx 19$ K per $-CH_2$ group (see dashed line). In contrast to the trends of the $T_b(N)$ plots, the value of the slopes a_1 of the linear $T_m(N)$ plots for the two types of alcohols as well as alkanes is also equal to about 19 K per $-CH_2$ group, but the extrapolated value of T_m^0 is equal to 43.4 K for alkanes and about 123.2 K for the two types of alcohols.

Table 1.3. Values of constants of $T_b(N)$ and $T_m(N)$ plots

Compound	Data	a_0 (K)	a_1 (K)	a_2 (K)	R^2
1-Alkanes	$T_b(N)$	64.1±7.8	60.4±3.3	−2.25±0.29	0.9963
	$T_m(N)$	43.4±9.2	20.3±1.4	—	0.9630
1-Alcohols	$T_b(N)$	315.8±1.2	19.0±0.2	—	0.9990
2-Alcohols	$T_b(N)$	299.0±2.4	18.8±0.4	—	0.9975

A measure of the difference in the behavior of successive analogues of alkanes and alcohols during the melting and evaporation processes in terms of their molecules is the temperature difference (T_b-T_m) as a function of the carbon number N in their molecules. This difference (T_b-T_m) is about 193 and 176 K for 1- and 2-alcohols, respectively, and is practically independent of the carbon number N. However, because of the quadratic dependence of T_b on N, the value of (T_b-T_m) increases enormously from the values of about 94 K for ethane to about 204 K for nonane and decane. Exceptions from the above general trends appear to be methane and methanol where the difference (T_b-T_m) is relatively low and is equal to 21 and 162 K, respectively.

We describe first the melting and evaporation entropies, $\Delta H_m/T_m$ and $\Delta H_b/T_b$, of the above organic compounds as a function of the number N of carbon atoms in their chemical formula, as illustrated in Figure 1.15. In the figure, the data of $\Delta H_m/R_GT_m$ as a function of the number N of carbon atoms in the chemical formula are shown for some simple alcohols and alkanes, with $N \leq 5$ and $N \leq 10$, respectively. It may be seen that $\Delta H_b/T_b \approx 13R_G$ for water and different types of alcohols and $\Delta H_b/T_b \approx 10R_G$ for the alkanes. The former and the latter values of the evaporation entropy are in agreement with the values reported above for associated liquids like water and alcohols and normal liquids such as alkanes. However, the data of $\Delta H_m/R_GT_m$ against N show that, except for methane and methanol, their values of higher alcohols and alkanes are higher than that for water. If the data for methane, butane and nonane are excluded, the data for alkanes may be represented by the linear relation:

$$\frac{\Delta H_m}{R_G T_m} = \frac{\Delta S_m^0}{R_G} + \frac{\Delta S_m^1}{R_G} N, \tag{1.18}$$

where the intercept $\Delta S_m^0/R_G = 0.965$ and the slope $\Delta S_m^1/R_G = 1.29$, with goodness-of-the-fit parameter $R^2 = 0.9872$. Except for pentanol, 2-propanol and glycerol, the data for alcohols also follow this relation. The above relation holds for linear alcohols and alkanes, and the observed deviations may be attributed to errors in the data and nonlinear (branched) nature of their chains. The linear dependence of $\Delta H_m/R_GT_m$ on carbon number N of alkanes and alcohols suggests that, starting from methane and methanol, the melting entropy ΔS_m of these liquids is additive with entropy increment $\Delta S_m^1 = 1.29R_G$ and the associated energy increment $\Delta H_m/N = 1.29R_GT_m$ per $-CH_2$ group.

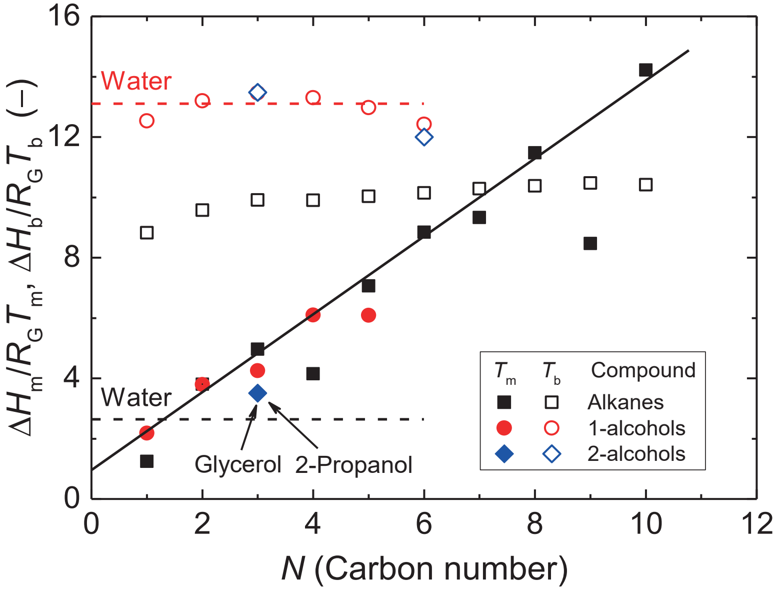

Figure 1.15. Data of $\Delta H_b/R_G T_b$ and $\Delta H_m/R_G T_m$ plotted as a function of the number N of carbon atoms in the chemical formula of some simple alcohols and alkanes. Values of $\Delta H_b/R_G T_b$ and $\Delta H_m/R_G T_m$ for the compounds are compared with the values for water shown as dashed lines. Linear plot represents data according to relation (1.18). Original data from Lide (1996/1997).

The constancy of $\Delta H_b/T_b$ for alcohols suggests that their evaporation enthalpy ΔH_b also increases linearly with the carbon number N (cf. Eq. (1.17), Table 1.3), and that the values of ΔH_b for the 1-alcohols are higher than those for the 2-alcohols by about 2 kJ·mol^{-1} (see Table 1.4), and may be calculated from the relation

$$\Delta E = \Delta H_b - \Delta H_b^* = \zeta R_G (T_b - T_b^*) = \zeta R_G (a_0 - a_0^*)\,, \qquad (1.19)$$

where ΔE is the energy difference, the different parameters without and with asterisks refer to the two types of alcohols, and the Trouton constant $\zeta = \Delta H_b/R_G T_b$ is assumed to be constant equal to 13 for alcohols and 10 for alkanes (cf. Figure 1.15). The lower enthalpy of 2-alcohols than that of 1-alcohols by about 2 kJ·mol^{-1} may be attributed to the branching of the linear C chain of the alcohols. From Figure 1.15 one observes that the Trouton constant ζ somewhat depends on the number N of carbon atoms in the chain length of alcohols and alkanes. For example, the value of the Trouton constant ζ for the alkanes slowly increases with their chain length N from 8.7 ultimately attaining a saturation value of 10.3 for $N \geq 9$ with an increase of about 1.6 in the Trouton constant ζ. With reference to methane, this increase in ζ corresponds to an increase in the evaporation energy $(\Delta H_b - \Delta H_b^{\text{meth}}) \approx 16$ kJ·mol^{-1} and an increase in the evaporation entropy $(\Delta S_b - \Delta S_b^{\text{meth}}) \approx 1.3$ J·mol^{-1}·K^{-1}. It is also interesting to note that substitution of an H atom of a 1-alkane by an OH group in the corresponding 1-alcohol is accompanied by an increase in the entropy $(\Delta S_b - \Delta S_b^*) = 3R_G = 25$ J·mol^{-1}·K^{-1}, and this increase in the entropy is practically independent of the number N of carbon atoms in the alcohol molecules.

Dismantling of molecules from a solid during its melting involves: (1) the cohesion energy E_{latt} of the lattice equal to the enthalpy change ΔH_{m}, and (2) the entropy change ΔS_{m} associated with the reorganization of molecules. Similarly, escape of molecules from a molecular liquid during its evaporation also involves: (1) the binding energy E_{liq} of molecules in the liquid equal to the enthalpy change ΔH_{b}, and (2) the entropy change ΔS_{b} associated with the reorganization of molecules during evaporation. For both melting and evaporation of a compound these contributions may be given by

$$\Delta H_{\mathrm{m,b}} = \Delta H_{\mathrm{m,b}}^{\mathrm{coul}} + \Delta H_{\mathrm{m,b}}^{\mathrm{van}} + \Delta H_{\mathrm{m,b}}^{\mathrm{sc}}, \tag{1.20}$$

$$\Delta S_{\mathrm{m,b}} = \Delta S_{\mathrm{m,b}}^{\mathrm{tr}} + \Delta S_{\mathrm{m,b}}^{\mathrm{rot}} + \Delta S_{\mathrm{m,b}}^{\mathrm{conf}}, \tag{1.21}$$

where $\Delta H_{\mathrm{m,b}}^{\mathrm{coul}}$, $\Delta H_{\mathrm{m,b}}^{\mathrm{van}}$ and $\Delta H_{\mathrm{m,b}}^{\mathrm{sc}}$ are contributions to $\Delta H_{\mathrm{m,b}}$ due to coulombian, van der Waals and hydrogen-type specific interactions, respectively, and $\Delta S_{\mathrm{m,b}}^{\mathrm{tr}}$, $\Delta S_{\mathrm{m,b}}^{\mathrm{rot}}$ and $\Delta S_{\mathrm{m,b}}^{\mathrm{conf}}$ are contributions to $\Delta S_{\mathrm{m,b}}$ due to translation, rotation and configuration of molecules during the melting or evaporation of the compound. In the case of molecular solids where $\Delta H_{\mathrm{m,b}}^{\mathrm{coul}} = 0$, $\Delta H_{\mathrm{m,b}}$ is determined by van der Waals and hydrogen-type interactions whereas $\Delta S_{\mathrm{m,b}}^{\mathrm{tr}} = \Delta S_{\mathrm{m,b}}^{0}$, and $\Delta S_{\mathrm{m,b}}^{1} = \Delta S_{\mathrm{m,b}}^{\mathrm{rot}} + \Delta S_{\mathrm{m,b}}^{\mathrm{conf}}$.

Increase in the length of the molecules of alcohols and alkanes results in increase in their molar volume and the chain flexibility. Therefore, both $\Delta H_{\mathrm{m,b}} = (\Delta H_{\mathrm{m,b}}^{\mathrm{van}} + \Delta H_{\mathrm{m,b}}^{\mathrm{sc}})$ and $\Delta S_{\mathrm{m,b}} = (\Delta S_{\mathrm{m,b}}^{\mathrm{rot}} + \Delta S_{\mathrm{m,b}}^{\mathrm{conf}})$ increase with an increase in the number N of $-\mathrm{CH_2}$ groups in the alcohol and alkane molecules (see Table 1.4). Consequently, depending on the relative changes in the values of $\Delta H_{\mathrm{m,b}}$ and $\Delta S_{\mathrm{m,b}}$ caused by the number N of $-\mathrm{CH_2}$ groups of alcohols and alkanes, their melting/boiling point $T_{\mathrm{m,b}} = \Delta H_{\mathrm{m,b}}/\Delta S_{\mathrm{m,b}}$ is expected to increase or decrease with increasing N. Assuming that the dependences of $\Delta H_{\mathrm{m,b}}$ and $\Delta S_{\mathrm{m,b}}$ on N are linear, i.e.

$$\Delta H_{\mathrm{m,b}} = \Delta H_{\mathrm{m,b}}^{0}(1+\alpha N), \qquad \Delta S_{\mathrm{m,b}} = \Delta S_{\mathrm{m,b}}^{0}(1+\beta N), \tag{1.22}$$

where $\Delta H_{\mathrm{m,b}}^{0}$ and $\Delta S_{\mathrm{m,b}}^{0}$ are the extrapolated values of $\Delta H_{\mathrm{m,b}}$ and $\Delta S_{\mathrm{m,b}}$ when $N = 0$, and α and β are constants characteristric of the series of alcohols and alkanes. Then, for the approximations $\alpha N \ll 1$ and $\beta N \ll 1$, one obtains Eq. (1.17) in the form

$$T_{\mathrm{m,b}} = T_{\mathrm{m,b}}^{0}[1+(\alpha-\beta)N-\alpha\beta N^{2}], \tag{1.23}$$

with $T_{\mathrm{m,b}}^{0} = \Delta H_{\mathrm{m,b}}^{0}/\Delta S_{\mathrm{m,b}}^{0} = a_0$, $T_{\mathrm{m,b}}^{0}(\alpha-\beta) = a_1$, and $T_{\mathrm{m,b}}^{0}\alpha\beta = a_2$. Elimination of β from the latter two relations gives

$$a_0 = T_{\mathrm{m,b}}^{0} = \frac{a_1\alpha + a_2}{\alpha^{2}}, \tag{1.24}$$

and

$$\alpha = \frac{a_1 + (a_1^2 + 4a_2 T^0_{\mathrm{m,b}})^{1/2}}{2T^0_{\mathrm{m,b}}} . \tag{1.25}$$

According to Eq. (1.25) the parameter α is mainly determined by the coefficient a_1 of Eq. (1.23) and the extrapolated temperature $T^0_{\mathrm{m,\,b}}$. From the values of a_i's of Table 1.3 one finds that the values of the parameter α are about 0.06 and 0.15 for the evaporation and melting of alcohols and about 0.075 and 0.46 for the evaporation and melting of alkanes.

As seen from Figure 1.14, during their evaporation the linear dependence is followed by 1- and 2-alcohols and the quadratic dependence by alkanes. This suggests that ΔS_{b} of alcohols is practically independent of N ($\beta \approx 0$) but its value for alkanes somewhat increases with N ($\beta > 0$). However, during the melting of alcohols and alkanes, although a linear increase in T_{m} occurs with N for $N > 3$, there is an initial small linear decrease in T_{m} for $N < 3$. Obviously, the latter trend is observed during the melting of solids made up of small molecules, whereas the former trend is observed with increasing length of the molecules of the solids. The initial small decrease in T_{m} for $N < 3$ for both alcohols and alkanes is related to the relatively poor increase in ΔH_{m} than that in ΔS_{m} with increasing N for $N < 3$. As argued below, these molecular solvents are known to be associated solvents involving hydrogen-like bonds between the molecules in the liquid state.

The branching of the chains of molecules of alcohols and alkanes ensures disorder higher than that in linear-chain molecules. This gives rise to a higher contribution of $\Delta S^{\mathrm{conf}}_{\mathrm{m,b}}$ of branched molecules to $\Delta S_{\mathrm{m,b}}$ of alcohols and alkanes than that due to linear molecules. This combined with lower values of $\Delta H_{\mathrm{m,b}}$ results in lower $T_{\mathrm{m,b}}$ of the nonlinear-chain compounds than those of the linear-chain compounds.

According to the hole model of liquids (see Section 1.4), thermal fluctuations due to an increase in the vibration of liquid molecules around their temporary equilibrium positions result in the formation of holes in the liquid. In the model it is assumed that the energy E_{D} required for the formation of holes in nonassociated liquids participating in their transport properties, such as self-diffusion and viscosity, is related to their melting temperature T_{m}, and is given by (Bockris and Reddy, 1970)

$$E_{\mathrm{D}} = \Delta H_{\mathrm{m}} = 3.7 R_{\mathrm{G}} T_{\mathrm{m}} . \tag{1.26}$$

It is easy to see from Eq. (1.26) that the relation $\Delta H_{\mathrm{m}}/T_{\mathrm{m}} = 3.7R_{\mathrm{G}}$ holds when $N = 2$ for alkanes and alcohols. For $N < 1$, the entropy $\Delta H_{\mathrm{m}}/T_{\mathrm{m}} < 3.7R_{\mathrm{G}}$; for $N \geq 3$, $\Delta H_{\mathrm{m}}/T_{\mathrm{m}} > 3.7R_{\mathrm{G}}$. This difference in the behavior of melting entropy $\Delta H_{\mathrm{m}}/T_{\mathrm{m}}$ of alcohols and alkanes as a function of their carbon number N is associated with the nature of the molecules diffusing away from the solid–melt interface during their melting from the solid state.

In liquids composed of small molecules like water and alcohols, the existance of structural entities in the form of clusters or of locally-ordered structures, such as

$(H_2O)_2$, $(H_2O)_3$, etc., should be taken into consideration. For example, due to the formation of hydrogen bond in the molecules of liquid water, the following geometrical configuration is possible:

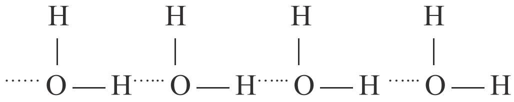

$$\cdots\overset{\displaystyle H}{\overset{|}{O}}-H\cdots\overset{\displaystyle H}{\overset{|}{O}}-H\cdots\overset{\displaystyle H}{\overset{|}{O}}-H\cdots\overset{\displaystyle H}{\overset{|}{O}}-H$$

In alcohols, in addition to the configuration for water, because of the presence of an –R group, especially in lower acohols, ring configuration, shown below, is also possible:

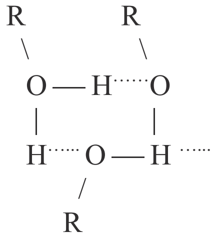

Liquids in which their molecules have a tendency to exist in configurations composed of two or more molecules are known as *associated liquids*. Because of the formation of locally-ordered structures in these liquids, their reduced melting enthalpy ΔH_m leads to a lower entropy $\Delta H_m/T_m$ than that in liquids without ordered structures. In liquids composed of larger molecules, the contribution E_{reorg} to the melting enthalpy ΔH_m of the liquid increases with the increasing length of their molecules. Consequently, the entropy $\Delta H_m/T_m$ of these liquids increases with the length of their molecules.

1.2. Properties of molecular and low-temperature ionic-liquid solvents

Solvents used in the preparation of solutions of different solutes may be classified into molecular and ionic liquids. Examples of the molecular solvents are water and many organic compounds existing as liquids under normal temperature and pressure conditions, whereas molten ionic compounds like NaCl above their melting points T_m and a diverse group of salts, composed of large organic structures as cations and organic or inorganic-based relatively small anions, existing in the liquid state at ordinary temperature and pressure conditions are examples of the ionic liquids. This classification is based on their specific conductivity σ, which is several orders of magnitude higher in ionic liquids than in molecular liquids such as water at 25 °C (see Chapter 6). With the exception of water which is an inorganic solvent, other solvents are usually organic or organic-inorganic liquids.

1.2.1. Molecular solvents

In terms of their chemical structures organic solvents may be classified as hydrocarbon, oxygenated and halogenated solvents. Hydrocarbon solvents are petroleum-based solvents containing hydrogen and carbon atoms in their molecular structure. Although these solvents can have complex chemical structures, they are of two main types: aliphatic, and aromatic solvents. Aliphatic solvents have a straight-chain hydrocarbon structure. Examples of aliphatic solvents are: gasoline, kerosene and hexane. Aromatic solvents contain a benzene ring structure. Examples include benzene, xylene and toluene. Oxygenated solvents contain oxygen in their molecular structure and are derived from petroleum products. Examples of oxygenated solvents are: alcohols, ethers, esters, glycol ethers, and ketones. Halogenated solvents, on the other hand, contain halogen atoms (such as fluorine, bromine, iodine or chlorine) in their molecular structure. Examples are: perchloroethylene, chlorinated fluorocarbons, and 1,1,1-trichloroethane.

All solvents used in the preparation of solutions of different solutes are composed of molecules of various sizes. Some of the commonly used solvents for preparing solutions of different inorganic and organic compounds and their properties are listed in Table 1.4.

The simplest solvent is water composed of water molecules (molecular weight 18) while butanol, glycerol and N-methyl-2-pyrrolidine (NMP), with molecular weights 74, 92 and 99, respectively, are solvents composed of relatively complex molecules. Some features of the different properties of these solvents may be noted:

(1) Water has relatively high density d, high viscosity η, high dielectric constant ε, high melting point T_m and high boiling point T_b than the corresponding properties of the lowest alcohols like methanol and ethanol.

(2) Simple alcohols have roughly the same density d at 20 °C, whereas melting point T_m and dielectric constant ε decrease and boiling point T_b and viscosity η increase with increasing molecular weight (MW).

(3) Normal alcohols like 1-proponol and 1-butanol have slightly higher density, higher dielectric constant ε, and higher boiling point T_b and melting point T_m than those of iso-alcohols 2-propanol and 2-butanol. However, the viscosity η of normal alcohols are lower than those of iso-alcohols.

(4) Other high carbon-containing solvents like ethylene glycol, glycerol and NMP have high density d, high viscosity η, high dielectric constant ε, and relatively high melting point T_m and boiling point T_b than those of simple alcohols.

(5) These solvents are poor conductors of electricity.

The above differences in the properties of the solvents are associated with the structure of their molecules which are electrically neutral. The structure of molecules determines not only the nature of interactions holding the molecules in the liquid state and their packing, but also determines their motion in the liquid state, processes of solidification and evaporation, and poor electrical conductivity. Because of relatively small sizes of the molecules of these solvents, they have relatively high vapor pressure. Many of them are even toxic and inflammable.

Depending on the structure of molecules composing different liquids, the above liquids may be classified as polar, nonpolar and apolar. Molecules of a polar liquid are uncharged with an overall dipole moment which may be the result of one individual polar bond within the molecule. Molecules of a nonpolar liquid are uncharged neutral with a zero dipole moment but contain bonds which are polar. Molecules of apolar liquids are neutral with an overall zero dipole moment. A measure of the polar or nonpolar nature of molecules composing a liquid is the value of its dielectric constant ε (see Table 1.4). The higher the polarity of molecules of a molecular liquid, the higher is the value of its ε.

Table 1.4. Properties of some commonly used solvents

Solvent[a]	MW[b]	d (g/cm^3)[c]	η (mPa s)[d]	ε (-)[c]	T_m (^{o}C)	ΔH_m (kJ/mol)	T_b (^{o}C)	ΔH_b (kJ/mol)
Water (H_2O)	18.0	0.9982	0.890	80.1	0 6.0	1	100	40.65
Acetone (C_2H_6CO)	50.08	0.790	0.306	21.01	−95.0	26.53	56.3	31.27
MeOH (CH_3OH)	32.04	0.7914	0.544	33.3	−97.6	3.18	64.6	35.21
EtOH (C_2H_5OH)	46.07	0.7893	1.074	25.3	−114.1	5.02	78.2	38.56
1-PrOH (C_3H_7OH)	60.10	0.8035	1.945	20.8	−126.1	5.2	97.2	41.44
2-PrOH (C_3H_7OH)	60.10	0.7855	2.038	20.18	−89.5	5.37	82.3	39.85
1-BuOH (C_4H_9OH)	74.12	0.8098	2.544	17.84	−89.8	9.28	117.7	43.23
2-BuOH (C_4H_9OH)	74.12	0.8063	3.096	17.26	−114.7	--	99.5	40.85
1-PeOH ($C_5H_{11}OH$)	88.15	0.8108	3.153	15.13	−78.9	9.83	138.0	44.36
1-HeOH ($C_6H_{13}OH$)	102.18	0.8188	4.590	12.5	−45.0	13.03	157.6	44.50
Ethylene glycol ($C_2H_6O_2$)	62.07	1.1088	16.1	41.4	−13.0	9.9	197.3	65.6
Glycerol ($C_3H_8O_3$)	92.09	1.2613	18.2	46.53	18.2	8.48	290	91.7
Benzene (C_6H_6)	78.11	0.8765	0.604	2.28	5.5	9.95	80.1	30.72
Toluene (C_7H_8)	92.14	0. 8670	0.560	2.38	−95.0	6.85	110.6	33.18
NMP (C_5H_9NO)	99.13	1.0230	1.667	32.55	−24.0	202	--	--
Acetonitrile (C_2H_3N)	41.05	0.7768	0.370	37.5	−43.8	8.17	81.6	29.75
DMSO (C_2H_6OS)	78.13	1.0958	2.012	4.7	19.0	8.69	189.0	52.90
1,4-Dioxane ($C_4H_8O_2$)	88.02	1.0269	1.180	2.2	11.8	12.84	101.5	39.80
γ-Butyrolactane ($C_4H_6O_2$)	86.09	1.1243	1.730	--	−43.4	6.47	204.6	55.60

Comments: [a] Abbreviations: MeOH – methyl alcohol, EtOH – ethyl alcohol, PrOH – propanol, BuOH – butanol; PeOH – pentanol; HeOH – hexanol; NMP - N-methyl-2-pyrrolidine; DMSO – dimethylsulfoxide; [b] MW – molecular weight, [c] 20^{o}C, [d] 25^{o}C. Other symbols are: density d, viscosity η, dielectric contant ε, boiling temperature T_b, melting temperature T_m, and enthalpy of melting ΔH_m.

1.2.2. Low-temperature ionic liquids

Low-temperature ionic liquids (ILs) are a diverse group of salts found in the liquid state at temperatures below 100 ^{o}C and are conductors of electricity. The main characteristic of ILs is molecular ion-pairs as their building blocks as opposed to molecules in the traditional solvents. Their characteristic features are negligible vapor pressure even at high temperature in contrast to traditional organic solvents which are volatile, high thermal stability, a large liquidus range determined by their low melting points and high decomposition points, a density higher for most ILs except for salts based on pyrrolidinium, dicyanodiamide and guanidinium than that of water, high viscosity about 1 to 3 orders of magnitude higher than that of molecular organic solvents, moderate specific conductivities, and miscibility with substances having a wide range of polarities. In this section the characteristic features of their properties are briefly described. For more details on the properties of ILs the reader is referred to the literature (Bittner et al., 2012; Handy, 2011; Marsh et al., 2004; Rooney et al., 2009; Zhang et al., 2006; 2014).

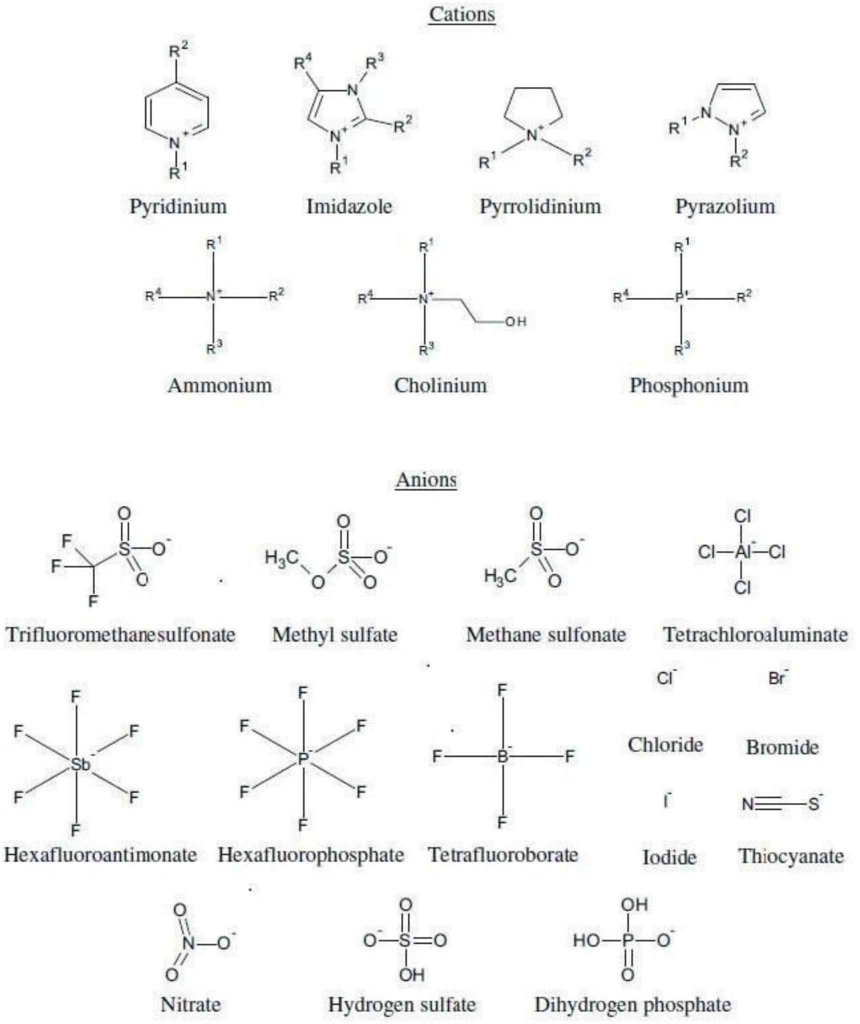

Figure 1.16. Most common cations and anions that form ionic liquids. Reproduced from Zhao (2017).

Figure 1.16 shows examples of most common cations and anions that form ionic liquids (Zhao, 2017). Cations in ILs are typically asymmetric organic structures, often containing nitrogen or phosphorus atoms with linear alkyl chains, such as ammonium, phosphonium, imidazolium (im), pyridinium (py) or pyrrolidinium (pyr) cations (Dong et al., 2014; Marsh et al., 2004; Mu and Han, 2014; Rooney et al., 2009; Zhang et al., 2006; Zhao, 2017). Examples of asymmetric organic cations are: alkylammonium, alkylphosphonium, 1,3-dialkylimidazolium, and 1-alkylpyridinium ions. Anions in ILs can be either organic or inorganic based compounds. Most common anions in ILs are: Br^-, Cl^-, hexafluorophosphate $[PF_6]^-$, tetrafluoroborate $[BF_4]^-$, bis(trifluoromethylsulfonyl)amide $[NTf_2]^-$, thiocyanate $[SCN]^-$, dicynamide $[DCA]^-$, tris(penta-fluoroethyl) $[FAP]^-$, trifluoromethane-sulfonate $[TfO]^-$, and methylsulfate $[C_1SO_4]^-$. The freedom in designing the organic cation (for example, by variation of the side chain length or by varying the substituents on the ring and/or on the chain) and the possible combination of cation and anion enable to obtain a huge number of different ionic liquids.

In addition to the interactions, such as hydrogen bonding and covalent, dipole–dipole and van der Waals interactions, existing in conventional organic solvents, ionic interactions (mutual electrostatic attraction or repulsion of charged particles) present in the ILs have a strong effect on their various properties (Crosthwaite et al., 2005, 2006; Dong et al., 2014; Freire et al., 2007a; Marsh et al., 2004; Mu and Han, 2014). For example, unlike ionic solids like NaCl in which ions are close-packed leading to high lattice energies E_{latt} and high melting points T_{m}, the ILs containing halide anions exist as liquids at ambient conditions because the bulkiness of the cations and anions prevents their packing despite strong electrostatic interaction between the ions. The ionic interactions in ILs make them miscible with various polar substances and the presence of the alkyl chain on the cation determines their solubility in less polar liquids (Mu and Han, 2014). Weaker interactions such as hydrogen bonding in ILs are believed to occur between an oxygen or halide atom on the anion and the hydrogen atoms on the imidazolium or pyridinium ring of the cation.

Compared to conventional molecular solvents, the chemical and physical properties of ILs strongly depend on the nature of the cations and anions composing them. The desired property of a particular IL is achieved by varying the length and branching of alkyl groups incorporated into cations. For example, in 1-alkyl-3-methylimidazolium hexafluorophosphate, $[C_n\text{mim}][PF_6]$ where n is an integer, change in the length of the 1-alkyl chain from 1 to 9 renders the liquid practically immiscible in water from miscible. Similarly, in the IL 1-alkyl-3-alkylimidazolium hexafluorophosphate, $[C_nC_m\text{im}][PF_6]$ where n and m are integers, replacement of the $[PF_6]^-$ anion by $[BF_4]^-$ enormously increases the solubility of the IL in water whereas its replacement by $[NTf_2]^-$ anion decreases the solubility in water. The physical properties such as density, melting point and viscosity of ILs strongly depend on the size or structure of cations and anions (Bittner et al., 2012; Hu and Peng, 2014; Rooney et al., 2009; Zhang et al., 2006). Ideally, the temperature when an IL melts from its solid phase or when it freezes from the disordered liquid form are expected to be the same (i.e. $T_{\text{m}} = T_{\text{f}}$), but it is frequently observed that these temperatures, T_{m} and T_{f}, differ from each other such that $T_{\text{m}} > T_{\text{f}}$

and that the reported values of the melting point T_m of some of the ILs in fact represent their T_g obtained during the cooling of their liquids. Therefore, the values of T_m for the ILs recorded during the heating of their solids are more reliable.

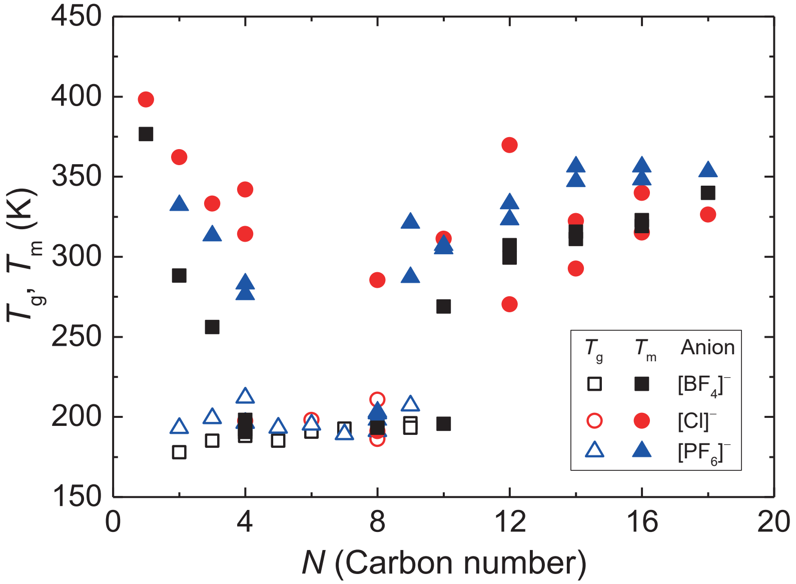

Figure 1.17. Phase transition temperature of various ILs with the number *N* of carbon atoms in alkyl chain of $[C_n mim]^+$ cations containing the anions X^-: $[PF_6]^-$, $[BF_4]^-$, and $[Cl]^-$. Carbon number *n* in the cation notation is denoted by *N* in the figure. Original data from Zhang et al. (2006).

The phase transition temperatures of ILs are determined by van der Waals forces and electrostatic interaction force, and the impact of the two forces plays different roles for different kinds of ILs (Marsh, 2004; Rooney et al., 2009; Hu and Peng, 2014; Zhang et al., 2006). The T_m of quaternary ammonium-type ionic liquid is governed by the van der Waals force rather than the electrostatic interaction force. In these ILs, the change of phase transition temperature with the anions is not so pronounced as with their cations. The ILs of imidazolium containing symmetric cations, such as 1,3-dimethylimidazolium (denoted as $[C_1mim]^+$), 1,3-diethylimidazolium ($[C_2eim]^+$), 1,2,3-trimethylimidazolium, and 1,2-dimethyl-3-ethylimidazolium, show higher melting points than those containing asymmetric cations containing longer alkyl chain length. Figure 1.17 shows, as an example, the experimentally obtained data of the T_m and T_g of ILs of $[C_n mim]^+$ cations containing the anions $[X]^-$: $[PF_6]^-$, $[BF_4]^-$, and $[Cl]^-$ as a function of the carbon number *N* in the cation chain. This carbon number *N* is represented by *n* in the notation of the cation formula (i.e. $n = N$). As seen from the figure, with the exception of some 5-6 of the erratic values of T_m for different ILs with $N = 4$, 8 and 10, T_m, as a rule, is higher than T_g and there are no T_m data for ILs with $5 \leq N \leq 7$. It may be noted that ILs with symmetric cations, such as

1,3-dimethyl-imidazolium, $[C_1mim]^+$, have the highest melting points, which initially decrease steeply with increasing alkyl-chain length in the branch of 1-alkyl-3-methyl-imdazolium, denoted as $[C_n mim][X]$, for N up to 4, and finally, when the carbon number N exceeds 8, the melting points T_m of the ILs increase slowly with the carbon number N.

As seen from Figure 1.17, the melting points T_m of the ILs composed of small and bulky alkyl-chain cations in the intervals of carbon number $N < 4$ and $N > 10$, respectively, strongly depend on the nature of the anion of the ILs, but their trends in the two intervals are different. In the former interval, the melting points T_m of the ILs decrease in the sequence of anions: $[Cl]^- > [PF_6]^- > [BF_4]^-$. However, in the latter interval, their T_m's decrease in the sequence of anions: $[PF_6]^- > [BF_4]^- > [Cl]^-$. The glass transition temperatures T_g of the above ILs in the alkyl-chain length N between 4 and 9 increases practically linearly with N and their values for the ILs containing $[PF_6]^-$ anions are higher than those of $[BF_4]^-$ anions, with probably an intermediate position for the $[Cl]^-$ ions.

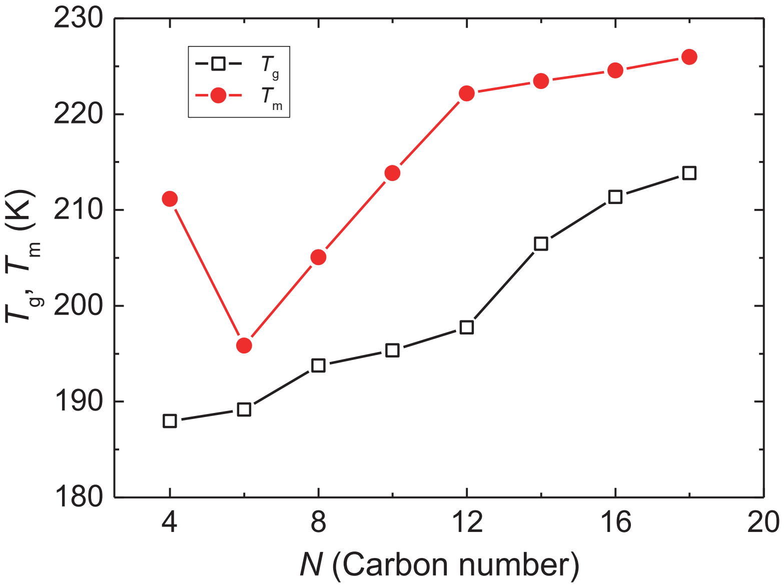

Figure 1.18. Variation in melting point T_m and glass transition temperature T_g of various N-alkyl-isoquinolinium bis((perfluoroethane)sulfonyl)imide ILs ($C_n$isoqBETI; $[C_nH_{2n+2}C_9H_6N]$-$[C_4F_{10}NO_4S_2]$) with the number N of carbon atoms in alkyl chain. Carbon number n in the cation notation is denoted by N in the figure. Original data from Zhang et al. (2006).

Figure 1.18 shows another example of the variation in the melting points T_m and glass transition temperatures T_g of various N-alkyl-isoquinolinium bis((perfluoroethane)sulfonyl)imide ILs (denoted as $C_n$isoqBETI; chemical formula: $C_nH_{2n+2}C_9H_6N][C_4F_{10}NO_4S_2]$) with the number N of carbon atoms in alkyl chain. Here the trend of the variation in the melting points T_m with the number N of carbon atoms is similar to that of [C$_n$mim][PF$_6$] described above but that of T_g steadily increases practically linearly with N. The increment ($\Delta T_g/\Delta N$) in T_g with N of the $-CH_2$ groups in the alkyl-chain length of the cations of the ILs of Figures 1.17 and 1.18 are also comparable. However, as expected for the temperatures of solid-to-liquid and liquid-to-solid transitions, $T_m > T_g$ in the entire N range.

Comparison of the melting points T_m of inorganic molten salts like NaCl (T_m = 1076.15 K) with those of the ILs like 1-alkyl,3-methylimidazolium chloride, [C$_n$mim][Cl] with 275 K < T_m < 400 K (see Figure 1.17), shows that the reduction in the T_m of ILs is caused by replacing the small inorganic cations by bulky organic cations. However, not all ILs composed of asymmetric cations are observed to melt at precisely-defined temperatures. The above behavior of the melting points of the ILs is associated with the molecular shape and symmetry of cations, electrostatic intermolecular interactions and their conformational and rotational degrees of freedom in the solid and liquid phases. As described above, these factors determine the values of contributions ΔH_m^{coul}, ΔH_m^{van} and ΔH_m^{sc} to the enthalpy of melting ΔH_m due to coulombian, van der Waals and hydrogen-type specific interactions, respectively, and contributions ΔS_m^{tr}, ΔS_m^{rot} and ΔS_m^{conf} to the entropy of melting $\Delta S_{m,b}$ due to translation, rotation and configuration of molecules during the melting of the compound (see Eqs. (1.20) and (1.21)). Since an increase in the alkyl-chain length leads to an increase in the molar volume V_M and the chain flexibility, they give positive contributions to ΔS_m^{conf} and ΔH_m^{van} and a negative contribution to ΔH_m^{coul}. Consequently, depending on whether the value of $\Delta H_m/\Delta S_m$ decreases or increases due to the competition between these factors with increasing number N of $-CH_2$ groups in the alkyl-chain length of the cations of ILs, their melting points $T_m = \Delta H_m/\Delta S_m$ decrease or increase in different N intervals (Hu and Peng, 2014).

The dominant forces determining the melting points of ILs with short alkyl-chain cations and rigid anions are electrostatic interactions, which are related to their lattice energies E_{latt} given by (Dong et al., 2014)

$$E_{latt} = 2\left(C_1 + \frac{C_2}{V_M^{1/3}}\right), \tag{1.27}$$

where V_M is their molar volumes in the lattice and is equal to the sum of the volumes V_M^+ and V_M^- of individual cations and anions, respectively, and C_1 and C_2 are empirical constants. Therefore, the melting point of ILs containing a particular anion or cation decreases with an increase in the molar volume V_M^+ or V_M^- of cations or anions. This behavior of T_m of ILs is observed for $N < 4$. However, the melting point of ILs containing rigid anions and long alkyl-chain cations is determined by weak short-range van der Waals interactions, which are related to the compactness of arrangement of alkyl chains in the IL structure. In these ILs the separation between alkyl chains decreases with increasing anion size (i.e. with decreasing the anion basicity). Therefore, the enthalpies of melting ΔH_m, and hence the melting points T_m, of these ILs composed of a particular type of cations or anions are expected to increase with increasing size of the anion or cation. This trend of T_m of long alkyl chains is observed for $N > 10$. This suggests that elongation of the chain length reverses the sequence of anions for the T_m's of the ILs with the short alkyl chains.

In contrast to the dominant role of coulombian and van der Waals interactions in the determination of the the melting points of different ILs in the ranges of alkyl chain length $N < 4$ and $N > 10$, respectively, the melting points in the interval $4 < N < 10$ is mainly determined by the enhanced contribution of the configurational entropy ΔS_m^{conf} of the alkyl chains. This configurational entropy contribution appears to be strongly related to the asymmerical nature of the alkyl chains and is observed when electrostatic interaction is damped by van der Waals-type interactions. As seen from Figures 1.17 and 1.18, these temperatures correspond to the T_g of the ILs and cover a wide alkyl-chain length range.

The density d of ILs decreases as the alkyl chain length in the cation increases up to a certain length, but, for a given cation, the density increases as the molecular weight M of the anion increases (Mu and Han, 2014; Rooney et al., 2009; Zhang et al., 2006; Zhao, 2017). As in molecular organic solvents, the density of ionic liquids decreases practcally linearly with increasing temperature (Marsh et al., 2004; Zhao, 2017). Trends opposite to those in density of ILs are observed in the case of their viscosity. The viscosity of ILs increases with an increase in the alkyl chain length and, for a given cation, the viscosity decreases in the following order of anions (Zhao, 2017): $[CH_3COO]^- > [PF_6]^- > [C_1SO_4]^- > [C_2SO_4]^- > [BF_4]^- > [OTf]^- > [NTf2]^-$. The viscosities of ILs are governed essentially by van der Waals interactions and H bonding (Rooney et al., 2009; Zhang et al., 2014; Zhao, 2017). In general, ILs composed of highly symmetric or almost spherical anions are more viscous and their viscosity decreases with increasing anionic asymmetry.

As examples of the effect of the size and structure of cations and anions, the values of densities d and viscosities η of some ILs at 25 °C are listed in Table 1.5. It may be noted that both the molar volume $V_M^{25} = M/d$ and the viscosity η of ILs composed of the same anion increase with an increase in the length of an alkyl group of the cation, but the molar volume V_M^{25} increases and the viscosity η decreases with an increase in the size of the anion of the ILs composed of the same cation. There is no direct relationship between V_M^{25} and η, but the values of η of the ILs are inversely proportional to their thermal expansivity α_P. This inverse relationship between η and α_P follows from the linear relationship between the fluidity $\phi = \eta^{-1}$ of nonassociated liquids and their molar volumes, given by the modified Batschinski equation (Hildebrand, 1971, 1977); see Section 5.2.1:

$$\phi = D\frac{(V_M - V_M^0)}{V_M^0}, \tag{1.28}$$

where V_M^0 is the molar volume of the liquid corresponding to the temperature T_0 when its fluidity ϕ approaches zero, and D is a proportionality constant characteristic of the liquid. The relative change in the molar volume $(V_M - V_M^0)/V_M^0$ of the ILs is related to their thermal expansivity α_P with reference to the volume V_M^0 when $\phi \to 0$. The volume change ($V_M - V_M^0$) of the liquid is the effective free volume of the liquid participating in viscous flow and the value of the parameter D/V_M^0 for an IL is related to different types of interactions between its ions.

Table 1.5. Densities and viscosities of some ILs at 25 °C

IL	MW	d (g·cm^{-3})	V_M^{25} (cm^3·mol^{-1})	η (mPa·s)	$10^4\alpha_P$ (K^{-1})	Source
[C$_4$mim][SCN]	197.3	1.0698	184.43	51.7	5.55	a
[C$_4$mpy][SCN]	208.2	1.0613	196.18	85.7	5.40	a
[C$_4$mpyr][SCN]	200.4	1.0248	195.56	109.5	5.04	a
[C$_4$mim][NTf$_2$]	430.4	1.4343	300.07	50.05	6.868	b
[C$_4$mpyr][NTf$_2$]	420.4	1.3946	301.45	76.73	6.307	c
[C$_2$py][NTf$_2$]	388.2	1.5320	253.36	39.76		d
[C$_4$py][NTf$_2$]	416.4	1.4560	285.97	60.55		d
[C$_6$py][NTf$_2$]	444.4	1.3820	321.58	245.33		d
[C$_4$py][BF$_4$]	223.0	1.2134	183.80	163.26		e
[C$_8$py][BF$_4$]	279.1	1.1127	250.85	233.50		e
[C$_1$C$_4$py][BF$_4$]	237.0	1.1811	200.69	196.20		f

a - Domańska and Królikowska (2012); b - Vraneś et al. (2014); c - Vraneś et al. (2015); d - Bittner et al. (2012); e - Mokhtarani et al. (2009); f - Heintz et al. (2005).

The validity of Eq. (1.28) is associated with the contributions of molar volumes V_M of individual cations and anions of ILs in their flow properties. In fact, different approaches of describing various properties of ILs are based on consideration of the existence of individual cations and anions in an IL (group contribution models) and identification of regions of cations and anions interacting with each other (quantitative structure–property relationship models). For example, assuming that the volumes of individual ions in an IL behave as an ideal mixture, usually known as group contribution method (GCM), Jacquemin et al. (2008) determined the effective molar volumes V_M(eff) and the densities d of ILs. Extended versions of the group contribution method have been used for the estimation and modeling of volumetric and flow properties of individual as well as binary mixtures of ILs: density (Zhao et al., 2017), viscosity (Gardas and Coutinho, 2008; Zhao et al., 2016a,b; Zhao and Jacquemin, 2017a), and electrical conductivity (Zhao and Jacquemin, 2017b). However, methods based on quantitative structure–property relationship (QSPR) consider appropriate selection of molecular descriptors relevant to the properties of ILs, as employed by Katritzky et al. (2002a,b), Eike et al. (2003), and Carrera and Aires-de-Sousa (2005) to predict the melting points of different ILs, and by Bini et al. (2008), Han et al. (2011) and Chen et al. (2013) to predict the viscosity and conductivity of ILs.

López-Martin et al. (2007) optimized the geometries of cations and anions separately using semi-empirical quantum mechanical calculations and classified descriptors in terms of size, symmetry and charge distribution in either the cation or the anion. These authors described one descriptor related to structural variation of the anion, defined by the degree of sphericity $s = (1-1/Z)q$, with Z as the coordination number of the central atom and q the charge of the anion, and three descriptors related to the charge, symmetry and size of the cation interacting with an anion. The authors found three structural regions for the calculation of the melting point T_m of ILs based on 1-alkyl-imidazolium cations as shown schematically in Figure 1.19. The first and the most important region, known as charge-rich region, is confined to the imidazolium ring of the cation (size about 0.4 nm) and is responsible for the ionic interaction. The second region, the symmetry-breaking region, characterizes the space where the chain grows (at about 0.55 nm) but the cation symmetry breaks and the coulombian interaction weakens with the chain length. Here the melting point of an IL decreases with an increase in the side-chain length. This region reflects poor packing of ions in the lattice. The third region, the hydrophobic region, corresponds to the point (beyond about 1.2 nm) where the side-chain length increases and involves increasing van der Waals forces with chain length. In this region, the melting point of the IL begins to increase with increasing chain length.

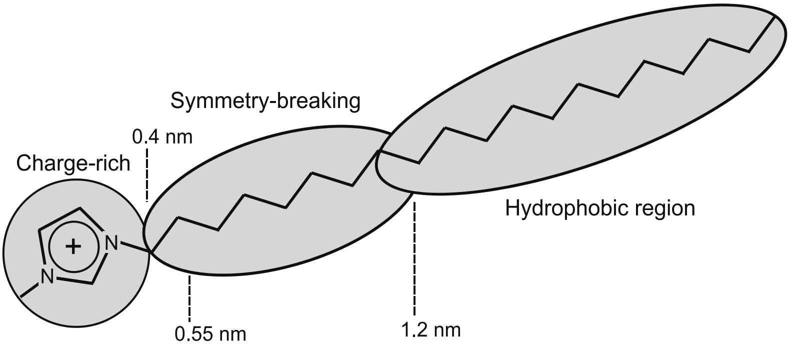

Figure 1.19. Schematic presentation of structural regions proposed in the calculation of the melting point T_m of ILs based on 1-alkyl-imidazolium cations. Adapted from López-Martin et al. (2007).

Temperature is an important factor that affects the viscosity of ILs. The viscosity decreases with an increase in the temperature of an IL. As in other liquids, the viscosity of ILs decreases with an increase in their temperature. The temperature dependence of the dynamic viscosity η of ionic liquid systems is sometimes described by an Arrhenius-type equation (see Chapter 5)

$$\eta = \eta_0 \exp\left(\frac{E_\eta}{R_G T}\right), \tag{1.29}$$

where η_0 is the viscosity of the liquid at $T \to \infty$ when the exponential term approaches unity, E_η is the activation energy for viscous flow. This relation holds for unassociated liquids, including molten electrolytes. However, it is found that the temperature dependence of the viscosity η of many ionic liquid follows the Vogel−Tammann−Fulcher (VTF) relation (Angell, 1991, 1995; see Chapter 5)

$$\eta = \eta_0^* \exp\left(\frac{B^*}{T - T_0}\right), \tag{1.30}$$

where $\eta_0{}^*$, B^* and T_0 are constant related to the glass-forming ability of an IL, and the ratio B^*/T_0 is a measure of the strength of mutual interaction between the liquid constituents.

Additives, whether organic solvents or ionic liquids, contained in ILs also have a pronounced effect on their different properties such as densities, viscosities and melting points. The effects of additives contained in the ILs on their properies are also explained using the above concepts. As discussed below, examples of such an interpretation are mixtures of ILs containing other solvents.

1.2.3. Mixtures of solvents

Commonly used molecular solvents such as water and conventional organic solvents can be classified as polar and nonpolar solvents. A polar solvent dissolves in other polar solvents, whereas a nonpolar solvent dissolves in other nonpolar solvents. In other words, it is the similarity in the chemical properties of the solvents that determines their mutual solubility. The process of two similar solvents dissolving in each other means that the two solvents are miscible. However, when two solvents do not dissolve in each other, they are known as immiscible solvents. For example, water and ethanol, and ethanol and *n*-butanol are completely miscible in all proportions, water and *n*-butanol are partly miscible, whereas water and oils are completely immiscible. In the case of partly miscible and immiscible solvents, the liquid of lower density appears on the top of the liquid of higher density.

Whether a molecular solvent is miscible or immiscible with another molecular solvent is associated with the formation of chemical bonds between the molecules of the two solvents and is intimately related to the chemical structure of their molecules. The simplest model to understand the mutual solubility of two solvents, say main solvent 1 containing another solvent 2 of concentration x_2 of fraction between 0 and 1, is the model of regular solutions, which assumes that the solution volume is the sum of the volumes of N_1 and N_2 molecules of individual components and they pack the solution volume simply by interchanging their positions. If w_{11}, w_{22} and w_{12} denote bond energies between pairs of molecules of solvent 1 and 1, cosolvent 2 and 2, and both solvents 1 and 2, respectively, the change in the bond energy w between the solution molecules in the solution may be given by

$$Zw = Z(w_{11} + w_{22} - 2w_{12}), \tag{1.31}$$

where Z is the number of nearest neighbors. The two solvents are mutually miscible when the enthalpy of solution $\Delta H_s = Zw/2 > 0$. This is possible when 1–2 interactions are stronger than 1–1 and 2–2 interactions (i.e. $2w_{12} > w_{11}+w_{22}$). They are poorly soluble when $\Delta H_s < 0$, i.e. 1–2 interactions are weaker than 1–1 and 2–2 interactions (i.e. $2w_{12} < w_{11}+w_{22}$).

We assume that the enthalpy of solution ΔH_s is a sum of the enthalpy of complete miscibility ΔH_m of the two types of molecules in the mixture of solvents and the enthalpy of mixing ΔH_mix due to the formation of 1–2 bonds at the expense of 2–2 bonds, i.e.

$$\Delta H_\mathrm{s} = \Delta H_\mathrm{m} + \Delta H_\mathrm{mix}\,, \tag{1.32}$$

where $\Delta H_\mathrm{m} = Z(w_{11}-w_{22})/2$ and $\Delta H_\mathrm{mix} = Z(w_{22}-w_{12})$. The enthalpy of mixing ΔH_mix of the solvent mixture is given by (Eggers et al., 1964)

$$\Delta H_\mathrm{mix} = \left(\frac{N_1 N_2}{N_1 + N_2} \right) w_{12} = N_\mathrm{A} x_2 (1 - x_2) w_{12}\,, \tag{1.33}$$

where N_A is the Avogadro number and x_2 denotes the molar concentration of the cosolvent 2.

The enthalpy of mixing ΔH_mix of the solvent mixture, as defined above, may serve as a measure of interactions between 1–1, 2–2 and 1–2 molecules. When $\Delta H_\mathrm{mix} > 0$, $w_{12} > (w_{11}+w_{22})$. However, when $\Delta H_\mathrm{mix} < 0$, $w_{21} < (w_{11}+w_{22})$. When $\Delta H_\mathrm{mix} = 0$ (i.e. $w_{12} = 0$), the two solvents are completely or ideally miscible. Thus, deviations from the complete miscibility behavior of two solvents are due to the nature of interactions between the molecules of the two solvents.

Eq. (1.33) predicts a maximum and a minimum value of ΔH_mix at cosolvent composition $x_2^* = 0.5$ for $w_{12} > 0$ and $w_{12} < 0$, respectively. It is usually observed that the value of x_2^* differs from 0.5. This deviation in the value of x_2^* from 0.5 is a consequence of consideration of a two-component system of unassociated molecules (Eggers et al., 1964). Association of molecules of components in the mixture leads to a decrease in their motion which results in a negative enthalpy of mixing ΔH_mix and an increase in x_2^*. An opposite effect is encountered in systems composed of an associated component and a more or less passive component. In this case mixing partially destroys association of atoms/molecules, which results in a positive enthalpy of mixing because rupturing of associated atoms/molecules requires consumption of heat. In such cases the value of the fraction x_2^* of the component of the system is also usually reduced below 0.5.

Changes in the molar volume V_M and the mutual miscibility, as defined by the temperature T_LLE of liquid–liquid equilibria (LLE), of solvent mixtures are the properties directly related to different types of interactions taking place between the molecules and ions of components of solvent mixtures, and are reflected by the values of the enthalpy of mixing ΔH_mix. The characteristic features of these properties of binary mixtures of molecular solvents and molecular solvents containing ionic liquids are described below using the above ideas of interactions in binary mixtures.

1.2.3.1. Interactions in mixtures of molecular solvents

As mentioned above, the miscibility of a molecular solvent in another molecular solvent is associated with the formation of chemical bonds between the molecules of the two solvents and is intimately related to the chemical structure of their molecules and their polarities. A solvent dissolves in another solvent when its molecules form chemical bonds with the molecules of the other solvent. A measure of formation of chemical bonds in a mixture of solvents of two or more solvents at a particular temperature is a change in the molar volume V_M, usually known as the excess molar volume V_M^E, of the mixture given by

$$V_M^E = V_M - V_M^{id} = \frac{x_1M_1 + x_2M_2}{d} - \left(\frac{x_1M_1}{d_1} + \frac{x_2M_2}{d_2} \right), \qquad (1.34)$$

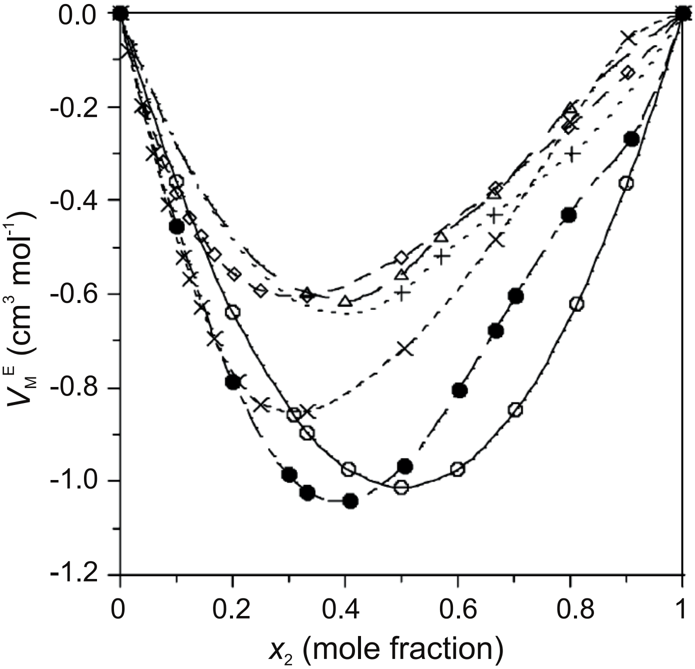

Figure 1.20. Variation of the excess molar volumes V_M^E for some monoalcohol−water binary mixtures with the mole fraction x_2 of different alcohols at 298.15 K: (○) methanol, (●) ethanol, (◊) 1-propanol, (×) 2-propanol, (+) 1-butanol, and (Δ) 2-butanol. Adapted from Herráez and Belda (2006).

where d is the density of the mixture, d_1 and d_2 are the densities of solvents 1 and 2 of mole fractions x_1 and x_2, respectively, and M_1 and M_2 are the molar masses of the pure solvents 1 and 2. When $V_M^E < 0$, there is a contraction in the mixture volume; but when $V_M^E > 0$, there is an expansion in the mixture volume (González et al., 2007; Herráez and Belda, 2006; Holguin et al., 2011). The larger the decrease in the V_M^E of the solution mixture, the stronger is the bonding between the molecules of the liquids, and vice versa.

Figure 1.20 shows, as an example, the variation in the excess molar volumes V_M^E

for some water–monoalcohol mixtures with the mole fraction x_2 of different alcohols, considered as cosolvents, at 298.15 K. It may be seen that: (1) the excess volume V_M^E is negative for all alcohols, (2) the deviation in the absolute value of V_M^E decreases with an increase in the carbon number N in the linear chain of the alcohol molecules, (3) the alcohol content x_2 resulting in the maximum volume contraction V_M^E decreases with an increase in the carbon number N in the alcohol molecule, and that (4) the alcohol content x_2 when the maximum excess molar volumes V_M^E in the mixture occurs decreases with an increase in the carbon number N in the alcohol molecule. Note that alcohols other than 1- and 2-butanols are miscible with water in the entire composition region but the latter are miscible only when x_2 exceeds about 0.5 and 0.3 mole fraction, respectively. In other words, the two forms of butanols have partial miscibility with water.

While binary mixtures of methanol and ethanol with water containing different compositions x_2 of the alcohol gives $V_M^E < 0$, binary mixtures of methanol or ethanol cosolvents contained in solvents like methyl acetate and ethyl acetate esters exhibit different trends. In the entire range of the cosolvent composition x_2, ester–methanol mixtures give $V_M^E < 0$, whereas ethanol–ester mixtures give $V_M^E > 0$ (González et al., 2007). Similarly, glycerol formal (i.e. 5-hydroxy-1,3-dioxane) mixtures with water and ethanol result in $V_M^E < 0$, but its mixtures with propylene glycol give $V_M^E > 0$ (Holguin et al., 2011).

The maximum variation in the excess molar volume V_M^E of a mixture of solvent 1 and cosolvent 2 depends on the temperature T of the solvent mixture. There is an insignificant variation in the value of V_M^E with temperature T of the binary mixtures of methanol and ethanol with water (González et al., 2007), but for other systems V_M^E is greatly influenced by the mixture temperature. With an increase in the temperature T, the positive values of V_M^E increase for the ester–ethanol mixture (González et al., 2007), the negative values of V_M^E decrease for the ester–methanol mixtures (González et al., 2007), and the negative values of V_M^E increase for the glycerol formal mixtures with ethanol (Holguin et al., 2011).

The above observation of the negative or positive values of excess molar volume V_M^E of different systems are associated with the nature of interactions w_{12} between the molecules of the mixture of the two solvents and the effect of temperature on these interactions (see Eq. (1.33)). As explained above, a negative excess molar volume V_M^E results due to various types of strong attractive interactions w_{12} between the molecules of the two solvents. These possible interactions involve charge transfer, dipole–dipole and dipole-induced interactions, and formation of hydrogen bonds between the molecules of the two components. These interactions result in the trapping of molecules of one of the solvents by those of the other in their vicinity, and is reflected by the cosolvent composition x_2 when V_M^E attains a maximum variation. However, a positive V_M^E is a result of weak dispersive forces which occur in all types of molecular interactions.

The trends of the variation of the maximum variation in V_M^E of different solvent–cosolvent mixtures with an increase in their temperature T are associated with the effect of temperature on different interactions between the molecules of the solvents. The main effect of an increase in the temperature of a solution mixture is to increase the thermal vibration of individual molecules as single entities, thereby decreasing their mutual interactions. This explains an increasingly lower variation in the maximum value of V_M^E of the water–methanol and water–ethanol mixtures by attractive interactions between the molecules of individual components with its increasing temperature. However, the consideration of vibration of individual molecules as single entities does not explain the opposite trends of increasingly higher positive values of V_M^E for mixtures of methyl or ethyl acetate with ethanol and increasingly lower negative values of V_M^E for mixtures of glycerol formal with ethanol with an increase in their temperature. A possible explanation of these opposite trends is that the molecules of methyl or ethyl acetate and glycerol formal cosolvents are composed of two different segments which, as a whole, show thermal behavior different from that of single entities.

Finally, it should be mentioned that strong attractive interactions leading to negative V_M^E in a binary mixture of solvents are an indication of compact packing of the molecules of the mixture, whereas weak dispersive forces imply loosening of molecular packing in the mixture.

1.2.3.2. Interactions in mixtures of ionic liquids and molecular solvents

Interactions in mixtures of ionic liquids with molecular solvents and other ionic liquids are more complex than those in mixtures of molecular liquids. Instead of interactions between the molecules in the mixture of the two molecular liquids, in the mixtures of solvents containing ionic liquids cations and anions of the ionic liquids are expected to interact with the molecules of molecular solvents and with the ionic parts of the ionic liquids. However, the general trends of the composition dependence of different physical properies of these mixtures are similar to those observed for mixtures of molecular liquids. Figure 1.21 illustrates, as an example, variation of the excess molar volumes V_M^E for $[C_4mim][C_8H_{17}SO_4]$–1-alcohol binary mixtures with the mole fraction x_2 of the IL in different solvents at 298.15 K.

It may be seen from Figure 1.21 that the values of V_M^E are negative in the entire range of $[C_4mim][C_8H_{17}SO_4]$–methanol mixture, with the minimum value of the V_M^E occurring at a particular x_2^* equal to 0.4 mole fraction. In contrast to methanol cosolvent, the values of V_M^E are positive for the mixtures of this IL with other alcohols over the entire composition range x_2 and the value of V_M^E increases with increasing alkyl-chain length. A similar behavior in the values of V_M^E with increasing chain length of alchohol molecules has been observed, among others, for $[C_1mim][CH_3SO_4]$–alcohol and $[C_4mim][CH_3SO_4]$–alcohol mixtures (Domańska et al., 2006b), $[C_4mim][SCN]$–alcohol mixtures containing 1-butanol, 1-pentanol and 1-hexanol as cosolvents (Domańska and Laskowska, 2009), and $[C_2mim][C_2H_5SO_4]$-–alcohol mixtures containing 1-alcohols with the alcohol alkyl number N between 3 and 10 (Domańska and Laskowska, 2008). However, in the case of the $[C_2mim][C_2H_5SO_4]$–alcohol mixtures it was observed (Domańska and Laskowska, 2008) that 1-propanol and 1-butanol cosolvents exhibit negative deviations in V_M^E from ideality in the entire composition but IL composition x_2^* corresponding to the minimum V_M^E shifts from 0.5 for 1-propanol to 0.6 for 1-butanol.

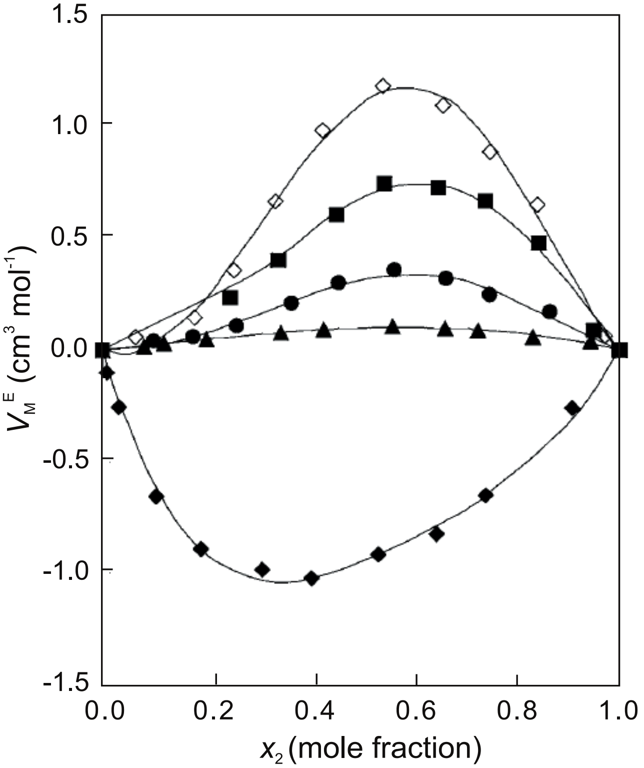

Figure 1.21. Variation of excess molar volumes V_M^E for [C_4mim][$C_8H_{17}SO_4$]−1-alcohol binary mixtures with the mole fraction x_2 of the IL in different alkyl-group in alcohols at 298.15 K: (♦) methanol, (▲) 1-butanol, (●) 1-hexanol, (■) 1-octanol, and (◊) 1-decanol. Solid lines represent best fit of the data according to Redlich−Kister relation. Adapted from Domańska et al. (2006b).

In contrast to the above trend, the highest investigated alcohols, 1-nonanol and 1-decanol cosolvents, exhibit positive deviations in V_M^E with IL composition x_2* shifting to higher values with an increase in the alkyl number N of the alcohol. However, for the alcohols in between the above two extremes, the deviations in V_M^E were observed to show sinusoidal curves such that the deviation in V_M^E is positive at low IL content x_2, followed by negative V_M^E at high IL content x_2 such the x_2 range of this negative V_M^E diminishes with increasing alkyl number N of the alcohol. Figure 1.22 shows an example of the above behavior for the [C_2mim][$C_2H_5SO_4$]−1-alcohol binary mixtures.

The above trends of variations of V_M^E of mixtures of ILs and molecular solvents with their composition are frequently observed for various systems. In the entire composition range, examples of IL−cosolvent mixtures exhibiting positive variations of V_M^E are: [C_4py][BF_4] and [C_8py][BF_4] in water at different temperatures between 283.15 and 333.15 K (Mokhtarani et al., 2009), [C_4pyr][NTf_2] in γ-butyrolactone (GBL) at different temperatures between 293.15 and 323.15 K (Vraneš et al., 2015); negative variations of V_M^E are: [C_4mim][NTf_2] in GBL at different temperatures between 293.15 and 323.15 K (Vraneš et al., 2014); sinusoidal variation in V_M^E are: [C$_4$mim][SCN], [C$_4$mpy][SCN], [C$_4$mpyr][SCN] and [C$_4$mpip][SCN] in water in the temperature range between 298.15 and 348.15 K (Domańska and Królikowska, 2012).

From the dependence of the excess molar volume V_M^E of different IL-alcohol systems on the IL content x_2 the following features may be noted:

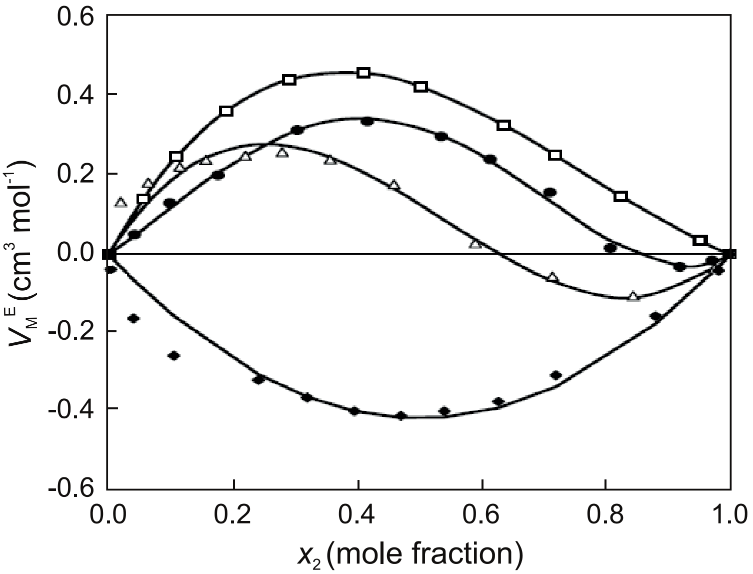

Figure 1.22. Variation of V_M^E for [C$_2$mim][C$_2$H$_5$SO$_4$]−1-alcohol binary mixtures with x_2 of the IL in different solvents at 298.15 K: (♦) 1-propanol, (Δ) 1-pentanol, (●) 1-heptanol, and (□) 1-nonanol. Solid lines represent best fit of the data according to Redlich−Kister relation. Adapted from Domańska and Laskowska (2008).

(1) The maximum deviation in V_M^E caused by the addition of a particular IL to higher homologues of normal linear alcohols increases with increasing alkyl-chain length of the alcohol molecules from its lowest, negative value for the lowest alcohol to positive values. For the [C$_1$mim][CH$_3$SO$_4$]−alcohol and C$_4$mim][CH$_3$SO$_4$]− alcohol mixtures, the value of the maximum deviation in V_M^E in the above IL-alcohol systems follows the order: methanol < 1-propanol < 1-butanol < 1-hexanol < 1-octanol < 1-decanol (Domańska and Laskowska, 2009; Domańska et al., 2006b).

(2) The maximum deviation in V_M^E caused by the addition of ILs of cations of different alkyl-chain length and anions of different sizes to a particular alcohol increases with increasing alkyl-chain length of the cation and increasing size of the anion. Examples of the former effect of the cation alkyl-chain length are [C$_1$mim][CH$_3$SO$_4$]−alcohol and [C$_4$mim][CH$_3$SO$_4$]−alcohol mixtures whereas those of the anion size are [C$_4$mim][CH$_3$SO$_4$]−alcohol and [C$_4$mim][C$_8$H$_{17}$SO$_4$]−alcohol mixtures (Domańska et al., 2006b).

(3) The value of IL content x_2* corresponding to the maximum deviation in V_M^E in an IL-alcohol system usually increases with increasing alkyl-chain length of the alcohol molecules. Examples are mixtures of [C_1mim][CH_3SO_4], [C_4mim][CH_3SO_4] and [C_4mim][$C_8H_{17}SO_4$] in alcohols (Domańska et al., 2006b).

(4) For the [C_2mim][$C_2H_5SO_4$]−alcohol mixtures which show sinusoidal variation of V_M^E with IL content x_2, the value of the maximum variation of V_M^E in different alcohols follows the trend observed above for the [C_1mim][CH_3SO_4]−alcohol and [C_4mim][CH_3SO_4]−alcohol mixtures (Domańska and Laskowska, 2008). However, the value of the IL content x_2^* corresponding to the maximum variation of V_M^E in different alcohols reveals two distinct regions of x_2* defined by $V_M^E < 0$ and $V_M^E > 0$. In the former case represented by 1-propanol and 1-butanol, x_2* = 0.45 and 0.70, respectively. In the latter case, x_2* < 0.4 and is represented by 1-pentanol and higher alcohols. Sinusoidal variation of V_M^E with IL content x_2, with two distinct regions of x_2* defined by $V_M^E < 0$ and $V_M^E > 0$, has been observed for mixtures of [C_8mim][BF_4] with 1-butanol at 298.15 K (Heintz et al., 2005) and for mixtures of different ILs [C_4mim][SCN], [C_4mpy][SCN], [C_4mpyr][SCN] and [C_4mpip][SCN] with water at various temperatures between 298.15 and 348.15 K (Domańska and Królikowska, 2012). The values of x_2* in the two V_M^E regions increase with increasing temperature.

(5) The value of the maximum deviation in V_M^E for a particular IL−alcohol system decreases with increasing temperature. Examples are: [C_4mim][SCN]−alcohol mixtures with 1-butanol, 1-pentanol and 1-hexanol (Domańska and Laskowska, 2008). This trend is similar to that observed for the IL−water system (Domańska and Królikowska, 2012).

The above observations may be explained using the concepts described above, where the solvents and cosolvents are assumed to be molecular and their molecules are considered spherical. However, the molecules of different ILs are elongated where the positive charge on a cation is separated by the negatively-charged anion by the chain of $-CH_2$ groups in between the two. Therefore, the structure of the IL may be considered to consist of four regions: positively-charged, symmetry-breaking, hydrobhobic, and negatively-charged regions. The former three regions define different segments of the cation of an IL molecule, as described in Figure 1.19, whereas the fourth region, referring to the anion of the IL molecule, ensures electrical neutrality to the molecule as a whole, Since the molecule of solvent 1 is capable of forming bonds with different segments of the IL molecule, the interaction energy w_{12} may be considered to be composed of contributions from different regions of the IL molecule, given by

$$w_{12} = (w_{12}^{+} + w_{12}^{\mathrm{sb}} + w_{12}^{\mathrm{hydr}} + w_{12}^{-}), \tag{1.35}$$

where the superscripts "+", "sb", "hydr", and "–" denote the contributions from the above regions. The contributions w_{12}^{+} and w_{12}^{-} involve the formation of hydrogen bonds between solvent molecules and the cation and anion, w_{21}^{sb} is associated with formation of π−π type bonds between solvent molecule and $-CH_2$ groups of the alkyl-chain of the IL cation, and w_{12}^{hydr} involves repulsion between the cation alkyl-chain and the solvent molecule. Therefore, the value of w_{12} depends on the relative contributions of these four contributions, implying that $w_{12} > 0$ when $(w_{12}^{+} + w_{12}^{\text{sb}} + w_{12}^{-}) > w_{12}^{\text{hydr}}$, and $w_{12} < 0$ when $(w_{12}^{+} + w_{12}^{\text{sb}} + w_{12}^{-}) < w_{12}^{\text{hydr}}$.

Using the above interaction energy contributions associated with different segments of an IL molecule in Eq. (1.35), one can explain the above observations. The first two features directly follow from the above inferences when $(w_{12}^{+} + w_{12}^{\text{sb}} + w_{12}^{-}) > w_{12}^{\text{hydr}}$ or $(w_{12}^{+} + w_{12}^{\text{sb}} + w_{12}^{-}) < w_{12}^{\text{hydr}}$. These features are directly connected with the affinity of O−H group of the alcohols to the formation of hydration bonds with different segments of an IL molecule and is related to the dielectric constant ε of the alcohols. Feature 3 of the shift in the IL composition x_2 is associated with the relative variation in $(w_{12}^{\text{hydr}} - w_{12}^{\text{sb}})$ with x_2. However, feature 4 of the sinusoidal variation in the excess molar volumes V_M^E for different ILs in water and alcohols may be attributed to the dependence of the interaction energy w_{12} on the IL composition x_2. This type of dependence involves the disruption of the structure of these solvents by the mixing of IL molecules, which at low IL compositions follows the relation $(w_{12}^{+} + w_{12}^{\text{sb}} + w_{12}^{-}) < w_{12}^{\text{hydr}}$. A typical example is the associated solvent like water, which shows sinusoidal variation of V_M^E in binary mixtures of various ILs composed of different cations over a wide range of temperatures (Domańska and Królikowska, 2012). A similar explanation holds in the case of variation of V_M^E for the binary mixtures of $[C_2mim][C_2H_5SO_4]$ contained in different 1-alcohols with IL content x_2, where the sinusoidal variation in not observed in lower alcohols like 1-propanol and 1-butanol and in higher alcohols 1-nonanol and 1-decanol (Domańska and Laskowska, 2008). The trends of decrease in the values of V_M^E and the shift in IL composition x_2 to higher values with an increase in the temperature of a solvent−IL binary mixture are a consequence of weaking of different interactions with increasing temperature.

Finally, it should be mentioned that increasing values of w_{12}^{+} and w_{12}^{-} involving hydrogen bonds between alcohol molecules and the positively-charged region of cations and negatively-charged anions of ILs lead to higher variations in the V_M^E of IL−alcohol systems.

1.2.3.3. Miscibility of ionic liquids and molecular solvents

Physical properties of ionic liquids comprise the properties of pure components as well as the properties of their mixtures with other solvents such as various molecular solvents. Among the various properties of mixtures of ionic liquids with other solvents, understanding of their phase behavior, such as vapor−liquid (VLE) and liquid−liquid equilibria (LLE), is important in using the ILs for chemical reactions and separation processes. The mutual solubility of ionic liquids with other solvents is determined by observing visually the temperatures when samples of IL−solvent mixtures of known compositions changes from one phase to two phases on cooling or from two phases to one phase on heating (Crosthwaite et al., 2004, 2005, 2006). The LLE temperature data on a variety of IL−solvent mixtures have been reported and discussed in the literature (Crosthwaite et al., 2004, 2005, 2006; Freire et al., 2007a; Heintz, 2005; Mu and Han, 2014). The ILs are mainly imidazolium-, pyridinium-, pyrrolidinium-, and piperidinium-based cations with anions like $[BF_4]^-$, $[PF_6]^-$, $[NTf_2]^-$, $[TfO]^-$ and $[DCA]^-$, whereas the molecular solvents, both polar as well as nonpolar, in the mixtures are: water, various 1-alcohols ($C_nH_{2n+2}OH$, with $3 < n < 12$), and benzene and toluene. These studies have shown that the mutual solubility of the IL−solvent mixtures depends on the cation, the substituents on the cation, the anion, and the solvent.

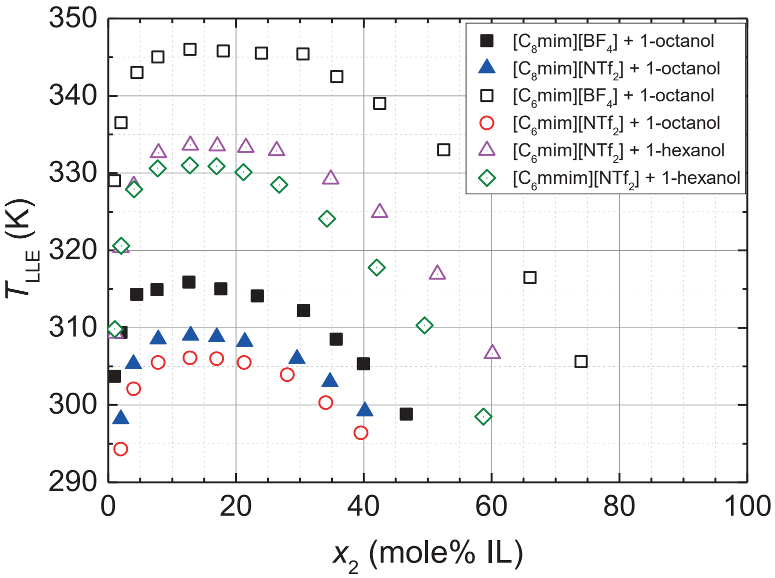

Figure 1.23. Variation of LLE temperatures T of 1-hexanol and 1-octanol mixtures containing some imidazolium-based ILs with IL content x_2 (mole %). Original data from Crosthwaite et al. (2005).

Figure 1.23 shows examples of the mutual solubility of $[C_nmim][BF_4]$, $[C_nmim][NTf_2]$, and $[C_nmmim][NTf_2]$ ILs with 1-hexanol and 1-octanol as a function of IL content x_2 in the mixtures. A general feature of all these solubility curves is that the T_{LLE} initially steeply increases and then, after passing through a maximum value of T_{LLE}, usually referred to as the upper critical solution temperature, corresponding to a particular value of x_2 (denoted hereafter as T^*_{LLE} and x^*_2, respectively) decreases with increasing x_2. Other features of the plots are summarized below.

Effect of alcohol chain length. The mutual solubility of IL−alcohol systems decreases with increasing alcohol chain length. Here the examples are both $[C_nmim][BF_4]$ and $[C_nmim][NTf_2]$ dissolved in 1-hexanol and 1-octanol, where changes in the maximum mutual-solubility temperature T^*_{LLE} are 14.1 and 27.5 K for [C_8mim][BF_4] and [C_6mim][NTf_2], respectively. A similar behavior has been observed for other systems such as [C_4mpy][NTf_2] and [C_2mim][NTf_2] in various alcohols (Crosthwaite et al., 2004, 2005, 2006; Heintz, 2005). Since increasing chain length of an alcohol renders it more aliphatic and hydrophobic, this increasing value maximum mutual-solubility temperature T^*_{LLE} is associated with the hydrophobicity of alcohols. In general, more hydrophobic the alcohol, the higher is the value of T^*_{LLE} and the lower is the IL solubility in the alcohol.

Effect of alkyl-chain length of cation. The mutual solubility of ILs of different of the alkyl-chain lengths in a particular alcohol decreases with increasing alkyl-chain length of the cations. An example here are the cations [C_6mim]$^+$ and [C_8mim]$^+$ dissolved in 1-octanol, where the maximum-temperature difference is 24.6 K. Similar trends have been reported, among others, for [$C_n$mim][BF_4] ILs, with $4 < n < 8$, in 1-butanol (Wu et al., 2003) and for [C_4mpy][NTf_2] and [C_6mpy][NTf_2] in 1-hexanol (Crosthwaite et al., 2006). This trend is associated with an increase in the van der Waals interactions (i.e. London dispersion forces) between the alkyl portions of the cation and the alcohol. The longer alkyl chain of the cation causes its hydrophobicity to match the hydrophobicity of the alcohol, thereby resulting in an increase in the maximum solubility temperature T^*_{LLE} with the hydrophobicity of the alkyl-chain. In other words, the longer the alkyl-chain length in the cation, the higher is the value of the T^*_{LLE} of the IL−alcohol mixture and lower is its mutual solubility in the alcohol.

Effect of anion. The mutual solubility of [$C_n$mim][NTf_2] is higher than that of [$C_n$mim][BF_4] in an alcohol. Here examples are the cations: [C_6mim]$^+$ and [C_8mim]$^+$, and the solvents are: 1-hexanol and 1-octanol. In 1-octanol the value of the maximum mutual-solubility temperature difference for [C_6mim][BF_4] is higher than that of [C_6mim][NTf_2] by 12.4 K and its value for [C_8mim][BF_4] is higher than that of [C_8mim][NTf_2] by 6.2 K. Similar trends have been observed for [C_4mim]$^+$- and [$C_n$mpy]$^+$-type cations in different alcohols (Crosthwaite et al., 2004, 2005, 2006). It was reported (Crosthwaite et al., 2004) that the mutual solubility of [C_4mim]$^+$- based ILs containing [NTf_2]$^-$, [BF_4]$^-$ and [PF_6]$^-$ with 1-butanol decreases in the sequence: [NTf_2]$^-$ > [BF_4]$^-$ > [PF_6]$^-$. [C_4mim][TfO] is miscible with alcohols (1-$C_nH_{2n+1}OH$, n = 2, 4, 6, and 8) at room temperature, and a phase split occurs with 1-dodecanol, but [C_4mim][DCA] is completely miscible with all the investigated alcohols. This suggests that the mutual solubility of imidazolium-based ionic liquids with alcohols follows the order: [DCA]$^-$ > [TfO]$^-$ > [NTf_2]$^-$ > [BF_4]$^-$ > [PF_6]$^-$. This decreasing mutual solubility of these ILs in alcohols implies that the value of their T^*_{LLE} follows an opposite order, i.e. [DCA]$^-$ < [TfO]$^-$ < [NTf_2]$^-$ < [BF_4]$^-$ < [PF_6]$^-$. The increase in the value of the temperature T^*_{LLE} of these ILs in an alcohol indicates that coulombian interactions between the cations and anions of the IL become increasingly strong with decreasing cation size, which in its turn results in a increasingly weak hydrogen bonding between the anion and the alcohol molecules. This means that increasing hydrogen bonding between the anion and the alcohol increases the mutual solubility of IL–alcohol mixtures.

Effect of addition of methyl group. The addition of a methyl group to [C_6min][NTf_2] increases the solubility of the IL in 1-hexanol, with small increase in the temperature T^*_{LLE}. However, beyond T^*_{LLE} the variation in T_{LLE} with an increase in the IL composition x_2 is much pronounced with the addition of the methyl group. In contrast to the [C_6min][NTf_2] in 1-hexanol, the behavior of [C_6py][NTf_2] and its counterparts, with one and two methyl groups, in 1-hexanol is somewhat different (Crosthwaite et al., 2006). In this case, the addition of a methyl group slightly decreases the solubility and increases the T^*_{LLE}. As in the case of [C_6min][NTf_2] and its higher counterpart, for these pyridinium-based ILs the variation in T_{LLE} beyond T^*_{LLE} with x_2 is much pronounced with the addition of the methyl group and the trends of the $T_{\mathrm{LLE}}(x_2)$ curves intersect at a particular value of x_2 such that the solubility of the alcohol in the IL increases with increasing number of methyl groups of the cation. The solubility of the ILs below their crossover composition x_2 in a solvent in these systems has an opposite behavior.

Apart from the effects of the factors described above, factors like substitution of an ethyl chain on the carbon atom as in [C_6C_1mpy]$^+$ and [C_6C_2mpy]$^+$ cations and different types of cations such as [C_4mpy]$^+$ and [C_4mim]$^+$ cations with the same anion also have strong effect on the $T_{\mathrm{LLE}}(x_2)$ behavior of ILs in an alcohol, and show crossover at some value of x_2 (Crosthwaite et al., 2006). A common feature of these ILs is that they are quite soluble in most alcohols and show a maximum solubility temperature T^*_{LLE}. However, they are poorly soluble in aliphatic hydrocarbons, aromatic compounds and water, and have broad solubility gaps with no directly determined T^*_{LLE} for the mixture (Freire et al., 2007a; Heintz, 2005). Since different types of interactions occur between the solvent molecules and the cations and anions of an IL, the liquid–liquid phase behavior of ILs with different solvents is determined by the relative strengths of cation–anion, cation–solvent, anion–solvent, and solvent–solvent interactions.

The simplest model to explain the liquid–liquid phase behavior of a binary mixture of an IL and a solvent is the nonrandom two-liquid (NRTL) model used by Crosthwaite et al. (2006). This model is based on the postulate that IL molecules behave as unassociated species mixed with solvent molecules in the mixture and that there are two parameters Δg_{12} and Δg_{21} related to the interaction strength between the solvent and IL molecules and between the IL and solvent molecules, respectively. These authors found that a linear temperature dependence of these interaction parameters in the NRTL equation satisfactorily describes the experimental data of the liquid–liquid phase behavior of pyridinium- and imidazolium-based ILs in alcohols. However, this model cannot be applied to predict or correlate liquid mixture behavior.

Traditional approaches for correlating or predicting the properties of liquid mixtures, such as EoS (equation of state) and GCMs (group contribution methods) like UNIFAC, are not useful for this purpose because they require a large collection of experimental data before their application (Marsh et al., 2004; Freire et al., 2007a). A major requirement in the field of ILs is to use a predictive method that can scan the possible combinations of ILs and their mixtures prior to making extensive experimental measurements. COSMO-RS (COnductor like Screening MOdel for Real Solutions) is a unique method used for predicting the thermodynamic properties of mixtures on the basis of unimolecular quantum chemical calculations for individual molecules (Klamt and Eckert, 2000). COSMO-RS model has been applied to the description of the LLE of mixtures of ILs with different molecular solvents (Domańska et al., 2006a; Freire et al., 2007a,b).

1.3. Structure of solvents

Different properties of solvents and solutions are associated with the structure of particles (i.e. atoms, molecules or ions) composing them and may broadly be grouped into three categories: (a) static properties, (b) transport properties, and (c) thermal properties. Density, refractive index, dielectric constant, and surface tension are essentially static properties and are connected with the statistical distribution of particles composing a liquid. Viscosity and electrical conductivity belong to transport properties and are associated with the motion of particles in the bulk liquid. In contrast to the viscosity of a liquid which is determined by the relative motion of all particles in the liquid, electrical conductivity is associated with the transport of charged particles. Thermal conductivity, thermal expansivity, freezing and evaporation of liquids fall in the category of thermal properties and are determined by the thermal motion of particles composing them. In fact, it is the structure of particles which ultimately interact with each other and decide their arrangement and instantaneous distribution in the liquid state and determine the properties of liquids.

Basic ideas of the structure of solvents are briefly described in this section. Processes involved in the formation of solutions and the structure of solutions are described in Sections 1.4 and 1.5.

1.3.1. Water and other common solvents

It was mentioned in Section 1.1.2 that a water molecule has a pair of free orbitals for the lone pair of electrons on the oxygen atom. This pair of two free orbitals on the oxygen atom gives an interesting feature to the structure of water. An individual water molecule is nonlinear with the H—O—H angle of about 104.5° and the distribution of the four pairs of electrons of the six electrons from oxygen and the two electrons from hydrogen atoms is in four approximately equivalent directions. However, although a water molecule is neutral electrically, it behaves as an electric dipole because the centers of its negative and positive charges do not coincide. From the viewpoint of charge distribution, a water molecule can equally be represented as an assembly of four charges (quadrupole) of equal magnitude q, a charge of $+q$ near each hydrogen atom and two charges each of value $-q$ near the oxygen atom.

The property of two free orbitals on the oxygen atoms of water molecules gives an open structure to ice lattice by forming electrostic bonds, known as hydrogen bonds, with hydrogen atoms of other water molecules such that each oxygen atom is tetrahedrally surrounded by four other oxygen atoms (Bockris and Reddy, 1970; Luck, 1974). The ice lattice consists of oxygen atoms lying in layers with each layer forming a network structure of open hexagonal rings composed of associated water molecules (see Figure 1.11). In between two oxygen atoms is a hydrogen atom which provides the hydrogen bonding. The distance between an oxygen atom and its own hydrogen atom is 0.096-0.102 nm whereas the distance between a hydrogen atom and an oxygen atom entering into a hydrogen bond is 0.174-0.180 nm. Thus, the network structure of associated water molecules contains interstitial regions between the tetrahedra, which are larger than the dimensions of a water molecule.

With an increase in temperature of the network water, a molecule breaks its hydrogen bonds with the network and can enter interstitial regions as a free unassociated water molecule without disturbing the network structure. Thus, in liquid water there are networks of associated water molecules as well as certain fraction of free, unassociated water molecules. With increasing temperature more free, unassociated water molecules are broken from the associated network structure such that the fraction of unassociated water molecules increases at the expense of associated water molecules of the network structure.

X-ray absorption (XAS) and x-ray Raman scattering (XRS) spectroscopies indicate that, in water, there is a considerable degree of short-range order characteristic of the tetrahedral hydrogen bonding in ice. The liquid water partly retains the tetrahedral bonding and the resulting network structure of crystalline structure of ice. Therefore, in liquid water, in addition to the associated water molecules in the network structure, there can be a certain fraction of structurally free, unassociated water molecules in interstitial regions of the network. A water molecule may break its hydrogen bonds with the network and subsequently move into the interstitial region, while another free unassociated water molecule may join the network. Thus, there exists a dynamic equilibrium between the free unassociated water molecules joining the water network structure and the associated water molecules leaving the network structure. This implies that clusters of water molecules cooperate to form networks and, simultaneously, the networks break down.

A measure of associated structure, or structuredness, of water is the average number of hydrogen bonds per water molecule present in the liquid (for the literature, see: Marcus, 2009). X-ray Raman absorption and scattering studies and computer calculations reveal the presence of strong and weak hydrogen bonds characterized by short and large O····H bond distances (less than 0.21 nm and up to 0.23 nm), respectively. The number of hydrogen bonds per water molecule at ambient conditions, estimated by different methods, lies between 3.1 and 3.6. Since two molecules are involved in each hydrogen bond, there are about 1.7 hydrogen bonds per water molecule at ambient conditions. Since the extent of hydrogen bonding persists even at high temperatures of the liquid water, its structuredness exists under these conditions

Apart from water, there are several liquids which are used in diverse applications.

A large many of them are molecular organic solvents such as alcohols. Relatively less is known about the structure of these liquids. Since the structures of molecules of various liquids are usually known, the general concepts similar to those for the structure of simple solvents like water are equally useful in understanding the structure and properties of these other molecular solvents (see also Section 1.1.5). However, different geometrical configurations of the molecules of the liquids imply that they indeed associate in the liquid state. The properties of liquid water, for example, are explained on the postulate that there exist structural entities in the form of clusters or of locally-ordered structures.

Investigation of interaction of alcohols with water molecules by various spectroscopic techniques and molecular dynamic simulation has drawn considerable interest in view of wide use of aqueous alcohol solutions in diverse industries (for example, see: Gong et al., 2016, and the literature cited therein). The main emphasis in these studies has been placed on understanding the interaction of hydroxyl and hydrocarbon groups with the solvent water and the functioning of water hydrogen-bond network. The results showed the following features (Gong et al., 2016):

(1) Mixing of alcohol with water leads to the softening of both O–H bond and O····H nonbond of water hydrogen-bond network through hydrogen-bond cooperative relaxation and associated charge polarization.
(2) Each of the dangling alcohol OH^- group (interacting with $\ddot{O}$: or $-H^+$) and $C-H^+$ group (interacting with $-H^+$ or $\ddot{O}$:) is equally capable of interacting with H_2O molecule in the form of $\ddot{O}{:}\leftrightarrow{:}\ddot{O}$ point compressor, $H^+\leftrightarrow H^+$ point breaker, and O····H–O hydrogen bond at the alcohol–water interface without charge sharing or new bond formation.
(3) The alcohol–water O····H–O bond formation leads to the solubility and hydrophilicity of the alcohol, the $H^+\leftrightarrow H^+$ breaker weakens the hydrogen network, and $\ddot{O}{:}\leftrightarrow{:}\ddot{O}$ compression shortens (strenghens) the O····H nonbond and lengthens (softens) the H–O bond.
(4) The H–O softening is associated with heat emission and depression of solution melting temperature whereas the O····H nonbond softening due to charge polarization lowers the critical frezing temperature.

In order to illustrate the relationship between the structure of liquids and their properties, we consider here the temperature dependence of the molar volume V_M (a static property) and the dynamic viscosity η (a flow property) of the following three simple molecular solvents: water, methanol and ethanol. The molar volume V_M of a liquid at given temperature and pressure conditions is defined as the ratio of the molar mass M of the liquid to its density d (i.e. $V_M = M/d$). It is related to the packing of the molecules of one mole of a solvent in its volume V and represents the average volume occupied per molecule, which comprises the volume of a molecule and free space around it. The volume V of a solvent under a given pressure p usually increases with temperature. Therefore, the average free volume per molecule of the liquid increases with temperature, and the temperature dependence of V_M of the liquid is a measure of this increase in the average free volume per molecule with increasing temperature. In contrast to this, the temperature dependence of the dynamic viscosity η of a liquid is related to the nature of kinetic entities, such as their dimensions, participating in their movement in the liquid. These kinetic entities participating in viscous flow may differ substantially from the molecules present in the liquid volume.

The dependence of the density d of solvents on their temperature T is usually observed to follow the second-order dependence (see Chapter 3). Therefore, one expects that the experimental data of the temperature dependence of the molar volume V_M of liquids can also be described by a similar second-order relation

$$V_M = V_M^0 + a_1(T - T_0) + a_2(T - T_0)^2 , \tag{1.36}$$

where V_M^0, a_1 and a_2 are empirical parameters, T is taken in K and T_0 = 273.15 K. Figure 1.24 shows the plots of V_M of the above three liquids as a function of T, with the values of the best-fit parameters listed in Table 1.6.

The parameters of the second-order relation contain information on the thermal expansivity of the liquids, which is associated with the thermal vibration of molecules in the liquid volume. However, to obtain an idea of the process of creation of empty space in the liquid volume with its temperature, following the concept of generation of

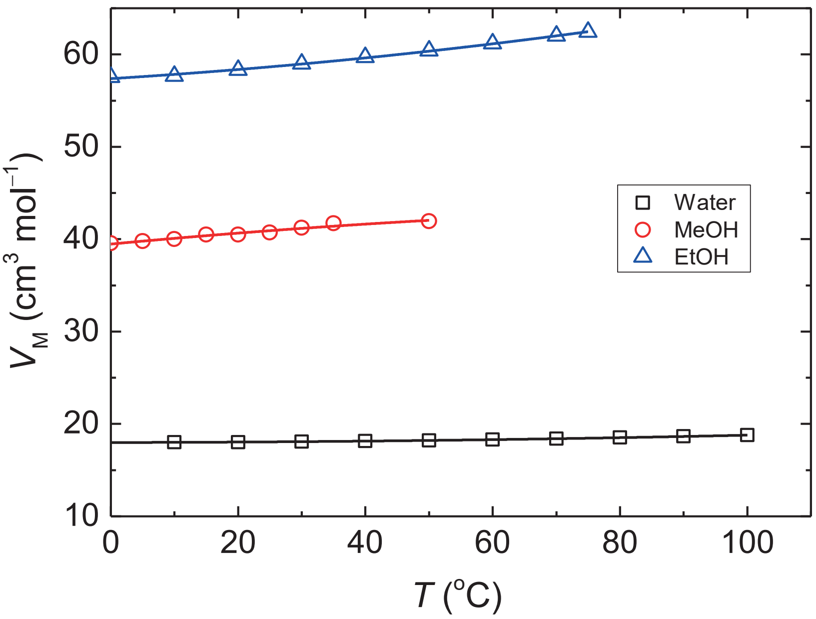

Figure 1.24. Dependence of molar volume V_M on temperature T of water, methanol and ethanol according to Eq. (1.36). Best-fit constants of the plots are given in Table 1.6. Sources of density data for water from Lide (1996/1997), for methanol from (open circles) www.EngineeringToolBox.com and (filled circles) www.ddbst.com/en, and for ethanol from (open triangles) www.ddbst.com/en and (filled triangles) www.celcius.process.com. Data accessed 12 January 2017.

Table 1.6. Values of constants of Eqs. (1.36) and (1.37)

Solvent	Eq. (1.36)				Eq. (1.37)		
	V_M^0 (cm^3·mol^{-1})	$10^2 a_1$ (cm^3··mol^{-1}K^{-1})	$10^4 a_2$ (cm^3·mol^{-1}·K^{-2})	R^2	$\Delta S_{th}/R_G$ (–)	ΔH_V (kJ·mol^{-1})	R^2
Water	17.993 (17.82)	0.098	0.697	0.9993	2.2633	16.3	0.9952
Methanol	39.473 (37.80)	6.445	−2.616	0.9489	2.4432	12.5	0.9476
					(3.2223)	(14.4)	(0.9719)
Ethanol	57.379 (55.95)	4.273	3.349	0.9969	2.9098	14.9	0.9905

vacancies in a crystal composed of similar atoms (for example, in metals), the change ΔV_M in the total molar volume V_M of the liquid may be given by an Arrhenius-type relation (for example, see: Dekker, 1964)

$$\frac{\Delta V_M}{V_M} = \left(1-\frac{V_M^0}{V_M}\right) = \left(\frac{\Delta V_M}{V_M}\right)^0 \exp\left(-\frac{\Delta H_V}{R_G T}\right), \qquad (1.37)$$

where ΔV_M is the contribution of vacancies to the total molar volume V_M of the liquid at temperature T from an initial reference volume V_M^0, ΔH_V is the energy required for the creation of a vacancy in the liquid, and the preexponentional term $(\Delta V_M/V_M)^0$ is related to the increase in the thermal entropy per vacancy by an amount ΔS_{th} such that $(\Delta V_M/V_M)^0 = \exp(\Delta S_{th}/R_G) \geq 1$. Since $V_M = V_M^0 + \Delta V_M$, the fraction of free volume due to vacancies in the reference volume V_M^0 is $(1-V_M^0/V_M)$.

Figure 1.25 shows the experimental $V_M(T)$ data of Figure 1.24 in the form of plots of $\ln(1-V_M^0/V_M)$ against T^{-1} according to Eq. (1.37), with the estimated values of $\ln(\Delta V_M/V_M)^0 = \Delta S_{th}/R_G$ and the activation energy ΔH_V included in Table 1.6. The dashed curve represents the best fit of the data for methanol excluding the point at 50° C (i.e. for $T^{-1} = 3.0945 \cdot 10^{-3}$ K^{-1}), with the estimated parameters given in the paretheses. The chosen values of V_M^0 for the three liquids are given in the parentheses in the second column of the table. These values are lower by about 1.0, 4.5 and 2.5% for water, methanol and ethanol, respectively, than their corresponding extrapolated values of V_M^0 at $T_0 = 273.15$ K. Note that these chosen values of V_M^0 for these liquids are different from their van der Waals molar volumes V_M^{vdW} and the intrinsic molar volumes V_M^{in}. For example, for water $V_M^{vdW} = 12.4$ cm^3·mol^{-1} and $V_M^{in} = 16.7$ cm^3·mol^{-1} (cf. Marcus, 2009).

If the data for methanol are considered in the wider temperature interval up to 50 °C, from Table 1.6 it may be seen that the value of the thermal entropy ΔS_{th} increases with the reference molar volume V_M^0 of the three liquids, but the values of their activation energy ΔH_V are comparable and are of the order of the hydrogen bond energy. The former observation is associated with the arrangement of molecules in the liquid, whereas the latter observation is related to the interactions between their molecules.

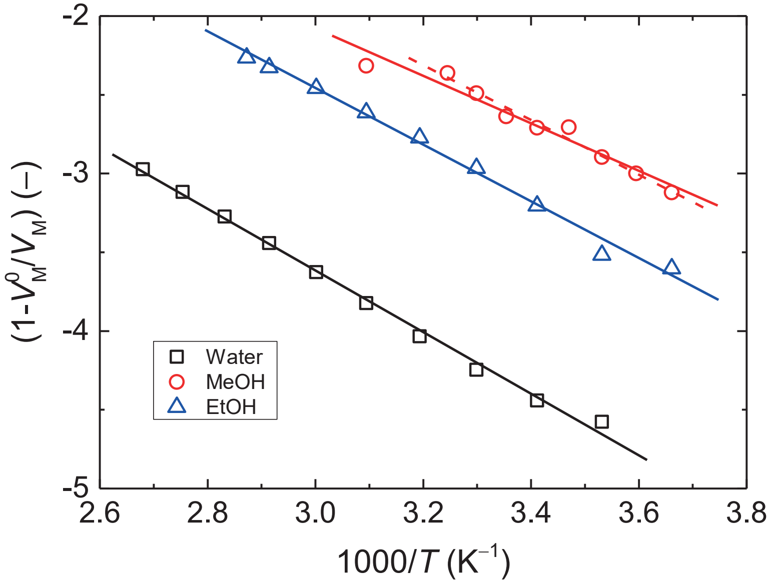

Figure 1.25. Plots of the above $V_M(T)$ data plotted as $\ln(1-V_M^0/V_M)$ against T^{-1} for water, methanol and ethanol according to Eq. (1.37). Solid curves represent the data in the entire temperature interval of the data. Dashed curve represents the best fit of the data for methanol without the point at 50° C (i.e. for $T^{-1} = 3.0945 \cdot 10^{-3}$ K^{-1}). Best-fit constants of the plots are given in Table 1.6. Estimated parameters for methanol in the narrow temperature interval are given in parentheses in the third row.

The temperature dependence of the viscosity η of the above solvents may be represented by Arrhenius-type relation (1.29) (Stokes and Mills, 1965; Bockris and Reddy, 1970; see also Chapter 5). Eq. (1.29) is derived using the hole theory of liquids (Bockris and Reddy, 1970). Eyring's transition state theory also gives a similar temperature dependence of the viscosity η of solvents, written in the form (Stokes and Mills, 1965; Horvath, 1985)

$$\eta = \frac{h_P N_A}{V_M^0} \exp\left(\frac{\Delta G^0}{R_G T}\right), \tag{1.38}$$

where V_M^0 is the molar volume of the solvent, h_P is the Planck constant, and ΔG^0 is the free activation energy for viscous flow of the solvent, given as

$$\Delta G^0 = \Delta H^0 - T\Delta S^0, \tag{1.39}$$

where ΔH^0 and ΔS^0 are the heat and the entropy of activation, respectively. For constant values of ΔS^0 and V_M^0, Eq. (1.38) reduces to Eq. (1.29) with $\Delta H^0 = E_\eta$ and $h_P N_A / V_M^0 \exp(-\Delta S^0/R_G) = \eta_0$. The main feature of Eq. (1.38) is that it provides a physical interpretation of the preexponential factor η_0 and the activation energy E_η.

According to Eq. (1.29) the dependence of $\ln\eta$ against $1/T$ gives a linear plot with intercept $\ln\eta_0$ and slope E_η/R_G. Figure 1.26 shows plots of $\ln\eta$ against $1/T$ for water, methanol and ethanol, with the corresponding intercepts $\ln\eta_0$ and slopes E_η/R_G, and the activation energy E_η and the constant E_η/R_GT_m calculated therefrom given in Table 1.7.

Two features may be noted from Table 1.7. First, the value of the activation energy E_η for viscous flow is the highest for water, the lowest for methanol and intermediate between these two values for ethanol. The difference in the values of E_η is due to the processes of creation of holes necessary for their subsequent motion in these solvents and are associated with the nature of chemical bonds in their structures. Second, the ratio E_η/R_GT_m is much higher than the expected value of 3.7 from the hole theory of liquids. The high values of E_η/R_GT_m are indicators of strong association of the molecules in these liquids. In fact, it is well known that liquid water is an associated liquid.

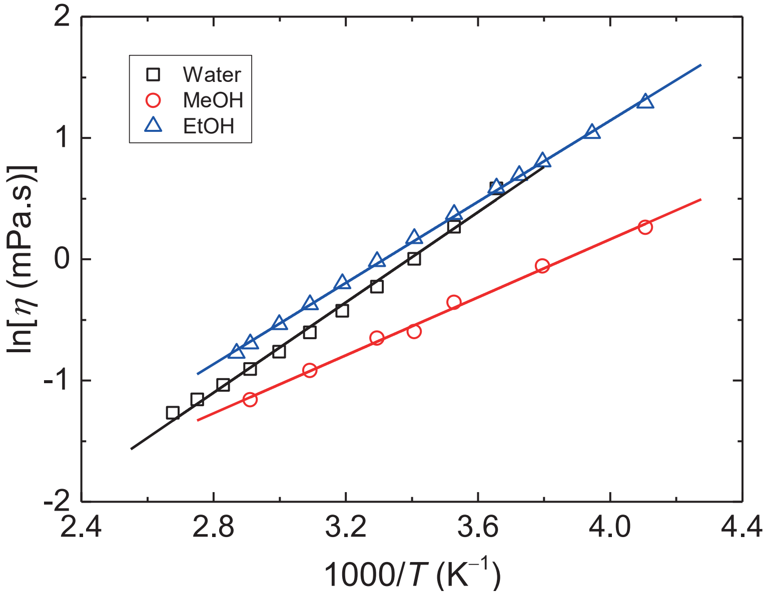

Figure 1.26. Dependence of $\ln\eta$ on T^{-1} for water, methanol and ethanol according to Eq. (1.29). Best-fit constants of the plots are given in Table 1.7. Sources of data: for water from Lide (1996/1997), for methanol from www.EngineeringToolBox.com and www.ddbst.com/en, and for ethanol from www.ddbst.com/en and www.celcius.process.com. Data for methanol and ethanol accessed 12 January 2017.

Table 1.7. Values of constants of Eq. (1.29)

Solvent	T_m (K)	$-\ln\eta_0$	$10^3E_\eta/R_G$ (K^{-1})	$10^{-3}\eta_0$ (mPa·s)	E_η (kJ·mol^{-1})	E_η/R_GT_m (–)
Water	273.15	6.3108	1.86078	1.817	15.45	6.81
Methanol	175.55	4.6206	1.19616	9.847	9.95	6.81
Ethanol	159.05	5.5499	1.67339	3.888	13.91	10.52

1.3.2. Ionic liquids

The properties of various materials depend on the structure of their molecules in different phases. Therefore, structural features of ILs concerning different types of interactions between cations and anions composing them have been extensively investigated using various approaches (for example, see: Dong et al., 2014; Matsumoto and Hagiwara, 2007; Shukla et al., 2011; Reichert et al., 2007).

X-ray scattering studies have been used to examine the structure of solid-state pyrrolidinium- and imidazolium-based ILs composed of cations of varying the alkyl-chain length and different anions (Dong et al., 2014; Matsumoto and Hagiwara, 2007; Reichert et al., 2007). These studies show that anions contact with the cation via H-bonds in the crystal structure but the alkyl-chain length has a strong effect on the packing of ions. However, the direct interaction between the delocalized positive charge on the cation and the anion is responsible for the dominant coulombian interaction between these ions than the C–H···· H-bonded cation–anion interaction. These H-bonds involved in the interactions of many ions in a bulk IL can be viewed to form a three-dimensional network as in liquid water. The network can be observed on a smaller nanometer scale or in an ion cluster in which nonhomogeneity of the local structure is found in ILs. Crystallographic studies indeed reveal that the H-bonded networks exist below melting points or at glass transition temperatures in many ILs (Matsumoto and Hagiwara, 2007; Reichert et al., 2007).

It is difficult to apply conventional techniques like single-crystal x-ray diffraction for the structural investigation of ILs in the liquid state at room temperature. Density Functional Theory (DFT), which is a quantum mechanical theory used to investigate the electronic structure of a molecule, is a versatile method for predicting the molecular structure and interactions present in a given molecule (Shukla et al., 2011). Vibrational spectroscopic techniques (infrared, Raman and NMR) have extensively been employed to analyze the existence and strength of H-bondings present in the liquid-phase of the common ILs (Dong et al., 2014; Giernoth, 2009; Matsumoto and Hagiwara, 2007). These studies have revealed that the modes of interaction in the liquid phase are almost identical with those encountered in the crystal structures of the ILs. Investigations of a variety of imidazolium salts containing weakly coordinated anions like $[BF_4]^-$ and $[PF_6]^-$ have demonstrated that each cation is surrounded by three anions (and vice versa), resulting in the formation of hydrogen-bonded ordered supermolecules in the liquid phase. Other evidences of the existence of associated structures in the ILs come from studies of their diffusion coefficients (Giernoth, 2009).

1.4. Models of liquid structure

In order to understand different properties of solvents, following the models for molten liquid electrolytes discussed by Bockris and Reddy (1970), different models may be considered. Since a liquid can be obtained either by melting its crystalline solid or by cooling its vapor, there are two ways of looking at the models of liquids.

Thus, there are *lattice-based* and *gas-based models* for a liquid. The main observation which a model should explain is an increase in the volume upon melting and roughly the same distance between the molecules in the crystalline and liquid phases. The volume increase with minor changes in the mean distance between the neighboring molecules suggests that melting of the crystalline solid introduces empty space into the liquid. It is the mode of description of this empty space that differentiates one model from another.

The simplest model of a liquid is based on the concept of injection of vacancies known as Schottky defects in a crystalline lattice. Vacancies are produced in the lattice by removal of atoms/molecules from lattice sites in the interior to the crystal surface (Figure 1.27a). Vacancies are produced randomly inside the crystal with simultaneous volume increase through displacement of removed atoms/molecules from lattice sites to the crystal surface. As the temperature of the solid is increased, the number of vacancies increases as a result of thermal motion of atoms/molecules of lattice sites and at the melting point they are so numerous in the lattice that the long-range order disappears. The vacancies are roughly of the size of displaced atoms/molecules. Since vacancies are produced at lattice sites, one refers to the *quasi-lattice model*.

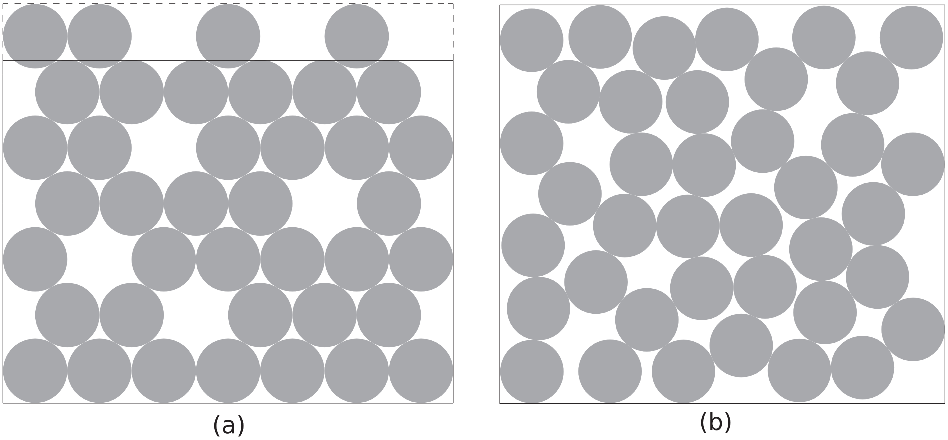

Figure 1.27. Schematic illustration of: (a) vacancies produced in crystal lattice, and (b) randomly located holes in a liquid.

When numerous vacancies are introduced in the crystalline lattice, the definition of crystalline lattice as a three-dimensional array of points no longer holds. Now atoms/molecules and vacancies of the molten system may be considered to be distributed randomly. In other words, the vacancies form empty regions, called *holes*, of various sizes, and atoms/molecules and differently-sized empty spaces are randomly close-packed in the liquid volume (Figure 1.27b). This is the so-called *hole* model. The process of formation of holes is somewhat similar to the formation of vacancies in the crystal lattice and is associated with the thermal motion of atoms/molecules constituting their clusters. However, in contrast to the creation of vacancies by removal of atom/molecule from far away sites in the interior of the lattice to the crystal surface, ions of clusters are displaced relative to each other by amounts similar to their displacement. Since thermal motion is random and occurs everywhere in the liquid volume, holes are also produced randomly in the liquid. However, holes continuously appear and disappear, move, coalesce to form large holes, and disintegrate into smaller holes.

When a gas transforms to the liquid state, the freedom of motion of its atoms/molecules is restricted such that the motion of each of its atoms/molecules is confined within its cell of identical volumes (Figure 1.28). This is the basis of the *simple cell theory*. Every atom/molecule has a free volume available for its motion. If V is the volume of the liquid containing N atoms/particles and V_0 is the volume of these atom/molecule considered as rigid spheres, the free volume v_f available to each atom/particle for its motion is

$$v_\mathrm{f} = \frac{V}{N} - v_0\,, \tag{1.40}$$

where V/N is the average volume available to each atom/particle, and $v_0 = V_0/N$ is the volume of each rigid spherical atom/molecule.

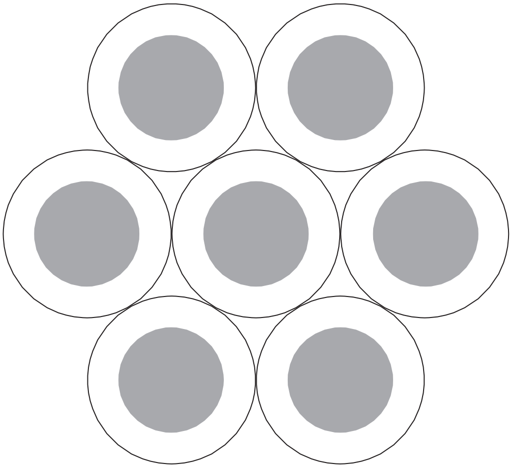

Figure 1.28. Free volume available for the motion of its atoms/molecules in a liquid.

The restriction in the motion of atoms/molecules to their cells does not explain transport properties of liquid, entropy of fusion, and volume expansion on melting. These difficulties are overcome in the *liquid free-volume theory*. According to this theory, the liquid free volume is not distributed equally to each atom/molecule but there is a statistical distribution of free volumes among them and thermal forces are responsible for the statistical distribution of these free volumes.

The movement of an atom/molecule from one position to another in the liquid not only results in the expansion of the cell of the moving atom/molecule and an increase in its energy, but leads to the contraction of the neighboring cell and a decrease in its energy. This explains the transport properties of liquids. An increase in the volume that occurs on melting implies an increase in the free volume. This means that, except for the free space in the liquid, the atoms/molecules have the same inter-neighbor distance.

The hole model explains most of the experimental observations. Some of the characteristics and predictions of this model are briefly described below.

The formation of holes in the liquid as a result of thermal fluctuations is due to an increase in the vibrations of the liquid molecules around their temporary equilibrium positions. According to the hole theory, the average hole radius r_h is given by (Bockris and Reddy, 1970)

$$r_\mathrm{h} = 0.51(k_\mathrm{B}T/\gamma)^{1/2}, \tag{1.41}$$

where k_B is the Boltzmann constant and γ is the surface tension of the melt. With the values of macroscopic surface tensions γ of different molten salts in Eq. (1.41), estimates of the values of r_h show that a typical hole is roughly of the size of an ion.

The dependence of self-diffusion coefficient D and viscosity η of simple liquid electrolytes on temperature T follows Arrhenius-type relation with activation energy E_D for diffusion and activation energy E_η for viscous flow, respectively, related to the melting point T_m by Eq. (1.26). This relation implies a relationship between the phenomena of diffusion and viscosity in liquids and is associated with the validity of the Stokes-Einstein relation

$$D = \frac{k_B T}{6\pi r \eta}, \tag{1.42}$$

where r is the radius of moving particles.

Among the different models of liquids, the hole model is found to be the most consistent model. In the case of ionic liquids, it satisfactorily explains the meaning of activation energy E_η for viscous flow as the work done in transferring a mole of particles from the surroundings of a hole into its interior, experimental compressibilities β and expansion coefficients α_V. It should be mentioned that relation (1.26) holds for nonassociated liquids in which transport processes, such as viscous flow, are determined by the enthalpy of hole formation. However, in associated liquids, such as water, with network structures, the transport process is determined by the energy required to rupture the bonds of the network.

1.5. Electrolyte and nonelectrolyte solutions

A solution is obtained by adding a solute to an appropriate solvent at a given temperature and pressure conditions. The solute may be made up of ions or molecules. The former type of solutes are known as ionic solutes, which are composed of charged atoms or groups of atoms with negative or positive charges. The latter type of solutes are molecular solutes composed uncharged neutral molecules which may be polar, nonpolar or apolar. The main requirement for the dissolution of a solute in a solvent is that the solute ions or molecules interact with the solvent molecules to liberate enough energy to break down the solvent structure.

Water is the most common solvent and dissolves different types of substances. It easily dissolves ionic salts like alkali halides, but there are many molecular substances that do not dissolve or poorly dissolve in water. Ionic salts are dissolved in water because polar water molecules attract the salt ions. However, the dissolution behavior of molecular solutes in water is determined by the extent of polarity of solute molecules. For example, sugars such as sucrose, $C_{12}H_{22}O_{11}$, dissolve in water mainly due to the attraction between negative and positive areas on O–H groups of polar sugar molecules and the polar H_2O molecules. The polar character of a sugar molecule is associated with a slight negative charge on the oxygen atom and a slight positive charge on the hydrogen atom of the O–H bonds in the sugars. This explains why polar solvents dissolve polar molecular solutes.

Ionic solutes dissolved in water or dismantled on melting show conduction of electrical current through the migration of the ions present in the solution. Such ionic solutes and their solutions are known as *electrolytes* and *electrolyte solutions*, respectively. In contrast to these ionic solutes, there is a large number of organic substances dissolved in pure water which show little conduction. Such solutes are composed of separate, neutral molecules and the bonding of atoms inside the neutral molecules is essentially nonionic. These solutes and their solutions are known as *nonelectrolytes* and *nonelectrolyte solutions*, respectively.

The above comparative behavior of electrical conduction of solutions is based on water alone used as a solvent. However, when a nonaqueous solvent is chosen to prepare the solution of an electrolyte, the conduction in the solution is reduced tremendously due to the suppressed solvation of its ions by the solvent molecules.

1.5.1. The solvation process

It is well known that ionic crystals, such as an NaCl or a KCl crystal, placed in solvent water dissolve in it. This process of dissolution of the ionic crystal is associated with the dismantling of the cation–anion bonds in the solid by solvent water such that the solute molecules in contact with the ionic solid enable the ions to move into the solvent resulting in an ionic solution. The solution is composed of solvated cations and anions separated by solvent molecules. The behavior of solvated ions in the solution is related to ion–solvent interactions.

When an ion is placed inside a solvent water, the spherically symmetrical electrical field of the ion is capable of tearing water dipoles out of the water structure by disrupting hydrogen bond between water molecules and orienting them with the appropriate charged end towards the central ion. These ion–dipole forces are the basis of ion–solvent interactions. Due to these interactions, some of the water molecules are trapped and oriented in the ionic field. The immobile water molecules in the immediate vicinity of an ion form its *primary solvation shell* or *sheath.* An ion also affects the solvent molecules outside the *primary solvation shell* in the immediate vicinity of the ion and are bonded with the firmly-trapped solvent molecules of the *primary solvation shell* by weak van der Waals forces. These molecules form a *secondary solvation shell*. Therefore, an ion in an infinitely dilute solution may be considered to be surrounded by a solvation cloud made up of primary and secondary solvation shells, as illustrated schematically in Figure 1.29a.

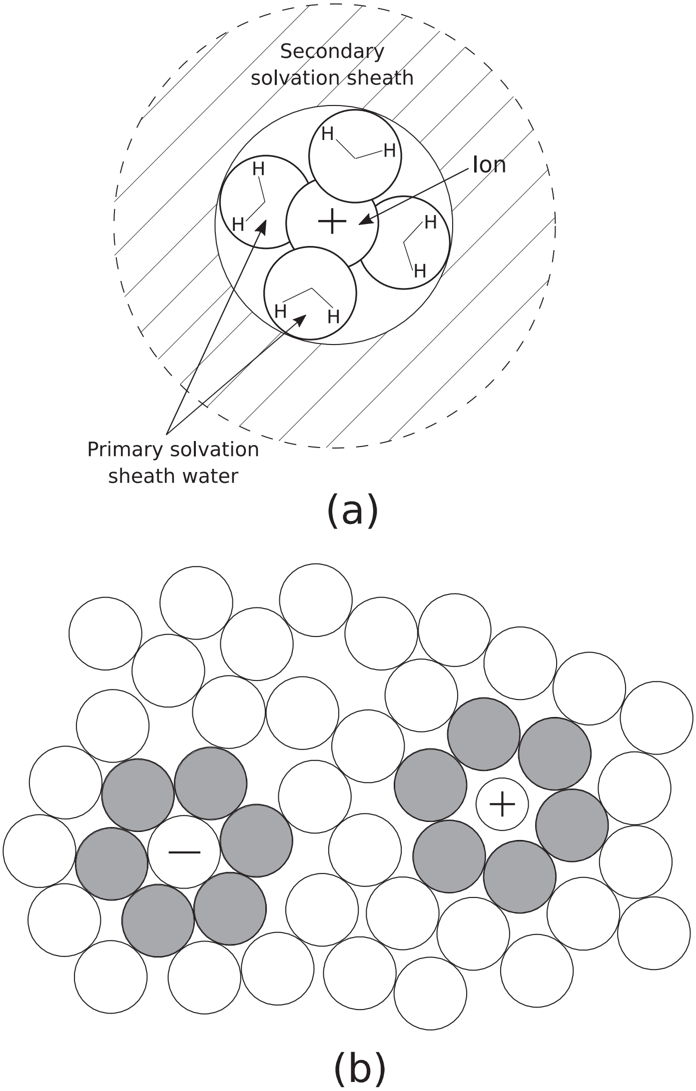

Figure 1.29. (a) Schematic illustration of primary and secondary regions of solvation of a monovalent cation. (b) Free water and immobile hydration water in primary solvation sheaths of ions shown as open and dark circles, respectively. Schematic (a) is based on an illustration in Bockris and Reddy (1970).

The question arises: why an ion is solvated in a solvent, and how the primary and secondary solvation shells look like. The process of solvation is described below, whereas the structure of solvation shells is discussed in the next section.

The process of solvation of ions in a solvent S is usually described by the Born model for ion–solvent interactions. In this model it is assumed that: (i) one molecule of a solute dissociates into ions I considered rigid spheres of radius r_i and charge z_iq, where q is the elementary charge and z_i is the valency of the ion i, (ii) the solvent is a continuum of dielectric constant ε_s, and (iii) the interactions between the solvent and the ions are entirely electrostatic. Then the free energy $\Delta G_\mathrm{I-S}$ of ion–solvent interactions per mole of ions is given by (Bockris and Reddy, 1970)

$$\Delta G_\mathrm{I-S} = -N_\mathrm{A} k_0 \frac{(z_i q)^2}{2r_\mathrm{i}}\left(1-\frac{1}{\varepsilon_\mathrm{s}}\right), \tag{1.43}$$

where the Avogadro number $N_\mathrm{A} = 6\cdot10^{23}$ ions per mole and the coulombian proportionality constant $k_0 = 9\cdot10^9$ Nm^{2}C^{-2}. Since $1 >> 1/\varepsilon_\mathrm{s}$ (for example, $\varepsilon_\mathrm{s} = 80$ for water), $\Delta G_\mathrm{I-S}$ is negative, which means that the ions are more stable in the solvent than in the vacuum and the solute is soluble in the solvent of a high dielectric constant. However, when the solvent is replaced by another solvent A of dielectric constant ε_a such that $\varepsilon_\mathrm{a} < \varepsilon_\mathrm{s}$, the corresponding free energy $|\Delta G_\mathrm{I-A}| < |\Delta G_\mathrm{I-S}|$, the ions become relatively less stable and the solute is less soluble in this solvent. Obviously, solute ions more stable in solvent S are more solvated than in solvent A.

In solutions containing small solute concentrations, dissociated ions acquire a particular time-average spatial distribution in the solution volume where the distance between the solvated ions is large and ion–ion interactions are insignificant. When the solute concentration is increased, the average distance between the ions decreases and ion–ion interaction become increasingly important. When the solute concentration is increased further, the water molecules bound to the solvated ions are not effective in dissolving ions further (Figure 1.29b). Then oppositely-charged ions come close to form neutral associated ion pairs. However, since the coulombian attractive forces $z_+z_-q^2/\varepsilon_\mathrm{s}r^2$ increase with decreasing dielectric constant ε_s of the solvent, for nonaqueous solvents of low dielectric constant ion-pair formation is favored. When the coulombian attractive forces are still strong, ion-pair dipoles may attract ions and form triple ions. Triple-ion formation has been suggested in solvents of $\varepsilon_\mathrm{s} < 15$, while formation of even still larger clusters of four, five or even more ions is possible in solvents of $\varepsilon_\mathrm{s} < 10$.

From the above discussion it follows that the structure of electrolyte solutions is determined by short-range forces like ion–solvent and ion–ion interactions. When the ion–solvent interactions are dominant as in the case of a medium of high dielectric constant, the species present are isolated solvated ions. When ion–ion interactions are dominating, ion association with the formation of new chemical species occurs with an increase in solute concentration, and at saturation the solution is basically a hydrated “molten phase”.

In the above picture of solvation of ions of an ionic solute immersed in a solvent, the solution is composed of randomly distributed solute ions which are surrounded by regions of immobile, strongly trapped solvent molecules around them and randomly distributed molecules of solvents in its remaining volume around the solvated molecules. With increasing solute concentration c, the concentration of solvated ions of the solute increases whereas the concentration of holes constituting the empty space in the solvent decreases. Therefore, the dependence of the properties of solutions of a solute on solute concentration c dissolved in a solvent is determined by the processes of solvation of solute ions and creation of holes.

It should be remembered that the solvated ionic entities participating in the properties of solutions are larger than the bare, unsolvated ions because of the firmly-trapped water molecules around them. Therefore, the radius of the kinetic entity participating in the transport properties of solutions is expected to change from one solvent to another because of changes in the structure of the solvation sheath. Since solvent molecules constitute the firmly-trapped solvation sheath, the sizes of these firmly-trapped solvent molecules mainly contribute to the changes in the radii of the solvated ions. For example, in the case of solvents water, methanol and ethanol where the size of their molecules increases in the order: water, methanol and ethanol, the radius of the solvated ions also increases in this order.

Finally, it should be mentioned that during the solvation of a solute extensive hydrogen-bonded structure of water, in general, responds to the presence of solute molecules and ions by spatial and orientational arrangements which result in an overall increase in the order of the solution. Interactions of ions with the dipole of water molecules lead to their solvation whereas hydrophobic interactions are the predominant factor in the solvation of nonpolar or apolar molecules. In an aqueous solution of polar solutes, their molecules break down the hydrogen-bonded arrangement of water and replace it by a spherically symmetrical non-hydrogen-bonded shell of water molecules. In a nonelectrolyte, there is no dissociation of its molecules and the solute molecules retain their unbroken identity.

1.5.2. Structure of primary and secondary solvation shells

It was mentioned above in Section 1.3.1 that the structured (or associated) structure of water is due to the extended hydrogen-bonded network and involves the average number of hydrogen bonds per water molecule in the liquid at ordinary temperatures is about 3.5 with O····H hydrogen-bond distance of about 0.23 nm. This implies that the average coordination number of a water molecule in the liquid is more than 4.0 expected from the regular tetrahedral hydrogen-bonded structure of ice. Intuitionally, it may be argued that replacement of a water molecule by an ion surrounded by the average number n_H of water molecules of the liquid water is possible without disturbing its structure when the ionic size is equal to about 0.23 nm of the O····H bond distance, but larger ions will distrupt the water structure. However, because of its electric field, the ion is capable of orienting water molecules due to ion–dipole interactions and disrupting the hydrogen bonds of the water structure. In general, small and positively-charged ions firmly bind the water molecules in their vicinity (structure-making ions) whereas large ions destroy the water structure (structure-breaking ions), but a certain number of water molecules, as a rule, remains around them distorting the water structure (solvation number).

There is huge literature devoted to the structure and dynamics of hydration of ions. Two authoritative reviews surveying diffraction, spectroscopic and computer simulation studies on this subject are readily available (Marcus, 2009; Ohtaki and Radnai, 1993). Experimental studies of ion hydration are based on x-ray and neutron diffraction techniques where fairly concentrated salt solutions of water-to-salt ratio between 4 and 40 were used. Various spectroscopic techniques, such as Raman and extended x-ray absorption fine structure (EXAFS) as well as nuclear magnetic resonance (NMR) and dielectric relaxation spectroscopic methods, have been used to investigate the structures of hydrated ions and their aqueous environment. Computer simulations used for ion hydration studies have been either independent or supporting diffraction and spectroscopic studies. A summary of ion–water distance $d_{\text{ion–W}}$ and coordination numbers n_{H1} and n_{H2} of the first and the second hydration shells of various ions is given in the review by Marcus (2009). The distance $d_{\text{ion–W}}$ in this review refers to the distance of the center of a water molecule from the center of the ions. This means that the first $d_{\text{ion–W}}$ distance denotes the thickness of the primary solvation shell whereas the second distance denotes the total thickness of the primary and secondary solvation shells.

The data of the ion–water distance $d_{\text{ion–W}}$ and the coordination number n_{H1} for the first solvation shells of different cations, reported by Marcus (2009), reveal that the values of $d_{\text{ion–W}}$ and n_{H1} increase from 0.194 nm and about 4.0 for Li^+ to 0.32 nm and about 9.0 for Cs^+, and the values of $d_{\text{ion–W}}$ and n_{H1} increase from 0.165 nm and about 4.0 for Be^{2+} to 0.281 nm and about 8.0 for Ba^{2+}. However, the value of $d_{\text{ion–W}}$ increases from 0.19 nm for Al^{3+} to 0.223 nm for Tl^{3+}, whereas n_{H1} for different trivalent cations remains essentially constant equal to 6.0. These trends of the distance $d_{\text{ion–W}}$ and the coordination numbers n_{H1} for the first hydration shell of cations are intimately related to the radii and electric charge (valency) of the ions. An increase in the valency of cation leads to a decrease is the value of $d_{\text{ion–W}}$ for neighboring cations (for example, compare Li^+ and Be^{2+}), but the increase in the coordination number n_{H1} of the cations with the distance $d_{\text{ion–W}}$ for the series of cations, as represented by $\Delta n_{\text{H1}}/\Delta d_{\text{ion–W}}$, strongly diminished with increasing cation valency. In contrast to the above trends related to the size and valency of cations, the values of $d_{\text{ion–W}}$ and n_{H2} of the second hydration shell are about 0.45±0.05 nm and 12 for various cations, irrespective of their size and valency.

The reported data of $d_{\text{ion–W}}$ and n_{H1} for different monovalent anions show that the values of $d_{\text{ion–W}}$ and n_{H1} for halides also increase with their size from 0.254 nm and 6.0 for F^- to about 0.40 nm and 8.0 for I^-, with $d_{\text{ion–W}}$ for these anions extending up to about 0.45±0.05 nm. The values of $d_{\text{ion–W}}$ for some complex monovalent anions are comparable with those for halides but their n_{H1} values lie between 2 and 4. The lower hydration number of complex anions is probably a consequence of opposing contributions of hydrophilic and hydrophobic parts of their constituents to the overall hydration. These observations imply that both primary and secondary solvation shells are present in halide ions but the hydration of the studied complex anions is confined essentially to the primary solvation shell.

The above trends are consistent with the nature of ion–solvent interactions and the concepts of the primary and the secondary solvation shells composed of immobile and loosely-attached layers of water molecules, respectively. The thickness of the secondary solvation shell may be estimated from the ion–water distances $d_{\text{ion–W}}$ of the primary and the secondary hydration shells of various ions. This thickness is practically constant equal to about 0.22 nm for both mono-, bi- and trivalent cations as well as halide-like anions, irrespective of their size, charge and valency. Comparison of this distance with the van der Waals radius of water molecule, equal to 0.17 nm, indeed suggests the loosely-bonded nature of this solvation layer of monomolecular thickness.

The strong tendency of cations to form secondary solvation shell in comparison with anions is associated with the polarization of positive charge of the H atoms of the O–H bonds due to the entrapped electrons of O atoms of the oriented water molecules by the electric field of the cations. Consequently, the positive charge of each polarized H atom of a pair of O–H bonds of the trapped water molecule can attract two water molecules around them, resulting in the secondary solvation shell. In contrast to the strong hydration effects of cations, the electric field of anions enable to develop weak bonds between them and the H atoms of the H–O bonds of water molecules. These trapped water molecules have their polarized lone-pair electrons of O atoms directed away from the anion, but these farther O atoms are not sufficiently strong to orient the water dipoles in their vicinity. This explains why anions are mainly surrounded by primary solvation shells alone.

The coordination of water molecules in the primary solvation shell of cations is usually 4 to 8 and the thickness of this solvation sheath lies between about 0.194 and 0.40 nm (cf. Marcus, 2009). Therefore, if the thickness of the secondary solvation is considered to be 0.195 nm instead of 0.22 nm mentioned above, one may take an ion–water distance $d_{\text{ion–W}} \approx 0.255$ nm of the primary solvation shell as the limiting thickness d_{lim} when an ion does not affect the water structure having a coordination number n_{H1} of 6. According to this criterion, ions with $d_{\text{ion–W}} < d_{\text{lim}}$ are structure makers and have $n_{\text{H1}} < 6$, whereas other ions with $d_{\text{ion–W}} > d_{\text{lim}}$ are structure breakers and have $n_{\text{H1}} > 6$. This classification appears to hold well for both cations and anions, but a somewhat higher value of d_{lim} is required for halides if the F^- ion is considered structure maker. Complex anions do not seem to fit into this classification.

The terms structure-making and structure-breaking behavior of ions associated with the effect of ions on the structure of water are usually used in the investigation of the concentration dependence of the viscosity η of aqueous solutions (see Chapter 5). The concentration dependence of viscosity η describing the structure-making and structure-breaking effects of the ions in the viscosity measurements is the sign of the so-called viscosity B_η coefficient and its temperature dependence defined by the temperature coefficient $\mathrm{d}B_\eta/\mathrm{d}T$.

The effects of ions on the structure of water are also described in terms of thermodynamic parameters representing the thermodynamic of solutions. Among these parameters are: the entropy of hydration of ions at infinite dilutions, structural entropy associated with changes in the structure of water beyond the hydration shell of ions, structural heat capacity, and the average number of hydrogen bonds per unit water existing in it. For details on this topic the reader is referred to Marcus (1994, 2009), where a list of various ions classified into structure breakers and structure makers on the basis of the average number of hydrogen bonds per unit water is also given.

Finally, it should be mentioned that the water-structure-affecting properties of ions have long been recognized in the precipitation of proteins from aqueous solutions of various ionic salts manifested typically at molar concentrations, where the protein precipitation effectiveness is related to the minimal concentration of the salt and is given by the empirical Hofmeister series (for example see: Gong et al., 2016; Marcus, 2009). The precipitation effects mediated by water are approximately additive over all the dissolved species and are dominated by the properties of the anions. For a cation, the decrease in the precipitation effectiveness of anions follows the series:

$$\mathrm{CO_3^{2-} > SO_4^{2-} > S_2O_3^{2-} > H_2PO_4^{-} > OH^{-} > F^{-} > HCOO^{-} > CH_3COO^{-} >} \\ \mathrm{> Cl^{-} > Br^{-} > NO_3^{-} > I^{-} > ClO_4^{-}}. \tag{1.44}$$

Thus, CO_3^{2-} is the most effective whereas ClO_4^- is least effective in the precipitation of proteins. For an anion, the effectiveness of cations has been reported to follow the series:

$$\mathrm{(CH_3)_4N^+ > Na^+ \approx K^+ > Cs^+ > Li^+ > NH_4^+ > Mg^{2+} > Ca^{2+} >> C(NH_2)_3^+}. \tag{1.45}$$

These two series of ions are, to some extent, similar to their structure-making and structure-breaking effects described above. Structure makers and structure breakers have also been known as kosmotropes and chaotropes.

1.5.3. Raman spectra and solution structure

As mentioned above, various spectroscopic techniques have been widely used for the investigation of structural characteristics of solutions and solvent mixtures. Among these techniques, Raman and infrared vibrational spectroscopy has been recognized as an important tool to study ionic and molecular interactions and the dynamic properties of ions and molecules in solutions. These studies of the solution structure are based on recording and interpretation of different Raman-active vibrations in the investigated system and involve all internal as well as external vibrations of the solvent and the solute (as individual ions as well as different type of ion pairs). In view of voluminous literature published on the Raman spectroscopic studies of solution structure, no attempt is made here to review different aspects of these studies. Instead, some examples of spectra of aqueous and alcoholic solutions of different types of solutes and the information derived therefrom are briefly presented below.

For bulk water under ambient conditions, wavenumbers centred at about 200 $\mathrm{cm^{-1}}$ and 3200 $\mathrm{cm^{-1}}$ are associated with the vibration mode of O····H nonbond and O–H bond, respectively. These low and high wavenumber regions, denoted as ν_L and ν_H, respectively, lie in the red and blue regions of the vibrational spectra. When an O–H bond of an associated water molecule becomes shorter during its vibration, the nonbond O····H segment of the associated molecule becomes longer. Then the O–H bond becomes stiffer, its characteristic phonon wavenumber undergoes a blue shift. In contrast to this, the O····H segment becomes softer, its characteristic wavenumber undergoes a red shift. Addition of an electrolyte to bulk water disrupts its network structure, such that the effects of dissolved solute are manifested in the Raman spectra in the form of apperance of new bands due to the dissolved ions and molecules of the salt and changes in the intensity of the bands of the solvent water.

Raman spectroscopy studies of the effects of different compunds on the structure of solvents have been reported: alkali halides in water (Gong et al., 2016), monovalent chlorides in water (Yoshimura and Kanno, 1996; Sokołowska, 1996), different monovalent anions in alcohols (Hidaka et al., 2003), ammonium chloride and sulfate in water (Mukhopadhyay and Dubey, 2017), various mono-, bi- and trivalent cations in water (R. Li et al., 2009), sodium, magnesium and calcium nitrates in water (K.-K. Li et al., 2012; Zhu et al., 2018), mono- and bivalent cation sulfates in water (Rull and Sobron, 1994; Rull et al., 1994, 1995), and carbohydrates in water (Paolantoni et al., 2008; Perticaroli et al., 2008). With appropriate computer programs and models, the positions and intensities of these experimentally recorded different bands are analyzed to establish contributions of possible vibration bands in a spectrum, i.e. deconvolution of spectrum (Gong et al., 2016; K.-K. Li et al., 2012; R. Li et al., 2009; Mukhopadhyay and Dubey, 2017; Zhu et al., 2018), and to optimize structures of molecular species in the solution, i.e. geometrical optimization of clusters (Mukhopadhyay and Dubey, 2017; Zhu et al., 2018).

The effects of a solute dissolved in a solvent by spectroscopic techniques are studied by comparing the positions, widths and heights of different bands appearing in its spectrum with reference to the positions of the bands observed due to the possible modes of vibrations of molecules of the neat solvent in its spectrum at a given temperature. In the low- and high-wavenumber regions covering the spectral range 30–4000 $\mathrm{cm^{-1}}$ of a Raman spectrum of neat water, these bands are known to appear at wavenumbers 50, 170, 3070, 3240, 3430, and 3606 $\mathrm{cm^{-1}}$. In the low-wavenumber region, the bands at 50 and 170 $\mathrm{cm^{-1}}$ are assigned to the H-bond (O····O····O unit) bending and H-bond (O····O unit) stretching intermolecular bonds. In the high-wavenumber region, the 3070 $\mathrm{cm^{-1}}$ band is assigned to the intermolecularly coupled vibrations moving in phase with one another, the 3240 $\mathrm{cm^{-1}}$ band is assigned to the O–H stretching vibrations of water molecule moving collectively in plane with its nearest and next nearest neighbors, the band centered at 3430 $\mathrm{cm^{-1}}$ is assigned to the partially H-bonded water, whereas the 3606 $\mathrm{cm^{-1}}$ band is due to the H-bonds of free water molecules. However, in these high-wavenumber regions deviations up to ± 20 $\mathrm{cm^{-1}}$ in the positions of the peaks in various studies have been observed.

Figure 1.30 shows the Raman spectra, using a confocal Raman spectrometer in the back-scattering configuration, of neat water and 2.1 M aqueous solutions of selected alkali halides MX in the spectral range 50–4000 $\mathrm{cm^{-1}}$ at room temperature. The spectra of Figure 1.30a were obtained from MI solutions with M = Na, K, Rb and Cs, whereas those of Figure 1.30b from NaX solutions with X = Cl, Br and I. As mentioned above, the spectral characteristics between 70–300 cm^{-1} and 50–4000 cm^{-1} are due to O····H and O–H stretching vibrations, respectively. Irrespective of the type of the ions, red shifting of ν_L and blue shifting of ν_H are consistently observed, implying O····H–O cooperative relaxation by the ionic field in the solution. However, the presence of ions reveals much pronounced effect on the bands of the Raman spectra in the high-wavenumber region than in the low-wavenumber region.

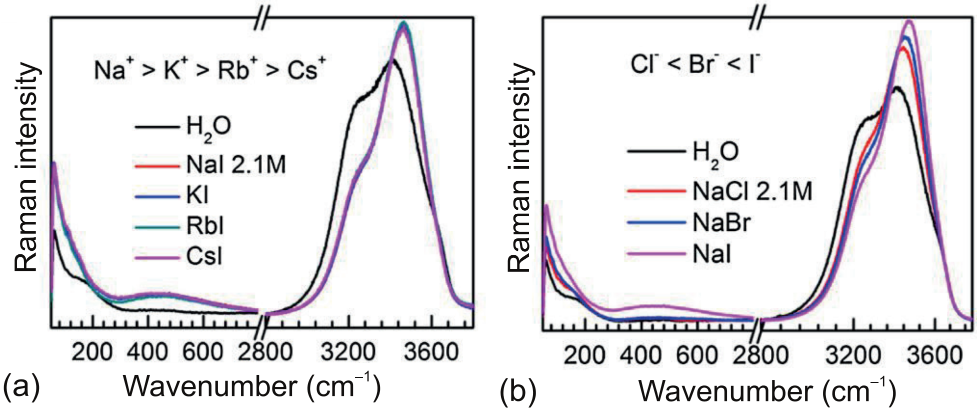

Figure 1.30. Raman spectra of neat water and 2.1 M aqueous solutions of selected alkali halides MeX in the spectral range 50–4000 cm^{-1}: (a) MeI with Me = Na, K, Rb and Cs, and (b) NaX with X = Cl, Br and I. Reproduced from Gong et al. (2016).

The obvious effect of the presence of a cation as well as an anion is that the peak centered at about 3450 cm^{-1} becomes more pronounced and is blue shifted. This implies that the pronounced behavior of this peak is associated with the formation of hydration shell around the ions. For the cations, the position and the intensity of the peak insignificantly differ from each other. In contrast to this behavior of cations, the position of the peak blue shifts and the peak intensity increases with their size, i.e. $Cl^- < Br^- < I^-$. These differences are due to their ability to form ion–water bonds.

Hydration of a cation shortens the O–H bond ($\Delta d_{HB} < 0$) due to electrostatic attraction between the positively charged ion and the lone-pair of the O atom of the H_2O molecule of the primary hydration shell. This shortening of the O–H bond is simultaneously accompanied by the lengthening of the weak H····O non-bond ($\Delta d_{NB} > 0$), as a result of polarization of positive charge on the H^+ of the H_2O molecule of the solvated cation. The Raman peak increases (blue shifts) in the former case, but the peak decreases (red shifts) in the latter case. The polarization increases the molecular order, which is inversely related to the half-width at the maximum height of a symmetrical band ($1/F_{WHM}$). However, for both cations and anions at a given concentration, the Raman wavenumber shift depends on the ratio R of the radius r_{ion}

and electronegativity difference χ of ions ($R = r_{\text{ion}}/\chi$), and increases in the sequence (Gong et al., 2016): I^- (2.2/2.5) > Br^- (1.96/2.8) > Cl^- (1.81/3.0) > F^- (1.33/4.0) for anions, and Na^+ (0.98/0.9) > K^+ (1.33/0.8) > Rb^+ (1.49/0.8) > Cs^+ (1.65/0.8) for cations, where the values of r_{ion} and χ for an ion are given in the parentheses.

Figure 1.31 shows another example of the Raman spectra of $NaNO_3$ bulk solutions in water at room temperature with various water-to-solvent ratio $R_{W:S}$ of 84.2–5.39 and supersaturated droplets with $R_{W:S}$ of 4.6–2.3, with saturation point corresponding to $R_{W:S}$ of 5.39. It may be seen that addition of the salt gives a new band at 1046.7 and another one at 3428 cm^{-1} with the presence of a shoulder at 3259 cm^{-1}. As mentioned above, the peak centered here at 3428 cm^{-1}, which blue shifts with an decrease in $R_{W:S}$, is associated with the O–H bond. However, the peak centered at 1046.7 cm^{-1} is due to the NO_3^- ions. This main peak, denoted as $\nu(NO_3^-)$, shifts from 1046.7 to 1049.9 cm^{-1} as the $R_{W:S}$ decreases from 84.2 to 5.39, and the peak position continues to increase from 1052.4 to 1054.7 cm^{-1} in the droplet region as the $R_{W:S}$ decreases down to 2.30. The position of the $\nu(NO_3^-)$ band depends on the solute concentration as well as on the type of the cation, but the height of this peak increases with decreasing $R_{W:S}$ (K.-K. Li et al., 2012; Zhu et al., 2018). The variation of the wavenumber of the $\nu_1(NO_3^-)$ band with $R_{W:S}$ is associated with the variation of water molecules surrounding an NO_3^- ion by the cation. Weakening of nitrate–water hydrogen bonding caused by the cations results in the $\nu_1(NO_3^-)$ band shifts to higher wavenumbers.

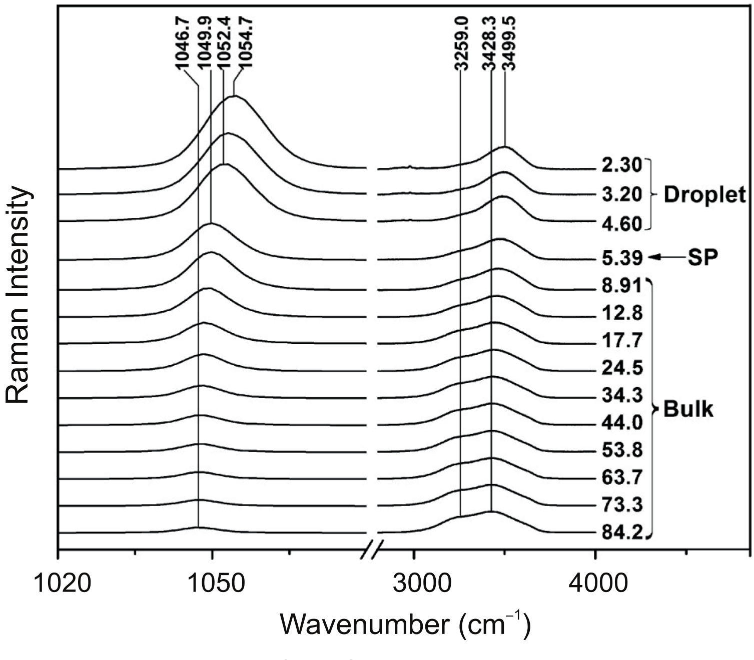

Figure 1.31. Raman spectra of $NaNO_3$ solutions in water at various water-to-solvent ratio $R_{W:S}$ at room temperature. Three spectra at the top are from droplets. Saturation point (SP) is denoted by arrow. After K.-K. Li et al. (2011).

The $\nu_1(NO_3^-)$ bands at wavelengths of 1046.7, 1049.0 and 1052.5 cm^{-1} are due to free NO_3^- ions, solvent-shared ion pairs (SIPs), and contact ion pairs (CIPs), whereas the peak located at 1058.0 cm^{-1} for $R_{W:S}$ below 1.0 is due to complicated CIP (CIP*) structures (see K.-K. Li et al., 2012). It was observed that: (1) the ratio I_{rel} of the intensities of the SIP, CIP and CIP* bands with respect to the intensity of the $\nu_1(NO_3^-)$ band increases with decreasing $R_{W:S}$ from 84.2 down to 8.86, and follows the sequence: I_{rel}(SIP) > I_{rel}(CIP) > I_{rel}(CIP*), indicating that free NO_3^- ions and SIPs are mainly formed in dilute solutions, and (2) for $R_{W:S} < 5.39$, I_{rel}(CIP*) > I_{rel}(SIP) > I_{rel}(CIP), implying that CIPs are mainly formed in the supersaturated solution.

As seen from Figure 1.31, the main peak of the water O–H stretching band from $NaNO_3$ solution increases with decreasing $R_{W:S}$ from 3428 to 3499 cm^{-1}. Component analysis of the main band and the shoulder at 3259 cm^{-1} showed (K.-K. Li et al., 2012) that the peak position at 3259 cm^{-1} remains unchanged but the main band is composed of two components C_1 and C_2 centered at 3259 and 3477 cm^{-1}, with full-width at half maximum F_{WHM} practically constant at 229 and 217 cm^{-1}, irrespective of $R_{W:S}$.

The relative proportions of weak and strong hydrogen bonds corresponding to the components C_1 and C_2 and of hydrogen and NO_3^- bands can be roughly estimated from the ratio of areas of the bands as a function of $R_{W:S}$. The ratio $A_{C1:C2}$ of the areas of the weak and strong bonds decreases from 0.86 to 0.17 with decreasing $R_{W:S}$ from 84.2 to 2.30 (K.-K. Li et al., 2012). This implies that the proportion of strong hydrogen bonds becomes lower with an increase in the concentration of ions. However, the ratio of the hydrogen and NO_3^- bands increases linearly with $R_{W:S}$ with a slope $A_{C1:C2}/R_{W:S} \approx 1.8$. This observation indicates that the Raman scattering cross-sections of water molecules and NO_3^- ions are insensitive to the structures of both ion pairs and hydrogen-bonding structures (K.-K. Li et al., 2012). This inference also implies that the perturbations caused in the weak and strong hydrogen bands at 3259 and 3477 cm^{-1}, respectively, by different anions of a common cation and by different cations of a common anion of electrolytes in aqueous solutions of a particular water-to-salt ratio $R_{W:S}$ are associated with the ability of hydration of the ions. In agreement with the above conclusion, from an investigation of the Raman OD stretching spectra of aqueous solutions of MCl (M = Li, Na, K, Rb and Cs) and R_4NCl (R = Me, Et and Pr) at $R_{W:S} = 16$, Yoshimura and Kanno (1996) reported that the area ratio $A_{C1:C2}$ gradually decreases from about 27 to 22.5 with an increase in cationic radius r_{ion} from 0.06 to 0.5 nm.

Due to their charge, the strong effect of ions on the O–H stretching vibrations of water molecules is revealed by the position and intensity of the main band components centered at 3259 and 3477 cm^{-1} in the high-wavenumber spectra. However, in aqueous solutions of nonelectrolytes such as carbohydrates (e.g. sucrose, $C_{12}H_{22}O_{11}$), the same sensitivity is not observed from their spectra in this region due to weak interactions between the OH groups of the carbohydrates and the O atoms of H_2O molecules. The Raman spectra of concentrated solutions of these compounds show only minor differences from that of neat water and the variations are similar for different sugar–water systems (for example, see: Perticaroli et al., 2008). For such systems, instead of Raman scattering spectra in the low-wavenumber region, analysis of depolarized Rayleigh scattering spectra in terms of imaginary part of the dynamical susceptibility χ" has been found to be very informative (Paolantoni et al., 2008; Perticaroli et al., 2008).

The imaginary part of the dynamical susceptibility χ" is the sum of quasi-elastic relaxation (QE) and inelastic vibrational (IE) contributions. For water, the QE relaxation contribution is due to the band below 25 cm^{-1}, but the IE contribution is due to vibrational modes: the H-bond (O····O····O unit) bending mode at about 60 cm^{-1} and the H-bond (O····O unit) stretching mode at 170 cm^{-1}. Therefore, the IE contribution to χ" is obtained by subtracting the QE contribution from the total χ". Figure 1.32 shows the χ" spectra of neat water and aqueous glucose solutions of three different concentrations at 25 °C. Obviously, dissolution of sugar to water leads to a decrease in the intensity of the 60 and 170 cm^{-1} bands of water and gives rise to new vibrational modes of glucose in the 250–500 cm^{-1} range. Similar trends were also observed (Perticaroli et al., 2008) for aqueous solutions of a monosaccharide (fructose), a disaccharide (trehalose), and an oligomer (dextran), and the intensities of these bands varied practically linearly with increasing sugar concentration.

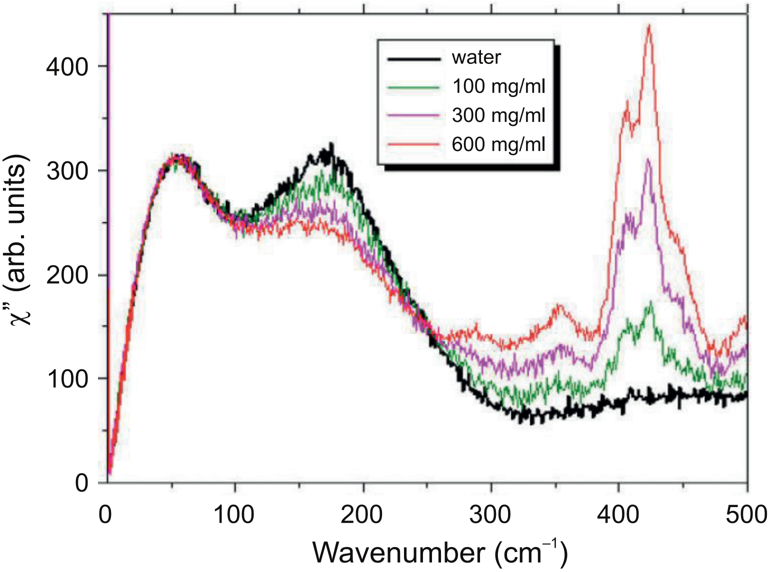

Figure 1.32. Susceptibility spectra of neat water and aqueous glucose solutions of three different concentrations at 25 °C. New vibrational modes of glucose appear in the 250–500 cm^{-1}. After Perticaroli et al. (2008).

The above observations suggest that the intensities of the 60 and 170 cm^{-1} bands are intimately connected with the effect of a carbohydrate on the local arrangement of H-bonded water molecules and that this effect is very pronounced on the 170 cm^{-1} band. The appearance of the 60 and 170 cm^{-1} bands has been attributed to the bending and stretching modes of vibration of a tetrahedral unit of five water molecules in the hydrogen-bonded network. Therefore, it may be argued that the decrease in the intensity of the 170 cm^{-1} band with increasing sugar concentration is due to increasing disruption of the local tetrahedral structure of water, and that the new bands of increasing intensities with increasing sugar concentration in the 250–500 cm^{-1} range are due to various types of interactions between different groups of sugar molecules and water.

References

Angell, C.A. (1991). Relaxation in liquids, polymers and plastic crystals: Strong/fragile patterns and problems. *J. Non-Cryst. Solids* **131-133**, 13-31.

Angell, C.A. (1995). Formation of glasses from liquids and biopolymers. *Science* **267**, 1924-1935.

Atkins, P.W. (1998). *Physical Chemistry*, 6th ed. Oxford University Press, Oxford.

Barrow, G.M. (1973). *Physical Chemistry*. 3rd ed. McGraw-Hill, New York.

Bini, R., M. Malvaldi, W.R. Pitner, and C. Chiappe (2008). QSPR correlation for conductivities and viscosities of low-temperature melting ionic liquids. *J. Phys. Org. Chem.* **21**, 622-629.

Bittner, B., R.J. Wrobel, and E. Milchert (2012). Physical properties of pyridinium ionic liquids. *J. Chem. Thermodyn.* **55**, 159-165.

Bockris, J.O'M., and A.K.N. Reddy (1970). *Modern Electrochemistry*, Vol. 1, Plenum Press, New York.

Bodo, E., and V. Migliorati (2011). Theoretical Description of Ionic Liquids. pp. 107-125. Chapter 5. In: S.T. Handy (Editor) (2011). *Ionic Liquids – Classes and Properties*. InTech, Rijeka, Croatia.

Carrera, G., and J. Aires-de-Sousa (2005). Estimation of melting points of pyridinium bromide ionic liquids with decision trees and neural networks. *Green Chem.* **7**, 20-27.

Chen, B.K., M.J. Liang, T.Y. Wu, and H.P. Wang (2013). A high correlate and simplified QSPR for viscosity of imidazolium-based ionic liquids. *Fluid Phase Equilibria* **350**, 37-42.

Crosthwaite, J.M., S.N.V.K. Aki, E.J. Maginn, and J.F. Brennecke (2004). Liquid phase behavior of imidazolium-based ionic liquids with alcohols. *J. Phys. Chem. B* **108**, 5113-5119.

Crosthwaite, J.M., S.N.V.K. Aki, E.J. Maginn, and J.F. Brennecke (2005). Liquid phase behavior of imidazolium-based ionic liquids with alcohols: effect of hydrogen bonding and non-polar interactions. *Fluid Phase Equilibria* **228-229**, 303-309.

Crosthwaite, J.M., M.J. Muldoon, S.N.V.K. Aki, E.J. Maginn, and J.F. Brennecke (2006). Liquid phase behavior of ionic liquids with alcohols: Experimental studies and modeling. *J. Phys. Chem. B* **110**, 9354-9361.

Dekker, A.J. (1964). *Solid State Physics*. MacMillan, London.

Domańska, U., and M. Królikowska (2012). Density and viscosity of binary mixtures of thiocyanate ionic liquids + water as a function of temperature. *J. Solution Chem.* **41**, 1422–1445.

Domańska, U., and M. Laskowska (2008). phase equilibria and volumetric properties of (1-ethyl-3-methylimidazolium ethylsulfate+alcohol or water) binary systems. *J. Solution Chem.* **37**, 1271–1287.

Domańska, U., and M. Laskowska (2009). Effect of temperature and composition on the density and viscosity of binary mixtures of ionic liquids with alcohols. *J. Solution Chem.* **38**, 779–799.

Domańska, U., and A. Marciniak (2005). Liquid phase behaviour of hexyloxymethyl-3-methylimida- zolium-based ionic liquids with hydrocarbons: The influence of anion. *J. Chem. Thermodyn.* **37**, 577–585.

Domańska, U., A. Pobudkowska, and F. Eckert, (2006a). (Liquid-liquid) phase equilibria of 1-alkyl,3-methylimidazolium methylsulfate with alcohols, ketones, or ethers. *J. Chem. Thermodyn.* **38**, 685-695.

Domańska, U., A. Pobudkowska, and A. Wiśniewska (2006b). Solubility and excess molar properties of 1,3-dimethylimidazolium methylsulfate, or 1-butyl-3-methylimidazolium methylsulfate, or 1-butyl-3-methylimidazolium octylsulfate ionic liquids with *n*-alkanes and alcohols: Analysis in terms of the PFP and FBT models. *J. Solution Chem.* **35**, 311–334.

Dong, K., Q. Wang, X. Lu, Q. Zhou, and S. Zhang (2014). Structure, interaction and hydrogen bond, pp. 1-38. In: Structures and Interactions of Ionic Liquids, S. Zhang, J. Wang, X. Lu, and Q. Zhou (Editors). *Structure and Bonding*, Vol. 151. Springer, Berlin, Heidelberg.

Eggers, D.F., N.W. Gregory, G.D. Halsey, B.S. Rabinovitch (1964). *Physical Chemistry*. Wiley, New York.

Eike, D.M., J.F. Brennecke, and E.J. Maginn (2003). Predicting melting points of quaternary ammonium ionic liquids. *Green Chem.* **5**, 323-328.

Freire, M.G., C.M.S.S. Neves, P.J. Carvalho, R.L. Gardas, A.M. Fernandes, I.M. Marrucho, L.N.M.B.F. Santos, and J.A.P. Coutinho (2007a). Mutual solubilities of water and hydrophobic ionic liquids. *J. Phys. Chem.* B **111**, 13082-13089.

Freire, M.G., L.N.M.B.F. Santos, I.M. Marrucho, and J.A.P. Coutinho (2007b). Evaluation of COSMO-RS for the prediction of LLE and VLE of alcohols + ionic liquids**.** *Fluid Phase Equilibria* **255**, 167-178.

Gardas, R.L., and J.A.P. Coutinho (2008). A group contribution method for viscosity estimation of ionic liquids. *Fluid Phase Equilibria* **266**, 195-201.

Giernoth, R. (2009). NMR spectroscopy in ionic liquids. *Topics in Current Chemistry*, **290**, 263-283.

Gong, Y., Y. Xu, Y. Zhou, C. Li, X. Liu, L. Niu, Y. Huang, X. Zhang, and C.Q. Sun (2017). Hydrogen bond network relaxation resolved by alcohol hydration (methanol, ethanol, and glycerol). *J. Raman Spectrosc*. **48**, 393-398.

Gong, Y., Y. Zhou, H. Wu, D. Wu, Y. Huang, and C.Q. Sun (2016). Raman spectroscopy of alkali halide hydration: hydrogen bond relaxation and polarization. *J. Raman Spectrosc*. **47**, 1351-1359.

González, B., N. Calvar, E. Gómez, and A. Domínguez (2007). Density, dynamic viscosity, and derived properties of binary mixtures of methanol or ethanol with water, ethyl acetate, and methyl acetate at T = (293.15, 298.15, and 303.15) K. *J. Chem. Thermodyn.* **30**, 1578-1588.

Halliday, D., R. Resnick, J. Walker (2001). *Fundamentals of Physics*, Part 5. Wiley, New York.

Han, C., G. Yu, L. Wen, D. Zhao, C. Asumana, and X. Chen (2011). Data and QSPR study for viscosity of imidazolium-based ionic liquids. *Fluid Phase Equilibria* **300**, 95-104.

Handy, S.T. (Editor) (2011). *Ionic Liquids – Classes and Properties*. InTech, Rijeka, Croatia.

Heintz, A. (2005). Recent developments in thermodynamic and thermophysics of non-aqueous mixtures containing ionic liquids. A review. *J. Chem. Thermodyn.* **37**, 525-535.

Heintz, A., D. Klasen, J.K. Lehmann, and C. Wertz (2005). Excess molar volumes and liquid-liquid equilibria of the ionic liquid 1-methyl-3-octyl-imidazolium tetrafluoroborate mixed with butan-1-ol and pentan-1-ol. *J. Solution Chem*. **34**, 1135-1144.

Herráez, J.V., and R. Belda (2006). Refractive indices, densities and excess molar volumes of monoalcohols + water. *J. Solution Chem.* **15**, 1315-1328.

Hidaka, F., Y. Yoshimura, and H. Kanno (2003). Anionis effects on Raman OD stretching spectra for alcoholic LiX (X = Cl^-, Br^-, I^-, ClO_4^-, NO_3^-, and CH_3COO^-). *J. Solution Chem.* **32**, 239-251.

Hildebrand, J.H. (1971). Motions of molecules in liquids: Viscosity and diffusivity. *Science* **174**, issue 4008, 490-493.

Hildebrand, J.H. (1977). *Viscosity and Diffusivity: A Predictive Treatment*. Wiley-Interscience, New York.

Holguin, A.R., D.R. Delgado, F. Martinez, M. Khoubnasabjafari, and A. Jouyban (2011). Study of some volumetric properties of glycerol formal + ethanol mixtures and correlation with the Jouyban-Acree model. *Rev. Acad. Colomb. Cienc*. **35**, 315-328.

Horvath, A.L. (1985). *Handbook of Aqueous Electrolyte Solutions: Physical Properties, Estimation and Correlation Methods*. Ellis Horwood, Chichester.

Hu, Y., and X. Peng (2014). Effect of structure of ionic liquids on their physical chemical properties, pp. 141-174. In: Structures and Interactions of Ionic Liquids, S. Zhang, J. Wang, X. Lu, and Q. Zhou (Editors). *Structure and Bonding*, Vol. 151. Springer, Berlin, Heidelberg.

Jacquemin, J., R. Ge, P. Nancarrow, D.W. Rooney, M.F. Costa Gomes, A.A.H. Padua, C. Hardcore (2008). Prediction of ionic liquid properties. I. Volumetric properties as a function of temperature at 0.1 MaP. *J. Chem. Eng. Data* **53**, 716-726.

Klamt, A., and F. Eckert (2000). COSMO-RS: a novel and efficient method for the a priori prediction of thermophysical data of liquids**.** *Fluid Phase Equilibria* **172**, 43-72.

Katritzky A.R., A. Lomaka, R. Petrukhin, R. Jain, M. Karelson, A.E. Visser, and R.D. Rogers (2002a). Correlation of the melting point of potential ionic liquids (imidazolium bromides and benzimidazolium bromides) using the CODESSA program. *J. Comp. Info. Comp. Sci*. **42**, 225-231.

Katritzky, A.R., A. Lomaka, R. Petrukhin, R. Jain, M. Karelson, A.E. Visser, and R.D. Rogers (2002b). QSPR correlation of the melting point for pyridinium bromides, potential ionic liquids. *J. Comp. Info. Comp. Sci.* **42**, 71-74.

Katritzky, A.R., R. Jain, A. Lomaka, R. Petrukhin, U. Maran, and M. Karelson (2001). Perspective on the relationship between melting points and chemical structure. Crystal Growth Des. **1**, 261-265.

Kittel, C. (1976). *Introduction to Solid State Physics*. Fifth edition. Wiley, New York.

Li, K.-K., S.-F. Pang, G. Zeng, F. Wang, and Y.-H. Zhang (2010). The structural independence of Raman scattering cross sections of $\nu_1(NO_3^-)$ and $\nu(H_2O)$. *J. Raman Spectrosc.* **41**, 338-343.

Li, R., Z. Jiang, Y. Guan, H. Yang, and B. Liu (2008). Effect of metal ion on the water structure studied by the Raman O–H stretching spectrum. *J. Raman Spectrosc.* **40**, 1200-1204.

Lide, D.R. (1996/1997). *Handbook of Chemistry and Physics*, 77th edition. CRC Press, Boca Raton, FL.

López-Martin, I., E. Burello, P.N. Davey, K.N. Seddon, and G. Rothenberg (2007). Anion and cation effects on imidazolium salt melting points: a descriptor modelling study. *Chem. Phy. Chem*. **8**, 690-695.

Luck, W.A.P. (Editor), (1974). *Structure of Water and Aqueous Solutions*, Verlag Chemie GmbH, Weinheim.

Marcus, Y. (1992). The structuredness of solvents. *J. Solution Chem*. **21**, 1217-1230.

Marcus, Y. (1994). Viscosity B-coefficients, structural entropies and heat capcities, and the effects of ions on the structure of water. *J. Solution Chem*. **21**, 831-848.

Marcus, Y. (2009). Effect of ions on the structure of water: structure making and breaking. *Chem. Rev*. **109**, 1346-1370.

Marsh, K.N., J.A. Boxal, and R. Lichtenthaler (2004). Room temperature ionic liquids – a review. *Fluid Phase Equilibria* **219**, 93-98.

Mokhtarani, B., A. Sharifi, H.R. Mortaheb, M. Miraei, M. Mafi, and F. Sadeghian (2009). Density and viscosity of pyridinium-based ionic liquids and their binary mixtures with water at several temperatures. *J. Chem. Thermodyn.* **41**, 323–339.

Mortimore, R.G. (2008). *Physical Chemistry*, 3rd edition, Elsevier, Amsterdam, Chap. 23.

Mu, T., and B. Han (2014). Structure and thermodynamic properties of ionic liquids, pp. 107-139. In: Structures and Interactions of Ionic Liquids, S.Zhang, J. Wang, X. Lu, and Q. Zhou (Editors). *Structure and Bonding*, Vol. 151. Springer, Berlin, Heidelberg.

Mukhopadhyay, A., and P. Dubey (2018). Investigation of solvation of ammonium salts: a Raman spectroscopy and ab initio study. *J. Raman Spectrosc*. **49**, 736-746.

Ohtaki, H., and T. Radnai (1993). Structure and dynamics of hydrated ions. *Chem. Rev*. **93**, 1157-1204.

Paolantoni, M., L. Gomez, D. Fioretto, M.E. Gallina, A. Morresi, P. Sassi, and F. Scarponi (2008). Structural and dynamic properties of glucose aqueous solutions by depolarized Raleigh scattering. *J. Raman Spectrosc.* **39**, 238-243.

Perticaroli, S., P. Sassi, A. Morresi, and M. Paolantoni (2008). Low-wavenumber Raman scattering from aqueous solutions of carbohydrates. *J. Raman Spectrosc.* **39**, 227-232.

Rooney, D., J. Jacquemin, and R. Gardas (2009). Thermophysical properties of ionic liquids. *Topics in Current Chemistry*, **290**, 185-212.

Rull, F., and F. Sobron (1994). Band profile analysis of the Raman spectra of sulphate ions aqueous solutions. *J. Raman Spectrosc*. **25**, 693-698.

Rull, F., Ch. Balarew, J.L. Alvarez, F. Sobron, and A. Rodroguez (1994). Raman spectroscopic study of ion association of aqueous magnesium sulphate solutions. *J. Raman Spectrosc.* **25**, 933-941.

Rull, F., F. Sobron, and O.F. Nielsen (1995). Dependence of concentration and temperature of the dynamics of SO_4^{2-} in Li_2SO_4, Na_2SO_4 and K_2SO_4 aqueous solutions studied by Raman spectroscopy. *J. Raman Spectrosc.* **26**, 663-668.

Sangwal, K. (1989). On the estimation of surface entropy factor, interfacial-tension, dissolution enthalpy and metastable zone-width for substances crystallizing from solution. *J. Cryst. Growth* **97**, 393-405.

Shukla, M., N. Srivastava, and S. Saha (2011). Interactions and transitions in imidazolium cation based ionic liquids. pp. 153-170. Chapter 7. In: S.T. Handy (Editor) (2011). *Ionic Liquids – Classes and Properties*. InTech, Rijeka, Croatia.

Sindt M., J.L. Mieloszynski, and J. Harmand (2011). Ionic liquids from (meth) acrylic compounds. pp. 81-104. Chapter 4. In: S.T. Handy (Editor) (2011). *Ionic Liquids – Classes and Properties.* InTech, Rijeka, Croatia.

Vraneš, M., S. Popović, A. Tot, N. Zec, and S. Gadžurić (2014). Density, excess properties, electrical conductivity of 1-butyl-1-methylimidazolium bis(trifluoromethylsulfonyl)imide + γ-butylrolactone binary mixtures. *J. Chem. Thermodyn.* **76**, 161-171.

Vraneš, M., A. Tot, S. Popović, N. Zec, S. Dožić, and S. Gadžurić (2015). Ideal and non-ideal behaviour of {1-butyl-1-methylpyrrolydinium bis(trifluoromethylsulfonyl)imide + γ-butylrolactone} binary mixtures. *J. Chem. Thermodyn.* **81**, 66-76.

Wright, M.R. (2007). *An Introduction to Electrolyte Solutions*. Wiley, Chichester.

Wu, C.-T., K.N. Marsh, A.V. Deev, and J.A. Boxall (2003). Liquid–liquid equilibria of room-temperature ionic liquids and butan-1-ol. *J. Chem. Eng. Data* **48**, 486–491.

Yoshimura, Y., and H. Kanno (1996). Cationis effects in the Raman OD stretching spectra of aqueous electrolyte solutions. *J. Raman Spectrosc.* **27**, 671-674.

Zhang, S., N. Sun, X. He, X. Lu, and X. Zhang (2006). Physical properties of ionic liquids: database and evaluation. *J. Phys. Chem. Ref. Data* **35**,1475-1517.

Zhang, S., J. Wang, X. Lu, and Q. Zhou (Editors) (2014). Structures and Interactions of Ionic Liquids. *Structure and Bonding*, Vol. 151. Springer, Berlin, Heidelberg.

Zhao, N. (2017). Evaluation of physical properties of ionic liquids. *PhD thesis*. Queen's University Belfast.

Zhao, N., and J. Jacquemin (2017a). New method based on the UNIFAC-VISCO model for the estimation of dynamic viscosity of (ionic liquid + molecular solvent) binary mixtures. *Fluid Phase Equilibria* **449**, 41-51.

Zhao, N., and J. Jacquemin (2017b). The development of the UNIFAC-CONDUCT as a novel approach for the estimation of the conductivity of pure ionic liquids. *Fluid Phase Equilibria* **449**, 60-67.

Zhao, N., J. Jacquemin, R. Oozeerally, and V. Degirmenci (2016a). New method for the estimation of viscosity of pure and mixtures of ionic liquids based on the UNIFAC-VISCO model. *J. Chem. Eng. Data* **61**, 2160-2169.

Zhao, N., R. Oozeerally, V. Degirmenci, Z. Wagner, M. Bendová, and J. Jacquemin (2016b). New method based on the UNIFAC-VISCO model for the estimation of ionic liquids viscosity using the experimental data recommended by mathematical gnostics. *J. Chem. Eng. Data* **61**, 3908-3921.

Zhao, N., H.B. Menegolla, V. Degirmenci, Z. Wagner, M. Bendová, and J. Jacquemin (2017). Group contribution method for the evaluation of volumetric properties of using experimental data recommended by mathematical gnostics. *Ind. Eng. Chem. Res.* **56**, 6827-6840.

Zhu, F., H. Zhou, X. Wang, Y. Zhou, H. Liu, C. Fang, and Y. Fang (2018). Raman spectroscopy and ab initio quantum chemical calculations of ion association behavior in calcium nitrate solution. *J. Raman Spectrosc.* **49**, 852-861.

2

SOLUBILITY OF ELECTROLYTES AND NONELECTROLYTES

Mixing of a solute with its solvent at given temperature and pressure conditions produces a mixture which can be homogeneous as well as heterogeneous depending on the capability of the solvent to devour the solute. The limiting concentration of the solute that can be taken up by the solvent keeping homogeneity of the mixture is called its solubility and the solution is referred to as saturated. Addition of more solute to the saturated solution simply remains undissolved in it because the pure solute is in equilibrium with the dissolved solute.

Dissolution of a crystalline solid in a solvent is a case of phase transformation of the solid to the liquid state (solution) and is associated with the dismantling of the long-range order of the arrangement of the building units in the solid by the solvent. The building units are cations and anions in ionic crystalline solids (electrolytes) and molecules in molecular crystalline solids (nonelectrolytes such as most organic compounds). In the dissolution process the solvent binds with the ions (or molecules) of the solid so that the solvated ions (or molecules) leave the solid and move into the solvent. It is these solute–solvent interactions (also referred to as solid–liquid interactions) that overcome the solid–solid (ionic or molecular) interactions holding the crystalline solid together and determine its dissolution in the solvent. There is a free energy change ΔG associated with the dissolution of the solute in the solution, which is equal to to the algebraic sum of: (1) the energy G_1 spent in the creation of a cavity or hole of the size of solute ions (or molecules) in the solvent and (2) the energy G_2 recovered in the transfer of an ion (or molecule) and the rearrangement of solvent molecules around the transferred ion (or molecule); i.e. $\Delta G = G_1 - G_2 < 0$. The free energy change ΔG approaches zero as the concentration approaches saturation. With reference to the initial state, this energy change ΔG for an ideal solution is taken as the standard free energy change ΔG^{o}.

There is a huge literature on the solubility of different types of crystalline solids in aqueous and nonaqueous solutions. Most of the publications on the solubility published before the early nineteen eighties deal with electrolytes in solvents like water and simple organic solvents such as alcohols. However, since then work on the investigation of the solubility of organic compounds in water and a variety of organic solvents has witnessed enormous progress from the standpoint of their usefulness as drugs. In this chapter different problems encountered in the field of solubility of different solids in individual solvents and binary solvent mixtures are described and discussed. After a short description of the methods of measurement of solubility and the units used to denote its value in the following section, brief description of distinction between ideal and real solutions is given in Section 2.2. Thermodynamics of solutions and theoretical models of solubility, and the effect of dielectric constant of solvents and their structure are presented in Sections 2.3 and 2.4, respectively. Finally, trends in studies of the solubility in solvent–cosolvent systems are surveyed in Section 2.5.

2.1. Solubility measurements

Saturated solutions of crystalline solids in their solvents at known temperatures are usually obtained by adding previously weighed amounts of the solid periodically to a known volume of the solvent contained in glass flasks and the solid–solvent mixture is mixed vigorously until the portion of the added solute is dissolved to yield a homogeneous mixture. A similar procedure to obtain the saturated solution of a crystalline solid in a solvent is based on feeding periodically known amounts of the solvent, by weight or volume, to the inhomogeneous solid–solvent mixture containing excess solid in it until the last traces of the solid are completely dissolved. From a knowledge of the mass of the solid dissolved in the volume of the solution, the solubility of the solid is calculated.

Another method of determination of the solubility of solids in individual solvents and solvent mixtures is based on recording the temperature of solid–solvent mixture of known composition during its controlled cooling or heating at a constant rate. In the case of a solid whose solubility in its solvent increases with temperature, crystallites of the solid begin to appear during the slow cooling of an undersaturated solution but they disappear during the slow heating of a solid–solvent mixture containing excess undissolved solid. The temperature when the crystallites begin to appear and disappear in the solution during its slow cooling and heating is an indicator of solution saturation. Since the appearance of crystallites occurs from supersaturated solutions, the temperature at which the crystallites are detected during slow cooling of a solution is *always* lower than the saturation temperature. Therefore, the temperature of disappearance of crystallitine solute during slow heating of the solution is considered reliable for the detection of its saturation temperature (Omar and Ulrich, 2006).

Traditionally, solid–solvent mixtures containing an excess amount of the solid in a known volume of the solvent in glass flasks are placed in a constant-temperature bath and stirred for suitable durations to ensure that an equilibrium is reached in the solution. Then the supernatant solutions are filtered at isothermal conditions to remove undissolved solid. Finally, from the samples of the saturated solution the solute solubility is determined by spectrophotometric or other convenient analytic procedures.

In the uv-vis spectrophotometric procedure, the solute concentrations are determined from interapolation of the values of absorbance of their diluted solutions at a known peak in the spectra in a standard curve of its concentration and absorbance in the same solvent system (Avila and Martinez, 2002; Delgado and Martinez, 2015; Martin et al., 1982; Sotomayor et al., 2013; Zhou et al., 2013). A similar procedure involves measurement of refractive indices of appropriately diluted solutions and their interpolation from previously constructed calibration curve for the salt in the same solvent (Jimenez and Martinez, 2006). Titration of saturated solutions of acids and salts with appropriate solutions serving as indicators is another procedure (Bravi and Mazzarotta, 1998; Manzurola and Apelblat, 2002). The commonly used procedure is based on evaporation of the solvent in a known volume of the saturated solution (Anuar et al., 2008; Borissova et al., 2009; Cui et al., 2017; Gharsallaoui et al., 2008; Huang et al., 2015; Li and Gao, 2018; Muñoz et al., 2016; O'Ciardha et al., 2011; Wu et al., 2012), where the amount of the solid dissolved in the known volume of the saturated solution is obtained from the difference in the masses of the saturated solution before and after solvent evaporation.

Laser monitoring system based on recording intensity of laser beam transmitted through a mixture of solute and solvent contained in a thermostated vessel maintained at a predefined temperature is another method for solubility measurements (Chen et al., 2014; Liu et al., 2014; Zhang et al., 2018). The initial solute–solvent mixture of known masses in the vessel may have the solute more or less than its solubility. The solution is stirred and the transmitted light intensity is recorded. When the solute in the solution is less than the solubility, small amounts of the solute are added after suiable intervals until the solution becomes saturated. However, when the solute in the solution is in excess, small amounts of the solvent are fed to the solution periodically until the last traces of the solute are completely dissolved in the solution. These stages of solid solubility are indicated by abrupt changes in the recorded levels of the laser beam intensity. Finally, from a knowledge of the mass of the solid contained in the volume of the solution at a particular temperature, its solubility is calculated.

Since dissolution of a solid in a solvent is associated with a change in the heat content of the solid–solvent system, solubility measurement has been made from changes in the heat content of the system using differential scanning calorimetry (Mohan et al., 2002). This procedure has been suggested for small masses of solid samples.

Most of the methods described above enable to determine solubilities of different substances reliably but are time-consuming. However, sophisticated techniques such as focussed-beam reflectance measurements (FBRM) (Kim and Kim, 2010; Nowee et al., 2008; O'Grady et al., 2007; O'Ciardha et al., 2011), attenuated total reflectance Fourier transform infrared (ATR-FTIR) spectroscopy (Barrett et al., 2010; Borissova et al., 2009; Danuwila and Berglund, 1997; Danuwila et al. 1994), and turbidimetry (Zhang et al., 2015; Zhu et al., 2003) have been used for quick solubility measurements at the expense of accuracy. Experimental equipments based on these techniques are commericially available.

FBRM is a probe-based instrument that measures *in situ* the time duration for a part of a monochromatic laser-beam reflected back up the probe to a detector by change in the size, shape and population of particles, whereas ATR-FTIR spectroscopy measures solution concentration by irradiating the solution with infrared light to produce an infrared spectrum, which is characteristic of the vibrational structure of the substance in contact with the ATR probe. To obtain information for the solubility of a solute in a particular solvent by these techniques, slurries of the solute in the solvent are prepared at some temperature by dissolving excess solute in the solvent at a temperature higher than the possible temperature of solubility measurement and then cooled down to a temperature lower than the saturation temperature. The solutions are heated at a low heating rate (< 0.1 K·min^{-1}) to record the saturation temperature. In the FBRM, with increasing temperature the fine chord counts (between 1 and 1000 nm) initially remain constant at some level, then decrease slowly and finally the count approaches zero at the saturation temperature. In the ATR-FTIR spectra on the other hand, the absorption peak height initially increases, attains a maximum value at the saturation temerature and then begins to decrease. In turbidimetry the turbidity of the solution is recorded using a turbidity probe inserted in the slurry during its slow heating. Disappearance of turbidity of the slurry is an indication of saturation temperature.

The solubility of a solute in its solution is the amount of the solute, which is in equilibrium with its solid phase, in a given volume or weight of solution or solvent. In volume and weight methods, solubility may be expressed as g solute per g solvent (weight fraction), g solute per 100 g solvent (weight percent; wt%), g equivalent or moles of solute per litre of solution (molarity), and moles of solute per kg solvent (molality). Molar and molal concentrations, denoted usually by c and m, respectively, are frequently used to express solute concentration in aqueous solutions, but the temperature dependence of solubility of various solutes in solutions is customarily expressed in mole fraction x.

The solubility x_i, expressed in mole fraction, of component i of a system composed of n components in a solution composed of individual solvents or their mixtures is given by

$$x_i = \frac{w_i / M_i}{\sum_{i=1}^{n} w_i / M_i}, \tag{2.1}$$

where w_i is the mass of component i and M_i is its molecular weight. However, the content f_j of a solvent in a mixture of j solvents in the solution is usually expressed as g of solvent per g of solvent mixture (weight fraction), g of solvent per 100 g of solvent mixture (weight percent; wt%), or in mole fraction given by

$$f_j = \frac{w_j / M_j}{\sum_{j=1}^{n} w_j / M_j}, \tag{2.2}$$

where w_j is the mass of solvent j and M_j is its molecular weight. Note that the solute content is not taken into account in the solvent content f_j, implying that the solvent content f_2 or f_3 is equal to x_2 or x_3 only in solutions containing low solute concentrations x_1.

2.2. Ideal and real solutions

The temperature dependence of the solute concentration of saturated solution (i.e. solubility) is predicted by the Le Chatelier principle which states that *any change in the variables that characterize the state of a system in equilibrium causes a shift in the position of equilibrium in a direction that tends to counteract the change in the variable under consideration*. Therefore, if dissolution is exothermic, solubility will decrease with an increase in temperature, and conversely, if dissolution is endothermic as is usually encountered, solubility will increase with temperature. $Ca(OH)_2$ and Li_2SO_4 are example of compounds whose solubility decreases with an increase in temperature of solvent water. In the temperature range between 0 and 100 °C in water, the solubility of sodium chloride, NaCl, insignificantly increases with temperature, but the solubilities of KNO_3 and $PbCl_2$ at 100 °C are several times higher than those at 0 °C. Figure 2.1 illustrates typical examples of the temperature dependence of solubility c_s for some common inorganic compounds in water in the temperature interval 0–100 °C. As seen from the figure, the solubilities of all compounds neither increase nor decrease steadily in the entire temperature interval. There are different compounds the solubility of which either increases or decreases in certain temperature intervals with an increase in temperature.

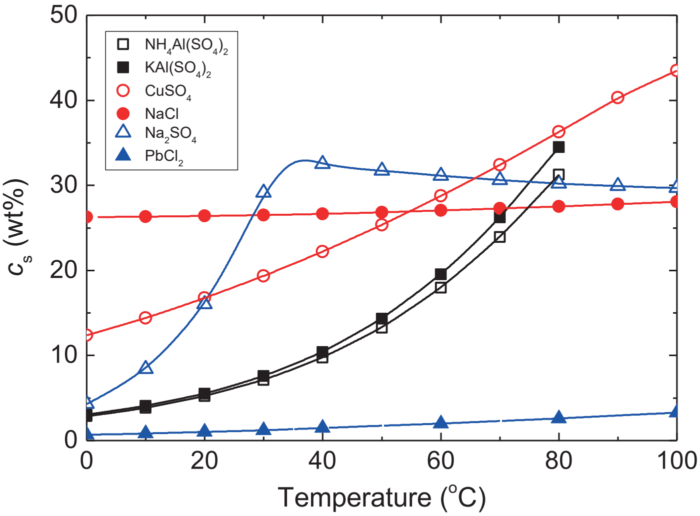

Figure 2.1. Typical examples of temperature dependence of solubility c_s for some common inorganic compounds in water in the temperature interval 0–100 °C. Original data for $CuSO_4$, NaCl, Na_2SO_4, $NH_4Al(SO_4)_2$ and $KAl(SO_4)_2$ are from Söhnel and Novotny (1985), and for $PbCl_2$ from Mullin (2001).

Smooth, continuous increase or decrease in the solubility of a compound with temperature means that the same solid phase is in equilibrium in the solution at all temperatures. However, break in the curve of solubility c_s of a compound in a given solvent as a function of temperature T indicates that a change in the solid phase in equilibrium has occurred in the saturated solution at this temperature. In Figure 2.1 examples of well-defined breaks are Na_2SO_4, $KAl(SO_4)_2$ and $NH_4Al(SO_4)_2$. The breaks are caused by the formation of hydrates containing different water molecules. A general trend of formation of hydrates of different salts in aqueous solutions is that the number of water molecules entering a compound decreases with increasing temperature. For example, $Na_2SO_4 \cdot 10H_2O$ is formed between 0 and 33 $^\circ$C and the salt solubility increases with temperature, but anhydrous Na_2SO_4 is formed above 33 $^\circ$C and the solubility decreases with increasing temperature. In contrast to only two phases of Na_2SO_4, with increasing solute concentration in the aqueous solution $MgSO_4$ forms dodecahydrate, heptahydrate, hexahydrate and monohydrate in the temperature intervals between 0 and –2 $^\circ$C, –2 and 52 $^\circ$C, 52 and 73 $^\circ$C, and 73 and 194 $^\circ$C, respectively. Note that –2 $^\circ$C is an eutectic point but 52 and 73 $^\circ$C are peritectic points.

Increasing or decreasing trends of the dependence of solubility c_s on temperature T are usually discussed in terms of positive or negative temperature coefficient of solubility (i.e. $\partial c_s/\partial T$) in a particular temperature range. Depending on the nature of solute–solvent system, the solubility coefficient can be high or low and can vary in different temperature intervals. It is the solute–solvent interaction that leads to the dissolution of the solute in the solution and decides the solubility.

As mentioned above, the temperature dependence of solubility of various solutes in solutions is customarily expressed in mole fraction x. Here we use x_s and x to denote solute solubility and solute concentration (frequently in mole fraction), respectively, but we use the general notation c to denote solute concentration. For the sake of clarity, the concentration units are mentioned whenever required.

2.2.1. Basic equations

The solubility of a compound is its equilibrium concentration x_s in the solute–solvent mixture at a particular temperature T. Therefore, the solubility depends on the thermodynamic stability of the solid phase as well as on the conditions in the solution. If some reference state is considered, the activity a of the solute at equilibrium is equal to its activity a_s in the solution. The Gibbs free energy change ΔG^o involved in the change of the solid phase of the solute to the liquid phase is given by

$$\Delta G^\mathrm{o} = -R_\mathrm{G} T \ln a_\mathrm{s}, \tag{2.3}$$

with R_G as the gas constant, and the solute activity $a_s = x_s\gamma_s$, where γ_s is the activity coefficient of the solute in the saturated solution. Using the Gibbs–Helmholtz equation

$$\frac{\mathrm{d}\Delta G^\mathrm{o}}{\mathrm{d}T} = -\Delta S^\mathrm{o} = \frac{\Delta G^\mathrm{o} - \Delta H^\mathrm{o}}{T}, \tag{2.4}$$

where ΔS^o is the entropy of the solution and ΔH^o is the enthalpy of solution (or dissolution), Eq. (2.3) may be written in the form of the van't Hoff equation

$$\frac{\mathrm{d}\ln x_\mathrm{s}}{\mathrm{d}T} = \frac{\Delta H^\mathrm{o}}{R_\mathrm{G}T^2} \,. \tag{2.5}$$

According to this relation the solubility of a solute is the same for all solutions and the enthalpy of dissolution $\Delta H^\mathrm{o} = \Delta H_\mathrm{m}$. Eq. (2.5) is usually expressed in the form of an Arrhenius-type relation

$$\ln x_\mathrm{s} = \frac{\Delta H_\mathrm{m}}{R_\mathrm{G}T_\mathrm{m}} - \frac{\Delta H_\mathrm{m}}{R_\mathrm{G}T} \,, \tag{2.6}$$

where ΔH_m is the enthalpy of melting, T_m is the melting temperature and $x_\mathrm{s} = 1$ for $T = T_\mathrm{m}$. This equation holds when molecules of solute and solvent are similar and are miscible in the entire concentration range. Solutions which follow Eq. (2.6) of the temperature dependence of solubility are called *ideal solutions*.

Real solutions are rarely ideal. However, they follow a relation similar to (2.6), i.e.

$$\ln x_\mathrm{s} = \frac{\Delta H_\mathrm{sol}}{R_G T_s} - \frac{\Delta H_\mathrm{sol}}{R_\mathrm{G}T} \,, \tag{2.7}$$

where the enthalpy of solution, denoted hereafter as ΔH_sol, is different from ΔH_m. Such solutions are known as *regular solutions*.

In ideal and regular solutions, the value of ΔH_m and ΔH_sol for the solutions are obtained from plots of $\ln x_\mathrm{s}$ against $1/T$, usually called as the van't Hoff plots, with intercept $A = \Delta H_\mathrm{m}/R_\mathrm{G}T_\mathrm{m}$ or $\Delta H_\mathrm{sol}/R_\mathrm{G}T_\mathrm{s}$ and slope $B = \Delta H_\mathrm{m}/R_\mathrm{G}$ or $\Delta H_\mathrm{sol}/R_\mathrm{G}$.

The temperature dependence of solubility x_s of a solute in a solution is also usually given by the empirical relation

$$\ln x_\mathrm{s} = a_1 + a_2 T + a_3 T^2 + \cdots, \tag{2.8}$$

where a_1, a_2, a_3, …, are constants and T is taken in K. In a narrow temperature interval, a linear relation has also been observed to represent the solubility data. In the case of solutes with $x_\mathrm{s} << 1$, linear and quadratic equations are also expected.

Plots of $\ln x_\mathrm{s}$ against $1/T$ for the different salts in water of Figure 2.1 are shown in Figure 2.2. In this figure the solubility is expressed in mole fraction of the anhydrous salts. As seen from the figure, for many substances the plots are straight lines representing a constant value of ΔH_sol for the substance in the entire temperature interval, but there are substances like Na_2SO_4, $KAl(SO_4)_2$ and $NH_4Al(SO_4)_2$, where the value of ΔH_sol is different in different temperature intervals for a substance and is indicated by the existence of transition points. In the case of Na_2SO_4, the value of ΔH_sol is even negative in the higher temperature interval. It is also observed that for substances which have a high temperature coefficient of solubility and are highly soluble, the plots of $\ln x_\mathrm{s}$ against $1/T$ do not yield straight lines as predicted by Eq. (2.7). This nonlinearity is possibly associated with the existence of several phase in a narrow range of temperature or with changes (association or dissociation of ions) taking place in the structure of solution.

Figure 2.3a and b illustrates examples of plots of lnx_s against $1/T$ for the solubility of *p*-terphenyl ($C_{18}H_{14}$) in benzene, dimethyl formamide (DMF) and methanol, and sulfomerazine ($C_{11}H_{12}N_4O_2S$) in water, methanol (MeOH) and 1-propanol (1-PrOH), respectively. The estimated values of the intercept *A* and the slope $B = \Delta H_{sol}/R_G$ from the plots and the corresponding values of the enthalpy ΔH_{sol} of solution are given in Table 2.1. Figure 2.4 shows another example of plots of lnx_s against $1/T$ for the solubility of cyromazine ($C_6H_{10}N_6$) in normal homologues of alcohols. The estimated values of constants intercept *A* and slope *B* of the plots are listed in Table 2.1. Values of constants *A* and *B* from the solubility data of cyromazine in water, acetone and acetic acid are also included in the table. The constants listed in the table are somewhat different from those reported by Zhang et al. (2018).

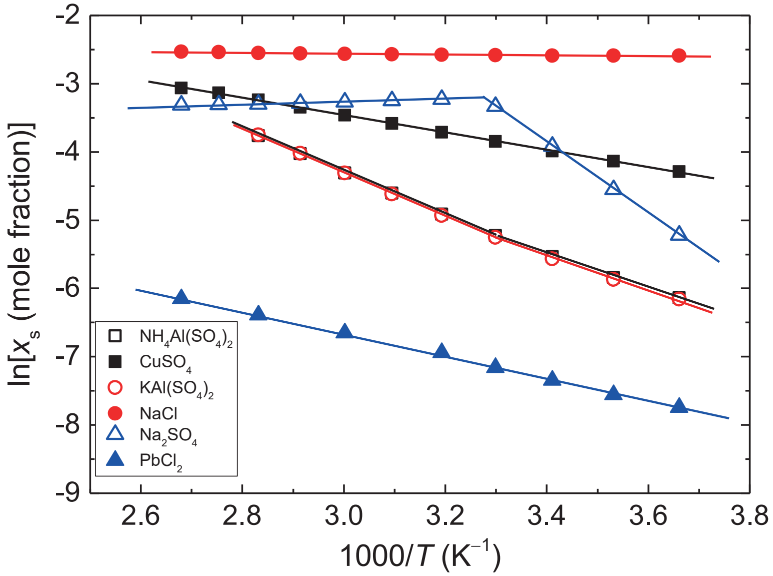

Figure 2.2. Plots of lnx_s against $1/T$ for different salts with data of Fig. 2.1.

The plots of the above figures for *p*-terphenyl, sulfomerazine and cyromazine in different solvents lead one to the inference that the solutions are regular. As seen from the table, the value of ΔH°_{sol} for a substance in different solvents differs from the enthalpy $\Delta H^{\circ-id}_{sol}$ of melting representing ideal solutions and $\Delta H^{\circ}_{sol} > \Delta H_m{}^{id}$ in some systems whereas $\Delta H^{\circ}_{sol} < \Delta H_m{}^{id}$ in others. These differences are intimately connected with the solvent of a compound and are associated with the nature of solute–solvent interactions. This aspect is discussed below.

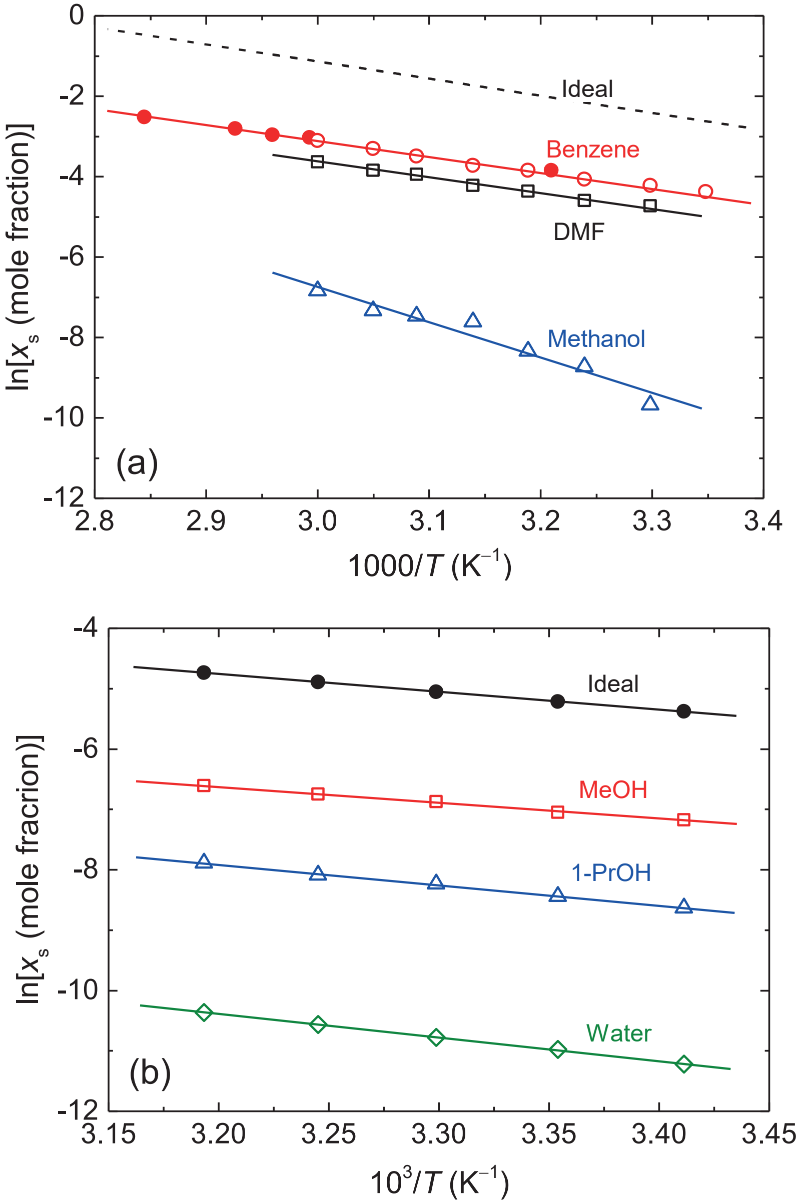

Figure 2.3. Plots of lnx_s against 1/T for (a) *p*-terphenyl and (b) sulfamerazine in different solvents. Solvents are indicated. Constants of the plots are listed in Table 2.1. Original data from: (a) Borecka et al. (1983), and (b) Delgado and Martinez (2014, 2015).

Table 2.1. Constant of Eq. (2.7) and values of $\Delta H^{\circ}_{\mathrm{sol}}$ and heat of mixing $\Delta H^{\circ}_{\mathrm{mix}}$ for *p*-terphenyl, sulfamerazine and cyromazine in different solvents

Substances	Solvent	*A*	$\Delta H^{\circ}_{\mathrm{sol}}/R_G$ (kK^{-1})	$\Delta G^{\circ}_{\mathrm{sol}}$ (kJ mol^{-1})	$\Delta H^{\circ}_{\mathrm{sol}}$ (kJ mol^{-1})	$\Delta H^{\circ}_{\mathrm{mix}}$ (kJ mol^{-1})
p-terphenyl[a]	Ideal	8.776	4.270	12.28	35.50	--
	Benzene	7.820	3.644	9.62	30.31	−5.19
	DMF	7.693	3.428	11.09	31.44	−4.06
	Methanol	20.10	8.660	21.15	74.32	38.82
Sulfamerazine[b]	Ideal	4.709	2.958	12.73	24.59	--
	Methanol	1.795	2.631	17.36	21.88	−2.71
	1-Propanol	2.965	3.400	20.80	28.27	3.68
	Water	2.114	3.907	27.16	32.48	7.89
Cyromazine[c]	Ideal	5.898	2.90	9.21	24.11	--
	Methanol	0.467	1.893	14.56	15.72	−8.39
	Ethanol	3.955	3.113	15.90	25.88	1.77
	1-Propanol	4.407	3.277	16.12	27.99	3.88
	1-Butanol	4.505	3.330	16.31	26.69	2.58
	1-Pentanol	4.521	3.353	16.46	27.88	3.77
	1-Hexanol	5.749	3.768	16.81	31.33	7.22
	1-Heptanol	9.283	4.998	18.11	41.56	17.45
	Acetone	0.321	2.257	17.96	18.77	−5.34
	Acetic acid	7.996	3.627	9.96	30.16	6.05
	Water	2.261	2.622	16.09	22.25	−1.86

[a] Borecka et al. (1982); [b] Delgado and Martinez (2014, 2015); [c] Zang et al. (2018).

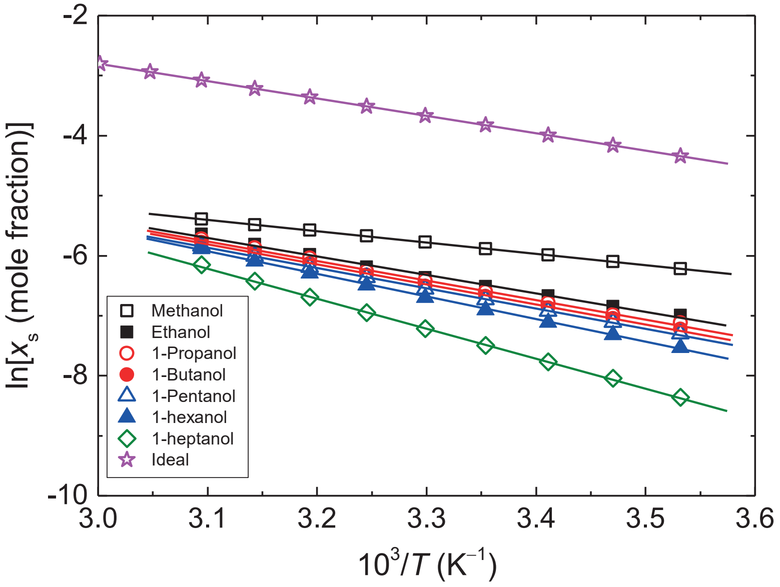

Figure 2.4. Plots of $\ln x_s$ against $1/T$ for cyromazine in homologues of normal alcohols. Solvents are indicated. Constants of the plots are listed in Table 2.1. Original data from Zhang et al. (2018).

2.2.2. Ideal and real solubilities

In ideal solutions the solution activity $a_s = x_s = 1$ and the Gibbs free energy of melting, ΔG_m, is zero at the melting point T_m (cf. Eq. (2.3)). Then the entropy of melting $\Delta S_m = \Delta H_m/T_m$ and Eq. (2.6) for the ideal solubility x_s^{id} of the substance may be written in the form

$$\ln x_s^{id} = -\frac{\Delta S_m}{R_G T}(T_m - T), \tag{2.9}$$

where ΔS_m has the units: J·mol^{-1}·K^{-1}, and the gas constant $R_G = 8.3145$ J·mol^{-1}·K^{-1}. Incorporation of the activity coefficient γ_s of the solution gives the real solubility of the substance as

$$\ln x_s = -\frac{\Delta S_m}{R_G T}(T_m - T) - \ln \gamma_s = -\frac{\Delta S_{sol}}{R_G T}(T_{sol} - T), \tag{2.10}$$

where ΔS_{sol} is the entropy of solution at T_{sol} and is given by: $\Delta S_{sol} = R_G A$. The entropy of fusion, ΔS_m, is equal to the entropy of the liquid minus entropy of the crystalline solid, denoted by S_L and S_S, respectively, given by (Yalkowsky and Valvani, 1980)

$$\Delta S_m = S_L - S_S = -R_G \ln\left(\frac{W_S}{W_L}\right) = -R_G \ln P_m, \tag{2.11}$$

where P_m is the ratio of the number of ways W_S of achieving the solid to the number of ways W_L of achieving the liquid. The entropy of fusion is the sum of contributions due to: (1) dismantling of solid arrangement to form the liquid (translational entropy), (2) randomization of orientation of molecules in the liquid (rotational entropy), and (3) internal conformation of molecules in the liquid (intenal or conformational entropy). Contributions of the latter entropies become important in long-chain molecules. It has been argued (Yalkowsky and Valvani, 1980) that the molecules of organic compounds having less than five units in their linear chains may be considered as rigid molecules, but the internal entropy of fusion, ΔS_{int}, of the compounds with more than five units in the linear chains of their molecules increases linearly with the number of carbon and heteroatoms in the chains.

Eq. (2.10) enables to predict the solubility of different substances from a knowledge of two parameters: ΔS_m and $\ln\gamma_s$ (Yalkowsky and Valvani, 1980). This relation represents ideal solubilities for solutes in solvents of similar polarity. However, the ideal solubility of a solute affects its solubility in a solvent and requires estimation of the activity coefficient γ_s. Since the work of Yalkowsky and Valvani (1980), prediction of the solubility of drugs in water has drawn enormous interest in the field of their design and discovery and the importance of octanol–water partition coefficient P, which is approximately equal to the activity coefficient γ_s of the solute in water-saturated octanol, has been recognized, with $\ln P$ as a criterion of drug's lipophilicity. A brief account of different models and their predictions of the solubility of pharmaceutical compounds in aqueous and nonaqueous solvents is given by Emami et al. (2015).

2.3. Thermodynamics of solutions

2.3.1. Temperature dependence of solubility

According to the thermodynamics of solutions at solid–solvent equilibrium, the solubility x_s of a substance in the solution at a given temperature T may be given by (Nordström and Rasmuson, 2009)

$$\ln x_\mathrm{s} = \frac{\Delta H_\mathrm{m}}{R_\mathrm{G}}\left(\frac{1}{T_\mathrm{m}} - \frac{1}{T}\right) + \frac{\Delta C_p}{R_\mathrm{G}}\left(\int_{T_\mathrm{m}}^{T} \frac{\mathrm{d}T}{T} - \frac{1}{T}\int_{T_\mathrm{m}}^{T} \mathrm{d}T\right) - \ln \gamma_\mathrm{s}\,. \tag{2.12}$$

In Eq. (2.12), ΔC_p is the difference between the molar heat capacity of the substance in the solid form and the molar heat capacity of the hypothetical supercooled melt solution, both at the equilibrium solution temperature T. When $(T_\mathrm{m}-T)/T_\mathrm{m} << 1$, the two terms contained in the second brackets are approximately equal and the ΔC_p term can be neglected. Then the solubility x_s of the substance reduces to the form of Eq. (2.6) and describes its ideal solubility.

The heat capacity ΔC_p of supercooled melts at temperatures significantly below T_m is usually not available. It is frequently assumed that ΔC_p is negligible, but it has been recognized that this is a poor assumption and is related to the entropy ΔS_m of melting. Following Nordström and Rasmuson (2009), we assume that

$$\Delta C_p = \sigma \Delta S_\mathrm{m}\,, \tag{2.13}$$

where σ is an empirical proportionality constant. Substitution of Eq. (2.13) in Eq. (2.12) gives

$$\ln x_\mathrm{s} = \frac{\Delta H_\mathrm{m}}{R_\mathrm{G}}\left[\frac{1-\sigma}{T_\mathrm{m}} - \frac{1-\sigma}{T} + \frac{\sigma}{T_\mathrm{m}}\ln\left(\frac{T}{T_\mathrm{m}}\right)\right] - \ln \gamma_\mathrm{s}\,, \tag{2.14}$$

where $0 < \sigma < 1$. Assuming that the change in $\ln\gamma_\mathrm{s}$ of saturated solution with temperature is negligible, from Eq. (2.14) one obtains

$$\Delta H_\mathrm{sol} = \Delta H_\mathrm{m}\frac{T}{T_\mathrm{m}}\left\{1 + \sigma \ln\left(\frac{T}{T_\mathrm{m}}\right)\right\} - R_\mathrm{G} T \ln x_\mathrm{s}\,, \tag{2.15}$$

which with Eq. (2.4) gives

$$\frac{\Delta G_\mathrm{sol} - \Delta H_\mathrm{sol}}{T} = -\Delta S_\mathrm{sol} = \frac{\Delta H_\mathrm{m}}{T_\mathrm{m}}\left\{1 + \sigma \ln\left(\frac{T}{T_\mathrm{m}}\right)\right\}, \tag{2.16}$$

where $\Delta G_\mathrm{sol} = -R_\mathrm{G} T \ln x_\mathrm{s}$.

Eq. (2.14) is the general solubility relation. According to this relation the molar solubility x_s of a solute in a solvent depends on the intrinsic properties (i.e. ΔH_m and T_m) of the solute and the nature of solute–solvent interactions (i.e. proportionality constant σ and activity coefficient γ_s). As seen from Eqs. (2.15) and (2.16), enthalpy and entropy of dissolution, ΔH_{sol} and ΔS_{sol}, also depend on these factors. The assumption of $\ln\gamma_s = 0$ (i.e. $\gamma_s = 1$) in Eq. (2.14) corresponds to the validity of Raoult's law. Depending on whether $\gamma_s < 1$ or $\gamma_s > 1$, negative or positive deviation from the Raoult's law behavior is predicted. The role of activity coefficient γ_s in these deviations is discussed by Nordström and Rasmuson (2009). However, the effect of heat capacity ΔC_p on molar solubility x_s and enthalpy ΔH_s and entropy ΔH_s of dissolution may be explained in terms of the proportionality constant σ with its possible values between 0 and 1. The condition $\sigma = 0$ implies that the effect of ΔC_p on solubility x_s is neglibible, but $\sigma = 1$ means that its effect on x_s is the maximum.

Eq. (2.14) may be written in the form of an Apelblat-type equation (Apelblat and Manzurola, 1999; Manzurola and Apelblat, 2002)

$$\ln x_s = A + \frac{B}{T} + C \ln T\,, \tag{2.17}$$

where

$$A = \frac{\Delta H_m}{R_G T_m}(1 - \sigma - \sigma \ln T_m) - \ln \gamma_s\,, \tag{2.18}$$

$$B = \frac{\Delta H_m (1-\sigma)}{R_G}\,, \tag{2.19}$$

$$C = \frac{\Delta H_m \sigma}{R_G T_m}\,. \tag{2.20}$$

When $T/T_m << 1$, Eq. (2.14) takes the form

$$\ln x_s = A + \frac{B}{T} + CT\,, \tag{2.21}$$

where

$$A = \frac{\Delta H_m}{R_G T_m} - \ln \gamma_s\,, \tag{2.22}$$

$$B = \frac{\Delta H_m (1-\sigma)}{R_G}\,, \tag{2.23}$$

$$C = \frac{\Delta H_m \sigma}{R_G T_m^2}\,. \tag{2.24}$$

When $\ln\gamma_s = 0$, with the constant $\sigma = 0$ Eq. (2.14) reduces to the equation of ideal solutions (see Eqs. (2.7) and (2.8)). However, when $\sigma = 1$ Eq. (2.14) may be written in the form of a Hildebrand-type relation (Hildebrand and Scott, 1962)

$$\ln x_\mathrm{s} = A + B \ln T\,, \tag{2.25}$$

where

$$A = -\frac{\Delta H_\mathrm{m}}{R_\mathrm{G} T_\mathrm{m}} \ln T_\mathrm{m}\,, \tag{2.26}$$

$$B = \frac{\Delta H_\mathrm{m}}{R_\mathrm{G} T_\mathrm{m}}\,. \tag{2.27}$$

Eqs. (2.7), (2.17), (2.21) and (2.25) are the commonly used equations describing the temperature dependence of solubility of various compounds.

Apart from the above equations, the following linear and quadratic relations are also employed (see Eq. (2.8)):

$$\ln x_\mathrm{s} = A + BT\,, \tag{2.28}$$

$$\ln x_\mathrm{s} = A + BT + CT^2\,. \tag{2.29}$$

In cases where $x_\mathrm{s} << 1$, these equations transform to linear and quadratic dependence of x_s on T.

Different solubility equations and values of enthalpy $\Delta H_\mathrm{s}/R_\mathrm{G}$ of solution following from these equations are summarized in Table 2.2.

Table 2.2. Commonly used solubility equations and corresponding $\Delta H_\mathrm{s}/R_\mathrm{G}$

Equation	$\ln x_\mathrm{s}$	$\Delta H_\mathrm{sol}/R_\mathrm{G}$
(2.7)	$A+BT^{-1}$	$-B$
(2.17)	$A+BT^{-1}+C\ln T$	$-B+CT$
(2.21)	$A+BT^{-1}+CT$	$-B+CT^2$
(2.25)	$A+B\ln T$	BT
(2.28)	$A+BT$	BT^2
(2.29)	$A+BT+CT^2$	BT^2+2CT^3

2.3.2. The λh model of Buchowski et al. (1980)

The third term on the right-hand side of Eq. (2.12) is the activity coefficient γ_s of saturated solution. Its value depends on the properties of both solute and solvent, the composition of the solution and the solution temperature. Expressions have been given for the calculations of the activity coefficient of different solutes in solutions (Hildebrand and Scott, 1950; Renon and Prausnitz, 1968; Wilson, 1964).

The ions or molecules of a solute are expected to exist as individual entities only in dilute solutions when the average distance between them is relatively large. In these situations alone the activity coefficient is unity. However, when solute concentration in the solution increases, the distance between the ions or molecules of the solute decreases and they begin to associate and form dimers, trimers and higher multimers. Consequently, the solute concentration in the solution is the sum of mole fractions of all of its multimers, Σx_i, present in it and is a measure of solute association. This process of solute association is related to the activity coefficient of the solution. According to the theory of ideal associated solutions, $\Sigma x_i = 1-\alpha_B$, where α_B is the activity of the solvent B. These arguments also hold in saturated solutions where the solubility of an associating solute in nonpolar solvents depends strongly on the activity coefficient γ_s in saturated solution, and the solubility curve deviates from the ideal.

Starting from the activity α_B of the solvent at saturation as an implicit function of temperature, Buchowski et al. (1980) derived the relation

$$\frac{\mathrm{d}\ln(1-\alpha_B)_{\mathrm{sat}}}{\mathrm{d}(1/T)} = \lambda h\,, \tag{2.30}$$

where

$$\frac{\alpha_B}{1-\alpha_B}\frac{x_A}{x_B} \equiv \lambda\,, \tag{2.31}$$

and the parameter

$$h = \frac{\Delta H_{\mathrm{m}} + \Delta H_{\mathrm{mix}}}{R_G} = \frac{\Delta H_{\mathrm{sol}}}{R_G}\,. \tag{2.32}$$

In Eq. (2.31) x_A and x_B are concentrations of solute A and solvent B, respectively, and λ is the mean association number defined as the mean value of solute molecules per multimer associate. Integration of Eq. (2.30) from T_m to T gives

$$-\ln(1-\alpha_B)_{\mathrm{sat}} = \lambda h\left(\frac{1}{T} - \frac{1}{T_m}\right). \tag{2.33}$$

Eq. (2.31) may be rewritten in the form

$$\lambda\left(\frac{1-x_A}{x_A}\right) = \frac{\alpha_B}{1-\alpha_B} = \frac{1}{1-\alpha_B} - 1\,, \tag{2.34}$$

which gives

$$-\ln(1-\alpha_B) = \ln\left[1+\lambda\left(\frac{1-x_A}{x_A}\right)\right]. \tag{2.35}$$

Finally, on replacing the concentration x_A of the solute by its solubility x_s in the solution, from Eqs. (2.33) and (2.35) one obtains

$$\ln\left[1+\lambda\left(\frac{1}{x_\mathrm{s}}-1\right)\right]=\lambda h\left(\frac{1}{T_\mathrm{m}}-\frac{1}{T}\right). \tag{2.36}$$

The values of constants λ and h are temperature independent but depend on the solute–solvent system. They are obtained by regressing the $x_\mathrm{s}(T)$ data for a system.

2.3.3. Apparent thermodynamic functions of solution

During the dissolution of a solute in a solvent, the thermodynamic functions of solution are changes involved in the standard Gibbs free energy G, the enthalpy H and the entropy S at equilibrium described by the Gibbs–Helmholtz equation in the form (see Eq. (2.4))

$$\Delta G_\mathrm{sol}^\mathrm{o}=\Delta H_\mathrm{sol}^\mathrm{o}-T\Delta S_\mathrm{sol}^\mathrm{o}. \tag{2.37}$$

The standard enthalpy change $\Delta H_\mathrm{sol}^\mathrm{o}$ of solution is usually obtained by plotting $\ln x_\mathrm{s}$ of a solute in the solution as a function of $1/T$ according to Eq. (2.7). However, the standard Gibbs free energy change $\Delta G_\mathrm{sol}^\mathrm{o}$ of the solution at equilibrium is related to the saturation temperature T which varies between some temperature interval. Therefore, a simple procedure involving the use the harmonic mean saturation temperature T_hm has been suggested to estimate $\Delta G_\mathrm{sol}^\mathrm{o}$ (Krug et al., 1976; Delgado and Martinez, 2014, 2015). The harmonic mean saturation temperature T_hm is determined by

$$T_\mathrm{hm}=\frac{n}{\sum_{i=1}^{n}(1/T)_i}, \tag{2.38}$$

where n is the number of saturation temperatures of solubility data. Then the calculated values of the slope $\Delta H_\mathrm{sol}^\mathrm{o}/R_\mathrm{G}$ and the intercept A_1 from plots of $\ln x_\mathrm{s}$ against $(1/T-1/T_\mathrm{hm})$ enable to obtain $\Delta H_\mathrm{sol}^\mathrm{o}$ and $\Delta G_\mathrm{sol}^\mathrm{o}$ according to the relations

$$\frac{\partial \ln x_\mathrm{s}}{\partial(1/T-1/T_\mathrm{hm})}=-\frac{\Delta H_\mathrm{sol}^\mathrm{o}}{R_\mathrm{G}}, \tag{2.39}$$

and

$$\Delta G_\mathrm{sol}^\mathrm{o}=-R_\mathrm{G}T_\mathrm{hm}\cdot A_1, \tag{2.40}$$

where

$$R_\mathrm{G}T_\mathrm{hm}A_1=R_\mathrm{G}T_\mathrm{hm}A-\Delta H_\mathrm{sol}^\mathrm{o}. \tag{2.41}$$

Eq. (2.39) follows from Eq. (2.7) where the saturation temperature T_s is replaced by T_hm. Then the entropy change $\Delta S_\mathrm{sol}^\mathrm{o}$ for solution at T_hm is given by Eq. (2.4), with T

replaced by T_{hm}.

It should be noted that $\Delta G^{\mathrm{o}}_{\mathrm{sol}}$ is different from $\Delta G^{\mathrm{o-id}}_{\mathrm{sol}}$ for ideal solution. The value of $\Delta G^{\mathrm{o-id}}_{\mathrm{sol}}$ is obtained from Eq. (2.40) taking the value of the intercept equal to $\Delta H^{\mathrm{o-id}}_{\mathrm{sol}} / R_{\mathrm{G}}$, where $\Delta H^{\mathrm{o-id}}_{\mathrm{sol}}$ is usually obtained experimentally using differential scanning calorimetry. The values of $\Delta G^{\mathrm{o}}_{\mathrm{sol}}$ and $\Delta H^{\mathrm{o}}_{\mathrm{sol}}$ calculated from the original solubility data of *p*-terphenol ($C_{18}H_{14}$), sulfamerazine ($C_{11}H_{12}N_4O_2S$) and cyromazine ($C_6H_{10}N_6$) in different solvents are summarized in Table 2.1 using the above procedure and note that their values for ideal solubility curves in the table refer to $\Delta G^{\mathrm{o-id}}_{\mathrm{sol}}$ and $\Delta H^{\mathrm{o-id}}_{\mathrm{sol}}$ with reference to the harmonic mean temperature T_{hm}. These data for *p*-terphenyl were obtained from its enthalpy of melting ΔH_{m} and melting temperature T_{m} reported by Chang (1983), whereas those for sulfamerazine and cyromazine were taken from Delgado and Martinez (2014, 2015) and Zhang et al. (2018), respectively.

From Table 2.1 one notes that the calculated value of the Gibbs free energy $\Delta G^{\mathrm{o}}_{\mathrm{sol}}$ for the dissolution of a compound in different solvents is either comparable or greater than the Gibbs free energy $\Delta G^{\mathrm{o-id}}_{\mathrm{sol}}$ for ideal solution. However, depening on the solvent, the enthalpy of solution $\Delta H^{\mathrm{o}}_{\mathrm{sol}}$ of a compound can be greater as well as lower than the enthalpy of solution $\Delta H^{\mathrm{o-id}}_{\mathrm{sol}}$ for its ideal solution. For the three compounds considered here, $\Delta H^{\mathrm{o}}_{\mathrm{sol}} > \Delta H^{\mathrm{o-id}}_{\mathrm{sol}}$ in most of the solvents, but there are some solvents where $\Delta H^{\mathrm{o}}_{\mathrm{sol}} < \Delta H^{\mathrm{o-id}}_{\mathrm{sol}}$. Examples of the latter are dissolution of *p*-terphenyl in benzene and DMF, sulfamerazine in methanol, and cyromazine in methanol, acetone and water. In the case of dissolution of cyromazine in acetone, both $\Delta G_{\mathrm{sol}} > \Delta G_{\mathrm{m}}{}^{\mathrm{id}}$ and $\Delta H^{\mathrm{o}}_{\mathrm{sol}} > \Delta H^{\mathrm{o-id}}_{\mathrm{sol}}$, but the changes in their values are not large.

Figure 2.5a and b shows the data of enthalpy $\Delta H^{\mathrm{o}}_{\mathrm{sol}}$ of solution and entropy-related term $T_{\mathrm{hm}}\,\Delta S^{\mathrm{o}}_{\mathrm{sol}}$ on Gibbs free energy change $\Delta G^{\mathrm{o}}_{\mathrm{sol}}$ of solution for *p*-terphenyl and sulfamerazine, respectively, in some selected solvents, whereas Figure 2.6 shows similar data for the dissolution of cyromazine in different solvents including higher homologues of methanol. The dashed horizontal lines in these figures show the values of $\Delta H^{\mathrm{o}}_{\mathrm{sol}}$ for the ideal solution behavior of the compound. The values of $T_{\mathrm{hm}}\,\Delta S^{\mathrm{o}}_{\mathrm{sol}}$ for the dissolution of the compounds in different solvents were calculated using Eq. (2.37). As seen from these figures, the value of $\Delta H^{\mathrm{o}}_{\mathrm{sol}}$ shows a general tendency to increase with increasing $\Delta G^{\mathrm{o}}_{\mathrm{sol}}$ for the dissolution of a compound in different solvents. These observations are associated with differences in the interactions between solute and solvent molecules in the solution during dissolution and are usually discussed in terms of apparent thermodynamic functions of mixing.

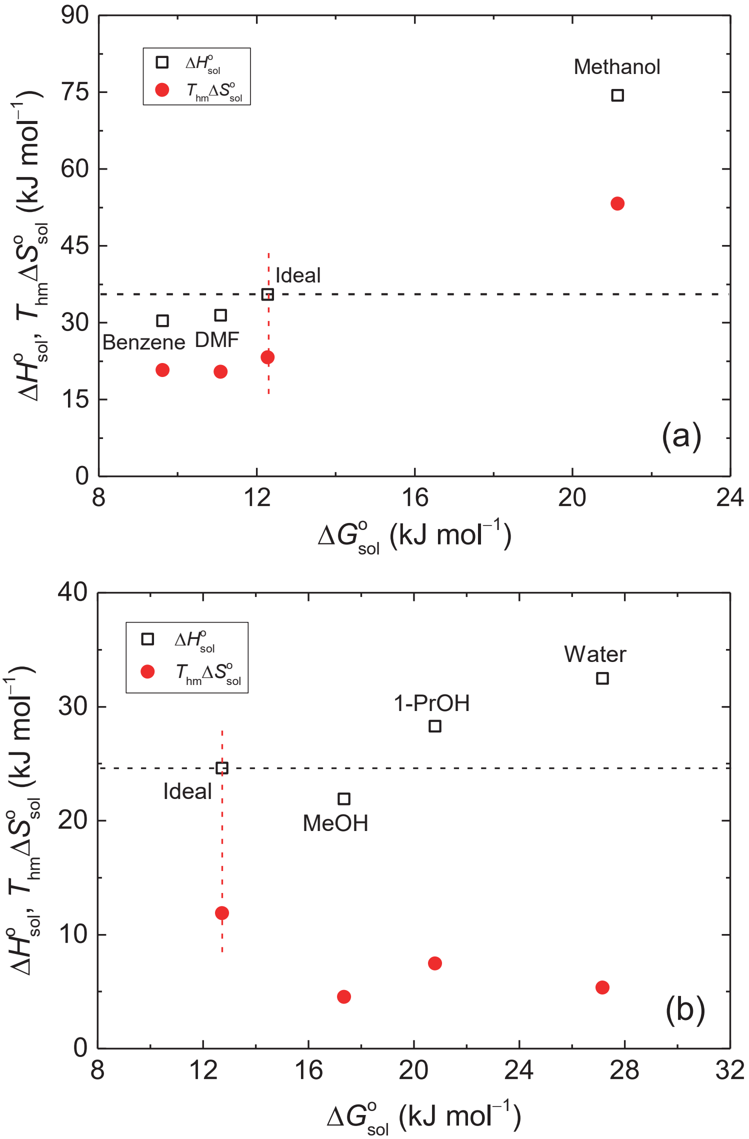

Figure 2.5. Dependence of ΔH^o_{sol} and $T_{hm}\Delta S_{sol}{}^o$ on Gibbs free energy change ΔG^o_{sol} of solution for (a) *p*-terphenyl and (b) sulfamerazine in selected solvents. Solvents are indicated in the plots. Data are from Table 2.1.

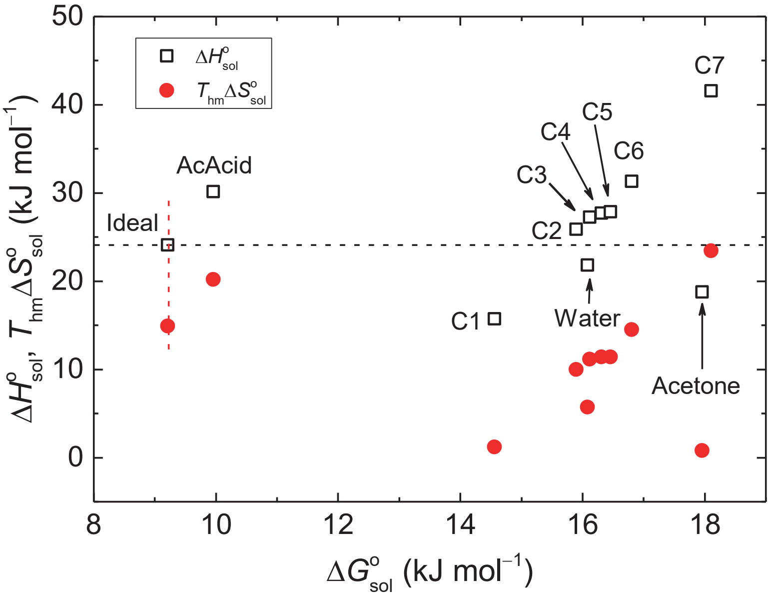

Figure 2.6. Dependence of ΔH^o_{sol} and $T_{hm}\Delta S_{sol}{}^o$ on Gibbs enthalpy ΔG^o_{sol} of solution for cyromazine in different solvents. Solvents are indicated in the plots. Data are from Table 2.1.

2.3.4. Apparent thermodynamic functions of mixing

Dissolution of a solute to yield its saturated solution of concentration x_s in a solvent is associated with phase change of the solid to liquid phase. This process occurs in successive steps involving fusion of the solute, cooling of the liquid solute to the saturation temperature, and mixing of the supercooled liquid solute with the solvent. These steps enable to write different thermodynamic functions of mixing as follows:

$$\Delta G^o_{sol} = \Delta G^{o-id}_{sol} + \Delta G^o_{mix}, \tag{2.42}$$

$$\Delta H^o_{sol} = \Delta H^{o-id}_{sol} + \Delta H^o_{mix}, \tag{2.43}$$

$$\Delta S^o_{sol} = \Delta S^{o-id}_{sol} + \Delta S^o_{mix}, \tag{2.44}$$

where ΔH^o_{mix}, ΔS^o_{mix} and ΔG^o_{mix} are changes in the enthalpy, entropy and Gibbs free energy of mixing, respectively, and ΔH^{o-id}_{sol}, ΔS^{o-id}_{sol} and ΔG^{o-id}_{sol} are changes in the enthalpy, entropy and Gibbs free energy of ideal solution, respectively, with reference to the harmonic mean temperature T_{hm}. Obviously, $\Delta H^o_{mix} \neq 0$, $\Delta S^o_{mix} \neq 0$ and $\Delta G^o_{mix} \neq 0$ for regular solutions, and $\Delta H^o_{mix} = 0$ and $\Delta S^o_{mix} \neq 0$ for ideal solutions. In other words, in regular solutions $\Delta H^o_{sol} \neq \Delta H^{o-id}_{sol}$.

The theoretical models of regular solutions are based on creating a mixture of two components one of which is a solvent and the other is a solute and the dimensions of atoms or molecules composing them are the same. However, real solutions are not so simple regarding the dimensions of atoms/molecules of components, the physical nature of their composition as well as the total number of components present in them. In aqueous solutions of salts for example, their molecules are dissociated into cations and anions which exist as solvated entities of dimensions differing from that of water molecules.

Ideal solution relationship approximates the behavior of regular systems for mixtures of chemically similar substances and applies at low solute concentrations. In ideal solutions the enthalpy $\Delta H^{\text{o}}_{\text{mix}}$ of mixing of the two components (solute and solvent) is zero and the entropy $\Delta S^{\text{o}}_{\text{mix}}$ of mixing is determined only by the mole fraction x_i of the components. Then (cf. Eq. (2.16))

$$\Delta S^{\text{o}}_{\text{mix}} = -R_{\text{G}} \ln x_i \, . \tag{2.45}$$

In regular solutions both these conditions are not fulfilled. The deviation of a regular solution from an ideal one is caused by the difference in the interaction energies between the molecules/ions of solute and solvent in the solution.

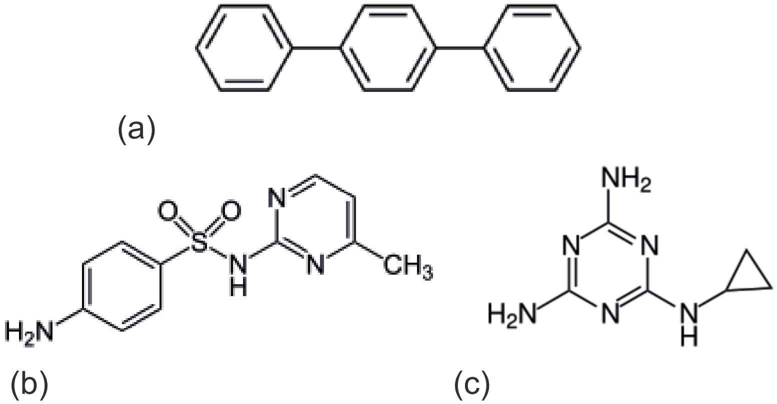

Figure 2.7. Molecular structures of (a) *p*-terphenyl, (b) sulfamerazine, and (c) cyromazine.

We consider here the data of enthalpies of mixing associated with the solubility of *p*-terphenol ($C_{18}H_{14}$), sulfamerazine ($C_{11}H_{12}N_4O_2S$) and cyromazine ($C_6H_{10}N_6$) in different solvents and note that all the three are organic compounds containing decreasing number of benzene-ring structures, as shown in Figure 2.7. The starting data of the standard Gibbs free energy change $\Delta G^{\text{o}}_{\text{mix}}$, the standard enthalpy change $\Delta H^{\text{o}}_{\text{mix}}$ and the standard entropy term $T_{\text{hm}}\Delta S^{\text{o}}_{\text{mix}}$ for mixing for the compounds in different solvents were obtained by using Eqs. (2.42), (2.43) and (2.44) with the values of the enthalpies $\Delta G^{\text{o}}_{\text{sol}}$ and $\Delta H^{\text{o}}_{\text{sol}}$ given in Table 2.1.

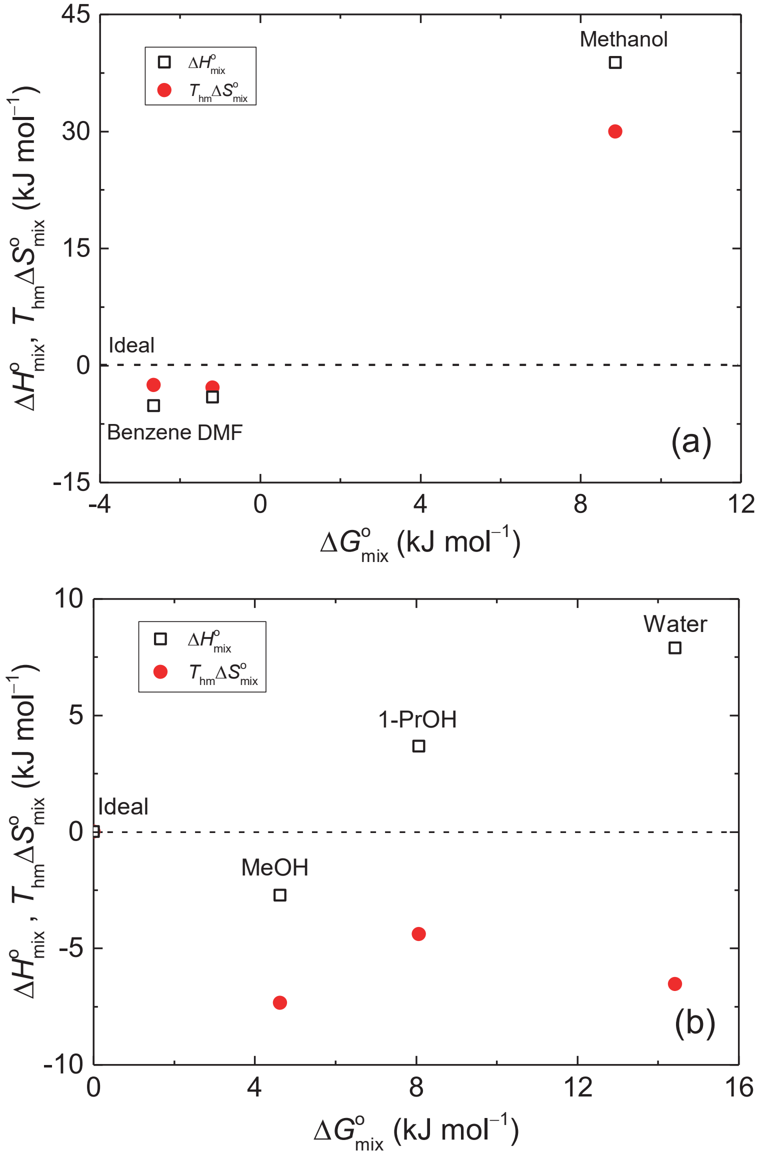

Figure 2.8. Data of $\Delta H^{o}_{\text{mix}}$ and $T_{\text{hm}}\Delta S^{o}_{\text{mix}}$ as a function of Gibbs free energy change $\Delta G^{o}_{\text{mix}}$ of mixing for (a) *p*-terphenyl and (b) sulfamerazine in different solvents, respectively. Original data from Table 2.1.

In regular solutions the value of $\Delta H^{o}_{\text{mix}}$ is as an indicator of solute–solvent, solute–solute and solvent–solvent interactions. When $\Delta H^{o}_{\text{mix}}$ is positive, the ideal solubility is higher than the real one. This means that solute–solute and solvent–solvent interactions are stronger than solute–solvent interactions. In this case, ionic/molecular pairs, triplets, quadruplets are likely to exist in solution. When $\Delta H^{\circ}_{\mathrm{mix}}$ is negative, the ideal solubility is lower than the real one, implying that solute–solvent interactions are stronger than the others.

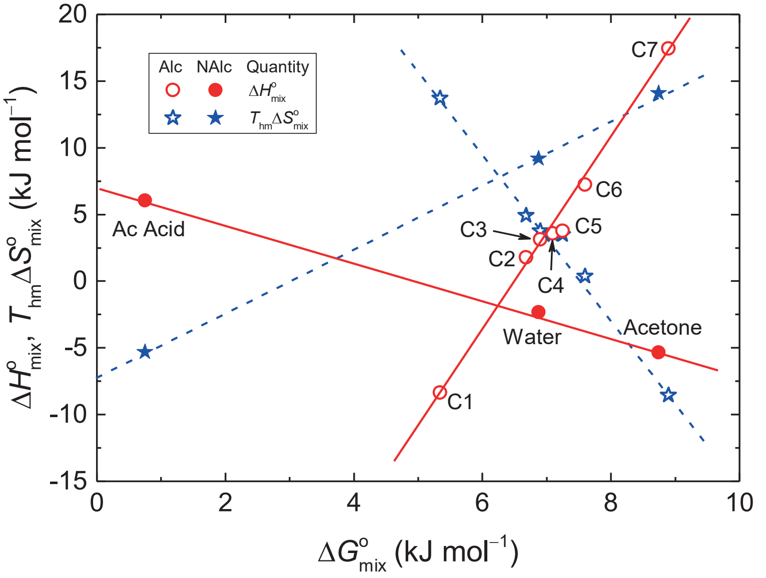

Figure 2.9. Plots of $\Delta H^{\circ}_{\mathrm{mix}}$ and $T_{\mathrm{hm}}\Delta S^{\circ}_{\mathrm{mix}}$ on Gibbs enthalpy change $\Delta G^{\circ}_{\mathrm{mix}}$ of mixing for cyromazine in different alcohol homologue and nonalcohol solvents. Linear relationships between $\Delta H^{\circ}_{\mathrm{mix}}$ and $\Delta G^{\circ}_{\mathrm{mix}}$ (solid lines) and between $T_{\mathrm{hm}}\Delta S^{\circ}_{\mathrm{mix}}$ and $\Delta G^{\circ}_{\mathrm{mix}}$ (dashed lines) for two groups of solvents may be noted. Solvents are indicated in the plots. Original data from Table 2.1.

Figure 2.8a and b shows the data of standard enthalpy change $\Delta H^{\circ}_{\mathrm{mix}}$ and standard entropy term $T_{\mathrm{hm}}\Delta S^{\circ}_{\mathrm{mix}}$ for mixing as a function of the standard Gibbs free energy change $\Delta G^{\circ}_{\mathrm{mix}}$ of mixing for *p*-terphenyl and sulfamerazine in different solvents, respectively. It may be seen from these figures that $\Delta H^{\circ}_{\mathrm{mix}}$ of the two solutes shows a general tendency to increase with increasing $\Delta G^{\circ}_{\mathrm{mix}}$ for different solvents but $T_{\mathrm{hm}}\Delta S^{\circ}_{\mathrm{mix}}$ shows a somewhat irregular trend. Figure 2.9 shows the data of $\Delta H^{\circ}_{\mathrm{mix}}$ and $T_{\mathrm{hm}}\Delta S^{\circ}_{\mathrm{mix}}$ as a function of $\Delta G^{\circ}_{\mathrm{mix}}$ for cyromazine in different alcohols and nonalcohols. In this case, one observes that the value of $\Delta H^{\circ}_{\mathrm{mix}}$ increases practically linearly with an increase in $\Delta G^{\circ}_{\mathrm{mix}}$ in *n*-alcohols but an opposite trend of decreasing $\Delta H^{\circ}_{\mathrm{mix}}$ in nonalcohols (i.e. acetone, acetic acid and water). In contrast to the trends of $\Delta H^{\circ}_{\mathrm{mix}}$ with $\Delta G^{\circ}_{\mathrm{mix}}$ mentioned above, with increasing $\Delta G^{\circ}_{\mathrm{mix}}$ the value of $T_{\mathrm{hm}}\Delta S^{\circ}_{\mathrm{mix}}$ decreases practically linearly in *n*-alcohols and increases linearly in nonalcohol solvents.

However, in the case of *n*-alcohols there is insignificant variation in the values of $\Delta H^{\circ}_{\text{mix}}$ and $T_{\text{hm}}\Delta S^{\circ}_{\text{mix}}$ with $\Delta G^{\circ}_{\text{mix}}$ for 1-propanol, 1-butanol and 1-pentanol (i.e. $3 < N < 5$). The causes of the above trends are associated with the structures of solute and solvent molecules. These trends are discussed below.

2.4. Effect of nature of solvents on solute solubility

It is well known that the solubility of inorganic salts decreases with a decrease in the dielectric constant ε of solvent as a result of weakening of solute–solvent interactions and increasing tendency of solvent and solute ions to self-associate. This observation of the effect of solvent on the solubility of inorganic salts is associated with the process of solvation of ions in the solvent, and is explained by the Born model for ion–solvent interactions (see Section 1.5.1; Eq. (1.43)). Since the free energy of ion–solvent interactions is related to the enthalpy of dissolution (Section 2.2), this model predicts that the solubility of an electrolyte decreases with a decrease in the dielectric constant ε of the solvent.

The relation between solubility m_s (expressed in molality) of an electrolyte and the dielectric constant ε of the solvent is of the form (Izmailov, 1970)

$$\ln m_s = \text{const} - \frac{(\beta - \beta' \mu)}{\varepsilon}, \tag{2.46}$$

where β and β' are constants, and μ is the dipole moment of a solvent. The constant β is much greater than β'. Therefore, the decrease in solubility with ε is determined by the value of the dipole moment μ of the solvent. Values of the dielectric constant ε and the dipole moment μ of some selected solvents are given in Table 2.3.

The dependence of $\ln m_s$ on $1/\varepsilon$ for AgCl and CsCl in alcohols $\mu \approx 1.7$ and ketones $\mu \approx 2.8$ is illustrated in Figure 2.10. As seen from the figure, the nature of the curves for AgCl and CsCl is the similar in alcohols and ketones. However, the value of the slope of the plots for AgCl and CsCl is different in alcohols and ketones due to a ifference in the value of μ, and the slopes of the straight lines for AgCl and CsCl are similar. Since the dipole moment μ of water is close to that of alcohols, the solubility of the salts follows the curve for alcohols but markedly differs from that for ketones.

The linear dependence of $\ln m_s$ against $1/\varepsilon$ is usually observed in a series of solvents with relatively high values of ε (ε exceeding about 15). In a series of solvents with very low ε, the experimental solubility is higher than the one predicted by Eq. (2.46). This deviation is due to the association of anions and cations of the salt to form ionic pairs, triplet, etc., such that the salt solubility is higher than that due to free ions. This feature is directly related to the positive enthalpy $\Delta H^{\circ}_{\text{mix}}$ of mixing discussed in the preceding subsection.

Table 2.3. Values of dielectric constant ε, dipole moment μ, and relative polarity of some selected solvents*

Solvent	Abbreviation	Chemical formula	Dielectric constant ε	Dipole moment μ	Relative polarity
Water	C0	H_2O	80	1.85	1
Methanol	C1; MeOH	CH_3OH	33	1.7	0.762
Ethanol	C2; EtOH	C_2H_5OH	24.3	1.7	0.654
1-Propanol	C3; PrOH	C_3H_7OH	22	1.68	0.617
1-Butanol	C4; BuOH	C_4H_9OH	17.5	1.7	0.586
1-Pentanol	C5	$C_5H_{11}OH$	14	1.7	0.568
1-Hexanal	C6	$C_6H_{13}OH$	12.5	1.65	0.559
1-Heptanol	C7	$C_7H_{15}OH$	12	1.7	0.549
1-Octanol	C8	$C_8H_{17}OH$	10.3	1.7	0.537
Acetone		CH_3COCH_3	20.7	2.69	0.355
Methylethyl ketone		$CH_3COC_2H_5$	18.5	2.78	0.327
Methylpropyl ketone		$CH_3COC_3H_7$	18.6	2.80	0.321
Benzene		C_6H_6	2.28	0	0.111
Dimethyl formamide	DMF	C_3H_7NO	38.3	3.82	0.386
Acetic acid	Ac acid	CH_3COOH	6.15	1.74	0.648

* Data of dielectric constant ε at 20 °C, and dipole moment μ in Debye. Relative polarity after Reichardt and Welton (2011).

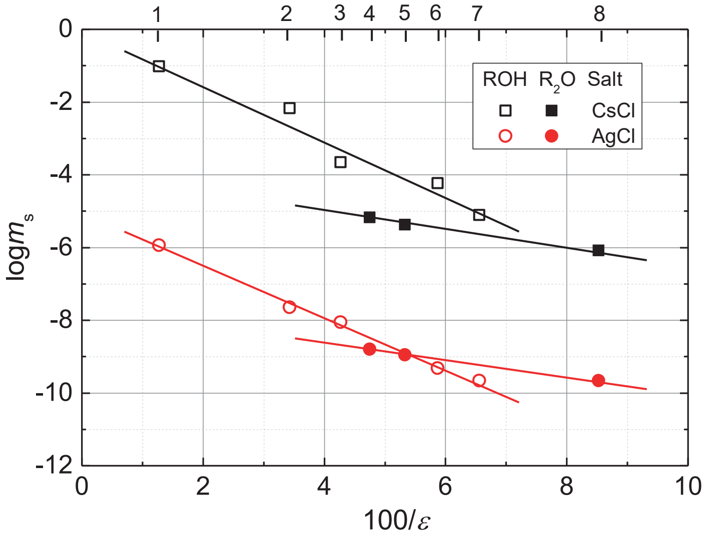

Figure 2.10. Dependence of logm_s on 1/ε for (1,2) CsCl and (3,4) AgCl in some (1,3) alcohols ROH and (2,4) ketones ROR'. At the upper side of 1/ε axis solvents are: (1) water, (2) methanol, (3) ethanol, (4) acetone, (5) methylethyl ketone, (6) butanol, (7) amyl alcohol, and (8) methylpropyl ketone. After Izmailov (1970).

Figure 2.11 shows another example of the dependence of logm_s of $Gd(IO_3)_2$ on 1/ε in H_2O+CH_3OH and $H_2O+C_2H_5OH$ mixtures. In both solvent mixtures, the linear dependence is observed in a narrow range of 1/ε lying below about 0.014 and 0.0135 (i.e. ε above about 70 and 74) for H_2O+CH_3OH and $H_2O+C_2H_5OH$ mixtures, respectively. However, above these $1/\varepsilon$ values the dependence shows increasingly pronounced deviation from the linearity with increasing $1/\varepsilon$ values in both mixtures and this deviation is lower in H_2O+CH_3OH mixture than in H_2O+C_2H_5OH mixtures. Since the dielectric constant ε of water is 80, it can be argued that the linear dependence is observed only in solution mixtures containing no more than 0.2 volume fraction of these cosolvent alcohols. The increasingly pronounced deviation from the linearity of $\log m_s$ of $Gd(IO_3)_2$ on $1/\varepsilon$ with increasing $1/\varepsilon$ values in the two mixtures is associated with the pronounced ability of the ions of this salt to form ionic associates with increasing alcohol content in the mixtures.

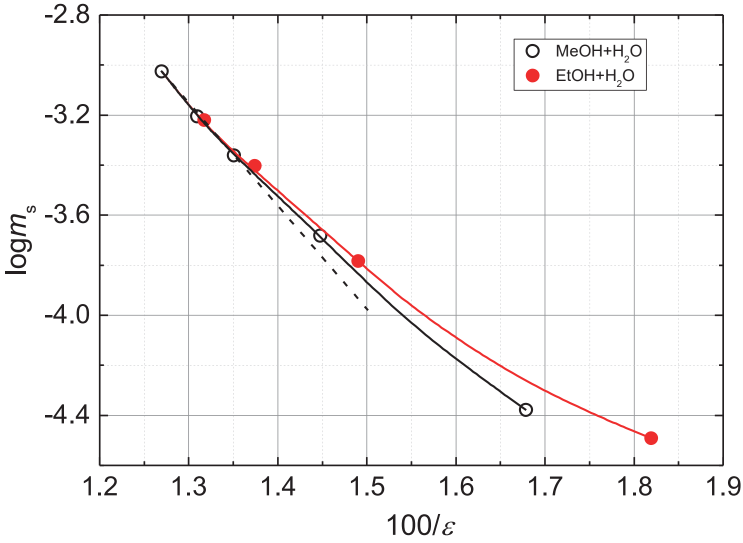

Figure 2.11. Dependence of $\log m_s$ of $Gd(IO_3)_2$ on $1/\varepsilon$ in H_2O+CH_3OH and H_2O+C_2O_5OH mixtures. In the figure CH_3OH and C_2O_5OH are denoted as MeOH and EtOH, respectively. After Miyamoto et al. (1985).

The dielectric constant ε of normal alcohols decreases with the number N of $-CH_2$ groups in their molecules but their dipole moment μ is practically independent of N (see Table 2.3). Therefore, the decreasing trend of the solubility of cyromazine in increasing series of normal alcohols, described above, suggests that the dielectric constant ε of the alcohols, rather than the dipole moment μ of their molecules, has the pronounced effect on the solubility of nonelectrolyte solutes. However, relation (2.46) cannot be used to describe the effect of the dielectric constant ε of solvents on the solubility of organic compounds (nonelectrolytes) because its derivation is based on mutual interactions between ions resulting from the dissociation of electrolyte by a solvent. Therefore, the behavior of solubility of organic compounds cannot be attributed directly to their dielectric constant ε and dipole moment μ.

In order to the understand the parameters that determine the dissolution behavior of nonelectrolyte solutes we analyze their thermodynamic functions of mixing obtained in different solvents. Figure 2.12 shows plots of calculated thermodynamic functions $\Delta G^{\mathrm{o}}_{\mathrm{mix}}$, $\Delta H^{\mathrm{o}}_{\mathrm{mix}}$ and $T_{\mathrm{hm}}\Delta S^{\mathrm{o}}_{\mathrm{mix}}$ of solution obtained from solubility data of cyromazine in the series of normal alcohols on the number N of –CH_2 groups in alcohol molecules. The $\Delta G^{\mathrm{o}}_{\mathrm{mix}}$ and $\Delta H^{\mathrm{o}}_{\mathrm{mix}}$ data of this figure are from Table 2.1 and the values of $T_{\mathrm{hm}}\Delta S^{\mathrm{o}}_{\mathrm{mix}}$ were calculated by using Eq. (2.37). In the figure, the data for $N = 0$ refers to the data for water.

It may be seen from the above figure that there is an insignificant increase in $\Delta G^{\mathrm{o}}_{\mathrm{mix}}$ for alcohols from ethanol to 1-pentanol (about 0.15 kJ·mol^{-1} per –CH_2 group) but methanol, 1-hexanol and 1-heptanol are exceptions from this trend.

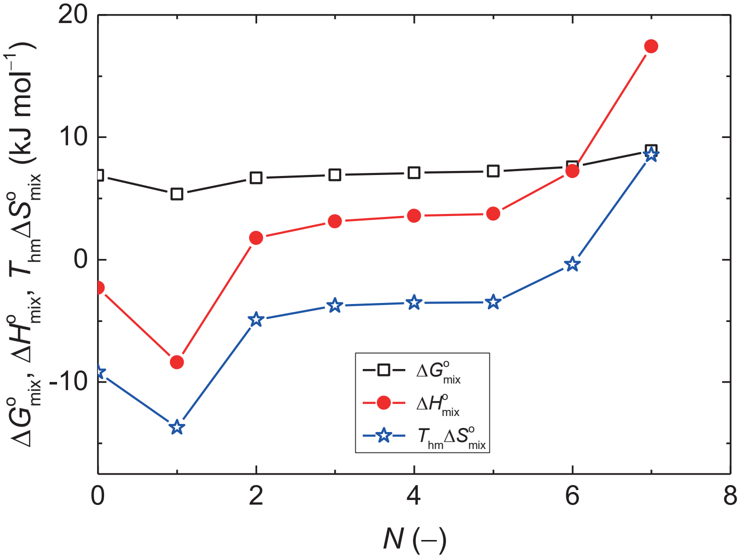

Figure 2.12. Dependence of calculated thermodynamic functions $\Delta G^{\mathrm{o}}_{\mathrm{mix}}$, $\Delta H^{\mathrm{o}}_{\mathrm{mix}}$ and $T_{\mathrm{hm}}\Delta S^{\mathrm{o}}_{\mathrm{mix}}$ mixing from solubility of cyromazine in different homologues of normal alcohols on the number N of –CH_2 groups in alcohol molecules. Original data from Zhang et al. (2018).

The value of $\Delta G^{\mathrm{o}}_{\mathrm{mix}}$ for water is comparable with that for 1-propanol, that for methanol and 1-hexanol differs from their neighbors by about twice the average increase of 0.15 kJ·mol^{-1} per –CH_2 group, but that for 1-heptanol is much higher. The $\Delta H^{\mathrm{o}}_{\mathrm{mix}}$ data also show similar trends but the differences are more pronounced for methanol, 1-hexagonol and 1-heptanol. These changes are compensated by the entropy term $T_{\mathrm{hm}}\Delta S^{\mathrm{o}}_{\mathrm{mix}}$.

The above observations cannot be explained directly in terms of dielectric constant ε of solvents and the dipole moment μ of their molecules. Another property of solvents affecting the dissolution behavior of organic compounds is the relative polarity of their molecules (see Table 2.3), and is intimately connected with the functional groups in the solvent molecules. Figure 2.13a shows the data of the calculated thermodynamic functions $\Delta G^{\circ}_{\mathrm{sol}}$, $\Delta H^{\circ}_{\mathrm{sol}}$ and $T_{\mathrm{hm}}\Delta S^{\circ}_{\mathrm{sol}}$ of solutions from the solubility of cyromazine in different alcohol homologues and nonalcohols (acetone, acetic acid and water) as a function of their relative polarity. From the figure a decrease in the values of the different functions in the alcohols with their increasing relative polarity may be discerned but no well-defined trend appears in the case of nonalcohol solvents. Figure 2.13b shows the data of the calculated thermodynamic functions of mixing $\Delta G^{\circ}_{\mathrm{mix}}$, $\Delta H^{\circ}_{\mathrm{mix}}$ and $T_{\mathrm{hm}}\Delta S^{\circ}_{\mathrm{mix}}$ from solubility of cyromazine in different homologues of normal alcohols as a function of their relative polarity. It may be seen that, with the exception of 1-heptanol, the value of each thermodynamic function of mixing decreases practically linearly with increasing relative polarity and the value for water corresponds to a relative polarity of about 0.7, which lies between the polarity for methanol and ethanol.

It may be seen from Figure 13b and Table 2.3 that the value of the relative polarity decreases with an increase in the number N of –CH_2 groups in the molecules of alcohol homologues from the highest of 0.76 for methanol down to the lowest value of 0.55 for heptanol. However, the value of each of the thermodynamic functions increases linearly with increasing number N of –CH_2 groups in the molecules of higher homologues of methanol up to hexanol, when their value abruptly increases for *n*-heptanol. Since the solubility of an organic solute such as cyromazine is determined by solute–solvent interactions, the above observations of the difference in the trends of decrease in the thermodynamic functions of mixing for its dissolution in different homologues of normal alcohols may be explained from consideration of the structure of their molecules in the solutions.

As in the case of different contributions in the entropy of melting of long-chain compounds (see Section 2.2.2), the entropy of dissolution may also be considered to be composed of contributions similar to those in melting. As in the case of their melting, we assume that the contribution of entropy due to internal conformation of the molecules in the solution becomes important during the dissolution of long-chain compounds. Then it may be argued that solvents composed of molecules having a few –CH_2 groups behave as rigid molecules (i.e. conformation- al entropy is zero), but the contribution of conformational entropy due to larger molecules increases with the number N of –CH_2 groups in the solution. Thus, the linear dependence of the thermodynamic functions of mixing for the dissolution of cyromazine in different homologues of normal alcohols in the solutions up to hexanol may be attributed to the length of the solvent molecules which behave as rigid units, but the abrupt increase thereafter to the flexibility of the solvent molecules in the solution.

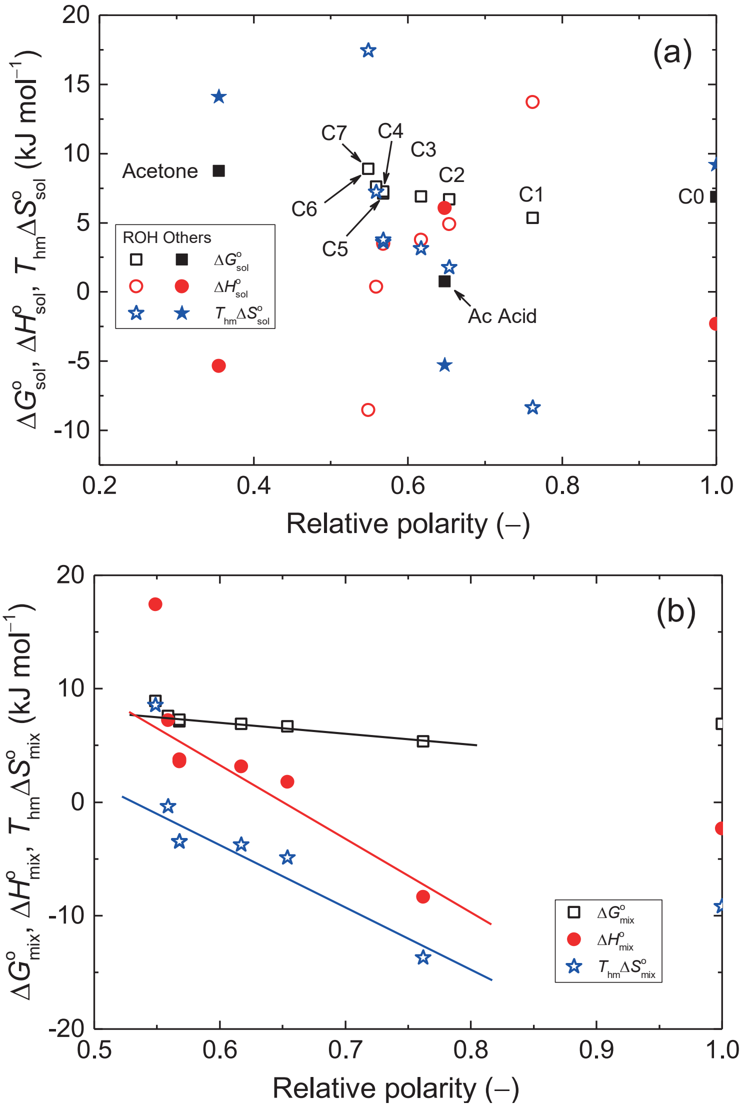

Figure 2.13. Dependence of (a) ΔG^o_{sol}, ΔH^o_{sol} and $T_{hm}\Delta S^o_{sol}$ of solution for cyromazine in different alcohol homologues and nonalcohols on the relative polarity of their molecules, and (b) ΔG^o_{mix}, ΔH^o_{mix} and $T_{hm}\Delta S^o_{mix}$ of mixing for cyromazine in alcohol homologues on the relative polarity of their molecules.

Figure 2.14 presents the dependence of parameters λ and h of the λh model for solubility of cyromazine in different homologues of normal alcohols on the number N of –CH$_2$ groups in alcohol molecules. The original data of λ and h for cyromazine are from Zhang et al. (2018). It may be noted from the figure that the values of λ and h are mutually related and their values are practically constant for alcohols between ethanol and pentanol. This behavior is clearly observed in the case of solutions where the value of h decreases and that of λ increases beyond pentanol and the value of h is higher and that of λ is lower for methanol than for its higher homologues. Physically, these trends mean that association of cyromazine molecules becomes increasingly pronounced in higher homologues of alcohols beyond pentanol and this process is accompanied by a decreasing value of h. In contrast to these trends in the highest alcohols hexanol and heptanol involving strong solute–solute interactions, the observed behavior of cyromazine in methanol suggests preferred solute–solvent interactions in the solution.

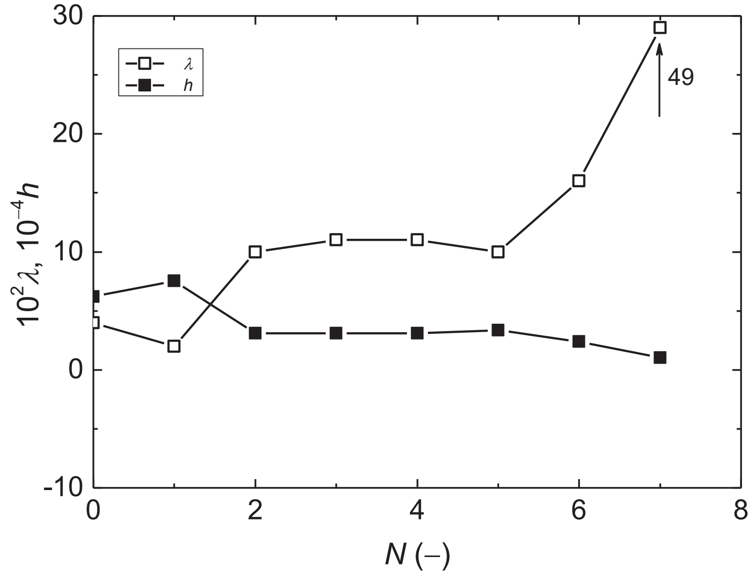

Figure 2.14. Dependence of parameters λ and h for solubility of cyromazine in different homologues of normal alcohols on the number of $–CH_2$ groups in alcohol molecules. Original data from Zhang et al. (2018).

Finally, it should be mentioned that the mutual compensation of the trends of λ and h on N observed above in Figure 2.14 is similar to that of the trends of $\Delta H^{\circ}_{\mathrm{mix}}$ and $T_{\mathrm{hm}}\Delta S^{\circ}_{\mathrm{mix}}$ on N seen in Figure 2.12.

2.5. Solubility of solutes in solvent–cosolvent systems

Real solutions composed of two components, one of which is a solvent and the other is a solute, were considered above. However, real solutions composed of more than two components are frequently required in different applications. These solutions may contain two or more solutes in a particular solvent or one solute in a mixture of two or more solvents. A general feature of the equilibrium concentration (solubility) of various solutes in individual solvents and their mixtures is that the temperature dependence of the solubility follows Eq. (2.14) described above for two-component (binary) systems composed of a particular solute dissolved in an isolated solvent.

At a given temperature, not only the solubility of different solutes in a particular solvent such as water is different but the solubility of the same solute in different solvents is different. For example, at room temperature common salt (NaCl) has a relatively high solubility in water but it is sparingly soluble in alcohols. Therefore, at a particular temperature the solubility of NaCl in solvent water can be reduced by mixing it with alcohols in various proportions. Another solvent, such as alcohols miscible with the first solvent in the above case, in which the solute is insoluble or poorly soluble is usually called a *nonsolvent* or *antisolvent*. Addition of antisolvents to saturated solutions of solutes dissolved in fairly-soluble solvents is the basis of processes of salting-out and drowning-in (antisolvent crystallization), whereas search for new solvents and mixtures of two or more solvents for chemical compounds in which they are relatively soluble is indispensable for the application of the compounds in food, pharmaceutical and chemical industries. When it is immaterial whether the solute has a solubility less or more in the other solvent than that in the first (reference) solvent, this other solvent is frequently referred to as a *cosolvent*.

Using the theoretical background of real solutions discussed above, some general features of the dependence of solubility of some inorganic and organic solutes on the temperature of mixtures of two solvents in different proportions and on the antisolvent content at different temperatures are presented below.

2.5.1. Simple additivity rule approach

The simplest model to describe the solubility x_s^m of a solute in the mixture of a solvent containing a cosolvent is based on the additivity rule of mixing involving summation of logarithms of equilibrium activities $a_s = x_s\gamma_s$ of the solute in the solvent and in the cosolvent, given by

$$\begin{aligned}\ln x_s^m\gamma_s^m &= (1-f_3)\ln x_{s2}\gamma_{s2} + f_3 \ln x_{s3}\gamma_{s3} = \\ &= \ln x_{s2} + f_3[\ln(x_{s3}/x_{s2})] + \ln\gamma_{s2} + f_3[\ln(\gamma_{s3}/\gamma_{s2})], \qquad (2.47)\end{aligned}$$

where the indices 2 and 3 with the solubility x_s and the activity coefficient γ_s denote their values from saturated solutions in neat solvent and neat cosolvent, respectively, γ_s^m and x_s^m denote the values of γ_s and x_s for solvent–cosolvent mixture, and $f_2 = (1–f_3)$ and f_3 are the fractions (usually expressed in weight, volume or mole fraction) of solvent and cosolvent in the mixture such that the sum of solvent and cosolvent fractions is unity. Following the result that $\ln(x_s+\beta_s)$, where β_s is a small correction factor as a measure of solute–solvent interaction, depends linearly on cosolvent content f_3 (Sangwal, 2010b; Sangwal et al., 2013), we assume that the activity coefficient γ_s of a saturated solution is related to solubility x_s by

$$\gamma_\mathrm{s} = 1 + \frac{\beta_\mathrm{s}}{x_\mathrm{s}}, \tag{2.48}$$

where β_s is an interaction parameter that accounts for the deviation of the saturated solution from ideal behavior. Then Eq. (2.47) takes the form

$$\ln\left[x_\mathrm{s}^\mathrm{m}\left(1+\frac{\beta_\mathrm{s}^\mathrm{m}}{x_\mathrm{s}^\mathrm{m}}\right)\right] = \ln x_{\mathrm{s}2} + f_3 \ln\left(\frac{x_{\mathrm{s}3}}{x_{\mathrm{s}2}}\right) + \ln\left(1+\frac{\beta_{\mathrm{s}2}}{x_{\mathrm{s}2}}\right) + f_3 \ln\left(\frac{1+\beta_{\mathrm{s}3}/x_{\mathrm{s}3}}{1+\beta_{\mathrm{s}2}/x_{\mathrm{s}2}}\right). \tag{2.49}$$

Using the van’t Hoff relation, Eq. (2.5), the above equation may be expressed as

$$\ln\left[x_\mathrm{s}^\mathrm{m}\left(1+\frac{\beta_\mathrm{s}^\mathrm{m}}{x_\mathrm{s}^\mathrm{m}}\right)\right] = A_2 + f_3(A_3 - A_2) - \left[\frac{\Delta H_{\mathrm{s}2}}{R_\mathrm{G}T} + f_3 \ln\left(\frac{\Delta H_{\mathrm{s}3} - \Delta H_{\mathrm{s}2}}{R_G T}\right)\right] + \\ + \ln\left(1+\frac{\beta_{\mathrm{s}2}}{x_{\mathrm{s}2}}\right) + f_3 \ln\left(\frac{1+\beta_{\mathrm{s}3}/x_{\mathrm{s}3}}{1+\beta_{\mathrm{s}2}/x_{\mathrm{s}2}}\right). \tag{2.50}$$

Eq. (2.50) describes the solubility of a solute in the solvent–cosolvent mixture as a function of cosolvent content f_3 and solution temperature T.

When the solvent–cosolvent mixture content is constant, Eq. (2.50) may be written as

$$\ln x_\mathrm{s}^\mathrm{m} = A_f^\mathrm{m} - \frac{\Delta H_{\mathrm{s}f}^\mathrm{m}}{R_\mathrm{G}T}, \tag{2.51}$$

where

$$A_f^\mathrm{m} = A_2 - f_3(A_3 - A_2) + \ln\left(\frac{1+\beta_{\mathrm{s}2}/x_{\mathrm{s}2}}{1+\beta_\mathrm{s}^\mathrm{m}/x_\mathrm{s}^\mathrm{m}}\right) + f_3 \ln\left(\frac{1+\beta_{\mathrm{s}3}/x_{\mathrm{s}3}}{1+\beta_{\mathrm{s}2}/x_{\mathrm{s}2}}\right), \tag{2.52}$$

$$\Delta H_{\mathrm{s}f}^\mathrm{m} = \Delta H_{\mathrm{s}2} + f_3(\Delta H_{\mathrm{s}3} - \Delta H_{\mathrm{s}2}), \tag{2.53}$$

and A_f^m is dimensionless but $\Delta H_{\mathrm{s}f}^\mathrm{m}$ has the units of energy ($\mathrm{J \cdot mol^{-1}}$). When the solution temperature T is constant, Eq. (2.50) takes the form

$$\ln\left[x_\mathrm{s}^\mathrm{m}\left(1+\frac{\beta_\mathrm{s}^\mathrm{m}}{x_\mathrm{s}^\mathrm{m}}\right)\right] = A_T + B_T f_3, \tag{2.54}$$

where

$$A_T = A_2 - \frac{\Delta H_{\mathrm{s}2}}{R_\mathrm{G}T} + \ln\left(1+\frac{\beta_{\mathrm{s}2}}{x_{\mathrm{s}2}}\right), \tag{2.55}$$

$$B_T = (A_3 - A_2) - \left(\frac{\Delta H_{s3} - \Delta H_{s2}}{R_G T} \right) + \ln \left(\frac{1 + \beta_{s3} / x_{s3}}{1 + \beta_{s2} / x_{s2}} \right), \tag{2.56}$$

and both A_T and B_T are dimensionless. It should be mentioned that during the derivation of Eq. (2.51) it is assumed that the logarithm terms of Eq. (2.52) are temperature independent. The deviation in the solubility behavior of the solute in the solvent–cosolvent mixture from that in individual solvent and cosolvent is associated with the logarithmic terms in these equations.

Eq. (2.51) of the temperature dependence of x_s^m is similar to Eq. (2.7) for the solubility of substances in single-solvent solutions. In fact, there are several evidences that the experimental solubility x_s^m of different substances in solvent–cosolvent mixtures of different cosolvent content follows Eq. (2.51). Eq. (2.54) predicts linear dependence of $\ln(x_s^m+\beta_s^m)$ on f_3 with intercept A_T and slope B_T at a given temperature T and both A_T and B_T are temperature dependent. Some examples are described below.

Figure 2.15a presents the data of the solubility x_s^m of ammonium oxalate [$(NH_4)_2C_2O_4$; abbreviated as AO] in solutions of water–acetone mixtures as a function of cosolvent acetone content f_3 at different temperatures T. Figure 2.15b shows the same data as plots of $\ln x_s^m$ against acetone content f_3 according to Eq. (2.54), with the interaction parameter $\beta_s^m = 0$ (dashed curves) and $\beta_s^m \neq 0$ (solid curves). It may be seen that the dependence of $\ln x_s^m$ on f_3, with $\beta_s^m = 0$, for AO solutions in Figure 2.15b is not strictly linear and the slope of the plot slowly increases with an increase in f_3, thereby showing a positive deviation from the linearity. However, introduction of a suitably-selected nonzero correction β_s^m to the solubility x_s^m ensures a linear dependence with a higher fitting parameter R^2.

Figure 16a shows another example of the dependence of solubility x_s^m of 2,4,6-trinitrotoluene ($C_7H_5N_3O_6$; TNT) in methanol–water mixtures on water content f_3 at different temperatures T, whereas Figure 2.16b shows the same data as plots of $\ln x_s^m$ against water content f_3 according to Eq. (2.54), with the interaction parameter $\beta_s^m = 0$ (dashed curves) and $\beta_s^m \neq 0$ (solid curves). The values of the parameters of Eq. (2.54), and the best-fit parameter R^2, for the two systems are given in Table 2.4.

It may be noted from Table 2.4 that the values of the parameters A_T and B_T in both systems when $\beta_s^m = 0$ show a general tendency to decrease with an increase in temperature but the decrease in B_T is relatively poor in comparison with that in A_T. These trends are predicted by relations (2.55) and (2.56). As seen from Table 2.4, the correction term β_s^m is nonzero at most temperatures and, except in the case of TNT dissolved in methanol–water at 293.15 K, its value usually exceeds 0. The correction factor $\beta_s^m \neq 0$ leads to a change in the values of both A_T and B_T at all temperatures, but the change introduced in A_T is relatively insignificant in comparison with that in B_T. These changes may also be explained qualitatively from consideration of different terms in Eqs. (2.55) and (2.56).

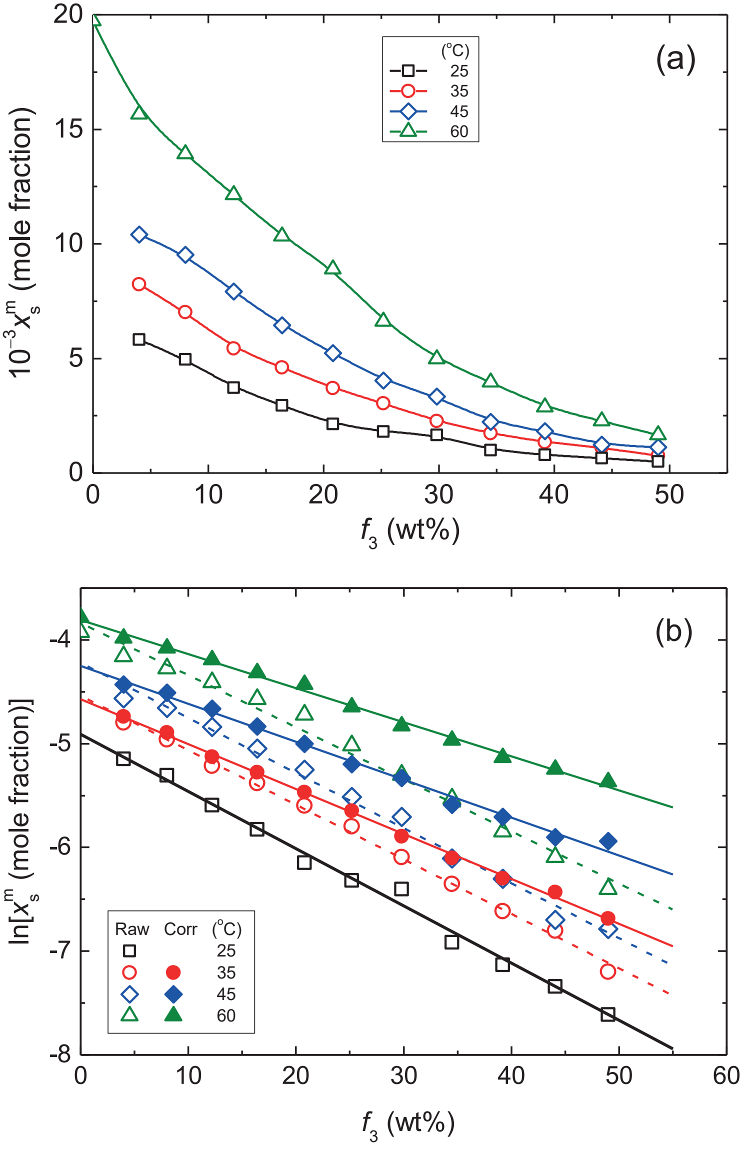

Figure 2.15. (a) Plots of x_s^m of AO in solutions of water–acetone mixtures against acetone content f_3 at different temperatures T. (b) Data of (a) shown as plots of $\ln x_s^m$ against f_3 without (dashed lines) and with correction factor β_s^m (solid lines) according to Eq. (2.54). Linear plots are drawn with the parameters given in Table 2.4. Adapted from Sangwal et al. (2013).

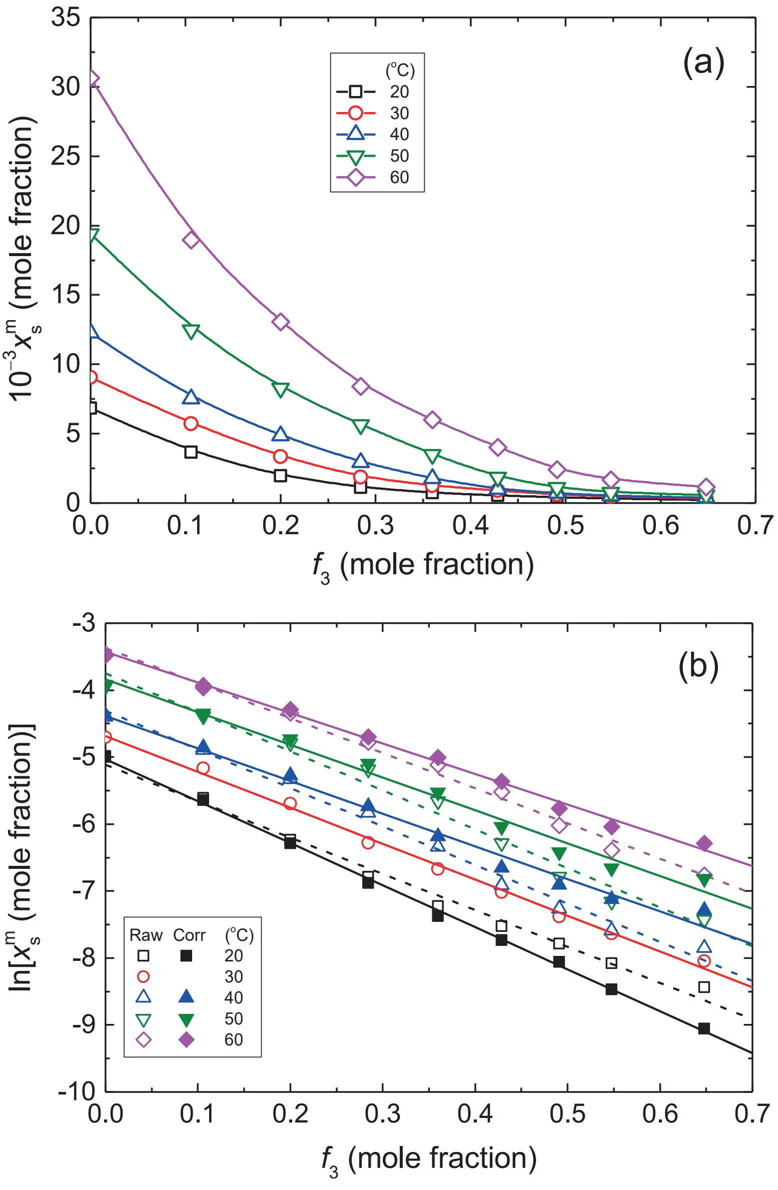

Figure 2.16. (a) Plots of x_s^m of TNT in solutions of methanol–water mixtures against water content f_3 at different temperatures T. (b) Data of (a) shown as plots of $\ln x_s^m$ against f_3 without (dashed lines) and with correction factor β_s^m (solid lines) according to Eq. (2.54). Linear plots are drawn with best-fit parameters given in Table 2.3. Original data from Chen et al. (2014).

Table 2.4. Values of constants of Eq. (2.54) for different systems

Solute	Mixture	T (K)	β_s^m	$-A_T$	B_T	R^2
AO	Water/acetone	298.15	--	4.911	5.507	0.9966
		303.15	--	4.709	5.480	0.9979
			0.00025	4.726	4.863	0.9986
		308.15	--	4.539	5.257	0.9984
			0.0005	4.573	4.332	0.9991
		313.15	--	4.371	5.454	0.9966
			0.002	4.345	3.306	0.9957
		318.15	--	4.222	5.308	0.9952
			0.002	4.239	3.328	0.9955
		323.15	--	4.107	4.981	0.9943
			0.002	4.104	3.398	0.9963
		333.15	--	3.837	5.019	0.9944
			0.002	3.807	3.283	0.9977
TNT	Methanol/water	293.15	--	5.117	5.423	0.9882
			−0.0001	5.029	6.276	0.9984
		303.15	--	4.685	5.362	0.9958
		313.15	--	4.309	5.756	0.9881
			0.0003	4.384	4.870	0.9823
		323.15	--	3.749	5.827	0.9796
			0.0005	3.839	4.894	0.9825
		333.15	--	3.369	5.241	0.9902
			0.0007	3.428	4.565	0.9936

It is usually observed that the dependence of the experimental solubility x_s^m of several inorganic and organic compounds on cosolvent content f_3 according to Eq. (2.54) is followed for low f_3 (< 0.4 mole fraction), but shows enormous deviations from the predicted dependence for high f_3. Figure 2.17a illustrates an example of this behavior where the solubility x_s^m of sulfamerazine in solutions of methanol–water and 1-propanol–water mixtures against solubility parameter δ_{mix} of the mixture is shown at two different temperatures T. The solubility parameter δ_{mix} of the mixture was calculated using the additive rule (see Eq. (2.62)) with the following values of the solubility parameter δ of solvent and cosolvent of the mixture: for water $\delta_3 = 47.8$ MPa$^{1/2}$, methanol $\delta_2 = 29.6$ MPa$^{1/2}$ and 1-propanol $\delta_2 = 24.5$ MPa$^{1/2}$. The original data used in the plots are from Delgado and Martinez (2014, 2015). The trends of these $x_s^m(\delta_{mix})$ plots are essentially similar to those of the $x_s^m(f_3)$ plots because δ_{mix} increases linearly with the cosolvent water content f_3 (see Eq. (2.63)).

From Figure 2.17a it may be seen that the solubility x_s^m of sulfamerazine in both mixtures increases with temperature but in the 1-propanol–water mixture the solubility initially increases and then decreases with increasing solubility parameter δ_{mix}, showing a maximum at each temperature corresponding to $\delta_{mix} \approx 38$ MPa$^{1/2}$. In contrast to the above trend of the solubility x_s^m with a maximum solubility in the 1-propanol–water mixture of a particular δ_{mix}, a maximum solubility is not observed in methanol–water mixture where the highest solubility is obtained in pure methanol alone. Irrespective of the temperature, in alcohol-rich mixtures the maximum solubility of sulfamerazine in methanol is about twice that in 1-propanol–water mixture. However, the order of the solubility of sulfamerazine is reversed in water-rich solutions such that its values are lower in the solutions of methanol–water mixture than those in 1-propanol–water mixture.

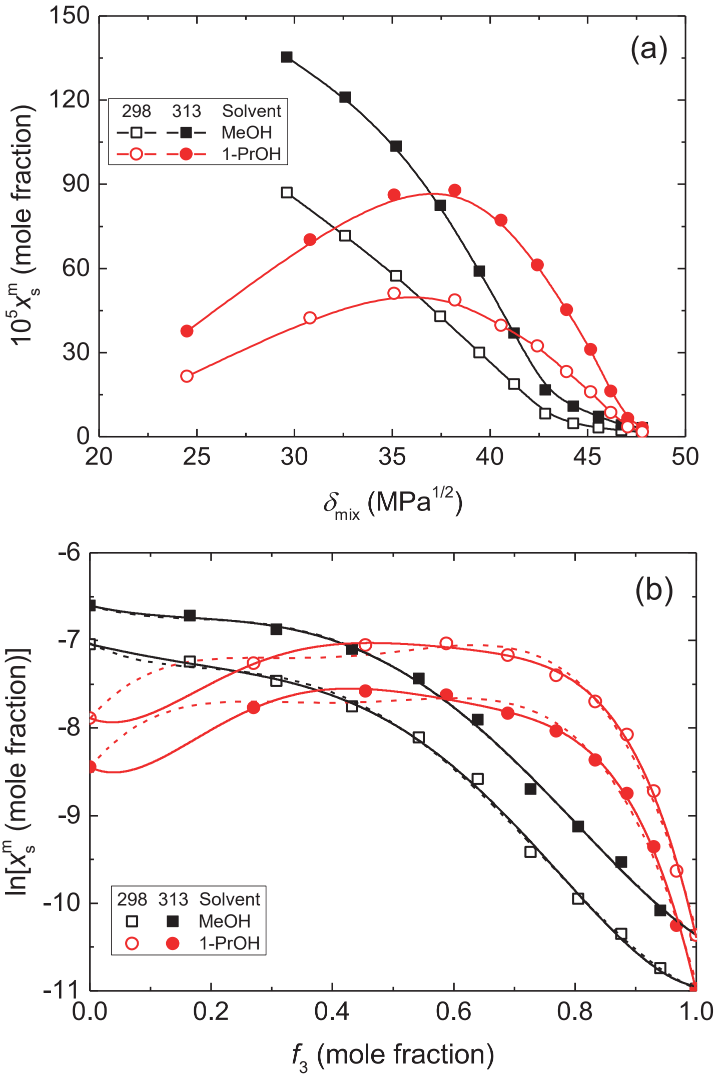

Figure 2.17. (a) Solubility x_s^m of sulfamerazine in solutions of methanol–water and 1-propanol–water mixtures against solubility parameter δ_{mix} of the mixture according to Eq. (2.68) at two different temperatures T. (b) Data of (a) shown in the form of plots of $\ln x_s^m$ against water content f_3 in methanol–water and 1-propanol–water mixtures. In (b) dashed and solid curves are drawn according to Eq. (2.65) with fourth- and fifth-order polynomials. Original data from Delgado and Martinez (2014, 2015).

Figure 2.17b shows plots of $\ln x_s^m$ of sulfamerazine against water content f_3 in solutions of methanol–water and 1-propanol–water mixtures. Differences in the trends of the plots of $\ln x_s^m$ against f_3 in the two mixtures are evident. In the methanol–water mixture $\ln x_s^m$ steadily decreases with increasing f_3 from its maximum value, but in the 1-propanol–water mixture $\ln x_s^m$ initially increases and then decreases after passing through a maximum at $f_3 \approx 0.5$ mole fraction. This type of anomalous solubility behavior of solutes in solvent–cosolvent mixtures is associated with different kinds of interactions between solute, solvent and cosolvent molecules in the solutions.

The above interactions between solute, solvent and cosolvent molecules in the solutions are reflected in the deviations of the experimental solubility $x_s^m(\text{exp})$ of real solutions from the calculated solubility $x_s^m(\text{cal})$ of ideal solutions following from the simple additive (or mixing) rule, i.e.

$$\Delta(\ln x_s^m) = [\ln x_s^m(\text{exp}) - \ln x_s^m(\text{cal})] = \ln x_s^m(\text{exp}) - \{\ln x_{s2} + f_3[\ln(x_{s3}/x_{s2})]\}\,. \quad (2.57)$$

This equation is another form of Eq. (2.47) where all terms containing various types of activity coefficients γ_s's are assumed to lead to the deviation $\Delta(\ln x_s^m)$. Some of the approaches advanced to explain the observed deviations in the solubility behavior of various systems are discussed below.

2.5.2. Extended Hildebrand solubility approach

When activity coefficients of solutions are not considered in Eq. (2.47), it reduces to the form of a linear relationship between $\ln x_s^m$ and f_3 introduced by Yalkowsky et al. (1972), usually referred to as log-linear model, to describe the solubility of some drugs in mixtures of water and nonaqueous cosolvents, where x_s^m denotes the solubility of the solute in moles per liter in the mixture, x_{s2} is its solubility in water, f_3 is the volume fraction of the cosolvent, and $\ln(x_{s3}/x_{s2})$ is a parameter representing the solubilizing power of the cosolvent for the solute. The value of the parameter $\ln(x_{s3}/x_{s2})$ depends on the polarity of the solute and the cosolvent. This linear relationship between $\ln x_s^m$ and f_3 holds in systems where the polarity of the solute is significantly lower than that of either of the solvents in the mixture, and applies when the Hildebrand solubility parameters δ_2 and δ_3 of both solvent components are much larger than the solubility parameter δ_1 of the solute. However, it is frequently observed that the relationship between $\ln x_s^m$ and f_3 is nonlinear (Martin et al., 1982; Delgado and Martinez, 2015). This nonlinear dependence of $\ln x_s^m$ on f_3 is described by the extended Hildebrand solubility (EHS) approach (Martin et al., 1982), which is discussed below.

In Eq. (2.14) the first term on the right-hand side, with the proportionality constant $\sigma = 0$, describes the temperature dependence of the ideal solubility x_s^{id} of a solid solute in a solvent and the second term equal to $\ln\gamma_s$ accounts for the nonideal behavior. When the solute is dissolved in a mixture of solvent containing a cosolvent, the nonideality of this solvent–cosolvent mixture is due to $\ln\gamma_s^m$, different from $\ln\gamma_s$. Then we may write the solute solubility x_s^m in the mixture in the form

$$\ln x_s^m = \ln x_s + \ln \gamma_s - \ln \gamma_s^m , \tag{2.58}$$

where x_s and γ_s denote the solubility and the activity coefficient of the solute in solvent and the superscript 'm' indicates their values in the solution mixture. This behavior of solute in the solvent–cosolvent mixture is described in terms of the Hildebrand solubility parameter δ_{mix} of the mixture, which is a polarily index frequently used in the study of nonelectrolyte drugs (Martin et al., 1982; Jouyban 2010; Hansen, 2007; Barton, 1991). The solubility parameter δ is square-root of the cohesion energy density of the compound (solute or solvent), and is defined as

$$\delta^2 = (\Delta H_v - R_G T)V_M , \tag{2.59}$$

where ΔH_v and V_M are the molar enthalpy of vaporization and the molar volume, respectively. According to the extended Hildebrand approach (see Martin et al., 1982), the activity-coefficient term $\ln\gamma_s^m$ of the solute in a solvent–cosolvent mixture may be given by

$$\ln \gamma_s^m = X(\delta_1^2 + \delta_2^2 - 2W) , \tag{2.60}$$

where $W = K\delta_1\delta_2$ is the interaction energy density of solute and solvent–cosolvent mixture, K is a solute–solvent interaction parameter, δ_1^2 and δ_2^2 are the cohesive energy densities of solute 1 and solvent 2, respectively, and, according to the regular solution theory, the parameter

$$X = \frac{V\phi_2^2}{R_G T} , \tag{2.61}$$

where V (cm^3·mol^{-1}) is the molar volume of the solute considered as a hypothetical supercooled liquid at saturation temperature, ϕ_2 is the volume fraction of neat solvent or solvent–cosolvent mixture in the saturation solution. The energy densities δ_1^2, δ_2^2 and W represent solute–solute, solvent–solvent and solute–solvent interaction energies, respectively. The parameter W accounts for the deviation of the system from the behavior of regular solutions. In the case of regular solutions, $W = \delta_1\delta_2$ in Eq. (2.60) to obtain the regular solution dependence

$$\ln x_s^m = \ln x_s + \ln \gamma_s - X(\delta_2 - \delta_1)^2 . \tag{2.62}$$

The mixture solubility parameter δ_{mix} is calculated using additivity of their volumes and is given by

$$\delta_{mix} = f_3\delta_3 + (1 - f_3)\delta_2 = \delta_2 + f_3(\delta_3 - \delta_2) , \tag{2.63}$$

where f_3 is the volume fraction of the cosolvent.

The interaction energy density W or $\ln\gamma_s^m/X$ is usually regressed in a polynomial on solvent solubility parameter δ or volume fraction f_2 of the solvent or f_3 of the cosolvent in the solvent–cosolvent mixture to obtain values of $\ln\gamma_s^m$ and $\ln x_s^m$. In the case of cosolvent volume fraction f_3, the values of $\ln\gamma_s^m/X$ are calculated from the relation

$$\frac{\ln \gamma_\mathrm{s}^\mathrm{m}}{X_\mathrm{cal}} = \frac{\ln x_\mathrm{s} + \ln \gamma_\mathrm{s} - \ln x_\mathrm{s}^\mathrm{m}}{X_\mathrm{cal}} = \frac{1}{X_\mathrm{cal}} \ln\left(\frac{x_\mathrm{s}^\mathrm{id}}{x_\mathrm{s}^\mathrm{m}}\right) = C_0 + C_1 f_3 + C_2 f_3^2 + C_3 f_3^3 + \ldots + C_n f_3^n \,. \tag{2.64}$$

If the power series is confined to the fourth degree, the extended Hildebrand equation takes the form

$$\ln x_\mathrm{s}^\mathrm{m} = X_0 - X \sum_{n=1}^{4} C f_3^n \,, \tag{2.65}$$

where

$$X_0 = \ln x_\mathrm{s}^\mathrm{id} - X C_0 \,, \tag{2.66}$$

C_0 is a regression constant, and C_i's are coefficients of regression analysis over the solvent–cosolvent mixture composition for the compound at a particular temperature. The parameter $X \approx 0.1$.

In order to describe the dependence of $\ln x_\mathrm{s}^\mathrm{m}$ on the solvent or cosolvent solubility parameter δ the deviation of the solution from the behavior of regular solutions the parameter W of Eq. (2.60) is calculated from the relation

$$W = \frac{1}{2}\left[(\delta_1^2 + \delta_2^2) - \frac{\ln \gamma_\mathrm{s}^\mathrm{m}}{X}\right] = \frac{1}{2}\left[(\delta_1^2 + \delta_2^2) - \frac{1}{X_\mathrm{cal}} \ln\left(\frac{x_\mathrm{s}^\mathrm{id}}{x_\mathrm{s}^\mathrm{m}}\right)\right]. \tag{2.67}$$

and then the values of the W parameter are regressed on δ_2 of solvent or δ_3 of cosolvent according to the polynomial of several orders. In terms of cosolvent solubility parameter δ_3 one may write

$$W = K_0 + K_1 \delta_3 + K_2 \delta_3^2 + K_3 \delta_3^3 + \cdots + K_m \delta_3^m \,, \tag{2.68}$$

and

$$\ln x_\mathrm{s}^\mathrm{m} = K_0 + 2X \sum_{n=1}^{m} K \delta_3^m \,, \tag{2.69}$$

where

$$K_0 = \ln x_\mathrm{s}^\mathrm{id} - X(\delta_2^2 + \delta_1^2) \,. \tag{2.70}$$

When $x_\mathrm{s}^\mathrm{m} << 1$, Eq. (2.69) reduces to the form

$$x_\mathrm{s}^\mathrm{m} = K_0^* + 2X \sum_{n=1}^{m} K \delta_3^m \,, \tag{2.71}$$

where $K_0^* = K_0 - 1$.

The experimental data of the solubility x_s^m of a solute in a solvent–cosolvent mixture as a function of cosolvent content f_3 and cosolvent solubility parameter δ_3 can be analyzed according to Eqs. (2.65) and (2.69), respectively. As an illustration Figure 2.17b shows the experimental $\ln x_s^m(f_3)$ data of sulfamerazine in solutions of methanol–water and 1-propanol–water mixtures, where dashed and solid curves are drawn in the form of Eq. (2.65) with fourth- and fifth-order polynomials. As seen from the best-fit plots, both fourth- and fifth-order polynomials represents the experimental $\ln x_s^m(f_3)$ data in the methanol–water mixture but fifth-order polynomial represents the experimental data better than the fourth-order polynomial in the 1-propanol–water mixture.

2.5.3. CNIBS/Redlich-Kister and Jouyban-Acree models

The log-linear model expressed by Eq. (2.47), based on the additive rule without consideration of activity coefficients of solutions, assumes, among others, that: (1) the number of molecules of solvent and cosolvent surrounding a solute molecules is the same, (2) the molar volume of solute in the solution does not differ from the molar volumes of the solvent and the cosolvent, (3) the solvent molecules in the solvent–cosolvent mixture behave in the same way as in the solvent and cosolvent individually, and (4) the free energy of transferring a solute to the solvent–cosolvent mixture is the algebraic sum of the free energies in the solvent and the cosolvent. However, most of these assumptions do not hold during the solubility of solutes in solvent mixtures and, therefore, as observed in numerous publications and examples presented above in Figures 2.15, 2.16 and 2.17, the log-linear model shows large deviations from the experimental data (Barzegar-Jalali and Jouyban-Gharamaleki, 1996, 1997).

The extended Hildebrand solubility (EHS) approach based on solubility parameters of solute, solvent and cosolvent was described above to describe the solubility of drugs. Apart from the EHS approach, several cosolvency models describing the solubility of solutes in mixed solvents have been reported in the literature (Jouyban and Acree, 2018; Jouyban-Gharamaleki and Acree, 1998; Jouyban-Gharamaleki et al., 1999). Despite different appearances of the equations of some of the theoretical models, using appropriate substitutions and rearrangements they can be transformed mathematically to the same model equation (Barzegar-Jalali and Jouyban-Gharamaleki, 1997).

Among the theoretical models, the combined nearly-ideal binary solvent/Redlich-Kister (CNIBS/R-K) model is based on thermodynamic consideration of contributions from both two- and three-body interactions during random mixing of components (Acree, 1992; Jouyban and Acree, 2018). According to this model, the solubility of a nonelectrolyte solute at temperature T in a solvent–cosolvent mixture may be given by (Jouyban and Acree, 2018)

$$\ln x_s^m = f_2(\ln x_{s2})_T + f_3(\ln x_{s3})_T + \\ + \frac{f_2 f_3}{R_G T}[M_0 + M_1(f_2 - f_3) + M_2(f_2 - f_3)^2 + M_3(f_2 - f_3)^3], \qquad (2.72)$$

where the indices 2 and 3 with the solubility x_s denote their values from saturated solutions in pure solvent and cosolvent, respectively, f_2 and f_3 are the fractions of solute 2 and cosolvent 3 in the mixture in the absence of the solute, M's are constants comprising different interaction energies, the subscript T indicates the solubility at temperature T, and $(f_2+f_3) = 1$. Eq. (2.72) describes the solute solubility as a function of solvent–cosolvent composition (i.e. f_2 and f_3) and solution temperature T. The above approach on which Eq. (2.72) is based is called the Jouyban–Acree model.

At a constant temperature T, R_GT is a constant and may be combined with the terms involving M's to obtain the well-known CNIBS/R-K equation

$$\ln x_s^m = f_2 \ln x_{s2} + f_3 \ln x_{s3} + f_2 f_3 \sum_{i=0}^{n} S_i (f_2 - f_3)^i , \tag{2.73}$$

where $S_i = M_i/R_GT$ and n may be 0, 1, 2 or 3. The third term on the right-hand side represents the excess Gibbs free energy change ΔG_{23}^{ex} of the system during the dissolution of a solute in the solvent–cosolvent mixture.

When $J_i = M_i/R_G$ and the solute solubility x_s is expressed by the van't Hoff relation, Eq. (2.72) may be written in the form (Jouyban et al., 2012, 2016):

$$(\ln x_s^m)_T = f_2\left(A_2 + \frac{B_3}{T}\right) + f_3\left(A_3 + \frac{B_3}{T}\right) + \frac{f_2 f_3}{T} \sum_{i=0}^{n} J_i (f_2 - f_3)^i , \tag{2.74}$$

where x_s^m is the solubility of the solute in the solvent mixture at T, the first two terms on the right-hand side represent the solute solubility in pure solvent 2 and cosolvent 3 of fractions f_2 and f_3, respectively, and A's and B's are constants of van't Hoff relation (2.5), J_i terms are constants of the model, and i is the number of solvents. The J_i terms may be calculated for $n = 2$ using a no-intercept least-square analysis of $[(\ln x_s^m)_T – f_2(A_2+B_2/T) – f_3(A_3+B_3/T)]$ against f_2f_3/T, $f_2f_3(f_2–f_3)/T$ and $f_2f_3(f_2–f_3)^2/T$. Obviously, for a two-solvent mixture from the solubility data the constants obtained are: A_1, B_1, A_2, B_2, J_0, J_1 and J_2. Then taking $f_3 = 1–f_2$, from Eq. (2.74) one obtains

$$(\ln x_s^m)_T = \left(A_2 + \frac{B_2}{T}\right) + f_3\left((A_3 - A_2) + \frac{(B_3 - B_2)}{T}\right) + \frac{(J_0 - J_1 + J_2)f_2}{T} + \\ + \frac{(-J_0 + 3J_1 - 5J_2)f_3^2}{T} + \frac{(-2J_1 + 8J_2)f_3^3}{T} + \frac{(-4J_2)f_3^4}{T} . \tag{2.75}$$

This equation upon rearrangement gives

$$T[(\ln x_s^m)_T - A_2] = B_2 + C_1 T f_3 + C_2 f_3 + C_3 f_3^2 + C_4 f_3^3 + C_5 f_3^4 , \tag{2.76}$$

where C's are parameters of the model, which may be calculated by regressing $T(\ln x_s^m)_T – A_2)$ against Tf_3. f_3, f_3^2, f_3^3 and f_3^4. Note that for a constant T the form of Eq. (2.76) is similar to that of Eq. (2.65).

The excess Gibbs free energy change $\Delta G_{23}{}^{\mathrm{ex}}$ in Eq. (2.73) is synonym of $\Delta G^{\mathrm{o}}_{\mathrm{mix}}$ for dissolution, which may be splitted into contributions from enthalpy and entropy of mixing, $\Delta H^{\mathrm{o}}_{\mathrm{mix}}$ and $\Delta S^{\mathrm{o}}_{\mathrm{mix}}$ using the Gibbs–Helmholtz equation. These excess thermodynamic functions F may be described by the polynomial relation (cf. Eq. (2.73))

$$F = A_0 + A_1 f_3 + A_2 f_3^2 + \cdots + A_n f_3^n , \tag{2.77}$$

where F denotes $\Delta G^{\mathrm{o}}_{\mathrm{mix}}$, $\Delta H^{\mathrm{o}}_{\mathrm{mix}}$ and $T\Delta S^{\mathrm{o}}_{\mathrm{mix}}$, and A's are regression parameters of the model.

It should be mentioned that the temperature dependence of the solubility $x_{\mathrm{s}}{}^{\mathrm{m}}$ of different solutes in solvent mixtures has also been represented by Apelblat equation (Zhou et al., 2013; Liu, B., et al., 2014; Dali et al., 2016):

$$\ln x_{\mathrm{s}}^{\mathrm{m}} = A_{\mathrm{m}} - \frac{B_{\mathrm{m}}}{T} + C_{\mathrm{m}} \ln T, \tag{2.78}$$

where A_{m}, B_{m} and C_{m} are model constants and the subscript m denotes the mixture. However, for binary solvent mixtures the Apelblat model does not reproduce the solubility data at any composition and temperature of interest (Jouyban et al., 2016).

Figure 2.18a and b shows the data of Figure 2.17b as dependence of the deviations $\Delta(\ln x_{\mathrm{s}}{}^{\mathrm{m}})$ in the experimental $\ln x_{\mathrm{s}}{}^{\mathrm{m}}(\mathrm{exp})$ from the calculated $\ln x_{\mathrm{s}}{}^{\mathrm{m}}(\mathrm{cal})$ by the additive rule (sum of terms $f_2 \ln x_{\mathrm{s}2}$ and $f_3 \ln x_{\mathrm{s}3}$ in Eq. (2.73)) for sulfamerazine in solutions of methanol–water and 1-propanol–water mixtures, respectively, on cosolvent water content f_3. Best-fit curves in the figures are drawn according to Eq. (2.73) with values of the constants S_i's given in Table 2.5. One observes some evident differences in the trends of the deviations in the plots of the two solvent mixtures due to the main solvent 2 and the solution temperature. With an increase in the cosolvent content f_3 in both solution mixtures, the deviation $\Delta(\ln x_{\mathrm{s}}{}^{\mathrm{m}})$ first increases and then decreases after passing through a maximum deviation at a particular value of the cosolvent content f_3. This value of f_3 is about 0.5 and 0.75 mole fraction for methanol–water and 1-propanol–water solutions, respectively, and is characteristic of the solvent mixture. In the two solvent mixtures, although one observes positive deviations in practically the entire range of water content f_3 at the two temperatures of the solubility measurements, small negative deviations may be discerned in the case of methanol–water mixtures at 298.15 K for methanol content less than about 0.1 mole fraction (i.e. $0.9 < f_3 < 1$). These observations of the deviations in the behavior of the plots of $\Delta(\ln x_{\mathrm{s}}{}^{\mathrm{m}})$ as a function of cosolvent content f_3 are associated with differences in the sizes of solvent and cosolvent molecules and solvent–cosolvent interactions.

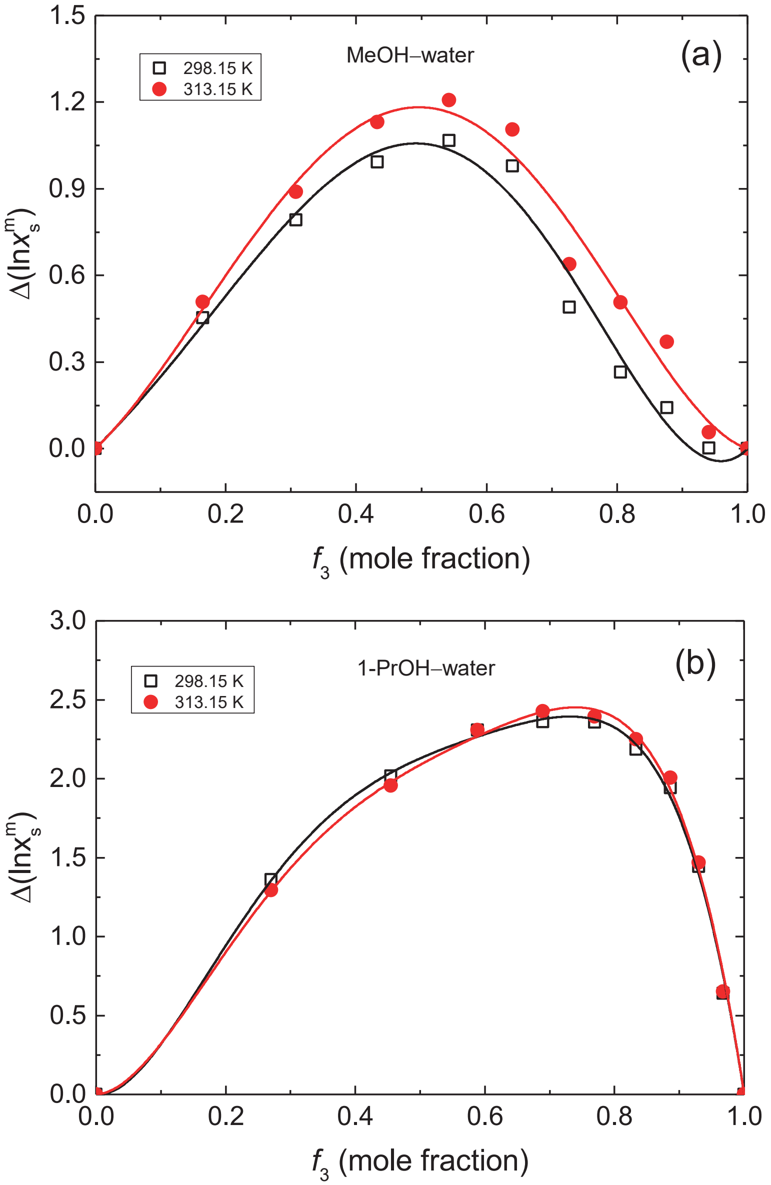

Figure 2.18. Plots of deviations $\Delta(\ln x_s^m)$ in the experimental $\ln x_s^m$(exp) of sulfamerazine in solutions of (a) methanol–water and (b) 1-propanol–water mixtures against water content f_3. Curves are drawn according to Eq. (2.73) with values of constants given in Table 2.5. Original data from Figure 2.17b.

Table 2.5. Values of constants of Eq. (2.73) for solubility of sulfamerazine in methanol–water and 1-propanol–water mixtures

Solvent	T (K)	Constants				R^2
-		S_0	S_1	S_2	S_3	
Methanol	298.15	4.22633	0.28803	−4.20450	1.95713	0.9715
	313.15	4.73909	0.12922	−3.27979	0.57279	0.9710
1-propanol	298.15	8.51509	−3.63080	4.70020	−9.90625	0.9962
-	313.15	8.35136	−4.52281	5.34470	−8.94848	0.9957

2.5.4. Thermodynamic functions of solution and mixing in ternary solutions

The thermodynamic functions ΔG^o, ΔH^o and $T\Delta S^\mathrm{o}$ of solution and mixing of a ternary system composed of a solute dissolved in a given solvent–cosolvent mixture of known cosolvent content f_3 are calculated from the plots of $\ln x_\mathrm{s}{}^\mathrm{m}$ against T^{-1} following the procedure described in Section 2.3.4 for binary solutions. In this section, the behavior of the thermodynamic functions of mixing as a function of cosolvent content f_3 in the solvent mixture for the following two systems is described: (1) ammonium oxalate (AO) dissolved in water–acetone mixtures, and (2) sulfamerazine dissolved in methanol–water and 1-propanol–water mixtures. The original data are from Sangwal et al. (2013) and Delgado and Martinez (2014, 2015), respectively. While calculating the values of $\Delta G^\mathrm{o}_\mathrm{sol}$ for the dissolution of AO, the values of enthalpy ΔH_m and temperature T_m of melting reported by Mosaad et al. (1995) were used.

Figure 2.19 shows the experimental data of the temperature dependence of the standard Gibbs free energy change $\Delta G^\mathrm{o}_\mathrm{mix}$, the standard enthalpy of mixing $\Delta H^\mathrm{o}_\mathrm{mix}$ and the corresponding entropy-related term $T_\mathrm{hm}\Delta S^\mathrm{o}_\mathrm{mix}$ for the solubility $x_\mathrm{s}{}^\mathrm{m}$ of ammonium oxalate in water and water–acetone mixtures as a function of cosolvent content f_3 (by weight) up to 0.55. The curves are drawn according to Eq. (2.77) with the constant listed in Table 2.6. As seen from the figure, the value of the standard Gibbs free energy change $\Delta G^\mathrm{o}_\mathrm{mix}$ steadily increases with increasing cosolvent content f_3 and is positive in the entire cosolvent range investigated in the study. The positive values of $\Delta G^\mathrm{o}_\mathrm{mix}$ are due to the fact that the experimental solubilities are lower than the ideal solubilities and the activity coefficient γ_s of the solutions is greater than unity in the entire studied f_3 range. Despite large variations, the estimated values of $\Delta H^\mathrm{o}_\mathrm{mix}$ and $T_\mathrm{hm}\Delta S^\mathrm{o}_\mathrm{mix}$ show trends different from that of $\Delta G^\mathrm{o}_\mathrm{mix}$. The mixing enthalpy $\Delta H^\mathrm{o}_\mathrm{mix}$ is positive for all acetone content f_3 and, with an increase in f_3, its value $\Delta H^\mathrm{o}_\mathrm{mix}$ increases from an initial value of 3.45 kJ·mol^{-1}, attains a maximum value at $f_3 \approx 0.25$ weight fraction, and finally approaches $\Delta G^\mathrm{o}_\mathrm{mix}$ for $0.4 \leq f_3 \leq 0.55$. The entropy term $T_\mathrm{hm}\Delta S^\mathrm{o}_\mathrm{mix}$ also shows a behavior similar to that of $\Delta H^\mathrm{o}_\mathrm{mix}$. Its value increases from an initial value of –0.86 kJ·mol^{-1}, attains a maximum value at $f_3 \approx 0.25$ weight fraction, and finally approaches zero for $0.4 \leq f_3 \leq 0.55$.

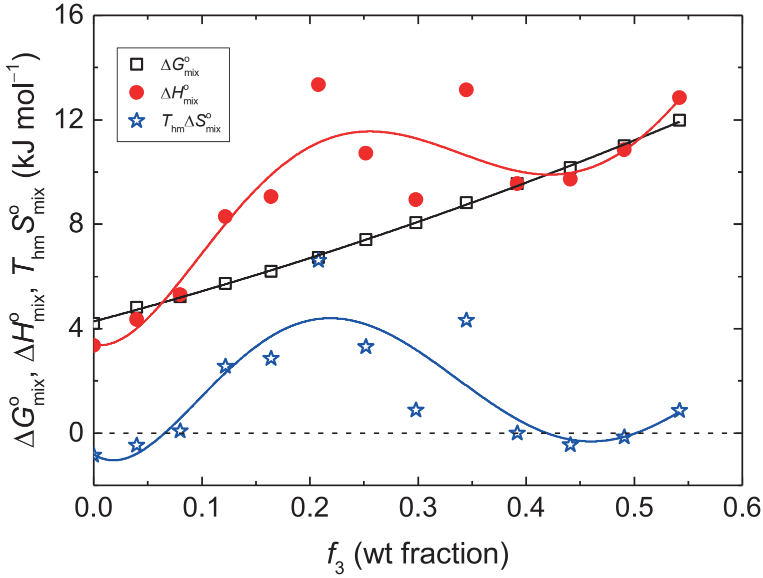

Figure 2.19. Dependence of calculated thermodynamic functions $\Delta G^{\text{o}}_{\text{mix}}$, $\Delta H^{\text{o}}_{\text{mix}}$ and $T_{\text{hm}}\Delta S^{\text{o}}_{\text{mix}}$ for the dissolution of AO in water–acetone mixture on acetone content f_3 at 303.15 K. Plots are drawn according to Eq. (2.77). Original data from Sangwal et al. (2013).

Figure 2.20a and b shows the experimental data of $\Delta G^{\text{o}}_{\text{mix}}$, $\Delta H^{\text{o}}_{\text{mix}}$ and $T_{\text{hm}}\Delta S^{\text{o}}_{\text{mix}}$ for the dissolution of sulfamerazine in methanol–water and 1-propanol–water mixtures, respectively, on water content f_3 at 303 K. Best-fit plots for the data are drawn according to Eq. (2.77) with the parameters given in Table 2.6. Well-defined differences in the plots of different functions in the two solvent mixtures may be noted from the figure. The value of $\Delta G^{\text{o}}_{\text{mix}}$ in the methanol–water mixture steadily increases with the cosolvent content f_3 (Figure 2.20a). The values of $\Delta H^{\text{o}}_{\text{mix}}$ and $T_{\text{hm}}\Delta S^{\text{o}}_{\text{mix}}$ also increase with f_3 approaching maximum values at $f_3 \approx 0.85$ mole fraction when it begins to decrease with an increase in f_3.

In contrast to the dissolution behavior of sulfamerazine in methanol–water mixture, the value of $\Delta G^{\text{o}}_{\text{mix}}$ in the 1-propanol–water mixture (Figure 2.20b) initially decreases and approaches a minimum value at $f_3 \approx 0.5$ mole fraction when it begins to increase with increasing f_3 and the increase is relatively steep for $f_3 > 0.8$ mole fraction. The values of $\Delta H^{\text{o}}_{\text{mix}}$ and $T_{\text{hm}}\Delta S^{\text{o}}_{\text{mix}}$ also decrease with an increase in f_3 and, after approaching minumum values at $f_3 \approx 0.5$ mole fraction, they attain maximum values at $f_3 \approx 0.8$ mole fraction when they begins to decrease with an increase in f_3.

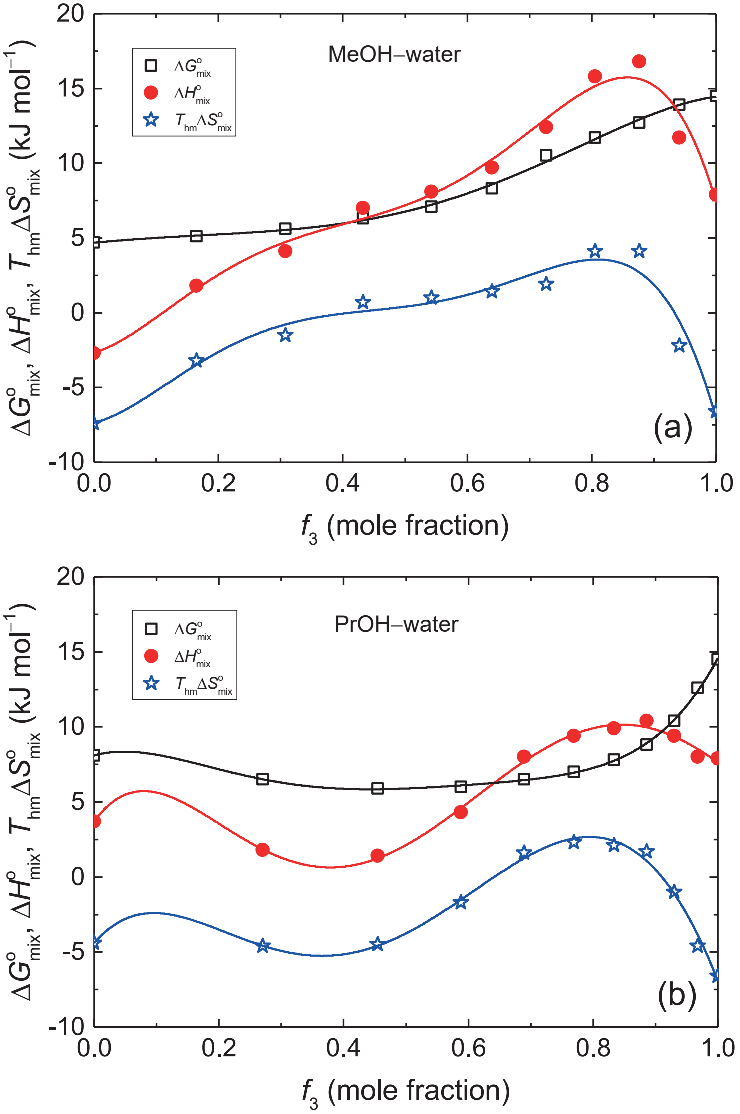

Figure 2.20. Plots of $\Delta G^{\mathrm{o}}_{\mathrm{mix}}$, $\Delta H^{\mathrm{o}}_{\mathrm{mix}}$ and $T_{\mathrm{hm}}\Delta S^{\mathrm{o}}_{\mathrm{mix}}$ for the dissolution of sulfamerazine in (a) methanol–water and (b) 1-propanol–water mixtures against water content f_3 at 303 K. Plots are drawn according to Eq. (2.77). Original data from Delgado and Martinez (2014, 2015).

Table 2.6. Values of constants of Eq. (2.77) for dissolution of AO and sulfamerazine

Function	Constants						R^2
-	A_0	A_1	A_2	A_3	A_4	A_5	
AO/water–acetone							
$\Delta G^{\circ}_{\mathrm{mix}}$	4.278	10.979	5.782	--	--	--	0.9992
$\Delta H^{\circ}_{\mathrm{mix}}$	3.394	−8.636	747.1	−3751.3	6677.4	−3941.5	0.7415
$T_{\mathrm{hm}}\Delta S^{\circ}_{\mathrm{mix}}$	−0.810	−26.63	864.7	−4261.0	7743.3	−4724.6	0.4735
Sulfamerazine/methanol–water							
$\Delta G^{\circ}_{\mathrm{mix}}$	4.688	3.833	−6.703	−2.002	52.11	−37.47	0.9951
$\Delta H^{\circ}_{\mathrm{mix}}$	−2.678	12.454	174.0	−720.1	1061.5	−517.7	0.9628
$T_{\mathrm{hm}}\Delta S^{\circ}_{\mathrm{mix}}$	−7.342	10.590	167.8	−688.2	980.0	−469.8	0.9046
Sulfamerazine/1-propanol–water							
$\Delta G^{\circ}_{\mathrm{mix}}$	8.099	11.479	−149.0	437.1	−517.9	224.8	0.9977
$\Delta H^{\circ}_{\mathrm{mix}}$	3.698	57.78	−499.3	1258.3	−1200.6	387.8	0.9855
$T_{\mathrm{hm}}\Delta S^{\circ}_{\mathrm{mix}}$	−4.401	48.28	−360.4	839.9	−697.5	167.2	0.9741

As seen from Figures 2.19 and 2.20, irrespective of the cosolvent content f_3, the Gibbs free energy change $\Delta G^{\circ}_{\mathrm{mix}}$ of mixing is positive in the three cases. The positive values of $\Delta G^{\circ}_{\mathrm{mix}}$ in these cases are due to the fact that the experimental solubilities are lower than the ideal solubilities and are associated with the activity coefficients γ_s of the systems. In ideal solubilities, the contributions $\Delta H^{\circ}_{\mathrm{mix}}$ and $T_{\mathrm{hm}}\Delta S^{\circ}_{\mathrm{mix}}$ to $\Delta G^{\circ}_{\mathrm{mix}}$ are positive. However, during the dissolution of solutes in solvent–cosolvent mixtures these contributions depend on the cosolvent content f_3 and can be positive as well as negative, depending on the region of cosolvent content f_3. For example, during the dissolution of AO in water–acetone mixture $\Delta H^{\circ}_{\mathrm{mix}}$ is positive in the entire f_3 range, but $T_{\mathrm{hm}}\Delta S^{\circ}_{\mathrm{mix}}$ is positive in the range of acetone content f_3 between 0.1 and 0.4 wt fraction. During the dissolution of sulfamerazine in methanol–water mixture $\Delta H^{\circ}_{\mathrm{mix}}$ is positive for water content $f_3 > 0.15$ mole fraction, but $T_{\mathrm{hm}}\Delta S^{\circ}_{\mathrm{mix}}$ is positive in the f_3 range between 0.3 and 0.93 mole fraction. In contrast to this, during the dissolution of sulfamerazine in 1-propanol–water mixture $\Delta H^{\circ}_{\mathrm{mix}}$ is positive in the entire f_3 range whereas $T_{\mathrm{hm}}\Delta S^{\circ}_{\mathrm{mix}}$ is positive only in a narrow range of f_3 between 0.65 and 0.90 mole fraction.

As described in Section 2.5.2, the solubility of a solute in an individual solvent depends on solute–solute, solvent–solvent and solute–solvent interactions. In Eq. (2.60) these solute–solute, solvent–solvent and solute–solvent interactions were represented by the solubility parameters δ_1, δ_2 and $W^{1/2}$, respectively. The δ_1 and δ_2

parameters are unfavorable for solubility whereas the $W^{1/2}$ parameter favors solubility. The dissolution of a solute in an individual solvent is determined by two processes: (1) breaking of solvent–solvent bonds by solute molecules, and (2) solvation of solute molecules involving the association of solvent molecules around them by forming solute–solvent bonds. The process of rupturing of solvent–solvent bonds involves the formation of cavities or voids in the solvent and is endothermic because energy is required in this process ($\Delta H^{\mathrm{o}}_{\mathrm{mix}} < 0$). This results in a decrease in the solute solubility. The process of formation of different types of solute–solvent bonds is exothermic. This results in an increase in the solute solubility. In a solvent–cosolvent mixture, apart from the above interactions, additional solvent–cosolvent, solute–cosolvent and cosolvent–cosolvent interactions also contribute to the solute solubility $x_{\mathrm{s}}^{\mathrm{m}}$. The net variation in the mixing enthalpy $\Delta H^{\mathrm{o}}_{\mathrm{mix}}$ is related to the contributions from changes in the different kinds of interactions with cosolvent content f_3. Below we consider the trends of variation of $\Delta H^{\mathrm{o}}_{\mathrm{mix}}$ with cosolvent content f_3 in the above examples of Figures 2.19 and 2.20.

The positive values of $\Delta H^{\mathrm{o}}_{\mathrm{mix}}$ for the dissolution of AO in water–acetone mixtures and sulfamerazine in 1-propanol-rich solutions in the entire investigated f_3 range (Figures 2.19 and 2.20b) suggest that the association of solvent molecules with the solute molecules by forming preferred solute–solvent bonds determines the dissolution process in these systems. In organic (nonelectrolyte) compounds the association of solvent molecules can take place around the solute molecules by van der Waals and Lewis acid–base interactions, but in electrolytes the association of solvent molecules occurs around their ions mainly by electrostatic interactions between the ions and the polar groups of solvent molecules. In cosolvent-rich solutions interactions between the cosolvent molecules become increasingly dominant with an increase in the cosolvent content f_3. This leads to a decrease in the values of $\Delta H^{\mathrm{o}}_{\mathrm{mix}}$ after attaining a maximum in different systems. In the case of dissolution of AO in water–acetone mixtures, after attaining a minimum value at acetone content $f_3 \approx 0.4$ wt fraction, the mixing enthalpy $\Delta H^{\mathrm{o}}_{\mathrm{mix}}$ begins to increase with an increase in the acetone content f_3 (see Figure 2.19). This trend is possible when acetone–acetone interactions become saturated such that their contribution attains a constant value but the other contributions still increase with increasing f_3. The negative values of $\Delta H^{\mathrm{o}}_{\mathrm{mix}}$ during the dissolution of sulfamerazine in pure methanol and methanol-rich solutions, as observed in Figure 2.20a, may be attributed to the dominant contribution of the process of formation of cavities or voids by the solute in these solutions.

2.5.5. Enthalpy–entropy compensation analysis

The mechanism responsible for the action of a cosolvent on the solubility of a solute is analyzed from plots of enthalpy $\Delta H^{\mathrm{o}}_{\mathrm{mix}}$ of mixing as a function of Gibbs free energy change $\Delta G^{\mathrm{o}}_{\mathrm{mix}}$ of mixing for the system. This type of analysis is usually referred to as enthalpy–entropy compensation analysis of solubility (Bustamante et al., 1998; Delgado and Martinez, 2013, 2014; Krug et al., 1976). A general feature of these plots is that the dependence of $\Delta H^{\mathrm{o}}_{\mathrm{mix}}$ on $\Delta G^{\mathrm{o}}_{\mathrm{mix}}$ is nonlinear and is unrelated to the increase in cosolvent content f_3.

Figure 2.21 shows plots of the enthalpy $\Delta H^{\mathrm{o}}_{\mathrm{mix}}$ of mixing and the corresponding entropy-related term $T_{\mathrm{hm}}\Delta S^{\mathrm{o}}_{\mathrm{mix}}$ as functions of the Gibbs free energy change $\Delta G^{\mathrm{o}}_{\mathrm{mix}}$ of mixing for the dissolution of AO in water–acetone mixture of different acetone content. Despite large scatter in the $\Delta H^{\mathrm{o}}_{\mathrm{mix}}$ and $T_{\mathrm{hm}}\Delta S^{\mathrm{o}}_{\mathrm{mix}}$ data, one observes that their values increase and then decrease with an increase in $\Delta G^{\mathrm{o}}_{\mathrm{mix}}$. This behavior may be correlated by the following regular polynomial:

$$F = a_0 + a_1(\Delta G^{\mathrm{o}}_{\mathrm{mix}}) + a_2(\Delta G^{\mathrm{o}}_{\mathrm{mix}})^2 + \cdots + a_n(\Delta G^{\mathrm{o}}_{\mathrm{mix}})^n , \tag{2.79}$$

where F denotes $\Delta H^{\mathrm{o}}_{\mathrm{mix}}$ and $T_{\mathrm{hm}}\Delta S^{\mathrm{o}}_{\mathrm{mix}}$, and a's are regression constants. Curves in the figure are drawn according to Eq. (2.79) with $n = 5$ and the constants given in Table 2.7. The increase in $\Delta H^{\mathrm{o}}_{\mathrm{mix}}$ with an increase in $\Delta G^{\mathrm{o}}_{\mathrm{mix}}$ suggests that the dissolution of AO in water-rich solutions is driven by enthalpy but the process becomes entropy controlled with the addition of acetone.

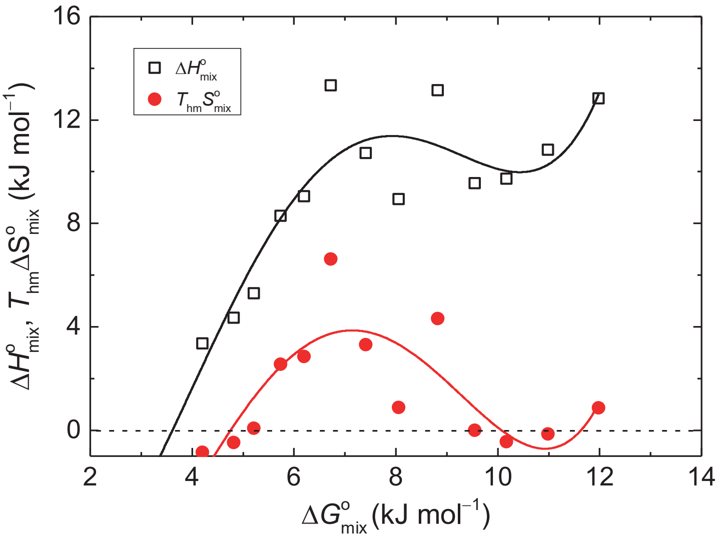

Figure 2.21. Plots of $\Delta H^{\mathrm{o}}_{\mathrm{mix}}$ and $T_{\mathrm{hm}}\Delta S^{\mathrm{o}}_{\mathrm{mix}}$ against Gibbs enthalpy change $\Delta G^{\mathrm{o}}_{\mathrm{mix}}$ of mixing in the dissolution of AO in water–acetone mixtures of different acetone content. Plots are drawn according to Eq. (2.79) with constants in Table 2.7. Original data in Figure 2.19.

Table 2.7. Values of constants of Eq. (2.79) for dissolution of AO and sulfamerazine

Function	Constants						R^2
-	A_0	A_1	A_2	A_3	A_4	A_5	
AO/water–acetone							
$\Delta H^{\circ}_{\text{mix}}$	0.0098	−8.2634	3.6152	−0.4209	0.01435	$-8.58 \cdot 10^{-5}$	0.8170
$T_{\text{hm}}\Delta S^{\circ}_{\text{mix}}$	0.0098	−9.2634	3.6152	−0.4209	0.01434	$-8.58 \cdot 10^{-5}$	0.4122
Sulfamerazine/methanol–water							
$\Delta H^{\circ}_{\text{mix}}$	−263.88	131.24	−24.33	2.121	−0.0836	0.0011	0.9877
$T_{\text{hm}}\Delta S^{\circ}_{\text{mix}}$	−265.96	131.58	−24.65	2.157	−0.0855	0.0012	0.9708
Sulfamerazine/1-propanol–water							
$\Delta H^{\circ}_{\text{mix}}$	−1064.76	543.41	−108.35	10.65	−0.5164	0.0099	0.9180
$T_{\text{hm}}\Delta S^{\circ}_{\text{mix}}$	−1043.94	531.22	−106.01	10.42	−0.5046	0.0096	0.9304

Figure 2.22a and b shows plots of the enthalpy $\Delta H^{\circ}_{\text{mix}}$ of mixing and the corresponding entropy-related term $T_{\text{hm}}\Delta S^{\circ}_{\text{mix}}$ as functions of the Gibbs free energy change $\Delta G^{\circ}_{\text{mix}}$ of mixing of sulfamerazine in methanol–water and 1-propanol–watermixtures, respectively, on water content f_3 at 303 K. In the plots pure solvent methanol and 1-propanol, and pure cosolvent are denoted by 0 and 1, respectively. If the data for 1-propanol-rich mixtures are excluded, the data may be described by the fourth-order polynomial of Eq. (2.79), with the values of the constants listed in Table 2.7.

As seen from Figure 2.22a, the value of $\Delta H^{\circ}_{\text{mix}}$ steadily increases nonlinearly with $\Delta G^{\circ}_{\text{mix}}$ from an initial value of -3.3 kJ·mol^{-1} for the solute solubility in pure methanol and, after attaining a maximum value of 16.8 kJ·mol^{-1} at $f_3 = 0.877$ mole fraction (for $\Delta G^{\circ}_{\text{mix}} = 12.7$ kJ·mol^{-1}), finally approaches a value of 7.9 kJ·mol^{-1} for the solubility in pure water. In the case of the 1-propanol–water mixture (Figure 2.22b), the trend of the dependence of $\Delta H^{\circ}_{\text{mix}}$ on $\Delta G^{\circ}_{\text{mix}}$ is somewhat different from that in the methanol–water mixture. From an initial value of 3.7 kJ·mol^{-1} for pure 1-propanol, the value of $\Delta H^{\circ}_{\text{mix}}$ slowly decreases to 1.8 kJ·mol^{-1} at water content $f_3 = 0.455$ mole fraction, then increases to a maximum value of 10.4 kJ·mol^{-1} at water content $f_3 = 0.769$ mole fraction, and finally decreases slowly and attains a value of 7.9 kJ·mol^{-1} in pure water. These trends suggest that in the composition range of methanol-water and 1-propanol-water mixtures where the slope of the dependence of $\Delta H^{\circ}_{\text{mix}}$ on $\Delta G^{\circ}_{\text{mix}}$ for the dissolution of sulfamerazine is positive, the dissolution process is enthalpy controlled and is probably associated with the better solvation of the solute. However, in water-rich mixtures of both methanol and 1-propanol where the slope is negative, the dissolution process is controlled by the entropy of mixing and is probably associated with the loosening of the structures of cosolvent water. The decrease in the value of $\Delta H^{\text{o}}_{\text{mix}}$ with the addition of cosolvent water to 1-propanol in 1-propanol-rich mixtures is also probably entropy driven involving the loosening of the structures of the solvent 1-propanol by water.

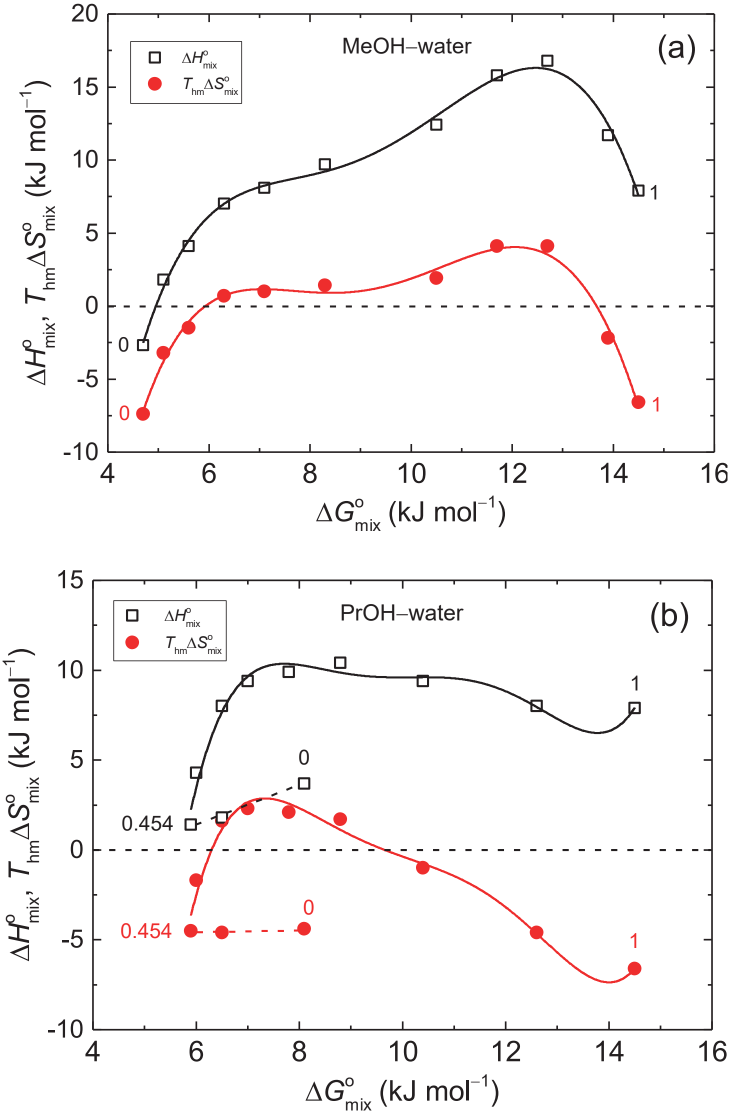

Figure 2.22. Plots of $\Delta H^{\text{o}}_{\text{mix}}$ and $T_{\text{hm}}\Delta S^{\text{o}}_{\text{mix}}$ against Gibbs enthalpy change $\Delta G^{\text{o}}_{\text{mix}}$ of mixing in the dissolution of sulfamerazine in (a) methanol–water and (b) 1-propanol–water mixtures on water content f_3 at 303 K. Plots are drawn according to Eq. (2.79). Original data from Delgado and Martinez (2014, 2015).

2.5.6. Preferential solvation of solute by solvents

A solute has a high solubility in the main solvent and relatively poor solubility in the cosolvent. Differences in the solubility of the solute in the solvent and cosolvent are associated with the differences in the ability of solvation of solute by the two. This is the basis of carrying out antisolvent crystallization where the more preferential solvation of solute molecules/ions by solvent molecules is replaced by the less preferential solvation of the solute molecules/ions by cosolvent molecules. Differences in the preferential solvation of the solute by the main solvent and the cosolvent in saturated mixtures are associated with some thermodynamic quantities (Delgado and Martinez, 2015; Jouyban et al., 2016; Marcus, 2002, 2008; Martinez et al., 2016).

In the discussion of the solubility of solute 1 in the main solvent 2 and the cosolvent 3 above it was implicitly assumed that the solute solubility is higher in the solvent than that in the cosolvent. However, this assumption is arbitrary and the solubility behavior of a solute in the mixture can be considered equally with reference to the solvent as well as the cosolvent. Denoting the solute as 1, and the reference solvent and the other solvent (cosolvent) as 2 and 3, respectively, the preferential solvation behavior of the solute is described by its solvation parameter defined as (Delgado and Martinez, 2015; Marcus, 2002, 2008; Jouyban et al., 2016; Martinez et al., 2016):

$$\delta x_{3,1} = x_{3,1}^{\mathrm{L}} - x_3 = -\delta x_{2,1}\,, \tag{2.80}$$

where $x_{3,1}{}^{\mathrm{L}}$ is the local mole fraction of cosolvent 3 in the environment near to the solute 1 and x_3 is its bulk mole fraction composition in the initial binary solvent mixture. If $\delta x_{3,1} > 0$, the solute is preferentially solvated by cosolvent 3. However, if $\delta x_{3,1} < 0$, the solute is preferentially solvated by the reference solvent 2. Values of $\delta x_{3,1}$ are obtained from the inverse Kirkwood-Buff integrals for the individual solvent components in terms of the thermodynamic quantities (Marcus, 2002, 2008):

$$G_{2,1} = R_{\mathrm{G}} T \kappa_T - V_1 + x_3 V_3 D / Q\,, \tag{2.81}$$

$$G_{3,1} = R_{\mathrm{G}} T \kappa_T - V_1 + x_2 V_2 D / Q\,, \tag{2.82}$$

where κ_T is the isothermal compressibility of the solvent mixtures (GPa^{-1}), V_2 and V_3 are the partial molar volumes of the solvents 2 and 3, respecively, and V_1 is the partial molar volume of the solute. The function D is the derivative of the standard molar Gibbs energies of transfer of solute from neat reference solvent 2 to the binary solvent mixtures, with respect to the solvent composition. The function Q involves the second derivative of the excess molar Gibbs energy of mixing of the two solvents with respect to the proportion of the reference solvent in the mixtures. These functions are given by

$$D = \left(\frac{\partial \Delta G^{\mathrm{o}}_{1,2\to 2+3}}{\partial x_3} \right)_{T,p} \tag{2.83}$$

$$Q = R_G T + x_2 x_3 \left(\frac{\partial^2 \Delta G_{2+3}^{\text{excess}}}{\partial x_2^2} \right)_{T,p} , \tag{2.84}$$

whereas the preferential solvation parameter is calculated from the relation

$$\delta x_{3,1} = \frac{x_2 x_3 (G_{3,1} - G_{2,1})}{x_2 G_{2,1} + x_3 G_{3,1} + V_{\text{cor}}} , \tag{2.85}$$

with the correlation volume V_{cor} obtained by

$$V_{\text{cor}} = 2522.5\left(r_1 + 0.1363[x_{2,1}^{\text{L}} V_2 + x_{3,1}^{\text{L}} V_3]^{1/3} - 0.085\right)^3 , \tag{2.86}$$

where the radius r_1 of the solute in nm is related to the partial molar volume V_1 of the solute and the Avogadro number N_A by

$$r_1 = \left(\frac{3 \cdot 10^{21} V_1}{4\pi N_A} \right)^{1/3} . \tag{2.87}$$

The Gibbs energy of transfer of solute from neat reference solvent 2 to binary solvent mixtures is given by

$$\Delta G_{1,2\to 2+3}^{\text{o}} = R_G T \ln\left(\frac{x_{1,2}}{x_{1,2+3}} \right) . \tag{2.88}$$

The value of $\Delta G_{1,2\to 2+3}^{\text{o}}$ is usually correlated according to a polynomial such as:

$$\Delta G_{1,2\to 2+3}^{\text{o}} = z_0 + z_1 f_3 + z_2 f_3^2 + z_3 f_3^3 , \tag{2.89}$$

where z's are empirical constants and f_3 ($\equiv x_3$) is the content of the cosolvent 3 in the solute-free solvent–cosolvent mixture.

Several examples of the analysis of the solvation behavior of various solutes in suitable solvent–cosolvent mixtures are known in the literature (Delgado and Martinez, 2015; Marcus, 2002, 2008; Jouyban et al., 2016; Martinez et al., 2016). An example of the analysis of the solvation behavior deduced from experimental solubility data of vanillin (solute 1) in solvent mixtures of water (main solvent 2) + propylene glycol (cosolvent 3) at two different temperatures is presented below

It is found (Delgado and Martinez, 2015; Jouyban et al., 2016; Martinez et al., 2016) that the values of the standard Gibbs energies $G_{2,1}$ and $G_{3,1}$ are negative in all solution mixtures indicating that this compound shows affinity for both solvents in the mixtures. The parameters used in the calculations are: molar volume of vanillin V_1 = 103.0 $\text{cm}^3 \cdot \text{mol}^{-1}$, r_1 = 0.344 nm. Figure 2.23 shows the Gibbs energy ΔG^{o} of transfer behavior of vanillin (1) from neat water (2) to water (2) + propylene glycol (3) mixtures as a function of propylene glycol content f_3 at 298 and 313 K. Obviously, the Gibbs energy ΔG^{o} smoothly decreases with increasing propylene glycol content f_3.

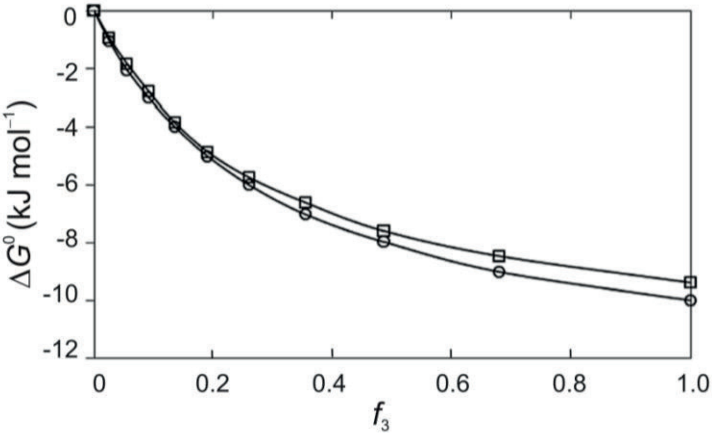

Figure 2.23. Gibbs energy ΔG^o of transfer of vanillin (solute 1) from neat water (solvent 2) to cosolvent mixtures of water (solvent 2) + propylene glycol (cosolvent 3) as a function of propylene glycol content f_3 at two temperatures: (circles) 298 K and (squares) 313 K. After Martinez et al. (2016).

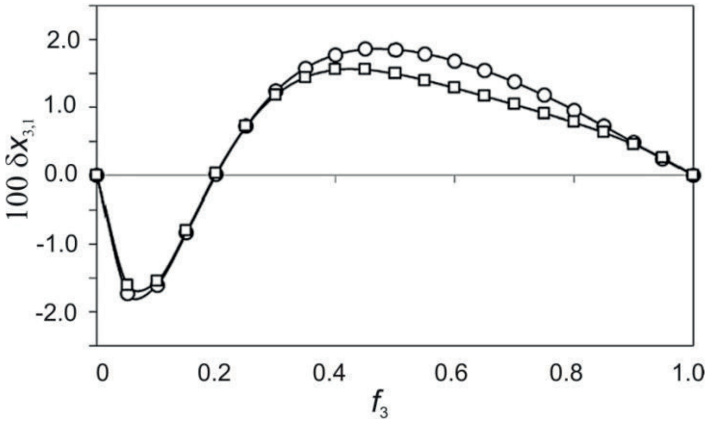

Figure 2.24. Dependence of preferential solvation parameter $\delta x_{3,1}$ on the content f_3 of cosolvent propylene glycol in water + propylene glycol mixtures at two temperatures: (circles) 298 K and (squares) 313 K. After Martinez et al. (2016).

Figure 2.24 shows the dependence of preferential solvation parameter $\delta x_{3,1}$ on propylene glycol content f_3 in water (2) + propylene glycol (3) cosolvent mixtures at 298 and 313 K. It may be noted that the variation of $\delta x_{3,1}$ is nonlinear with the propylene glycol content f_3 in the solvent mixture. Addition of propylene glycol to water leads to make the parameter $\delta x_{3,1}$ negative initially approaching a minimum value at $f_3 = 0.05$ in the mixture. In these water-rich mixtures, the lowering of the net $\delta x_{3,1}$ to negative values is probably associated with the hydrophobic hydration around the nonpolar groups of vanillin. In the mixture composition $0.20 < f_3 < 1.0$, the local mole fraction of cosolvent propylene glycol is higher than that of water. In this range of solvent mixture composition the increase in the solubility of solute vanillin is likely to be associated with the breaking of the ordered structure (hydrogen bonds) of water around the nonpolar moieties of solute which increases the solvation of vanillin and exhibits a maximum value at f_3 = 0.45. From the figure one also notes that the magnitude of preferential solvation by propylene glycol and water diminishes with an increase in temperature.

References

Anuar, N., W.R.W. Daud, K.J. Roberts, S.K. Kamarudin, and S.M. Tasirin (2009). An examination of the solution chemistry, nucleation kinetics, and polymorphic behavior of aqueous phase batch crystallized L-isoleucine at the 250 mL scale size. *Cryst. Growth Des.* **9**, 2853-2862.

Acree W.E. Jr (1992). Mathematical representation of thermodynamic properties. Part 2. Derivation of the combined nearly ideal binary solvents(NIBS)/Redlich-Kister mathematical representation from a two-body and three-body interactional model. *Thermochimica Acta* **198**, 71-79.

Apelblat, A., and E. Manzurola (1999). Solubilities of *o*-acetylsalicylic, 4-aminosalicylic, 3,5-dinitrosalicylic, and*p*-toluic acid, and magnesium-DL-aspartate in water from T = (278 to 348) K. *J. Chem. Thermodyn.* **31**, 85-91.

Avila, C.M., and F. Martinez (2002). Thermodynamic study of the solubility of benzocaine in some organic and aqueous solvents. *J. Solution Chem*. **31**, 975-985.

Barata, P.A., and M.L. Serrano (1997). Thermodynamic representation of the solubility of potassium dihydrogen phosphate (KDP) + water + alcohol systems. *Fluid Phase Equilibria* **141**, 247-263.

Barrett, M., M. McNamara, H.-X. Hao, P. Barrett, and B. Glennon (2010). Supersaturation racking for the development, optimization and control of crystallization processes. *Chem. Eng. Res. Des.* **88**, 1108–1119.

Barton, A. (1991). *Handbook of Solubility Parameters and Other Cohesion Parameters*. 2nd Edition. CRC Press, New York.

Barzegar-Jalali, M., and A. Jouyban-Gharamaleki (1996). Models for calculating solubility in binary solvent systems. *Int. J. Pharm.* **140**, 237-246.

Barzegar-Jalali, M., and A. Jouyban-Gharamaleki (1997). A general model from theoretical cosolvency models. *Int. J. Pharm.* **152**, 247-250.

Borecka, B., K. Sangwal, M. Rak, and A. Lipiński (1983). Growth characteristics of *p*-terphenol crystals from some organic solvents. *J. Cryst. Growth* **65**, 518-523.

Borissova, A., S. Khan, T. Mahmud, K.J. Roberts, J. Andrews, P. Dallin, Z.-P. Chen, and J. Morris (2009). In situ measurement of solution concentration during the batch cooling crystallization of L-glutamic acid using ATR-FTIR spectroscopy coupled with chemometrics. *Cryst. Growth Des.* **9**, 692-706.

Bravi, M., and B. Mazzarotta (1998). Primary nucleation of citric acid monohydrate: influence of selected impurities. *Chem. Eng. J.* **70**, 197-202.

Buchowski, H., A. Ksiazczak, and S. Pietrzyk (1980). Solvent activity along a saturation line and solubility of hydrogen-bonding solids. *J. Phys. Chem.* **84**, 975-979.

Bustamante, P., S. Romero, A. Pena, B. Escalera, and A. Reillo (1998). Nonlinear enthalpy−entropy compensation for the solubility of drugs in solvent mixtures: paracetamol, acetanilide and nalidixic acid in dioxane−water. *J. Pharm. Sci.* **87**, 1590-1596.

Chang, S.S. (1983). Heat capacity and thermodynamic properties of p-terphenyl: study of order-disorder transition by automated high-resolution adiabatic calorimetry, *J. Chem. Phys.* 79, 6229-6236

Chen, L.-Z., F.-Z. Zhou, and J.-L. Wang (2014). Solubilities of 2,4,6-trinitrotoluene in methanol and binary mixtures of methanol + water from 293.15 to 333.15 K. *J. Solution Chem.* **43**, 2163-2169.

Cui, Y.-D., S.-J. Xu, S.-G. Wu, S.-C. Du, Y. Cao, Y.-F. Chen, L. Liu, W.-B. Dong, and J.-B. Gong (2017). Temperature and solvent dependent thermodynamic behavior of tetrabromobisphenol A. *J. Mol. Liquids* **241**, 150-162.

Danuwila, D.D., and A.K. Berglund (1997). ATR FTIR spectroscopy for in situ measurement of supersaturation. *J. Cryst. Growth* **179**, 185-193.

Danuwila, D.D., B.L. Carroll, and A.K. Berglund (1994). An investigation of the applicability of attenuated total reflection infrared spectroscopy for measurement of solubility and supersaturation of aqueous citric acid solutions. *J. Cryst. Growth* **137**, 561-568.

Delgado, D.R., and F. Martinez (2013). Solubility and solution thermodynamics of sulfamerazine and sulfamethazine in some ethanol + water mixtures. *Fluid Phase Equilibria* 360, 88-96.

Delgado, D.R., and F. Martinez (2014). Solubility and solution thermodynamics of some sulfonamides in 1-propanol + water mixtures. *J. Solution Chem*. 43, 836-852.

Delgado, D.R., and F. Martinez (2015). Solution thermodynamics and preferential solvation of sulfamerazine in methanol + water mixtures. *J. Solution Chem.* **44**, 360-377.

Emami, S., A. Jouyban, H. Valizadeh, and A. Shayanfar (2015). Are crystallinity parameters critical for drug solubility prediction? *J. Solution Chem.* **44**, 2297-2315.

Gharsallaoui, A., B. Roge, and M. Mathlouthi (2008). Water-disaccharides interactions in saturated solution and the crystallisation conditions. *Food Chemistry* **106**, 1329-1339.

Hansen, C.M. (2007). *Hansen Solubility parameters*. 2nd Edition. Taylor and Francis, Boca Raton.

Hildebrand, J.H., and R.L. Scott (1962). *Regular Solutions*. Prentice-Hall, New Jersey.

Izmailov, N. A. (1970). *Electrochemistry of Solutions*, Khimiya, Moscow, in Russian.

Jimenez, J.A., and F. Martinez (2006). Temperature dependence of the solubility of acetaminophen in propylene glycol + ethanol mixtures. *J. Solution Chem.* **35**, 335-352.

Jouyban, A., and W.E. Acree Jr. (2018). Mathematical derivation of the Jouyban-Acree model to represent solubility data in mixed solvents at various temperatures. *J. Mol. Liquids* **256**, 541-547.

Jouyban, A., W.E. Acree Jr., and F. Martinez (2016). Modeling the solubility and preferential solvation of gallic acid in cosolvent + water mixtures. *J. Mol. Liquids* **224**, 502-506.

Jouyban, A., M.A.A. Fakhree, and W.E. Acree Jr. (2012). Comments on "Measurement and correlation of solubility of (Z)-2-(2-Aminothiazol-4-yl)-2-methoxyaminoacetic acid in different pure solvents and binary mixtures of water + (ethanol, methanol, or glycol)". *J. Chem. Eng. Data* **57**, 1344-1345.

Jouyban-Gharamaleki, A., and W.E. Acree (1998). Comparison of models for describing multiple peaks in solubility profiles. *Int. J. Pharm.* **167**, 177-182.

Jouyban-Gharamaleki, A., L. Valee, M. Barzegar-Jalali, B.J. Clark, and W.E. Acree Jr. (1999). Comparison of various cosolvency models for calculating solubility in water-cosolvent mixtures. *Int. J. Pharm.* **177**, 93-101.

Kim, D.-Y., and K.-J. Kim (2010). Correlation between quantity of defect and supersaturation in RDX crystallization using γ-butyrolactone and water as solvent. *Chem. Eng. Res. Des.* **88**, 1461-1466.

Krug, R.R., W.G. Hunter, and R.A. Grieger (1976). Enthalpy-entropy compensation. 2. Separation of the chemical from the statistical effects. *J. Phys. Chem.* **80**, 2341-2351.

Manzurola, E., and A. Apelblat, (2002). Solubilities of L-glutamic acid, 3-nitrobenzoic acid, p-toluic acid, calcium-L-lactate, calcium gluconate, magnesium-DL-aspartate, and magnesium-L- lactate in water. *J. Chem. Thermodyn.* **34**, 1127-1136.

Martin, A., P.L. Wu, A. Adjei, R.E. Lindstrom, and P.H. Elworthy (1982). Extended Hildebrand solubility approach and the log linear solubility equation. *J. Pharm. Sci.* **71**, 849-856.

Martinez, F., A. Jouyban, and W.E. Acree Jr. (2016). Further comments on "Solubility and thermodynamic behavior of vanillin in propane-1,2-diol + water mixtures at different temperatures". *Food Chem.* **196**, 757-759.

Marcus, Y. (2002). Solvent Mixtures: Properties and Selective Solvation. Marcel Dekker, New York.

Marcus, Y. (2008). On the preferential solvation of drugs and PAH in binary solvent mixtures. *J. Mol. Liquids* **140**, 61-67.

Miyamoto, H., H. Shimura, and K. Sasaki (1985). Solubilities of rare earth iodates in aqueous and aqueous alcoholic solvent mixtures. *J. Solution Chem.* **14**, 485-497.

Mohan, R., H. Lorenz, and A.S. Myerson (2002). Solubility measurement using differential scanning calorimetry. *Ind. Eng. Chem. Res.* **41**, 4854-4862.

Mosaad, M.M., A. El-Shawarby, Z.H. El-Tanahy, and M.M. Abdel-Kader (1995). Electrical and thermal properties of ammonium and potassium oxalates. *J. Mater. Sci.: Mater. Electronics* **6**, 235-239.

Muñoz, M.M., M.A. Peña, O.A. Almanza, A. Jouyban, M. Martinez, and W.E. Acree Jr. (2016). Solubility and apparent specific volume at saturation of some pharmaceutical salts in methanol + water mixtures at 298.15 K. *J. Mol. Liquids* **220**, 842-847.

Mullin, J.W. (2001). *Crystallization*, 4nd Edition, Butterworths-Heinemann, London.

Nordström, F.L., and A.C. Rasmuson (2009). Prediction of solubility curves and meting properties of organic and pharmaceutical compounds. *Eur. J. Pharm. Sci*. **36**, 330-344.

Nowee, S.M., A. Abbas, J.A. Romagnoli (2008). Antisolvent crystallization: Model identification, experimental validation and dynamic simulation. *Chem. Eng. Sci.* **63**, 5457-5467.

O'Ciardha, C.T., P.J. Frawley, N.A. Mitchell (2011). Estimation of the nucleation kinetics for the anti-solvent crystallisation of paracetamol in metanol/water solutions. *J. Cryst. Growth* **328**, 50-57.

O'Grady, D., M. Barrett, E. Casey, B. Glennon (2007). The effect of mixing on the metastable zone width and nucleation kinetics in the anti-solvent crystallization of benzoic acid. *Chem. Eng. Res. Des* **85**, 945-952.

Omar, W., and J. Ulrich (2006). Solid liquid equilibrium, metastable zone, and nucleation parameters of the oxalic acid-water system. *Cryst. Growth Des*. **6**, 1927-1930.

Renon, H., and J.M. Prausnitz (1968). Local compositions in thermodynamic excess functions for liquid mixtures**.** *AIChE J.* **14**, 135-144.

Reichardt, C., and T. Welton (2011). *Solvents and Solvent Effects in Organic Chemistry*. 4th Ed. Wiley-VCH.

Sangwal, K., E. Mieniczek-Brzóska, and S. Barylska (2013). Solubility of ammonium oxalate in water-acetone mixtures and metastable zone width of their solutions. *Chem. Eng. Res. Des.* **92**, 491-499.

Sotomayor, R.G., A.R. Holguin, A. Romdhani, F. Martinez, and A. Jouyban (2013). Solution thermodynamics of piroxicam in some ethanol + water mixtures and correlation with the Jouyban-Acree model. *J. Solution Chem.* **42**, 358-371.

Söhnel, O., and P. Novotny (1985). *Densities of Aqueous Solutions of Inorganic Substances*. Academia, Prague.

Wilson, G.M. (1964). Vapor-liquid equilibrium. XI. A new expression for the excess free energy of mixing. *J. Am. Chem. Soc.* **86**, 127-130.

Yalkowsky, S.H., G.L. Flynn, and G.L. Amidon (1972). Solubility of nonelectrolytes in polar solvents. *J. Pharm. Sci.* **61**, 983-984.

Yalkowsky, S.H., and S.C. Valvani (1980). Solubility and partitioning I: Solubility of nonelectrolytes in water. *J. Pharm. Sci.* **69**, 912-922.

Zhang, P.-S., R. Zhao, C. Zhang, T. Li, and B. Ren (2018). Solubility determination and correlation of cyromazine in sixteen pure solvents and mixing properties of solutions. *Fluid Phase Equilibria* **375**, 77-88.

Zhang, Y., Y. Jiang, D. Zhang, Y. Qian, X.Z. Wang (2015). Metastable zone width, crystal nucleation and growth kinetics measurement in anti-solvent crystallization of β-artemether in the mixture of ethanol and water. *Chem. Eng. Res. Des.* **95**, 187-194.

Zhao, Y.-Q., W.-W. Liu, X.-Q. Pei, and D.-R. Yao (2017). Refinement of the theoretical solubility model and prediction of solute solubility in mixed solvent systems. *Fluid Phase Equilibria* **437**, 43-55.

Zhou, J.-Y., H.-L. Fu, H. Cao, C.-C. Lu, C. Jin, T. Zhou, M.-J. Liu, and Y.-L. Zhang (2013). Measurement and correlation of florfenicol in binary 1,2-propanediol+water mixtures from 293.15 K to 316.15 K. *Fluid Phase Equilibria* **360**, 118-123.

Zhu, Y., D. Youssef, C. Porte, A. Rannou, M.P. Delpancke-Olgetree, B.L.M. Lung-Somarriba (2003). Study of the solubility and the metastable zone of 1,3-dihydrozyacetone for the drowning-out process. *J. Cryst. Growth* **257**, 370-377.

3

DENSITY OF SOLVENTS AND SOLUTIONS

The density *d* of a substance is defined as its mass per unit volume. It is commonly expressed in g/cm^3 or kg/m^3. It is one of the main quantities characterizing a solvent and solution. Densities of liquid mixtures and homogeneous solutions are used to determine partial molar volumes and excess molar volumes of their individual components, which provide information about interactions taking place between the ions/molecules in the mixtures and solutions. Density data are required not only in determining the concentration of a solute in some solution or in achieving a particular supersaturation in crystal growth, but also in estimating kinematic viscosity and refractivity of a liquid. Since the density of solutions is intimately connected with their concentration, densities of feed solution and mother liquors are necessary in calculations of establishing material balances and equipment volumes for crystallization processes. For practical purposes, concentration and temperature dependences of densities of solutions are usually expressed by empirical functions (Horvath, 1985; Söhnel and Novotný, 1985).

Systems for which densities have been studied widely as functions of different experimental conditions may be grouped into the following categories: (1) various types of individual solvents for the preparation of solutions, (2) mixtures of individual solvents, and (3) solutions of various substances dissolved in individual solvents and their mixtures. In the first category of systems are simple liquids like water, various alcohols and organic solvents available in the liquid state under normal conditions. Other individual solvents are organic salts having melting points below room temperature, known as room-temperature ionic liquids (ILs), as substitutes for organic solvents. Mixtures of solvents, one of which is the main solvent and the other is a cosolvent, form another category. The last category of systems comprise solutions of solutes, which may be electrolytes and nonelectrolytes, dissolved in individual solvents and their mixtures. The chemical constitution of individual solvents and the nature of bonds between their molecules in the volume determine the absolute values of the densities of these solvents and the temperature dependence of their densities. In the case of solvent mixtures, composition and temperature dependences of their densities are determined by processes involving different types of interactions between solvent and cosolvent molecules. Similarly, the dependence of density of solutions on their concentration and temperature is governed by interactions between solute ions/molecules and solvent molecules. Binary mixtures of two solvents and binary solutions composed of a solute dissolved in a solvent are the simplest systems for understanding different interactions that determine the value of their density as a function of experimental conditions.

The present chapter is devoted to an overview of different types of observations related to the investigation of densities of single-component solvents, mixtures of solvents and solutions of electrolytes and nonelectrolytes. No attempt is made to survey the entire literature on the subject. Examples are selected simply to serve as illustrations on various topics for discussion.

After a brief description of experimental methods of measurement of densities in the next section, basic concepts of densities of solvent mixtures and solutions, molar volumes, excess molar volumes, and apparent molar volumes, and commonly used equations of temperature and concentration dependence of densities are described in Section 3.2. Then chemical-constituent and temperature dependence of organic solvents (with alcohols as their representatives) and low-temperature ionic liquids (ILs), composition and temperature dependence of solvent mixtures, and different aspects of densities of electrolyte and nonelectrolyte solutions are presented in Sections 3.3, 3.4 and 3.5, respectively. Observations of the temperature dependence of densities of saturated solutions in the neighborhood of their saturation temperatures in undersaturated and supersaturated regions are presented in Section 3.6. Finally, some models for calculating the densities as functions of concentration and temperature dependence of solutions are described in Section 3.7.

3.1. Density measurements

Widely different methods are used for determining densities of liquids. Among the commonly used techniques in the laboratory are the buoyancy method, the displacement principle and the pycnometer method. These methods have their advantages and disadvantages. The main disadvantage of these techniques is that the measurements are manual and time-consuming. However, during the last three decades digital densimeters based on vibrating tubes and buoyancy principle have been available commercially and used for density measurements. Examples of authors using different methods of density measurements are listed below: hydrostatic balance by weighing a float (Frej et al., 1998; Sokołowski and Sangwal, 1983; Szwczyk and Sangwal, 1988), aerometers (Petrova et al., 2010), density/specific gravity meter (Herraez and Belda, 2006; Zhang S., et al., 2006), pycnometer (Ali et al., 2006; Kawahara and Tanford, 1966; Mahajan and Mirgane, 2013; Mohiuddin and Ismail, 1996; Nain et al., 2011; Ortega, 1982; Rooney et al., 2009; Sharma et al., 2007; Zhang S., et al., 2006), oscillating/vibrating tube densimeters (Albuquerque et al., 1996; Bajic et al., 2013; Francesiconi and Ottani, 2007; Fucaloro et al., 2007; Rooney et al., 2009; Singh et al., 2013; Šegatin and Klofutar, 2004), and weighing a constant volume of ILs (Bittner et al., 2012).

3.2. Basic concepts of density of solutions

As discussed in Chapter 1, at a given pressure p, with an increase in temperature T every solidified material first transforms to the liquid form at a temperature T_m and this liquid thereafter begins to boil at temperature T_b and transforms to the vapor phase.

Conversely, with a slow decrease in temperature a material initially existing in the vapor phase condenses into the liquid phase at the temperature T_b, and the cooling of the liquid later solidifies at the temperature T_m and remains in this phase. These phase transformations are associated, among others, with changes in the volumes of these phases and may be understood from consideration of the average distance between their atoms/molecules of the compound. In the case of melting of solids, increase in their volume is insignificant (about 10%). Consequently, the average distance between their atoms/molecules before and after melting remains practically unchanged.

The volume thermal expansion coefficient α_V of liquids is one-order higher than that in the solids state due to differences in the nature of interactions between atoms/molecules in the two states, which ultimately determine the difference between the physical properties of liquids from those of solids. In contrast to the long-range interactions between the atoms/molecules in the solid state, short-range interactions are involved in the liquids, but the average distance between the atoms/molecules in the both phases increases with temperature. Consequently, the temperature dependence of decrease in the density d of liquids is higher than that of solids.

Molecules/ions of a solid dissolved at a particular temperature in the solvent decrease its volume due to surrounding solvent molecules. This results in a decrease in the solution volume, which increases with the solute concentration. Therefore, in contrast to the effect of temperature, the density d of the solution increases with an increase in the concentration of the solute.

3.2.1. Apparent partial molar volume of solute

The total volume V of a multicomponent system composed of n_i moles of ith component of its volume V_i may be given by

$$V = \sum_{i=1}^{j} n_i V_i \,, \tag{3.1}$$

where the partial molar volume V_i of the ith component of the total components j at constant temperature T and pressure p conditions is

$$V_i = \left(\frac{\partial V}{\partial n_i} \right)_{n_i, T, p} . \tag{3.2}$$

For a two-component mixture of n_1 and n_2 moles of components 1 and 2, the so-called apparent molar volume is defined as

$$\Phi_\mathrm{v} = \frac{(V - n_1 V_{\mathrm{M1}})}{n_2} = \frac{(V - x_1 V_{\mathrm{M1}})}{x_2} \,, \tag{3.3}$$

where V_{M1} is the molar volume of component 1 of the mixture and x_1 and x_2 are concentrations of solvent and solute in the mixture in mole fractions, respectively. When the molar volume is expressed in terms of densities and molecular weights, one may write the above equation in the form

$$\Phi_{\mathrm{v}} = \frac{1}{n_2}\left(\frac{n_1M_1 + n_2M_2}{d} - \frac{n_1M_1}{d_1}\right), \tag{3.4}$$

where d_1 is the density of the solvent, d is the density of the solution, and M_1 and M_2 are the molecular weights of solvent 1 and solute 2, respectively. When the solution composition is expressed in molality m (i.e. moles of solute in 1 kg solvent) such that $n_2 = m_2$ and $n_1 = 1/M_1$, Eq. (3.4) takes the form

$$\Phi_{\mathrm{v}} = \frac{d_1 - d}{dd_1m_2} + \frac{M_2}{d}, \tag{3.5}$$

but when the solution composition is expressed in molarity c_2 (i.e. moles of solute per liter of solution) such that $n_2 = c_2$ and $n_1 = (d{-}c_2M_2)/M_1$, one obtains

$$\Phi_{\mathrm{v}} = \frac{10^3(d_1 - d)}{d_1c_2} + \frac{M_2}{d_1}. \tag{3.6}$$

The partial molar volume of solute and solvent in a binary solution may be obtained from Eq. (3.3) of Φ_{v} as

$$V_{\mathrm{M}2} = \left(\frac{\partial V}{\partial n_2}\right)_{n_i,T,p} = \Phi_{\mathrm{v}} + n_2\left(\frac{\partial \Phi_{\mathrm{v}}}{\partial n_2}\right)_{n_1,T,p}, \tag{3.7}$$

$$V_{\mathrm{M}1} = \frac{V - n_2V_{\mathrm{M}2}}{n_1} = \frac{1}{n_1}\left[n_1V_{\mathrm{M}1} + n_2^2\left(\frac{\partial \Phi_{\mathrm{v}}}{\partial n_2}\right)_{n_1,T,p}\right]. \tag{3.8}$$

Obviously, at infinite dilution (i.e. $n_2 \to 0$), from (3.7) one has

$$V_{\mathrm{M}2}^{\mathrm{o}} = \Phi_{\mathrm{v}}^{\mathrm{o}}, \tag{3.9}$$

which means that the partial molar volume $V_{\mathrm{M}2}^{\mathrm{o}}$ of a solute at infinite dilution is equal to its apparent molar volume $\Phi_{\mathrm{v}}^{\mathrm{o}}$ at infinite dilution.

The apparent molar volume Φ_{v} changes with the square-root of molar concentration c_2 of an electrolyte following Masson's empirical relation (Redlich and Rosenfeld, 1931)

$$\Phi_{\mathrm{v}} = \Phi_{\mathrm{v}}^{\mathrm{o}} + S_{\mathrm{v}}c_2^{1/2}, \tag{3.10}$$

where $\Phi_{\mathrm{v}}^{\circ} \equiv V_{\mathrm{M}2}^{\mathrm{o}}$ of the solute, and S_{v} is the slope of the $\Phi_{\mathrm{v}}(c_2^{1/2})$ plot. The above relation adequately describes the concentration dependence of Φ_{v} of different solutes over a wide temperature and concentration range. It is found (Couture and Laidler, 1956; Millero, 1970, 1972) that the values of $\Phi_{\mathrm{v}}^{\circ}$ and S_{v} are additive for several salt solutions. In view of the additive behavior of $\Phi_{\mathrm{v}}^{\circ}$ and S_{v}, the above equation has been found useful in estimating the densities of unknown concentrated solutions.

To calculate the slope S_{v} of the $\Phi_{\mathrm{v}}(c_2^{1/2})$ plots for different electrolyte solution systems, Redlich and Meyer (1964) proposed an equation of the type

$$\Phi_v = \Phi_v^o + S_v c_2^{1/2} + b_v c_2 , \tag{3.11}$$

where the constant S_v of Masson's equation (3.10) results from the Debye–Hückle theory of interionic interactions in electrolyte solutions for dilute solutions whereas the constant b_v is an empirical parameter representing deviation from the Debye–Hückle theory slope S_v at high concentrations from the square-root dependence. Experiments also show that in some cases the square-root term in Eq. (3.11) dominates the linear term, while in others the converse is true.

Experimental data of the dependence of Φ_v on solute concentration c_2 in solutions show that the values of the theoretical slope S_v and the deviation constant b_v strongly depend on temperature. For example, in the case of aqueous NaCl solutions, the slope S_v increases regularly with increasing temperature but the deviation constant b_v is positive at low temperature and becomes negative at high temperatures (Millero, 1970). These results are related to the effect of temperature on the structure of the hydrated ions (i.e. on the structure of water between the interactiong ions) and are associated with cation–anion interactions involving the formation of ionic pairs (Desnoyer et al., 1969; Millero, 1970, 1972). This subject is discussed in Section 3.5.3.

For aqueous systems of 1:1 electrolytes, a theoretical value of 1.868 $\text{cm}^3\cdot\text{mol}^{-3/2}\cdot\text{L}^{1/2}$ at 25 °C has been assigned for S_v (Redlich and Meyer, 1964). Experimental results show that S_v depends not only on solvent but also on solute and solution temperature (Härtling et al., 1981; Lowe et al., 1973; Mecklenburg and Seidel, 1983: Millero, 1970; Skabichevski, 1972). Similarly, according to the theory (Redlich and Meyer, 1964), $\Phi_v°$ should be a function of solvent only, but experimentally it is observed that its value depends on solvent as well as solute.

Figure 3.1 shows, as an example, the dependence of apparent molar volume Φ_v of two substituted ammonium chlorides, $(CH_3)_3HNCl$ and $(CH_3)_3(C_6H_5)NCl$, in dimethylsulfoxide (DMSO) at 318 K on $c_2^{1/2}$. The original $\Phi_v(c_2)$ data are from Mecklenburg and Seidel (1983), who investigated several substituted ammonium halides in DMSO solvent and obtained the values of $\Phi_v°$ and S_v from their data for solute concentration $c_2 > 0.01$ $\text{mol}\cdot\text{L}^{-1}$. The linear plots in the figure represent the $\Phi_v(c_2^{1/2})$ data with the values of $\Phi_v°$ and S_v for $c_2^{1/2} > 0.15$ $\text{mol}^{1/2}\cdot\text{L}^{-1/2}$ (i.e. $c_2 > 0.02$ $\text{mol}\cdot\text{L}^{-1}$), indicated by asterisk in Table 3.1. The pronounced effect of the choice of the c_2 range for the analysis of the $\Phi_v(c_2^{1/2})$ data on the values of $\Phi_v°$ and S_v is also shown in the table for $c_2^{1/2} > 0.10$ $\text{mol}^{1/2}\cdot\text{L}^{-1/2}$ of the $(CH_3)_3HNCl$ solute.

It may be seen from Figure 3.1 that the $\Phi_v(c_2^{1/2})$ data deviate hyperbolically from the expected linear dependence for $c_2^{1/2}$ below about 0.15 $\text{mol}^{1/2}\cdot\text{L}^{-1/2}$ (i.e. $c_2 < 0.02$ $\text{mol}\cdot\text{L}^{-1}$). The hyperbolic deviations increase with decreasing concentration and are associated with measurement errors in solution densities at low solute concentrations and are strongly affected by temperature (Härtling et al., 1981; Mecklenburg and Seidel, 1983). It has been proposed (Härtling et al., 1981) that these deviations are due to perturbation of molecular distribution in the solvent caused by solute ions. Therefore, data of the apparent molar volume Φ_v against $c_2^{1/2}$ are analyzed to calculate the value of the partial molar volume $\Phi_v°$ at infinite dilution and the slope S_v in the linear part of the plots, omitting data of hyperbolic deviations at low concentrations. The value of the partial molar volume $\Phi_v°$ of the solute at infinite dilution is obtained by extrapolation of the linear plot to $c_2^{1/2} = 0$.

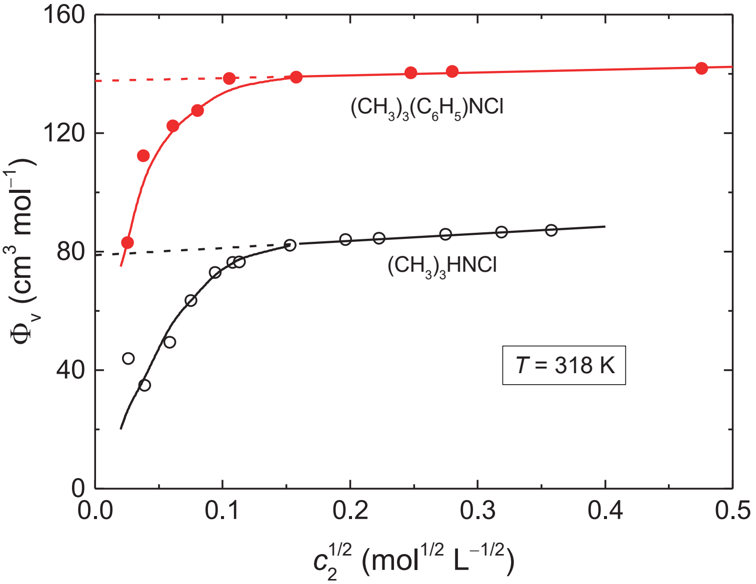

Figure 3.1 Example of dependence of apparent molar volume Φ_v of two substituted ammonium chlorides, $(CH_3)_3HNCl$ and $(CH_3)_3(C_6H_5)NCl$, in dimethylsulfoxide (DMSO) at 318 K on $c_2^{1/2}$. The plots are drawn with the values of $\Phi_v°$ and S_v given in Table 3.1. Original data from Mecklenburg and Seidel (1983).

Table 3.1. Constants of $\Phi_v°$ and S_v of Eq. (3.10) for two substituted ammonium chlorides

Substance	Curve	$c_2^{1/2}$ (mol$^{1/2}$·L$^{-1/2}$)	$\Phi_v°$ (cm^3·mol^{-1})	S_v (cm^3·mol$^{-3/2}$·L$^{1/2}$)	R^2
$(CH_3)_3HNCl$	Lower	> 0.15*	78.87±0.60	24.01±2.30	0.9558
		> 0.10	71.66±1.87	49.18±8.35	0.9249
$(CH_3)_3(C_6H_5)NCl$	Upper	> 0.15*	137.56±0.49	9.62±1.72	0.9762

The lower concentration limit beyond which the "expected" linear dependence is considered for the examination of the $\Phi_v(c_2^{1/2})$ data is chosen arbitrarily. As noted in case of the $(CH_3)_3HNCl$ solute, a lower concentration limit of this arbitrarily chosen value of $c_2^{1/2}$ frequently leads to a poorer fit of the data with higher values of the slope S_v in the linear part of the plots and relatively lower extrapolated values of the partial molar volume Φ_v^o at infinite dilution. When a higher concentration limit is taken, the fit of the data is improved and a lower value of the slope S_v and somewhat higher extrapolated value of Φ_v^o are obtained (see Table 3.1). However, a higher value of Φ_v° and a lower value of S_v for the $(CH_3)_3(C_6H_5)NCl$ solute than those for the $(CH_3)_3HNCl$ solute are obviously due to the larger size of the molecules of the former than that of the latter.

In the case of very high concentrations of electrolytes, higher terms may be added to Eq. (3.11). Then

$$\Phi_v = \Phi_v^o + S_v c_2^{1/2} + b_{v1} c_2 + b_{v2} c_2^{3/2} + b_{v3} c_2^2 , \tag{3.12}$$

where b_v's are empirical constants. It should be noted that $S_v = 0$ in the case of nonelectrolyte solutions. Therefore, the $c^{1/2}$ and $c^{3/2}$ terms in Eqs. (3.11) and (3.12) are zero. Then Eqs. (3.11) and (3.12) reduce to linear and quadratic dependences, respectively. These dependences are also explained in terms of compability and incompability of solvated molecules to orient other molecules present in the solution; see Section 3.5.4.

3.2.2. Molar volumes and excess molar volumes

In recent years, for the interpretation of concentration dependence of density d of solvent mixtures and solutions concepts of molar volumes V_M for a binary mixture, ideal molar volumes V_M^{id} from the additive rule and excess molar volumes ΔV_M have been defined according to the following relations (Albuquerque et al., 1996; Herráez and Belda, 2006; Zhao C., et al., 2005):

$$V_M = \frac{x_1 M_1 + x_2 M_2}{d} , \tag{3.13}$$

$$V_M^{id} = \frac{x_1 M_1}{d_1} + \frac{x_2 M_2}{d_2} , \tag{3.14}$$

and

$$\Delta V_M = \frac{x_1 M_1 + x_2 M_2}{d} - \left(\frac{x_1 M_1}{d_1} + \frac{x_2 M_2}{d_2} \right) = \\ = \frac{M_1 + x_2 (M_2 - M_1)}{d} - \left[\frac{M_1}{d_1} + x_2 \left(\frac{M_2}{d_2} - \frac{M_1}{d_1} \right) \right] , \tag{3.15}$$

where the different symbols have been defined above. The excess molar volume ΔV_M defined here has the same sense as the apparent molar volume Φ_v defined above and depends on the cosolvent content in solvent mixtures and solute concentration x_2.

For the analysis of solvation behavior of solutes, another approach has also been developed (Fucaloro et al., 2005, 2007). This approach is based on consideration of molar volume V_M for a binary mixture as the sum of partial molar volumes V_1 and V_2 of solvent and solute, respectively, given by Eq. (3.14), expressed in the form

$$V^* = \frac{V_\mathrm{M}}{x_1} = V_1 + rV_2\,, \tag{3.16}$$

and an analogous function V_id* from the ideal molar volume $V_\mathrm{M}{}^\mathrm{id}$ as the sum of partial molar volumes $V_1{}^\mathrm{o}$ and $V_2{}^\mathrm{o}$ of solvent and solute, respectively, at infinite dilution, i.e.

$$V_\mathrm{id}^* = \frac{V_\mathrm{M}^\mathrm{id}}{x_1} = V_1^* + rV_2^*\,, \tag{3.17}$$

to define a new excess function

$$\Delta V^* = V^* - V_\mathrm{id}^* = (V_1 - V_1^*) + r(V_2 - V_2^*)\,, \tag{3.18}$$

where the differences $(V_1 – V_1{}^*)$ and $(V_2 – V_1{}^*)$ are the excess partial molar volumes associated with the solvent and the solute, respectively. The partial molar volumes of the solvent and the solute are determined by fitting V^* as a function of r.

3.2.3. Some equations of temperature and solute-concentration dependence of density of solutions

Combining Eqs. (3.6) and (3.10) one obtains an equation relating the density d and the apparent molar volume Φ_v to the concentration c of electrolytes in the form

$$d = d_0 + (M_2 - d_0\Phi_\mathrm{v}^\mathrm{o})c_2 - S_\mathrm{v} d_0 c_2^{3/2}\,. \tag{3.19}$$

This equation was first proposed by Root (1933) and is usually referred to as Root's equation. Similarly, combining Eqs. (3.6) and (3.12) one gets

$$d = d_0 + (M_2 - d_0\Phi_\mathrm{v}^\mathrm{o})c_2 - S_\mathrm{v} d_0 c_2^{3/2} - b_\mathrm{v1} d_0 c_2^2 - b_\mathrm{v2} d_0 c_2^{5/2} - b_\mathrm{v3} d_0 c_2^3\,. \tag{3.20}$$

Note that in the case of nonelectrolyte solutions, $S_\mathrm{v} = 0$. Then the above equation becomes a simple third-order equation.

In the above equations of the concentration dependence of the density d of binary mixtures the constants $\Phi_\mathrm{v}{}^\mathrm{o}$, d_0, S_v and b_v's are functions of temperature. However, since the forms of these temperature dependences are not known, different empirical equations of temperature and concentration dependences have been proposed (Horvath, 1985; Söhnel and Novotný, 1985).

The density of a solution of a particular concentration c_2 decreases with an increase in temperature T (taken in °C), and is given by empirical relations (Gleim et al., 1969; Maksimova, 1965; Zhang Y., et al., 2013)

$$d = d_0 + a_1T + a_2T^2 + a_3T^3 + a_4T^4\,, \tag{3.21}$$

$$d = d_0^1 + b_1(T - T_0)\,, \tag{3.22}$$

where a's and b_1 are constants, d_0 is the density of the solvent (system) at $T = 0$ and $d_0{}^1$

is the density of solvent (system) at $T = T_0$. The magnitudes of the constants a's of Eq. (3.21) usually follow the sequence:

$a_1 > a_2 >> a_3 >> a_4$.

Therefore, in practice it is considerd sufficient to use the linear and square terms of Eq. (3.21), especially in the case of a narrow range of temperature used for measurements. The latter equation, Eq. (3.22), is essentially identical with the former because the b_1T_0 term can also be described by a higher T term of Eq. (3.21). Since the term $a_1T/d_0 << 1$, Eq. (3.21) may also be written in the form

$$d = d_0 \exp(a_1 T / d_0) = d_0 \exp(\alpha T), \tag{3.23}$$

where the constant $a_1/d_0 = \alpha$, and corresponds to the thermal expansivity of the solution.

Sangwal (1987), and Szewczyk and Sangwal (1988) observed that the equation

$$d = d_0 \exp[\Omega (T - \theta)^2], \tag{3.24}$$

satisfactorily reproduces the temperature dependence of liquids and electrolyte solutions. In this equation d_0, θ and Ω are constants characteristic of a solvent or solution and their values usually increase with solute concentration. Using Taylor's expansion one finds a connection between the above equation and Eq. (3.21).

The concentration dependence of density of an electrolyte solution of solute concentration c_2 at a given temperature T is usually given by (Maksimova, 1965; Skabichevskii, 1975)

$$d = d_0 + a_5 c_2 + a_6 c_2^2, \tag{3.25}$$

where a_5 and a_6 are constants, such that $a_5 >> a_6$ when the solute concentration c_2 is expressed in mol·L^{-1}. This equation is similar to Eq. (3.19) due to Root in which the $c_2^{3/2}$ term is replaced by the square term. When the c_2^2 term is negligible small, one may also write Eq. (3.25) in the form

$$d = d_0 + \frac{c_2}{A_1 + A_2 c_2}, \tag{3.26}$$

where A_1 and A_2 are new constants and $A_1 >> A_2$.

In comparison with the contribution of the positive c_2 term, the contribution of the c_2^2 term in Eq. (3.25) to the density d of a solution is relatively small and usually negative. Therefore, the c_2^2 term may be a considered as a truncation of Taylor's series up to the third term. When all subsequently decreasing c_2, c_2^2, ... c_2^i terms are considered, Eq. (3.25) may be expressed in the power-law form (Misztal and Sangwal, 1999)

$$d = d_0 + A c_2^p, \tag{3.27}$$

where the new constant $A \approx a_5$ and the exponent $p < 1$.

Equation (3.25) satisfactorily represents the densities of aqueous solutions of different electrolytes in a wide range of molar concentration c_2. Some authors have also used this equation taking concentration of the electrolyte as mole fraction x_2, wt% W_2, ionic strength I, and molality m. Different equations proposed for the solute concentration dependence of density of solutions are surveyed in the literature (Horvath, 1985).

3.2.4. The packing coefficient *K* of solutions

When the c_2^2 term is negligibly small in comparison with the linear c_2 term in Eq. (3.25), the solution density d can be given by the additive rule

$$d = x_1 d_1 + x_2 d_2 = d_1 + x_2(d_2 - d_1) = d_1 + \frac{x_2}{V_2}\left(M_2 - \frac{V_2}{V_1}M_1\right), \tag{3.28}$$

where d_1 and d_2 are the densities of solvent 1 and solute 2, respectively, M_1 and M_2 as their molecular weights (g per mole), V_1 and V_2 their volumes, and x_1 and $x_2 = (1-x_1)$ are the mole fractions of solvent and solute in the solution. Note that the solute concentration here is taken in mole fraction x_2. Using the relationship between the mole fraction x_2 and the molar concentration c_2 of the solute 2, i.e.

$$x_2 = \frac{M_1 c_2}{1000\,d + c_2(M_1 - M_2)} \approx 10^{-3} c_2\,, \tag{3.29}$$

with reference to one mole of solvent and solute volumes V_1 and V_2, one may write Eq. (3.28) in the form

$$d = d_1 + 10^{-3} c_2 (M_2 - KM_1)], \tag{3.30}$$

where the packing coefficient K is a measure of deviation in the ratio V_2/V_1 from unity. Reichardt (1970) derived a similar expression from an analysis of the experimental data of the densities of aqueous solutions of various 1:1, 2:1 and 3:1 electrolytes and observed that the above linear dependence is followed when the packing coefficient K is constant or when $M_2 >> KM_1$ does not remain constant for a binary system.

Following Reichardt (1970), we assume that introduction of a molecule of the electrolyte MX to the solvent leads to its solvation by expanding the volume of solvent volume by a quantity equal to v_1, such that each solute molecule displaces a certain number of solvent molecules, given by: $K = v_1/v_{20}$, where the volume of free solvent molecule in the solvent is v_{20}. In real solutions, the solvent volume v_2 differs from v_{20}. Then for the situation when the concentration is taken in weight percent w, substitution of the above value of K in Eq. (3.30) gives

$$d = \frac{100 v_2}{\frac{v_1}{M_1} w + \frac{v_2}{M_2}(100 - w)}\,. \tag{3.31}$$

From Eq. (3.30) it follows that

$$d = \frac{100}{100 + \dfrac{M_2 K w}{M_1} - w}. \tag{3.32}$$

Elimination of d from Eqs. (3.31) and (3.32) gives

$$K = n_2\left(\frac{v_2}{v_{20}} - 1\right) + \frac{v_1}{v_{20}}, \tag{3.33}$$

where n_2 is the number of moles of the solvent surrounding one mole of the electrolyte. According to this equation, in solutions of relatively low structural packing where $v_2 > v_{20}$, $K > v_1/v_{20}$. When $v_2 \approx v_{20}$, $K \approx v_1/v_{20}$ = constant. However, when $v_2 < v_{20}$, $K < v_1/v_{20}$.

The value of the packing coefficient K for different systems may be estimated from the experimental data of concentration dependence of their densities. From this type of examination of the $d(w)$ data for concentrations w of aqueous solutions of exceeding 8 to 10% up to near saturation, Reichardt (1970) observed that with increasing solute concentration the coefficient K sharply increases for densely packed solutions for which v_2/v_{20} lies between about 1.7 and 5.2, but the increase is relatively insignificant for loosely packed solutions where v_2/v_{20} is close to unity. In the former class of systems are practically all of the examined 2:1 and 3:1 salts, while in the latter class are 1:1 salts. These different increasing trends of the coefficient K are associated with the concentration dependence of solvent volume v_2, with v_2/v_{20} as a measure of the increase with solute concentration.

3.3. Chemical-constituent and temperature dependence of solvents

3.3.1. Water and organic solvents

Densities of organic liquids at ambient temperatures lie in a wide range from about 0.6 to 3.3 $g \cdot cm^{-3}$ and are related to their chemical constituents. In general, liquids of low molecular weights have low density whereas those of high molecular weights have high density, and the density of a substance decreases with increasing temperature. Density data for various organic solvents are easily available (e.g. Lide, 1996/1997).

In this section some general features of the density of organic liquids are discussed from a consideration of their chemical constituents and temperature taking normal- and iso-alcohols, denoted hereafter as 1- and 2-alcohols, respectively, up to decanol ($C_{10}H_{21}OH$) as representives of organic solvents. Normal alcohols may be considered as higher homologues of the lowest alcohol methanol with one $-CH_2$ group attached in a series to the H atom of a water molecule H–OH, whereas iso-alcohols are higher homologues of iso-butanol where one of its $-CH_2$ groups is attached in the side position. Therefore, formally these alcohols may be represented as $OH{-}H\cdots(-CH_2)_N$ with the interger $N \geq 1$ for 1-alcohols and with $N \geq 3$ for 2-alcohols. Evidently, $N = 0$

denotes water whereas $1 < N < 3$ refers to the lowest alcohols for these two homologues of alcohols and $N = 10$ represents decanol.

The density d of the 1- and 2-alcohols measured at a given temperature increases with increasing number N of the $-CH_2$ group. Figure 3.2 shows the plots of the $d(N)$ data for the above alcohols at 20 °C. As seen from the above figure, the dependence of d on N is not strictly linear but follows the empirical relation

$$d = d_0 + d_1 N(1 - \lambda N)\,, \tag{3.34}$$

where d_0 is the extrapolated value of d when $N = 0$, d_1 is the slope of the $d(N)$ plot representing increase in the density per $-CH_2$ group, and the parameter λ accounts for the interactions between neighboring $-CH_2$ groups. In the above equation, the first and the second derivatives, $\mathrm{d}d/\mathrm{d}N$ and $\mathrm{d}^2 d/\mathrm{d}N^2$, represent an increase and a decrease in the density d due to the addition of a $-CH_2$ group and the interactions between neighboring $-CH_2$ groups, respectively.

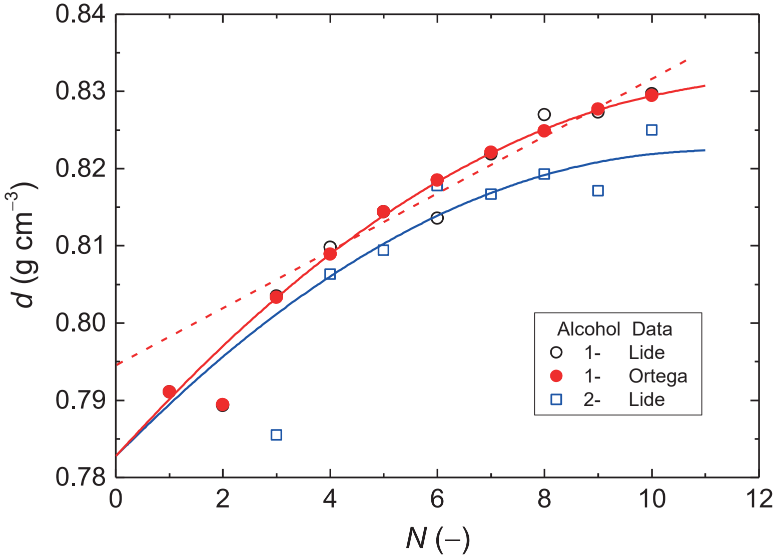

Figure 3.2. Plots of density d of 1- and 2-alcohols as a function of the number N of $-CH_2$ groups. Solid curves are drawn according to the constants of Table 3.2. Curves represent data of Ortega and Lide, respectively. Dashed curve represents linear dependence for 1-alcohols.

Table 3.2. Constants of Eq. (3.34) for alcohols

Substances	d_0 (g·cm^{-3})	$10^3 d_1$ (g·cm^{-3})	$10^3\, d_1\lambda$ (g·cm^{-3})	λ (–)	R^2
1-alcohols	0.7945	3.72	–	–	0.9648
	0.7828	7.827	0.315	0.040	0.9972
2-alcohols	0.7128	7.129	0.320	0.045	0.8480

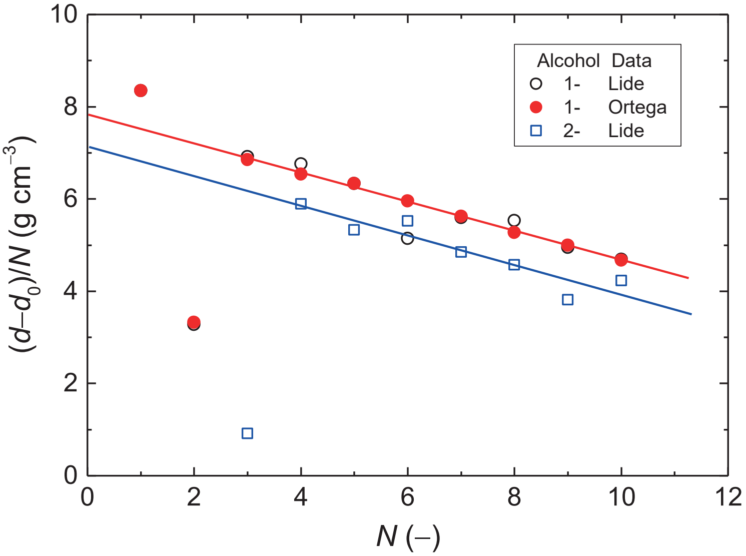

Figure 3.3. Plots of $(d–d_0)/N$ against N of $–CH_2$ groups. Best-fit constants of the plots for 1- and 2-alcohols given in Table 3.2 are for the data of Ortega and Lide, respectively. Data for methanol and ethanol and 2-propanol were omitted during analysis.

Eq. (3.34) may be used to analyze the $d(N)$ data of Figure 3.2 for the two types of alcohols from the plots of $(d–d_0)/N$ against N, with an appropriately chosen value of d_0, with intercept d_1 and slope $d_1\lambda$. Figure 3.3 shows such plots with the values of the constants d_0, d_1 and $d_1\lambda$, and the calculated values of the parameter λ, listed in Table 3.2. While analyzing the data, data for methanol and ethanol in 1-alcohols and 2-propanol in 2-alcohols were omitted. In Figure 3.2 the curves are drawn for the data with the constants of Table 3.2.

With the exception of the lowest alcohols of the two homologues, the density d of an alcohol composed of N $–CH_2$ group in its molecule is the sum of an extrapolated density d_0 of an imaginary (hypothetical) alcohol of $k = 0$ and incremental density d_k of the successive $–CH_2$ groups, i.e.

$$d = d_0 + \sum_{k=1}^{N} d_k \ . \tag{3.35}$$

This relation explains the first term of Eq. (3.35), but the second term involving the λ parameter accounts for increasing repulsion between the neighboring molecules of an alcohol with increasing number N of $–CH_2$ groups in its molecule.

The increasing density d of higher homologues of alcohols with the number N of $–CH_2$ groups in their molecules may be related to their molar volumes $V_M = d/M$, where M is the molecular weight of the alcohols. Figure 3.4 shows that the dependence of the molar volume V_M of 1- and 2-alcohols on the number N of $–CH_2$ groups in their molecules is linear. The plot represents the $V_M(N)$ data for the 1- alcohols, with an intercept $V_{M0} = 24.8$ cm^3·mol^{-1} and a slope 16.6 cm^3·mol^{-1} per $–CH_2$ group. However, the slope dV_M/dN for the 2-alcohols is insignificantly higher than that for the 1-alcohols.

From Table 3.2 it may be noted that the values of d_0 and d_1 for the 2-alcohols are lower than those for the 1-alcohols. Moreover, the value of the slopes $d_1\lambda$ is practically constant for the two types of the alcohols and does not depend on the type of the alcohols. However, the value of the mutual interaction parameter λ for the 2-alcohols is higher than that for the 1-alcohols. These trends of the alcohols are related to the higher molar volumes V_M of the former than those of the latter, and are directly associated with differences in the compactness of the molecules of the alcohols.

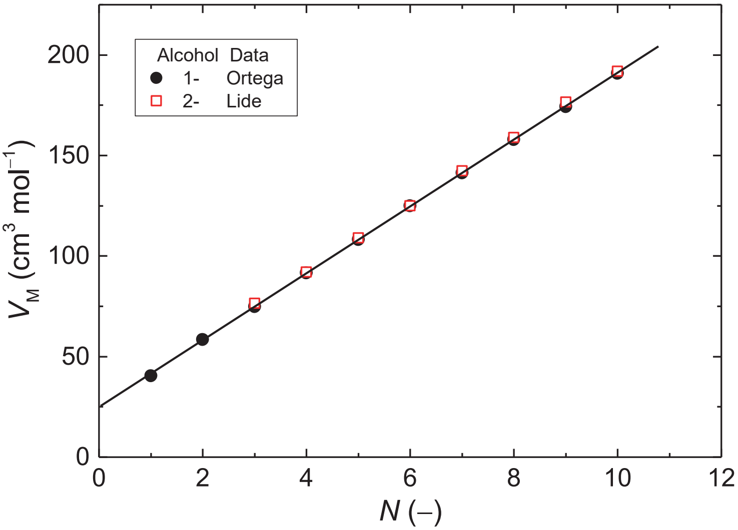

Figure 3.4. Dependence of molar volumes V_M of 1- and 2-alcohols on the number N of $-CH_2$ groups. Best-fit linear plot represents $V_M(N)$ data based on density data from Ortega for 1-alcohols.

The density d of the two types of alcohols at 20 °C is related to their boiling point T_b and melting point T_m. Since the density d of a substance is related to its molar volume V_M, it is tempting to correlate T_b and T_m of the alcohols to their molar volumes V_M. Figure 3.5 shows plots of T_b and T_m of 1- and 2-alcohols against their their molar volumes V_M. With the exception of methanol, T_b and T_m of the 1- and 2-alcohols increases linearly with their molar volumes V_M. In view of relatively large scatter in the $T_m(V_M)$ data for 2-alcohols, these data were not analyzed. However, it seems that the $T_m(V_M)$ plot for these 2-alcohols has a slope similar to that of the 1-alcohols with a value of the intercept T_{m0} somewhat lower than that of the 1-alcohols. The values of the intercept $T_{b,m0}$ and the slope $dT_{b,m}/dV_M$ for both $T_b(d)$ and $T_m(d)$ plots are listed in Table 3.3. Since the temperatures T_b and T_m are related to the enthalpies ΔH_b and ΔH_m of evaporation and melting, it may be concluded that the relationship between the density d of alcohols and their boiling and melting points T_b and T_m is associated with the the enthalpies ΔH_b and ΔH_m per molar volume and the value of the intercept $T_{b,m0}$ is associated with threshold values of ΔH_b and ΔH_m for an alcohol.

The deviation in the density d of series of alcohols with the number N of $-CH_2$ groups in their constitution from the linear behavior (Figure 3.2), and the linear dependence of their boiling point T_b and melting point T_m on the molar volumes V_M (Figure 3.5) are due to the nature of self-association of the alcohol molecules which increases with the number N of $-CH_2$ groups. The higher the number N of $-CH_2$ groups in an alcohol, the higher is the self-association of its molecules. However, self-association in alcohols involves relatively weak van der Waals interactions between alcohol molecules whereas self-association in water involves strong hydrogen bonds.

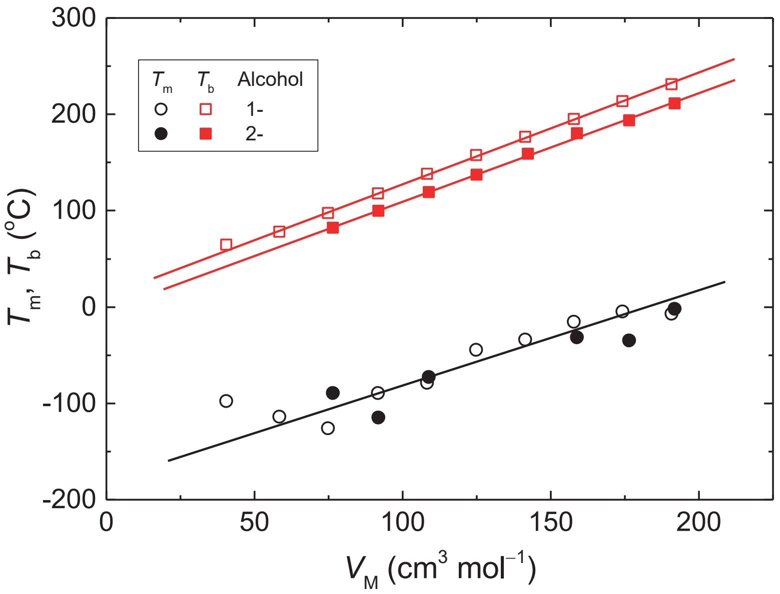

Figure 3.5. Relationship between boiling point T_b and melting point T_m of 1- and 2-alcohols and their molar volumes V_M at 20 °C. Methanol was excluded from analysis. Best-fit plots are drawn with constants listed in Table 3.3. The data of T_b and T_m are from Lide, but those of d for 1- and 2-alcohols are from Ortega (1982) and Lide (1996/1997), respectively. See text for details.

Table 3.3. Values of intercept $T_{b,m0}$ and slope $dT_{b,m0}/dV_M$ for alcohols

Data	Alcohol	$T_{b,m0}$ (°C)	$dT_{b,m}/dV_M$ (°C·mol·cm^{-3})	R^2
$T_b(V_M)$	1-	11.36±1.15	1.160±0.009	0.9995
	2-	−3.25±2.893	1.127±0.021	0.9975
$T_m(V_M)$	1-	−180.8±12.3	0.992±0.093	0.9331

From the extrapolated density $d_0 = 0.7828$ g·cm^{-3} of the hypothetical alcohol of $k = 0$ (Figure 3.3 and Table 3.2) and its molar volume V_{M0} = = 24.8 cm^3·mol^{-1} (Figure

3.3) one finds its molecular weight $M_0 = 19.4$ g·mol^{-1}, which is close to that of water. A lower density d_0 and a higher molar volume V_{M0} of this hypothetical water-like alcohol implies that the average distance between its molecules is about 10% higher than that of water molecules in the solvent. This difference is associated with the nature of intermolecular interaction in alcohols and water. Hydrogen bonds dominate in the water structure but van der Waals interactions are mainly present in organic compounds, including alcohols.

The density of simple liquids, including alcohols, decreases with an increase in temperature and frequently follows Eq. (3.21) (Gurevich and Bednov, 1972; Nayar and Kudchadker, 1973; Ortega, 1982). Ortega (1982) investigated the temperature dependence of the density d of normal alcohols from methanol to decanol and found that his $d(T)$ data follow Eq. (3.23) and the α coefficient of this equation coincides with the average coefficient of thermal expansion. He also found that the value of the α coefficient does not remain constant for all alcohols but slowly decreases with increasing number of N of $-CH_2$ groups in the molecule of an alcohol. This implies that the value of the α coefficient of these alcohols depends on the nature of molecules composing them. Since the addition of a $-CH_2$ group to the series of alcohols changes their molecular weight M and molar volumes V_M, the dependence of α on N may be attributed to the changes in their molecular weight M and molar volume V_M.

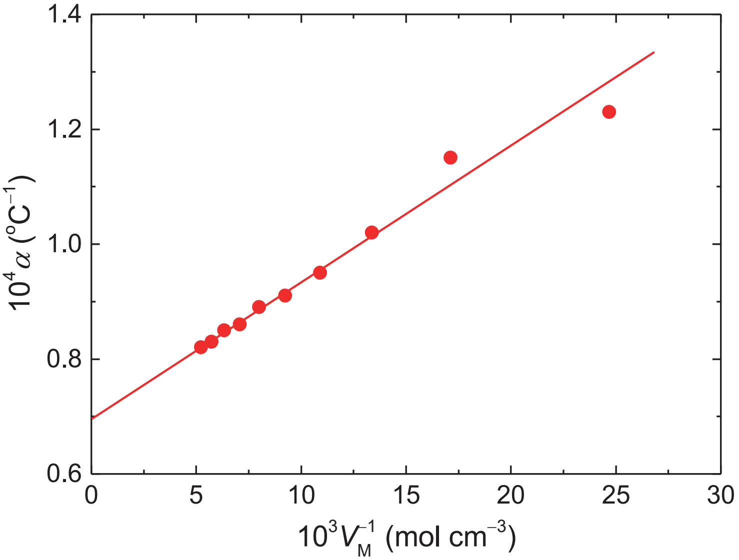

Figure 3.6. Relationship between the α coefficient of different alcohols and the inverse of their molar volumes V_M. Data for methanol and ethanol were omitted during analysis. See text for details. Original data of α coefficients from Ortega (1982).

Figure 3.6 shows that the α coefficient for the above alcohols increases linearly with the inverse of their molar volume V_M with an intercept $6.9\cdot10^{-5}$ (°C^{-1}) and a slope

$2.4 \cdot 10^{-3}$ (mol·cm^{-3}·°C^{-1}). The linear relationship may be attributed to the thermal vibration of molecules of the liquid because the thermal expansivity α of liquids is a result of amplitudes of vibration of its molecules in the liquid volume. Therefore, one expects that lighter molecules composing a lower alcohol will have larger amplitude of vibration around their saddle points than the heavier molecules of higher alcohols. The slope of the $\alpha(V_M^{-1})$ plot is a consequence of increasing amplitudes of vibrations of the molecules of alcohols of decreasing molar volume where the value of the intercept corresponds to the thermal expansivity of an alcohol composed of $N \to \infty$.

3.3.2. Low-temperature ionic liquids

Experimental data of the density *d* of ILs based on various cations combined with a variety of simple as well as complex anions have been reported. Among the cations are: imidazolium (im), pyridinium (py), pyrrolidium (pyrr), isoquinolium (isoq), ammonium, phosphonium and sulfonium, whereas the anions, among others, are: halides, nitrate, sulfate, hexafluorophophate (PF_6), tetrafluoroborate (BF_4), tosylate (Tos), trifluoromethanesulfonate (OTf), bis(trifluoromethylsulfonyl)imide (NTf_2), and tris(pentafluoroethyl)trifluorophosphate (FAP). From these data the following features have been observed (Bittner et al., 2012; Jacquemin et al., 2008; Rooney et al., 2009; Zhang S., et al., 2006):

(1) The densities of most of the ILs are higher than that of water and, depending on the anion and cation, the values lie between 0.9 and 1.7 at 25 °C and 0.1 MPa.
(2) The value of the density *d* of ILs containing a given anion decreases with the number N_C of carbon atoms of the alkyl group in the cation, but its value for the ILs of the same cation usually increases with the complexity of the anion.
(3) The density of an IL decreases linearly with increasing temperature, but the rate of this decrease is much lower than that for molecular organic solvents.

As with molecular solvents, the above observations are related to the molar volume V_M of the ILs. However, it should be noted that, in contrast to the increase in the density *d* of molecular solvents with the number *N* of $-CH_2$ groups, the density of ILs composed of the same anion decreases with the number N_C of carbon atoms in the alkyl group of the cation. This apparent anomaly between the trends of the dependence of *d* on *N* of molecular solvents and N_C of ILs is associated with the relatively small increase in the molar mass *M* of ILs with increasing N_C. The molar mass *M* of an IL is equal to the sum of the molar masses M_C and M_A of its cation and anion, respectively, and $M_C >> M_A$. Consequently, in the case of ILs, their molar volume $V_M = M/d$ also increases with increasing N_C.

3.4. Composition and temperature dependence of density of solvent mixtures

The density of mixtures of two solvents 1 and 2 varies in a large range and the trend of variation in the density of solvent 1 strongly depends on the nature of cosolvent 2. Since the density of a solvent is intimately connected with its chemical constitution, the trend of the density of a solvent−cosolvent mixture depends on the interaction between the molecules of the solvent and the cosolvent.

Density measurements have been reported on different systems: water in selected normal alcohols at 293.15 and 298.15 K (Herráez and Belda, 2006; Khimenko, 1969; Šegatin and Klofutar, 2004); methanol in ethanol and 1,2-ethanediol (Albuquerque et al., 1996); mixtures of protic−protic solvents (methanol in ethanol, propanol and butanol, and ethanol in water), aprotic−aprotic solvents (acetonitrile in dimethylformamide, dimethylsulfoxide and 1,4-dioxane; abbreviations for the former three solvents are: AN, DMF and DMSO), and aprotic−protic solvents (DMF and AN in water and some aliphatic alcohols) at temperatures between 298.15 and 308.15 K (El-Dossoki, 2007), mixtures of poly(ethylene glycol) (PEG) and poly(propylene glycol) (PPG) (Francesiconi and Ottani, 2007), octan-2-ol in *n*-octane, *n*-decane, *n*-dodecane and *n*-tetradecane (Mahajan and Mirgane, 2013), eucalyptol in *o*-xylene, *m*-xylene and toluene at temperatures between 303.15 and 313.15 K (Sharma et al., 2007), butanoic acid in propanoic and 2-methyl-propanoic acids between 293.15 and 313.15 K (Bahadur et al., 2013), 1,2-propanediol and 1,3-propanediol in PEG200 and PEG400 between 288.15 and 333.15 K (Bajić et al., 2013), *o*-, *m*- and *p*-xylenes (C_8H_{10}) in benzaldehyde (C_7H_6O) and nitrobenzene ($C_6H_5NO_2$) between 298.15 and 318.15 K (Rafiee and Frouzesh, 2016), methanol, ethanol, *n*-propanol and *n*-butanol in pyridine between 293.15 and 323.15 K (Dikio et al., 2012), benzene, toluene, mesitylene and phenylacetonitrile in N-methylacemide at 308.15 K (Ranjith Kumar et al., 2009), glycerol formal (5-hydroxy-1,3-dioxane isomer) in ethanol at temperatures between 278.15 and 313.15 K (Holguin et al, 2011), mixtures of tert-butylmethylether (MTBE) and *n*-heptane in ethanol and 1- and 2-propanols at 293.15 K (Budeanu et al., 2015); 2-4-6-8-tetramethyl-2,4,6,8-tetraethenylcyclotetrasiloxane (D_4^{Vi}) in ethylbenzene, and *o*, *m* and *p*-xylenes at temperatures between 288.15 and 328.15 K (Zhang Y., et al., 2013). Density data of mixtures of water in various alcohols are also available in the handbook (Lide, 1996/1997).

In the published literature on density measurements, two types of aspects have been discussed: (1) molar volumes and excess molar volumes, and (2) limiting partial molar volumes of cosolvents. In the former case the excess behavior, calculated from the experimental $d(x_2)$ data using Eq. (3.15), has usually been analyzed using Redlich−Kister relation (3.36), whereas in the latter case the limiting partial molar volumes, calculated from the experimental $d(x_2)$ data using Eq. (3.6), have been analyzed using Redlich−Meyer relation (3.11).

3.4.1. Excess molar volumes

In this section some general features of the behavior of the composition dependent density d of binary solvent–cosolvent mixtures are described and discussed taking the following two groups of systems as representative examples:

(1) The first two homologues of normal alcohols (i.e. methanol and ethanol, denoted hereafter as MeOH and EtOH, respectively) as solvents 1 containing water cosolvent 2.

(2) Ethanol and 1,2-ethanediol solvents 1 containing methanol 2 as cosolvent.

The experimental $d(x_2)$ data for the mixtures are analyzed using excess density Δd and excess molar volume ΔV_M as a function of cosolvent content x_2 and Redlich–Kister relation

$$\Delta Y = x_1 x_2 \sum_{j=0}^{n} a_j (x_2 - x_1)^j = x_2 (1 - x_2) \sum_{j=0}^{n} a_j (2x_2 - 1)^j \ , \tag{3.36}$$

where ΔY denotes the excess quantities Δd and ΔV_M, a_j is the standard deviations, and j is an integer. The excess density is given by (cf. Eq. (3.28))

$$\Delta d = d - [d_1 + x_2 (d_2 - d_1)], \tag{3.37}$$

and the excess molar volume ΔV_M is given by (3.15).

Figure 3.7a,b shows the dependences of density d of MeOH–H_2O and EtOH–H_2O mixtures at 20 °C on water content x_2 in MeOH and EtOH, and EtOH–MeOH and 1,2-ethanediol–MeOH mixtures at 25 °C on MeOH content x_2 in the mixtures, respectively. In Figure 3.7a the $d(x_2)$ data from Khimenko (1969) for $x_2 < 0.28$ mole fraction are presented to show that the data from two sources for a solvent mixture may lead to $\Delta d(x_2)$ and $\Delta V_\mathrm{M}(x_2)$ data substantially different from each other (see below). It may noted that the density d of the above solvent mixtures does not depend linearly on x_2 but may be described by a quadratic relation with the constants given in Table 3.4 (cf. Eq. 3.41)). It was observed that the fit of the $d(x_2)$ data somewhat improves with a higher-order polynomial such that the values of fitting parameters listed in Table 3.4 are somewhat changed. The deviations in d as represented by the excess density Δd are shown in Figure 3.8a,b, which illustrates the dependences of excess density Δd of MeOH–H_2O and EtOH–H_2O mixtures at 20 °C, and EtOH–MeOH and 1,2-ethanediol–MeOH mixtures at 25 °C on cosolvent content x_2, respectively. It may be seen again that Δd does not depend linearly on x_2, but usually passes through a minimum in Figure 3.8a and a maximum in Figure 3.8b at a certain x_2 typical of the cosolvent. The best-fit plots of the $\Delta d(x_2)$ data according to Redlich–Kister relation (3.36) are drawn in the figures with the constants listed in Table 3.5.

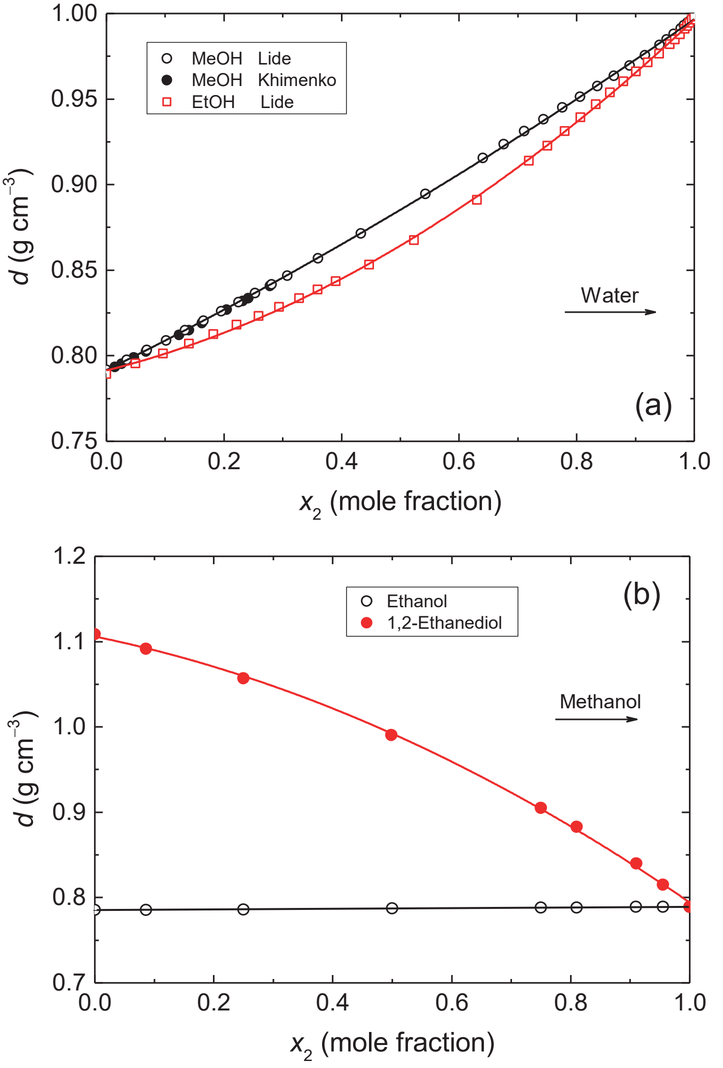

Figure 3.7. Dependences of density *d* of (a) MeOH–H_2O and EtOH–H_2O mixtures at 20 °C on water content x_2 in MeOH and EtOH, and (b) EtOH–MeOH and 1,2-ethanediol–MeOH mixtures at 25 °C on MeOH content x_2 in the mixtures. Note that *d* does not depend linearly on x_2 in the above solvent mixtures. Plots represent data according to Eq. (3.41) with constants listed in Table 3.4. In (a) $d(x_2)$ data from Khimenko (1969) are shown for comparison alone. Original data from (a) Lide (1996/1997) and Khimenko (1969), and (b) Albuquerque et al. (1996).

Table 3.4. Constants of Eq. (3.41) for $d(x_2)$ data of alcohol mixtures

Mixture	d_0^x (g·cm^{-3})	b_1 (g·cm^{-3})	b_2 (g·cm^{-3})	R^2
MeOH–H_2O	0.7916	0.1697	0.0054	0.9998
EtOH–H_2O	0.7914	0.0866	0.1185	0.9997
EtOH–MeOH	0.7852	0.0033	0.0007	0.9988
1,2-ethanediol–MeOH	1.1061	−0.1438	−0.1681	0.9992

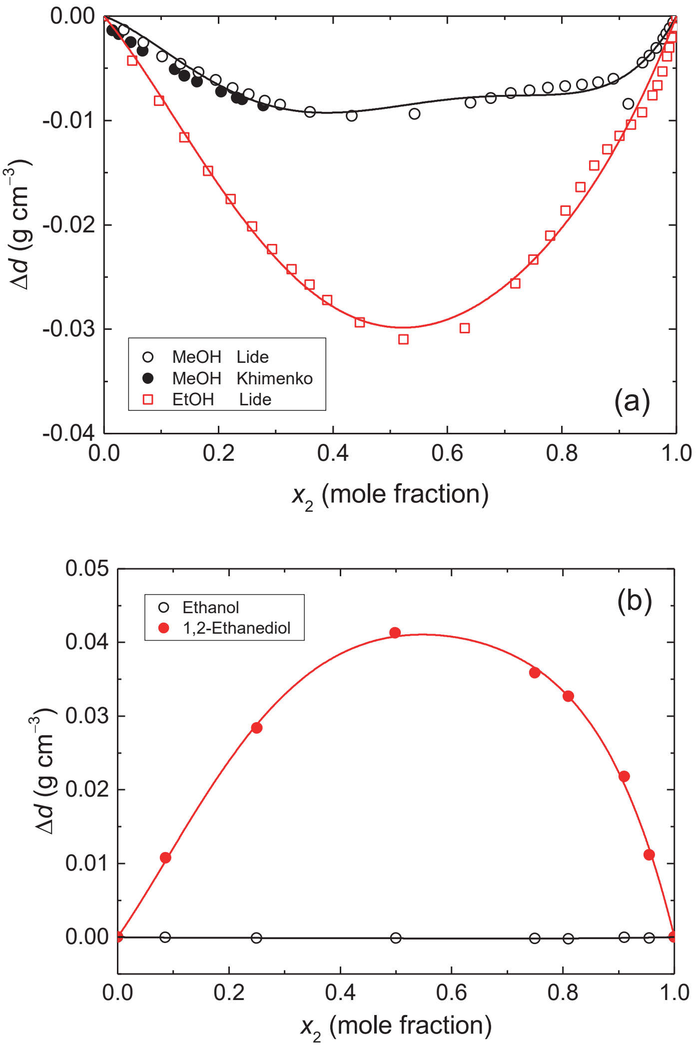

Figure 3.8. Dependences of excess density Δd of (a) MeOH–H_2O and EtOH–H_2O mixtures at 20 °C, and (b) EtOH–MeOH and 1,2-ethanediol–MeOH mixtures at 25 °C on cosolvent content x_2. Note that Δd does not depend linearly on x_2, but passes through a maximum at a certain x_2 typical of the cosolvent. Curves are drawn according to Redlich–Kister relation (3.36) with constants of Table 3.4. Original data given in Figure 3.7a and b. In (a) $\Delta V_M(x_2)$ data obtained from $d(x_2)$ data of Khimenko (1969) were not considered for analysis.

Table 3.5. Constants of Eq. (3.36) for $\Delta d(x_2)$ data of alcohol mixtures

Mixture	a_0 (g·cm^{-3})	a_1 (g·cm^{-3})	a_2 (g·cm^{-3})	a_3 (–)	R^2
MeOH–H_2O	0.0349	0.0153	−0.0250	−0.0553	0.9434
EtOH–H_2O	−0.1192	−0.0116	0.0147	−0.2737	0.9812
EtOH–MeOH	−0.00064	−0.00044	0.00062	−0.00022	0.6230
1,2-ethanediol–MeOH	0.1633	−0.02128	0.04432	−0.0782	0.9976

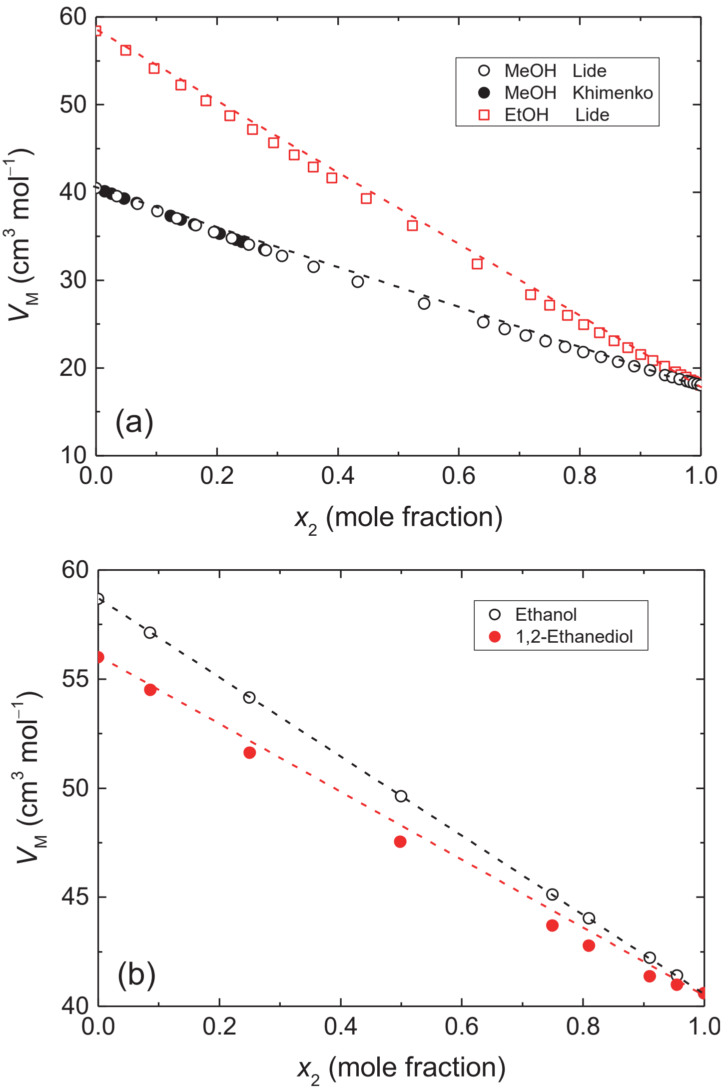

Figure 3.9. Dependences of molar volume V_M of (a) MeOH–H_2O and EtOH–H_2O mixtures at 20 °C, and (b) EtOH–MeOH and 1,2-ethanediol– MeOH mixtures at 25 °C on cosolvent concentration x_2. Dashed lines represent additive rule. Note that experimental V_M shows negative deviation from the additive rule. Original data from Figure 3.7a and b.

Figure 3.9a,b presents the dependences of molar volume V_M of MeOH–H_2O and EtOH–H_2O mixtures at 20 °C, and MeOH–EtOH and MeOH–1,2-ethanediol mixtures at 25 °C on cosolvent concentration x_2, respectively. As indicated by the dashed lines represented by the additive rule, the experimental V_M shows negative deviations from the additive rule. The deviations in V_M, represented by ΔV_M, are shown in Figure 3.10a,b, which presents the dependences of excess molar volume ΔV_M of MeOH–H_2O and EtOH–H_2O mixtures at 20 °C, and EtOH–MeOH and 1,2-ethanediol–MeOH mixtures at 25 °C on cosolvent content x_2. One notes once again that ΔV_M in the above mixtures does not depend linearly on x_2. The best-fit plots for the above $\Delta V_M(x_2)$ data are drawn according to Redlich–Kister relation (3.36) with the constants given in Table 3.6.

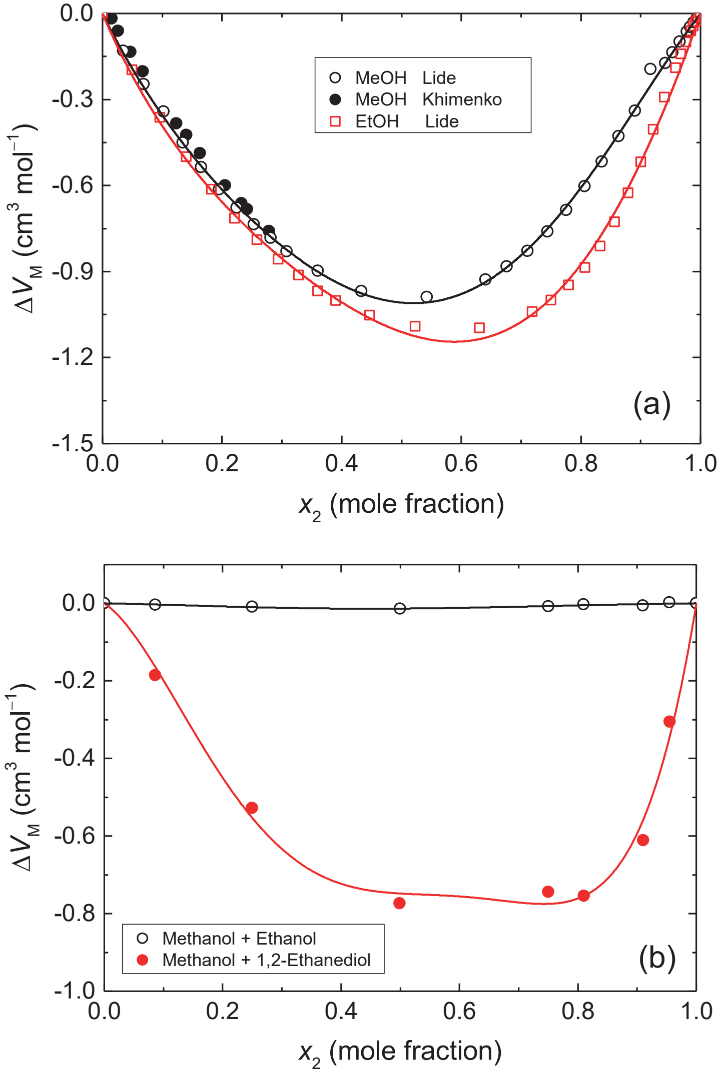

Figure 3.10. Dependences of excess molar refraction ΔV_M of (a) MeOH–H_2O and EtOH–H_2O mixtures at 20 °C, and (b) EtOH–MeOH and 1,2-ethanediol– MeOH mixtures at 25 °C on cosolvent content x_2. Note that ΔV_M does not depend linearly on x_2. Plots represent Redlich–Kister relation (3.36) with constants given in Table 3.6. In (a) $\Delta V_M(x_2)$ data obtained from $d(x_2)$ data of Khimenko (1969) were not considered for analysis.

Table 3.6. Constants of Eq. (3.36) for $\Delta V_M(x_2)$ data of alcohol mixtures

Mixture	a_0 ($cm^3 \cdot mol^{-1}$)	a_1 ($cm^3 \cdot mol^{-1}$)	a_2 ($cm^3 \cdot mol^{-1}$)	a_3 ($cm^3 \cdot mol^{-1}$)	R^2
MeOH–H_2O	−4.0334	−0.3731	0.5868	1.1369	0.9983
EtOH–H_2O	−4.4436	−1.4612	−0.9644	−0.9131	0.9957
EtOH–MeOH	−0.0538	−0.0538	0.0195	−0.0158	0.7404
1,2-ethanediol–MeOH	−2.9923	−0.1803	−2.1970	−4.0044	0.9862

3.4.2. Apparent partial molar volumes

Understanding of factors responsible for changes in volumetric properties of strongly associated systems composed of mixtures of organic liquids such as different alcohols and mixtures of water and organic liquids is an important aspect of density measurements of different systems. In comparison with the above procedure of analysis of excess molar volumes, investigation of apparent partial molar volumes is more informative. Here some results on the limiting partial molar volumes of cosolvent (water) in different solvents (*n*-alcohols), as examples of solvent–cosolvent mixtures, are described, following the ideas from Šegatin and Klafutar (2004).

We recall that the partial molar volume Φ_v of component 2 added to the main component 1 is calculated by using Eq. (3.6) and, from the dependence of Φ_v on the concentration c_2 of components 2 using linear or quadratic form of Eq. (3.12), values of the limiting partial molar volume Φ_v^o (denoted as V_2^o) of component 2 in the main components are calculated. During the analysis of water–alcohol mixtures, the square-root term in these equations is omitted because water–alcohol mixtures are nonelectrolytes. Then, from the calculated values of the limiting partial molar volume Φ_v^o, the deviation $\Delta\Phi_v$ in the calculated limiting molar volume Φ_v^o from the molar volume Φ_v^o(pure) of pure component 2 is calculated (i.e. $\Delta\Phi_v = \Phi_v^o(\text{pure}) - \Phi_v^o$). The deviation $\Delta\Phi_v$ is a measure of solvent–cosolvent interactions. When the deviation $\Delta\Phi_v$ is negative ($\Delta\Phi_v < 0$, or $\Phi_v^o(\text{pure}) > \Phi_v^o$), solvent–cosolvent interactions are attractive. However, when $\Delta\Phi_v > 0$, solvent–cosolvent interactions are repulsive. The more the deviation in Φ_v^o from Φ_v^o(pure), the higher are the attractive or repulsive solvent–cosolvent interactions, depending on whether $\Delta\Phi_v < 0$ or $\Delta\Phi_v > 0$.

Mixing of a cosolvent with a solvent can cause a change in the limiting partial molar volume Φ_v^o, denoted hereafter as V_2^o, of the cosolvent due to a difference in the size of component molecules and various interactions between the components. In the water–alcohol mixtures, attractive interactions occur by the formation of hydrogen bonds between alcohol–alcohol, alcohol–water and water–water molecules, but repulsive interactions take place between water molecules and alkyl group of alcohols. In general, attractive interactions lead to a reduction in the molar volume V_2^o, whereas repulsive interactions lead to an increase in V_2^o. Thus, it may be argued that the partial molar volume V_2^o of water increases in hydrophobic solvents and is larger than the molar volume V_2^o(water) of pure water. As shown in Figure 3.11, the calculated values of limiting partial molar volume V_2^o of water in some 1-alcohols increase with an increase in the molar volumes V_{M1} of the *n*-alcohols at 298.15 K. The molar volume of pure water is 18.068 $cm^3 \cdot mol^{-1}$. Therefore, if the molecules composing a liquid are considered as hard spheres, it may be inferred that water molecules fit more or less in the voids between the spheres of alcohols when the volumes of the molecules of the alcohols are large. The smaller values of V_2^o of water in the lower alcohols can be attributed mainly to the formation of strong hydrogen bonds between water and alcohol molecules.

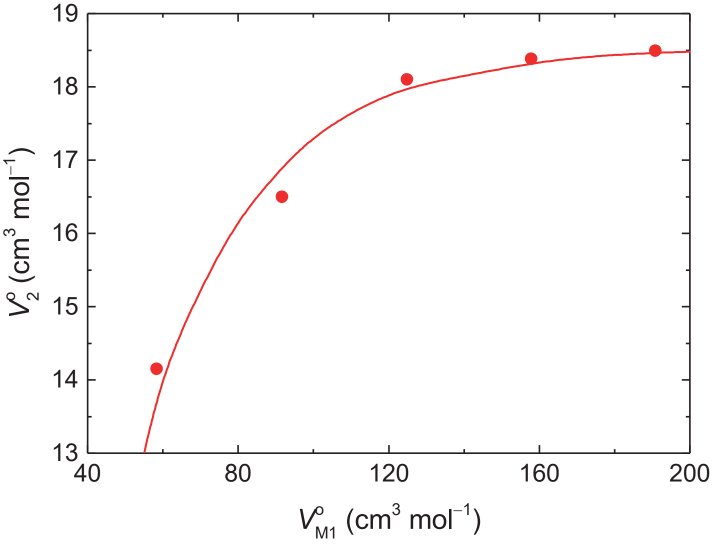

Figure 3.11. Limiting partial molar volume V_2^o of water in some *n*-alcohols as a function of molar volumes V_{M1}^o of 1-alcohols at 298.15 K. Adapted from Šegatin and Klafutar (2004).

The partial molar volume V_2^o of water in alcohols at infinite dilution is the sum of the volume V_{void} of the void space created by the addition of 1.0 mol of water to the alcohol and the van der Waals volume V_W of water (Šegatin and Klafutar, 2004):

$$V_2^o = V_W + V_{void}, \tag{3.38}$$

where $V_W = 12.4$ $cm^3 \cdot mol^{-1}$. With reference to Figure 3.11, one finds that V_{void} and the ratio V_{void}/V_W increase with increasing molar volume V_{M1}^o of the alcohols, which implies that they increase with increasing hydrophobicity of the solvent.

Šegatin and Klafutar (2004) calculated the packing density of a solute in the solution, defined as the ratio V_W/V_2^o, and observed that the packing density of water decreases gradually with increasing V_{M1}^o of an alcohol from a value of 0.88 for ethanol to 0.67 for *n*-decanol. Although these extreme values of 0.88 and 0.67 are somewhat higher than the values of 0.70 and 0.57 for random close-packed distribution of spheres, it may be concluded that the decreasing values of the packing density are a result of increasing void space V_{void} and approach the lowest extreme in higher *n*-alcohols.

If water and alcohol molcules are considered hard spheres, the limiting partial molar volume V_2^{o} of water may also be analyzed by the scaled particle theory (French and Criss, 1981; Pierotti, 1976; Šegatin and Klafutar, 2004). According to this theory, the limiting partial molar volume V_2^{o} of a solute is given by

$$V_2^{\mathrm{o}} = V_{\mathrm{cav}} + V_{\mathrm{inter}} + \beta_T^o R_{\mathrm{G}} T \ , \tag{3.39}$$

where $\beta_{\mathrm{T}}^{\mathrm{o}}$ is the isothermal compressibility of the solvent at the temperature T, R_{G} is the gas constant, V_{cav} is the volume of cavity formation in the solvent by thermal fluctuations, and the contribution V_{inter} to the volume V_2^{o} due to intermolecular interactions is given by

$$V_{\mathrm{inter}} = V_{\mathrm{disp}} + V_{\mathrm{dip}} + V_{\mathrm{ind}} \, , \tag{3.40}$$

where V_{disp} , V_{dip} and V_{ind} are the contributions of dispersive, dipole–dipole and inductive interactions, respectively, to the volume V_{inter} due to intermolecular interactions. In Eq. (3.39), both V_{cav} and $\beta_{\mathrm{T}}^{\mathrm{o}} R_{\mathrm{G}} T$ are positive quantities but V_{inter}, which accounts for the contraction of the cavity due to attractive intermolecular solute–solute interactions, is a negative quantity. Estimations of V_{cav} and V_{inter} for *n*-hexane, *n*-octane and *n*-decane (see Šegatin and Klafutar, 2004) also showed that both V_{cav} and $-V_{\mathrm{inter}}$ decrease, whereas V_2^{o} of water in the *n*-alcohols increases with their increasing hydrophobicity.

Šegatin and Klafutar (2004) also examined the trends of V_2^{o} of water in different alcohols according to the fluctuation theory of Kirkwood and Buff (1951) which treats the aggregation behavior of solute in a solvent. In this theory, a dimensionless parameter N_{22} is a measure of the aggregation number representing the excess of solute molecules in the surrounding of a solute molecule at infinite dilution. The main finding of this analysis is that introduction of water to an alcohol leads to the rupturing of self-associated alcohol molecules, resulting in the formation of smaller aggregates of alcohol molecules than those in the pure alcohol. The alcohol aggregates are bonded to water molecules such that a certain number of alcohol molecules is bonded to each water molecule. These clustering processes are intensified with the increasing chain length of the *n*-alcohol molecule.

3.5. Densities and molar volumes of solutions

3.5.1. Solute concentration dependence of densities of solutions

In this section two ionic salts, NaCl and KCl, and two sugars, sucrose and D-glucose, are first considered as representative examples of inorganic and organic compounds which are solutes dissolved in water as their solvent. Water as a solvent for the preparation of solutions of different types of solutes is attractive because they are reasonably soluble in it and, therefore, are suitable for the investigation of various interactions involved in the aqueous solutions from analysis of the dependences of the density of aqueous solutions of the above compounds on solute concentration and solution temperature using different equations presented in Section 3.2. The original data of the density *d* of solutions as a function of concentration x_2 are taken from Lide (1996/1997).

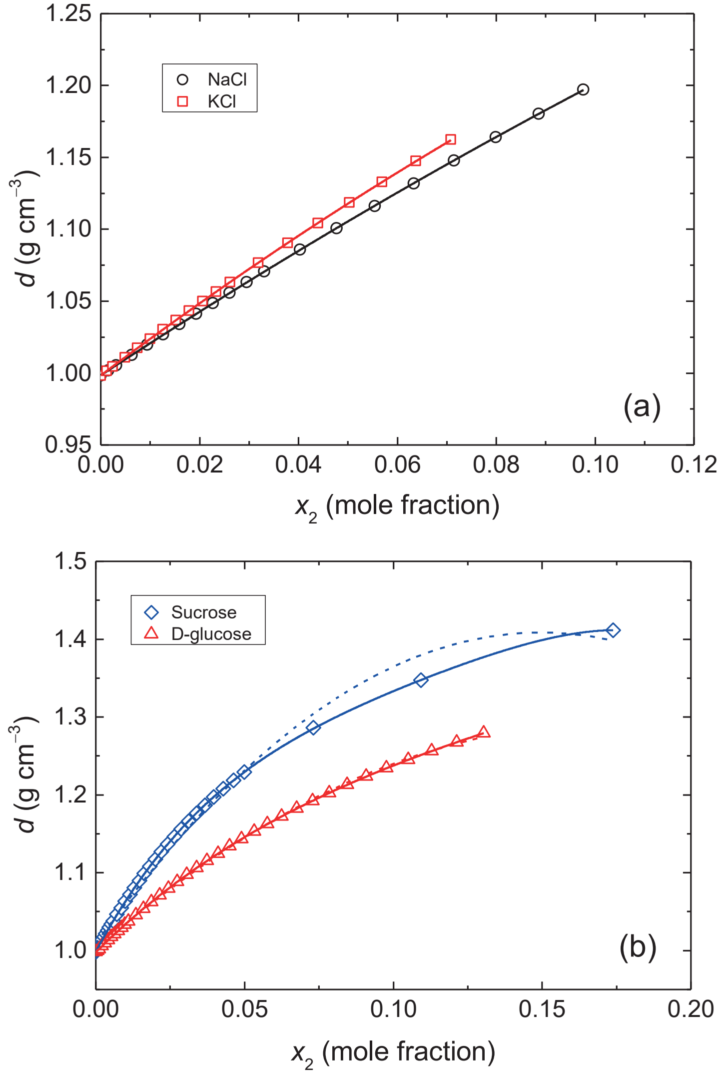

Figure 3.12. Dependence of density *d* of aqueous solutions of (a) NaCl and KCl, and (b) sucrose and D-glucose on solute concentration x_2. Dashed and solid curves represent plots according to Eq. (3.41), with constants listed in Table 3.7. Original data from Lide (1996/1997).

Figure 3.12a and b shows the dependence of density *d* of aqueous solutions of NaCl and KCl, and sucrose and D-glucose at 20 °C on solute concentration x_2, respectively. As in the case of the dependence of the densities *d* of binary solvent–cosolvent mixtures of different alcohols on cosolvent content x_2 described above, the density d of aqueous solutions of these compounds also does not increase linearly with solute concentration x_2. Instead, the density of the solution in a compound deviates from the linearity such that it appears to approach a maximum value at some value of the solute concentration x_2. The $d(x_2)$ data for aqueous NaCl and KCl solutions may be represented satisfactorily by a quadratic relation but those for aqueous sucrose and D-glucose solutions are described better by a polynomial relation (cf. Eq. (3.20))

$$d = d_0 + b_1 x_2 + b_2 x_2^2 + \ldots + b_n x_2^n, \tag{3.41}$$

where d_0 is the density of the solution corresponding to $x_2 \to 0$, b's are constants and n is an integer. Solid curves in Figure 3.12a and b are drawn according to the polynomial relation, respectively, whereas dashed curves in Figure 3.12b represent the data according to the quadratic relation. The constants of the best-fit curves for the above $d(x_2)$ data are listed in Table 3.7.

Table 3.7. Constants of Eq. (3.41) for $d(x_2)$ data of aqueous solutions of selected solutes

Solute	d_0 (g·cm^{-3})	b_1 (g·cm^{-3})	b_2 (g·cm^{-3})	b_3 (g·cm^{-3})	b_4 (g·cm^{-3})	R^2
NaCl	0.99848	2.25485	−2.28406			0.99999
KCl	0.99842	2.58223	−3.84836			0.99999
Sucrose	1.0089	5.34348	−17.86349			0.99132
	0.99874	7.1056	−65.99012	366.097	−822.707	0.99999
D-glucose	1.0088	3.37227	−9.78948			0.99946
	0.99818	3.7965	−20.42134	77.21232	−130.4995	1

An indicator of deviation from the linear dependence of d on x_2 is the value of the constant b_1 listed in Table 3.7. For the above solutions the different solutes show the following trend of increasing deviation: NaCl < KCl < D-glucose < sucrose. This observed trend is intimately related to their solubility and is associated with the increasing solute–solute interactions which begin to dominate over the solute–solvent interactions at high solute concentrations x_2.

In order to study the temperature dependence of density of solutions of known concentrations and their concentration dependence at known temperatures in terms of the thermal expansivity coefficient α of Eq. (3.23) or of a_1 of Eq. (3.21) and constants a_5 and a_6 of Eq. (3.25) or of A and p of Eq. (3.27) it is convenient to use density difference (d–d_0) or relative density $d_\mathrm{r} = d/d_0$ rather than d itself and take solute concentration in mole fraction x_2. In the case of concentration dependence of solutions, Eq. (3.25) may be written in the form

$$\left(\frac{d}{d_0} - 1\right)\frac{1}{x_2} = \frac{a_5}{d_0} + \frac{a_6}{d_0} x_2, \tag{3.42}$$

whereas Eq. (3.27) in the logarithmic form

$$\ln\left(\frac{d}{d_0}-1\right)=\ln\left(\frac{A}{d_0}\right)+p\ln x_2\,. \tag{3.43}$$

Note that $a_5/d_0 = b_1$ and $a_6/d_0 = b_1$ in Eq. (3.42). According to these relations experimental data of $[(d/d_0)-1]/x_2$ against x_2 and $\ln[(d/d_0)-1]$ against $\ln x_2$ for aqueous solutions at particular temperatures enable to obtain the values of different constants and discuss the nature of solute–solvent interactions. For this purpose, the density data for aqueous solutions of the four solutes at 20 °C considered above and new density data for aqueous solutions of five electrolytes at 25 and 50 °C were analyzed. The density data for the solutions are taken from Söhnel and Novotný (1985) and from Lide (1996/1997). It should be mentioned that, except for NaCl, the other four solutes with the new data are hydrated salts. The densities d_s of different solutes in the solid state are taken from Lide (1996/1997).

Figure 3.13 shows plots of $\ln[(d/d_0)-1]$ against $\ln x_2$ according to Eq. (3.43) for the data of all solutes. Dashed lines in these figure are drawn with a slope $p = 1$ such that they represent the data at low concentrations, but in Figure 3.13b dashed lines are drawn to represent the data at 25 °C. It may be observed from Figure 3.13a that the slope p of the plots is unity only at concentrations x_2 corresponding to $\ln[(d/d_0)-1]$ lying below about -3. However, later the value of the slope steadily decreases with solute concentration x_2 and the decrease in the slope p, as determined by $\mathrm{d}p/\mathrm{d}x_2$, with x_2 is directly related to the solubility of the solute in the solvent. For example, the decrease in $\mathrm{d}p/\mathrm{d}x_2$ with x_2 is enormous for aqueous sucrose and D-glucose solutions in comparison with that for NaCl and KCl solutions. The decrease in the slope appears to approach the value of $\ln[(d/d_0)-1]$ corresponding to the concentration $x_2 = 1$ for these solutes of density d_s in the solid state. A similar trend may also be noted from the plots of Figure 3.13b but the trend is not so well defined because of a narrow range of solute concentration x_2 for these data. In this figure solid lines present the best fit of the data with values of the intercept $\ln(A/d_0)$ and the slope p listed in Table 3.8. The molar mass M_2 of anhydrous solutes is also included in the table.

Figure 3.14 shows, as typical examples, plots of $[(d/d_0)-1]/x_2$ against x_2 according to Eq. (3.42) for the data of aqueous solutions of the selected electrolytes. If the data at very low concentrations (x_2 below about 0.003 mole fraction) are ignored, the dependence of $[(d/d_0)-1]/x_2$ on x_2 is linear. However, except for $KAl(SO_4)_2$, the slopes a_6/d_0 of the plots are negative for all other solutes.

From Table 3.8 the following features may be noted:

1. As expected from Eq. (3.27), the exponent $p < 1$ from the $d(x_2)$ data for most of the compounds. The data at 50 °C for $KAl(SO_4)_2$ show an anomalous behavior.
2. The value of the constant A/d_0 of Eq. (3.43) is lower than that of the constant a_6/d_0 of Eq. (3.42) for NaCl, Na_2SO_4 and $CuSO_4$, and their values are comparable for $NH_4Al(SO_4)_2$ and $KAl(SO_4)_2$.
3. Irrespective of the temperature, the values of A/d_0 and a_5/d_0 for these solutes increase in the sequence: $NaCl < Na_2SO_4 < CuSO_4 < NH_4Al(SO_4)_2 < KAl(SO_4)_2$. A similar trend appears to be followed by the constant a_6/d_0 of Eq. (3.42) and the

exponent p of Eq. (3.43).

(4) The values of A/d_0 and a_5/d_0 for different solutes are usually higher at 25 °C than those at 50 °C.

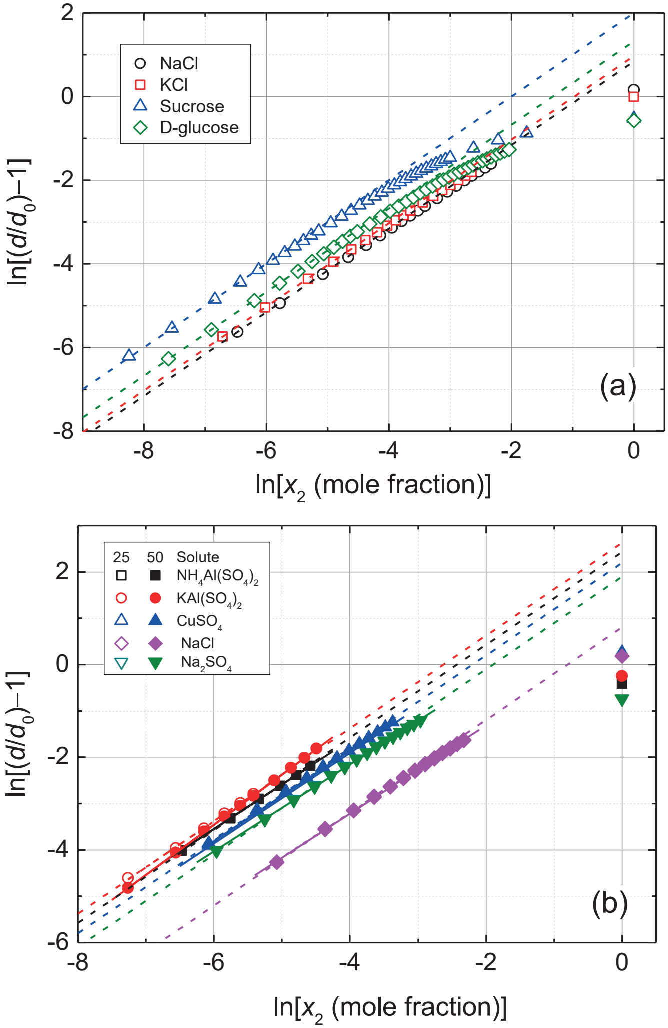

Figure 3.13. Plots of $\ln[(d/d_0)–1]$ against $\ln x_2$ of aqueous solutions of (a) NaCl, KCl, sucrose and D-glucose and (b) some selected electrolytes according to Eq. (3.43). Dashed lines in both figures represent linear dependence of slope $p = 1$ but solid lines represent best-fit plots of the data with the constants listed in Table 3.8. Original data in (a) and (b) are from Lide (1996/1997), and from Söhnel and Novotný (1985), respectively.

The anomalous behavior of $p > 1$ in the case of the data at 50 °C for $KAl(SO_4)_2$ is probably associated with the anomalous data themselves. Features (2) and (3) are mainly associated with the solubility of the solutes, which increases in the order mentioned above, and is mainly associated with the dominant contribution of the solute molar mass M_2 in the $(M_2 - d_0\Phi_v^o)$ term of Eq. (3.20). Feature (4) is associated with a decrease in the density d of solutions with increasing temperature.

Table 3.8. Constants of Eqs. (3.42) and (3.43) for different aqueous solutions

Solute	M_2	Temp.	Eq. (3.42)			Eq. (3.43)			
	(g·mol^{-1})	(°C)	a_5/d_0	$-a_6/d_0$	R^2	$\ln(A/d_0)$	A/d_0	p	R^2
NaCl	58.44	25	2.28	5.08	0.973	0.6265	1.871	0.9575	0.9995
		50	2.25	4.62	0.962	0.5856	1.796	0.9508	0.9998
Na_2SO_4	142.04	25	7.03	30.9	0.974	1.7069	5.512	09576	0.9998
		50	6.88	33.6	0.953	1.6027	4.966	0.9389	0.9997
$CuSO_4$	159.60	25	9.26	48.0	0.968	2.0076	7.445	0.9631	0.9997
		50	8.80	77.1	0.993	2.0076	7.445	0.9783	0.9999
$NH_4Al(SO_4)_2$	237.14	25	11.70	92.2	0.678	2.3433	10.416	0.9831	0.9999
		50	11.85	53.7	0.734	2.2118	9.132	0.9603	0.9999
$KAl(SO_4)_2$	258.20	25	13.19	369	0.910	2.5645	12.995	0.9910	0.9989
		50	11.88	−517	0.992	3.0385	20.874	1.0828	0.9999

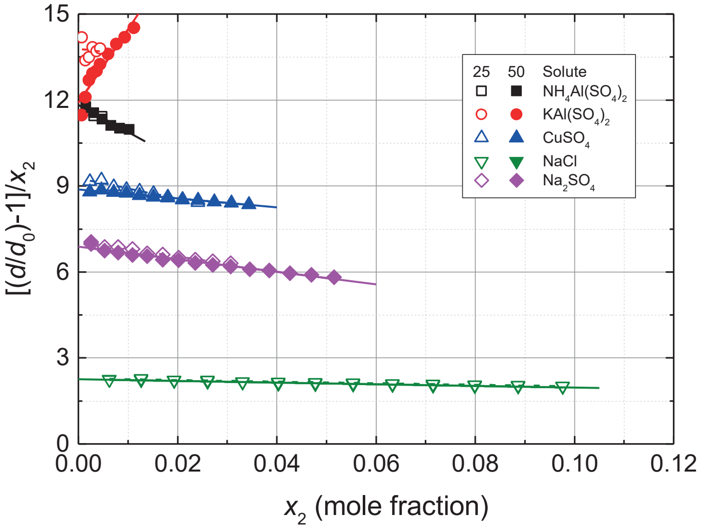

Figure 3.14. Plots of $[(d/d_0)-1]/x_2$ against solution concentration x_2 of aqueous solutions of selected electrolytes according to Eq. (3.42), with constants listed in Table 3.8.

3.5.2. Solute-concentration dependence of molar volumes of solutions and molar volumes at infinite dilution

The behavior of the $d(x_2)$ data for the above four solutes was analyzed from consideration of the molar volumes V_M of the solutions calculated by using Eq. (3.13) and excess molar volume ΔV_M using Eq. (3.15). Figure 3.15a and b shows the dependence of the molar volume V_M of aqueous solutions of NaCl and KCl, and sucrose and D-glucose on solute concentration x_2. The $V_M(x_2)$ data were analyzed by using linear and quadratic functions (see Eq. (3.12)). Solid curves in Figure 3.15a and b show the best fit of the data according to the quadratic relation, whereas dashed curves in Figure 3.15b represent best-fit plots according to linear relation. The constants of the plots are listed in Table 3.9. In view of concentration of solute here in mole fraction x_2 for the analysis of the $d(x_2)$ data, the constants b_{v1} and b_{v3} of Eq. (3.12) are distinguished by b_{V1} and b_{V3}, repectively, and $\Phi_v^o = V_{M0}$.

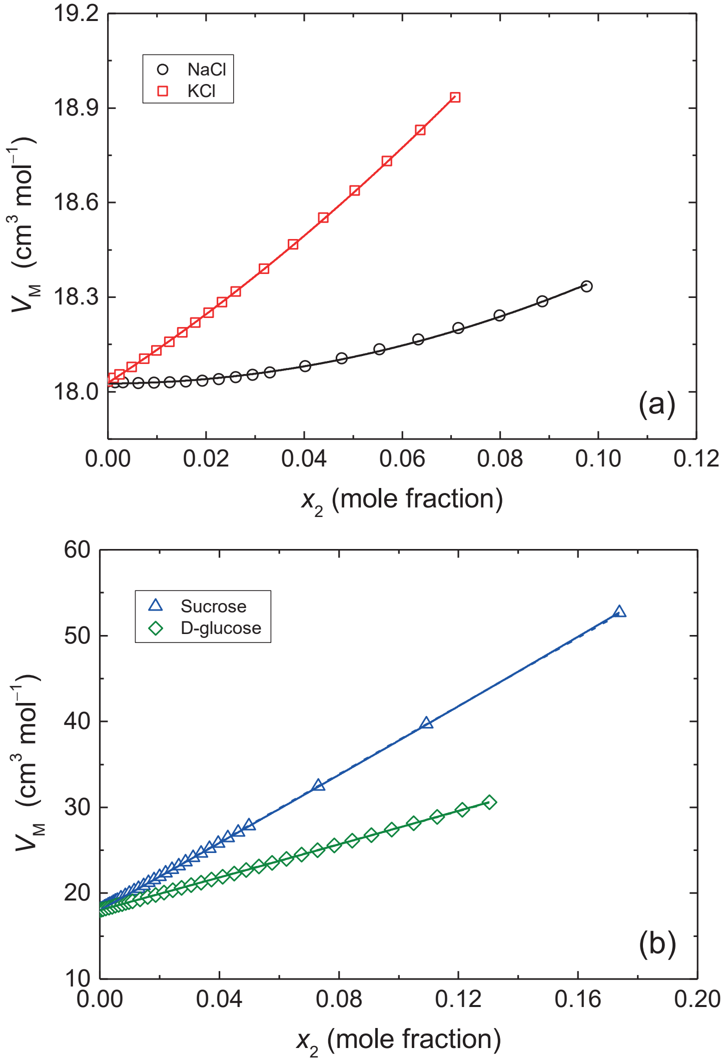

Figure 3.15. Dependence of molar volume V_M of aqueous solutions of (a) NaCl and KCl, and (b) sucrose and D-glucose at 20 °C on solute concentration x_2. Dashed and solid curves represent plots according to linear and quadratic relations, respectively, with constants listed in Table 3.9. Original data from Figure 3.11.

Table 3.9. Constants of Eq. (3.12) for $V_M(x_2)$ data of aqueous solutions of selected solutes*

Solute	V_{M0} (g·cm^{-3})	b_{V1} (cm^3·mol^{-1})	b_{V3} (cm^3·mol^{-1})	R^2
NaCl	18.026	0.0736	32.293	0.9980
KCl	18.028	10.115	36.573	0.9999
Sucrose	17.968	198.694		0.9999
	18.020	194.699	27.640	1
D-glucose	17.968	96.276		0.9999
	18.027	94.482	15.867	1

* Constants are denoted here by b_V's.

It may be observed from the above table that the data of aqueous NaCl and KCl solutions are better represented by the quadratic dependence but in the case of sucrose and D-glucose solutions the data are also described reasonably well by the linear dependence. In the latter solutions, the value of the b_{V1} parameter obtained by the linear relation is higher than that obtained by the quadratic relation by no more than 2%. However, if the constant b_{V1} is taken as an indicator of solute–solute interactions, its value increases in the sequence: NaCl, KCl, D-glucose and sucrose. This trend is the same as that observed above in the case of the $d(x_2)$ data.

Figure 3.16 shows the dependence of excess molar volume ΔV_M of aqueous solutions of the above solutes on solute concentration x_2. As in the case of the $d(x_2)$ and $V_M(x_2)$ plots, the excess molar volume ΔV_M does not depend linearly on x_2. With increasing solute concentration x_2, the value of ΔV_M decreases steadily for NaCl and KCl in the entire studied range of x_2, it decreases and attains a limiting and practically constant value of about -0.15 cm^3·mol^{-1} for $0.08 < x_2 < 1.4$ of D-glucose, while it decreases first and then, after showing a minimum value of -0.15 cm^3·mol^{-1} at $x_2 \approx 0.05$ mole fraction, increases for sucrose. Obviously, the behavior of NaCl and KCl is completely different from that of sucrose but that of D-glucose lies in between the two previous groups.

The $\Delta V_M(x_2)$ data for the solutes were analyzed by using Redlich–Kister relation (3.36) with the limiting values of different a_j parameters kept fixed between -10 and 10 and with changed values of the a_3 parameters kept between -100 and 100. The best-fit values of the different parameters for the former and the latter iteration of the $\Delta V_M(x_2)$ data are listed in Table 3.10. The sum Σa_j of the parameters for these limiting iteration values of the parameters is also included in the table.

From Table 3.10 it may be seen that the parameters of the fit of the $\Delta V_M(x_2)$ data for all four solutes improves in the case of the latter iteration and the sum Σa_j is somewhat decreased. The decrease in the sum Σa_j is about 2% for NaCl and KCl solutions and about 5% for sucrose and D-glucose solutions. However, these changes are insignificant in the general trend of the sum Σa_j of the parameters for the four solutes, which in the order of decreasing changes in Σa_j follows the sequence: KCl, NaCl, sucrose and D-glucose.

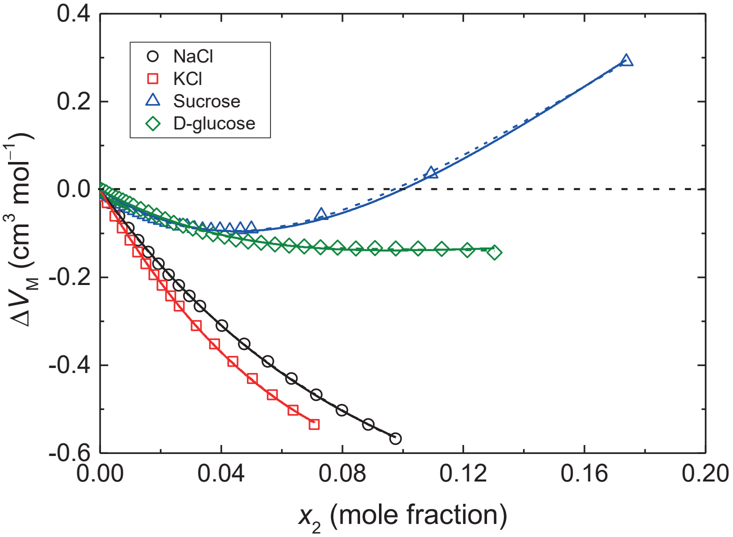

Figure 3.16. Dependences of excess molar volume ΔV_M of aqueous solutions of (a) NaCl and KCl, and (b) sucrose and D-glucose on solute concentration x_2. Note that ΔV_M does not depend linearly on x_2. Plots represent Redlich-Kister relation (3.36) with constants in Table 3.10.

Table 3.10. Constants of Eq. (3.36) for $\Delta V_M(x_2)$ data of some aqueous solutions

Solute	a_0 (cm^3·mol^{-1})	a_1 (cm^3·mol^{-1})	a_2 (cm^3·mol^{-1})	a_3 (cm^3·mol^{-1})	Σa_j (cm^3·mol^{-1})	R^2
NaCl	−5.41452	2.82085	3.01809	−10	−9.57558	0.99968
	−10	7.95945	9.37288	−17.08651	−9.75418	0.99995
KCl	−1.20677	0.76246	−1.60306	−10	−12.04677	0.99964
	−9.72320	10	9.11942	−21.60219	−12.20597	0.99980
Sucrose	3.05628	3.29464	−0.88322	−10	−4.53230	0.99753
	5.09671	−10	23.10036	−23.00162	−4.80455	0.99918
D-glucose	−3.21489	4.85906	4.54477	−10	−3.81106	0.99673
	−6.88271	10	8.12486	−15.29583	−4.05368	0.99837

The plots of $\ln[(d/d_0)-1]$ against $\ln x_2$ of aqueous solutions of different solutes with a slope $p = 1$ enable to determine, by extrapolation of the plots from the experimental $d(x_2)$ data in Figure 3.13, down to lower the values of $\ln[(d/d_0)-1]$ for infinitely dilute solutions ($x_2 \to 0$) and to highly concentrated solutions ($x_2 \to 1$), denoted hereafter as $\ln[(d/d_0)-1]_0$ and $\ln[(d/d_0)-1]_{x2=1}$, respectively, and examine their relationship with the nature of the solutes. However, it is impossible to obtain the values of $\ln[(d/d_0)-1]_0$ at infinite dilution from the plots of Figure 3.13. Therefore, a solute concentration corresponding to $\ln x_2 = -9$ (i.e. $x_2 = 1.2\cdot10^{-4}$ mole fraction) was taken as the reference concentration of infinite dilution. The feature here is that the values of $\ln[(d/d_0)-1]_{x2=1}$ obtained by extrapolation of the plots from the experimental data do not correspond to the values of $\ln[(d_s/d_0)-1]$ for the solutes in the solid state and are always higher than the latter. Therefore, the anticipated deviation $\ln[(d/d_0)-1]_{x2=1}-\ln[(d_s/d_0)-1]$ in the value of $\ln[(d_s/d_0)-1]$ from the extrapolated value of $\ln[(d/d_0)-1]_{x2=1}$ for the solutes was considered for the analysis. As a measure of the values of the above quantities molar volumes $V_{Ms} = M_2/d_s$ of the solutes were taken.

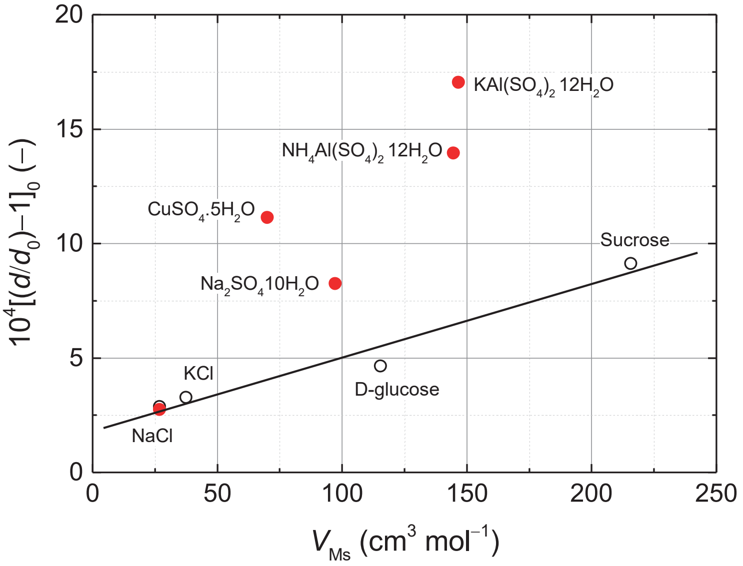

Figure 3.17. Relationship between $[(d/d_0)-1]_0$ at infinite dilution ($\ln x_2 = -9$, i.e. $x_2 = 1.2\cdot10^{-4}$ mole fraction) of aqueous solutions of different solutes and their molar volume V_{Ms}. Original data from Figure 3.13.

Figure 3.17 shows the data of $[(d-d_0)-1]_0$ at infinite dilution ($\ln x_2 = -9$, i.e. $x_2 = 1.2\cdot10^{-4}$ mole fraction) of aqueous solutions of different solutes and their molar volume V_{Ms}. The data are derived from Figure 3.13. It may be noted that the value of $[(d-d_0)-1]_0$ increases with an increase in V_{Ms} of the solutes. For solutes, which are unhydrous in the solid state, the value of $[(d-d_0)-1]_0$ increases practically linearly with intercept $1.8\cdot10^{-4}$ and slope $3.0\cdot10^{-6}$ mol·cm^{-3}. One may also note a similar trend with a somewhat higher slope for the hydrous salts.

Figure 3.18 shows the relationship between anticipated deviation $\ln[(d/d_0)-1]_{x2=1}-\ln[(d_s/d_0)-1]$ in the value of $\ln[(d_s/d_0)-1]$ for hypothetical aqueous solutions of concentration $x_2 = 1$ of different solutes and their molar volume V_{Ms}. Once again one finds that the deviation increases with the increasing molar volume V_{Ms} and the behavior of the solutes without and with water molecules in their crystalline state is different from each other.

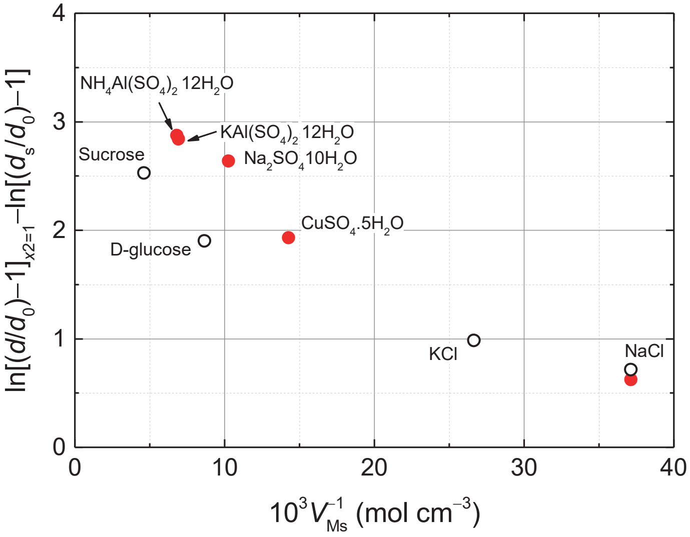

Figure 3.18. Relationship between anticipated deviation $[(d/d_0)-1]_{x2=1}-[(d_s/d_0)-1]$ in the value of $\ln[(d_s/d_0)-1]$ for hypothetical aqueous solutions of concentration $x_2 = 1$ of different solutes and inverse of their molar volume V_{Ms}. Original data from Figure 3.13.

3.5.3. Apparent molar volumes of electrolyte solutions

In this section some general features of apparent molar volumes Φ_v of electrolyte solutions as a function of solute concentration c_2 and solution temperature T are presented. Aqueous solutions of simple ionic salts such as NaCl and KCl are taken as typical examples for analysis of the experimental data of apparent molar volumes and discussion of physical interpretation of constants of the different $\Phi_v(c_2)$ relations. Comments on the values of the constants of the $\Phi_v(c_2)$ relations for some other ionic organic compounds used as sweeteners and drugs and the effect of temperature on the values of the constants are also made. Discussion of the $\Phi_v(c_2)$ data on NaCl and KCl electrolytes is based on the original $d(c_2)$ data from Lide (1996/1997), those on sweeteners Na saccharin and K acesulfame from Klofutar et al. (2006), whereas those on drugs Methyl orange, Propranalol HCl, Procaine HCl, Pilocarpene HCl, and Ephedrine HCl from Iqbal and Verrall (1989).

Figure 3.19 shows the $\Phi_v(c_2)$ data for aqueous NaCl and KCl solutions in the form of the dependence of Φ_v on $c_2^{1/2}$ according to Eq. (3.10). It may be seen that the $\Phi_v(c_2^{1/2})$ plot for NaCl solutions may be represented by this relation satisfactorily in the entire concentration range but the plot for KCl solutions the dependence is followed well only up to $c_2 < 0.8$ mol·L^{-1}. In the latter case, the plot begins to exhibit positive deviation from the above dependence for c_2 exceeding about 0.8 mol·L^{-1} due the dominance of the $b_{v1}c$ term (see Eq. (3.12)). Then cation–anion interactions begin to dominate the ion–solvent interactions (see below). The best-fit values of the limiting apparent molar volumes Φ_v^o and the constant S_v for these two systems are listed in Table 3.11. The molar volumes V_{M2} of NaCl and KCl salts are 26.93 and

37.50 $cm^3 \cdot mol^{-1}$, respectively, and are given in the parentheses in the first column of the table. Included in the table are also the constants of Eq. (3.10) for aqueous solutions of other compounds.

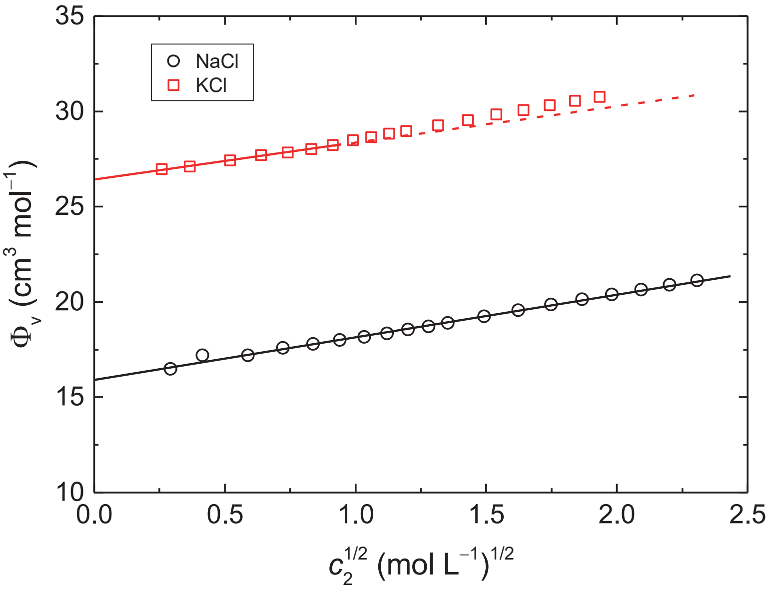

Figure 3.19. Dependence of Φ_v of NaCl and KCl on $c_2^{1/2}$ at 20 °C on c_2. Original data from Lide (1996/1997).

Table 3.11. Constants of $\Phi_v°$ and S_v of Eq. (3.10) for some aqueous electrolyte solutions

Substance	T (°C)	c_2 range	$\Phi_v°$	S_v	b_{v1}	Ref.
-			($cm^3 \cdot mol^{-1}$)	($cm^3 \cdot L^{1/2} \cdot mol^{-3/2}$)	($cm^3 \cdot L \cdot mol^{-2}$)	
NaCl (26.93)	20	Entire	15.924	2.238		a
KCl (37.50)	20	< 0.00 M	26.421	1.937		a
Na saccharin	25	Entire	113.19	1.833	$-5.05 \pm 0.28^*$	b
K acesulfame	25	Entire	107.58		0.39 ± 0.05	b
Na salicylate	25	Entire	93.40	1.20		c
Methyl orange	25	Entire	227.58	−11.12		c
Propranalol HCl	25	< 0.06 m	245.14	0.86		c
Procaine HCl	25	Entire	225.84	−1.61		c
Pilocarpene HCl	25	Entire	193.34	−1.05		c
Ephedrine HCl	25	Entire	168.79	0.29		c

Constant $b_{v2} = 4.76 \pm 0.23$ $cm^3 \cdot L^{3/2} \cdot mol^{-5/2}$.
[a] This work. [b] Klofutar et al. (2006). [c] Iqbal and Verrall (1989).

The limiting apparent molar volume $V_2°$ of an electrolyte is usually lower than the molar volume V_{M2} of the solid calculated from its molecular weight M and density d_s.

The value of V_2^{o} of the electrolyte is equal to the sum of its ionic contributions, denoted hereafter as V_+^{o} and V_-^{o} corresponding to cations and anions, respectively. Couture and Eyring (1956) found that, with reference to the molar volume $V_{\mathrm{H}}{}^+$ of hydrogen ion equal to zero, the limiting partial molar volumes V_+^{o} and V_-^{o} of cations and anions of a given value of the charge z follow the empirical relations

$$V_{2+}^{\mathrm{o}} = 16 + 4.9r^3 - 26z_+ , \tag{3.44}$$

$$V_{2-}^{\mathrm{o}} = 4 + 4.9r^3 - 14z_- , \tag{3.45}$$

respectively. However, when it is assumed that $V_{\mathrm{H}}{}^+ = -6$ cm^3·mol^{-1}, the above equations yield

$$V_2^{\mathrm{o}} = V_+^{\mathrm{o}} + V_-^{\mathrm{o}} = 20 + 4.9(r_+^3 + r_-^3) - 20(z_+ + z_-) , \tag{3.46}$$

where $z_\pm$ is the valence of an ion and r is its radius. The volume $V_\pm = (4\pi/3)r_\pm^3$ of an ion of crystallographic radius $r_\pm$ (expressed in Å) is equal to $2.5r_\pm^3$ cm^3·mol^{-1} and is about one-half of the value $4.9r_\pm^3$ of the above equations. Then Eq. (3.46) takes the form

$$V_2^{\mathrm{o}} = 20 + 1.95(V_+ + V_-) - 20(z_+ + z_-) . \tag{3.47}$$

In the case of a 1:1 electrolyte, with $V_\pm = 2.5r_\pm^3$, the above equation becomes

$$V_2^{\mathrm{o}} = 1.95(V_+ + V_-) - 20 . \tag{3.48}$$

Obvously, in the above equations the limiting molar volume V_2^{o} of an electrolyte depends on the charge z on its ions and on their size r.

It may be noted that the total volume of the ions of electrolytes in aqueous solutions as given in Eq. (3.47) is approximately twice the volume based on their crystallographic radii. This difference is associated with the solvation of ions in the solution because the volume occupied by an ion in the solution is the sum of (1) its intrinsic volume and (2) the constriction of water molecules in its neighborhood.

The limiting partial molar volume $V_{2\,\mathrm{ion}}^{\mathrm{o}}$ of an ion is the sum of different contributions usually given by (Millero, 1970, 1972)

$$V_{2\,\mathrm{ion}}^{\mathrm{o}} = V_{\mathrm{int}}^{\mathrm{o}} + V_{\mathrm{elect}}^{\mathrm{o}} + V_{\mathrm{disord}}^{\mathrm{o}} + V_{\mathrm{str}}^{\mathrm{o}} , \tag{3.49}$$

where $V_{\mathrm{int}}^{\mathrm{o}}$ is the intrinsic volume associated with the geometrical volume of the ion, usually calculated from the crystal volume, $V_{\mathrm{elect}}^{\mathrm{o}}$ is the electrostriction partial molar volume due to charge of the ion, $V_{\mathrm{disord}}^{\mathrm{o}}$ is the disordered or the void-space molar volume of the ion, and $V_{\mathrm{str}}^{\mathrm{o}}$ is the structured partial molar volume of the ion. The intrinsic volume $V_{\mathrm{int}}^{\mathrm{o}}$ is the volume of the ion inpenetrable to the solvent molecules is approximately equal to the van der Waals volume V_{W} of the solvent, the disordered or void-space volume is related to the radius r of the ion, given by the empirical relation (Millero, 1972)

$$V^{\mathrm{o}}_{\mathrm{disord}} = (A_0 - 2.52)r^3, \tag{3.50}$$

where the constant $A_0 = 4.48$ $\mathrm{cm^3 \cdot mol^{-1} \cdot Å^{-3}}$ and assuming that the ion is a hard sphere, its radius is obtained from V_{W} according to the relation (De Ligny and van der Veen, 1972)

$$2r = \left(\frac{6V_{\mathrm{W}}}{\pi N_{\mathrm{A}}}\right)^{1/3}, \tag{3.51}$$

where N_{A} is the Avogadro number. The electrostriction partial molar volume $V^{\mathrm{o}}_{\mathrm{elect}}$ is given by the empirical relation (Millero, 1972)

$$V^{\mathrm{o}}_{\mathrm{elect}} = -\frac{B_0 z^2}{r}, \tag{3.52}$$

where the constant $B_0 = 13.0$ $\mathrm{cm^3 \cdot Å \cdot mol^{-1}}$ and z is the valency of the ion. The contribution $V^{\mathrm{o}}_{\mathrm{str}}$ due to the structure of the ion may be assessed from the difference between $V^{\mathrm{o}}_{2\mathrm{ion}}$ and other contributions. Its value is -38.2 $\mathrm{cm^3 \cdot mol^{-1}}$ for saccharin nitranion and -37.59 $\mathrm{cm^3 \cdot mol^{-1}}$ for acesulfame nitranion (Klofutar et al., 2006).

The short-range behavior of an ion may be discussed from the difference ($V^{\mathrm{o}}_{2\mathrm{ion}} - V_{\mathrm{W}}$) for the ion. When ($V^{\mathrm{o}}_{2\mathrm{ion}} - V_{\mathrm{W}}$) < 0, the ion may be considered as an electrostatic positive solvating ion. However, ($V^{\mathrm{o}}_{2\mathrm{ion}} - V_{\mathrm{W}}$) > 0, the ion may be considered as a negative solvating ion. Thus, the ions of the salts of the former category, such as NaCl and KCl, organize the bulk water structure around them by attracting water molecules which act as dipoles and cause electrostriction in water. However, in sodium saccharin and potassium acesulfame, while $\mathrm{Na^+}$ and $\mathrm{K^+}$ ions cause electrostriction in water structure, solvation of the anions is associated with their structure-breaking effect due to their poor fit into the tetrahedral structure of water and their possible hydrophobic behavior due to the distribution of the negative charge on them. Consequently, the large size and the diffuse charge of these anions result in their weak hydration. Therefore, disorganization of the water structure while organizing a part of the water molecules due to attraction of nitranions and water molecules can result in an overall constriction of aqueous solutions of salts like sodium saccharin and potassium acesulfame. A similar explanation may be given for the other electrolytes.

At very low solute concentrations the dependence of apparent partial molar volume Φ_{v} on solute concentration c_2 in aqueous solutions is adequately represented by the Debye–Hückel limiting law. After the initial Debye–Hückel limiting law range of concentrations of electrolytes, when the solute concentration is increased, the solvated ions come closer. Then the solvation shells around the ions begin to overlap and result in positive deviations from the limiting law. The interactions between the trapped water molecules surrounding the ions is related to the magnitude of the ion–water interactions. Therefore, the temperature dependence of the deviations results due to changes in the structure of trapped water between the interacting solvated ions.

In the range of high concentrations, positive deviations in the $\Phi_v(c_2^{1/2})$ plots from the Debye–Hückel limiting law is represented by the deviation parameter b_v. This parameter is related to the formation of ion pairs and larger aggregates involving cation–anion interactions, and its value is an indicator of the strength of these interactions. These cation–anion interactions become increasingly weak with increasing temperature such that the deviation parameter ultimately become negative.

The effect of temperature on the limiting partial molar volumes $V_{2\text{ion}}^{\text{o}}$ of ions may be explained from consideration of the last three contributions, i.e. $V_{\text{elect}}^{\text{o}}$, $V_{\text{disord}}^{\text{o}}$ and $V_{\text{str}}^{\text{o}}$, of Eq. (3.48); cf. Millero (1970, 1972). At low temperatures the last two contributions are the predominant factors where ion–solvent interactions determine the structure of water. At high temperatures the first contribution, $V_{\text{elect}}^{\text{o}}$, is the predominant factor. Here the larger temperature dependence on $V_{2\,\text{ion}}^{\text{o}}$ is due to its effect on the water molecules trapped by the ions involving the dominance of solvent–solvent interactions over ion–solvent interactions.

The dependence of the apparent partial molar volume Φ_v on the solute concentration c_2 in aqueous solutions may be interpreted in terms of cosphere overlap or structural interaction model (Desnoyer et al., 1969; Gurney, 1954), in which the characteristics of the cospheres depend on the structure, shape, size and hydrophobicity of the electrolyte ions. According to this model, two solute molecules will attract each other if their structural influences or tendencies to orient water molecules are compatible with each other, and, conversely, they will repel each other if their influences or tendencies are incompatible with each other. At low concentrations of the 1:1 electrolytes where the long-range coulombian attractive interactions between cations and anions take place, the concentration dependence of their apparent partial molar volume Φ_v is given by the Debye–Hückel limiting law with a slope S_v equal to 1.868 $\text{cm}^3\cdot\text{mol}^{-3/2}\cdot\text{L}^{1/2}$. The experimental values of the slope S_v for NaCl, KCl and sodium saccharin are close of this theoretical value of this slope S_v. The value of S_v equal to 1.20 $\text{cm}^3\cdot\text{mol}^{-3/2}\cdot\text{L}^{1/2}$ for aqueous sodium salicylate solutions is lower than the Debye–Hückel limiting law slope S_v. This lower value of S_v for this system is probably due to a larger c_2 range used than the concentration range where the Debye–Hückel limiting law holds. Relatively low values, and negative values, of S_v for other systems are associated with the hydrophobicity of solute molecules where solute–solute interactions occur by overlapping of hydration spheres engulfing some part of the solute molecules. In this concentration one encounters linear dependence of Φ_v on c_2.

3.5.4. Apparent molar volumes of nonelectrolyte solutions

In this section some general features of apparent molar volumes Φ_v of nonelectrolyte solutions as a function of solute concentration c_2 and solution temperature T are presented taking aqueous solutions of sucrose and D-glucose as examples. Results of analysis of the $\Phi_v(c_2)$ data for some compounds used as sweeteners and drugs are also briefly discussed. Discussion of the $\Phi_v(c_2)$ data on sucrose and D-glucose nonelectrolytes is based on the original $d(c_2)$ data from Lide (1996/1997), on lysozyme from Millero et al. (1976), on sweetener aspartame (Asp) from Klofutar et al. (2006), whereas on drugs L-triptophan (Trip) and phenol (PhOH) are from Iqbal and Verrall (1989).

Figure 3.20a and b shows the $\Phi_v(c_2)$ data for aqueous sucrose and D-glucose solutions, respectively, in the form of the dependence of Φ_v on c_2 according to the polynomial relation following from Eq. (3.12) for solutions of nonelectrolytes. It may be seen that the $\Phi_v(c_2)$ data show anomalous deviations for both systems below 0.1 mol·L^{-1}. This trend is similar to that observed in the plots of $\Phi_v(c_2^{1/2})$ data for many different systems, including aqueous solutions of substituted ammonium chlorides shown in Figure 3.1. Therefore, these $\Phi_v(c_2)$ data were analyzed for $c_2 > 0.1$ mol·L^{-1}. The $\Phi_v(c_2)$ data for aqueous sucrose solutions may be described satisfactorily by a quadratic relation while those of aqueous D-glucose solutions by a polynomial equation of the fourth order. The constants of the plots for the two systems are given in Table 3.12. The molar volumes V_{M2} of sucrose and D-glucose are 215.69 and 115.48 cm^3·mol^{-1}, respectively, calculated from their molecular weights M and densities d, and are given in the parentheses in the first column of the table. This table also includes values of constants of Eq. (3.12) for the $\Phi_v(c_2)$ data of some other systems, where the constant b_{v1} of constant of Eq. (3.12) is obtained from a linear dependence.

It should be mentioned that Millero et al. (1976) also observed linear concentration dependence of Φ_v in the case of aqueous lysozyme solutions at different temperatures. This linear solute-concentration dependence of Φ_v for aqueous lysozyme, aspartame, L-tryptophan and phenol solutions is due to narrow concentration range (< 0.25 m) whereas the quadratic and polynomial relations are followed for sucrose and D-glucose solutions at concentration c_2 below 3.25 and 4.4 mol·L^{-1}, respectively. Since the aqueous solution concentration in molality m (mol·kg^{-1}) is approximately equal to molarity M (mol·L^{-1}) at low solute concentrations, the values of the constant b_{v1} for aspartame, L-tryptophan and phenol are given in Table 3.12 in cm^3·L·mol^{-2} units.

The volumetric behavior of nonelectrolyte solutions is associated with the formation of solvated molecules in solutions and the mutual interaction between these solvated molecules. Both of these processes are related to the chemical nature of the constituents of the molecules of the electrolyte in the solid state. These solute molecules in the solution form a homogeneous mixture of solvated molecules and solvent molecules such that the mutual interaction between them increases with increasing solute concentrations. The situation resembles that of different types of interactions involved in mixtures of two solvents composed of cosolvent 2 dissolved in solvent 1 (see Section 3.4.2).

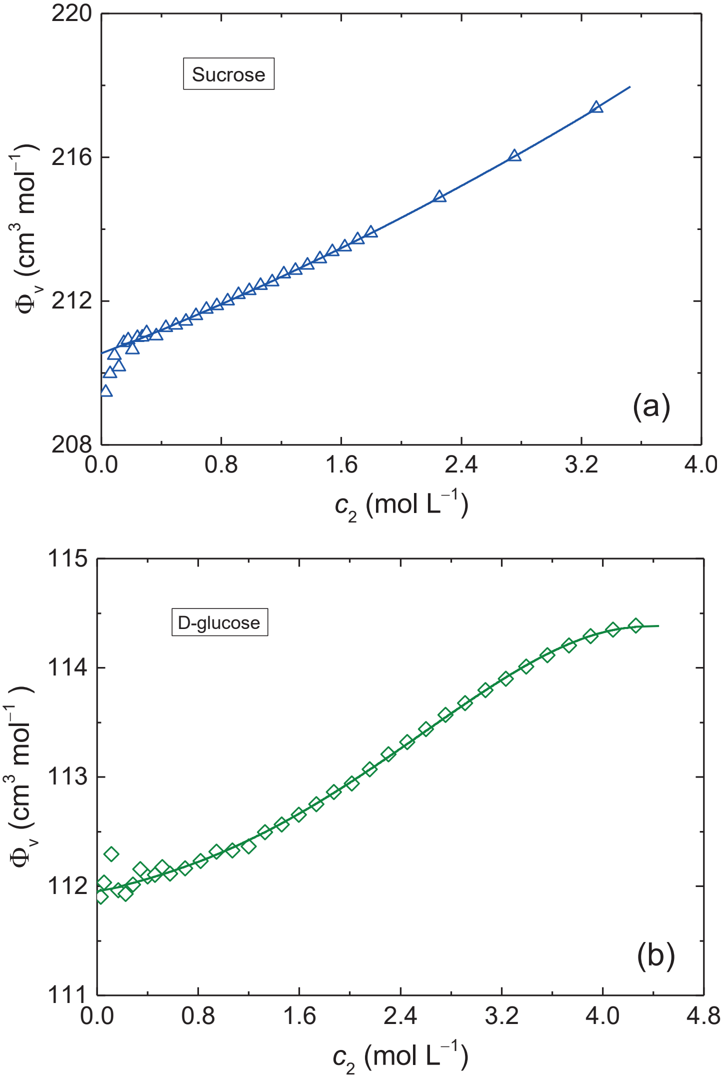

Figure 3.20. Dependence of Φ_v of (a) sucrose and (b) D-glucose at 20 °C on c_2. Original data from Lide (1996/1997).

As discussed in Section 3.4.2, the limiting apparent molar volume $\Phi_v^o = V_2^o$ of a nonelectrolyte at infinite dilution of the solution is the sum of the volume V_{cav}^o of cavity formation in the solution due to the intrinsic size of the solute and solvent molecules, the interaction volume V_{inter}^o due to different types of solute–solvent intermolecular interactions, and a correction term $\beta_T^o R_G T$ due to change in the standard state from gaseous to liquid state (see Eqs. (3.39) and (3.40)). Dipole–dipole interactions between polar or charged groups of molecules and polar water molecules in the form of hydrogen bonds and induced-dipole–dipole interactions are the main contribution to the interaction volume $V^{\circ}_{\mathrm{inter}}$. Apart from these interactions, hydrophobic interaction occurs between nonpolar parts of solute molecules and water molecules. The former two interactions are attractive in nature but hydrophobic interactions are repulsive.

Table 3.12. Constants of $\Phi_v°$ and b_v's of polynomial form of Eq. (3.12) for some aqueous nonelectrolyte solutions*

Substance	$\Phi_v°$ ($cm^3 \cdot mol^{-1}$)	b_{v1} ($cm^3 \cdot mol^{-2} \cdot L$)	b_{v3} ($cm^3 \cdot mol^{-3} \cdot L^2$)	b_{v5} ($cm^3 \cdot mol^{-4} \cdot L^3$)	b_{v7} ($cm^3 \cdot mol^{-5} \cdot L^4$)	Ref.
Sucrose (215.69)	210.522	1.636	0.1317			a
D-glucose (115.48)	119.947	0.268	0.0648	0.0472	−0.0108	a
Aspartame	216.37	−8.6				b
L-tryptophan	144.24	0.59				c
Phenol	85.20	−0.64				c

* Temperatures in the studies as in Table 3.11. [a] This work.; [b] Klofutar et al. (2006); [c] Iqbal and Verrall (1989).

The cavity formation volume V°_{cav} and $\beta_T{}^{\circ} R_G T$ term are positive quantities whereas the interaction volume $V^{\circ}_{\mathrm{inter}}$ is negative due to shrinking of cavities by intramolecular attraction forces in the liquid volume. However, as observed in the case of aqueous aspartame solution (Klofutar et al., 2006), the interaction volume $V^{\circ}_{\mathrm{inter}}$ is about one-tenth of the value of V°_{cav} . Therefore, the main contribution to the limiting apparent molar volume $V_2{}^{\circ}$ of a nonelectrolyte is from V°_{cav} . This inference is corroborated by the observation that the experimental values of $\Phi_v{}^{\circ}$ for sucrose and D-glucose are approximately equal to their molar volumes V_{M2} calculated from the molecular weight M and the density d (see Table 3.12).

As discussed in Sections 3.2.1 and 3.4.3, positive deviations in the $\Phi_v(c_2{}^{1/2})$ plots for electrolyte solutions from the Debye–Hückel limiting law occur in the range of high solute concentrations. This deviation is represented by the deviation parameter b_v, which is related to the formation of ion pairs and larger aggregates involving cation–anion interactions. A similar interpretation applies in the case of the effect of concentration and temperature on the slope b_{v1} of the $\Phi_v(c_2)$ plots of aqueous nonelectrolyte solutions, where dipole–dipole, induced-dipole–dipole and hydrophobic interactions take place. When dipole–dipole and induced-dipole–dipole attractive interactions mainly contribute to the interaction volume $V^{\circ}_{\mathrm{inter}}$, they are steadily suppressed with increasing nonelectrolyte concentration c_2 by forming solute aggregates in the solution volume. This results in an increase in the limiting apparent molar volume $V_2{}^{\circ}$ of the nonelectrolyte and positive values of the slope b_{v1} in the $\Phi_v(c_2)$ plot. This is the situation in the case of sucrose, D-glucose and L-tryptophan solutions, where dipole–dipole and induced-dipole–dipole attractive interactions are dominant. However, when hydrophobic interactions mainly contribute to $V^{\circ}_{\mathrm{inter}}$, their contribution to $V_2{}^{\circ}$ increases with increasing solute concentration c_2, such that the value of V_2° decreases with an increase in c_2. This results in a negative value of b_{v1}. This is the possible situation for aspartame and phenol, where hydrophobic interactions between the nonpolar solute molecules and polar water molecules are dominant.

The effect of temperature on the values of V_2° and b_{v1} for a nonelectrolyte solution depends on its effect on the interaction volume V_{inter}° and the correction term $\beta_T^\circ R_G T$ of Eq. (3.36). Irrespective of the nature of interactions, they become increasingly weak with increasing temperature. Consequently, the contribution of V_{inter}° decreases with increasing temperature whereas the correction term $\beta_T^\circ R_G T$ increases with increasing temperature. This means that the effect of temperature on the interaction volume V_{inter}° is opposite to that of the correction term $\beta_T^\circ R_G T$. Therefore, depending on the relative contribution of these two terms in infinitely dilute solutions, the value of V_2° is expected to increase as well as decrease with an increase in temperature. However, it is observed that the limiting apparent molar volume V_2° for different aqueous nonelectrolyte solutions, as a rule, increases with an increase in temperature (for example, see: Klofutar et al., 2006). This implies that the contribution of the correction term $\beta_T^\circ R_G T$ to V_2° is greater than that of the interaction volume V_{inter}°.

The increasing or decreasing trend of the apparent molar volume Φ_v, as reflected by the deviation parameter b_{v1}, is determined by the temperature dependence of relative contribution $\Delta(V_{\text{inter}}^\circ - \beta_T^\circ R_G T)$ resulting from the temperature dependence of V_{inter}° and $\beta_T^\circ R_G T$. When the change in V_{inter}° with increasing temperature exceeds the corresponding change in $\beta_T^\circ R_G T$ such that $\Delta(V_{\text{inter}}{}^\circ - \beta_T^\circ R_G T) > 0$ (i.e. $\Delta V_{\text{inter}}^\circ > \Delta\beta_T^\circ R_G T$), Φ_v increases with increasing temperature, leading to a positive b_{v1}. However, when $\Delta(V_{\text{inter}}^\circ - \beta_T^\circ R_G T) < 0$, the value of Φ_v decreases with increasing temperature and $b_{v1} < 0$.

Klofutar et al. (2006) reported data of the limiting apparent molar volume V_2° and the deviation constant b_{v1} as a function of temperature of aqueous aspartame solutions. Their data show that both V_2° and b_{v1} increase with increasing temperature and that b_{v1} is negative at low temperature and attains positive values with increasing temperature. These observations may be explained along the above lines.

3.5.5. Concentration and temperature dependence of different constants of solutions

As mentioned in preceding sections, the concentration and temperature dependences of solutions of different solutes are usually described by quadratic equations but the dominant contributions in these relations come from the linear terms in T and c_2 in Eqs. (3.21) and (3.25). These are the constant a_1 in Eq. (3.21) and the constant a_5 in Eq. (3.25). The a_1 constant of Eq. (3.21) increases with the solute concentration c_2, whereas the a_5 coefficient of Eq. (3.25) increases with the solution temperature T. Related to the a_1 constant is the thermal expansivity $\alpha = a_1/d_0$ for the solutions of known concentration c_2 and the constant $A = a_5/d_0$ for the solutions of known temperature T. Therefore, it is expected that α is a function of solute concentration c_2 and the constant A is a function of solution temperature T.

The original data of a_1 and d_0 for different concentrations c_2 for aqueous potassium bichromate (Sokolowski and Sangwal, 1983) and lithium iodate solutions (Szewczyk and Sangwal, 1988) and those for aqueous sodium nitrate and sodium thiosulfate solutions (Mohiuddin and Ismail, 1996) have been reported from analysis of the $d(T)$ data using quadratic and linear dependences, respectively. From these reported $a_1(c_2)$ and $d_0(c_2)$ data the thermal expansivity α for the solutions of different concentrations c_2 were calculated. Figure 3.21 illustrates these data of the thermal expansivity α of aqueous solutions as a function of solute concentration c_2. It may be seen that the value of α for different solutes increases with their concentration c_2 in the solutions, following the linear relation

$$\alpha = \alpha_0 + \alpha_1 c_2 , \tag{3.53}$$

where the values of the constants α_0 and α_1 are related to the solute (see Table 3.13).

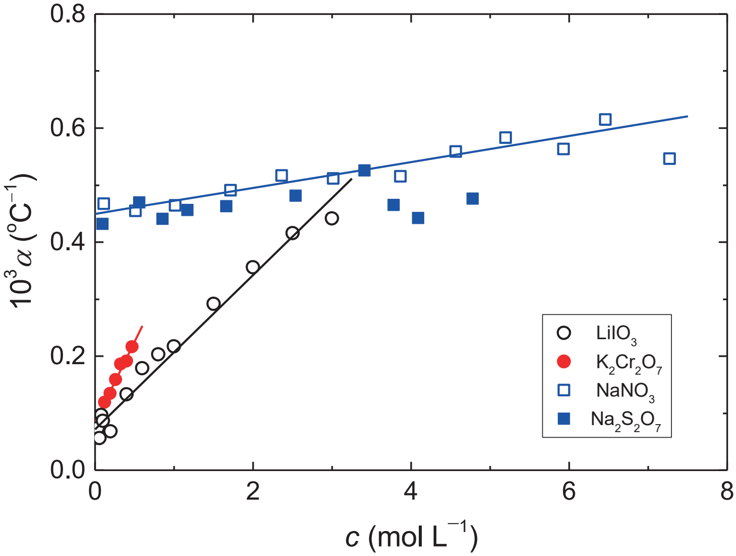

Figure 3.21. Dependence of parameter α on solute concentration c_2 of aqueous $LiIO_3$, $K_2Cr_2O_7$, $NaNO_3$ and $Na_2S_2O_7$ solutions. Plots are drawn according to Eq. (3.52) with constants listed in Table 3.13. Data for $LiIO_3$ are from Szewczyk and Sangwal (1988), for $K_2Cr_2O_7$ from Sokolowski and Sangwal (1983), and for $NaNO_3$ and $Na_2S_2O_7$ from Mohiuddin and Ismail (1996).

As seen from Figure 3.21, the constant α_0 for sodium thiosulfate is somewhat lower than that for sodium nitrate but the value of the slope α_1 for the two solutes is practically the same. Since the molar volume V_M of a solution at a particular temperature increases with solute concentration c_2 (see Eq. (3.12)), it may be concluded that these constants are related to the molar volume V_{Ms} of the solute (see Section 3.2). However, in the case of potassium bichromate and lithium iodate solutions, the high values of the slope α_1 may be due to the relatively high contribution of the c_2-term, which resulted in low values of a_1 at low concentrations.

Table 3.13. Constants α_0 and α_1 of Eq. (3.53) for different aqueous electrolyte solutions

Salt	$10^4\alpha_0$ (°C^{-1})	$10^4\alpha_1$ (L·mol^{-1}· °C^{-1})	R^2
$NaNO_3$	4.45±0.008	0.23±0.02	0.9144
$LiIO_3$	0.72±0.06	1.35±0.05	0.9788
$K_2Cr_2O_7$	0.84±0.06	2.82±0.02	0.9752

The parameters a_5/d_0 and A/d_0 for the solutions of a solute depend on solution temperature T but are usually analyzed in a relatively narrow temperature range where they decrease practically linearly with temperature. However, in a wider range of temperature, the constant A follows an Arrhenius-type relation (Misztal and Sangwal, 1999)

$$A = A_0 \exp(-E_{\mathrm{d}} / R_{\mathrm{G}}T) , \tag{3.54}$$

where the exponential factor A_0 and the activation energy E_{d} are related to the solute–solvent system. However, the value of E_{d} is relatively low of the order of a few kJ·mol^{-1}.

3.6. Density of saturated, undersaturated and supersaturated solutions

Depending on the temperature dependence of solubility, the density of saturated electrolyte solutions increases, decreases or first increases and then decreases with an increase in temperature. Such dependences, based on experimental data from Söhnel and Novotný (1985), are shown for some typical salts in Figure 3.22. The density decreases with an increase in temperature for those salts whose solubility changes insignificantly (e.g. NaCl) or whose solubility decreases with an increase in temperature. When the solubility of a salt increases markedly, the density of its solution also regularly increases, as seen for alums and $CuSO_4$. When the solubility of a salt first increases markedly and then either decreases or increases insignificantly, the density of its solution first increases and then decreases, as for Na_2SO_4. Sudden discontinuities in the curves of density of saturated solutions against their saturation temperature are associated with phase transitions of a salt.

As described in Section 3.2.3, the temperature dependence of solvents and solutions of constant concentrations is usually represented by Eqs. (3.21) and (3.23), where their empirical constants d_0 and a_1 are closely related to the thermal expansivity α of the solution ($\alpha = a_1/d_0 = \mathrm{d}d/\mathrm{d}T$). The values of both d_0 and a_1 increase with increasing solution concentration but the variation in d_0 with solution concentration is much smaller than that in a_1. Therefore, it is observed that the value of the thermal expansivity α of the solutions increases with an increase in solute concentration x_2 and the dependence of α on x_2 is determined by the nature of the solute dissolved in a solvent (see Figure 3.21).

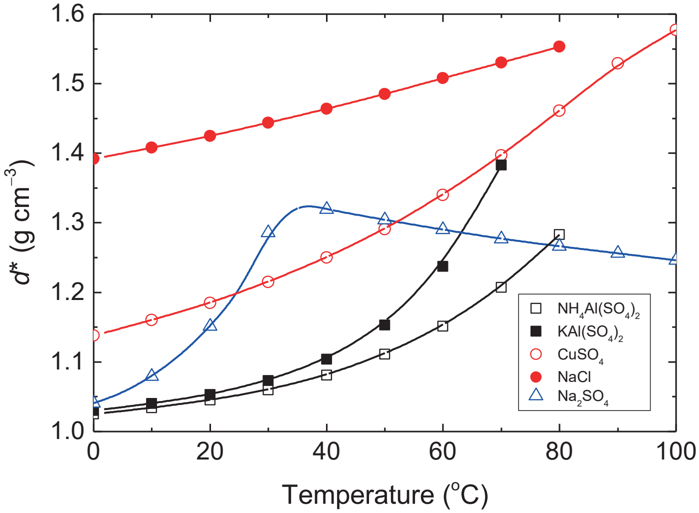

Figure 3.22. Dependence of density d^* of aqueous saturated solutions of some electrolytes on their saturation temperature T. Original data from Söhnel and Novotný (1985).

The temperature dependence of density d^* is relatively more complicated than that for constant-concentration solutions because of simultaneous variation of solution concentration c_2 with saturation temperature T_s. However, in the temperature interval in which the density d^* of saturated solutions of a salt increases or decreases, their temperature dependence follows the empirical relation (Karniewicz et al., 1982; Sokolowski, 1981; Szewczyk et al., 1985)

$$d^* = d_0^* + a_1^* T_s + a_2^* T_s^2 , \tag{3.55}$$

where d_0^* is the density of the solution saturated at $T_s = 0$, a_1^* and a_2^* are empirical constants, and the temperature T_s is taken in °C. In this equation, $d_0^* > d_0$, and a_1^* and a_2^* are different from a_1 and a_2 of Eq. (3.21). This dependence is similar to that for constant-concentration solutions, usually with $a_1^* >> a_1^*$. Therefore, when $a_1^* T_s << d_0^*$, which is often observed, Eq. (3.55) may be written in the form

$$d^* = d_0^* \exp(a_1^* T_s / d_0^*) = d_0^* \exp(\alpha^* T_s) , \tag{3.56}$$

where $\alpha^* = a_1^*/d_0^*$.

It is well known that the density d of solutions of a solute at a particular temperature increases with the solute concentration x_2 (for example, see Figure 3.12). Therefore, it is expected that the density d^* of saturated solutions of a solute increases with an increase saturation temperature T_s and their expansivity $\alpha^* = a_1^*/d_0^*$ increases with the solubility x_2^* of salts of positive temperature coefficient of solubility for solutions whose density d^* increases with temperature T_s, while it is negative for saturated solutions of salts whose density d^* (and solubility x_2^*) decreases or poorly increases with temperature T_s. Since $d_0^* > 0$, the sign of the parameter a_1^* is directly related to the trend of the thermal expansivity α^* of the saturated solutions with solute concentration c_2^*. Obviously, for a salt which exhibits phase changes and the density d^* of its saturated solution first increases and subsequently decreases at a particular temperature of phase transition, the value of a_1^* increases with saturation concentration c_2^* in the former temperature interval whereas its value decreases with an increase in c_2^* in the latter interval. It is thus implied that a change in the value of the parameter $(a_1^*T_s/d_0^*)$ of Eq. (3.56) reflects phase changes of the solute molecules in the solution and is directly connected with the extent of their solvation and the temperature dependence of the solute solubility. Consequently, the density d^* of saturated solutions of a solute is expected to be related to its solubility x_2^* in the solution.

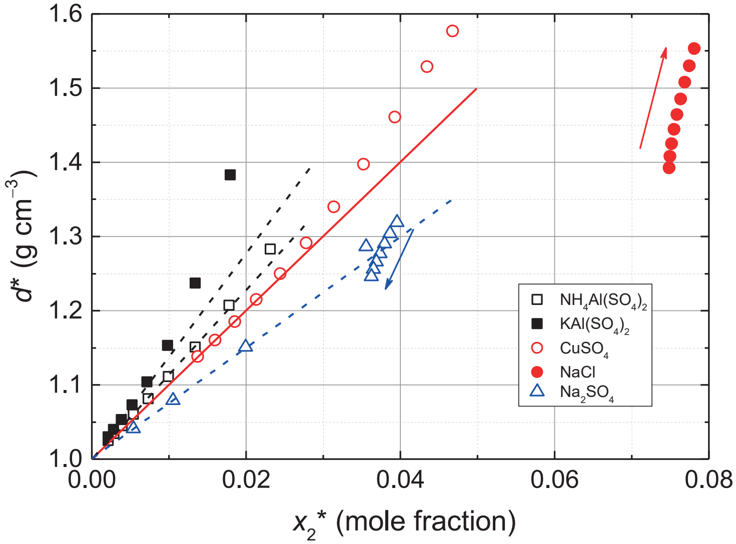

Figure 3.23. Relationship between density d^* and solubility x_2^* of aqueous solutions of different electrolytes. Solid line represents initial data for $CuSO_4$ solutions with slope 10. For Na_2SO_4 and NaCl solutions arrows indicate increasing solution temperature. Original data from Söhnel and Novotný (1985).

Figure 3.23 shows the relationship between density d^* and solubility x_2^* of the salts of Figure 3.22 in water. As in the case of unsaturated solutions, it is interesting to analyze the above data of the density d^* of saturated solutions of different solutes on their solubility x_2^* according to Eq. (3.41), with its parameters d_0, $b_1 = a_5/d_0$ and $b_2 = a_6/d_0$ (cf. Eq. (3.42)) for saturated solutions with added asterisks (i.e. d_0^*, b_5^* and b_6^*,

A^*) to distinguish them from those for constant-temperature undersautated solutions. It may be seen that the $d^*(c_2^*)$ data for the above solutions of solutes other than NaCl may be described by a polynomial dependence with the intercept $d_0^* \approx 1$ and the slope b_1^* lying between 7.5 and 14 for different solutes, the value of b_1^* increasing in the order: $Na_2SO_4 < CuSO_4 < NH_4Al(SO_4)_2 < KAl(SO_4)_2$. This trend is the same as that observed in the case of constant-temperature solutions discussed in Section 3.5.1. The observed increasing trend of b_1^* is partly associated with increasing temperature coefficient of solubility c_2^*. For example, although $CuSO_4$ has the lowest temperature coefficient of solubility among the above salts, it is an exception from the above trend.

The above values of b_1^* for saturated solutions are much higher than those of b_1 obtained from $d(x_2)$ data for constant-temperature solutions (see Table 3.8), and is probably associated with the increased contribution of $(d_0\Phi_v^o)$ for saturated solutions in the $(M_2 - d_0\Phi_v^o)$ term of Eq. (3.20) such that the main contribution comes from the molar mass M_2 of the anhydrous solute. One also notes that the parameter b_2^*, as indicated by deviation from the linear $d^*(c_2^*)$ plots, is positive in contrast to the negative values of b_2 for constant-temperature solutions (see Table 3.8).

The $d^*(c_2^*)$ data for saturated solutions of different solutes may equally be analyzed according to Eqs. (3.25) and (3.27) rewritten in the form of Eqs. (3.42) and (3.43). It was found that Eq. (3.42) is inadequate to describe the data due to contributions from terms higher than the quadratic term of Eq. (3.41), but the dependence of the density d^* of saturated solutions of different solutes on their solubility x_2^* may be described by Eq. (3.43) satisfactorily, as shown in Figure 3.24, with the best-fit parameters and goodness-of-the-fit parameter R^2 listed in Table 3.14.

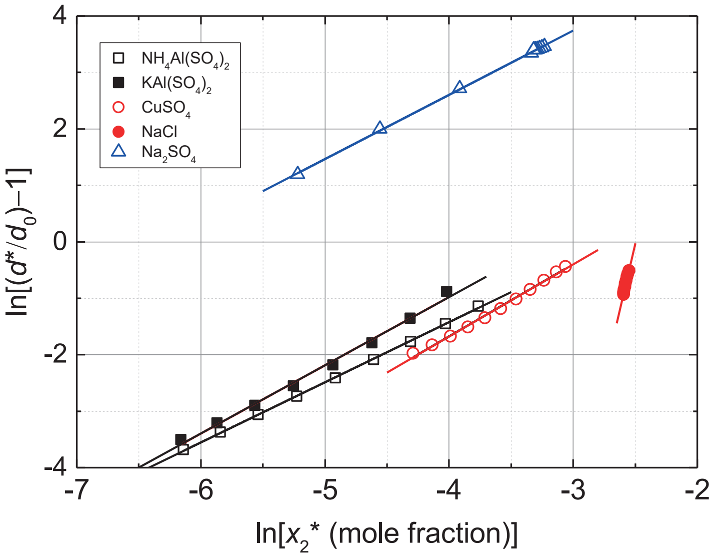

Figure 3.24. Plots of $\ln[(d^*/d_0)-1]$ against $\ln x_2^*$ for aqueous solutions of some selected electrolytes according to Eq. (3.42). Best-fit constants of the plots are listed in Table 3.14. Original data from Söhnel and Novotný (1985).

Table 3.14. Constants of Eq. (3.43) for different aqueous saturated electrolyte solutions

Salt	M_2 (g·mol^{-1})	ln(A^*/d_0)	A^*/d_0	p	R^2
$KAl(SO_4)_2$	258.20	3.858	47.36	1.209	0.9925
$NH_4Al(SO_4)_2$	237.14	2.838	17.08	1.065	0.9995
$CuSO_4$	159.60	3.436	31.06	1.278	0.9949
Na_2SO_4	142.04	7.150	1274	1.137	0.9993
NaCl	58.44	23.66	$1.89\cdot10^{-10}$	9.475	0.9741

It may be noted from Figure 3.24 and Table 3.14 that the $d^*(c_2^*)$ data for $NH_4Al(SO_4)_2$ and Na_2SO_4 solutions are described much better than those for $KAl(SO_4)_2$ and $CuSO_4$ solutions, and that the value of the exponent p for the latter solutions at low values of saturation concentrations c_2^* is comparable with that of the former solutions in their entire c_2^* interval. However, as expected for saturated solutions, $p > 1$ in all cases, and, if the two pairs of solutions are considered, the values of the p and $\ln(A^*/d_0)$ appear to increase with decreasing molar mass M_2 of the solutes.

It was mentioned above that the value of the parameter a_1^* for a solute–solvent system does not remain constant in a particular temperature interval in which the solubility increases or decreases but this increase or decrease is enormous and is intimately connected with the temperature coefficient of solubility of solutes in the solvent. In the temperature interval in which the solute solubility increases or decreases, the $d^*(T)$ data for different solute–solvent systems can also be described by Eq. (3.24), where the values of the constants d_0, θ and Ω are unique for the system (Sangwal, 1987). The value of d_0 is related to the solute solubility in the solvent whereas that of Ω depends on the temperature coefficient of solubility. The temperature θ for a solute–solvent system is not related to the solute solubility but a dimentionless parameter $\Omega = \Omega/\theta^2$ is a measure of the behavior of different solutes in a solvent.

Some experimental data (Karniewicz et al., 1982; Sokolowski, 1981; Szewczyk et al., 1985) of the temperature dependence of density of solutions saturated at particular temperatures below and above the saturation temperature T_s are available. These ranges of temperature correspond to supersaturation and undersaturation regions of solutions, respectively. It is found that in some cases (Sokolowski, 1981) the curves of the temperature dependence of the density of solutions saturated at particular temperatures show discontinuities at the saturation points, while in other solutions (Karniewicz et al., 1982; Szewczyk et al., 1985) their density does not show discontinuities at the saturation points and is a linear function of temperature given by Eq. (3.22) in the entire range of undersaturation as well as supersaturation. The argument of changes in the structure of species present given for the temperature dependence of density of solutions is also applicable here. However, the question of reorganization of solutions still remains unsettled.

3.7. Models for calculations of densities

Various empirical equations have been proposed in the literature to describe the dependence of the density of electrolytes on their concentration and solution temperature (Horvath, 1985; Söhnel and Novotný, 1985). Some models have also been proposed to predict the density of electrolyte solutions (Horsak and Slama, 1986; Kumar, 1986; Patwardhan and Kumar, 1986; Theilander and Gren, 1989). In this section two simple models are presented. The first model was proposed by Horsak and Slama (1986), but the second one is proposed here.

3.7.1. Model based on additive rule for molar volumes

In this model proposed by Horsák and Sláma (1986), the density d of an electrolyte solution is described in terms of the molar mass M of the solution and the molar volume V_M of the electrolyte (i.e. $d = M/V_M$; see Eq. (3.13)), where the molar mass M is calculated by the simple additive rule:

$$M = x_2 M_2 + (1 - x_2) M_1 , \tag{3.57}$$

and the molar volume V_M is calculated according to the relation

$$V_M = x_2 V_2^o + (1 - x_2) V_1^o + \kappa x_2 \frac{1 - x_2}{1 + x_2} , \tag{3.58}$$

where κ is an empirical parameter describing changes in the volume of solvent water due to solute–solvent interactions and the solute mole fraction $x_2 = 1 - x_1$, with x_1 as the solvent mole fraction. The last term on the right hand side is associated with the deviation of the dependence of V_M on solute concentration x_2 from the additive rule due to solute–solvent interactions. The mole fraction concentration x_2 of the solute is given by

$$x_2 = \frac{n_2}{n_1 + \nu n_2} , \tag{3.59}$$

where n_1 and n_2 are the number of moles of the solvent and the solute, respectively, per 1000 g of solvent water, the number n_1 of the solvent water

$$n_1 = \frac{1000}{M_1} = 55.51 \text{ mol}, \tag{3.60}$$

and ν is the number of ions formed from the dissociation of one molecule of the electrolyte. If the salt molar volume V_M and the empirical constant κ are represented by the contributions of positively- and negatively-charged ions, Eq. (3.58) may be rewritten as

$$V_M = x_2(V_{2+}^o + V_{2-}^o) + (1-x_2)\left[V_1^o + (\kappa_+ + \kappa_-)\frac{x_2}{1+x_2}\right]. \tag{3.61}$$

where V_{2+}^o and V_{2-}^o are the partial molar volumes of cations and anions, respectively.

In the above equation partial molar volumes V_{2+}^o and V_{2-}^o of cations and anions and the constants κ_+ and κ_- are obtained by trial and error. The estimated values of these quantities for various ions of single-electrolyte in aqueous solutions are listed by Horsák and Sláma (1986), and by Lam et al. (2008). From the published values of the partial molar volumes V_{2+}^o and V_{2-}^o of different cations and anions, one finds that they are entirely different from their limiting partial molar volumes. For example, the published values for Na+, K+ and Cl^- ions give values of the molar volumes for NaCl and KCl higher by about 50% than those estimated from their limiting partial molar volumes calculated from the $\Phi(c_2)$ data at 25 °C.

Lam et al. (2008) extended the above model and used it to calculate the densities of aqueous solutions of single and double electrolytes. These authors compared the results of densities d of ternary systems obtained by the above model with those obtained by other models (Kumar, 1986; Patwardhan and Kumar, 1986; Theilander and Gren, 1989), and found that the extended model predicts values of densities of different systems satisfactorily.

Several models, proposed for the estimation of densities d of ILs, are also based on consideration of effective molar volumes of ions at 298.15 K and 0.1 MPa, where it is assumed that the ions behave as an ideal mixture (for example, see: Esperança et al., 2006; Jacquemin et al., 2008a; Rebelo et al., 2007; Zhao N., et al., 2017). This approach has been extended to include the effect of pressure using the commonly used Tait equations (Jacquemin et al., 2008b; Zhao N., et al., 2017).

3.7.2. Model based on additive rule for densities

The starting point of this model for the description of density of a binary solution using the additive rule for the densities of solvent and solute given by Eq. (3.28) and the idea that (1) the solute ions/molecules are solvated with their volumes larger than those of their bare entities, (2) the solvated ions/molecules shrink in size with increasing solute concentration, and (3) the solvation sheath around the ions/molecules decreases in size with increasing temperature whereas the solvent volume increases with increasing solution temperature. We assume that: (1) the decrease in the additional volume δ of the solvation sheath around the solvated ions/molecules with solute concentration x_2 and solution temperature T, and (2) the increase in the solvent volume V_1 with solution temperature T are linear, according to the relations:

$$\delta \propto x_2 = V_{20}kx_2\,, \tag{3.62}$$

$$\delta = \delta_0(1-\beta T)\,, \tag{3.63}$$

$$V_1 = V_{10}(1+\alpha T)\,, \tag{3.64}$$

where k and β are constants, α is the thermal expansivity of the solvent, δ_0 is the value of the additional volume δ of the solvation sheath at $T = 0$, and V_{10} and V_{20} are the volumes of the solvent and the solvated solute ions/molecules at $T = 0$. Using Eqs. (3.64) and (3.65) one may write Eq. (3.28) in the form

$$d = \frac{d_{10}}{1+\alpha T} + x_2 \frac{d_{20}}{(1+\alpha T)[1+kx_2(1-\beta T)]}\left[(1+\alpha T)+[1+kx_2(1-\beta T)]\frac{d_{10}}{d_{20}}\right], \tag{3.65}$$

where $d_{10} = M_1/V_{10}$ and $d_{20} = M_2/V_{20}$. Since $\alpha T << 1$ and $kx_2(1-\beta T) << 1$, the above equation takes the following forms

$$d = d_0 - [A_1B_1(1-kx_2]T + [B_2 - A_1B_1 - (A_2 + B_1)]T^2 + (A_1B_2 - A_2B_2)T^3 + A_2B_2T^4\,, \tag{3.66}$$

$$d = d_0^x + b_1x_2 + b_2x_2^2 + b_3x_2^3\,, \tag{3.67}$$

where

$$d_0 = d_{10} + (1-k_2x_2)^2, \tag{3.68}$$

$$d_0^x = d_{10}(1-\alpha T)^2, \tag{3.69}$$

$$A_1 = \alpha - kx_2(\beta - \alpha)\,, \tag{3.70}$$

$$A_2 = \alpha\beta kx_2\,, \tag{3.71}$$

$$B_1 = kx_2\beta\frac{d_{10}}{d_{20}} - \alpha(1+kx_2)\,, \tag{3.72}$$

$$B_2 = \alpha\beta\frac{d_{10}}{d_{20}}\,, \tag{3.73}$$

$$b_1 = d_{20}(1-\alpha)\left(1-\alpha\beta T^2\frac{d_{10}}{d_{20}}\right), \tag{3.74}$$

$$b_2 = kd_{20}(1-\alpha)\left(1+\alpha T-\beta T\frac{d_{10}}{d_{20}}\right) - [1+(\alpha-\beta)T-\alpha\beta T^2]\left(1-\alpha\beta T^2\frac{d_{10}}{d_{20}}\right), \tag{3.75}$$

$$b_3 = k^2d_{20}[1+(\alpha-\beta)T-\alpha\beta T^2]\left(1+\alpha T-\beta T\frac{d_{10}}{d_{20}}\right). \tag{3.76}$$

It may be noted that analysis of experimental data using Eqs. (3.66) and (3.67) enables to obtain the values of their constants. With the values of these constants, using Eqs. (3.68) through (3.76) one can obtain the values of parameters like δ, α and β and discuss the nature of processes involved in the concentration and temperature dependence of density.

References

Albuquerque, L., C. Ventura, and R. Goncalves (1996). Refractive indices, densities, and excess properties for binary mixtures containing methanol, ethanol, 1,2-ethanediol, and 2-methoxyethanol. *J. Chem. Eng. Data* **41**, 685-688.

Ali, A., S. Hyder, S. Sabir, D. Chand, and A.K. Nain (2006). Volumetric, viscometric, and refractive index behaviour of α-amino acids and their groups' contribution in aqueous D-glucose solution at different temperatures. *J. Chem. Thermodyn.* **38**, 136-143.

Bahadur, I., N. Deenadayalu, P. Naidoo, and D. Ramjugernath (2013). Densities, speed of sound, and refractive index measurements for the binary systems (butanoic acid + propanoic acid, or 2-methyl-propanoic acid) at T = (293.15 to 313.15) K. *J. Chem. Thermodyn.* **57**, 203-211.

Bajić, D.M., G.R. Ivaniš, Z.P. Visak, E.M., Živković, S.P. Šerbanović, and M.Lj. Kijevčanin (2013). Densities, viscosities, and refractive indices of the binary systems (PEG200 + 1,2-propanediol, + 1,3-propanediol) and (PEG400 + 1,2-propanediol, + 1,3- propanediol) at (288.15 to 333.15) K and atmospheric pressure: measurement and modelin. *J. Chem. Thermodyn.* **57**, 510-529.

Bittner, B., E.J. Wrobel, and E. Milchert (2012). Physical properties of pyridinium ionic liquids. *J. Chem. Thermodyn.* **55**, 159-165.

Budeanu, M.M., V. Dumitrescu, and O. Pantea (2015). Excess molar volume and volume study of ternary mixtures of *tert*-butylmethylether and *n*-heptane with alcohols at 293.15 K. *Rev. Chim. (Bucharest)* **66**, 1227-1231.

Couture, A.M., and K.J. Laidler (1956). The partial molal columes of ions in aqueous solutions. 1. Dependence of charge and radius. *Can. J. Chem.* **34**, 1209-1216.

De Ligny, C.L., and H.G. van der Veen (1972). A test of Pierotti's theory for the solubility of gases in liquids, by means of literature data of solubility and entropy of solution. *Chem. Eng. Sci.* **27**, 391-401.

Desnoyer, J.E., M. Arel, G. Perron, and C. Jolicoeur (1969). Apparent molal volumes of alkali halides in water at 25°. Influence of structural hydration interactions on the concentration dependence. *J. Phys. Chem.* **73**, 3347-3351.

Dikio, E.D., S.M. Nelana, D.A. Isabirye, and E.E. Ebenso (2012). Density, dynamic viscosity and derived properties of binary mixtures of methanol, ethanol, *n*-propanol, and *n*-butanol with pyridine at T = (293.15, 303.15, 313.15 and 323.15) K. Intern. *J. Electrochem. Soc.* **7**, 11101-11122.

El-Dossoki, F.I. (2007). Refractive index and density measurements for selected binary protic-protic, aprotic-aprotic, and aprotic-protic systems at temperatures from 298.15 to 308.15 K. *J. Chinese Chem. Soc.* **54**, 1129-1137.

Esperança, J.M.S.S., H.J.R. Guedes, M. Blesic, L.P.N. Rebelo (2006). Densities and derived thermodynamic properties of ionic liquids. 3. Phosphonium-based ionic liquids over an extended pressure range. *J. Chem. Eng. Data.* **51**, 237-242.

Francesiconi, R., and S. Ottani (2007). Correlation of density and refractive index for liquid binary mixtures containing polyglycols. Use of the group contributions in Lorentz–Lorenz, Glastone–Dale and Vogel equations to evaluate the density of mixtures. *J. Mol. Liquids* **133**, 123-133.

Frej, H., M. Jakubczyk, and K. Sangwal (1998). Density, surface tension, refraction index of aqueous ammonium oxalate solutions from 293 K to 333 K. *J. Chem. Eng. Data* **43**, 158-161.

French, R.N., and C.M. Criss (1981). Effect of solvent on the partial molal volumes and heat capacities of nonelectrolytes. *J. Solution Chem.* **10**, 713-740.

Fucaloro, A.F., Y. Pu, K. Chu, A. Wlliams, and K. Conrad (2007). Partial molar volumes and refractions of aqueous solutions of fructose, glucose, mannose, and sucrose at 15.00, 20.00 and 25.00 °C. *J. Solution Chem.* **36**, 61-80.

Fucaloro, A.F., A. Zanella, A. Widjaja, S. Widjaja (2005). Partial molar volumes and refractions of cobalt complexes. Part I: Homologous series of hexaaminecobalt(III) complexes. *J. Solution Chem.* **34**, 1357-1370.

Gleim, V.G., A.N. Vishnevetskaya, and V.Ya. Khentov (1969). Effect of temperature on the physico-chemical characteristics of aqueous solutions of sodium chloride, phosphide and silicate during their mutual presence. *Zh. Fiz. Khimii* **43**, 510-512, in Russian.

Gurevich, B.S., and V.M. Bednov (1972). Effect of temperature dependence of density and viscosity of aromatic substances. *Zh. Fiz. Khimii* **46**, 2673-2674, in Russian.

Gurney, R.W. (1954). *Ionic Processes in Solutions*. McGraw Hill, New York.

Härtling, C., T. Mecklenburg, and W. Seidel (1981). Abweichungen im Konzentrationsverlauf scheinbarer Molvolumina und Viskositäten bei hochverdünnten Elektrolytlösungen. *Ber. Bunsenges. Phys. Chem.* **85**, 1012-1016.

Herráez, J.V., and R. Belda (2006). Refractive indices, densities and excess molar volumes of monoalcohols + water. *J. Solution Chem.* **15**, 1315-1328.

Holguin, A.R., D.R. Delgado, F. Martinez, M. Khoubnasabjafari, and A. Jouyban (2011). Study of some volumetric properties of glycerol formal + ethanol mixtures and correlation with the Jouyban-Acree model. *Rev. Acad. Colomb. Cienc.* **35**, 315-328.

Horsak, I. and I. Slama (1986). Densities of aqueous electrolyte solutions. A model for a data bank. *J. Chem. Eng. Data* **31**, 434-437.

Horvath, A.L. (1985). *Handbook of Aqueous Electrolyte Solutions: Physical Properties, Estimation and Correlation Methods*. Ellis Horwood, Chichester.

Iqbal, M., and R.E. Verrall (1989). Apparent molar volume and adiabatic compressibility of aqueous solutions of some drug compounds at 25°C. *Can. J. Chem.* **67**, 727-735.

Jacquemin, J., R. Ge, P. Nancarrow, D.W. Rooney, M.F. Costa Gomes, A.A.H. Padua, and C. Hardcore (2008a). Prediction of ionic liquid properties. I. Volumetric properties as a function of temperature at 0.1 MaP. *J. Chem. Eng. Data* **53**, 716-726.

Jacquemin, J., P. Nancarrow, D.W. Rooney, M.F. Costa Gomes, P. Husson, V. Mayer, A.A.H. Padua, and C. Hardcore (2008b). Prediction of ionic liquid properties. I. Volumetric properties as a function of temperature and pressure. *J. Chem. Eng. Data* **53**, 2133-2143.

Karniewicz, J., W. Kolasiński, and J. Szewczyk (1982). Some properties of lithium formate solutions near the saturation temperature. *J. Cryst. Growth* **57**, 462-465.

Kawahara, K., and C. Tanford (1966). Viscosity and density of aqueous solutions of urea and guanidine hydrochloride. *J. Biolog. Chem.* **241**, 3228-3232.

Kirkwood, J.G., and F.P. Buff (1951). The statistical mechanical theory of solutions. I. *J. Chem. Phys.* **19**, 774-778.

Klofutar, C., J. Horvat, and D. Rudan-Tasić (2006). Apparent molar volumes and apparent molar expansivity of sodium saccharin, potassium acesulfame and aspatame. *Acta Chim. Slov.* **53**, 274-283.

Kumar, A. (1986). Prediction of densities of concentrated brines by Pitzer theory. *J. Chem. Eng. Data* **31**, 19-20.

Lide, D.R. (1996/1997). *Handbook of Chemistry and Physics*, 77th edition. CRC Press, Boca Raton, FL.

Lowe, B.M., N.A. MacGil, and J.M. Prichard (1973). Conductivities and densities of aqueous solutions of quaternary ammonium iodides containing pentyl and ethoxyethyl groups. *J. Chem. Eng. Data* **18**, 220-223.

Luck, W.A.P. (1967). Spectroscopic studies concerning the structure and the thermodynamic behaviour of H_2O, CH_3OH and C_2H_5OH. *Disc. Faraday Soc.* **43**, 115-127.

Mahajan, A.R., and S.R.Mirgane (2013). Excess molar volumes and viscosities for the binary mixtures of n-octane, n-decane, n-dodecane and n-tetradecane with octan-2-ol at 298.15 K. *J. Themodyn.* 571918-11.

Maksimova, I.M. (1965). On the question of origin of densities of aqueous solutions. *Zh. Fiz. Khimii* **59**, 551-554, in Russian.

Mecklenburg, T. and W. Seidel (1983). Apparent molar volumes of some substituted ammonium halides in dimethylsulfoxide. *Z. Phys. Chem. N. F.* **156**, 69-80.

Millero, F.J. (1970). The apparent and partial molal volume of aqueous sodium chloride solutions at various temperatures. *J. Phys. Chem.* **74**, 356-362.

Millero, F.J. (1972). Partial molar volumes of electrolytes in aqueous solutions. In: *Water and Aqueous Solutions: Structure, Thermodynamics and Transport Properties*, R.N. Horne (Editor). Wiley, New York. Chapter 13, pp. 519-595.

Millero, F.J., G.K. Ward, and P. Chetirkin (1976). Partial specific volume, expansibility, compressibility, and heat capacity of aqueous lysozyme solutions. *J. Biolog. Chem.* **251**, 4001-4004.

Misztal, R., and K. Sangwal (1999). Analysis of the concentration and temperature dependence of densities of aqueous alkali halide solutions: a new power-law approach. *Cryst. Res. Technol.* **34**, 769-775.

Mohiuddin, S., and K. Ismail (1996). Temperature and concentration dependence of the viscosity of aqueous sodium nitrate and sodium thiosulphate electrolyte systems. *Fluid Phase Equilibria* **123**, 231-243.

Nain, A.K., R. Pal, and R.K. Sharma (2011). Volumetric, ultrasonic, and viscometric behaviour of l-histidine in aqueous-glucose solutions at different temperatures. *J. Chem. Thermodyn.* **43**, 603-612.

Nayar S., and A,P. Kudchadker (1973). Densities of some organic substances. *J. Chem. Eng. Data* **18**, 356–357.

Ortega, J. (1982). Densities and refractive indices of pure alcohols as a function of temperature. *J. Chem. Eng. Data* **27**, 312-317.

Patwardhan, V., and A. Kumar (1986). A unified approach for prediction of thermodynamic properties of aqueous mixed-electrolyte solutions. Part I: Vapor pressure and heat of vaporization. *AIChE Journal*. **32**, 1429-1428.

Pierotti, R.A. (1976). A scaled particle theory of aqueous and nonaqueous solutions. *Chem. Rev.* **76**, 717-726.

Rafiee, H.R., and F. Frouzesh (2016). The study of partial and excess molar volumes for binary mixtures of nitrobenzene and benzaldehyde with xylene isomers from T = (298.15 to 318.15) K and P = 0.087 MPa. *J. Adv. Res. (Cairo University)* **7**, 769-780.

Ranjith Kumar, B., B. Satyanarayana, S. Asra Banu, K. Amara Jyothi, T. Savitha Jyostna, and N. Satyanarayana (2009). *Indian J. Pure Appl. Phys*. **47**, 511-516.

Rebelo, L.P.N., J.N.C. Lopes, J.M.S.S. Esperança, H.J.R. Guedes, J. Łachwa, V. Najdanovic-Visak, and Z.P. Visak (2007). Accounting for the unique, doubly dual nature of ionic liquids from a molecular thermodynamic and modeling standpoint. *Acc. Chem. Res.* **40**, 1114-1121.

Redlich, O., and A.T. Kister (1948). Algebraic representation of thermodynamic properties and classification of solutions. *Ind. Eng. Chem.* **40**, 345-348.

Redlich, O., and D.M. Meyer (1964). The molal volumes of electrolytes. *Chem. Rev.* **64**, 221.

Redlich, O., and P. Rosenfeld (1931). Das partielle molare Volumen von gelösten Elektrolyten. I. *Z. Phys. Chem.* **155**, 65-74.

Reichardt, A.A. (1970). Relationship between density of electrolyte solutions and their molar concentration. *Zh. Fiz. Khimii* **44**, 437-439, in Russian.

Rooney, D., J. Jacquemin, and R. Gardas (2009). Thermophysical properties of ionic liquids. *Top. Curr. Chem.* **290**, 185-212.

Root, W.C. (1933). An equation relating density and concentration. *J. Am. Chem. Soc.* **55**, 850–851.

Sangwal, K. (1987). A new equation for the temperature dependence of density of saturated aqueous solutions of electrolytes. *Cryst. Res. Technol.* **22**, 789-792.

Sharma,, S., P.B. Patel, R.S. Patel, and J.J. Vora (2007). Density and comparative refractive index study on mixing properties of binary liquid mixtures of eucalyptol with hydrocarbons at 303.15, 308.15 and 313.15 K. *E-J. Chem.* **4**, 343-349.

Singh, S., M. Aznar, and N. Deenadayalu (2013). Densities, speed of sound, and refractive indices for binary systems of 1-butyl-3-methylimidazolium methyl sulphate ionic liquid with alcohols at T = (298.15, 303.15, 308.15, and 313.15) K. *J. Chem. Thermodyn.* **57**, 238-247.

Skabichevskii, P.A. (1972). Apparent molar volumes of lithium salts in methyl and isoamyl alcohols. *Zh. Fiz. Khimii* **46**, 531-532, in Russian.

Sokolowski, T. (1981). Physical properties of aqueous solution of sodium sulphate. *J. Cryst. Growth* **52**, 829-831.

Sokolowski, W. and K. Sangwal (1983). Some physical properties of dilute and concentrated aqueous solutions of potassium bichromate. *Z. Phys. Chem. N. F.* **158**, 157-165.

Söhnel, O., and P. Novotný (1985). *Densities of Aqueous Solutions of Inorganic Substances*. Academia, Prague.

Szewczyk, J., and K. Sangwal (1988). Density, refractive index, and specific refraction of aqueous lithium iodate solutions. *J. Chem. Eng. Data* **33**, 418-423.

Szewczyk, J., W. Sokołowski, and K. Sangwal (1985). Some physical properties of saturated, supersaturated, and undersaturated aqueous potassium bichromate solutions. *J. Chem. Eng. Data* **30**, 243-246.

Šegatin, N., and C. Klofutar (2004). Limiting partial molar volumes of water in 1-hexanol, 1-octanol, 1-decanol, and cyclohexane at 298.15 K. *Monatschefte für Chemie* **135**, 161-172.

Theilander, H., and U. Gren (1989). A simple algorithm for the estimation of the density of aqueous solutions containing two or more different salts. *Computers Chem. Eng.* **13**, 419-424.

Zhang, S., N. Sun, X. He, X. Lu, and X. Zhang (2006). Physical properties of ionic liquids: database and evaluation. *J. Phys. Chem. Ref. Data* **36**, 1475-1517.

Zhang, Y., H. Dong, Y. Yue, and C. Wu (2013). Effect of temperature and composition on the density, refractive index, and excess quantities of binary mixtures of 2,4,6,6-tetramethyl-2,4,6,8-tetraethenylcyclotetrasiloxane with aromatic hydro- carbons. *J. Chem. Thermodyn.* **57**, 114-130.

Zhao, C., P. Ma, and J. Li (2005). Partial molar volumes and viscosity B-coefficients of arginine in aqueous glucose, sucrose, and L-ascorbic acid solutions at T = 298.15 K. *J. Chem. Thermodyn.* **37**, 37-42.

Zhao, N., H.B. Menegolla, V. Degirmenci, Z. Wagner, M. Bendová, and J. Jacquemin (2017). Group contribution method for evaluation of volumetric properties of ionic liquids using experimental data recommended by mathematical gnostics. *Ind. Eng. Chem. Res*. **56**, 6827-6840.

4

REFRACTIVE INDEX OF SOLVENTS AND SOLUTIONS

Refractive index is a useful tool to differentiate between different types of gemstones, due to the unique refractive behavior of the molecules composing them. The refractive index is also an important property of the components of any optical instrument that uses refraction. It determines the focusing power of lenses, the dispersive power of prisms, and generally the path of light through the system. It is frequently used to identify a particular substance in the solution, assess its purity, or measure its concentration. It is commonly used to measure the concentration of solutes in aqueous solutions. A typical example is the determination of sugar content from its aqueous solutions. Refractive index is used to control supersaturation of systems during industrial crystallization and to study nucleation processes during crystallization from solutions. Refractive index measurements are also of interest in the fields of pharmaceutical research and in photonic applications of polymer systems.

Refractive index is an important property of pure liquids, liquid mixtures and solutions of electrolytes and nonelectrolytes. Refractive index data of various systems, combined with density measurments, as a function of composition and temperature provide knowledge of complex molecular interactions occurring between the molecules of the components composing them and reflect the extent of deviation from their nonideal behavior.

In view of widely different applications of refractive index measurements of various substances in the solid and liquid states, understanding of the basic processes of the dielectric constant ε and refractive index n of matter in relation to its composition received enormous interest in the last century both theoretically and experimentally. This period also witnessed main development in the field, but subsequent studies carried out during the last four decades have essentially been concentrated on the applied aspects of the basic concepts. The subject was surveyed by Böttcher and Bordewijk (1978), whereas the basic concepts may be found in textbooks devoted to physical chemistry (for example, see: Eggers et al., 1964) and solid state physics (for example, see: Dekker, 1964; Kittel, 1976).

In the present chapter different types of issues associated with the experimental data of refractive indices of simple solvents, solvent mixtures and solutions containing inorganic and organic solutes as functions of their chemical constitution, composition and temperature are described using examples of different systems published in the literature. After presenting the basic ideas of refractive index measurements in Section 4.1 and the theoretical description of the concepts of polarization of molecules and various expressions of polarizability and molar refraction in Section 4.2, relationships between: (1) the refractive index and density of solvents, solvent mixtures and solutions, (2) their molar refractions and chemical composition, and (3) deviations in the refractive indices and molar refractions from simple additivity rule are discussed in Sections 4.3 through 4.6. Finally, the behavior of refractive index of near-saturated solutions is described in Section 4.7. No attempt is made to survey the literature published so far in the field. The main emphasis here is to look for the science in the published data of refractive index measurements of solvents and solutions.

4.1. Measurement of refractive index of materials

The refractive index or index of refraction, traditionally denoted by n, of a medium is a dimensionless number for the material and describes how light propagates through it. Its concept applies to the three states of matter and to all types of wave phenomena such as entire electromagnetic spectrum from x-rays to radio waves and the sound waves. In the former case, the refractive index of a medium uses the velocity of light with vacuum as the reference medium. However, in the case of sound, the sound velocity is used with a reference medium other than vacuum.

Refractive index of a material is a measure of bending, or refraction, of a ray of light when it enters it and is described by Snell's law of refraction given by the relation

$$\frac{n_2}{n_1} = \frac{\sin \theta_1}{\sin \theta_2}, \tag{4.1}$$

where θ_1 and θ_2 are the angles of incidence and refraction, respectively, of a ray crossing the interface between two materials (media) 1 and 2 with refractive indices n_1 and n_2. Since the velocity of light in vacuum is c, the refractive index n_2 of the refracting material, which is essentially the ratio n_2/n_1 in Eq. (4.1), is 1. Since the velocity of light is the highest in vacuum, n is always greater than 1.

The refractive index of a medium may also be defined as

$$n = \frac{v}{c}, \tag{4.2}$$

where c is the velocity of light in the vacuum and v is the phase velocity of light in the medium. Similarly, the refractive index n of the medium is related to the wavelength λ of light and is given by

$$n = \frac{\lambda_0}{\lambda}, \tag{4.3}$$

where λ_0 is the wavelength of light in vacuum. The above relations imply that vacuum has a refractive index of 1, and that the frequency ν, which is the ratio v/λ, of the wave is not affected by the refractive index of the medium. This means that the refractive index of a medium may be considered as a parameter by which the velocity and the wavelength of light in a medium are reduced with respect to its value in vacuum.

According to Planck's relation, the energy E of a photon of light and its frequency ν are related, i.e. $E = h\nu$, where h is the Planck constant. Since refractive index affects the wavelength, white light entering the medium results in a difference in the bending angle of the refracted rays, thereby splitting the white light into its constituent colors. Therefore, due to the dependence of the refractive index on the wavelength of light used for its measurement, it is measured with monochromatic light. A common practice is to use the sodium D-line wavelength 589 nm. The refractive index measured at this wavelength is usually denoted by n_D. The temperature of measurements is usually 20 °C or 25 °C.

The refractive index of electromagnetic radiation is related to the relative permittivity (or relative dielectric constant) ε_r of a material and its relative permeability μ_r, i.e.

$$n = (\varepsilon_r \mu_r)^{1/2}, \tag{4.4}$$

where ε_r and μ_r of the material are defined with respect to vacuum. Most naturally occurring materials are nonmagnetic at optical frequencies. Then μ_r is very close to 1, and $\varepsilon_r \approx n^2$.

The refractive index of a material depends on the chemical constitution of molecules/ions composing the material, the temperature of measurement, and the wavelength of light used. The last factor is controlled by selecting a known source of light of a particular wavelength such as sodium D-line. The former two factors, on the other hand, determine the density of substances in the solid and liquid states. Therefore, the refractive index of substances usually increases with their density. However, there does not exist a general linear relation between the refractive index and the density of different substances. This is due to the fact that the density of substances is determined by the general packing of molecules/ions in the volume. Ethanol, which has a higher refractive index but a lower density than that of water, is a typical example of liquids that violate the general correlation between density and refractive index.

The refractive index of liquids or solids is measured with refractometers, which typically measure the angle of refraction or the critical angle for total internal reflection. Various laboratory refractometers are commercially available.

4.2. Theoretical background

4.2.1. Dielectric constant and polarizability of materials

When a dielectric material lies in an electric field of strength E, it induces an electrical dipole moment in it per unit volume. This resulting dipole moment per unit volume is called the polarization P of the material. The polarization P of a substance and the applied electric field strength E are related by

$$\frac{\varepsilon - 1}{4\pi} E = P, \tag{4.5}$$

where ε is the dielectric constant of the material. The polarization P of the material is described in terms of the properties of the ions/atoms and molecules composing it. In order to describe the polarization P of the material on molecular basis, it is assumed that it is composed of two parts: (i) induced polarization P_α caused by the displacement of the electrons with respect to the positive charges (electronic polarization) and of atoms or groups of atoms relative to each other (atomic polarization), and (ii) orientation polarization P_μ caused by the orientation of the permanent dipoles. Hence the above equation may be written as

$$\frac{\varepsilon-1}{4\pi}E = P_\alpha + P_\mu = \sum_j N_j \alpha_j (E_i)_j + \sum_j N_j \left(\frac{\mu_j^2 (E_\mathrm{d})_j}{3k_\mathrm{B}T} \right), \tag{4.6}$$

where N_j is the number of particles j per unit volume, α_j is the scalar polarizability of the particle j, μ_j is the permanent dipole moment of the particle, E_i is the average field strength, the so-called internal or local field, acting upon the particle j, E_d is the part of the electric field which tends to orient the permanent dipoles, and the index j refers to the jth type of particles. Induced polarization P_α is essentially temperature-independent polarization of molecules but orientation polarization P_μ is dependent on temperature due to the permanent dipole moment of molecules.

Eq. (4.6) is the so-called Debye formula for the static dielectric constant of a gas. This equation has been observed to apply well for several organic substances in the gaseous state where a given atom or molecule “sees” only the external field but does not see the fields produced by the dipoles on other particles. However, in solids and liquids the latter contribution cannot be neglected. In these substances one takes into account the additional field, the internal or local field, produced by the dipoles on other particles in their volume due to long range interactions. This internal field E_i is given by

$$E_\mathrm{i} = \frac{\varepsilon+2}{3}E\,. \tag{4.7}$$

Then substitution of this equation in Eqs. (4.6) gives

$$\frac{\varepsilon-1}{\varepsilon+2} = \frac{4\pi}{3} \sum_j N_j \alpha_j (E_i)_j + \sum_j N_j \left(\frac{\mu_j^2 (E_\mathrm{d})_j}{3k_\mathrm{B}T} \right). \tag{4.8}$$

For a polar substance, when E_i and E_d are not distinguished from each other and when one uses the equation of Lorentz field for both E_i and E_d, Eq. (4.8) may be written as

$$\frac{\varepsilon-1}{\varepsilon+2} = \frac{4\pi}{3} \sum_j N_j \left(\alpha_j + \frac{\mu_j^2}{3k_\mathrm{B}T} \right). \tag{4.9}$$

For a nonpolar system (i.e. $P_\mu = 0$) , Eq. (4.9) reduces to the form

$$\frac{\varepsilon-1}{\varepsilon+2}=\frac{4\pi}{3}\sum_j N_j\alpha_j\ , \tag{4.10}$$

for cases when the internal field in homogeneously polarized matter is considered as the field in a virtual spherical cavity. This field is called the Lorentz field, and Eq. (4.9) is the well-known Clausius–Mossotti equation. Eq. (4.8) relates the dielectric constant ε of induced polarization with the total polarization of the molecule to which both electronic and atomic polarization contribute, whereas Eq. (4.9) also includes contribution of orientation of atoms of the molecule to the dielectric constant.

For cases where Clausius–Mossotti equation holds, the molar polarization P is a constant for a given substance and is an additive quantity for mixtures:

$$P=\left(\frac{\varepsilon-1}{\varepsilon+2}\right)\frac{M}{d}=\sum_j x_jP_j\ , \tag{4.11}$$

with

$$P_j=\left(\frac{\varepsilon_k-1}{\varepsilon_k+2}\right)\frac{M_j}{d_j}=\frac{4\pi}{3}N_{\mathrm{A}}\alpha_j\,, \tag{4.12}$$

where d and M are the density and the molar mass of the substance, the index j refers to the values of d and M of the component j, and N_{A} is the Avogadro number.

The values of the molar polarization of nonpolar compounds deviate from those for dilute gases. They are interpreted by considering the environment of a single molecule in a dielectric continuum. Then the deviations in the molar polarization of molecules of the substance from that of the dilute gas is accounted for by a factor h_{j} for each component in the mixture and is determined by the polarizabilty α_j and radius r_j of the molecule and the dielectric constant ε of the substance. Then the molar polarization is given by (Böttcher and Bordewijk, 1978):

$$P_j=\left(\frac{\varepsilon-1}{\varepsilon+2}\right)\frac{M_j}{d_j}=\frac{4\pi}{3}N_{\mathrm{A}}\alpha\frac{9\varepsilon}{(\varepsilon+2)[2\varepsilon+1-2(\alpha_j/r_j^3)(\varepsilon-1)]}=h_jP_{0,j}\,, \tag{4.13}$$

where $P_{0,j}$ is the ideal polarization of the j molecule given by Eq. (4.12) and the parameter

$$h_j=\frac{9\varepsilon}{(\varepsilon+2)[2\varepsilon+1-2(\alpha_j/r_j^3)(\varepsilon-1)]}\,, \tag{4.14}$$

with the corrected Clausius–Mossotti equation

$$\frac{\varepsilon-1}{12\pi\varepsilon}=\sum_j\frac{N_{\mathrm{A}}\alpha_j}{2\varepsilon+1-2(\alpha_j/r_j^3)(\varepsilon-1)}\ . \tag{4.15}$$

Note that, for ε slightly different from unity, $h_j\approx 1$. For larger values of ε, the parameter h_j is a function of α_j/r_j^3 and is always less than 1.

Eq. (4.15) may be rewritten in the form

$$\frac{(\varepsilon-1)(2\varepsilon+1)}{12\pi\varepsilon}=\sum_j \frac{N_\mathrm{A}\alpha_j}{1-f_j\alpha_j}=\sum_j N_\mathrm{A}\alpha_j^* \ , \tag{4.16}$$

where

$$\alpha_j^*=\frac{\alpha_j}{1-f_j\alpha_j} \ , \tag{4.17}$$

and

$$f_j=\frac{2}{r_j^3}\left(\frac{\varepsilon-1}{2\varepsilon+1}\right). \tag{4.18}$$

For a single substance, Eq. (4.16) may be rewritten in the form

$$\frac{12\pi\varepsilon d}{(\varepsilon-1)(2\varepsilon+1)}=\frac{1}{\alpha^*}=\frac{M}{N_\mathrm{A}}\left(\frac{1-f\alpha}{\alpha}\right)=\frac{M}{N_\mathrm{A}}\left\{\frac{1}{\alpha}-\frac{2}{r^3}\left(\frac{\varepsilon-1}{2\varepsilon+1}\right)\right\}. \tag{4.19}$$

According to Eq. (4.18) a plot of $1/\alpha^*$ against $2(\varepsilon–1)/(2\varepsilon+1)$ gives a straight line with intercept $M/N_\mathrm{A}\alpha$ and slope $M/N_\mathrm{A}r^3$.

4.2.2. Polarizability and radius of ions and molecules of materials

Dielectric constant ε and refractive index n of a substance at higher frequencies (e.g. at optical frequencies), where orientation atomic polarizations do not follow the changes in the electric field, are related according to the Maxwell relation as: $\varepsilon = n^2$. Using this relation one may calculate molar refraction R_M of a mixture of j components of density d and molar mass M from Eqs. (4.10) and (4.12) in the following form:

$$R_\mathrm{M}=\left(\frac{n^2-1}{n^2+2}\right)\frac{M}{d}=\sum_j x_j R_{\mathrm{M}j} \ , \tag{4.20}$$

where

$$R_{\mathrm{M}j}=\left(\frac{n_j^2-1}{n_j^2+2}\right)\frac{M_j}{d_j}=R_{\mathrm{M}0}^*+\frac{R_{\mathrm{M}1}^*}{T}=\text{constant} \ , \tag{4.21}$$

such that

$$R_{\mathrm{M}0}^*=\frac{4\pi N_\mathrm{A}}{3}\sum_i \alpha_i \ , \qquad R_{\mathrm{M}1}^*=\frac{4\pi N_\mathrm{A}}{9}\sum_i \frac{\mu_i^2}{k_\mathrm{B}} \ . \tag{4.22}$$

In the above equations, x_j is the composition of component j and the subscript j denotes the component j. This additivity rule is followed by several mixtures obeying Eq.

(4.21) known as the Lorentz–Lorenz relation, but there are many systems of pure liquid mixtures and mixtures of two solutes dissolved in the same solvent that the experimental values are higher than those given by the additivity rule. This is explained by the formation of polar molecular complexes (Böttcher and Bordewijk, 1978).

The molar refraction R_M of a binary mixture of substances at a particular temperature T may be analyzed using Eq. (4.20) taking the molar mass M of the mixture using additivity rule and the experimental values of density d. Then one expects a linear dependence of R_M of the mixture on the concentration x_2 of component 2 with intercept R_M0 corresponding to $x_2 = 0$ and slope $R_\mathrm{M1} = (4\pi N_\mathrm{A}/3)(\alpha+\mu^2/k_\mathrm{B}T)$, where N_A is the Avogadro number. However, this procedure does not provide a direct method to estimate polarizability α and dipole moment μ of particles composing the mixture because the $(\mu^2/k_\mathrm{B}T)$ term is temperature dependent. The contributions of α and μ of the components of a mixture may be separated by plotting R_M of the mixture on T^{-1} and then, by analyzing the data of the intercept $(4\pi N_\mathrm{A}/3)\Sigma\alpha_j$ and the slope $(4\pi N_\mathrm{A}/9)\Sigma(\mu_j^2/k_\mathrm{B})$ as a function of x_2, one may determine the contributions of polarizability α_j and dielectric moment μ_j of individual component j of the mixture. The slope $(4\pi N_\mathrm{A}/9)(\mu_j^2/k_\mathrm{B})$ of plot of R_M against T^{-1} corresponds to the dipole moment measured in units of 10^{-18} esu·cm per molecule.

For a mixture of substances, the corrected Clausius–Mossotti equation, Eq. (4.15), provides an alternative procedure for the analysis of the refractive index data at a particular temperature to estimate the polarizability α_j and ionic radius r_j of particles composing the mixture. This procedure employs Eq. (4.16) rewritten in the form

$$\frac{(n^2-1)(2n^2+1)}{12\pi n^2} = \sum_j \frac{N_j\alpha_j}{1-f_j\alpha_j} = \sum_j N_j\alpha_j^* , \tag{4.23}$$

where

$$\frac{1}{\alpha_k^*} = \frac{1-f\alpha}{N_\mathrm{A}\alpha} = \frac{12\pi n^2 d}{(n^2-1)(2n^2+1)} = \frac{M}{N_\mathrm{A}}\left\{\frac{1}{\alpha_k} - \frac{2(n^2-1)}{r_k^3(2n^2+1)}\right\}, \tag{4.24}$$

where N_j has been replaced by the Avogadro number N_A. According to this equation, usually known as Böttcher's relation, a linear plot of $1/\alpha^*$ against $2(n^2-1)/(2n^2+1)$ from the data of the refractive index n of the mixture enables to estimate the polarizability α_j and ionic radius r_k of particles composing the mixture from the intercept $1/\alpha_j$ and the slope $1/r_j^3$ of the plot.

It should be mentioned that when the term (n^2+2) for a series of compounds or for a mixture is practically independent of the compounds or mixture and the polarization α of their molecules differs insignificantly from each other, Eq. (4.20) reduces to the Drude law:

$$\frac{n^2-1}{d} = \frac{4\pi(n^2+2)N_\mathrm{A}\alpha}{3M} = \text{constant} . \tag{4.25}$$

However, when the term

$$\frac{4\pi(n^2+2)d}{3M}N_{\mathrm{A}}\alpha << 1,$$

Eq. (4.19) takes the form of the Gladstone–Dale law:

$$\frac{n-1}{d}=\frac{2\pi(n^2+2)N_{\mathrm{A}}\alpha}{3M}=\text{constant}\ . \tag{4.26}$$

According to the Drude and Gladstone–Dale laws a plot of n^2 or n against d for the $n(d)$ data for a system is expected to yield a straight line of intercept 1 and slope $4\pi(n^2+2)N_{\mathrm{A}}\alpha/3M$ or $4\pi(n^2+2)N_{\mathrm{A}}\alpha/3M$. However, these laws hold when the term $(n^2+2)\alpha/M$ remains constant in the range of n measurements for a system. In practice, depending on the increasing or decreasing trend of $(n^2+2)\alpha/M$ in the measurement range of the refractive index n of the system, the value of the intercept can differ from unity and can even attain negative values (see below).

In the case of organic solvents, Eykman's empirical equation (Ortega, 1982; Riddick et al., 1986)

$$\frac{n^2-1}{n+0.4}\frac{1}{d}=K\ , \tag{4.27}$$

is also frequently used. The constant K of Eq. (4.27) is independent of temperature, but its value increases with increasing molar mass M of the solvent.

4.3. Refractive index of individual solvents

4.3.1. Dependence of refractive index on chemical composition of solvents

The refractive index n of a solvent depends on its chemical composition as well as on the measurement temperature and is intimately connected with the density d of the solvent. In organic solvents of the same homologous series such as normal alcohols, their refractive index n at a given temperature increases with an increase in the number N of $-CH_2$ groups in the alcohols (e.g. with molar mass M of solvent), as illustrated in Figure 4.1 for 1- and 2-alcohols at 20 °C. The $n(N)$ data for the two types of alcohols follow the empirical relation

$$n=n_1-A_1\exp(B_1N), \tag{4.28}$$

where n_1, A_1 and B_1 are empirical constants. Here n_1 is the extrapolated value of n when $N=\infty$ and corresponds to the limiting value of A_1, whereas A_1 is the value of n when $N=0$. The best-fit constants for the data at 20 °C reported by Ortega (1982) are: $n_1 = 1.4408$, $A_1 = 0.154$ and $B_1 = -0.326$ (with $R^2 = 0.9980$). The above data may also be represented by the empirical polynomial relation

$$n = \sum_{q=0}^{n} A_q N^q \; , \tag{4.29}$$

where q is a positive integer and A_q are best-fit constants. However, among these two empirical relations, the former relation is more informative in terms of the best-fit constants because it describes the $n(N)$ data for both 1- and 2-alcohols satisfactorily by a single linear dependence of $\ln(n_1 – n)$ on N of the same intercept $\ln A_1$ and slope B_1 with appropriately chosen values of n_1 for the two types of alcohols. Figure 4.2 presents the above $n(N)$ data as plot of $\ln(n_1 – n)$ against N, with intercept $\ln A_1 = –1.89418$ (i.e. $A_1 = 0.150$) and slope $B_1 = –0.29385$ for both 1- and 2-alcohols such that the chosen value of $n_1 = 1.444$ and 1.440 for 1- and 2-alcohols, respectively. As in Figure 4.1, the linear dependence represents the data reported by Ortega (1982), with $R^2 = 0.9967$. The lower value of the refractive index n_1 corresponding to $N = \infty$ for the 2-alcohols is associated with a higher molecular disorder due to the attachment of one of its $–CH_2$ groups in the side positions of their structure than that in the 1-alcohols composed of all $–CH_2$ groups arranged in series.

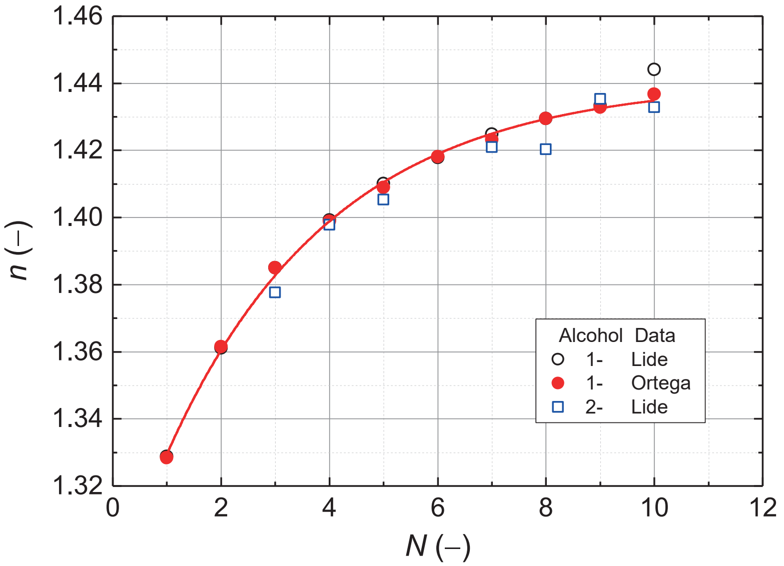

Figure 4.1. Refractive index n of pure 1- and 2-alcohols at 20 °C as a function of number N of $–CH_2$ groups in their chemical formula. Solid line represents entire data, due to Ortega (1982), for 1-alcohols according to Eq. (4.28). Original data from Lide (1996/1997) and Ortega (1982).

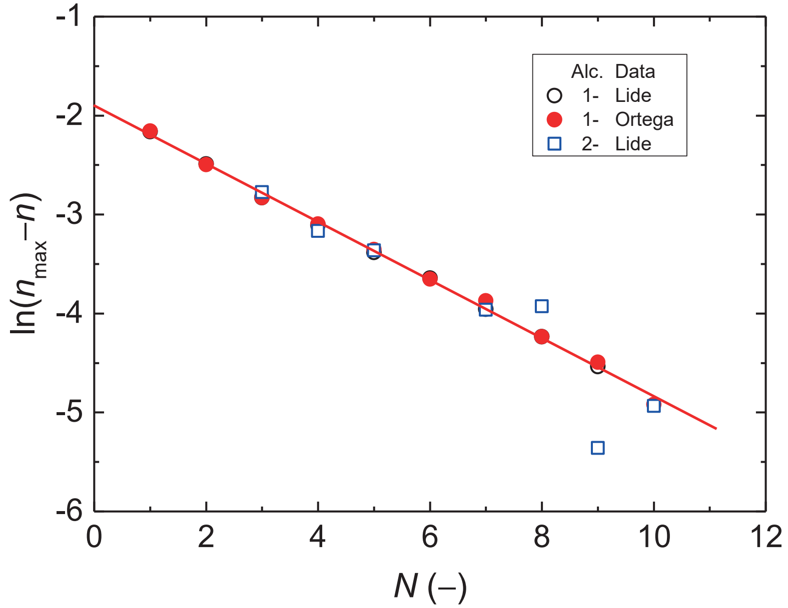

Figure 4.2. Plot of $\ln(n_1–n)$ against N for 1- and 2-alcohols at 20 °C according to Eq. (4.28). Linear dependence represents data reported by Ortega (1982), with constants n_1, A_1 and B_1 given in the text.

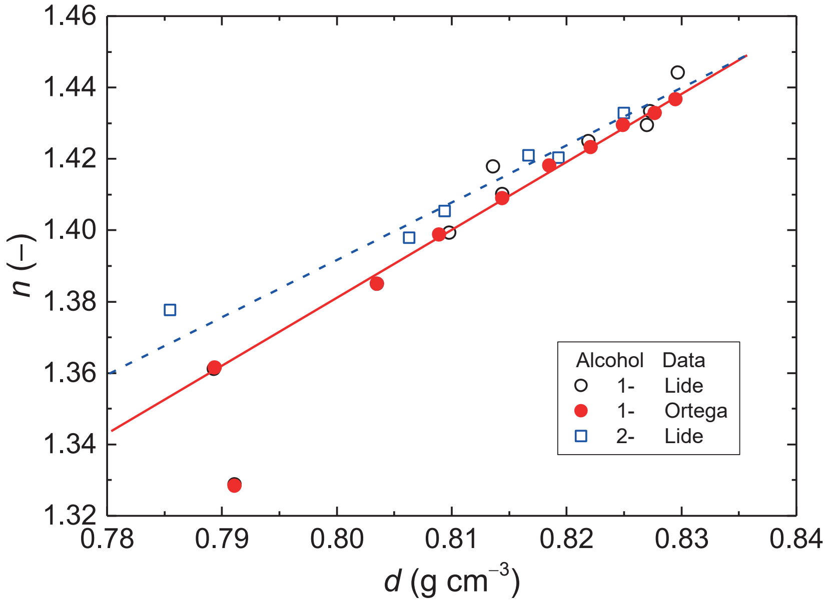

Figure 4.3. Refractive index n of pure 1- and 2-alcohols at 20 °C as a function of their corresponding density d. Solid and dashed line represent data of 1- and 2-alcohols, respectively. For 1-alcohols, data from Ortega (1982) were considered without methanol. Original data from Lide (1996/1997) and Ortega (1982).

The above trends of the $n(N)$ data imply that the refractive index n of a solvent is related to the molar mass M of the solvent for a particular series of solvents. Since the density d of a solvent at a particular temperature is related to its molar mass M, one also expects that the value of the refractive index n of organic solvents of a series is related to their densities d. As an example, the experimental data of the refractive index n of pure 1- and 2-alcohols at 20 °C as a function of their corresponding density d are shown in Figure 4.3. These data may be represented by the linear relation

$$n = n_2 + A_2 d\,, \tag{4.30}$$

where the constants are: $n_2 = -0.1461$ and $A_2 = 1.9089$ cm^3/g for 1-alcohols, and $n_2 = 0.1687$ and $A_2 = 1.5273$ cm^3/g for 2-alcohols. During the analysis, data for methanol were omitted. In Eq. (4.30), n_2 is the extrapolated value of n when $d = 0$, and the slope A_2 is an indicator of the ordering of the molecules in the series of these solvents. Higher value of A_2 for 1-alcohols than that for 2-alcohols implies more order in the former that that in the latter. It should be mentioned here that, although the form of this equation is similar to that of the Gladstone–Dale law (see Eq. (4.26)), the value of $n_2 < 1$ for both series of alcohols implies that the M/d ratio strongly increases with increasing molar mass M of the series of these alcohols.

The refractive index n of various substances, including liquids, decreases with increasing temperature T and usually follows the linear dependence:

$$n = n_3 - A_3 T\,, \tag{4.31}$$

where the intercept n_3 and the slope A_3 are constants characteristic of the substance. The value of the constant n_3 corresponds to $T = 0$ and depends on the unit of temperature. The value of A_3 is about $4 \cdot 10^{-4}$ K^{-1} for all normal alcohols up to 1-decanol (Ortega, 1982).

The refractive index n of solvents is also related to their boiling point T_b and melting pont T_m of alcohols. As in the case of the $n(N)$ data, the $n(T_\mathrm{b})$ and $n(T_\mathrm{m})$ data for the alcohols also follow the empirical relation

$$n = n_\mathrm{max} - A_\mathrm{b,m} \exp(B_\mathrm{b,m} T_\mathrm{b,m})\,, \tag{4.32}$$

where n_max, $A_\mathrm{b,m}$ and $B_\mathrm{b,m}$ are best-fit constants for the data. As in the case of Eq. (4.28), the value of $A_\mathrm{b,m}$ represents the value of n corresponding to $T_\mathrm{b,m} = 0$ but the value of the constant n_max and the value of $A_\mathrm{b,m}$ corresponding to n_max represent an alcohol with $N = \infty$. Figure 4.4 shows the $n(T_\mathrm{b})$ and $n(T_\mathrm{m})$ data in the form of the dependence of $\ln(n_\mathrm{max} - n)$ for the above value of $n_1 = 1.444$ on T_b. The solid line represents the best fit of the $n(T_\mathrm{b})$ data for the 1-alcohols at 20 °C reported by Ortega (1982), with intercept $\ln A_\mathrm{b} = -1.2385$ (i.e. $A_\mathrm{b} = 0.290$) and slope $B_\mathrm{b} = -0.01546$, $R^2 = 0.9935$, whereas the dashed line represents the $n(T_\mathrm{m})$ data with a slope $B_\mathrm{m} = B_\mathrm{b}$ and intercept $\ln A_\mathrm{m} = -4.50$.

It may be noted from Figure 4.4 that the $n(T_\mathrm{b})$ data for 2-alcohols are equally represented well by Eq. (4.32). The $n(T_\mathrm{m})$ data for various alcohols also show trends similar to those for the $n(T_\mathrm{b})$ data of the alcohols, but the linear dependence, represented by the dashed line with intercept $\ln A_\mathrm{m} = -4.5$ (i.e. $A_\mathrm{m} = 0.011$) and slope $B_\mathrm{m} = -0.01546$, is observed mainly for alcohols between butanol and nonanol.

Obviously, $A_b/A_m \approx 26$.

The boiling point of various compounds, taken in kelvin, is related to their enthalpy of vaporization ΔH_b and defines the vaporization entropy $\Delta H_b/T_b$ according to Trouton's rule. For hydrogen-bonded liquids such as water and alcohols, which behave as associated liquids, the vaporization entropy $\Delta H_b/T_b \approx 13.2R_G \approx 110$ kJ/mol·K. A similar relation exists between melting entropy ΔH_m and melting point T_m. These constant values of $\Delta H_b/T_b$ and $\Delta H_m/T_m$ explain the observed dependence of n on T_b and T_m for the alcohols. This observation implies that the increment in n is associated with the increment in the vaporization enthalpy ΔH_b and meling enthalpy ΔH_m of succeeding alcohols and is related to the nature of bonds between their molecules.

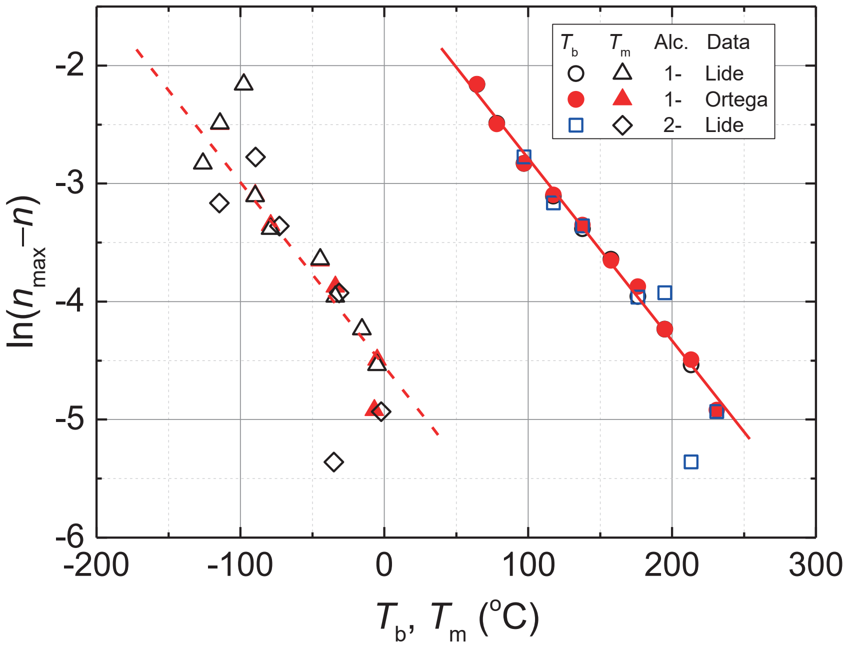

Figure 4.4. Plot of ln(n_{max}–n) from $n(N)$ data at 20 °C against T_b and T_m of pure 1- and 2-alcohols at atmospheric pressure. Solid and dashed lines represent data for 1-alcohols from Ortega (1982). Data of T_b and T_m for the alcohols and of n and T_b for 2-alcohols are from Lide (1996/1997). See text for details.

4.3.2. Molar refraction and chemical composition of solvents

Molar refraction R_M of 1- and 2-alcohols at 20 °C as a function of the number N of $–CH_2$ groups in their chemical formula is presented in Figure 4.5. The $R_M(N)$ data for the two series of alcohols follow the linear dependence

$$R_M = R_{M0} + R_{M1}N, \tag{4.33}$$

where the intercept R_{M0} is the extrapolated value of R_M when $N = 0$, and the slope R_{M1} represents the increment in R_M per $-CH_2$ group. These constants are: R_{M0} = 3.626 $cm^3 \cdot mole^{-1}$ and R_{M1} = 4.6327 $cm^3 \cdot mole^{-1}$ per $-CH_2$ group, which give the polarizability $\alpha_0 = 1.44 \cdot 10^{-24}$ cm^3 and the polarizability increment $\alpha_1 = 1.84 \cdot 10^{-24}$ cm^3 per $-CH_2$ group at 20 °C (see below).

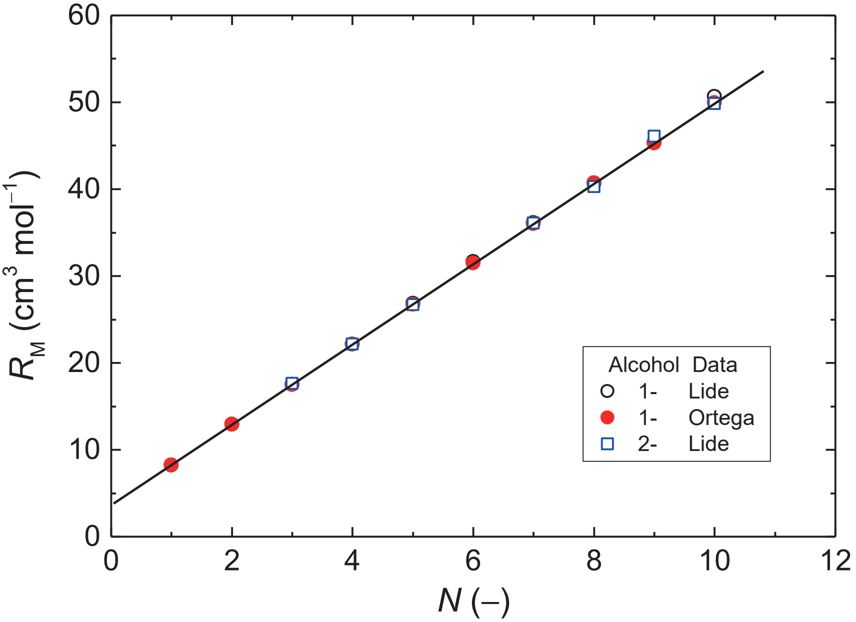

Figure 4.5. Dependence of molar refraction R_M of 1- and 2-alcohols at 20 °C on the number *N* of $-CH_2$ groups in their chemical formula according to Eq. (4.33). Solid line is drawn with data of 1-alcohols after Ortega (1982).

As mentioned above in Section 4.2.2, the refractive index *n* of various substances, including liquids, depends on their temperature *T*. Therefore, the molar refraction R_M for the substance may also be expected to change with temperature. As in the case of representation of the $n(T)$ data by relation (4.31), the temperature dependence of molar refraction R_M of these liquids also follows the empirical linear relation

$$R_M = R_M^* - A^*T, \tag{4.34}$$

where the intercept R_M^* represents the value of R_M corresponding to $T = 0$ and the slope A^* represents the change in R_M of the solution with *T*. It is usually found that $A^*/R_M^* << 1$. Therefore, instead of Eq. (4.34), plots of R_M against T^{-1} according to Eq. (4.22) provide useful information about the nature of the particles present in them. Figure 4.6 shows the data of molar refraction R_M of different 1-alcohols as a function of measurement temperature T in the form of Eq. (4.22), with the values of the polarizability α and the dipole moment contribution μ^2/k_B, calculated from the intercept $4\pi N_A\alpha/3$ and the slope $4\pi N_A\mu^2/3k_B$ of the plots according to Eq. (4.9), of the molecules of different alcohols presented in Figure 4.7a and b, respectively, as a function of the number N of $-CH_2$ groups in their chemical formula.

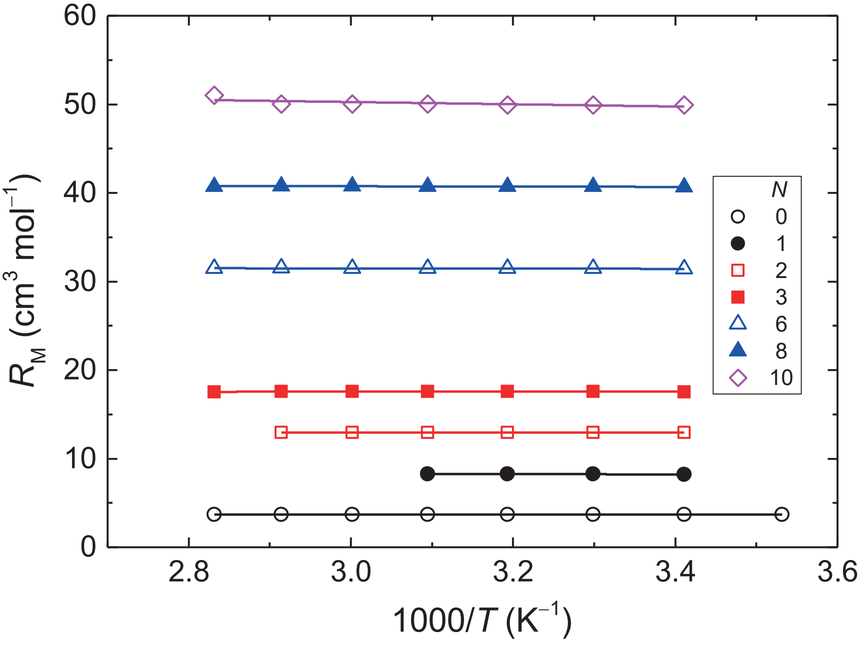

Figure 4.6. Data of molar refraction R_M of different 1-alcohols as a function of T^{-1} according to Eq. (4.21). Original data for R_M from Ortega (1982) for different alcohols and from Lide (1996/1997) for water with $N = 0$. See text for details.

As seen from Figure 4.7a, the polarizability α of molecules of the alcohols increases linearly with the number N of $-CH_2$ groups composing them, and follows the linear relation

$$\alpha = \alpha_0 + \alpha_1 N\,, \tag{4.35}$$

with the intercept $\alpha_0 = 1.469 \cdot 10^{-24}$ cm^3 corresponding to $N = 0$, and the slope $\alpha_1 = 1.861 \cdot 10^{-24}$ cm^3 per $-CH_2$ group ($R^2 = 0.9998$) corresponding to $T \to \infty$. These values of α_0 and α_1 are about 1% higher than those obtained from the $R_M(N)$ data at 20 °C above. As expected for these data, the values of $\alpha \approx r^3$ for the molecules of the alcohols. In contrast to the $\alpha(N)$ trend, the $\mu^2 < 0$ at least for higher alcohols (see Figure 4.7b). This negative value of μ^2 is probably due to the scatter in the original experimental data.

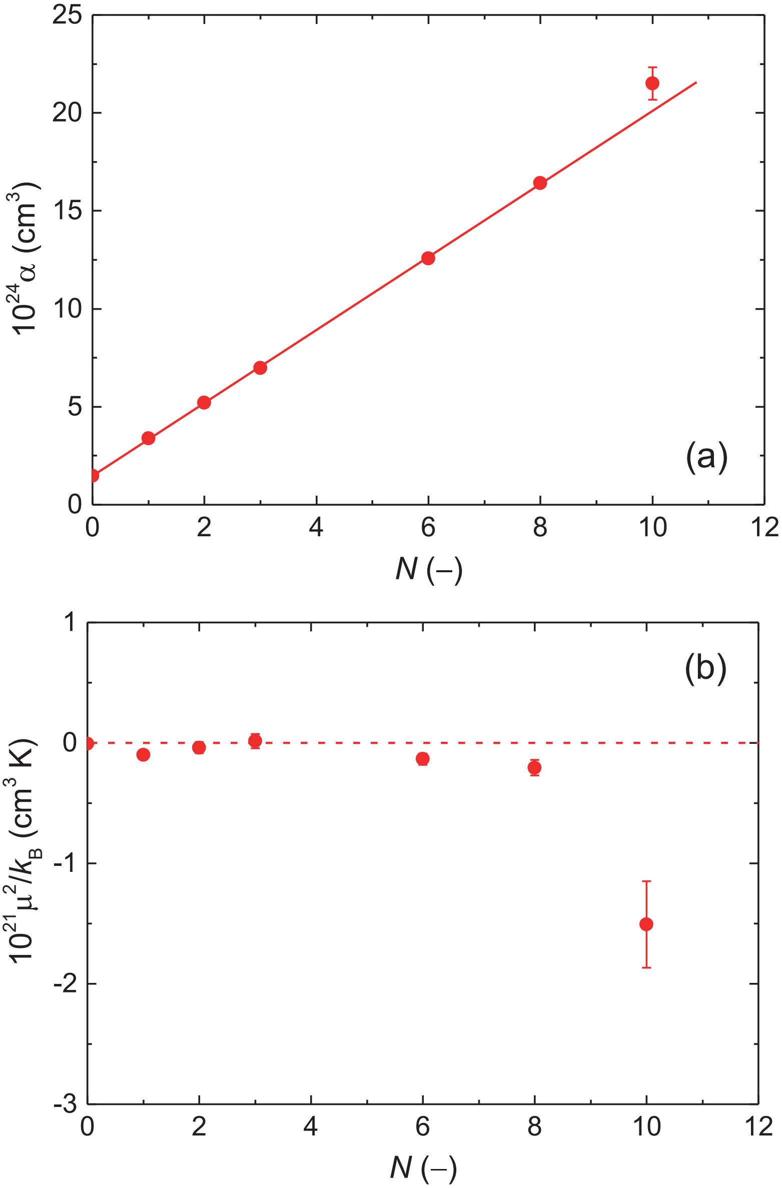

Figure 4.7. Relationship between (a) polarizability α and (b) dipole moment parameter μ^2/k_B of molecules of different 1-alcohols as a function of number N of $-CH_2$ groups in their chemical formula. In (a) Eq. (4.35) is followed.

Finally, it should be mentioned that the molar volume V_M of 1-alcohols increases linearly from an initial value of $V_M^o = 24.81$ cm^3·mol^{-1} for $N = 0$ with slope $dV_M/dN =$ 16.63 cm^3·mol^{-1} per $-CH_2$ group (see Section 3.3). This implies that the value of the polarizability α of the molecules of alcohols is associated with their molar volume V_M, and increases linearly with the V_M of the alcohols.

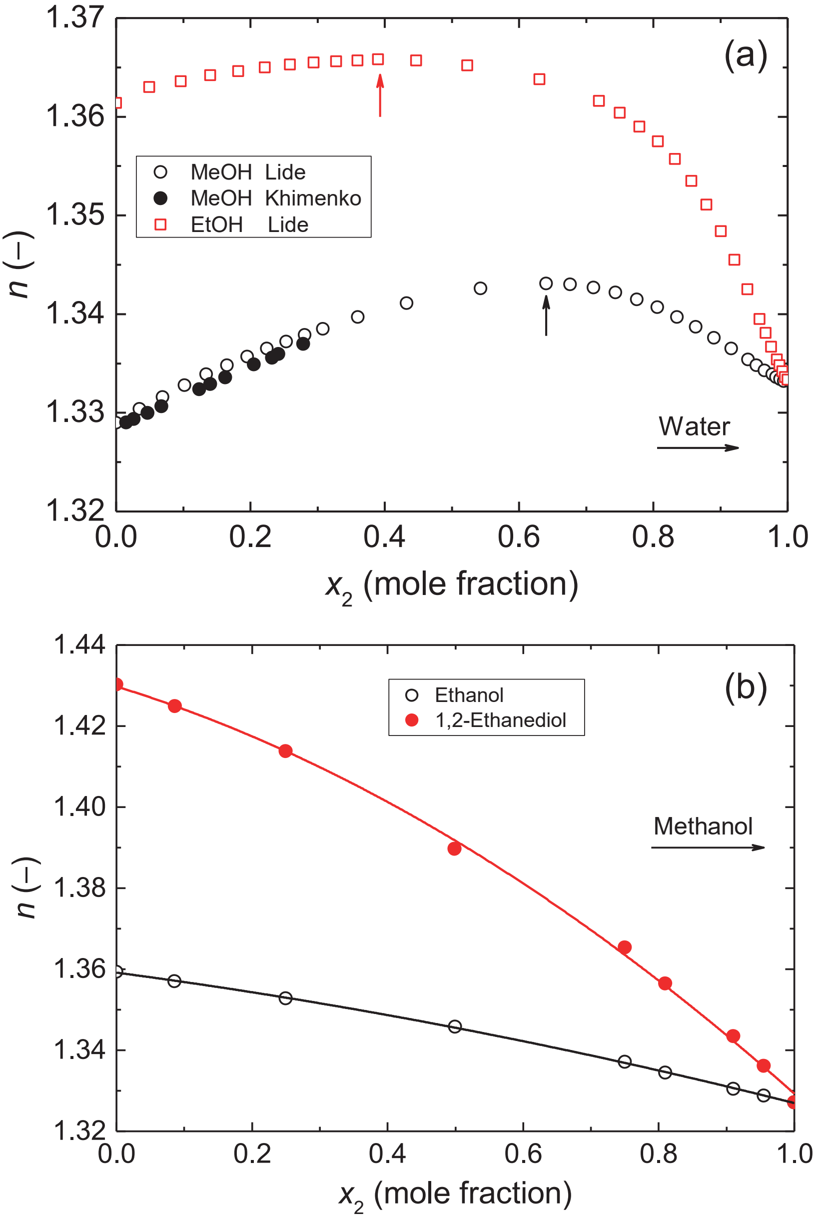

Figure 4.8. Dependences of refractive index n of (a) MeOH–H_2O and EtOH–H_2O mixtures at 20 °C on water content x_2 in the mixtures, and (b) EtOH–MeOH and 1,2-ethanediol–MeOH mixtures at 25 °C on MeOH content x_2 in the mixtures. Note that n does not depend linearly on x_1 but passes through a maximum at a certain water content typical of the alcohol in (a) but n steadily decreases from the n_1 of a pure solvent to the value n_2 for pure MeOH cosolvent with increasing MeOH content x_2. Cosolvent concentration corresponding to the maximum n_{max} are indicated by arrows. Original data from (a) Lide (1996/1997) and Khimenko (1969), and (b) Albuquerque et al. (1996).

4.4. Refractive index of solvent mixtures

4.4.1. Composition dependence of refractive index and molar refraction of solvent mixtures

It is well known that the refractive index n of binary mixtures of solvents containing simple as well as complex organic and ionic-liquid solvents at a particular temperature usually changes nonlinearly with an increase in the cosolvent content x_2 in the mixture (Albuquerque et al., 1996; Bahadur et al., 2013; Chandami et al., 2016; El-Dossoki, 2007; Francesconi and Ottani, 2007; Herráez and Belda, 2006; Maharolkar et al., 2010; Sharma et al., 2007; Singh et al., 2013). The value of their refractive index n of binary mixtures of solvents shows deviations from the linear dependence following from the additivity rule:

$$n = x_1 n_1 + x_2 n_2 = n_1 + (n_2 - n_1) x_2 = \sum_{i=1}^{2} x_i n_i \ , \tag{4.36}$$

where x and n are the mole fraction and the refractive index of the components i of a binary mixture, and $(x_1+x_2) = 1$. This relation predicts a linear dependence of n on x_2, with intercept n_1 and slope $(n_2–n_1)$. The slope $(n_2–n_1)$ of the $n(x_2)$ plot is positive when $(n_2–n_1) > 0$ and negative when $(n_2–n_1) < 0$. Deviations from the linear dependence are associated with the formation of molecular complexes between solvent and cosolvent molecules.

Figure 4.8 shows two examples of the dependence of the refractive index n on the content x_2 of cosolvent H_2O added to solvents MeOH and EtOH at 20 °C and on the content x_2 of cosolvent MeOH added to solvents EtOH and 1,2-ethanediol at 25 °C. The original data in Figure 4.8a are from Lide (1996/1997) and Khimenko (1969), whereas those of Figure 4.8b are from Albuquerque et al. (1996).

It may be noted from the figure that the refractive index n of the above mixtures does not show linear dependence on the composition x_2 of the cosolvent in accordance with the additivity rule. In Figure 4.8a, with increasing x_2 the value of n initially increases from n_1 and then, after going through a maximum value $n_{\max}$, indicated by arrows, at a certain water content $x_{2\max}$ typical of the alcohol, steadily decreases and approaches n_2 at $x_2 = 1$. However, as seen from the $n(x_2)$ data for methanol–water system, the value of n reported in two different studies may differ substantially from each other. In Figure 4.8b on the other hand, the value of n of the solvent mixture steadily decreases from an initial value of n_1 for the pure solvent with increasing methanol content x_2 and attains a value of n_2 at $x_2 = 1$. The data of Figure 4.8b may be described by the quadratic relation

$$n = n_0 + a_1 x_2 + a_2 x_2^2 = \sum_{i=0}^{2} a_i x_2^i \ , \tag{4.37}$$

where $n_0 = a_0$ denotes the refractive index of the pure solvent, a_i's are empirical constants related to the solvent–cosolvent mixture, and i is an integer. The values of the constants of Eq. (4.37) for the above binary mixtures are listed in Table 4.1.

Table 4.1. Values of the constants of Eq. (4.37) for $n(x_2)$ data

System	n_0	$-a_1$	$-a_2$	a_2/a_1	R^2
Ethanol–methanol	1.3592	0.0222	0.0009	0.04	0.9996
1,2-ethanediol–methanol	1.4298	0.0518	0.0488	0.94	0.9984

From Figure 4.8a it may be seen that each plot of the data of n against x_2 may be considered to be composed of two segments of plots below and after the cosolvent content $x_{2\max}$ corresponding to the maximum refractive index n. The trend of the $n(x_2)$ plot in the concentration range $x_2 > x_{2\max}$ is similar to that of Figure 4.8b, whereas the trend of the plot in the concentration range $0 < x_2 < x_{2\max}$ is opposite to that of Figure 4.8b. The $n(x_2)$ data in the two concentration intervals may be described by Eq. (4.37), with the difference that the constant $a_1 > 0$ and $a_1 < 0$ in the cosolvent concenration ranges $x_2 > x_{2\max}$ and $0 < x_2 < x_{2\max}$, respectively. The observation of maximum value $n_{\max}$ at $x_{2\max}$ may be attributed to the formation of relatively stable complexes like $(CH_3OH)_2(H_2O)$ and $(C_2H_5OH)_2(H_2O)_3$ for MeOH–H_2O and EtOH–H_2O systems, respectively. According to this concept, the refractive index $n_{\max}$ of the complex is higher than n_1 of the solvent 1 and n_2 of the cosolvent 2, and the formation of these complexes with the solvent molecules leads to an increase in n up to $n_{\max}$ whereas their dissipitation with increasing x_2 beyond $x_2 > x_{2\max}$ results in a decrease in n. The capability of formation and dissipitation of the complex with increasing cosolvent concentration x_2 is determined by the parameters a_1 and a_2/a_1. The higher the values of a_1 and a_2/a_1 for a solvent–cosolvent system, the higher are these capabilities. A similar explanation applies for binary systems involving the presence of individual solvent and cosolvent molecules without forming relatively stable complexes. The parameter a_1 is related to the difference $(n_2–n_1)$ between the n's of the mixture according to the additivity rule, whereas the parameter b/a is associated with the deviation from the additivity rule due to the nature of disorder or order in the binary solvent–cosolvent mixture.

Figure 4.9a and b shows the dependence of the above data of the refractive index n of MeOH–H_2O and EtOH–H_2O mixtures at 20 °C, and EtOH–MeOH and 1,2-ethanediol–MeOH mixtures at 25 °C on their corresponding density d. As in Figure 4.8, the original data in Figure 4.9a are from Lide (1996/1997) and Khimenko (1969), and in Figure 4.9b are from Albuquerque et al. (1996). It may be noted that the refractive index n of the MeOH–H_2O and EtOH–H_2O mixtures does not show linear dependence on d but passes through a maximum at a certain d typical of the cosolvent (Figure 4.9). As in the $n(x_2)$ plots of Figure 4.8a, the maxima in these $n(d)$ plots occur at $x_{2\max}$ values of 0.64 and 0.39 mole fractions of methanol and ethanol, respectively. It may be noted that the linear dependence of n on d following from the Gladstone–Dale law is followed only in a narrow d range but the width of this d range for the water cosolvent is larger for methanol than that for ethanol. This trend is similar to that observed in the $n(x_2)$ plots of Figure 8a. The similarity in the trends of the $n(x_2)$ plots with those of the $n(d)$ plots for these systems suggests that the processes involved in these trends are the same. However, in contrast to the nonlinear dependence observed

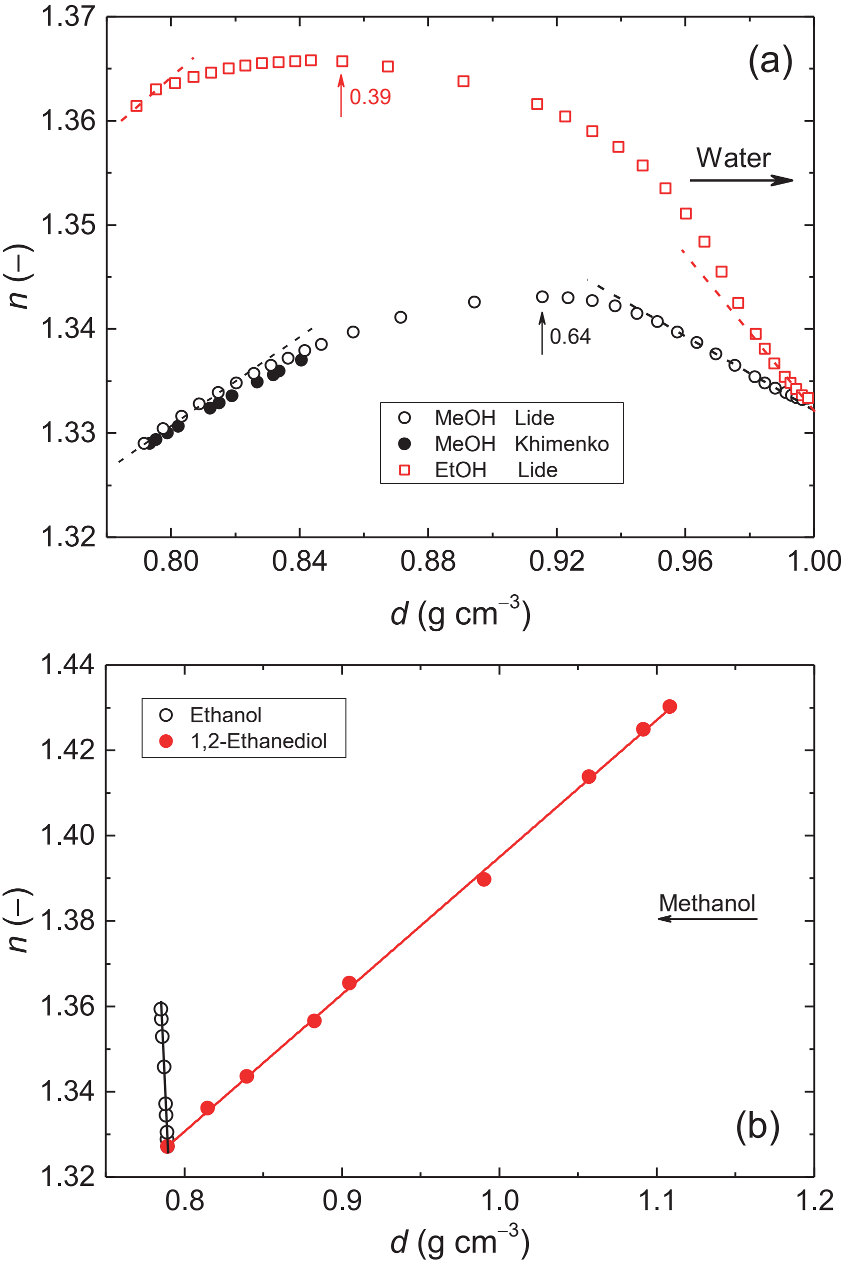

Figure 4.9. Dependences of refractive index *n* of (a) MeOH–H_2O and EtOH–H_2O mixtures at 20 °C, and (b) EtOH–MeOH and 1,2-ethanediol–MeOH mixtures at 25 °C on their corresponding density *d*. Note that *n* does not depend linearly on *d* but passes through a maximum at a certain *d* typical of the alcohol in (a). In (a) densities *d* of mixtures corresponding to their maximum *n* are indicated by arrows. Original data from (a) Lide (1996/1997) and Khimenko (1969), and (b) Albuquerque et al. (1996). See text for detail.

for alcohol–water mixtures in Figure 4.9a, the $n(d)$ data for the EtOH–MeOH and 1,2-ethanediol–MeOH mixtures in Figure 4.9b follow the linear dependence (4.30), with the constants: $n_2 = 7.614$ and $A_2 = -7.965$ cm^3/g for EtOH–MeOH mixtures ($R^2 = 0.9998$), and $n_2 = 1.0733$ and $A_2 = 0.3216$ cm^3/g for 1,2-ethanediol–MeOH mixtures ($R^2 = 0.9993$).

The above trends of the $n(d)$ plots for binary mixtures may be explained qualitatively on the assumption that: (1) both the polarizability α and the molar mass M of a binary mixture may be described by the simple additivity rule, and (2) the polarizability α of molecules of a solvent increases with the molar mass M of the solvent. Then α/M for the mixture may be expressed in the form

$$\frac{\alpha}{M} = \frac{\alpha_1 + (\alpha_2 - \alpha_1)x_2}{M_1 + (M_2 - M_1)x_2} \approx$$

$$\approx \frac{\alpha_1}{M_1}\left[1 + \left\{\left(\frac{\alpha_2 - \alpha_1}{\alpha_1}\right) - \left(\frac{M_2 - M_1}{M_1}\right)\right\}x_2 - \left(\frac{(\alpha_2 - \alpha_1)(M_2 - M_1)}{\alpha_1 M_1}\right)x_2^2\right], \tag{4.38}$$

where subscripts 1 and 2 denote solvent and cosolvent, respectively, and $(\alpha_2 - \alpha_1)/\alpha_1 << 1$ and $(M_2 - M_1)/M_1 << 1$ and are positive quantities. Obviously, depending on the relative contributions of the $(\alpha_2 - \alpha_1)/\alpha_1$ and $(M_2 - M_1)/M_1$ terms for the components of the mixture, the contributions of the x_2 and x_2^2 terms are opposite to each other. The x_2^2 term is small at low values of x_2. Therefore, the value of α/M is expected to decrease as well as increase linearly with an increase in x_2 but the contribution of the x_2^2 terms becomes pronounced at high x_2. When the x_2^2 term is insignificant in Eq. (4.38), from the Gladstone–Dale law one obtains

$$n = 1 + \left(C_1 \frac{\alpha}{M}\right)d = 1 + C_1 \frac{\alpha_1}{M_1}(1 + C_2 x_2)d\,, \tag{4.39}$$

where $C_1 = 2\pi(n^2+2)N_A/3$ and C_2 represents the term in the curly brackets of Eq. (4.38). This relation predicts a linear increase in n with d when $0 < C_2x_2 << 1$, but n decreases with an increase in d when $C_2x_2 < 0$.

Data of deviations in the values of the refractive index n of different solvent mixtures from the additivity rule are frequently analyzed using the traditional Redlich–Kister polynomial relation (Redlich and Kister, 1948)

$$\Delta Y = Y - (x_1 Y_1 + x_2 Y_2) = x_1 x_2 \sum_{i=0}^{j} k_i (x_2 - x_1)^i\,, \tag{4.40}$$

where ΔY denotes the deviation in the experimentally measured refractive index n from the additivity rule, Y_1, Y_2 and Y denote the refractive indices of solvent, cosolvent and mixture, respectively, the concentration $x_2 = (1-x_1)$, i is an integer and k_i's are the so-called interaction coefficients. Data of the dependences of excess refractive index Δn of MeOH–H_2O and EtOH–H_2O mixtures at 20 °C, and of MeOH–EtOH and MeOH–1,2-ethanediol mixtures at 25 °C on cosolvent content x_2 are shown in Figure

4.10a and b, respectively. In Figure 4.10a, the $n(x_2)$ data from Lide (1996/1997) were analyzed. Values of the constants k_i obtained by regression analysis of the $\Delta n(x_2)$ data according to Eq. (4.40) and the goodness-of-the-fit parameter R^2 are given in Table 4.2.

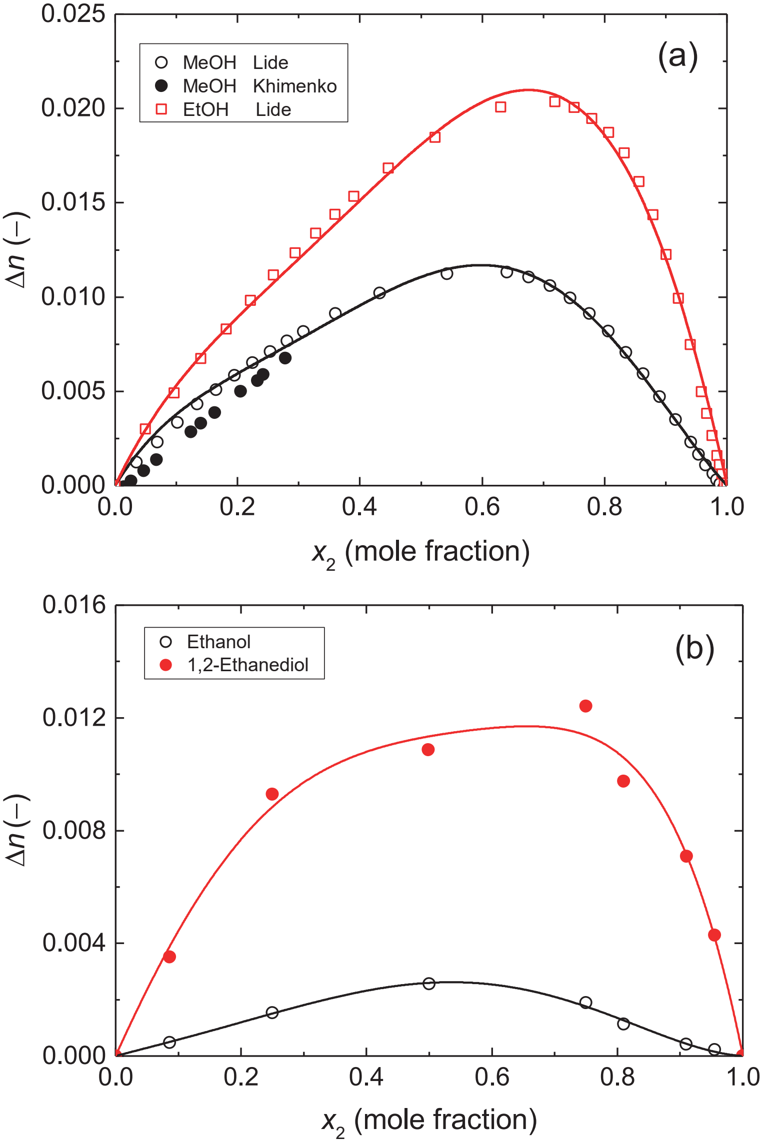

Figure 4.10. Dependences of excess refractive index Δn of (a) $MeOH–H_2O$ and $EtOH–H_2O$ mixtures at 20 °C, and (b) EtOH–MeOH and 1,2-ethanediol–MeOH mixtures at 25 °C on cosolvent content x_2. Note that Δn does not depend linearly on x_2, but passes through a maximum at a certain x_2 typical of the cosolvent. Curves are drawn according to Redlich–Kister relation (4.40) with constants of Table 4.2. Original data in Figure 4.8a and b.

Table 4.2. Values of the constants *k*'s of Eq. (4.40) for $\Delta n(x_2)$ and $\Delta R_M(x_2)$ data

System	k_0	k_1	k_2	k_3	R^2
$\Delta n(x_2)$ data					
Methanol–water	0.04758	0.00991	−0.00785	0.01667	0.9995
Ethanol–water	0.05704	−0.00458	−0.00282	0.04237	0.9993
Ethanol–methanol	0.01039	−0.00250	−0.00675	0.00469	0.9899
1,2-ethanediol–methanol	0.04538	−0.00789	0.03414	−0.02264	0.9780
$\Delta R_M(x_2)$ data					
Methanol–water	−2.2213	−0.04402	0.15464	0.25335	0.9995
Ethanol–water	−0.79435	−0.01199	0.04893	0.12552	0.9997

It may be noted that the maximum relative deviations in Δn are not enormous and are merely 0.9 and 1.6% for MeOH–H_2O and EtOH–H_2O mixtures at 20 °C, respectively. However, the maximum relative deviations $\Delta n/n$ are even much smaller and are 0.15 and 0.9% in the case of EtOH–MeOH and 1,2-ethanediol– MeOH mixtures at 25 °C, respectively. This observation means that the relative deviation in Δn is directly related to the difference in the densities *d* and molar masses *M* of a solvent–cosolvent mixture. The larger the difference in these *d* and *M*, the larger is the value of Δn.

Figure 4.11a and b shows the dependences of molar refraction R_M for MeOH–H_2O and EtOH–H_2O mixtures at 20 °C, and for EtOH–MeOH and 1,2-ethanediol–MeOH mixtures at 25 °C on the cosolvent content x_2, respectively. In contrast to the refractive indices *n* of different solvent mixtures on the content x_2 of cosolvents presented above, the dependence of their molar refractions R_M on cosolvent content x_2 appears to follow the linear relation (see below)

$$R_M = x_1 R_{M1} + x_2 R_{M2} = R_{M1} + (R_{M2} - R_{M1}) x_2 , \tag{4.41}$$

where R_{M1} and R_{M2} are the molar refractions of pure solvents and cosolvents, respectively. This relation is another form of the additivity rule of Eq. (4.20). The slope of the $R_M(x_2)$ plot is determined by the difference (R_{M2}–R_{M1}). The deviations ΔR_M in the values of the observed R_M from those calculated by (4.41) for the above mixtures of the two cosolvents as a function of cosolvent content x_2 are presented in Figure 4.12. The *k* constants of the Redlich–Kister relation (4.40) for alcohol–water mixtures are included in Table 4.2. In view of unusually high deviations ΔR_M for the methanol cosolvent x_2 = 0.5 mole fraction in Figure 4.11b, the *k* values for this cosolvent are not given in the table.

It should be mentioned that the deviation $\Delta R_M < 0$ for both types of solvent mixtures practically in the entire x_2 range, but the change in ΔR_M in the entire x_2 range is relatively small in the case of cosolvent methanol (see Figure 4.12b) in comparison with that in the covalent water (see Figure 4.12a). The maximum relative deviation $\Delta R_M/R_M$ is 0.4% for both alcohol solvents in Figure 4.12a, whereas this deviation is about 0.3% for the two solvents in the methanol content x_2 with the exception of the data at $x_2 = 0.5$ mole fraction (Figure 4.12b). These small relative deviations $\Delta R_M/R_M$ may partly be associated with measurement errors in the *n* and *d* data for the mixtures. In view of these insignificant deviations from the additivity rule, the dependence of R_M on x_2 for the above mixtures may be considered linear.

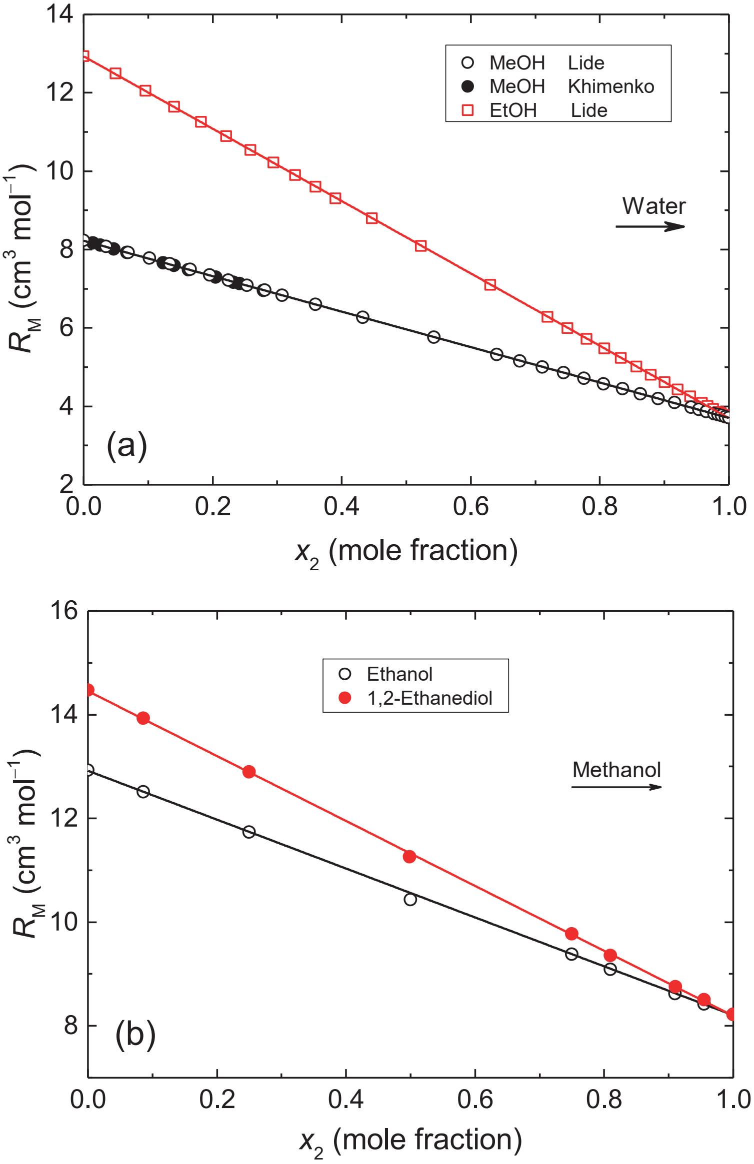

Figure 4.11. Dependences of molar refraction R_M of (a) MeOH–H_2O and EtOH–H_2O mixtures at 20 °C, and (b) EtOH–MeOH and 1,2-ethanediol–MeOH mixtures at 25 °C on cosolvent concentration x_2. Linear dependence is observed in (b), but experimental R_M shows insignificant negative deviation from the additivity rule in (a). Original data from Figure 4.8a and b.

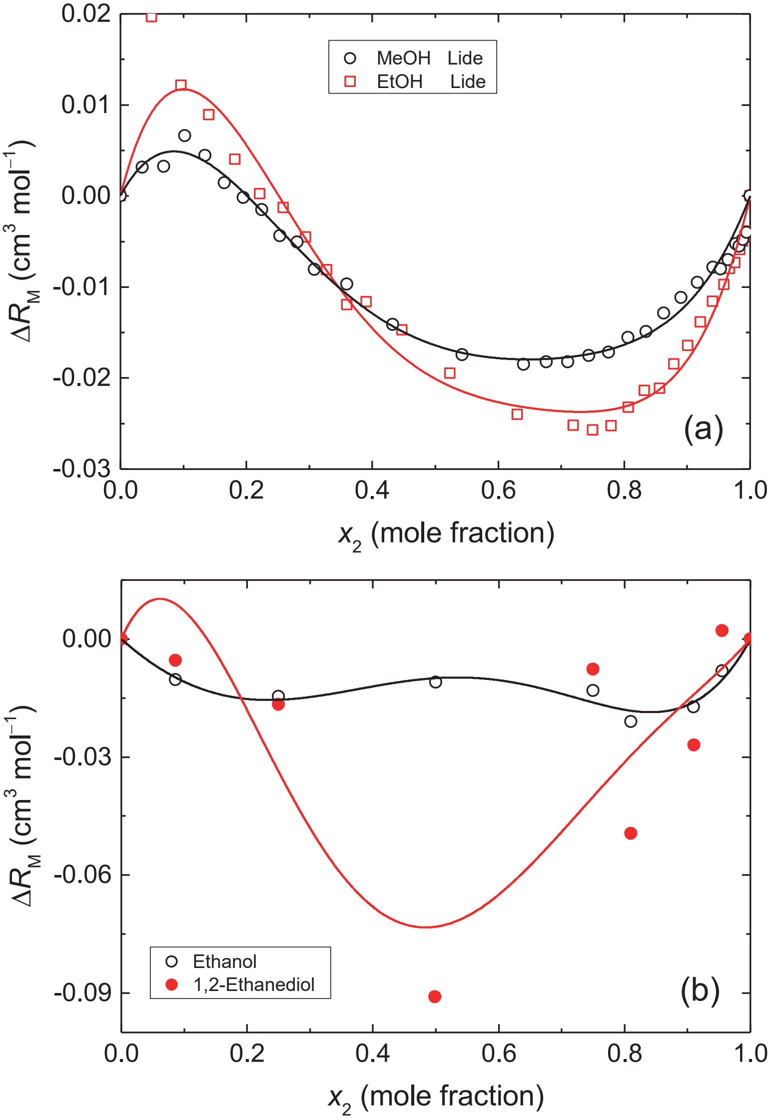

Figure 4.12. Dependences of excess molar refraction ΔR_M of (a) MeOH–H_2O and EtOH–H_2O mixtures at 20 °C, and (b) EtOH–MeOH and 1,2-ethanediol–MeOH mixtures at 25 °C on cosolvent content x_2. Note that ΔR_M does not depend linearly on x_2, but passes through a minimum at $x_2 \approx 0.7$ mole fraction in (a). Plots in (a) represent Redlich–Kister relation (4.40) with constants of Table 4.2.

4.4.2. Temperature dependence of refractive index and molar refraction of solvent mixtures

It is usually observed (Ali et al., 2006; Bahadur et al., 2013; Bajić et al., 2013; Herráez and Belda, 2006; Sharma et al., 2007; Singh et al., 2013; Zhang et al., 2013; Živković et al., 2014) that the refractive index n of pure individual solvents ($x_2 = 0$) as well as solvent–cosolvent mixtures of given cosolvent compositions x_2 decreases with an increasing temperature. For these systems in the temperature range of measurements, the value of n decreases practically linearly with increasing temperature T, following Eq. (4.31). Typical examples representing the dependence of n on temperature T for pure methanol and ethanol and their mixtures containing $x_2 = 0.333$ mole fraction of water are shown in Figure 4.13a. The data are from Herráez and Belda (2006). The plots the figure are drawn with the constants n_3 and A_3 listed in Table 4.3. The intercept n_3 corresponds to the extrapolated value of n at 0 °C.

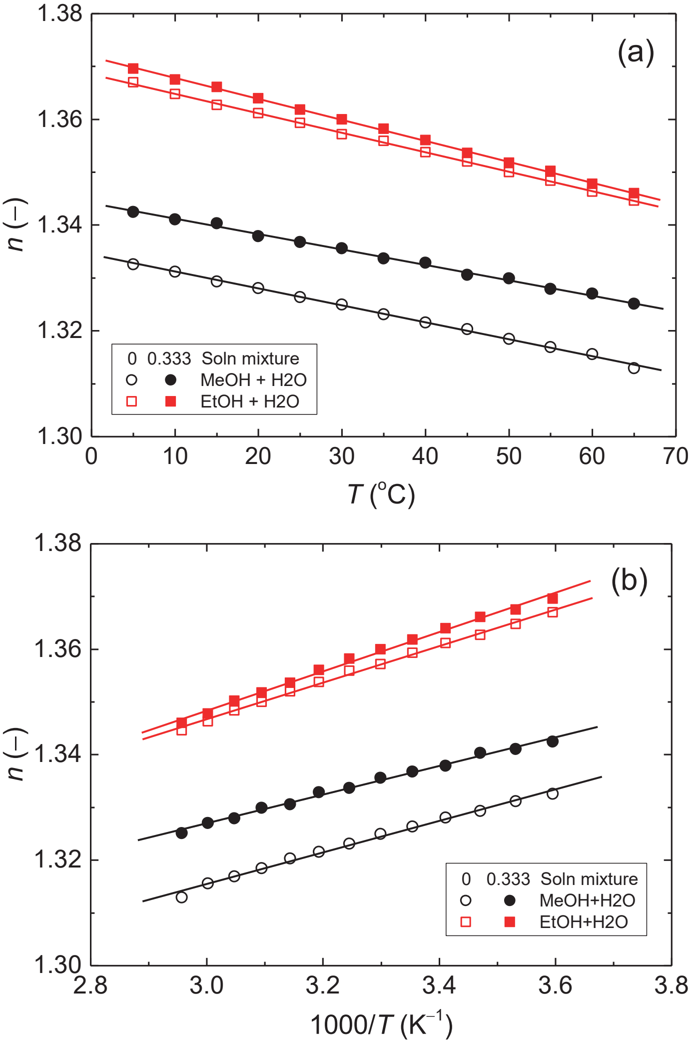

Figure 4.13. Examples representing dependence of (a) refractive indices n of pure methanol and ethanol and their mixtures containing $x_2 = 0.333$ mole fraction of water on temperature T according to Eq. (4.31), and (b) n on T^{-1} according to Eq. (4.42). Linear plots are drawn in (a) and (b) with the constants in Table 2.3. Original data from Herráez and Belda (2006).

Table 4.3. Values of constants of Eqs. (4.31) and (4.42)

Solvent	x_2	Eq. (4.31)			(Eq. (4.42)		
-	(mole frac.)	n_3	$10^4 A_3$ (K^{-1})	R^2	A	$10^5 B$	R^2
MeOH–water	--	1.3344	3.193	0.9978	1.2256	2..996	0.9921
	0.333	1.3441	2.897	0.9965	1.2452	2.724	0.9929
EtOH–water	--	1.3685	3.681	0.9992	1.2426	3.471	0.9967
	0.333	1.3718	3.963	0.9991	1.2366	3.725	0.9942

The value of n for a system is related to the entities responsible for refraction of light. Therefore, it may be expected that a better measure reflecting the nature of these entities in the system would be to analyze the data of the temperature dendence of its molar refraction R_M according to Eq. (4.21). However, due to lack of absence of data on the density d of these substances corresponding to the temperatures of measurement of their n, an alternative procedure is to analyze the $n(T)$ data according to the empirical relation

$$n = A + \frac{B}{T}, \tag{4.42}$$

where the intercept A and the slope B are obtained from the plots of n against T^{-1}. The parameter A corresponds to the value of n when $T \to \infty$. The usefulness of this relation is associated with the fact that in the investigated temperature range the molar refraction $R_M = (n^2-1)M/(n^2+2)d \approx \lambda n$, where the proportionality constant λ is practically a constant for a system. The value of λ is 2.78, 6.17 and 9.48 for water, methnol and ethanol, respectively. Figure 4.13b shows the $n(T)$ data of Figure 4.13a as plots of n against T^{-1} according to Eq. (4.42), with the parameters A and B included in Table 4.3.

From Table 4.3 one notes differences in the values of n_3 and A and A_3 and B due to differences in the temperature units. Irrespective of these differences, the values of n_3 for the slope A_3 of the $n(T)$ data for alcohols and their mixtures with 0.333 mole fraction of water suggest that the addition of cosolvent water to methanol leads to a decrease in the value of the parameter A_3 but its addition to ethanol increases it. Similar trends may be observed from the values of A and B. These trends are due to differences in the values of the polarizability α and the dielectric constant μ of these two solvents and their mixtures with water (cf. Eq. (4.21)).

4.5. Refractive index and molar refraction of solutions

4.5.1. Some general trends

The refractive index n and the molar refraction R_M of solutions of different solutes in different solvents at a constant temperature strongly depend on their concentration (Ali et al., 2006; Durou et al., 1973; Frej et al., 1998; Fucaloro et al., 2007; Szewczyk and Sangwal, 1988). It is observed that the dependence of n of the solution on solute concentration c_2 (mole·L^{-1}) usually follows quadratic relation (4.37) or its linear form with the constant $a_2 = 0$ (Durou et al., 1973; Frej et al., 1998; Fucaloro et al., 2007; Szewczyk and Sangwal, 1988), whereas the dependence of R_M on c_2 usually follows the linear dependence (4.41) (Ali et al., 2006; Chandami et al., 2016).

Here some general trends of the refractive index n and the molar refraction R_M of solutions as a function of the solute concentration are described. For this purpose, aqueous solutions of two inorganic compounds, NaCl and KCl, and two organic compounds, sucrose and D-glucose, are taken as examples. These four compounds are fairly soluble in water. Basic information on the molar mass M, density d and refractive index n_s of these compounds in the solid state is given in Table 4.4. The n_s values refer to wavelength 489.3 nm of yellow sodium line. The original data for the aqueous solutions at 20 °C are taken from Lide (1996/1997). In view of the unknown value of n_s for D-glucose, it was assumed that its value is similar to that for sucrose. The values of molar volume V_{Ms} and the Gladstone–Dale law parameter $(n_s–1)/d_s$ calculated from these data for the compounds are also listed in Table 4.4.

Table 4.4. Basic information of compounds

Compound	M	d_s (g·cm^{-3})	n_s	V_{Ms} (cm^3·mol^{-1})	$(n_s–1)/d_s$ (cm^3·g^{-1})
Water	18.0	0.9982^a	1.3333	18.03	0.3339
NaCl	58.443	2.17	1.5441	26.93	0.2507
KCl	74.551	1.988	1.4903	37.50	0.2466
Sucrose	342.296	1.587	1.5376	215.69	0.3387
D-glucose	180.156	1.54	1.5376	116.98	0.3491

^{a} 20 °C

It was observed that the dependence of refractive index n of aqueous solutions of NaCl and KCl, and sucrose and D-glucose on their concentration c_2 (mole·L^{-1}) in the solutions at 20 °C may indeed be represented satisfactorily by Eq. (4.37). The slope of the $n(c_2)$ plots slowly increases with increasing c_2 in all of the four solutions, but this trend is better observed in the case of sucrose and D-glucose. In the case of aqueous NaCl and KCl solutions, the fit of the data was also observed to be reasonabe with a linear dependence (with $b = 0$). For solutions concentration $c_2 = 1$ mole·L^{-1}, the estimated values of the refractive index $n_{\max}$ from the quadratic relation are: 1.5276, 1.4932, 1.5441 and 1.5345 for NaCl, KCl, sucrose and D-glucose, respectively. With the exception of NaCl solutions where $n_{\max} < n_s$ by 1%, the values of $n_{\max}$ are in good agreement with the estimated values of n_s for KCl and sucrose solutions. Since in solvent water Na$^+$ ions are known as structure makers whereas K$^+$ and Cl$^-$ ions have negligible effect on water structure, the above trends in $n_{\max}$ and n_s are associated with the solvation characteristics of these solutes in water.

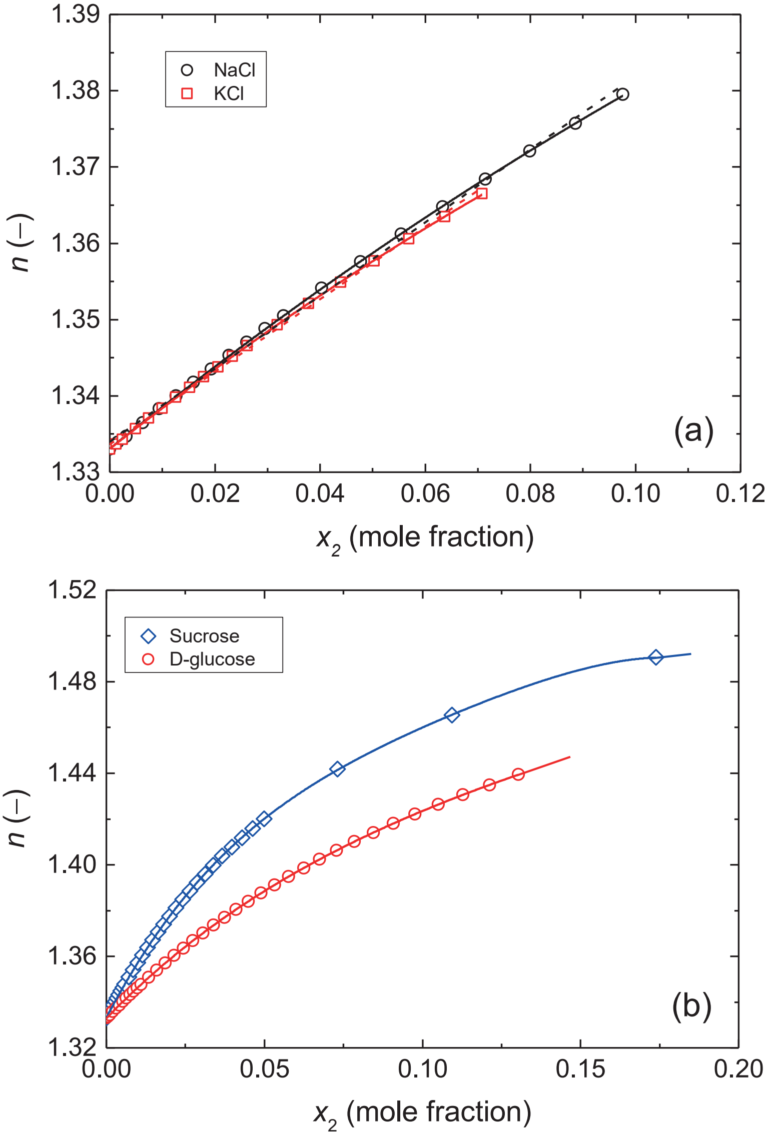

Figure 4.14. Dependence of refractive index n of aqueous solutions of (a) NaCl and KCl, and (b) sucrose and D-glucose on their content x_2 in the solutions at 20 °C. Note that the slope of the $n(x_2)$ plots slowly increases with increasing solute x_2 in these solutions. Best-fit constants of Eq. (4.37) are given in Table 4.5. Original data from Lide (1996/1997).

The $n(c_2)$ data for different solution systems may be analyzed with reference to the concentration c_2 expressed in solute mole fraction x_2. Figure 4.14a and b shows the dependence of refractive index n of aqueous solutions of NaCl and KCl, and sucrose and D-glucose on their x_2 in the solutions at 20 °C. It was found that the $n(x_2)$ data for these solutions may indeed be represented satisfactorily by the polynomial form of Eq. (4.37), with $i = 2$ for NaCl and KCl solutions and $i = 4$ for sucrose and D-glucose solutions. The best-fit plots of the data are drawn according to Eq. (4.37) with the constants listed in Table 4.5. The dashed lines in Figure 14a represent the fit of the $n(x_2)$ data for NaCl and KCl solutions according to the linear dependence with the parameters included in the table.

Table 4.5. Values of the constants of Eq. (4.37) for $n(x_2)$ data of Fig. 4.14

System	n_0	a_1	a_2	a_3	a_4	R^2
NaCl	1.33309	0.55325	−0.81261			0.99998
	1.33298	0.47927				0.99792
KCl	1.33307	0.54234	−1.01688			0.99996
	1.33367	0.47510				0.99818
Sucrose	1.33317	2.64504	−23.90816	130.4749	−290.522	0.99999
D-glucose	1.33298	1.42055	−7.50684	28.59685	−50.41285	1

It may be noted from Table 4.5 that the fit of the $n(x_2)$ data for NaCl and KCl solutions according to the linear dependence deteriorates in comprison with that from the quadratic relation. However, in the range of low x_2 for the solutes, the parameter a_1 increases in the sequence: KCl < NaCl < D-glucose < sucrose. This trend is similar to that followed by the Gladstone–Dale law parameter $(n_s-1)/d_s$, and suggests that the dependence of n on x_2 at low x_2 is intimately related to their solid-state molar volume V_{Ms}, but the trend for NaCl and KCl is reversed.

Figure 4.15a and b shows the relationship between the refractive index n of aqueous solutions of NaCl and KCl and of sucrose and D-glucose and their density d at 20 °C. the original data are taken from Lide (1996/1997). The $n(d)$ data for the four solution systems may be described satisfactorily by linear relation (4.30), with the best-fit constants given in Table 4.6.

From Table 4.6 the following features may be noted:

(1) As expected from Eq. (4.30), the calculated refractive index n_2^* of water corresponds to $d = 0.9982$ g·cm^{-3} for different systems.
(2) The constants n_2 and A_2 of Eq. (4.30) are inversely related. The higher the value of A_2, the lower is the value of n_2. The parameter A_2 increases in the sequence: KCl < NaCl < D-glucose ≈ sucrose. This observation again suggests that n is related to the molar volume V_{Ms} of the solutes.
(3) For the aqueous solutions considered here, a value of $A_2 = 0.33$ cm^3·g^{-1} corresponds to $n_2 = 1$ of the Gladstone–Dale law. However, the Gladstone–Dale law parameter $(n_s-1)/d_s > A_2$ for NaCl and KCl solutions but $(n_s-1)/d_s < A_2$ for sucrose and D-glucose solutions. This implies that the difference (n_2-1) for different solution systems in a solvent is determined by the nature of the properties of the dissolved solute in it.
(4) For the two groups of the compounds the value of n_2 for each group is related to their solid state density d_s.

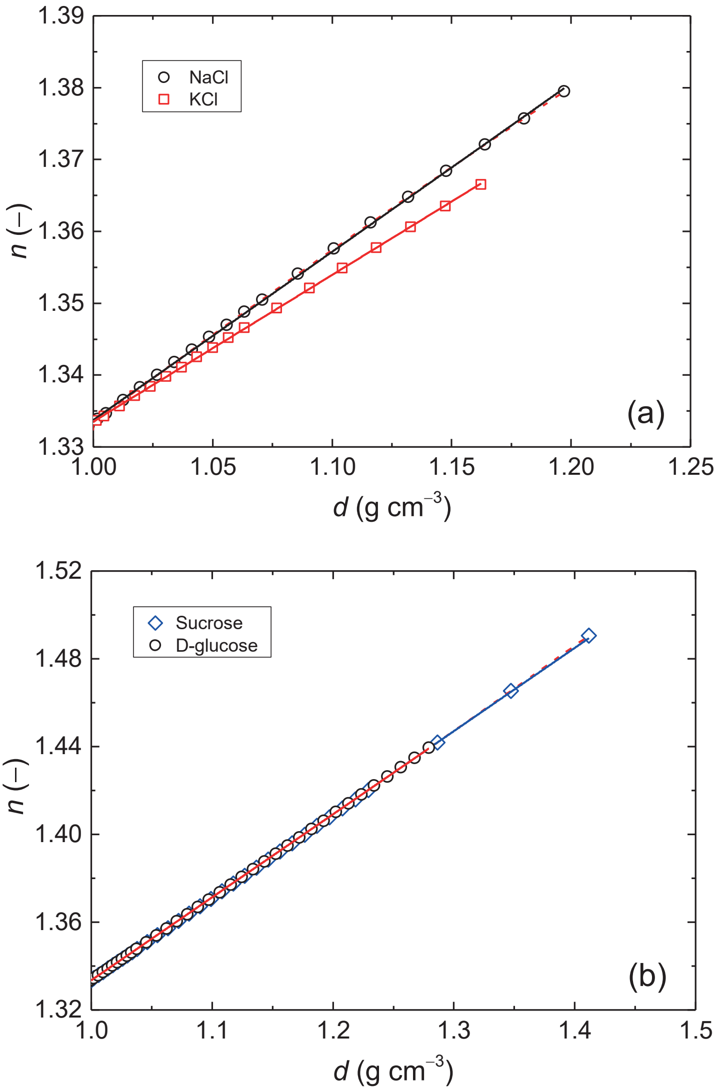

Figure 4.15. Dependence of refractive index n of aqueous solutions of (a) NaCl and KCl, and (b) sucrose and D-glucose on their density d at 20 °C. Note linear dependence of n on d for these systems according to Eq. (4.30) with the constant listed in Table 4.6. Original data from Lide (1996/1997).

Table 4.6. Values of the constants of Eq. (4.30) for $n(d)$ data

System	n_2	A_2 ($\mathrm{cm^3{\cdot}g^{-1}}$)	n_2^*	d ($\mathrm{g{\cdot}cm^{-3}}$)	R^2
NaCl	1.09949	0.23425	1.33323	2.17	0.99975
KCl	1.12936	0.20416	1.33315	1.988	0.99989
Sucrose	0.95415	0.37915	1.33262	1.587	0.99993
D-glucose	0.95532	0.37819	1.33283	1.540	0.99999

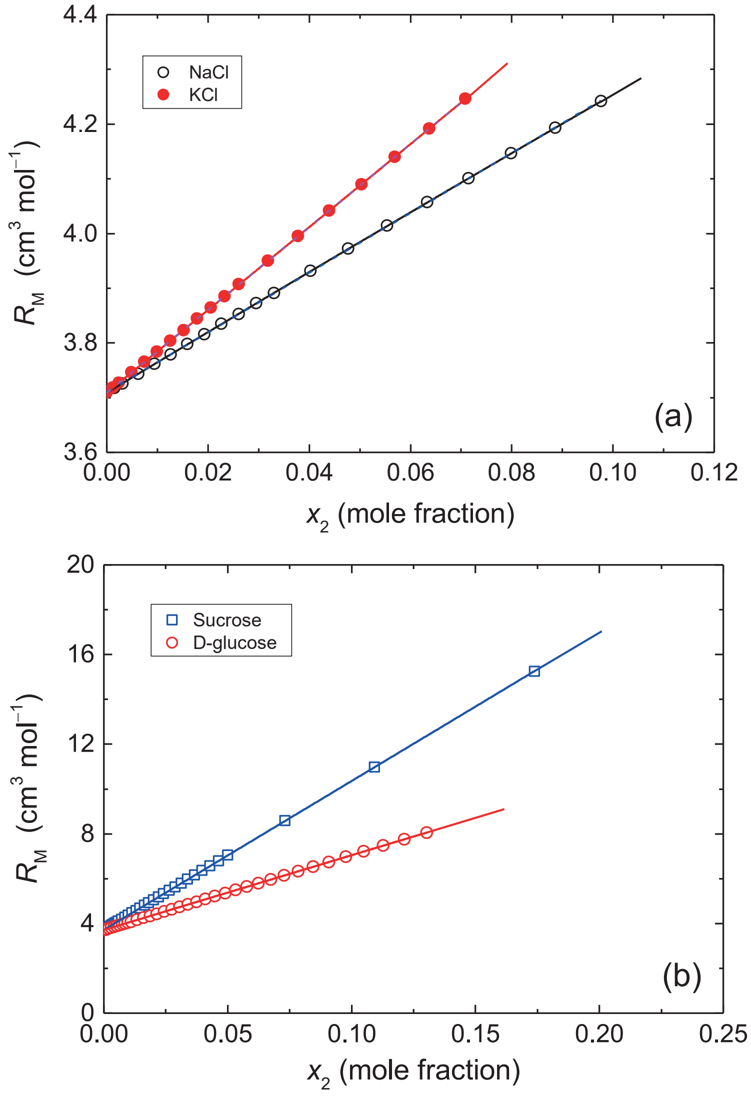

Figure 4.16. Dependence of molar refraction R_M of aqueous solutions of (a) NaCl and KCl and (b) sucrose and D-glucose on solute concentration x_2 at 20 °C. Plots are drawn according to Eq. (4.37) with the best-fit values of constants listed in Table 4.7.

Figure 4.16a and b presents the data of the molar refraction R_M of aqueous solutions of NaCl and KCl and of sucrose and D-glucose on the solute concentration x_2, respectively. As in the case of the $n(x_2)$ data, the $R_M(x_2)$ data may be presented by a quadratic relation similar to (4.37), with the corresponding best-fit constants R_{M0}, a_{M1} and a_{M2} for the $R_M(x_2)$ data. However, in the case of aqueous sucrose and D-glucose solutions, the data are better represented by the linear dependence (with $a_{M2} = 0$) similar to Eq. (4.41) used for solvent–constant mixtures. The best-fit values of the constants according to Eq. (4.37) with R_{M0}, a_{M1} and a_{M2} as well as with a_{M1} alone are listed in Table 4.7.

Using the values of the constants of Eq. (4.37) for the $R_M(x_2)$ data, values of the molar refraction $R_{M2} = (a_{M1}+R_{M1})$ corresponding to the solute concentration $x_2 = 1$ may be calculated. These values of R_{M2} and the values of the solid-state molar refraction R_{Ms} from the n_s, d_s and M_s data of Table 4.4 are also given in Table 4.7. From this table it may be seen that the values of R_{M2} obtained from the constants of the linear dependence are somewhat higher than those from the constants of the quadratic dependence. The trends of the values of n_{max} and R_{M2}, and somewhat higher goodness-of-the-fit parameter R^2 (see Tables 4.5 and 4.7), indicate that the quadratic dependence is more realistic in reproducing the $n(x_2)$ and $R_M(x_2)$ data of solutions of these two types of solutes. However, similar values of R_{M0} obtained for these solutes by using the linear dependence suggests that this linear relationship also cannot be ignored entirely.

Table 4.7. Values of the constants of Eq. (4.37) for $R_M(x_2)$ data

System	R_{M0} ($cm^3 \cdot mol^{-1}$)	a_{M1} ($cm^3 \cdot mol^{-1}$)	$-a_{M2}$ ($cm^3 \cdot mol^{-1}$)	R^2	R_{M2} ($cm^3 \cdot mol^{-1}$)	R_{Ms} ($cm^3 \cdot mol^{-1}$)
NaCl	3.7090	5.5594	1.0763	1	8.192	8.50
	3.7102	5.4614		0.9999	9.172	
KCl	3.7091	7.5477	0.4439	1	10.813	10.85
	3.7088	7.5771		1	11.286	
Sucrose	3.7153	66.4273		0.9999	70.143	67.42
D-glucose	3.7125	33.3501		1	37.063	36.57

From Table 4.7 it may be noted that the parameter a_{M1} and the molar refraction R_{Mmax} of a solute in their solutions changes in the order: NaCl < KCl < D-glucose < sucrose. This order is the same as the order of their molar refraction R_{Ms} in the solid state. This observation implies that the values of a_{M1} and R_{M2} for the solutions of these solutes are related to the molar volumes V_{Ms}. One observes that $R_{M2} = \pi V_{Ms}$ for all solutions. This means that the term $(n^2-1)/(n^2+2)$ for these solutes is constant (see Eq. (4.21)). Since $R_{M2} \approx R_{Ms}$, it may be concluded that ions and molecules of solutes are the refracting entities in the solutions. In electrolytes like NaCl and KCl, both cations and anions contribute to R_{M2}. From the individual contributions of cations and anions to R_{M2}, the polarizabilities α_+ and α_- of the ions may be determined using Eq. (4.22).

The value of R_{Mmax} of a solute obtained from the linear dependence of the $R_M(x_2)$ data is somewhat higher than its R_{Ms}. This observation is associated with small deviations in the observed R_M from the predicted values by the additivity rule. Assuming that the maximum refractive index n_{max} of a solute and the refractive index n_0 of the solvent of its solution, and the corresponding maximum molar refraction R_{Mmax} and the molar refraction R_{M0}, follow additivity rule, the excess refractive index Δn and the excess molar refraction ΔR_M were calculated for the different systems. Figure 4.17a and b shows the $\Delta n(x_2)$ and $\Delta R_M(x_2)$ data for these systems, respectively. The trends of these $\Delta n(x_2)$ and $\Delta R_M(x_2)$ data show that there is a solute concentration x_2^* when the deviations Δn and ΔR_M for a solute attain maximum values.

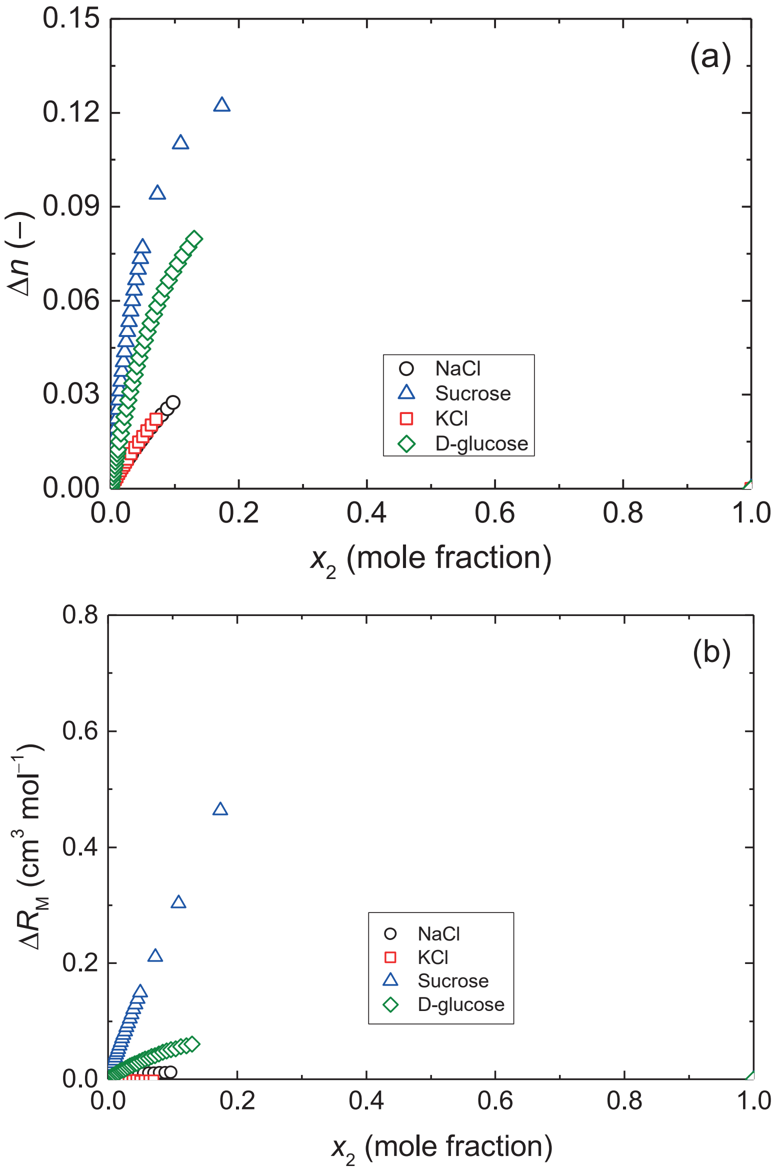

Figure 4.17. Dependence of (a) excess refractive index Δn and (b) excess molar refraction ΔR_M of aqueous solutions of different solutes on their content x_2 in the solutions at 20 °C. Original data from Lide (1996/1997).

4.5.2. Dependence of refractive index and molar refraction of solutions on their temperature

As in the case of solvents, refractive indices of solutions of known concentrations show noticeable decrease with an increase in temperature and are observed to follow quadratic relation (Szewczyk and Sangwal, 1988)

$$n = n_3 - A_3T - B_3T^2, \tag{4.43}$$

where n_3, A_3 and B_3 are constants characteristic of the concentration x_2 of the solute in the solution. The value of the constant n_3 corresponds to $T = 0$ and depends on the unit of temperature, whereas $A_3 >> B_3$. It is observed (Szewczyk and Sangwal, 1988) that the values of n_3 and A_3 increase whereas that of B_3 decreases with an increase in solute concentration x_2. In many cases, especially in solutions containing high solute concentrations, the B_3 term is very small and may be neglected. Then Eq. (4.43) reduces to relation (4.31).

In this section the trends of the temperature dependence of the refractive index and the molar refraction of solutions are discussed taking the experimental $n(T)$ data on aqueous solutions of ammonium oxalate ($(NH_4)_2CO_2$; abbreviated as AO) and $LiIO_3$ as examples. Figure 4.18 shows the $n(T)$ data for water, and aqueous solutions of ammonium oxalate and lithium iodate of selected concentrations x_2 on their temperature T. The original data for water, ammonium oxalate and lithium iodate from Lide (1996/1997), Frej et al. (1998) and Szewczyk and Sangwal (1988), respectively. The $n(T)$ data may be represented according to empirical dependence (4.31), with the constants listed in Table 4.8.

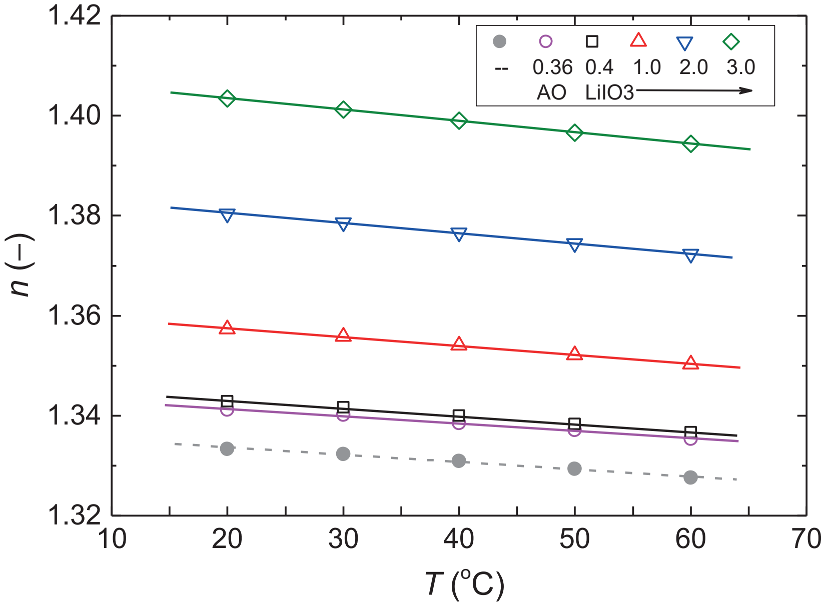

Figure 4.18. Dependence of refractive index n of water, and aqueous solutions of ammonium oxalate and lithium iodate of selected concentrations on their temperature T. Linear plots are drawn with constants listed in Table 4.8. Concentration in the inset in mol·L^{-1}. Original data for water, ammonium oxalate and lithium iodate from Lide (1996/1997), Frej et al. (1998) and Szewczyk and Sangwal (1988), respectively.

Table 4.8. Values of constants of Eq. (4.31) for $n(T)$ data

System	10^2x_2 (mole fraction)	n_3	10^4A_3 ($^{\circ}C^{-1}$)	R^2
Water	--	1.3365	1.451	0.9868
AO-water	0.661	1.3444	1.473	0.9912
$LiIO_3$-water	0.724	1.3462	1.578	0.9954
	1.821	1.3610	1.770	0.9976
	3.692	1.3847	2.035	0.9979
	5.632	1.4080	2.273	0.9998

As mentioned above, the values of constants n_3 and A_3 obtained from the $n(x_2)$ data for $LiIO_3$ solutions increase with solute concentration x_2 whereas their values differ for $LiIO_3$ and AO solutions of comparable concentrations x_2. However, in view of the empirical nature of the constants n_3 and A_3 of Eq. (4.43) to describe the $n(x_2)$ data, the observed trends of their increase with x_2 do not provide useful information about the nature of entities involved in refraction.

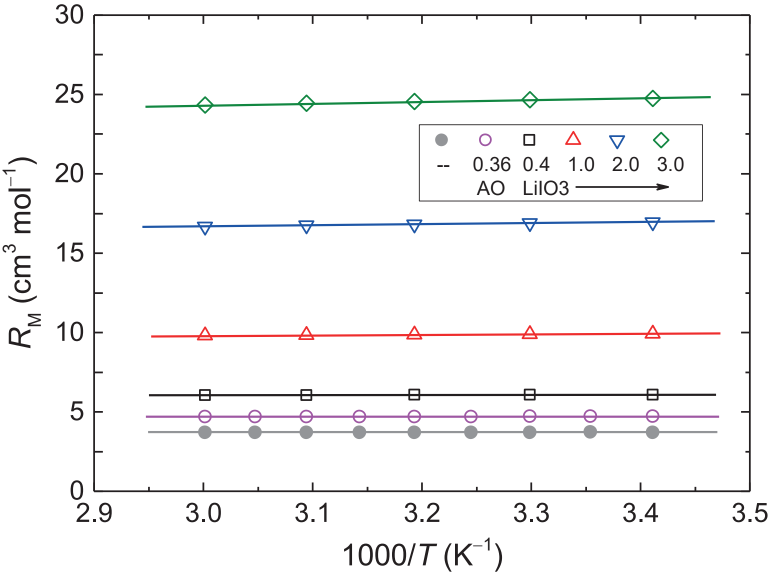

Figure 4.19. Data of molar refraction R_M of water, and aqueous solutions of ammonium oxalate and lithium iodate of selected concentrations x_2 on $1/T$ according to relation (4.21), with constants R_{M0}^* and R_{M1}^* given in Table 4.9. Concentration in the inset in mol·L^{-1}.

As in the case of normal alcohols and their mixtures, the temperature dependence of molar refraction R_M of water, and aqueous solutions of ammonium oxalate and lithium iodate of selected concentrations x_2 also follow linear relation (4.34). Figure 4.19 shows the data of molar refraction R_M of water, and aqueous solutions of ammonium oxalate and lithium iodate of selected concentrations x_2 on $1/T$, according to Eq. (4.21), with the best-fit constants R_M^* and A^* of the linear plots given in Table

4.9. The calculated values of the polarzability α and the dipole moment parameter μ^2/k_B of the particles in the substances are shown as a function of solute concentration x_2 in Figure 4.20.

Table 4.9. Values of the constants of Eq. (4.21) for $R_M(T)$ data

System	10^2x_2 (mole frac.)	R_{M0}^* (cm^3·mol^{-1})	$10^{24}\alpha$ (cm^3)	$10^3R_{M1}^*$ (cm^3·mol^{-1}·K)	μ (D)	R^2
Water	--	3.632	1.436	0.024	1.79	0.3402
AO-water	0.66	4.552	1.80	0.047	2.50	0.9432
$LiIO_3$-water	0.724	5.734	2.267	0.104	3.71	0.9945
	1.821	8.958	3.542	0.285	6.13	0.9944
	3.692	14.780	5.844	0.641	9.19	0.9920
	5.632	21.123	8.352	1.070	11.87	0.9967

From Figure 4.20 one finds that the polarizability α and the dipole moment parameter μ^2/k_B of the particles in aqueous solutions increase linearly with solute concentration x_2 and that the values of both α and μ^2/k_B depend on the dissolved solute in the solvent. The values of α and μ are also included in Table 4.9. Assuming that $\alpha = r^3$, their radius r increases from 0.113 nm for water to 0.203 nm for the highest $x_2 = 0.0563$ mole fraction of aqueous $LiIO_3$ solution. The dipole moment μ of the particles also behaves in a similar manner. The value of μ for water agrees well with the value given in the literature whereas the highest value for aqueous $LiIO_3$ solutions is comparable with the values of salts in the solid state (for example, see Lide, 1996-1997).

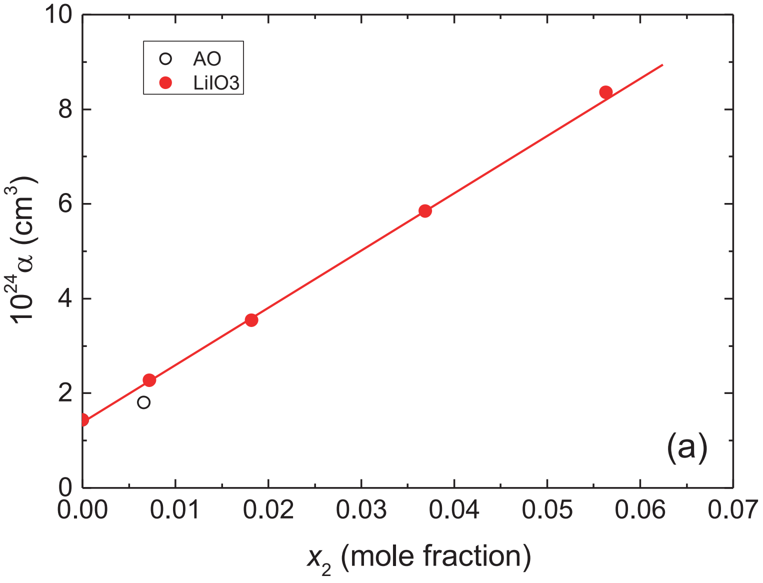

(Continued)

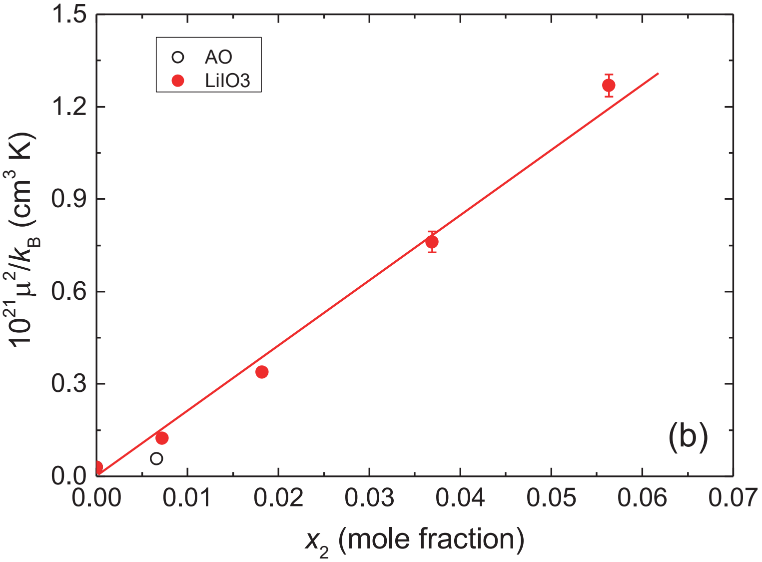

Figure 4.20. Plots of (a) polarizability α and (b) dipole moment parameter μ^2/k_B of Eq. (4.22) against solute concentration x_2. Both dependences are linear.

4.6. Böttcher's relation for analysis of refractive index data of binary systems

As mentioned in Section 4.2, Lorentz–Lorenz relation does not give information on size and polarization of molecules in pure liquids and ions in solutions at a given temperature. However, Böttcher's formula enables to deduce these parameters from the plot of $1/\alpha^*$ against $2(n^2-1)/(2n^2+1)$.

The dependence of $1/\alpha^*$ on $2(n^2-1)/(2n^2+1)$ holds both for pure substances as well as for mixtures of substances. In the case of pure substances, their temperature or pressure is changed but in the case of mixtures it is their concentration. For pure liquids, $1/\alpha^* = 12\pi n^2 N_A/(n^2-1)(2n^2+1)$. Therefore, plot of $12\pi n^2/(n^2-1)(2n^2+1)$ against $2(n^2-1)/(2n^2+1)$ is expected to yield a straight line with slope $1/r^3$ and intercept $1/\alpha$. In the case of mixtures of substances, the values of $1/\alpha_k^*$ for given particles (molecules or ion) in the solution can be calculated from Eq. (4.24), provided that the polarizabilities and radii of all other species (ions of an electrolyte and molecules of the liquid) are known. From the linear part of the plot, α and r may be calculated.

Böttcher's method has been verified for a number of materials, which serve as examples of calculations of the polarizability and radius of water molecules, carbon tetrachloride molecules and several ions from solutions. Figure 4.21 illustrates an example of the dependence of $1/\alpha^*$ on $2(n^2-1)/(2n^2+1)$ for MeOH with increasing water content in the mixture of water content below 0.18 wt fraction. This example is taken from Khimenko (1969), where the density of methanol–water mixture was changed by increasing the water content. It may be seen that the dependence is linear.

For the methanol molecules, this plot gives their polarizability $\alpha = 0.030$ nm^3 and radius $r = 0.195$ nm.

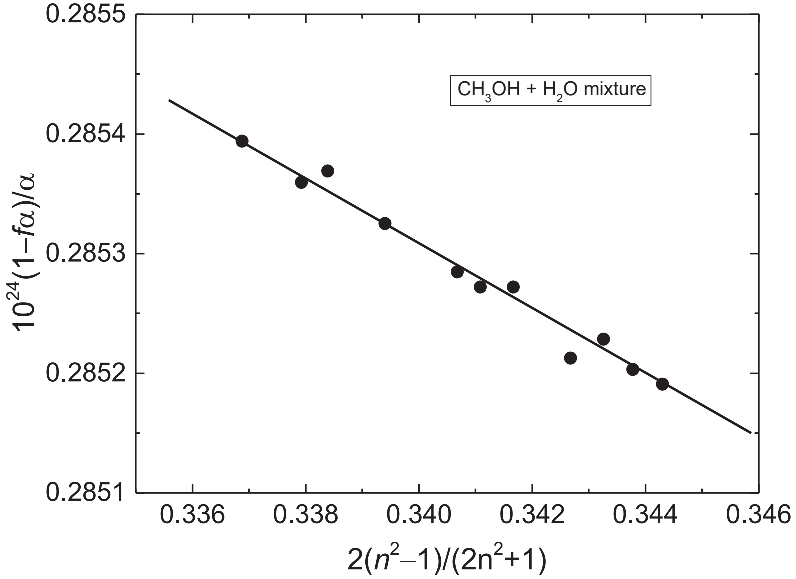

Figure 4.21. Dependence of $1/\alpha^*$ on $2(n^2-1)/(2n^2+1)$ for MeOH with increasing water content in the mixture of water content below 18 wt%. Direction of increasing water content is indicated by arrow. Adapted from Khimenko (1969).

Figure 4.22a and b presents two other examples of the plots of $1/\alpha^*$ against $2(n^2-1)/(2n^2+1)$ for aqueous NaCl and $[(C_2H_5)4N]I$ solutions, respectively, containing different concentrations of CH_3OH in the solvent water. It may be seen from the plots that there is a steep decrease in $1/\alpha^*$ initially, but at higher concentrations a well-defined linear dependence may be distinguished. Addition of CH_3OH to the solvent leads to the steep decrease at a higher concentration, but at still higher concentrations the curve joins the curve for pure water. From the linear parts of the curves, the polarizabilities and radii of Cl^- and $[(C_2H_5)_4N]^+$ ions may be estimated to be $\alpha = 0.0276$ nm^3 and $r = 0.164$ nm, and $\alpha = 0.135$ nm^3 and $r = 0.277$ nm, respectively. These estimated values of r are roughly equal to the crystallographic radii of these ions.

Böttcher's method is based on the assumption that an ion or a molecule has a fixed r which is independent of density d (i.e. temperature and concentration), and that r is equal to the size of an ion or a molecule. Referring back to the plots of Figures 4.21 and 4.22, one finds that in the nonlinear part of the curve (i.e. at low concentrations) r is zero initially, but its value increases with an increase in the salt concentration until the linear part where r approaches the crystallographical radius of the ion.

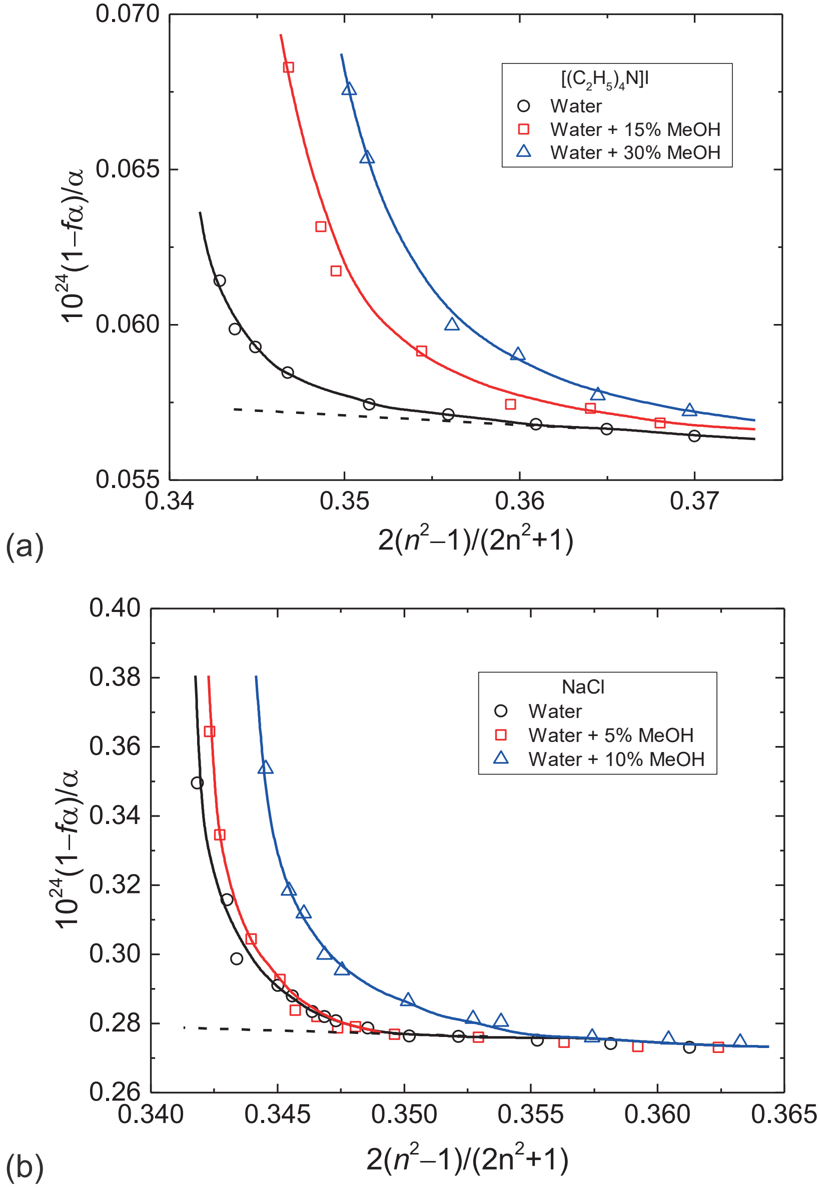

Figure 4.22. Dependence of $1/\alpha^*$ on $2(n^2-1)/(2n^2+1)$ for (a) aqueous NaCl solutions and (b) aqueous [(C$_2$H$_5$)$_4$N]I solutions containing two different MeOH content. Direction of increasing solute concentration is indicated by arrow. Adapted from Khimenko (1969).

In the lattice-based models of liquids and electrolytes the size of vacancies and holes is roughly the size of molecules and ions composing them. The applicability of Böttcher's formula to liquids and concentrated solutions provides a connection between refractive index and structure of liquids and solutions.

4.7. Refractive index of saturated, undersaturated and supersaturated solutions

The dependence of the refractive index *n* of saturated solutions on their temperature may also be expressed by relation (4.43) and usually the constants A_3 and B_3 are positive for fairly and highly soluble salts and $A_3 >> B_3$ (Szewczyk et al., 1985).

Refractive index of solutions saturated at particular temperatures is a linear function of temperature around saturation points in undersaturated and supersaturated regions, and is represented by Eq. (4.31). However, there are experimental results (Akhutin et al., 1964) which show that there are breaks at saturation points in the $n(t)$ plots for aqueous solutions of electrolytes. Figure 4.23 shows, as an example, the temperature dependence of refractive index *n* of aqueous NaI solutions of two different saturation concentrations. Dashed line in the figure shows saturation concentrations. However, no discontinuities were found in other cases (Böttcher and Bordewijk, 1978; Karniewicz et al., 1982; Szewczyk et al., 1985). The former observations indicate structural reorganization of species present in solution at saturation points, while the latter ones imply that the nature of species present in the undersaturated and supersaturated regions is the same.

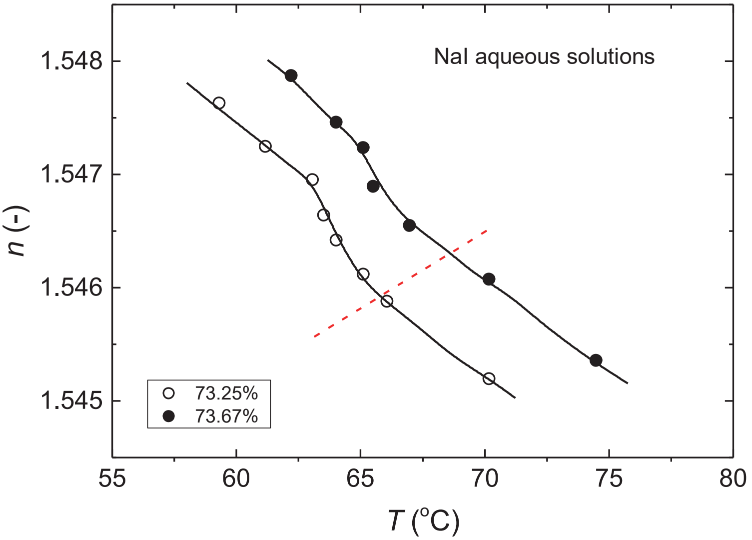

Figure 4.23. Temperature dependence of refractive index *n* of aqueous NaI solutions of two different saturation concentrations. Dashed line shows saturation concentrations. Adapted from Akhutin et al. (1964).

Akhutin et al. (1964) plotted the refractive index data for different salts in aqueous solutions, according to Böttcher's formula, Eq. (4.19). Their plots showed that the values of slope $M/N_A r^3$ are usually greater in the undersaturated region than those in the supersaturated region, whereas the intercept $M/N_A\alpha$ in the undersaturated region is smaller than that in the supersaturated region. This means that the size r of species is smaller in the undersaturated region than that in the supersaturated region, while their polarizability α is greater in the undersaturated region. If one considers the possible association of ions with increasing concentration, it is expected that the size r and the polarizability α of species increase in the supersaturated region in agreement with the results reported by Akhutin et al. (1964). However, judging from the available experimental data the question of structural reorganization at saturation point of electrolyte solutions is unsettled.

References

Akhutin, A.V., T.A. Komarova, and N.A. Figurovskii (1964). Refractrometric investigation of supersaturated solutions of electrolytes. *Zh. Fiz. Khimii* **38**, 387-395 (in Russian).

Albuquerque, L., C. Ventura, and R. Goncalves (1996). Refractive indices, densities, and excess properties for binary mixtures containing methanol, ethanol, 1,2-ethanediol, and 2-methoxyethanol. *J. Chem. Eng. Data* **41**, 685-688.

Ali, A., S. Hyder, S. Sabir, D. Chand, and A.K. Nain (2006). Volumetric, viscometric, and refractive index behaviour of α-amino acids and their groups' contribution in adqueous D-glucose solution at different temperatures. *J. Chem. Thermodyn.* **38**, 136-143.

Bahadur, I., N. Deenadayalu, P. Naidoo, and D. Ramugernath (2013). Density, speed of sound, and refractive index measurements for the binary systems (butanoic acid + propanioc acid, or 2-methyl-propionic acid) at T = (293.15 to 313.15) K. *J. Chem. Thermodyn.* **57**, 203-211.

Balić, D.M., G.R. Ivaniš, Z.P. Visak, E.M. Živković, S.P. Šerbanović, and M.Lj.. Kijevčanin (2013). Densities, viscosities and refractive indices of the binary systems (PEG200 +1,2-propanediol, +1,3-propanediol) and (PEG400 + 1,2-propanediol, +1,3-propanediol) at T = (288.15 to 333.15) K and atmospheric pressure: Measurements and modeling. *J. Chem. Thermodyn.* **57**, 510-529.

Böttcher, C.J.F., and P. Bordewijk (1978). *Theory of Electric Polarization*, 2nd edition, Vol. II, Elsevier, Amsterdam, Chapter XII.

Chandami, A.S., P.P. Chaudhari, and M.P. Wadekar (2016). Determination of refractive index, density, molar refraction and polarizability constant of substituted N,N'-bis(salicyliden)-arylmethanediamines in different binary mixture refractrometrically. *Adv. Appl. Science Research* **7**(3), 120-126.

Dekker, A.J. (1964). *Solid State Physics*. MacMillan, London. Chapter 6.

Durou, C., J.-C. Giraudou, and C. Moutou (1973). Refractive indices of aqueous solutions of $CuSO_4$, $ZnSO_4$, $AgNO_3$, KCl, and H_2SO_4 for He-Ne laser light at $\theta = 25^oC$. *J. Chem. Eng. Data* **18**, 289-290.

Eggers, D.F., N.W. Gregory, G.D. Halsey, and B.S. Rabinovitch (1964). *Physical Chemistry*. Wiley, New York. Chapter 16.

El-Dossoki, F.I. (2007). Refractive index and density measurements for selected binary protic-protic, aprotic-aprotic, and aprotic-protic systems at temperatures from 288.15 to 308.15 K. J. *Chinese Chem. Soc.* **54**, 1129-1137.

Francesconi, R., and S. Ottani (2007). Correlation of density and refraction index for liquid binary systems containing polyglycerols. Use of the group contributions in the Lorentz-Lorenz, gladstone-Dale and Vogel equations to evaluate the density of mixtures. *J. Mol. Liquids* **133**, 125-133.

Frej, H., M. Jakubczyk, and K. Sangwal (1998). Density, surface tension, refraction index of aqueous ammonium oxalate solutions from 293 K to 333 K. *J. Chem. Eng. Data* **43**, 158-161.

Fucaloro, A.F., Y. Pu, K. Cha, A. Williams, and K. Conrad (2007). Partial molar volumes and refractions of aqueous solutions of fructose, glucose, mannose, and sucrose at 15.00, 20.00 and 25.00 °C. *J. Solution Chem.* **36**, 61-80.

Herráez, J.V., and R. Belda (2006). Refractive indices, densities and excess molar volumes of monoalcohols + water. *J. Solution Chem.* **15**, 1315-1328.

Karniewicz, J., W. Kolasiński, and J. Szewczyk (1982). Some properties of lithium formate solutions near the saturation temperature. *J. Cryst. Growth* **57**, 462-465.

Khimenko, M.T. (1969). Study of refractometric data for the calculation of polarizability and radius od particles. *Zh. Fiz. Khimii* **43**, 1961 (in Russian).

Kittel, C. (1976). *Introduction to Solid State Physics*. Wiley, New York. Chapter 13.

Lide, D.R. (1996/1997). Handbook of Chemistry and Physics, 77th edition. CRC Press, Boca Raton, FL.

Maharolkar, A.P., Y. Sudke, S. Kamble, A. Tidar, A.G. Murugkar, S.S. Patil, P.W. Khirade, and S.C. Mehrotra (2010). Densities, viscosities and refractive indices of n-butanol + allyl chloride mixtures at 298 K. *Intern. J. Chem.* **2**, 250-260.

Ortega, J. (1982). Densities and refractive indices of pure alcohols as a function of temperature. *J. Chem. Eng. Data* **27**, 312-317.

Redlich, O., and A.T. Kister (1948). Algebraic representation of thermodynamic properties and classification of solutions. *Ind. Eng. Chem.* **40**, 345-348.

Riddick, J.A., W.B. Bunger, and T.K. Sakano (1986). *Organic Solvents: Physical Properties and Methods of Purification*, 4th edition, Wiley-Interscience, New York.

Sharma, S., P.B. Patel, R.S. Patel, and J.J. Vora (2007). Density and comparative refractive index study on mixing properties of binary liquid mixtures of eucalyptol with hydrocabons at 303.15, 308.15 and 313.15 K. *E-Journal Chem.* **4**, 343-349.

Singh, S., M. Aznar, and N. Deenadayalu (2013). Density, speed of sound, and refracive indices for binary mixtures of 1-butyl-3-methylimidazolium metyl sulphate ionic liquid with alcohols at T = (298.15, 303.15, and 313.15) K. *J. Chem. Thermodyn.* **57**, 238-247.

Szewczyk, J., and K. Sangwal (1988). Density, refractive index, and specific refraction of aqueous lithium iodate solutions. *J. Chem. Eng. Data* **33**, 418-423.

Szewczyk, J., W. Sokołowski, and K. Sangwal (1985). Some physical properties of saturated, supersaturated, and undersaturated aqueous potassium bichromate solutions. *J. Chem. Eng. Data* **30**, 243-246.

Zhang, Y., H. Dong, Y. Yue, and Ch. Wu (2013). Effect of temperature and composition on the density, refractive index, and excess quantities of binary mixtures of 2,4,6,8-tetramethyl-2,4,6,8-tetraetheneylcyclotetrasiloxane with aromatic hydro- carbons. *J. Chem. Thermodyn.* **57**, 114-130.

Živković, E.M., M.Lj.. Kijevčanin, I.R. Radović, and S. P. Šerbanović (2014). Viscosities and refractive indices of binary systems acetone+1-propanol, acetone+1,2-propanediol and acetone+1,3-propanediol. *Chem. Ind. Chem. Eng. Q.* **20**, 441-455.

5

VISCOSITY OF SOLVENTS AND SOLUTIONS

Every liquid under expansion or compression by an external stress across any element of its surface experiences an internal resistance due to the motion of one portion of the liquid tangentionally with respect to an adjacent portion. A measure of this internal resistance in the liquid is its viscosity. Liquids characterized by high internal resistances are known as viscous. The viscous behavior of different liquids is intimately connected with their densities. For example, common alcohols like methanol and ethanol composed of simple molecules are characterized by both low viscosities and densities (i.e. less viscous and less dense), whereas the alcohol glycerol composed of large molecules has high viscosity and density (i.e. highly viscous and highly dense). However, the relationship between liquid viscosity and density is not so simple as implied from the above examples of liquids.

Viscosity of liquids is a valuable property in academic research and industrial application. Viscosity data are indispensable for the verification and development of theoretical models of the liquid structure, and for the control and planning of fluid flow, and mass and heat transfer processes in various industries. Thermodynamic functions and parameters of liquid mixtures and electrolyte solutions are equally important for understanding different types of intermolecular interactions in them.

There is a huge published literature on the viscosities of individual simple as well as complex liquids (such as ionic liquids consisting of large asymmetric organic cations and organic or inorganic anions), mixtures of two or more liquids, and electrolyte and nonelectrolyte solutions. The investigated liquids and solvents used for solutions usually have their melting points below 100 $^{\circ}$C. While the interest in the investivation of the viscosities in the nineteen fifties and sixties was mainly confined to simple commonly-available solvents and their mixtures and to aqueous electrolyte solutions, studies during the last two decades have been devoted to complex liquids and their mixtures. The viscosity measurements have been carried out as functions of temperature and mixture or solvent composition.

In their monograph on the viscosities of electrolyte solutions, Stokes and Mills (1965) discussed different theoretical aspects of viscosities covering the literature published up to 1963. They reviewed measurement techniques and different viscosity equations, and compiled the then-available viscosity data. In his handbook, Horvath (1985) devoted a chapter to review various equations for the estimation and correlation of viscosities for aqueous electrolyte solutions. According to him, despite "numerous expressions for the viscosities of aqueous electrolyte solutions, there are no simple and reliable methods for estimating viscosity without the need of some knowledge on the physical properties of the solutions".

In their book, Viswanath et al. (2007) described developments in the theories of viscosities of liquids and commonly used methods for the estimation and correlation of viscosities of liquids and solutions. These authors also collected the viscosity–temperature data for more than a thousand liquids. Since the contents of the chapters of the latter two books mainly deal with the estimation and correlation of viscosities and the first book described the theoretical developments of viscosities five decades ago, it is desired to review the present status of studies on the viscosities of solvents and solutions.

In this chapter various aspects of viscosities of liquids, liquid mixtures and nonelectrolyte and electrolyte solutions are reviewed, with emphasis on the underlying science behind the observations. After a brief introduction to the physical concepts of viscosity and measurement techniques in the following section, different problems associated with the viscosities of single-component liquids, binary liquid mixtures, and nonelectrolyte and electrolyte solutions are discussed in Sections 5.2, 5.3 and 5.4, respectively. Ionic *B* coefficients and their relationship between solution structure are described in Sections 5.5 and 5.6. Finally, characteristic features of viscosities of aqueous saturated electrolyte solutions are discussed in Section 5.7.

5.1. Definitions and measurements of viscosities

5.1.1. Viscosities and liquid flow

Viscosities of liquids are expressed in two different forms: dynamic or absolute viscosity η and kinematic viscosity $\nu = \eta/d$, where *d* is the density of the liquid. Basic ideas of these two viscosies are described below.

Dynamic viscosity η is defined as a shearing stress τ_y per unit area per unit velocity gradient v/z within the liquid, where *v* is the velocity of relative movement of one layer of the liquid over its neighboring layer and *z* is the interlayer distance. This relation may be explained from Figure 5.1, which shows schematically two layers ABCD and EFGH of the liquid which are parallel to each other in the *x*–*y* plane and are perpendicular to the *z* axis at a distance *c*. We assume that the layers have lengths *a* and *b* in the *x* and *y* axes, respectively. We consider that the lower layer EFGH of the liquid is held immobile and a force F_y applied in the *y* direction shifts the upper layer ABCD to the new position A'B'C'D' equal to Δy in the direction *y* in time Δt. The relative sliding of the layers causes a shear flow rate $\varepsilon_R = (\Delta y/\Delta t)/z$ in this system of layers, which is proportional to the shear stress $\tau_y = F_y/ab$. Since by definition

$$\varepsilon_R = \phi \tau_y , \tag{5.1}$$

where ϕ is a proportionality constant, called the fluidity of the liquid, the dynamic viscosity η (i.e. $\eta = \phi^{-1}$) may be given by the relation

$$\eta = \frac{\tau_y}{\varepsilon_R} = \frac{F_y}{ab}\frac{c}{u_y} , \tag{5.2}$$

where $u_y = (\Delta y/\Delta t)$ is the relative velocity of the gliding layer in the *y* direction. From

Eq. (5.2) it follows that the liquid viscosity η is inversely proportional to the velocity u_y of the gliding layer and that u_y is a measure of the liquid fluidity ϕ.

The dimensions of dynamic viscosity η are: $M \cdot L^{-1} \cdot T^{-1}$. In the old CGS units, the dimensions of viscosity η are: $g \cdot cm^{-1} \cdot s^{-1}$ or Poise (P). However, in the MKS units, they are: $kg \cdot m^{-1} \cdot s^{-1} = N \cdot m^{-2} \cdot s$ or Pa·s. The viscosities of most common liquids lie between $2 \cdot 10^{-4}$ and 1 Pa·s and a majority of them have values close to 10^{-3} Pa·s. Since these are very small values, in practice mPa·s is commonly used. The absolute viscosity of water at 20 °C is approximately 1 mPa·s. Note that 1 mPa·s = 1 cP.

The kinematic viscosity ν, which is η/d, is expressed in centistokes (cSt) which is $0.01\ cm^2 \cdot s^{-1} = 10^{-6}\ m^2 \cdot s^{-1}$.

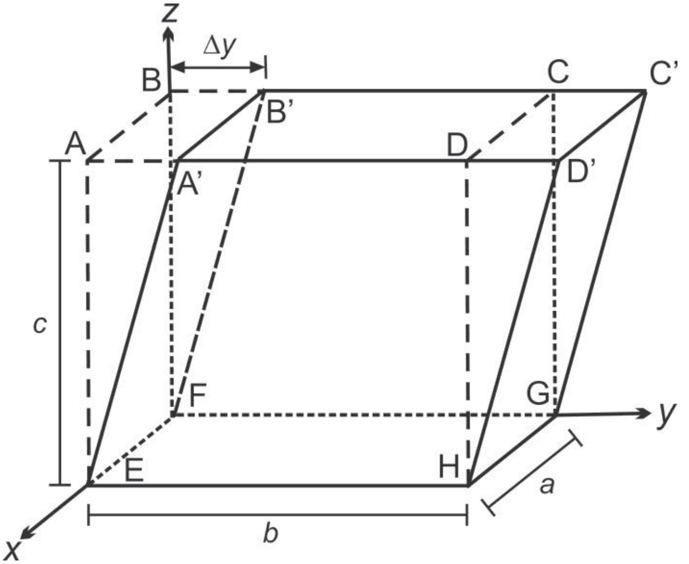

Figure 5.1. Schematically illustration of displacement of layer ABCD over immobile layer EFGH of a liquid. Layers are parallel to each other in the *x*–*y* plane and are perpendicular to the *z* axis at a distance *c*.

Viscosity η of liquids strongly depends on their flow characteristics, which are usually divided into the three categories (Viswanath et al., 2007): (1) Newtonian, (2) time-independent non-Newtonian, and (3) time-dependent non-Newtonian. The distinction between Newtonian and non-Newtonian liquids may be understood from Eq. (5.1) relating the applied shear stress τ (τ_y above in Eq. (5.2)) and the resulting shear rate ε_R, as represented in Figure 5.2. The slope $\Delta\tau/\Delta\varepsilon_R$ of the plot for a liquid is a measure of its viscosity η. The higher the slope $\Delta\tau/\Delta\varepsilon_R$ of the plot for the liquid, the higher is its viscosity η and the lower is its fluidity ϕ, and vice versa.

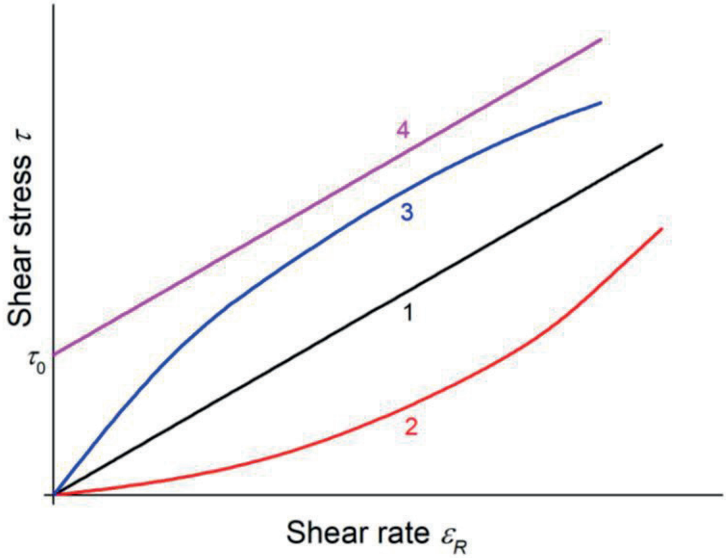

Figure 5.2. (1) Newtonian, and (2-4) non-Newtonian liquids as represented by relationship between applied shear stress τ and resulting shear rate ε_R. Non-Newtonian liquids are: (2) dilatant, (3) pseudoplastic, and (4) Bingham plastic. Adapted from Viswanath et al. (2007).

A liquid is said to be Newtonian when the applied shear stress τ linearly increases with the shear rate ε_R, i.e. when the viscosity η of liquid remains constant and is independent of the applied shear stress τ (Curve 1). In non-Newtonian liquids, their viscosity η depends on the applied shear stress and time. In the case of time-dependent non-Newtonian liquids, the viscosity of some liquids decreases and that of the others increases with increasing shear strain rate $\varepsilon_{R,}$ as shown by Curves 2 and 3, respectively, in Figure 5.2. The former type of liquids are called pseudoplastic, whereas the latter are called dilatant. There are also liquids, such as Bingham plastics, which show a flow behavior (i.e. $\varepsilon_R > 0$) only beyond a threshold value τ_0 of shear stress (Curve 4).

5.1.2. Viscosity measurements and their reproducibility

Precise experimental data of viscosities of solvents and solutions and reproducibility in their measurements from difference sources are important issues in academic research and in their usefulness in designing optimum operational conditions for efficiency of industrial products. For example, turbulent flow is undesirable in an industrial process and in the selection of capillary diameter for the design of capillary viscometers. Turbulent and laminar flow of a liquid in a tube of diameter w in such processes is determined by the Reynolds number Re given by

$$\mathrm{Re} = \frac{uwd}{\eta}, \tag{5.3}$$

where u is the liquid flow velocity. Laminar flow occurs for Re below about 2,000, but for Re beyond about 4,000 the liquid flow is turbulent.

Viscometers (also sometimes called viscosimeters) are instruments used for the measurement of the viscosity of liquids. Broadly, they are classified into the following categories: (1) capillary viscometers, (2) rotational viscometers, (3) falling ball viscometers, (4) vibrational or oscillating viscometers, and (5) ultrasonic viscometers. There are also some viscometers which combine the features of the above two or three categories of viscometers. Several viscometers are also automated for continuous viscosity measurements and for process control. There are many viscometers named after the pioneers in the field of viscosity measurements as well as after the manufacturers of automated and modified versions of known viscometers, mainly Ubbelohde and Hoppler viscometers. Examples of the former are: Ostwald, Ubbelohde and Hoppler viscometers, whereas those of the latter, inter alia, are: Cannon–Ubbelohde, Cannon–Fenske, Schott–Geräte, Brookfield, and Stabinger viscometers and Anton Paar AMVn falling-ball viscometer. For more information on different types of viscometers the reader is referred to the literature (Gupta, 2014; Viswanath et al., 2007). A list of commercial manufacturers of viscometers is also available (Gupta, 2014).

As mentioned above, precision in the measured value of the viscosity η of a liquid at a particular temperature and reproducibility in its measured values by different workers are important problems related to the published visocosity data. Table 5.1 lists an example of viscosities η of water, methanol, ethanol and 1-propanol measured at 298.15 K by different authors using different versions of Ubbelohde viscometers. The precision in measurements is up to third-decimal place. It may be seen from the table that the values of the viscosity for water from two sources are comparable but those reported by Herráez and Belda (2004) for the three alcohols are lower than those reported by González et al. (2007) and Pang et al. (2007). Figure 5.3 shows more data of the viscosity η of water as a function of increasing concentration x_2 of methanol, ethanol and 1-propanol at 298.15 K from different sources. The data are from Herráez and Belda (2004) for the three alcohol cosolvents, from González et al. (2007) for methanol and ethanol, and from Pang et al. (2007) for 1-propanol.

Table 5.1. Viscosities η of water, methanol, ethanol and 1-propanol from different sources at 298.15 K*

Water	Methanol	Ethanol	1-propanol
0.890[a]	0.545[a]	1.082[a]	1.947[b]
0.891[c]	0.553[c]	1.076[c]	1.946[c]

* Viscosity units: mP·s; [a] Gonzalez et al. (2007); [b] Pang et al. (2007); [c] Herraez and Belda (2004).

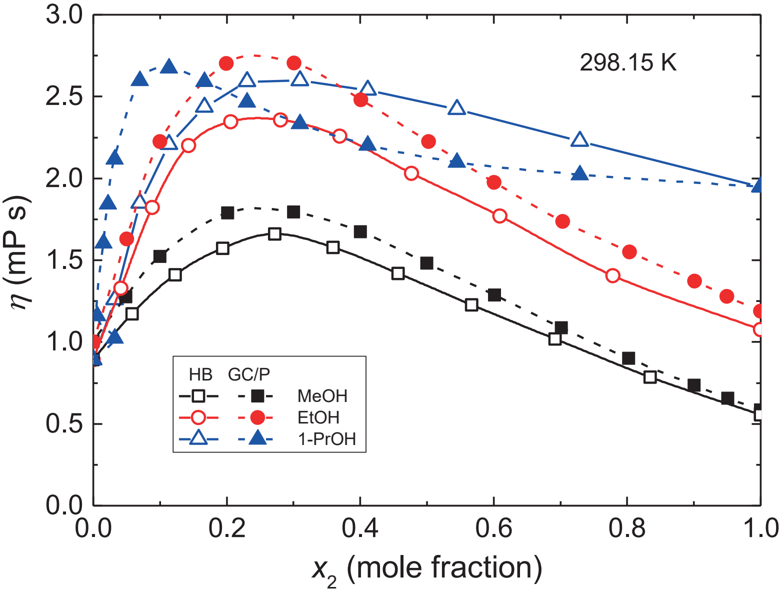

Figure 5.3. Viscosity η of water containing different contents x_2 of methanol, ethanol and 1-propanol at 25 °C as a function of alcohol content x_2. Data denoted by HB (continuous lines) for the three alcohols are from Herráez and Belda (2004), and GC/P (dashed lines) for methanol and ethanol are from González et al. (2007) and for 1-propanol from Pang et al. (2007).

It may be noted that the viscosity data of the water–methanol and water–ethanol mixtures reported by González et al. (2007) are higher than those by Herráez and Belda (2004), and that the relative difference is about 10% for the maximum value $\eta_{\max}$ of η at $x_2 \approx 0.25$ mole fraction. However, despite a difference in the values of η for various values of x_2, a general feature of these mixtures is that, with an increase in the alcohol content x_2, their viscosity η initially increases, attains a maximum value $\eta_{\max}$ at $x_2 \approx 0.25$ mole fraction, and then slowly decreases and approaches the value of the viscosity η_2 of pure alcohols. The general behavior of increasing 1-propanol content x_2 in water is similar to the above water–alcohols, but the data from the two sources differ both in the absolute values of the viscosity η at its different x_2 and in the value of x_2 for the appearance of the maximum value $\eta_{\max}$ in the water–1-propanol mixture. For this system, $\eta_{\max}$ appears at x_2 of about 0.25 and 0.15 mole fraction for the $\eta(x_2)$ data reported by Herráez and Belda (2004) and Pang et al. (2007), respectively.

The observed discrepancies in the values of the viscosities of individual solvents and water–alcohol mixtures of different compositions usually show systematic trends. These systematic trends of the discrepancy involved in viscosity data suggest that they result mainly from the measurements but differences in the composition x_2 of water–1-propanol of appearance of the maximum $\eta_{\max}$ may also be caused partly by the experimental conditions for the measurements. In view of the above, one should be cautious in the selection of experimental data of viscosities of individual liquids and their mixtures for their analysis.

5.2. Viscosities of single-component systems

Single-component systems include a variety of solvents, with their melting point usually below 100 °C, such as water, different organic liquids like common alkanes, alcohols and ketones, complex molecular organic liquids, and ionic liquids consisting of large asymmetric cations and inorganic and organic anions. Investigations of the physicochemical properties of ionic liquids have drawn enormous interest during the last two decades because they are environment-friendly solvents due to their negligible vapor pressure in comparison with traditional volatile organic solvents. Moreover, ionic liquids are known as designed solvents because their desired physiochemical properties can be achieved by changing the constitution of their molecules using changed structure of the cations and/or anions.

Different features of viscosities of liquids are described taking normal alcohols and their higher homologues as examples. The viscosities of the liquids are discussed in relation to the measurement temperature, chemical constitution of the liquid molecules and their physical properties.

5.2.1. Basic concepts and equations

The temperature dependence of viscosity η of several liquids (i.e. solvents and solutions) usually follows an Arrhenius-type relation (Stokes and Mills, 1965; Bockris and Reddy, 1970)

$$\eta = \eta_0 \exp\left(\frac{E_\eta}{R_\mathrm{G} T}\right), \tag{5.4}$$

where η_0 is the viscosity of the liquid at $T \to \infty$ when the exponential term approaches unity, E_η is the activation energy for viscous flow, and R_G is the gas constant (R_G = 8.3145 J·mol^{-1}·K^{-1}). Eq. (5.4) is similar to that for the temperature dependence of diffusion of *simple* liquids, including simple molten electrolytes, where their particles do not associate into pairs, triplets or network structures. The analogous behavior of the temperature dependence of self-diffusion and viscosity of simple liquids implies that the basic mechanism of self-diffusion and viscous flow is the same. It has been observed (Bockris and Reddy, 1970) that the activation energy for viscous flow and self-diffusion, E_η and E_D, respectively, for simple electrolytes is related to their melting point T_m, i.e.

$$\frac{E_\eta}{R_\mathrm{G}} \approx \frac{E_\mathrm{D}}{R_\mathrm{G}} = 3.7 T_\mathrm{m}\,. \tag{5.5}$$

The derivation of Eq. (5.4) and the validity of Eq. (5.5) are based on the hole theory of liquids (Bockris and Reddy, 1970). In this theory, size, distribution and free energy of formation of holes in liquids are calculated on the assumption that the kinetic entity involved in the transport process moves into a hole or cavity of radius r and that the work of formation of a hole in the liquid is given by the work required in forming the hole against the surface tension γ of the liquid. This work is the free energy ΔG° of activation for the flow process.

According to the hole theory of liquids, movement of molecules in a liquid is associated with the relative contribution of enthapies of formation of holes in its volume and jumping of molecules by rupturing of the bonds of the liquid network structure. In nonassociated liquids, it is the enthalpy of hole formation that determines the flow of their molecules. However, in associated liquids, the energy required in rupturing the bonds between the molecules of the liquid network structure determines their flow.

Eyring's transition state theory also describes the temperature dependence of the viscosity η of liquids in a form similar to that of Eq. (5.4). In the derivation of the final equation according to this theory, it is postulated that the liquids have a lattice-like structure containing a certain number of holes of dimensions of the order of their building entities (i.e. molecules, atoms or ions) and that these entities of the liquid jump from one "equilibrium" lattice position into a hole in its neighboring position during viscous flow. In the process of their jumping from one equilibrium position to another in the liquid structure, these kinetic entities pass through an activated or transition state to which various thermodynamic quantities are related. The final equation is of the form (Glasstone et al., 1941; Feakins et al., 1974; Horvath, 1985; Stokes and Mills, 1965)

$$\eta = \frac{h_{\mathrm{P}} N_{\mathrm{A}}}{V_{\mathrm{M}}} \exp\left(\frac{\Delta G^{\circ}}{R_{\mathrm{G}} T} \right), \tag{5.6}$$

where ΔG° is the Gibbs free activation energy for viscous flow of the liquid, h_{P} is the Planck constant ($h_{\mathrm{P}} = 6.626 \cdot 10^{23}$ J·s), V_{M} is the molar volume of the liquid ($V_{\mathrm{M}} = M/d$, with M as the molar mass and d as the liquid density), and N_{A} is the Avogadro number ($N_{\mathrm{A}} = 6.022 \cdot 10^{23}$ mol^{-1}). Physically, the molar volume $V_{\mathrm{M}} = \lambda^3 N_{\mathrm{A}}$, where λ is the average distance between the building entities of the liquid. A similarity of Eq. (5.6) with (5.2) may be noted by taking $a = b = c = \lambda$. Intermolecular interactions present in a liquid determine the concentration of holes in it, and the value of the Gibbs free activation energy ΔG° for viscous flow. Consequently, the concentration of holes is expected to be a fraction of the liquid molar volume V_{M}.

The energy ΔG° is related to the enthalpy ΔH° and the entropy ΔS° of activation for viscous flow, i.e.

$$\Delta G^{\circ} = \Delta H^{\circ} - T\Delta S^{\circ}. \tag{5.7}$$

The values of the Gibbs free activation energy ΔG° at different temperatures T are obtained from Eq. (5.6) rewritten in the form

$$\Delta G^{\circ} = R_{\mathrm{G}} T \ln\left(\frac{\eta V_{\mathrm{M}}}{h_{\mathrm{P}} N_{\mathrm{A}}} \right), \tag{5.8}$$

the enthalpy ΔH° of activation for viscous flow from the relation (cf. Eq. (5.6))

$$\Delta H^{\mathrm{o}} = R_{\mathrm{G}}\left[\frac{\mathrm{d}\ln(\eta V_{\mathrm{M}})}{\mathrm{d}(1/T)}\right], \tag{5.9}$$

and the entropy of activation

$$\Delta S^{\mathrm{o}} = \frac{\Delta H^{\mathrm{o}} - \Delta G^{\mathrm{o}}}{T}. \tag{5.10}$$

Obviously, when $\Delta S^{\mathrm{o}} = 0$, $\Delta H^{\mathrm{o}} = \Delta G^{\mathrm{o}}$ at a temperature T. Since usually $\Delta S^{\mathrm{o}} > 0$, $\Delta H^{\mathrm{o}} > \Delta G^{\mathrm{o}}$. Consequently, for a particular value of the Gibbs free energy ΔG^{o}, a higher value of ΔH^{o} is associated with a higher value of ΔS^{o}.

The entropy of activation for viscous flow, ΔS^{o}, is a measure of structural order of the liquid. High ΔS^{o} values indicate more structural order in the liquid and great structural breakdown in its flow (poor fluidity). However, low ΔS^{o} values indicate less structural order in the liquid and poor structural breakdown in its flow (high fluidity). Structural breakdown in the viscous flow of a liquid is related to the extent of ease in the creation of holes in the liquid during its flow. The easier the creation of holes in the liquid during its flow, the higher is its structural breakdown.

The main feature of Eq. (5.6) is that it provides physical interpretation of the preexponential factor η_0 and the activation energy E_η. Eq. (5.6) coincides with Eq. (5.4) when the molar volume V_{M} of the liquid is temperature independent. Then the preexponential factor $\eta_0 = h_{\mathrm{P}}N_{\mathrm{A}}/V_{\mathrm{M}}$ and the activation energy $E_\eta = \Delta H^{\mathrm{o}}$.

It is well known that both the density d and the viscosity η of a liquid increase with a decrease in their temperature T. In other words, both the molar volume $V_{\mathrm{M}} = M/d$ and the fluidity $\phi = \eta^{-1}$ of the liquid increase with increasing temperature. However, it is observed that the value of fluidity ϕ of some liquids increases linearly with increasing molar volumes V_{M} whereas its value for others slowly increases nonlinearly with increasing molar volume V_{M} such that the relative increase in ϕ with V_{M} (i.e. $\partial\phi/\partial V_{\mathrm{M}}$) increases with increasing V_{M} (and increasing temperature T) from an initial value of $\partial\phi/\partial V_{\mathrm{M}} = 0$ corresponding to a particular value of molar volume V_{M}^0 at a temperature T_0. The value of the threshold volume V_{M}^0 is characteristic of the liquid when its viscosity η approaches infinity and is determined by its chemical constitution. This means that the change in the viscosity η of a liquid with temperature is associated with an effective molar volume $V_{\mathrm{M}}(\mathrm{eff}) = V_{\mathrm{M}} - V_{\mathrm{M}}^0$, and, depending on the chemical constitution of the liquid, its value increases linearly or nonlinearly with an increase in temperature T since V_{M} increases with T. In the temperature interval between 25 and 80 °C, for a variety of common liquids like water and *n*-alcohols up to 1-tetradecanol the effective molar volume $V_{\mathrm{M}}(\mathrm{eff}) = V_{\mathrm{M}} - V_{\mathrm{M}}^{25} < 0.1V_{\mathrm{M}}^{25}$, implying that only a part of the molar volume V_{M}^{25} of a liquid at 25 °C participates in its flow behavior. The molar volume difference $(V_{\mathrm{M}} - V_{\mathrm{M}}^0)$ of the liquid, which is the free volume participating in the flow behavior, is mainly determined by different types of interactions in it. For different liquids the ratio $V_{\mathrm{M}}(\mathrm{eff})/V_{\mathrm{M}}^{25}$ is related to their thermal expansion.

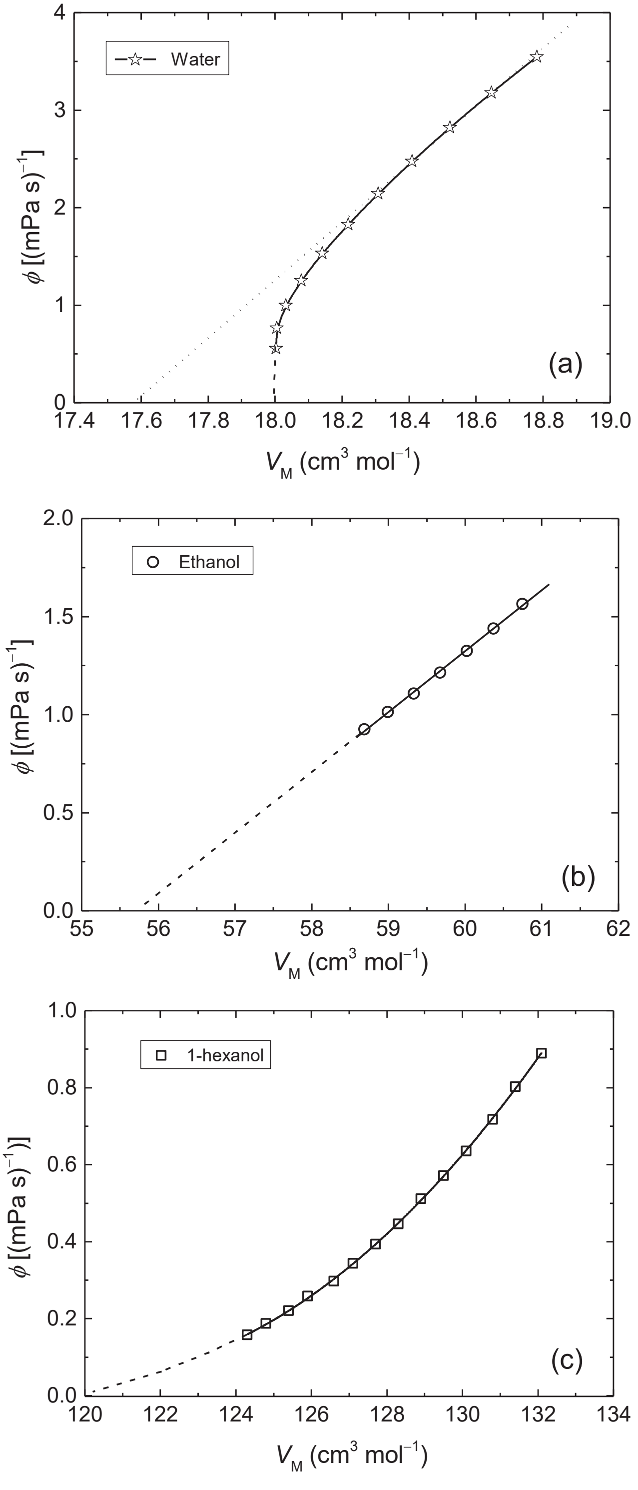
Water
(a)
φ [(mPa s)$^{-1}$]
0
1
2
3
4
17.4
17.6
17.8
18.0
18.2
18.4
18.6
18.8
19.0
V_M (cm^3 mol^{-1})
Ethanol
(b)
φ [(mPa s)$^{-1}$]
0.0
0.5
1.0
1.5
2.0
55
56
57
58
59
60
61
62
V_M (cm^3 mol^{-1})
1-hexanol
(c)
φ [(mPa s)$^{-1}$)]
0.0
0.2
0.4
0.6
0.8
1.0
120
122
124
126
128
130
132
134
V_M (cm^3 mol^{-1})

(Continued)

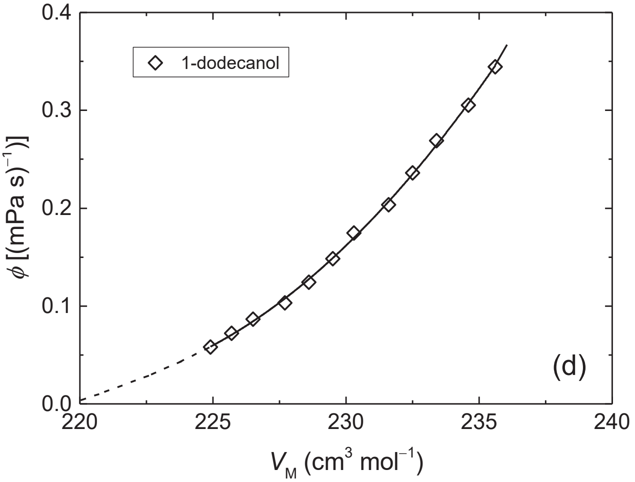

Figure 5.4. Typical examples of plots of fluidity ϕ of (a) water, (b) ethanol, (c) 1-hexanol and (d) 1-dodecanol against their molar volumes V_M at different temperatures T. Density and viscosity data used for water are from Lide et al. (1996/1997) and for ethanol are from Assael and Polimatidou (1994), whereas for 1-hexanol and 1-dodecanol are from Liew et al. (1993). Curves in (b-d) represent best fit of the data with V_M^0 as the extrapolated value of V_M corresponding to $\phi = 0$.

The value of the molar volume V_M^0 for a liquid may be obtained from a plot of the experimental data of its fluidity $\phi = \eta^{-1}$ as a function of its molar volume V_M at various temperatures according to Eq. (5.6) by extrapolating the curve to $\phi = 0$. Typical examples of determination of V_M^0 from plots of fluidity ϕ of water and three alcohols against their molar volumes V_M at different temperatures T are shown in Figure 5.4. With the exception of water where its fluidity ϕ abruptly tends to drop to zero with V_M below about 10 °C and it is difficult to represent the data by a linear or polynomial relation, curves are drawn from the best fit of the data using low- and high-order polynomial relations. This threshold molar volume V_M^0, frequently referred to as the intrinsic molar volume, is the liquid volume at which its molecules are so crowded that they inhibit their diffusion and flow. Values of molar mass M, intrinsic molar volume V_M^0 and molar volume V_M^{25} at 25 °C, extrapolated temperatures T_0 when $\phi = 0$, melting points T_m and boiling points T_b for water and *n*-alcohols up to tetradecanol are listed in Table 5.2. Here V_M^0 is the extrapolated value of the molar volume of a liquid corresponding to zero fluidity, and V_M^{25} is the value of the molar volume of the liquid calculated from its density d.

From Table 5.2 one observes that the values of all quantities show an increasing trend with an increase in the molar mass M of the liquid. The temperature T_0 of the liquid when its fluidity is zero is close to the melting point T_m. However, it is interesting to note that $T_m \approx T_0$ for water, $T_m < T_0$ for alcohols below 1-octanol, and $T_m > T_0$ for higher alcohols.

Table 5.2. Values of parameters M, $V_M{}^0$ and $V_M{}^{25}$, and temperatures T_0 and T_m for water and some n-alcohols

Solvent	M (g·mol^{-1})	$V_M{}^0$ (cm^3·mol^{-1})	$V_M{}^{25}$ (cm^3·mol^{-1}	T_0 (K)	T_m (K)^c	T_b (K)^c
Water	18.0	18.0	18.05^c	273	273.15	373.15
Methanol	32.08	37^a	40.74^d	226	176.09	337.75
Ethanol	46.07	56^a	58.67^d	259	159.05	351.35
1-propanol	60.1	74^a	75.17^d	258	147.05	370.35
1-butanol	74.12	88^a	92.04^d	265	158.45	372.65
1-pentanol	88.15	106	108.7	271	194.25	411.05
1-hexanol	102.18	116^b	125.4^b	262	228.55	430.75
1-octanol	130.23	151^b	158.4^b	260	257.65	468.25
1-decanol	158.28	185^b	191.4^b	267	280.05	504.25
1-dodecanol	186.34	219^b	224.9^b	284	297.15	532.15
1-tetradecanol	214.39	253^b	--	287	312.65	562.15

^{a} Ortega (1982); ^{b} Liew et al. (1993); ^{c} Lide (1996/1997); ^{d} Assael and Polimatidou (1994).

In the nineteen seventies, Hildebrand (1971, 1977) advanced the above concepts to explain the observed relationship between the fluidity $\phi = \eta^{-1}$ of different liquids and their relative expansion $(V_M - V_M{}^0)/V_M{}^0$, written in the form

$$\phi = D\frac{(V_M - V_M^0)}{V_M^0}\,, \tag{5.11}$$

where D is a proportionality constant with the units: (mPa·s)$^{-1}$, and $(V_M - V_M{}^0)$ is the effective molar volume V_M(eff) of the liquid with reference to the threshold molar volume $V_M{}^0$ when $\phi = 0$. Instead of the symbol B for the proportionality constant traditionally used in the original papers, here we have used the symbol D in order to avoid confusion with the viscosity B coefficient described in Section 5.4. According to Eq. (5.11) plot of fluidity ϕ of a liquid against its molar volumes V_M at different temperatures is expected to give a straight line of slope $D/V_M{}^0$ and, when extrapolated to $\phi = 0$, the value of $V_M{}^0$. Hildebrand and his colleagues have explored the applicability of this equation for various liquids, diluted gases and vapors, and liquid metals in a series of papers, which were later collected in the monograph (Hildebrand, 1977). In the context of the fluidity of liquids, we summarize the important findings of these studies below.

The linear relationship between ϕ and V_M holds over ranges of temperature from very low up nearly to the boiling points of simple liquids of various types, but there are liquids of relatively simple chemical composition (like 1-propanol, n-hexane, n-decane and n-heptadecane) as well as of long chemical formulae, such as perfluoro-tributyl-amine, $(C_4F_9)_3N$ with boiling pont T_b = 177 °C, and perfluoro-N-methyl-morpholine, C_5ONF_{11} with T_b = 50 °C, which show deviations from the linear dependence at low temperatures caused by increasingly hindered motion of liquid molecules during their cooling. The hindered motion of molecules in the liquid near its freezing point is associated with increasing order developing in it during cooling. This deviation from linearity in the region of low fluidity occurs for substances of unsymmetrical molecules which gain full freement of movement when the liquid is expanded somewhat more after melting.

The threshold molar volume V_M^0 is a "corresponding states" fraction of the critical molar volume V_M^c and is equal to the molar volume of the solid where the molecules are free to rotate as they do in the liquid. For normal alkanes the ratio $V_M^0/V_M^c \approx 0.30$. The ratio of molar volumes V_M^b of several simple liquids at their boiling point T_b to their critical volumes V_M^c is 0.377. This means that $V_M^0 \approx 0.796V_M^b$.

The value of the D parameter decreases linearly with increasing number N of carbon atoms of normal alkanes from C_3H_8 to $C_{20}H_{42}$ with a slope $\Delta D/\Delta N$ equal to about 0.47 but this slope is 8 from CH_4 to C_3H_8. The D values for cycloalkanes are somewhat lower and for branched alkanes are somewhat higher than those of the normal alkanes. The value of the D parameter is related to the absorption of energy during the collision of liquid molecules in the transfer of their momentum. It is expected that molecules with rotational inertia would lose more energy during collision than molecules without it. Absence of rotational inertia of molecules of CH_4 to C_3H_8 explains the steep decrease in D in these liquids in constrast to higher normal alkanes whose molecules can absorb energy by their bending where the energy loss is proportional to their chain length (i.e. N of carbon atoms). Thus, the mass, flexibility or inertia of rotation of molecules of a liquid determine the value of the D parameter.

Molar volume V_M of liquids is a function of their temperature as well as chemical constitution. Therefore, Eq. (5.11) may be applied to explain temperature and concentration dependence of fluidity. This equation indeed explains the fluidity behavior of nonassociated liquids where the constant D is temperature independent (Hildebrand, 1971, 1977). For these liquids, the activation energy E_D for self-diffusion is equal to the activation energy E_η for viscous flow. In the case of associated liquids, the proportionality constant D depends on temperature. We assume that the temperature dependence of the constant D follows an Arrhenius-type relation

$$D = D_0 \exp\left(-\frac{\Delta E_\eta}{R_G T}\right), \tag{5.12}$$

where ΔE_η is the activation energy for this dependence and D_0 is its preexponential factor. Physically, the activation energy ΔE_η is related to the nature of intermolecular interactions in the liquid (see below). Combination of Eqs. (5.11) and (5.12) gives

$$\eta = \frac{V_M^0}{D_0(V_M - V_M^0)_0} \exp\left(\frac{E_D + \Delta E_\eta}{R_G T}\right), \tag{5.13}$$

where the dependence of the effective molar volume $V_M(\text{eff}) = (V_M - V_M^0)_0$ of the liquid is described by an Arrhenius-type equation with activation barrier E_D and preexponention factor $(V_M - V_M^0)_0$. Eq. (5.13) is similar to Eyring's relation (5.6) with $(E_D + \Delta E_\eta) = \Delta G^\circ$ and $V_M^0/D_0(V_M - V_M^0)_0 = hN_A/V_M = \eta_0$.

An equation similar to Eq. (5.13) was first given by Liew et al. (1994) to explain the fluidity $\phi = \eta^{-1}$ of normal alcohols, and was applied to describe the dependence of fluidity ϕ of binary liquid mixtures on their composition (Manfredini et al., 2002).

Nonassociated liquids such as hydrocarbons involve predominantly weak van der Waals-type interactions which are of the order of thermal energy k_BT. Therefore, the activation energy ΔE_η is essentially zero, and Eq. (5.13) reduces to the Hildebrand equation, Eq. (5.11). However, in the case of alcohols and polyhydroxy liquids, intermolecular interactions mainly involve hydrogen bonds. Therefore, the value of the activation energy ΔE_η in these liquids is of the order of hydrogen bonds.

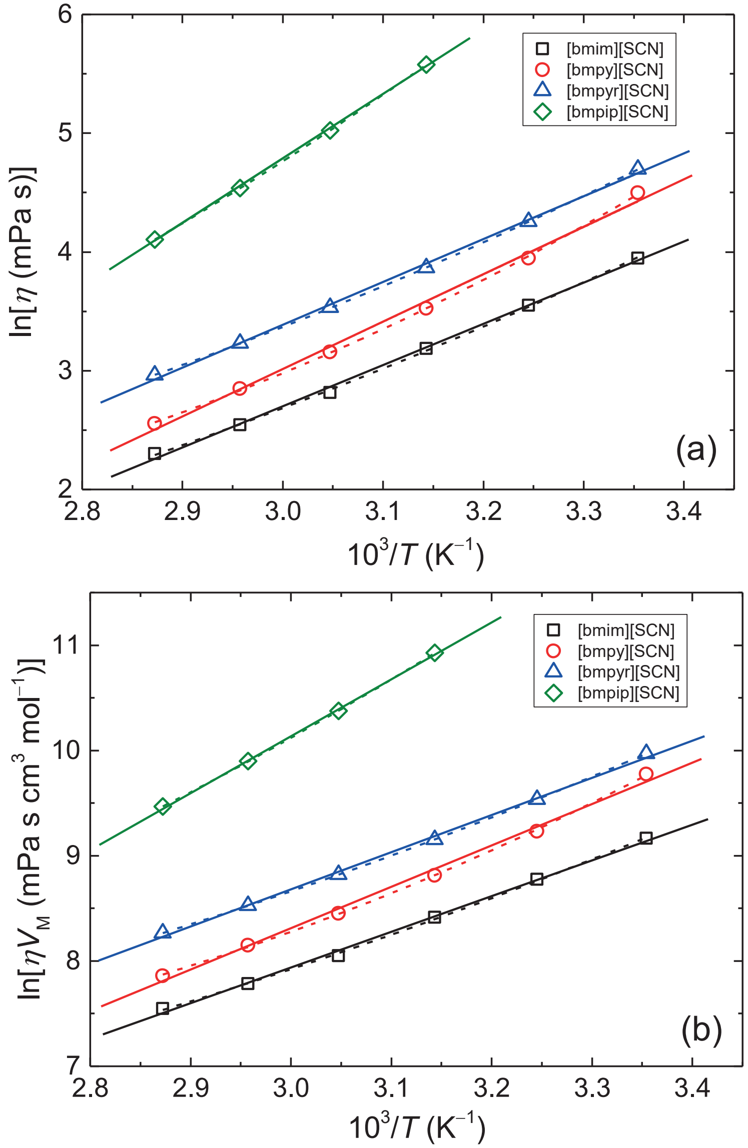

Figure 5.5. Examples of nonlinear plots of (a) $\ln\eta$ and (b) $\ln(\eta V_M)$ against $1/T$ for some ionic liquids showing nonlinear behavior indicated by dashed curves. Linear plots are drawn according to Eqs. (5.4) and (5.6), respectively. Data from Domańska and Królikowska (2012).

Although the temperature dependence of viscosity of individual liquids is often described by the Arrhenius-type equation, Eq. (5.4), it is observed that the $\ln\eta(1/T)$ curves for many single-component liquids markedly deviate from linearity in the entire range of temperature T. This nonlinear behavior of the plots of $\ln\eta$ against $1/T$ for some single-component ionic liquids is shown in Figure 5.5a. However, liquids which show the nonlinear behavior in the plots of $\ln\eta$ against $1/T$ also reveal a similar behavior in their plots of $\ln(\eta V_M)$ against $1/T$ (see Figure 5.5b).

The Arrhenius-type and non-Arrhenius-type behavior of liquids is related to the nature of interactions between their molecules. These differences are easily revealed (Angell, 1995) when the liquid temperature T is scaled with the glass temperature T_g (10^{12} Pa·s at T_g; 0.1 Pa·s = 1 poise). Liquids like SiO_2 and GeO_2, characterized by strong directional (covalent) bonds show an Arrhenius-type behavior of the viscosity η between T_g and the high-temperature limit when $\eta = 10^{-3}$ Pa·s for many liquids. These liquids are called *strong liquids*. Liquids characterized by simple nondirectional Coulomb interactions or weak van der Waals interactions in substances with many π electrons (usually aromatic substances) form the other extreme of *fragile liquids*. In fragile liquids viscosity changes in a strongly non-Arrhenius manner between the low and high viscosity limits.

The above classification of strong and fragile liquids is related to the sensitivity of the liquid structure to temperature changes (Angell, 1991, 1995). Strong liquids have a built-in resistance to structural changes with temperature changes. Fragile liquids, on the other hand, form glassy state structure that easily collapses with little provocation from thermal excitation. Strong liquids are characterized by very small jump ΔC_p in their heat capacity C_p at T_g, whereas fragile liquids show large jumps in ΔC_p.

The $\eta(T_g/T)$ data for different liquids can be well represented by a modified form of the Vogel–Tammann–Fulcher (VTF) relation (cf. Angell, 1991, 1995)

$$\eta = \eta_0 \exp\left(\frac{B^*}{T - T_0}\right), \tag{5.14}$$

rewritten in the form

$$\eta = \eta_0 \exp\left(\frac{\Psi T_0}{T - T_0}\right), \tag{5.15}$$

where the parameter $\Psi = B^*/T_0$ is a measure of the strength of mutual interaction between the liquid constituents and $T_g > T_0 > 0$. For a system following the Arrhenius relation, $\Psi = \infty$. The parameter Ψ is related to the temperature T_0 according to the simple dependence:

$$\frac{T_g}{T_0} = 1 + \frac{\Psi}{\ln(\eta_g/\eta_0)}, \tag{5.16}$$

where $\ln(\eta_g/\eta_0) \approx 39$ and the values of the liquid viscosity η at T_g and T_0 are η_g and η_0, respectively. The temperature T_0, called the Vogel temperature, refers to the ideal glass transition state when the movement of liquid constituents is totally frozen. The temperature ratio T_0/T_g has values of 0 and 1 when the corresponding strength parameter Ψ of the liquid is equal to ∞ and 0 and corresponds to *strong* and *fragile* liquids, respectively. Therefore, the ratio T_0/T_g may be considered as a measure of fragility of a system.

The non-Arrhenius behavior of viscosities of liquids is associated with the cooperative relaxation of their constituent molecules/atoms and is described by the Adam–Gibbs (AG) equation (Adam and Gibbs, 1965):

$$\eta = \eta_0 \exp\left(\frac{B^*}{T\Delta S_c} \right), \tag{5.17}$$

where the constant B^* is related to the free energy of the system, and ΔS_c is the configurational entropy. ΔS_c is related to the configurational heat capacity which is the difference ΔC_p between the heat capacities between the supercooled liquid and the extrapolated glass in the temperature interval from T_0 to some temperature T, and is given by the relation

$$\Delta S_c = \int_{T_0}^{T} \frac{\Delta C_p}{T} \mathrm{d}T\,, \tag{5.18}$$

which leads to different forms of Eq. (5.17), depending on the dependence of ΔC_p on T. When ΔC_p is a constant independent of T, from Eq. (5.18) one has: $\Delta S_c \propto \ln(T_0/T) \approx (1-T_0/T)$. Then Eq. (5.17) transforms to VTF relation (5.14) in a narrow range of temperature such that T is close to T_0 (Angell and Bressel, 1972). In a wide range of temperature when $\Delta C_p \propto 1/T$, $\Delta S_c \propto (T_0-T)/T_0T$, which on substitution into (5.17) gives the VTF relation with the constant $B^* \propto T_0$ (Angell and Bressel, 1972). With reference to the difference in the heat capacities of supercooled liquid and glass at temperature T_0, the decrease in the constant B^* with increasing T_0 has also been proposed to follow the linear dependence (Mahuiddin and Ismail (1982):

$$B^* = B_0^*(1 - B_1T_0)\,, \tag{5.19}$$

where $B_0{}^*$ and B_1 are constants characteristic for a system.

Finally, it should be mentioned that Eq. (5.14), which is derived from the free-volume theory, also describes other transport properties, such as conductance, of a variety of glass-forming liquids, including concentrated solutions, which become very viscous on cooling to their liquidus temperatures and which can be supercooled into the vitreous state (Angell, 1966; Angell and Bressel, 1972).

5.2.2. Individual homologues of normal alcohols

5.2.2.1. Temperature dependence of viscosities of normal alcohols

According to Eq. (5.4) the dependence of $\ln\eta$ against $1/T$ gives a linear plot with intercept $\ln\eta_0$ and slope E_η/R_G. Figure 5.6 shows plots of $\ln\eta$ against $1/T$ for water and

n-alcohols from methanol to 1-pentanol and higher even alcohols from 1-hexagonal to 1-tetradecanol, with the corresponding intercepts $\ln\eta_0$ and slopes E_η/R_G given in Table 5.3. The slope E_η/R_G is used to define an Arrhenius activation temperature T^* (i.e. $T^* = E_\eta/R_G$), and another temperature referred to as Arrhenius temperature T_A, defined as $T_A = E_\eta/R_G\ln\eta_0$ (cf. Eq. (5.4)). Following Messaâdi et al. (2015), the values of T_A were calculated using the units of viscosity η as Pa·s. The values of these temperatures T^* and T_A, the preexponential factor η_0, the activation energy E_η, the parameter E_η/R_GT_m of Eq. (5.5) and another boiling-point related parameter E_η/R_GT_b, calculated from the values of E_η/R_G, are also included in the table.

It may be seen from Table 5.3 that the value of the slopes E_η/R_G increases whereas that of the intercept $\ln\eta_0$ decreases with an increase in the number N of $–CH_2$ groups in the alcohols. However, as seen from the dependence of E_η/R_G and $\ln\eta_0$ on the number N of $–CH_2$ groups in alcohol molecules shown in Figure 5.7, the changes in these parameters are relatively high up to 1-propanol and later approach practically saturation values of about 3.35 kK and −8.6 for 1-decanol, 1-dodecanol and 1-tetradecanol. The values of E_η/R_G and $\ln\eta_0$ for water, represented by $N = 0$ in the figure, lie between those for ethanol and 1-propanol.

As seen from Table 5.3, the value of the activation energy E_η for viscous flow increases whereas that of the pre-exponential factor η_0 decreases with an increase in the number N of $–CH_2$ groups in the alcohols up to 1-decanol. For the alcohols considered here, with increasing N the overall increase in the value of E_η from methanol to tetradecanol is 3 fold but the corresponding decrease in η_0 is about 40 fold. These trends in the values of E_η and η_0 with increasing number N of $–CH_2$ groups in the alcohols are due to the processes of creation of holes necessary for their subsequent motion in these solvents and are associated with the nature of chemical bonds in their structures.

From Table 5.3 one also observes that, with increasing number N of $–CH_2$ groups in the alcohols, the parameter E_η/R_GT_m increases from a value of about 7 for methanol, approaches a maximum value of 14.6 for 1-propanol and 1-butanol and then decreases attaining a value of 10.9 for 1-tetradecanol. These observed values of the E_η/R_GT_m parameter are much higher than the expected value of 3.7 of the hole theory of liquids (see Eq. (5.5)), but are comparable with the values of the parameter $\Delta H_v/R_GT_b \approx 10.5$ for various substances according to the Trouton rule, where ΔH_v is the heat of vaporization. Therefore, one may take the E_η/R_GT_m parameter as a measure of manifestation of the heat of vaporization, ΔH_v, involved in the creation of holes in the liquid alcohols.

To understand the above trend, one may also consider the entropy of melting, $\Delta S_m = \Delta H_m/T_m$, of the alcohols in relation to their chain length. According to Yalkowsky and Valvani (1980), the entropy of melting, ΔS_m, is the sum of contributions due to: (1) dismantling of solid arrangement to form the liquid (translational entropy ΔS_{trans}), (2) randomization of orientation of molecules in the liquid (rotational entropy ΔS_{rot}), and (3) internal conformation of molecules in the liquid (internal or conformational entropy ΔS_{int}). The translational entropy ΔS_{trans} contributes to the total entropy of melting, ΔS_m, for different types of molecules, but this contribution is relatively small in comparison with contributions from ΔS_{rot} and ΔS_{int}. The rotational entropy ΔS_{rot} of melting is a component of the total entropy of melting, ΔS_m, of all nonspherical molecules, and ΔS_{rot} and ΔS_{trans} are the only contributions to the total entropy of melting, ΔS_m, for rigid molecules.

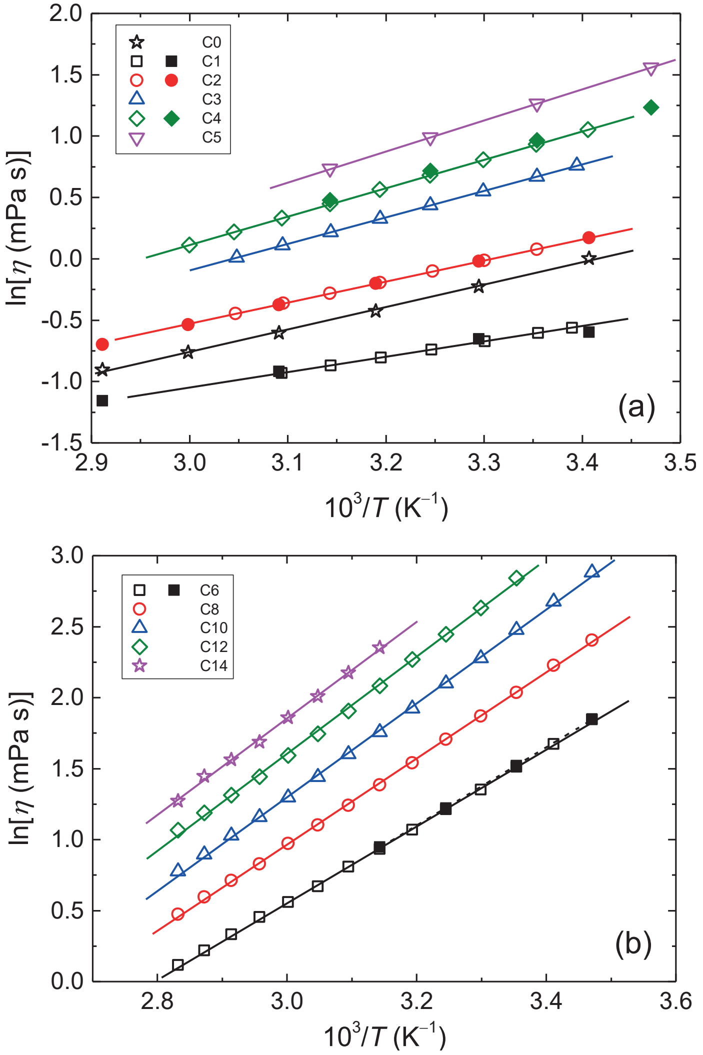

Figure 5.6. Dependence of lnη on 1/T for (a) water and various normal alcohols up to 1-pentanol, and (b) 1-hexanol and its higher homologues. Solid plots represent data of open points. Dashed curve for 1-hexanol represents filled points. Best-fit constants of the plots according to Eq. (5.4) are listed in Table 5.3. Sources of data: for water from Lide (1996/1997), for methanol, ethanol, 1-propanol and 1-butanol from Assael and Polimatidou (1994), for 1-butanol, 1-pentanol and 1-hexanol from D'Aprano et al. (1979), and for 1-hexanol and higher alcohols from Liew et al. (1993). Filled points for methanol and ethanol from Sangwal (2018), and for 1-butanol and 1-hexanol from D'Aprano et al. (1979).

Table 5.3. Values of constants of Eq. (5.4)

Solvent	T_m (K)[a]	$-\ln\eta_0$	$E_\eta/R_G =$ T^* (kK)	T_A (K)	$10^{-3}\eta_0$ (mPa·s)	E_η (kJ·mol^{-1})	E_η/R_GT_m (–)	E_η/R_GT_b (–)	Data
Water	273.15	6.3108	1.8608	140.8	1.817	15.45	6.8	4.99	a
		6.2440	1.8283	139.0	1.981	15.2	6.7	4.90	b
Methanol	175.55	4.6206	1.1962	103.8	9.847	9.95	6.8	3.55	c
		4.8014	1.2508	106.8	8.218	10.4	7.1	3.70	b
Ethanol	159.05	5.5499	1.6734	134.3	3.888	13.91	10.5	4.76	c
		5.6530	1.7091	136.1	3.507	14.21	10.7	4.86	b
1-propanol	147.05	6.5762	2.1604	160.2	1.393	17.96	14.7	5.83	c
1-butanol	158.45	6.8313	2.3155	168.5	1.079	19.25	14.6	6.21	c
		6.7859	2.3110	168.8	1.129	19.21	14.6	6.20	d
1-pentanol	194.25	7.1845	2.5204	178.9	0.758	20.96	13.0	6.13	d
1-hexanol	228.55	7.7077	2.7524	188.3	0.449	22.88	12.0	6.39	d
		7.5291	2.6958	186.7	0.537	22.41	11.8	6.26	e
1-octanol	257.65	8.1148	3.0272	201.5	0.229	25.17	11.7	6.46	e
1-decanol	280.05	8.6017	3.3012	212.9	0.184	27.45	11.8	6.55	e
1-dodecanol	297.15	8.6463	3.4174	219.7	0.176	28.41	11.5	6.42	e
1-tetradecanol	312.65	8.3617	3.4050	223.0	0.234	28.31	10.9	6.06	e

[a] Lide (1996/1997); [b] Sangwal (2018); [c] Assael and Polimatidou (1994); [d] D'Aprano et al. (1979); [e] Liew et al. (1993).

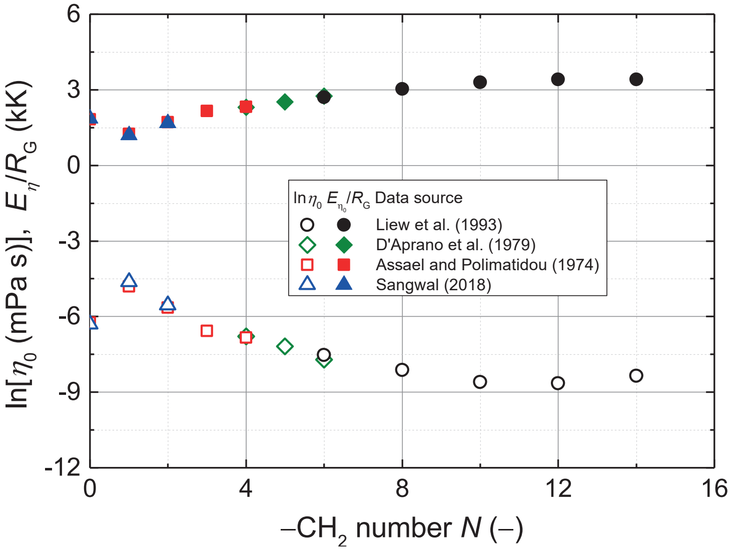

Figure 5.7. Dependence of slope E_η/R_G and intercept lnη_0 on the number N of –CH$_2$ groups in alcohol molecules. N = 0 denotes water.

Contribution of internal entropy ΔS_{int} to the total entropy ΔS_m becomes important in the case of long-chain molecules of flexible configuration (Yalkowsky and Valvani, 1980). The molecules of organic compounds having less than five units in their linear chains behave as rigid molecules, but the internal entropy of melting, ΔS_{int}, of the compounds with more than five units in the linear chains of their molecules increases linearly with the number of carbon and heteroatoms in the chains. However, due to the flexibility of linear chains, the molecules interact with each other, leading to a decrease in ΔS_{int} with increasing N. Consequently, depending on the number N of $-\mathrm{CH}_2$ groups in the alcohols, their entropy of melting, ΔS_{m}, initially increases and then decreases after going through a maximum value. Therefore, the $E_\eta/R_{\mathrm{G}}T_{\mathrm{m}}$ parameter may be taken as a measure of the reorganization of molecules in these alcohols in terms of their entropy of melting, ΔS_{m}.

In contrast to the trends of $E_\eta/R_{\mathrm{G}}T_{\mathrm{m}}$ with increasing number N of $-\mathrm{CH}_2$ groups in the alcohols, the $E_\eta/R_{\mathrm{G}}T_{\mathrm{b}}$ parameter practically remains constant equal to 6.38 ± 0.18 for all alcohols with N between 4 and 12. The differences in the trends of the $E_\eta/R_{\mathrm{G}}T_{\mathrm{m}}$ and $E_\eta/R_{\mathrm{G}}T_{\mathrm{b}}$ parameters as a function of the number N of $-\mathrm{CH}_2$ groups in the alcohols are due to the state of the alcohol molecules in the melt and the vapor phase. The entropy of melting, $\Delta S_{\mathrm{m}} = \Delta H_{\mathrm{m}}/T_{\mathrm{m}}$, involves three contributions associated with rupturing of bonds between the molecules in the solid state and their reorganization in the liquid, but the entropy of vaporization, $\Delta S_{\mathrm{v}} = \Delta H_{\mathrm{v}}/T_{\mathrm{b}}$, is mainly determined by the energy required to dismantle the bonds between the molecules of the liquid and the nature of the bond. Relatively low values of the $E_\eta/R_{\mathrm{G}}T_{\mathrm{b}}$ parameter for alcohols with $N < 4$ are likely to be due the rigidity of their molecules in comparison with higher alcohols composed of flexible molecules. These ideas are consistent with the concepts of formation of a holes in analogy with that of a bubble in the liquid (Bockris and Reddy, 1970).

The value of $E_\eta/R_{\mathrm{G}}T_{\mathrm{m}}$ for water is similar to that for methanol but the value of $E_\eta/R_{\mathrm{G}}T_{\mathrm{b}}$ is comparable with that for ethanol. These observations are probably due to the opposite effects of their structure in the liquid state and the entropy of vaporization. A similar extent of reorganization (association) of the molecules of liquid water and methanol explains similar value of $E_\eta/R_{\mathrm{G}}T_{\mathrm{m}}$ for these liquids. Similar values of the entropy of vaporization, $\Delta S_{\mathrm{v}} = \Delta H_{\mathrm{v}}/T_{\mathrm{b}}$, for water and ethanol, on the other hand, explains the latter observation. However, the values of E_η and η_0 for water are higher than those for ethanol. This difference is due to differences in the structure of these solvents and is associated with the nature of bonds between the molecules of a liquid during viscous flow.

5.2.2.2. Enthalpy and entropy of activation for viscous flow

In order to understand processes involved in the viscous flow of the above liquids it is necessary to analyze the viscosity data using Eq. (5.6) of Eyring's formalism and the data of molar mass M and molar volumes $V_{\mathrm{M}}{}^{0}$ and $V_{\mathrm{M}}{}^{25}$ given in Table 5.2. The values of the Gibbs free activation energy ΔG^{o} were calculated for viscosity at 25 °C (298.15 K) using Eq. (5.8), whereas the values of the enthalpy of activation, ΔH^{o}, for viscous flow for the liquids were determined from plots of $\ln(\eta V_{\mathrm{M}})$ against T^{-1}. In the latter case, the plot of $\ln(\eta V_{\mathrm{M}})$ against T^{-1} for a liquid in the investigated range of temperature gives a linear dependence of intercept $\ln(\eta V_{\mathrm{M}})_0$ and slope $\Delta H^{\mathrm{o}}/R_{\mathrm{G}}$ (see Eq. (5.9)). Figure 5.8 shows as typical examples of the plots of $\ln(\eta V_{\mathrm{M}})$ against T^{-1} for water and alcohols from methanol up to 1-pentanol. The calculated values of the Gibbs free activation energy ΔG^{o} using Eq. (5.8) and those of the intercept $\ln(\eta V_{\mathrm{M}})_0$ and the slope $\Delta H^{\mathrm{o}}/R_{\mathrm{G}}$ from the plots of $\ln(\eta V_{\mathrm{M}})$ against T^{-1} according to Eq. (5.9) for water and different alcohols are listed in Table 5.4. In view of a small number of data points, the values of $\ln(\eta V_{\mathrm{M}})_0$ and $\Delta H^{\mathrm{o}}/R_{\mathrm{G}}$ calculated from the plots of $\ln(\eta V_{\mathrm{M}})$ against T^{-1} for 1-butanol (dased line) and 1-pentanol are not given in the table. Similarly, 1-tetradecanol with its melting point $T_{\mathrm{m}} = 39.5$ °C (313.65 K) is excluded from the analysis. The values of the enthalpy ΔH^{o} of activation calculated from the slopes $\Delta H^{\mathrm{o}}/R_{\mathrm{G}}$ are given in the last column whereas those of the activation energy E_η of activation for viscous flow are included in the parentheses in the fourth column of ΔG^{o}.

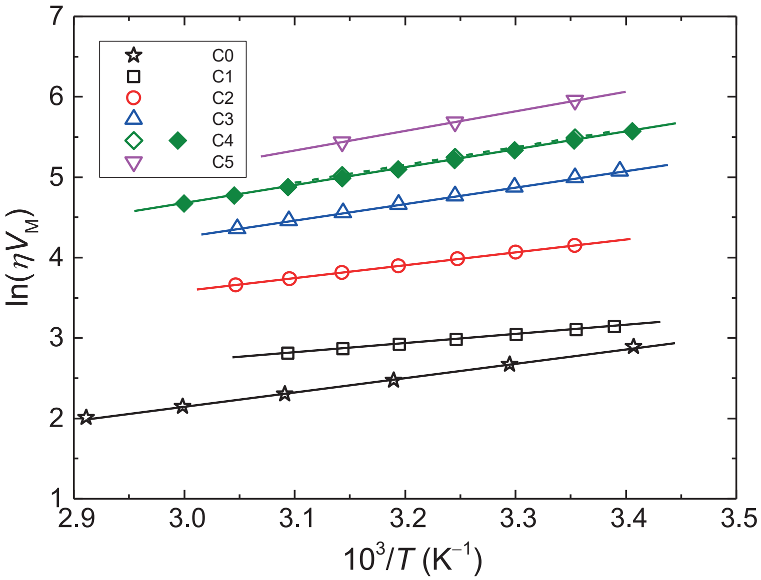

Figure 5.8. Plots of $\ln(\eta V_{\mathrm{M}})$ against T^{-1} for water and alcohols from methanol up to 1-pentanol. Best-fit constants of the plots according to Eq. (5.6) are listed in Table 5.4. Viscosity and density data for water are from Lide (1996/1997) and cover temperature interval between 293 and 343 K. Viscosity and density data for methanol, ethanol, 1-propanol and 1-butanol represented by solid lines in temperature range between 290 and 334 K are from Assael and Polimatidou (1994), but data for 1-butanol (dased line) and 1-pentanol are from D'Aprano et al. (1979) and Ortega (1982), respectively.

To account for the effect of the densities of the alcohols on their viscosities, the dependence of kinematic viscosity $\nu = \eta/d$ on temperature T following from Eq. (5.6) is usually analyzed. This procedure also gives linear plots of $\ln(\eta/d)$ against T^{-1}, with slopes $\Delta H^{\mathrm{o}}/R_{\mathrm{G}}$ comparable with those obtained from the $\eta(T)$ data but with intercepts $\ln(\eta/d)_0 = (\ln\eta_0 - \ln d)$. The values of these intercepts $\ln(\eta/d)_0$ are also included in Table 5.4. Since the molar volumes V_{M} of the alcohols are related to their densities d, this procedure gives the same values of $\Delta H^{\circ}/R_G$ as those obtained from the slopes of the plots of $\ln(\eta V_M)$ against T^{-1} according to Eq. (5.9) but the values of the intercept $\ln(\eta/d)_0$ are lower than those of $\ln(\eta V_M)_0$ by the factor $\ln M$, where M is the molar mass of the alcohols.

Table 5.4. Molar volume V_M^{25} and viscosity η^{25} at 25 °C, ΔG°, and Arrhenius parameters for water and alcohols

Solvent	V_M^{25} ($\mathrm{cm^3 \cdot mol^{-1}}$)	η^{25} (mP·s)	ΔG° (E_η) ($\mathrm{kJ \cdot mol^{-1}}$)	$-\ln(\eta/d)_0$	$-\ln(\eta V_M)_0$	$\Delta H^{\circ}/R_G$ (kK)	ΔH° ($\mathrm{kJ \cdot mol^{-1}}$)
Water	18.05[a]	0.891[a]	9.17 (15.2)	6.1021	3.2118	1.7867	14.85
Methanol	40.74[b]	0.5484[b]	9.98 (10.4)	4.1653	0.6983	1.1326	9.42
Ethanol	58.67[b]	1.081[b]	12.57 (14.21)	5.0355	1.2054	1.5970	13.28
1-propanol	75.17[b]	1.915[b]	14.60 (17.96)	6.0190	1.9230	2.0610	17.14
1-butanol	92.04[b]	2.626[b]	15.89 (19.25)	6.2960	1.9857	2.2285	18.53
1-pentanol	--	--	--	6.6885	2.2095	2.4341	20.24
1-hexanol	125.4[c]	4.5406[c]	18.01 (22.48)	7.0059	2.3791	2.6007	21.62
1-octanol	158.4[c]	7.6596[c]	19.89 (25.17)	7.6167	2.7474	2.9371	24.42
1-decanol	191.4[c]	11.9154[c]	21.45 (27.45)	8.1142	3.0499	3.2125	26.71
1-dodecanol	224.9[c]	17.1701[c]	22.76 (28.41)	8.1601	2.9325	3.3279	27.67
1-tetradecanol	--	--	--	7.8627	2.4949	3.3099	27.52

[a] Lide (1996/1997); [b] Assael and Polimatidou (1994); [c] Liew et al. (1993).

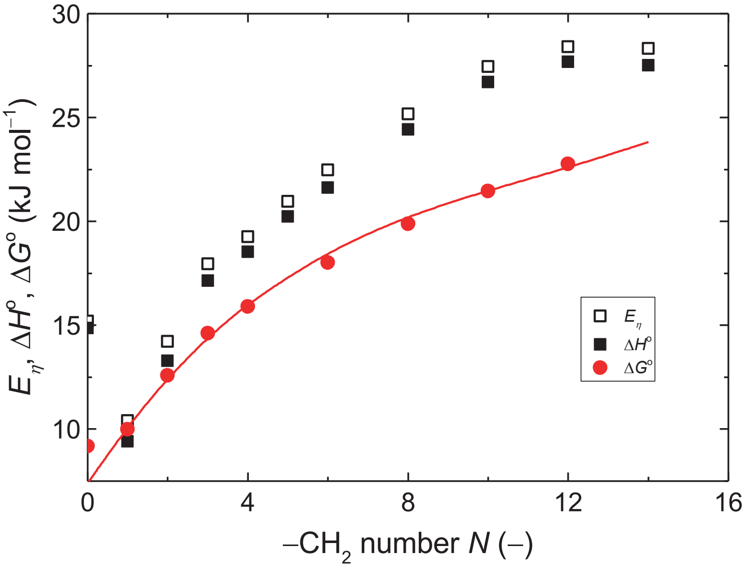

Figure 5.9. Dependence of activation energy E_η, Gibbs free energy ΔG° and enthalpy of activation ΔH° of viscous flow on the number N of $-CH_2$ groups in alcohol molecules. Best-fit curve for the $\Delta G^{\circ}(N)$ data for the alcohols is shown according to relation (5.17). Data for water, corresponding to $N = 0$, are also shown.

Figure 5.9 compares the values of activation energy E_η, Gibbs free energy ΔG^o and enthalpy of activation ΔH^o for viscous flow as a function of the number N of $-\mathrm{CH}_2$ groups in alcohol molecules. From the figure one notes that $E_\eta > \Delta H^\mathrm{o}$. Both of these energies increase with increasing N such that the difference $(E_\eta - \Delta H^\mathrm{o})$ between them also increases with N. With the exception of methanol where $\Delta H^\mathrm{o} < \Delta G^\mathrm{o}$, $\Delta H^\mathrm{o} > \Delta G^\mathrm{o}$ for the remaining alcohols.

The values of both E_η and ΔH^o increase with increasing N and approach limiting values equal to about 28.3 and 27.5 kJ·mol^{-1}, respectively, for $N \geq 12$ (see Figure 5.10). The relative increase in E_η and ΔH^o per $-\mathrm{CH}_2$ group decreases with the number N of $-\mathrm{CH}_2$ groups and there is essentially no increase for $N \geq 12$. It is interesting to note that the difference $(E_\eta - \Delta H^\mathrm{o})$ in the energies E_η and ΔH^o for the alcohols is practically constant equal to 0.8 kJ·mol^{-1}, but the relative increase $(E_\eta - \Delta H^\mathrm{o})/\Delta H^\mathrm{o}$ decreases exponentially with N from about 10% for methanol to about 4.8% for 1-propanol and 2.6% for 1-dodecanol. In contrast to the above trends for alcohols, in the case of water the energy difference $(E_\eta - \Delta H^\mathrm{o})$ is 0.35 kJ·mol^{-1} and the relative increase $(E_\eta - \Delta H^\mathrm{o})/\Delta H^\mathrm{o}$ is about 2.4%. This value of $(E_\eta - \Delta H^\mathrm{o}) = 0.35$ kJ·mol^{-1} is less than one-half the value observed for alcohols but the relative increase $(E_\eta - \Delta H^\mathrm{o})/\Delta H^\mathrm{o}$ is comparable with that observed for 1-dodecanol.

The dependence of the Gibbs free energy ΔG^o of activation for viscous flow on the number N of $-\mathrm{CH}_2$ groups in the alcohol molecules may be described by the third-order relation (see the curve in Figure 5.9)

$$\Delta G^\mathrm{o} = a_0 + a_1 N + a_2 N^2 + a_3 N^3 , \tag{5.20}$$

with $a_0 = 7.4$ kJ·mol^{-1}, $a_1 = 2.94$ kJ·mol^{-1}, $a_2 = 0.22$ kJ·mol^{-1} and $a_3 = 0.0067$ kJ·mol^{-1}. The value of 7.4 kJ·mol^{-1} represents the extrapolated value of ΔG^o corresponding to a hypothetical alcohol with $N = 0$.

The difference $(\Delta H^\mathrm{o} - \Delta G^\mathrm{o})$ between the enthalpy of activation, ΔH^o, and the Gibbs free energy ΔG^o of activation for viscous flow increases with an increase in the number N of $-\mathrm{CH}_2$ groups in the alcohol molecules from an initial value of -0.56 kJ·mol^{-1} for methanol (see Figure 5.10). These trends are associated with the fact that the different energies are mutually related. To analyze these relationships the term $T\Delta S^\mathrm{o} = (\Delta H^\mathrm{o} - \Delta G^\mathrm{o})$, representing the entropy ΔS^o of activation for viscous flow at 25 °C, was calculated using Eq. (5.10) from the data of ΔH^o and ΔG^o listed in Table 5.4. Figure 5.10 shows the data of the enthalpy of activation ΔH^o and the entropy-related term $T\Delta S^\mathrm{o}$ as a function of the Gibbs free energy ΔG^o for viscous flow of water and *n*-alcohol homologues. Obviously, both ΔH^o and $T\Delta S^\mathrm{o}$ increase linearly with ΔG^o according to the relation

$$y = y_0 + y_1 \Delta G^\mathrm{o} , \tag{5.21}$$

where y denotes ΔH^o and $T\Delta S^\mathrm{o}$, and y_0 and y_1 are constants. In a $y(\Delta G^\mathrm{o})$ plot, y_0 represents its intercept and y_1 its slope. The value of y_0 corresponds to the value of y

when $\Delta G^o = 0$. The values of constants y_0 and y_1 for the $\Delta H^o(\Delta G^o)$ and $T\Delta S^o(\Delta G^o)$ data of Figure 5.10 are given in Table 5.5.

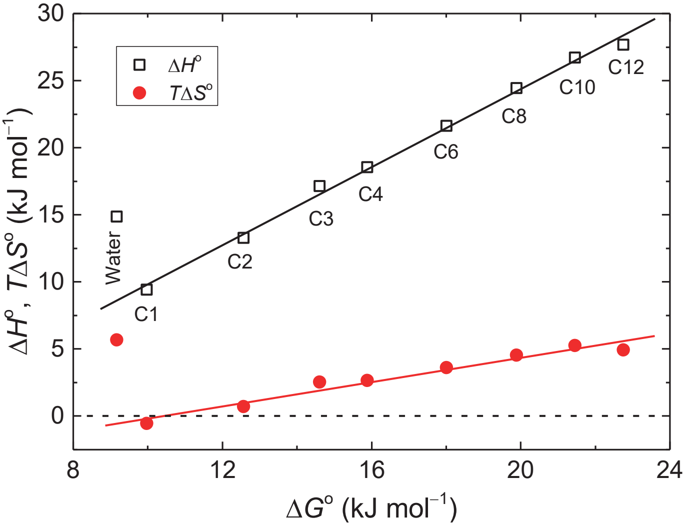

Figure 5.10. Dependence of enthalpy of activation ΔH^o and entropy-related term $T\Delta S^o$ on Gibbs free energy ΔG^o for viscous flow of water and *n*-alcohol homologues. For alcohols the dependences are linear according to Eq. (5.21) with constants given in Table 5.5.

Table 5.5. Values of constants y_0 and y_1 of Eq. (5.21)

Data	$-y_0$ (kJ·mol^{-1})	y_1 (–)	R^2
$\Delta H^o(\Delta G^o)$	4.721±0.067	1.454±0.039	0.9950
$T\Delta S^o(\Delta G^o)$	4.721±0.067	0.454±0.039	0.9512

It is interesting to compare the values of ΔH^o and $T\Delta S^o$ for water with those calculated for the hypothetical alcohol with $N = 0$ from Eq. (5.21) with the constants given in Table 5.5 and $\Delta G^o = 7.4$ kJ·mol^{-1}. For this alcohol the calculated values are: $\Delta H^o = 6.0$ kJ·mol^{-1} and $T\Delta S^o = -1.36$ kJ·mol^{-1}. Obviously, these values are much lower than those obtained for water (see Figure 5.10). One also finds that $T\Delta S^o = -0.56$ kJ·mol^{-1} for methanol in contrast to $T\Delta S^o > 0$ for higher alcohols such that $T\Delta S^o$ increases linearly with the number N of $-CH_2$ groups in the alcohol molecules.

The above observations may be understood from a consideration of the processes involved in viscous flow (see Section 5.2.1). The Gibbs free energy ΔG^o for viscous flow involves two contributions: (1) creation of a hole in the vicinity of an entity that jumps to occupy it, and (2) jumping of the entity to occupy the hole created in its vicinity. Since $\Delta G^o = (\Delta H^o - T\Delta S^o)$ and ΔS^o is a measure of structural order of the liquid, increasing values of $T\Delta S^o > 0$ for alcohols higher than ethanol suggests that the viscous flow of these alcohols is determined by contribution (2) and the structural disorder in the liquid increases with an increase in the number N of $-CH_2$ groups in their molecules. A similar behavior is encountered in the case of water where $T\Delta S^o > 0$. However, $T\Delta S^o < 0$ for methanol indicates that the process of creation of holes (contribution (1)) determines its flow and is related to less structural order in the liquid.

5.2.2.3. Relationship between different Arrhenius parameters for water and alcohols

From Tables 5.3 and 5.4 one observes that the data of E_η/R_G against $\ln\eta_0$, $\Delta H^o/R_G$ against $\ln(\eta/d)_0$ and $\Delta H^o/R_G$ against $\ln(\eta V_M)_0$ for the viscous flow of various *n*-alcohol homologues are mutually related. Figure 5.11 shows the relationship between E_η/R_G and $\ln\eta_0$, $\Delta H^o/R_G$ and $\ln(\eta/d)_0$ and between $\Delta H^o/R_G$ and $\ln(\eta V_M)_0$ for viscous flow of water and *n*-alcohol homologues. It may be seen that, if 1-dodecanol and 1-tetradecanol are excluded, the data for the alcohols may be described by the linear dependence:

$$Y = b_0 - b_1 \ln X \, , \tag{5.22}$$

where Y denotes E_η/R_G or $\Delta H^o/R_G$, X denotes η_0, $(\eta/d)_0$ or $(\eta V_M)_0$, and b_0 and b_1 are constants, which represent intercept and slope of the linear plots. Curves 1, 2 and 3 represent the data of E_η/R_G against $\ln\eta_0$, $\Delta H^o/R_G$ against $\ln(\eta/d)_0$, and $\Delta H^o/R_G$ against $\ln(\eta V_M)_0$, respectively, for the alcohols, whereas the best-fit values of the constants b_0 an b_1 for the plots are given in Table 5.6.

It should be noted that the constant b_0 in Table 5.6 is the maximum value of Y^* when $\ln\eta = 0$, and $-b_0/b_1 = \ln X^*$ is the maximum value of $\ln X$ when $Y = 0$. The maximum value of Y^* corresponds to the lowest value of $\ln X$ when Y begins to deviate from the linearity. This value of Y^* represents the point of intersection of dashed horizontal lines with the linear plots, as shown in Figure 5.11. Oviously, since both b_0 and b_1 are nonzero quantities, $\ln X^*$ is always nonzero. From the values of $\ln X^* = -b_0/b_1$, the calculated values of X^* equal to $\eta_0{}^*$, $(\eta/d)_0{}^*$ and $(\eta V_M)_0{}^*$ are also given in Table 5.6.

The differences in the behavior of the $\ln\eta[T^{-1}]$ and $\ln(\eta/d)[T^{-1}]$ data for the alcohols and that of the data for the alcohols and water in Figure 5.11 are essentially associated with the value of the intercept b_0 of the plots because the slope b_1 of the plots is a constant equal to 537±10 K and is independent of the data. These slopes of the plots correspond to the limiting temperature T_b^{lim} for the alcohols and are comparable with the boiling point $T_b = 532$ K of dodecanol (see Table 5.2). In contrast to the constancy of the slope b_1 of the plots, their intercept b_0 is related to the nature of the chemical bonds in the compounds and to the data. The lower value of E_η/R_G for water than that from the plot of E_η/R_G against $\ln\eta_0$ for alcohols is probably due to differences in the bonds between the molecules of water and alcohols.

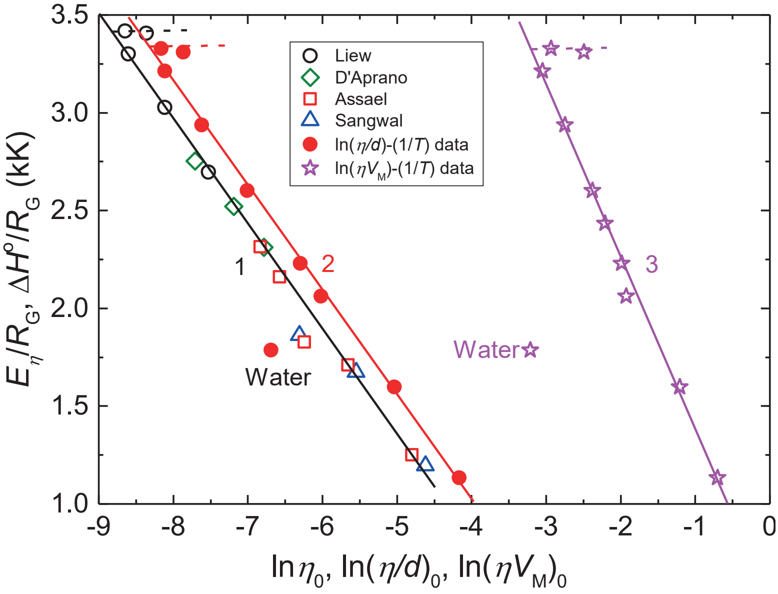

Figure 5.11. Relationship between (1) E_η/R_G and $\ln\eta_0$, (2) $\Delta H^o/R_G$ and $\ln(\eta/d)_0$, and (3) $\Delta H^o/R_G$ and $\ln(\eta V_M)_0$ for viscous flow of water and *n*-alcohol homologues. Constants of linear relationships, Eq. (5.22), for the alcohols are given in Table 5.6. Data from Tables 5.3 and 5.4.

Table 5.6. Constants b_0 and b_1 of Eq. (5.22) for curves of Figure 5.11

Data	Curve	$-b_0$ (kK)	b_1 (kK)	R^2	$-b_0/b_1$	X^*	r (nm)
$\ln\eta\ [T^{-1}]$	1	1.333	0.538	0.9966	2.478	0.0839 mP·s	0.124
$\ln(\eta/d)[T^{-1}]$	2	1.128	0.536	0.9969	2.104	0.122 mP·s·(cm³·g⁻¹)	0.124
$\ln(\eta V_M)[T^{-1}]$	3	0.492	0.881	0.9925	0.557	0.573 mP·s·(cm³·mol⁻¹)	0.113

The higher value of the intercept b_0 for curve 2 of $E_{\eta/d}/R_G$ against $\ln(\eta/d)_0$ than that for curve 1 of E_η/R_G against $\ln\eta_0$ for the same alcohols is due to the data used for the analysis. The higher intercept of curve 2 results in a higher value of $\ln(\eta/d)_0$ than those of curve 1 but this increase in the value of the intercept is accompanied by a lower value of the maximum $\Delta H^o/R_G$ of curve 2 than that of $E_{\eta/d}/R_G$ of curve 1. In fact, curve 2 overlaps curve 1 when $[\ln\eta_0 - \ln(\eta/d)_0] = -0.55$ and $(E_\eta - \Delta H^o)/R_G = 0.09$ kK. This implies that a lower value of the enthalpy ΔH^o of viscous flow obtained from the kinematic viscosity η/d of a liquid than that of E_η obtained from its dynamic viscosity η results in the value of $\ln(\eta/d)_0$ which is higher than $\ln\eta_0$. However, apart from differences in the absolute values of the Arrhenius parameters from the two types of the data, they give essentially the same information.

Using the values of b_0 and b_1 from the $\ln\eta(T^{-1})$ data given in Table 5.6, the limiting temperature $T_b^{\text{lim}} = 532$ K, and the lowest attainable value of $\ln\eta_0^{\text{lim}} = -8.85$ (i.e. $\eta_0^{\text{lim}} = 1.43\cdot10^{-4}$ mP·s) for 1-dodecanol (cf. Figure 5.11), one obtains

$$\frac{E_\eta}{R_G T_b^{\lim}} = 6.37\,. \tag{5.23}$$

Similarly, from the $\ln(\eta/d)[T^{-1}]$ data, with the lowest attained value of $\ln(\eta/d)_0^{\lim} = -8.3$ [i.e. $(\eta/d)_0^{\lim} = 2.48\cdot10^{-4}$ mP·s·(cm^3·g^{-1})] for 1-dodecanol, one obtains $\Delta H^o/R_G T_b^{\lim} = 6.20$. These values of $E_\eta/R_G T_b$ and $\Delta H^o/R_G T_b^{\lim}$ are comparable with the constant value of $E_\eta/R_G T_b$ equal to 6.38±0.18 for different alcohols from 1-butanol up to 1-dodcacanol (Table 5.3). This constancy implies that the activation energy E_η for viscous flow of these alcohols is mainly related to their boiling pont T_b and is about 40% of their enthalpy of vaporization. Using the constancies of $E_\eta/R_G T_b^{\lim}$ and $\Delta H^o/R_G T_b^{\lim}$, the relation between E_η/R_G and $\ln\eta_0$ for n-alcohols may be written in the form

$$\frac{E_\eta}{R_G T_b} = 6.37 - \ln\frac{\eta_0^*}{\eta_0^{\lim}}\,, \tag{5.24}$$

and

$$\frac{\Delta H^o}{R_G T_b} = 6.20 - \ln\left[\frac{(\eta/d)_0^*}{(\eta/d)_0^{\lim}}\right], \tag{5.25}$$

where the values of E_η, ΔH^o, T_b, $\ln\eta_0^*$ and of $\ln(\eta/d)_0^*$ refer to a particular alcohol.

From the values of $X^* = \eta_0$, $(\eta/d)_0$ and $(\eta V_M)_0$ listed in Table 5.6 and the preexponential factor hN_A/V_M of Eq. (5.6), one can calculate the smallest radius r_{h0} of the holes participating in the viscous flow of n-alcohols provided that the value of the volume $(V_M)_0$ corresponding to X^* is known. Since the radius of a spherical cavity of radius $r = (3V_M/4\pi)^{1/3}$ and the density $d = M/V_M$, we use the relation: $(V_M)_0 = hN_A/\eta_0$, assuming that $(\eta/d)_0 = \eta_0/d_0 = \eta_0\cdot(V_M/M)_0 = \eta_0\cdot(V_M)_0/M_0$ and $(\eta V_M)_0 = \eta_0\cdot(V_M)_0 = hN_A = 0.399$ mPa·s·(cm^3·mol^{-1}), where M_0 is the molar mass corresponding to the molar volume $(V_M)_0$ and d_0 is the density of the liquid of molar mass M_0 and molar volume $(V_M)_0$. The values of these smallest radii r_{h0} are included in Table 5.6. Obviously, these holes are of atomic dimensions.

The values of E_η/R_G and boiling point T_b given in Tables 5.3 and 5.2, respectively, show that for n-alcohols from 1-butanol up to 1-dodecanol, $E_\eta/R_G T_b$ is practically constant equal to 6.38±0.18 but its value decreases for lower alcohols with decreasing number N of $-CH_2$ groups in their molecules. This suggests that, although relation (5.24) holds for all normal alcohols up to dodecanol, the validity of linearity between $E_\eta/R_G T_b$ and $\ln(\eta_0^*/\eta_0^{\lim})$ is determined both by the activation energy E_η for viscous flow and the threhold $\ln\eta_0^*$. A similar conclusion can drawn from Eq. (5.25). From Eqs. (5.24) and (5.25) one can also explain the difference between E_η and ΔH^o.

The viscosity η of a liquid at different temperatures increases with its density d, which, in turn, decreases with increasing temperature following an Arrhenius-type dependence with the activation energy ΔE_η for self-diffusion (see Section 5.2.1). Then using Eqs. (5.11) and (5.12) the relationship between the limiting molar volume V_M^0 of the liquid when its fluidity $\phi = 0$ may be given in the form

$$V_M^0 = kV_M^{0*} \exp\frac{E_\eta^*}{R_G T_0}, \tag{5.26}$$

where k embraces constants related to D_0 of Eq. (5.12) and the term exp(6.37) of Eq. (5.24), and the activation energy $E_\eta^* = E_\eta - \Delta E_\eta$ (cf. Eq. (5.12)). In Eq. (5.26), T_0 denotes the limiting temperature of the liquid of the lowest attainable viscosity η_0^*, and V_M^{0*} is the lowest liquid molar volume V_M^0 of the liquid. Combination of Eq. (5.26) with (5.4) gives

$$\eta = A^* \exp\left(\frac{B^*}{T_0 - T}\right), \tag{5.27}$$

where $A^* = \ln[\eta_0^* \exp(6.37)]$, and $B^* = E_\eta T/R_G T_0$. This equation is similar to Eq. (5.14) used to describe the transport properties of glass-forming liquids which become very viscous on cooling down to their liquidus temperatures.

5.2.2.4. The Arrhenius temperature and model equations for viscosities of liquids

Eq. (5.4) may be expressed as

$$\ln\eta = \ln\eta_0 + \frac{E_\eta}{R_G T} = T^*\left(\frac{1}{T} - \frac{1}{T_A}\right), \tag{5.28}$$

where the Arrhenius activation temperature $T^* = E_\eta/R_G$ and the Arrhenius temperature $T_A = E_\eta/R_G\ln\eta_0$. From Tables 5.2 and 5.3, one observes the general relation: $T_A < T_m < T_b << T^*$. A similar trend may be observed from Table 1 in the paper by Messaâdi et al. (2015), who investigated the relationship between the Arrhenius temperatures T_A of 75 different liquids, their activation energies E_η for viscous flow and preexponential factors $\ln\eta_0$, and proposed model equations for viscosities of liquids. The results of this study are described below.

The Arrhenius temperatures T_A of various liquids are mutually related to their activation energies E_η for viscous flow and preexponential factor $\ln\eta_0$ and follow the relations (Messaâdi et al., 2015):

$$E_\eta = -\alpha\ln(1 - \beta T_A), \tag{5.29}$$

$$E_\eta = -31.3576 - 0.24845\ln\eta_0, \tag{5.30}$$

where α and β are positive constants. From Eq. (5.29) rewritten in the form

$$T_A = \frac{1 - \exp(E_\eta/\alpha)}{\beta}, \tag{5.31}$$

and the relation $T_A = E_\eta/R_G\ln\eta_0$, one obtains

$$\ln \eta_0 = -\frac{\beta E_\eta}{R_\mathrm{G}[1-\exp(-E_\eta/\alpha)]}, \tag{5.32}$$

and, with E_η is a function of $\ln\eta_0$, its reciprocal expression

$$E_\eta = -\frac{(R_\mathrm{G}/\beta)\ln \eta_0 + \alpha}{1-\exp(R_\mathrm{G}\gamma/\beta \ln \eta_0)}, \tag{5.33}$$

where γ is an adjustable parameter.

According to Eq. (5.31), the limiting value of the Arrhenius temperature T_A, $T_\mathrm{A}^* = 1/\beta$ when $E_\eta = \infty$. The experimental data of the dependence of E_η on T_A according to Eq. (5.29) gave $T_\mathrm{A}^* = 330.03\pm4.36$ K. This value corresponds to the lowest value of the boiling point T_b of the the studied liquids. With this limiting Arrhenius temperature T_A^*, Eqs. (5.29), (5.31), (5.32) and (5.33) may be written as

$$E_\eta = -\alpha_0 R_\mathrm{G} T_\mathrm{A}^* \ln\left(1-\frac{T_\mathrm{A}}{T_\mathrm{A}^*}\right), \tag{5.34}$$

$$T_\mathrm{A} = \left[1-\exp\left(\frac{E_\eta}{\alpha_0 R_\mathrm{G} T_A^*}\right)\right] T_\mathrm{A}^*, \tag{5.35}$$

$$\ln \eta_0 = -\frac{E_\eta}{R_\mathrm{G} T_\mathrm{A}^*\left[1-\exp\left(-\frac{E_\eta}{\alpha_0 R_\mathrm{G} T_A^*}\right)\right]}, \tag{5.36}$$

$$E_\eta = -\frac{(R_\mathrm{G} T_\mathrm{A}^*)[\ln \eta_0 + \alpha]}{1-\exp\left(\frac{R_\mathrm{G} T_A^* \ln \eta_0}{\gamma_0}\right)}, \tag{5.37}$$

where $\alpha_0 = 9.894\pm0.536$ and $\gamma_0 = (44.86\pm1.91)\cdot10^3$ are two dimensionless constants.

Messaâdi et al. (2015) calculated the values of E_η and $\ln\eta_0$ using Eqs. (5.37) and (5.36), respectively, and compared them with their experimental values. The authors observed good agreement between the two.

Substitution of Eqs. (5.36) and (5.37) in Eq. (5.28) gives the following one-parameter relations (Messaâdi et al., 2015):

$$\ln \eta = -\frac{E_\eta}{R_\mathrm{G} T_\mathrm{A}^*\left[1-\exp\left(-\frac{E_\eta}{\alpha_0 R_\mathrm{G} T_A^*}\right)\right]} + \frac{E_\eta}{R_\mathrm{G}}\frac{1}{T}, \tag{5.38}$$

$$\ln\eta = \ln\eta_0 - \frac{(R_\mathrm{G}T_\mathrm{A}^*)[\ln\eta_0 + \alpha_0]}{1 - \exp\left(\dfrac{R_\mathrm{G}T_A^*\ln\eta_0}{\gamma_0}\right)}\frac{1}{T}, \tag{5.39}$$

where $T_\mathrm{A}^* = 330.03 \pm 4.36$ K and the dimensionless constants $\alpha_0 = 9.894 \pm 0.536$ and $\gamma_0 = (44.86 \pm 1.91) \cdot 10^3$.

5.2.3. Low-temperature ionic liquids

Viscosities of a large number of organic solvents is relatively low and lie between 0.2 and 10 mPa·s at room temperature. In comparison with organic solvents, low-temperature ionic liquids (ILs) have a wide range of viscosities varying from about 15 to 800 mPa·s at room temperature (Rooney et al., 2009). Commonly investigated ILs are composed of cations based on imidazolium, pyridinium, pyrrolidinium and piperidinium, abbreviated hereafter as “im”, “py”, “pyr” and “pip”, respectively, and a variety of anions ranging from simple ions like halides and complex organic and inorganic-based radicals. Some of the common anions are: acetate $[\mathrm{CH_3COO}]^-$, thiocyanate $[\mathrm{SCN}]^-$, methylsulfate $[\mathrm{C_2SO_4}]^-$ (also denoted as $[\mathrm{MeSO_4}]^-$), ethylsulfate $[\mathrm{C_2SO_4}]^-$ (or $[\mathrm{EtSO_4}]^-$), hexafluorophosphate $[\mathrm{PF_6}]^-$, trifluoromethanesulfonate $[\mathrm{CF_3SO_3}]^-$, bis(trifluoromethylsulfonyl)imide $[\mathrm{NTf_2}]^-$, and tetrafluoroborate $[\mathrm{BF_4}]^-$. Figure 5.12 illustrates the viscosities of common ILs composed of two cations, 1-alkyl-3-methylimidazolium and alkyl-1-methylpyridinium, denoted as $[\mathrm{C}_n\mathrm{mim}]^+$ and $[\mathrm{C}_n\mathrm{mpy}]^+$, respectively, containing alkyl chain length with $n = 2$, 4, 6 and 8 and different anions at 25 °C.

It may be seen from the figure that the viscosity of an IL composed of the same anion increases with the alkyl chain length n of a cation, but that of the series of the same cation strongly depends on the type of the anion of the IL. For example, in the series $[\mathrm{C}_n\mathrm{mim}][\mathrm{NTf_2}]$ the viscosity at 25 °C increases steadily from 29.0 to 108.4 mPa·s whereas in the series $[\mathrm{C}_n\mathrm{mim}][\mathrm{PF_6}]$ it increases from 172.3 to 677.4 mPa·s. The increment $\mathrm{d}\eta/\mathrm{d}n$ in the viscosity η of the ILs with their chain length n shows the trend: $[\mathrm{NTf_2}]^- < [\mathrm{CF_3SO_3}]^- < [\mathrm{BF_4}]^- < [\mathrm{EtSO_4}]^- < [\mathrm{MeSO_4}]^- < [\mathrm{PF_6}]^- < [\mathrm{CH_3COO}]^-$. This general trend of the viscosity of ILs is related to the symmetry of the anion. ILs having highly symmetric anions are more viscous and the viscosity decreases with an increase in the asymmetry of the anion. It is also observed (Domańska and Królikowska, 2012; Rooney et al., 2009) that the viscosity of ILs having a common anion and a similar alkyl chain on the cation at a particular temperature changes in the order: $[\mathrm{C}_n\mathrm{mpip}]^+ > [\mathrm{C}_n\mathrm{mpyr}]^+ > [\mathrm{C}_n\mathrm{mpy}]^+ > [\mathrm{C}_n\mathrm{mim}]^+$, and the increment $\mathrm{d}\eta/\mathrm{d}n$ in the viscosity of these ILs having a common anion and a similar alkyl chain on the cation also changes in the same order. These trends of variation of viscosity are attributed to the ability of anion to form weak hydrogen and/or van der Waals bonds with the cation.

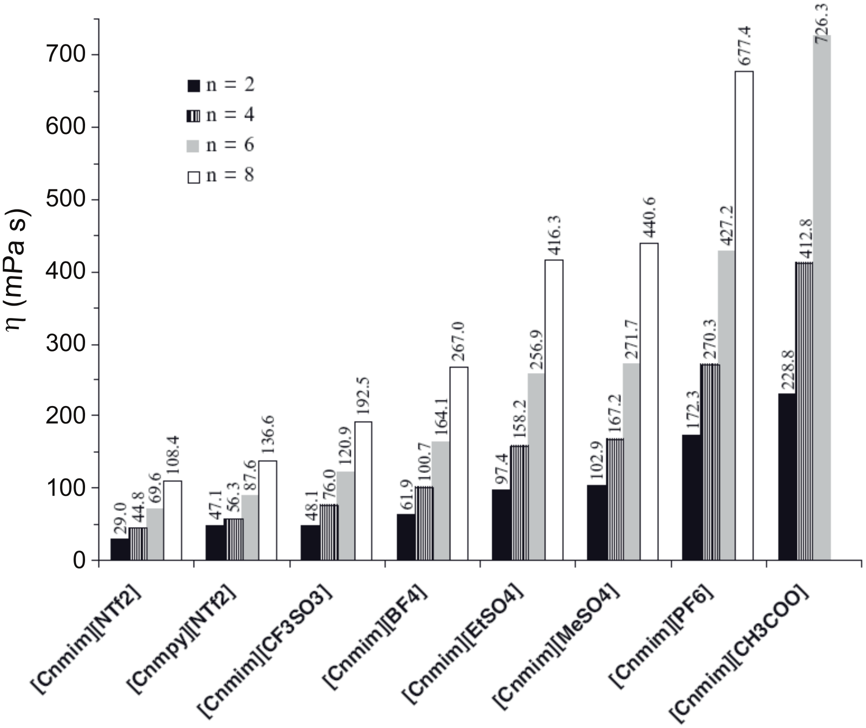

Figure 5.12. Viscosities of common ILs composed of $[C_n\text{mim}]^+$ and $[C_n\text{mpy}]^+$ containing alkyl chain length with n = 2, 4, 6 and 8 and different anions at 25 °C. Reproduced from Rooney et al. (2009).

As in the case of water and various organic liquids, the viscosity of ILs decreases with increasing temperature (Domańska and Królikowska, 2012; Domańska and Laskowska, 2009; Mokhtarani et al., 2009; Rooney et al., 2009; Vraneš et al., 2014, 2015), and is usually described by the VTF relation, Eq. (5.14). It has been found that the values of the ideal glass transition temperature T_0 for different ILs usually exceeds 150 K and the constant $B^* > 0$. Since the strength parameter $\Psi = B^*/T_0$ for a system, these values of the constant B^* and T_0 of Eq. (5.14) for different ILs imply that they are fragile liquids.

Here it should be mentioned that the presence of even low concentrations of impurities like chlorides strongly affects the viscosity of the ionic liquids and there is an enormous increase in the magnitude of the viscosity with the concentration of chloride (Seddon et al., 2000).

5.3. Viscosities of binary liquid mixtures

Investigations of viscosities of binary mixtures are of practical and theoretical interest in the range of their mutual miscibility. Therefore, viscosities of a wide variety of binary liquid mixtures have been studied. Examples of different binary mixtures are: water and alcohols (D'Aprano et al., 1979; Feakins et al., 1993; Ganzález et al., 2007; Herráez and Belda, 2004; Pang et al., 2007), water and nonionic organic compounds (Das et al., 2013, 2015; Koohyar et al., 2012; Messaâdi et al., 2012; Ouerfelli et al., 2012), alcohols and alkanes (Jimenez et al., 1998; Mahajan and Mirgane, 2013; Manfredini et al., 2002), alcohols and nonionic organic compound (Dikio et al., 2012; Mohammad et al., 2014; Živković et al., 2014), cyclic and aromatic hydrocarbons (Ranjith Kumar et al., 2009), water and ionic liquids (Domańska and Królikowska, 2012; Mokhtarani et al., 2009), and organic solvents and ionic liquids (Ciocirlan et al., 2016; Domańska and Laskowska, 2009; Heintz et al., 2002; Vraneš et al., 2014, 2015).

5.3.1. Basic concepts and equations

As in the case of the temperature dependence of viscosities of individual liquids discussed above, the dependence of the viscosities of binary liquid mixtures on temperature also usually follows Eqs. (5.4) and (5.6). Another general feature of most of the binary liquid mixtures is that their viscosity η measured at a constant temperature also does not follow the linear dependence according to the additivity rule for viscosities and usually shows enormous deviations from the linear behavior. Moreover, neither the values of the activation energies E_η and ΔG^o of Eqs. (5.4) and (5.6) of the temperature dependence of the viscosities η of the mixtures nor their viscosities η measured at a given temperature depend linearly on the concentration, taken in weight fraction w_2, volume fraction v_2 or mole fraction x_2, of liquid 2 (second liquid) added to liquid 1 (first liquid). Frequently they change nonlinearly showing a maximum or minimum at some concentration of the second solvent.

The nonlinear behavior of the viscosity η of liquid mixtures has drawn enormous interest regarding formulation of suitable mathematical equations capable of describing the available experimental viscosity data reliably and understanding of the possible causes of the nonlinearity. In this section the science behind these nonlinear dependences of the viscosities η of liquid mixtures on their composition is described. The thermodynamic properties like the energies E_η and ΔG^o associated with these nonlinear dependences of the viscosities η of liquid mixtures are also discussed.

A simple interpretation of the nature of viscosity of binary liquid systems versus their composition follows from Eyring's transition-state theory (see Section 3.2.1). The approach advanced below is similar to that used by Goldsack and Franchetto (1977, 1978) for the analysis of alkali halide solutions. According to this theory, the viscosity η of the mixture may be given by

$$\eta = \frac{h_\mathrm{P} N_\mathrm{A}}{V_\mathrm{M}} \exp\left(\frac{\Delta G^\mathrm{o}}{R_\mathrm{G} T}\right), \tag{5.40}$$

where V_M and ΔG^o are the molar volume and the free energy of activation of holes in the binary mixture, respectively. The sum of x_1 and x_2 mole fractions of liquid 1 and 2, respectively, in a binary mixture is always unity, i.e.

$$x_1 + x_2 = 1. \tag{5.41}$$

Therefore, when the values of V_{M} and ΔG^{o} for the mixture are the sums of contributions of solvent 1 and solvent 2, defined by

$$V_{\mathrm{M}} = (1-x_2)V_{\mathrm{M1}} + x_2 V_{\mathrm{M2}} = V_1\left[1 + x_2\left(\frac{V_{\mathrm{M2}} - V_{\mathrm{M1}}}{V_{\mathrm{M1}}}\right)\right], \tag{5.42}$$

and

$$\Delta G^{\mathrm{o}} = (1-x_2)\Delta G_1^{\mathrm{o}} + x_2 \Delta G_2^{\mathrm{o}} = \Delta G_1^{\mathrm{o}}\left[1 + x_2\left(\frac{\Delta G_2^{\mathrm{o}} - \Delta G_1^{\mathrm{o}}}{\Delta G_1^{\mathrm{o}}}\right)\right], \tag{5.43}$$

Eq. (5.40) gives

$$\eta = \frac{\eta_1}{1 + x_2 V}\exp(x_2 E). \tag{5.44}$$

In the above equations, h_{P} is the Planck constant, N_{A} is the Avogadro number, V_{M1} and V_{M2} are the molar volumes of the holes of the individual liquids 1 and 2 in the mixture, respectively, ΔG_1^{o} and ΔG_2^{o} are the corresponding molar free energies of activation for creating the holes, the dimensionless free energy E of activation for the creation of holes in the mixture

$$E = \frac{\Delta G_2^{\mathrm{o}} - \Delta G_1^{\mathrm{o}}}{\Delta G_1^{o}}, \tag{5.45}$$

the corresponding dimensionless molar volume V of the holes in the mixture

$$V = \frac{V_{\mathrm{M2}} - V_{\mathrm{M1}}}{V_{\mathrm{M1}}}, \tag{5.46}$$

and the viscosity η_1 of solvent 1 is given by

$$\eta_1 = \frac{h_{\mathrm{P}} N_{\mathrm{A}}}{V_{\mathrm{M1}}}\exp\left(\frac{\Delta G_1^{\mathrm{o}}}{R_{\mathrm{G}} T}\right). \tag{5.47}$$

Note that the values of V and E are constant for a binary mixture and depend on its temperature.

Eq. (5.44) reduces to (5.47) when $x_2 = 0$. It also takes the form of Eq. (5.4) when

$$\frac{1}{\eta_0} = \frac{V_{\mathrm{M1}}}{h_{\mathrm{P}} N_{\mathrm{A}}}(1 + x_2 V), \tag{5.48}$$

$$E_\eta = \Delta G_1^{\mathrm{o}}(1 + x_2 E). \tag{5.49}$$

However, depending on the values of V and E, Eq. (5.44) is expected to describe maxima as well as minima in the viscosity versus composition curves of mixtures. The values of V and E may be obtained from the experimental viscosities at fixed temperatures of binary solvent mixtures as a function of their composition using the rearranged form of Eq. (5.44) as

$$\ln\left\{\frac{\eta}{\eta_1}(1+x_2V)\right\}=x_2E. \tag{5.50}$$

This relation predicts a linear dependence of function $\ln[(\eta/\eta_1)(1+x_2V)]$ against x_2, if the value of V is chosen correctly.

In the above treatment, the dimensionless free energy E of activation for the creation of holes in the mixture (Eq. (5.45)) and the dimensionless volume V associated with E (Eq. (5.46)) are thermodynamic quantities involved in the viscosities of binary solvent mixtures, and Eq. (5.50) holds in the region of low x_2 values, say for $x_2 < 0.1$ mole fraction of solvent 2. An analogous procedure may be adopted to analyze the viscosity η of the liquid mixture rich in solvent 1.

It is usually observed that the viscosity η of binary mixtures of miscible liquids 1 and 2 of composition x_1 and x_2 at different temperature T changes nonlinearly with the content x_2 of liquid 2 in the main liquid 1. To account for this nonlinear behavior of the experimental $\eta(x_2)$ data in the intermediate x_2 region, a modified form of Eq. (5.44) based on the power-law dependence for non-Newtonian liquids and the Eyring's transition-state theory has been proposed using additive contribution from each component (Pang et al., 2007).

When the viscosity η of the liquid mixture at a given temperature is equal to the sum of individual contributions due to the two liquids, one talks of ideal mixture. The viscosity η^{id} of an ideal liquid mixture containing x_1 and x_2 mole fractions of the two liquids is given by the linear additivity rule, i.e.

$$\eta^{\mathrm{id}}=(\eta_1x_1+\eta_2x_2), \tag{5.51}$$

where η_1 and η_2 are the viscosities of the pure individual liquids 1 and 2, respectively. In order to describe the $\eta(x_2)$ data in the entire x_2 region, one has to consider the deviation $\Delta\eta$ in the measured experimental viscosity η of a liquid mixture from the ideal behavior, given by

$$\Delta\eta=\eta-\eta^{\mathrm{id}}=\eta-(\eta_1x_1+\eta_2x_2). \tag{5.52}$$

The simplest relation of the dependence of the viscosity η of a liquid mixture as a function of its composition x_1 or x_2 follows from Eq. (5.51), expressed as

$$\eta=(x_1\eta_1+x_2\eta_2)+\Delta\eta, \tag{5.53}$$

where emphasis is placed on describing the dependence of viscosity difference $\Delta\eta$ on x_1 or x_2. This difference is usually analyzed by the Redlich–Kister polynomial (Redlich and Kister, 1948)

$$\Delta\eta = Y^{\mathrm{E}} = x_1 x_2 \sum_{i=0}^{n} A_i (x_1 - x_2)^i \,, \qquad (5.54)$$

where n is an integer usually less than 4, A_i's are constants, and Y^{E} is usually called as an excesss parameter. When $n = 0$ in Eq. (5.54), the maximum deviation occurs at $x_1 = x_2 = 0.5$. However, the position of the maximum is shifted to a lower value of x_2 (or a higher value of x_1) with increasing n. Then one may write Eq. (5.53) in the form

$$\eta = (x_1\eta_1 + x_2\eta_2) + x_1 x_2 \sum_{i=0}^{n} A_i (x_1 - x_2)^i \,, \qquad (5.55)$$

Another approach is based on expressing the variation by a power-law function of x_2 (Herráez et al., 2008); i.e.

$$\eta = \eta_1 + (\eta_2 - \eta_1) x_2^{\sum_{i=0}^{n} B_i x_2^i} \,, \qquad (5.56)$$

where, as in Eq. (5.54), n is an integer and B_i's are constants. This equation explains systematic increase or decrease in the mixture viscosity η with x_1 or x_2 but is unsatisfactory for mixtures which show maxima or minima.

Some other empirical models involving one, two or three parameters used for the determination of the viscosities of liquid mixtures are given below.

(1) One-parameter models:

$$\eta = x_1^2\eta_1 + x_2^2\eta_2 + 2x_1x_2\eta_{12} \,, \qquad \text{Hind et al. (1960),} \qquad (5.57)$$

$$\ln\eta = (x_1 \ln\eta_1 + x_2 \ln\eta_2) + x_1x_2G_{12} \,, \qquad \text{Grunberg and Nissan (1949),} \qquad (5.58)$$

$$\ln(\eta V_{\mathrm{M}}) = [x_1 \ln(\eta_1 V_{\mathrm{M1}}) + x_2 \ln(\eta_2 V_{\mathrm{M2}})] + x_1x_2 \frac{W}{R_{\mathrm{G}}T} \,,$$

$$\text{Katti and Chaudhri (1964),} \qquad (5.59)$$

where G_{12} and W are fitting parameters.

(2) Two-parameter models:

$$\ln(\eta V_{\mathrm{M}}) = [x_1 \ln(\eta_1 V_{\mathrm{M1}}) + x_2 \ln(\eta_2 V_{\mathrm{M2}})] + x_1x_2[\alpha_1 + \alpha_2(x_1 - x_2)] \,,$$

$$\text{Heric and Brewer (1967),} \qquad (5.60)$$

$$\ln\nu = x_1^3 \ln\nu_1 + 3x_1^2x_2 \ln Z_{21} + x_2^3 \ln\nu_2 - \ln\left(x_1 + x_2\frac{M_2}{M_1}\right) +$$

$$+ 3x_1^2x_2 \ln\left(\frac{2}{3} + \frac{M_2}{3M_1}\right) + 3x_1x_2^2 \ln\left(\frac{1}{3} + \frac{2M_2}{3M_1}\right) + x_2^3 \ln\left(\frac{M_2}{M_1}\right) \,,$$

$$\text{McAllister (1960),} \qquad (5.61)$$

where $\nu = \eta/d$ is the kinematic viscosity of the liquid mixture, d is its density, the subscripts 1 and 2 with η and d denote the viscosity and the density of liquids 1 and 2, respectively, and M_1 and M_2 are the molar masses of the liquids.

(3) Three-parameter model:

$$x_1(x_1 + B_{12}x_2)(\eta - \eta_1) + A_{21}x_2(B_{21}x_1 + x_2)(\eta - \eta_2) = 0\,,$$

Auslander (1964), (5.62)

where B_{12}, B_{21} and A_{21} are empirical constants.

Comparison of fit of the experimental data for the viscosities of different liquid mixtures reveals that the viscosities calculated for some systems by one equation have a better correlation than those calculated for other systems by another equation but the correlation coefficient for a system improves with the number of fitting parameters (Herráez et al., 2008). The main limitation of the above equations is that they are empirical. However, among these relations, Redlich–Kister polynomial, Eq. (5.54), to analyze the dependence of the excess function Y^E or its reduced function Y^E/x_1x_2 on the composition x_1 or x_2 of the liquid 1 or 2 in their mixture provides useful information on the nature of complexes formed in the mixtures (for example, see: Das et al., 2013, 2015; Messaädi et al., 2012). For the purpose of analysis of the data of viscosities of the mixtures, different equations described in the preceding section are used.

5.3.2. Viscosities of molecular solvent mixtures

Here the general features of binary mixtures of simple molecular solvents are considered, where the dependence of the viscosity η of binary solvent mixtures on their composition and temperature is discussed.

5.3.2.1. Composition dependence of viscosities of molecular solvent mixtures

Figure 5.13 shows an example of the dependence of the viscosity η of water containing increasing concentration x_2 of methanol and ethanol at 25 °C. In the figure, the data denoted by open points are from Herráez and Belda (2004) and those denoted by filled points are from González et al. (2007). It may be noted that, despite a difference in the values of η for various values of x_2, a general feature of these mixtures is that, with an increase in the alcohol content x_2, their viscosity η initially increases, attains a maximum value $\eta_{\max}$ at $x_2 \approx 0.25$ mole fraction, and then slowly decreases and approaches the value of the viscosity η_2 of pure alcohols.

The $\eta(x_2)$ data of Figure 5.13 can be described by the n-th order polynomial:

$$\eta = \sum_{i=0}^{n} a_n x_2^n\,, \qquad (5.63)$$

where a_n's are empirical constants and n is an integer. Solid and dashed curves in the figure are drawn according to fourth- and fifth-order polynomials, respectively, with the best-fit contants listed in Table 5.7. It may be seen from the plots that the data of the mixtures, reported by Herráez and Belda (2004), are well described by the fourth-order polynomial, but the fit of the data reported by González et al. (2007) is somewhat improved when the fifth-order polynomial is used. This approach has been used to correlate the viscosity data of aqueous solutions of 1-propanol and 2 propanol at temperatures between 293.15 and 333.15 K (Pang et al., 2007).

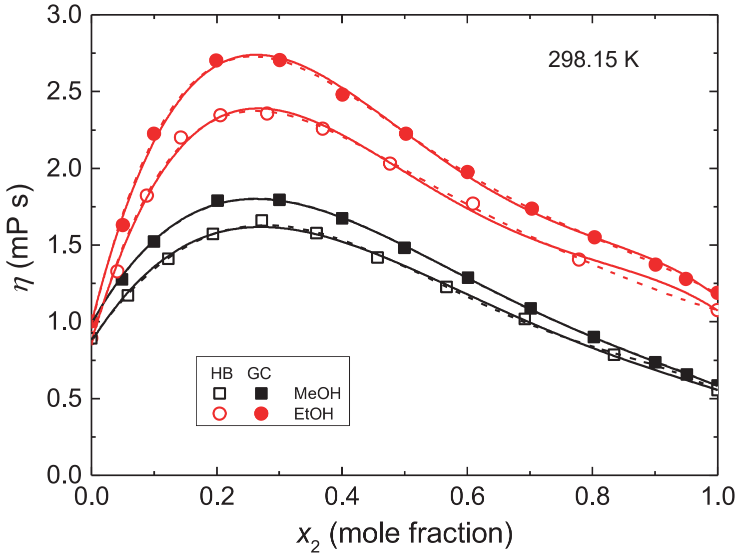

Figure 5.13. Dependence of viscosity η of water containing different contents x_2 of methanol and ethanol at 25 °C as a function of alcohol content x_2. Data denoted by HB and GC are from Herráez and Belda (2004), and González et al. (2007), respectively. Solid and dashed curves are drawn according to fourth- and fifth-order polynomials, respectively, with the best-fit contants listed in Table 5.7.

Table 5.7. Best-fit contants of polynomial for different water–alcohol mixtures

Mixture	Data	a_0	a_1	a_2	a_3	a_4	a_5	R^2
water–methanol	HB[a]	0.87019	6.50611	−17.84038	16.19739	−5.17574	--	0.9951
		0.88291	5.77692	−11.71521	−16.61266	15.77991	−8.56115	0.9964
	GC[b]	0.98688	7.3220	−20.79302	19.65605	−6.59071	--	0.9888
		0.98922	7.20055	−19.82278	16.94318	−3.49253	−1.23893	0.9987
water–ethanol	HB[a]	0.87163	13.96936	−41.92478	45.47592	−17.32071	--	0.9925
		0.85325	14.97567	−50.74047	72.16552	−49.79174	−13.61266	0.9930
	GC[b]	0.98882	16.27451	−49.24857	53.59315	−20.44710	--	0.9888
		0.96993	17.24999	−57.05623	75.44155	−45.40522	9.97972	0.9964

[a] Herráez and Belda (2004); [b] González et al. (2007).

The occurrence of a maximum viscosity $\eta_{\max}$ at $x_2 \approx 0.25$ mole fraction of an alcohol implies that one alcohol molecule is surrounded by three water molecules. This is associated with the dominance of solvation of alcohol molecules (i.e. water–alcohol interactions) involving hydrogen bonds, which results in maximum increase in the average size of the molecular aggregate. The motion of these aggregates leads to an increase in the viscosity of the water–alcohol mixture. More availability of water for $x_2 < 0.25$ mole fraction and more availability of an alcohol for $x_2 > 0.25$ mole fraction lead to the formation of competing water–water and alcohol–alcohol interactions, respectively, thereby decreasing the average size of the molecular aggregate participating in viscous flow. These changes in the average dimensions of the molecular aggregates also frequently result in changes in the density d of a water–alcohol mixture, but these changes may be insignificant in other mixtures.

Beyond the maximum viscosity $\eta_{\max}$ of a liquid mixture, the relative decrease in the viscosity η with the content x_2 of a liquid mixture is intimately connected with the size of liquid 2 molecules. Figure 5.14 shows, as an example, the maximum viscosities $\eta_{\max}$ of water–alcohol mixtures and the corresponding viscosities η_2 of pure alcohols as a function of the number N of $-CH_2$ groups in their molecules (also see Table 5.5). In the figure, the maximum viscosity $\eta_{\max}$ for 1-butanol in its mixtures with water denotes its saturation limit corresponding to 0.5 mole fraction, but addition of water to 1-pentanol results in a decrease in its viscosity. This means that 1-butanol can attach one water molecule to its molecule, but 1-pentanol is practically immiscible with water at 25 °C.

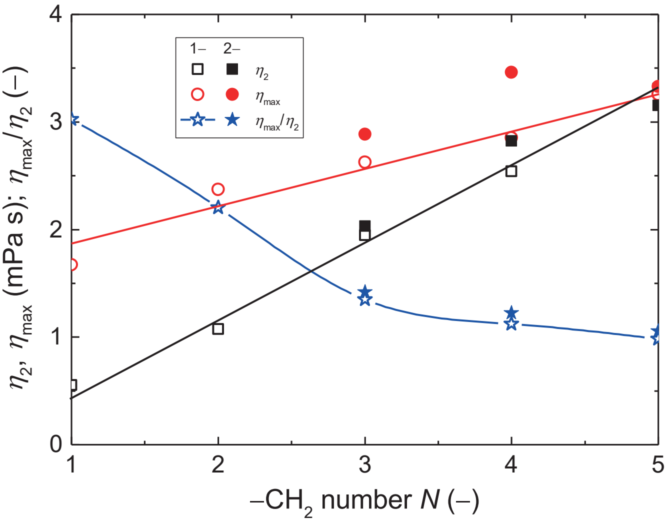

Figure 5.14. Plots of viscosities η_2 of pure 1- and 2-alcohols, maximum viscosities $\eta_{\max}$ of water–alcohol mixtures, and ratio $\eta_{\max}/\eta_2$ as a function of the number N of $-CH_2$ groups in their molecules. Open and filled points denote 1- and 2-alcohols, respectively. Data from Herráez and Belda (2004).

As seen from Figure 5.14, the viscosity η_2 of pure alcohols and the maximum viscosity η_{max} of water–alcohol mixtures increase practically linearly whereas the difference ($\eta_{max}-\eta_2$) for the alcohols decreases with increasing N and both linear plots tend to converge for $N = 5$ (i.e. for 1-pentanol). This behavior is associated with the decreasing number of attached water molecules per alcohol molecule with the increasing number N of $-CH_2$ groups in it. Since the difference ($\eta_{max}-\eta_2$) for the alcohols is related to the chemical constitution of alcohol molecules, the ratios η_{max}/η_2 and $(\eta_{max}-\eta_2)/\eta_2$ for an alcohol may be taken as measures of its solvation ability. The η_{max} and η_2 data for 1- and 2-alcohols up to $N = 5$ reveal that 2-alcohols in water have higher solvation ability than 1-alcohols in it (see Herráez and Belda, 2004).

The dependence of viscosity η of binary mixtures of molecular solvents on the content x_2 of one of the solvents, say solvent 2, is usually analyzed by using the Redlich–Kister polynomial (5.54) in terms of deviations $\Delta\eta$ in the experimental viscosity η from the ideal viscosity η^{id} determined by Eq. (5.52). From the sign of the viscosity deviation the nature of interaction between the molecules of the two solvents is discussed (for example, see González et al., 2007).

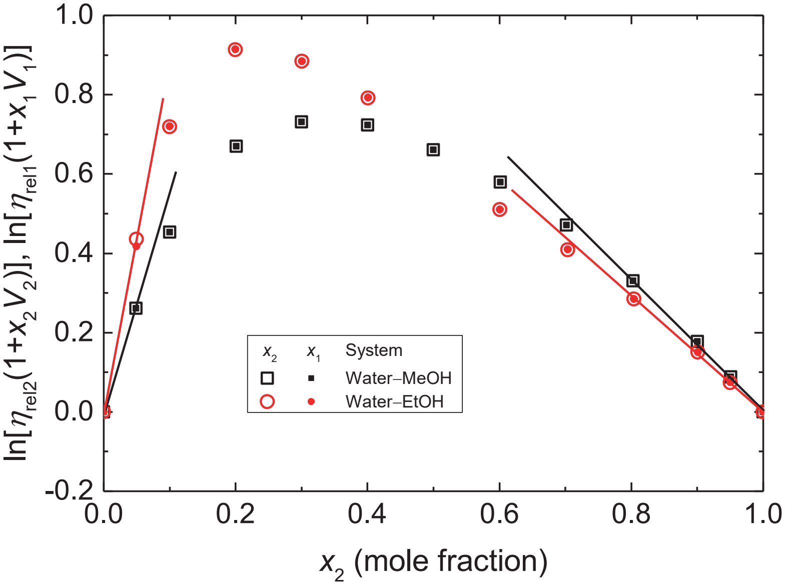

Figure 5.15. Plots of $\ln[(\eta/\eta_1)(1+x_2V_2)]$ against x_2 (large open points) and $\ln[(\eta/\eta_2)(1+x_1V_1)]$ against x_1 for water-rich and alcohol-rich mixtures of water–methanol and (squares) water–ethanol mixtures (circles), respectively, according to Eq. (5.50). Original data from González et al. (2007). Values of constants V_1 and V_2, and E_1 and E_2 of the plots are listed in Table 5.8. See text for details.

The viscosity data of water-rich and alcohol-rich mixtures may be analyzed according to Eyring's theory using Eq. (5.50). In view of a wide range of compositions of these mixtures, the original data at 25 °C reported by González et al. (2007) were used for the analysis. The terms $\ln[(\eta/\eta_2)$ for $x_2 = 0$ and $\ln[(\eta/\eta_1)$ for $(1–x_1) = x_2 = 1$ of Eq. (5.50) are zero. Therefore, these limiting values of $\ln[(\eta/\eta_1)(1+x_2V_2)] = 0$ and $\ln[(\eta/\eta_2)(1+x_1V_1)] = 0$ ensure a reliable procedure to determine the values of V_2 and V_1 while analyzing the data of water-rich and alcohol-rich mixtures according to Eq. (5.50). Here V_2 and V_1 denote the values of V of Eq. (5.50) for water-rich and alcohol-rich mixtures of composition x_2 and $x_1 = 1–x_2$, respectively. Figure 5.15 shows plots of $\ln[(\eta/\eta_1)(1+x_2V_2)]$ against x_2 (large open points) and $\ln[(\eta/\eta_2)(1+x_1V_1)]$ against x_1 (small filled points) for water-rich and alcohol-rich mixtures, respectively. As seen from the figure, the two sets of calculated data overlap each other when the values of V_1 and V_2 are correctly chosen. The values of the slopes E_2 and E_1 for the water-rich and alcohol-rich mixtures were calculated from the first two and the last four viscosity measurements, respectively. In view of the limited data considered for the calculation of E_2 for water-rich mixtures these values represent their lower limit. The values of the viscosities η_1 and η_2 of pure solvents, and the selected values of V_1 and V_2 and the corresponding values of the slope E_1 and E_2 of the linear plots are listed in Table 5.8.

Table 5.8. Values of constants V_1 and V_2, and E_1 and E_2 of Eq. (5.50).

System	Water-rich region			Alcohol-rich region		
	η_1	V_2	E_2	η_2	V_1	E_1
Water–methanol	0.890	0.6328	5.366	0.545	–0.388	1.673
Water–ethanol	0.890	–0.178	8.151	1.082	0.216	1.461

The values of V and E are related to the viscosity B coefficient of solute–solvent systems and to the volume V of the entities participating in viscous flow (see Section 5.4.3). However, this aspect will not be discussed here for these solvent–cosolvent binary systems.

5.3.2.2. Temperature dependence of viscosities of binary molecular solvent mixtures

The viscosity η and the quotient ηV_M of solvent mixtures of different second solvent content x_2 on mixture temperature T also follow Eqs. (5.4) and (5.9). Figure 5.16a and b shows typical examples of plots of $\ln(\eta/d)$ against T^{-1} for water–methanol and water–ethanol mixtures, respectively, containing different contents x_2 of alcohols, according to Eq. (5.9). The data of viscosity η and molar volume V_M for water, alcohols and their mixtures used in the plots are from González et al. (2007). The best-fit constants $\ln(\eta/d)_0$ and $\Delta H^o/R_G$ of the plots for various x_2 of methanol and ethanol in the mixtures are given in Table 5.9. The values of $\ln(\eta/d)_0$ and $\Delta H^o/R_G$ from plots similar to those in Figure 5.9 for pure alcohols based on the data published by Assael and Polimatidou (1994) are also included in the table.

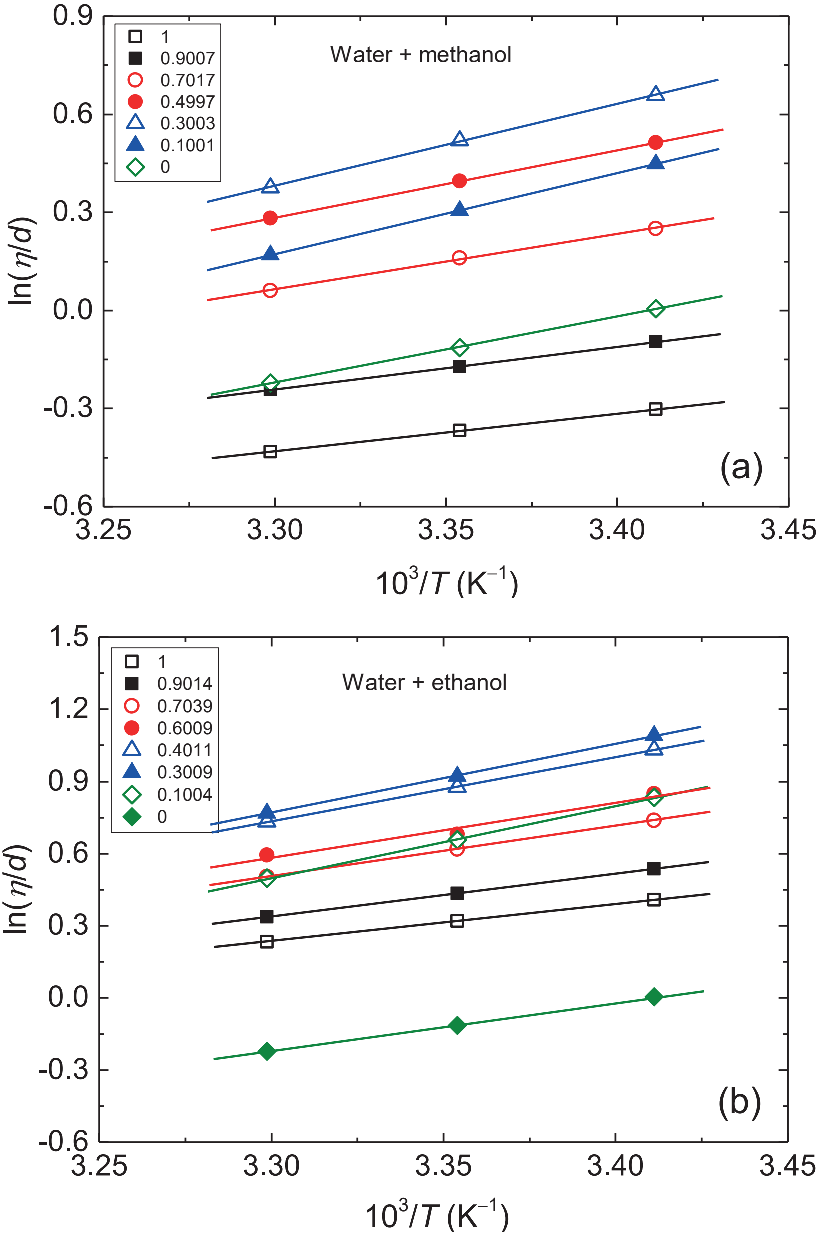

Figure 5.16. Plots of $\ln(\eta/d)$ against T^{-1} for (a) water–methanol and (b) water–ethanol mixtures containing different contents x_2 of alcohol, given in insets. Data from González et al. (2007). Constants of linear plots are listed in Table 5.9.

Table 5.9. Values of V_M^{25}, η^{25} and Arrhenius parameters $\ln(\eta V_M)_0$ and $\Delta H^o/R_G$ for two water-alcohol mixtures

Mixture	x_2 (mole frac.)	V_M^{25} (cm^3·mol^{-1})	η^{25} (mP·s)	ΔG^o (kJ·mol^{-1})	$-\ln(\eta/d)_0$	$\Delta H^o/R_G$ (kK)	ΔH^o (kJ·mol^{-1})
Water–MeOH	0	18.053^a	0.891^a	9.17	6.1021	1.7867	14.85
		18.053^b	0.890^b	9.17	6.8593	2.0117	16.73
	0.0488	19.155^b	1.121^b	9.89	7.1170	2.1618	17.97
	0.1001	20.317^b	1.317^b	10.43	8.0118	2.4802	20.62
	0.2014	22.612^b	1.542^b	11.09	7.9048	2.5026	20.81
	0.3003	24.852^b	1.554^b	11.34	7.9073	2.5114	20.88
	0.4016	27.124^b	1.463^b	11.41	7.0474	2.2454	18.67
	0.4997	29.368^b	1.309^b	11.33	6.5045	2.0574	17.10
	0.6015	31.674^b	1.150^b	11.20	6.0070	1.8775	15.61
	0.7017	33.944^b	0.987^b	10.99	5.5054	1.6880	14.03
	0.8027	36.231^b	0.821^b	10.70	5.0764	1.5133	12.58
	0.9007	38.451^b	0.677^b	10.37	4.5727	1.3124	10.91
	0.9510	39.590^b	0.607^b	10.17	4.4366	1.2420	10.33
	1	40.70^b	0.545^b	9.87	4.2179	1.1478	9.54
		40.74^c	0.5484^c	9.98	4.1653	1.1326	9.42
Water–EtOH	0	18.053^a	0.891^a	9.17	6.1021	1.7867	14.85
		18.053^b	0.890^b	9.17	6.8888	2.0117	16.73
	0.0501	20.084^b	1.388^b	10.54	8.4999	2.6403	21.95
	0.1004	22.126^b	1.860^b	11.50	9.3595	2.9877	24.84
	0.1999	26.166^b	2.300^b	12.44	8.7631	2.8799	23.94
	0.3009	30.267^b	2.275^b	12.78	8.7009	2.8700	23.86
	0.4011	34.335^b	2.115^b	12.91	8.0308	2.6563	22.09
	0.6009	42.447^b	1.659^b	12.83	6.9022	2.2684	18.86
	0.7039	46.628^b	1.531^b	12.87	6.3890	2.0894	17.73
	0.8039	50.688^b	1.380^b	12.82	5.8501	1.9031	15.82
	0.9014	54.647^b	1.232^b	12.72	5.5088	1.7720	14.73
	0.9499	56.616^b	1.153^b	12.65	5.2461	1.6764	13.94
	1	58.65^b	1.082^b	12.58	4.8535	1.5423	12.82
		58.67^c	1.081^c	12.57	5.0355	1.5970	13.28

[a] Lide (1996/1997); [b] Gonzalez et al. (2007); [c] Assael and Polimatidou (1994).

It should be mentioned that the effects of addition of component 2 to component 1 in binary liquid mixtures are usually discussed from the trends of the dependence of the activation energy E_η for viscous flow on the preexponential factor η_0 of Eq. (5.4) (Ciocirlan et al., 2016; Das et al., 2013, 2015; Mohammad et al., 2014; Messaâdi et al., 2012; Ourtfelli et al., 2012). However, here we examine the relationship between the slopes $\Delta H^o/R_G$ and the intercepts $\ln(\eta/d)_0$ of the plots of $\ln(\eta/d)$ against T^{-1} instead of the relationship between the slopes E_η/R_G and the intercepts $\ln\eta_0$ of the Arrhenius-type plots of $\ln\eta$ against T^{-1} according to Eq. (5.4). This is due to the fact that the dependence of $\ln(\eta/d)$ against T^{-1} provides a link between Arrhenius-type relation (5.4) and Eyring's relation (5.6). As pointed out before in Section 5.2.2, the values of the plots of both $\ln(\eta/d)$ against T^{-1} and $\ln(\eta V_M)$ against T^{-1} for various mixtures of molar volumes M give the same slope $\Delta H^o/R_G$ but the intercepts of the former plots are higher than those of the latter by the term $\ln M$. In addition to discussion of the relationship between $\Delta H^{o}/R_G$ and $\ln(\eta/d)_0$, dependences of Gibbs free energy ΔG^{o} and enthalpy ΔH^{o} of activation for viscous flow of water–alcohol mixtures on alcohol content x_2 and relationships between enthalpy ΔH^{o} of activation and ΔG^{o} and between entropy-related term $T\Delta S^{o}$ and ΔG^{o} are also discussed.

It may be seen from Table 5.9 that the values of molar volume V_M and viscosity η of the three solvents at 25 °C, denoted as V_M^{25} and η^{25}, respectively, from the two sources are comparable but the values of the intercept $\ln(\eta V_M)_0$ and the slope $\Delta H^{o}/R_G$ of the plots of Figure 5.16 are somewhat higher than those from the plots of Figure 5.9. Consequently, the values of the enthalpy ΔH^{o} of activation for the three solvents obtained from the data of González et al. (2007) are higher than those from the data of Assael and Polimatidou (1994). The difference in the values of ΔH^{o} for the alcohols are insignificant in contrast to that for water where they differ by 12%. These differences in ΔH^{o} for these solvents are due to errors in the measurements of their densities d and viscosities η in a relatively narrow temperature range between 20 and 30 °C. However, if the errors in the measurement are considered to be systematic, one may analyze the data of Gibbs free energy ΔG^{o} and enthalpy ΔH^{o} of activation for viscous flow as a function of content x_2 of liquid 2. The values of ΔH^{o} for different x_2 were calculated from the values of $\Delta H^{o}/R_G$ listed in Table 5.9 whereas those of the corresponding ΔG^{o} were calculated from the values of molar volume V_M^{25} and viscosity η^{25} of the mixtures at 25 °C using Eq. (5.8). The calculated values of ΔG^{o} and ΔH^{o} for different content x_2 of methanol and ethanol are included in Table 5.9.

Figure 5.17 illustrates changes in the enthalpy of activation ΔH^{o} and the Gibbs free energy ΔG^{o} for viscous flow of water–methanol and water–ethanol mixtures as a function of alcohol content x_2. The data are taken from Table 5.9 and are obtained from analysis of $\eta(T^{-1})$ data reported by Gonzalez et al. (2007). As in the case of the $\eta(x_2)$, the $\Delta H^{o}(x_2)$ and $\Delta G^{o}(x_2)$ data can also be represented by the polynomial of Eq. (5.63), with the values of the constants given in Table 5.10. As seen from the table, the $\Delta H^{o}(x_2)$ and $\Delta G^{o}(x_2)$ data for water–methanol mixtures can be represented satisfactorily by the fourth-order polynomial. The $\Delta G^{o}(x_2)$ data for water–ethanol mixtures are also well represented by the fourth-order polynomial, but the $\Delta H^{o}(x_2)$ data for these mixtures are better presented by the fifth-order polynomial.

A lower value of the ratio a_1/a_0 for the water–methanol mixtures than that for water–ethanol mixtures indicates that water–methanol interactions are weaker than water–ethanol interactions. Similarly, a lower value of $-a_2/a_1$ for water–methanol mixtures than that for water–ethanol mixtures indicates that methanol–methanol interactions are stronger than ethanol–ethanol interactions.

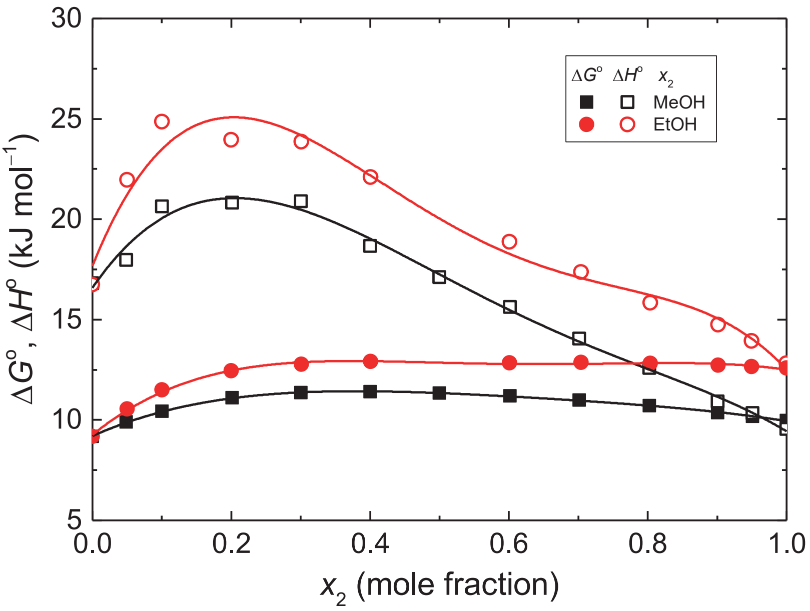

Figure 5.17. Change in Gibbs free energy ΔG^o and enthalpy of activation ΔH^o for viscous flow of water–methanol and water–ethanol mixtures as a function of alcohol content x_2. Curves represent best fit of the data according to fourth-order polynomial with constants listed in Table 5.10.

Table 5.10. Best-fit contants of Eq. (5.63) for $\Delta H^o(x_2)$ and $\Delta G^o(x_2)$ data of different alcohol–water mixtures

Mixture	Data	a_0	a_1	$-a_2$	a_3	$-a_4$	R^2
MeOH–water	$\Delta G^o(x_2)$	9.1993	15.3867	36.4993	35.3032	13.4475	0.9981
	$\Delta H^o(x_2)$	16.5787	50.4351	176.0235	192.9215	74.4810	0.9899
EtOH–water	$\Delta G^o(x_2)$	9.2552	28.0981	76.1962	86.2475	34.9042	0.9943
	$\Delta H^o(x_2)$	17.6574	86.4216	318.9380	394.9860	167.6162	0.9580

Figure 5.18 shows variations in the enthalpy of activation ΔH^o and the entropy-related term $T\Delta S^o$ for water–methanol and water–ethanol mixtures containing different alcohol content x_2 with Gibbs free energy ΔG^o for viscous flow. Directions of increasing alcohol content x_2, indicated by arrows, show that the value of the enthalpy ΔH^o for the two types of mixtures initially increases rapidly, then, after approaching a maximum value at $x_2 \approx 0.3$ mole fraction for water–methanol mixture and at $x_2 \approx 0.1$ mole fraction for water–ethanol mixture, decreases slowly with an increase in the Gibbs free energy ΔG^o up to the maximum value of ΔG^o equal to about 11.3 and 12.9 kJ·mol^{-1} at $x_2 \approx 0.35$ and 0.4 mole fraction for water–methanol and water–ethanol mixtures, respectively, when ΔH^o begins to decrease nonlinearly with decreasing ΔG^o. Trends similar to the plots of ΔH^o against ΔG^o are also shown by the plots of $T\Delta S^o$ against ΔG^o. With an increase in x_2 beyond the above maximum values of ΔG^o, the

decrease in ΔH^{o} with decreasing ΔG^{o} occurs in a narrow ΔG^{o} for water–ethanol mixtures in comparison with that for water–methanol mixtures. This observation is consistent with the above inference that methanol–methanol interactions are stronger than ethanol–ethanol interactions. These differences in the interactions are associated with the differences in the entropies of the two types of the mixtures.

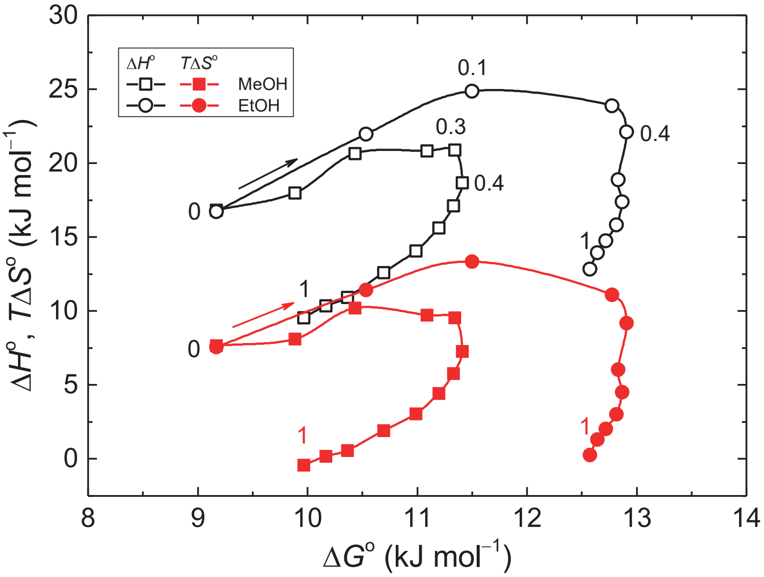

Figure 5.18. Change in enthalpy of activation ΔH^{o} (open points) and entropy-related term $T\Delta S^{\text{o}}$ (filled points) with Gibbs free energy ΔG^{o} for viscous flow of ethanol–water (squares) and ethanol–water mixtures (circles) containing different alcohol content x_2. Directions of increasing alcohol content x_2 for the two types of mixtures are indicated by arrows. Values of alcohol content x_2 corresponding to highest values of ΔG^{o} and ΔH^{o} are indicated.

Although the values of both Gibbs free activation energy and enthalpy of activation ΔH^{o} for a solvent mixture depend on the composition x_2 of solvent 2, the dependence of ΔG^{o} on x_2 for different systems is usually analyzed in terms of the data of the excess Gibbs free energy ΔG^{oE} at temperature T as a function of x_2 according to the Redlich–Kister relation (5.54). The excess ΔG^{oE} is calculated from the relation

$$\Delta G^{\text{oE}} = R_{\text{G}}T\left[\ln\left(\frac{\eta}{d}\right) - \sum_{i=1}^{n} x_i \ln\left(\frac{\eta_i}{d_i}\right)\right], \tag{5.64}$$

where η and d are the viscosity and density of the mixture. Using the UNIQUAC equation based on Eq. (5.64), with known values of η_i and d_i for individual components i of a mixture and the values of ΔG^{oE} the calculated viscosity data for the mixture may be correlated with its experimental data (González et al., 2007).

5.3.2.3. Relationship between activation energies and preexponential factors for binary molecular solvent mixtures

It was shown in Figure 5.11 that the values of $\Delta H^o/R_G$ of homologues of *n*-alcohols decrease linearly with increasing $\ln(\eta/d)_0$ for homologues of *n*-alcohols. It is interesting to examine the behavior of the data of $\Delta H^o/R_G$ against $\ln(\eta/d)_0$, given in Table 5.9, for different alcohol content x_2 in water–methanol and water–ethanol mixtures. Figure 5.19 shows the variation in the values of $\Delta H^o/R_G$ as a function of $\ln(\eta/d)_0$ with increasing alcohol content x_2 in water indicated by arrows starting from pure water (i.e. $x_2 = 0$) to pure alcohol (i.e. $x_2 = 1$).

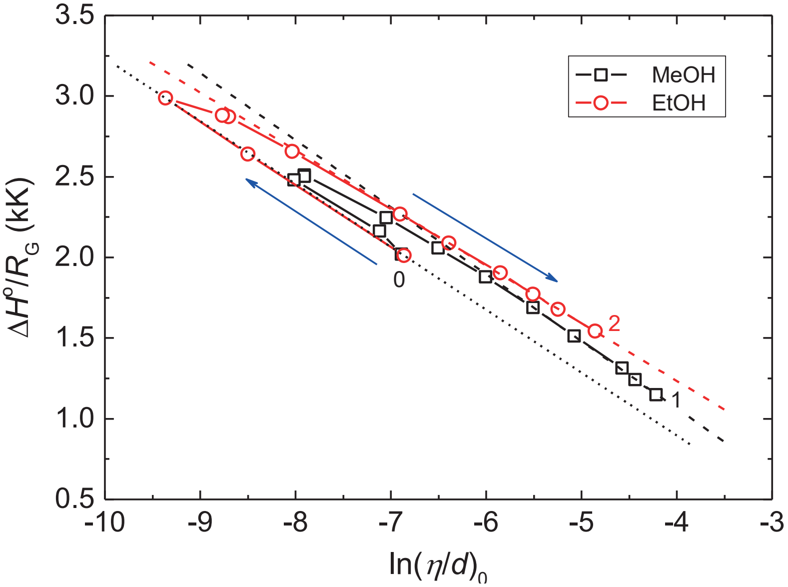

Figure 5.19. Relationship between $\Delta H^o/R_G$ and $\ln(\eta/d)_0$ for viscous flow of water–methanol and water–ethanol mixtures illustrating interruption at alcohol content $x_2 \approx 0.1$ mole fraction. Slopes of water-rich and alcohol-rich are indicated by dotted and dashed lines

From the above figure it may be noted that the data of $\Delta H^o/R_G$ as a function of $\ln(\eta/d)_0$ for water-rich and alcohol-rich solutions follow the same linear dependence described by Eq. (5.25) with slope b_1. In the linear range of composition x_2, the data for water-rich and methanol-rich solutions have practically the same slope equal to 0.393 kK but the data for ethanol-rich solutions have a lower slope equal to 0.350 kK. These values approximately correspond to the boiling points T_b of water and ethanol, respectively. However, the linear relationship between $\Delta H^o/R_G$ and $\ln(\eta/d)_0$ for water-rich solutions is interrupted at x_2 equal to 0.1 mole fraction corresponding to the limiting values of $\ln(\eta/d)_0$ of −8.0118 and −9.3595 [i.e. $\ln(\eta V_M)_0 = -5.1214$ and -6.4691 or $(\eta V_M)_0 = 5.97\cdot10^{-2}$ $1.55\cdot10^{-3}$ mPa·s·(cm^3·mol)] for methanol and ethanol cosolvents, respectively. This type of interruptions at specific mixture compositions are frequently observed in the plots of E_η against $\ln\eta_0$ of different binary liquid mixtures like 1,4-dioxane–water (Ouerfelli et al., 2012), N,N-dimethylacetamide–water (Das et al., 2013) and isobutyric-acid–water systems (Das et al., 2015). Since the values of E_η against $\ln\eta_0$ of the liquids are intimately related to ΔH° and $\ln(\eta/d)_0$, the origin of these interruptions in the two cases is the same.

An example of the relationship between E_η against $\ln\eta_0$ for 1,4-dioxane–water mixture illustrating the appearance of three interruptions corresponding to dioxane content x_2 equal to 0.08, 0.23 and 0.91 mole fractions is shown in Figure 5.20. The origin of the interruptions or breaks in the plots of activation energy E_η for viscous flow as a function of x_2 has been attributed to critical composition of the mixture separating distinct composition intervals of different clusters of associated molecules (for example, see: Das et al., 2013, 2015; Ouerfelli et al., 2012). The lowest value of $\ln\eta_0$ corresponding approximately to 0.08 mole fraction of dioxane indicates disruption of the hydrogen bonding network of water structure by hydrophobic hydration. This dioxane content of 0.08 mole fraction represents the formation of $10C_4H_8O_2{\cdot}H_2O$ clusters, followed by $4C_4H_8O_2{\cdot}H_2O$ clusters at $x_2 \approx 0.23$ mole fraction until $x_2 \approx 0.91$ corresponding to $C_4H_8O_2{\cdot}H_2O$ clusters.

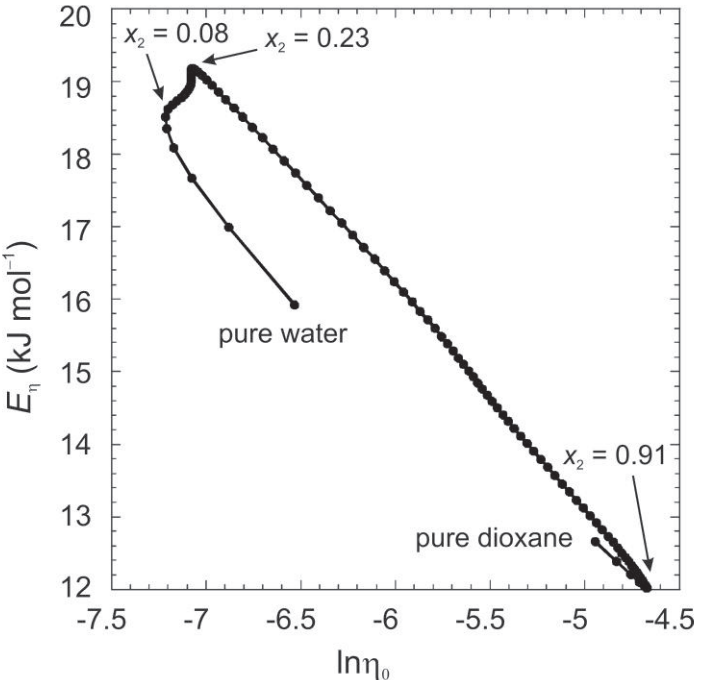

Figure 5.20. Relationship between E_η against $\ln\eta_0$ for 1,4-dioxane–water mixture illustrating the appearance of three interruptions at dioxane content x_2 equal to 0.08, 0.23 and 0.91 mole fractions. After Ouerfelli et al. (2012).

In order to have a better idea of the formation of clusters in the entire range of mixture composition, the data of E_η against $\ln\eta_0$ as a function of cosolvent content x_2 (Das et al., 2015; Ouerfelli et al., 2012) are discussed. Moreover, partial molar contributions Y_1 and Y_2 to E_η as well as $\ln\eta_0$ of the binary mixtures rich in liquid 1 and 2, respectively, are analyzed considering their thermodynamic functions defined as (Das et al., 2015; Ouerfelli et al., 2012)

$$Y_1(x_2) = Y_1^0(x_2) + (1 - x_2)\frac{\partial Y(x_2)}{\partial x_2}, \tag{5.65}$$

$$Y_2(x_2) = Y_2^0(x_2) - x_2\frac{\partial Y(x_2)}{\partial x_2}, \tag{5.66}$$

where $Y_1^0(x_2)$ and $Y_2^0(x_2)$ denote the values of $Y_1(x_2)$ when $x_2 = 0$. Figure 5.21 shows the dependences of the partial molar activation energies $E_{\eta 1}$ (filled circles) and $E_{\eta 2}$ (open circles) calculated according to Eqs. (5.65) and (5.66), respectively, on dioxane content x_2 in the 1,4-dioxane–water mixture. Following Ouerfelli et al. (2012), these observations are explained below.

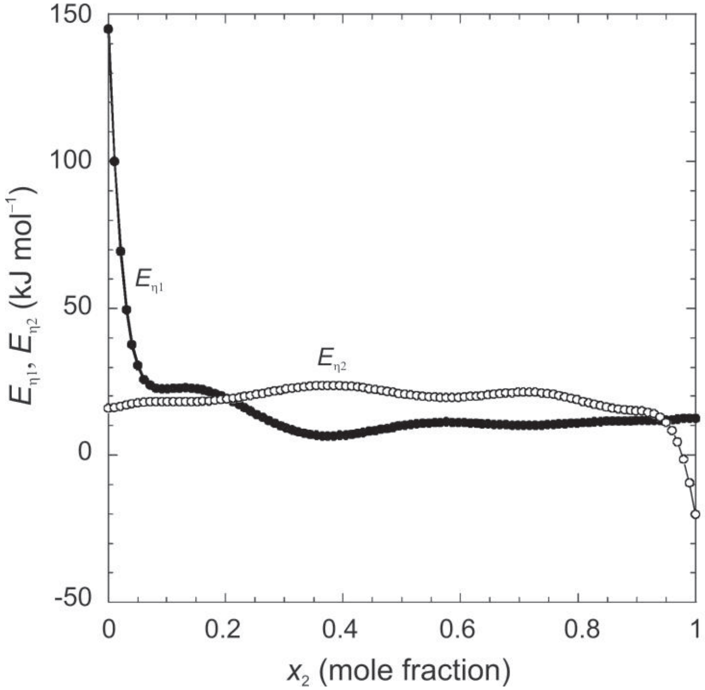

Figure 5.21. Dependence of the partial activation energies $E_{\eta 1}$ and $E_{\eta 2}$ calculated according to Eqs. (5.65) and (5.66), respectively, on dioxane content x_2 in the 1,4-dioxane–water mixture. After Ouerfelli et al. (2012).

The partial molar activation energy $E_{\eta 1}$ of dioxane abruptly decreases from a high value and after $x_2 \approx 0.05$ mole fraction changes slightly until it approaches a value of about 12 kJ·mol^{-1} for pure dioxane. This behavior indicates that in the water-rich mixture dioxane promotes the formation of clusters of water in which dioxane strenghens the water structure until $x_2 \approx 0.23$ mole fraction where the water network is broken. In contrast to the behavior of $E_{\eta 1}$ with x_2, the partial molar activation energy $E_{\eta 2}$ of water decreases insignificantly and has values slightly higher than that of pure water lying between 16 and 20 kJ·mol^{-1} up to $x_2 \approx 0.9$ mole fraction when it decreases steeply to negative values in the dioxane-rich region. The above results suggest that dioxane breaks the hydrogen bonds in the water structure in water-rich solutions but weak bonds between dioxane and water molecules may be formed in the mixtures containing high dioxane content. Consequently, dioxane molecules in water-rich mixtures are not integrated into the layers of water molecules but water molecules in dioxane-rich mixtures are easily incorporated in the layers of dioxane molecules. In these water-rich and dioxane-rich regions the size and shape of the incorporating molecules is likely to play important role.

The individual contribution of the components of a binary mixture of liquids to the activation energy E_η for viscous flow may be analyzed from the plot of the partial molar activation energies $E_{\eta 1}$ and $E_{\eta 2}$ in the entire composition range. For example, when the data of $E_{\eta 1}$ and $E_{\eta 2}$ for different dioxane content x_2 in the above water–dioxane mixture are presented as the plot of values of $E_{\eta 1}$ against their corresponding $E_{\eta 2}$, one obtains the delimitation of concentration domains of water and dioxane at $x_2 \approx 0.37$ mole fraction corresponding approximately to a cluster of composition $10C_4H_8O_2 \cdot 17H_2O$ (Ouerfelli et al., 2012). The dioxane content below and above $x_2 \approx 0.37$ mole fraction demarcates the former and the latter domains, respectively.

5.3.3. Viscosities of binary mixtures containing ionic liquids

The commonly investigated cosolvents with ionic liquids are water and various organic solvents (Ciocirlan et al., 2016; Domańska and Królikowska, 2012; Domańska and Laskowska, 2009; Heintz et al., 2002; Mokhtarani et al., 2009; Seddon et al. 2000; Vraneš et al., 2014, 2015). As in the case of mixtures of molecular solvents, the viscosity η of a binary mixture of an IL in water and molecular organic solids strongly depends on its concentration x_2 in the mixture as well as on the temperature T. However, the trends of the variation of η with x_2 for these mixtures significantly differ from those of the trends of the molecular solvents. An example illustrating the dependence of η of water–[bmim][SCN] mixture at different temperatures between 298.15 and 348.15 K on the concentration x_2 of [bmim][SCN] is shown in Figure 5.22. Here [bmim][SCN] is 1-butyl-3-methylimidazolium thiocyanate.

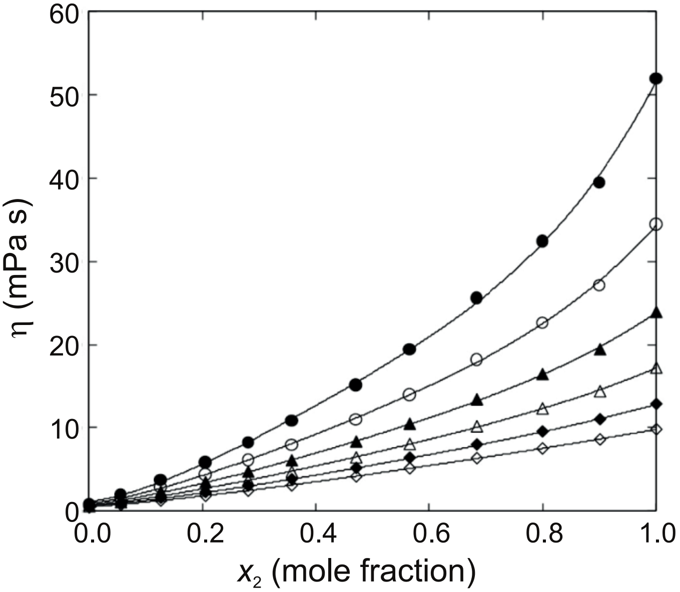

Figure 5.22. Dependence of η of water–[bmim][SCN] mixture on the concentration x_2 of [bmim][SCN] at different temperatures: (●) 298.15, (○) 308.15, (▲) 318.15, (△) 328.15, (♦) 338.15 and (◊) 348.15 K. After Domańska and Królikowska (2012).

It may be seen from the figure that the value of η steadily increases with x_2 at all temperatures and may be represented by a polynomial dependence similar to polynomial (5.63), with empirical constants a_i, to describe the $\eta(x_2)$ data of molecular solvent mixtures. However, in contrast to the maxima in the $\eta(x_2)$ plots of molecular solvent mixtures (see Figure 5.13), no maxima are observed in these plots of Figure 5.22 and there is enormous increase in η with increasing concentration x_2 of the IL (and decreasing concentration x_1 of water) in concentrated solutions of the IL in water. This trend is associated with the ion–dipole interactions and/or hydrogen bonding between the cation of the IL and the solvent water molecules in the water–[bmim][SCN] mixture. Addition of water to an IL results in the weakening of strong hydrogen bondings between its cations and anions, thereby increasing the mobility of ions and lowering the viscosity of the mixture. Similarly, an increase in temperature leads to the weakening of these bonds, which results in an increase in the mobility of ions and a decrease in the viscosity of the mixture of a particular composition. This effect of an increase in the temperature of a solvent–IL mixture on the plots of its viscosity η as a function of the IL concentration x_2 is reflected by decreasing trends of the absolute values of the constants a_i of polynomial (5.63).

It is interesting to note that the above trend of the $\eta(x_2)$ plots of Figure 5.22 is very similar to that observed in Figure 5.25 for aqueous solutions of sucrose and sodium nitrate, which follow Eq. (5.44); see Section 5.4.3. This suggests that the $\eta(x_2)$ of solvent–IL mixtures may also be described by an exponential function.

Another way of analysis of the viscosity η of solvent–IL mixtures is to consider the IL as a solvent and water and other organic solvents as cosolvent. Then the viscosity η may be observed to decrease with an increase in the concentration x_1 of the solvent 1 such that the resulting $\eta(x_1)$ plot is a mirror image of the $\eta(x_2)$ plot of Figure 5.22 about the η-axis and $x_1 = 1–x_2$. Using this procedure, Seddon et al. (2000) investigated the effect of water and several other solvents (ethanenitrile, trimethylethanenitrile, 2-propenenitrile, 1-methylimidazole, toluene, 1,4-dimethylbenzene, and 1,2-dimethoxyethane) on the viscosity of [C$_4$mim][BF$_4$] and [C$_4$mim][PF$_6$] and observed that the data of relative viscosity η_{rel} of the IL–cosolvent mixtures at 20 °C against the molar fraction x_1 of cosolvent indeed follow a single exponential equation with the constant 4.35 for [C$_4$mim][BF$_4$] and 5.26 for [C$_4$mim][PF$_6$]. This suggests that all of the investigated solvents have a similar effect on the viscosity of the ionic liquid.

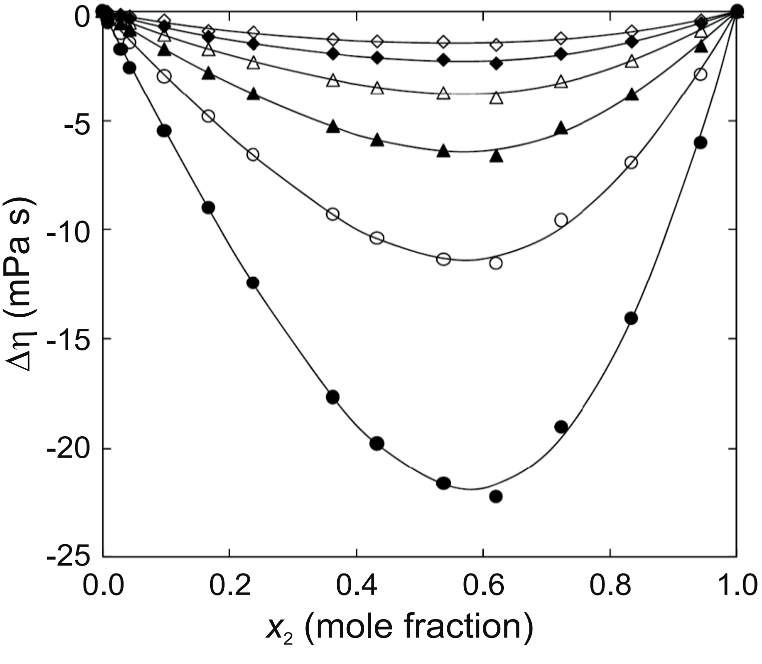

Figure 5.23. Plots of deviation $\Delta\eta$ in the viscosity η for water–[bmim][SCN] mixture as a function of x_2 of IL at different temperatures: (●) 298.15, (○) 308.15, (▲) 318.15, (∆) 328.15, (♦) 338.15 and (◊) 348.15 K. After Domańska and Królikowska (2012).

The nonlinear dependence of the experimental viscosity η of IL mixtures of different solvents on IL concentration x_2 at a given temperature is usually discussed from analysis of its deviation $\Delta\eta$ from the ideal viscosity η^{id} calculated by the additivity rule (see Eq. (5.52)) using Redlich–Kister polynomial relation (5.54). Figure 5.23 shows an example of the plots of deviation $\Delta\eta$ in the viscosity η of water–[bmim][SCN] mixture as a function of x_2 of IL at different temperatures. It may be seen that maximum deviation in $\Delta\eta$ occurs at $x_2 \approx 0.6$ mole fraction at all temperatures, but the maximum deviation decreases with increasing temperature. This behavior of the $\Delta\eta(x_2)$ plots is associated with the weakening of the hydrogen bonds between its cations and anions with an increase in the mixture temperature.

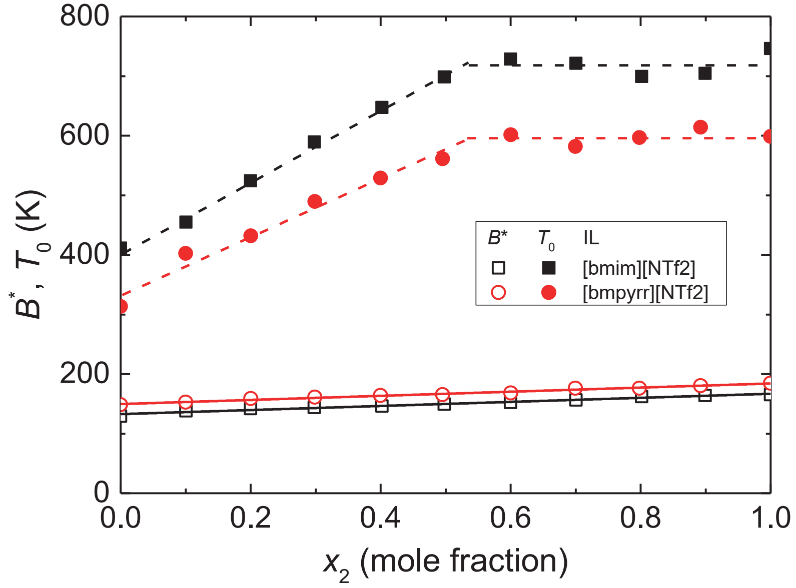

Figure 5.24. Dependence of B^* parameter and T_0 for GBL–[bmim][NTf$_2$] and GBL–[bmpyr][NTf$_2$] systems on IL concentration x_2. Note that T_0 increases linearly with x_2 in the entire x_2 range but this linear increase in B^* is only for $0 < x_2 < 0.5$.Original data from Vraneš et al. (2014, 2015).

As in the case of neat ILs, it is observed (Ciocirlan et al., 2016; Domańska and Królikowska, 2012; Domańska and Laskowska, 2009; Vraneš et al., 2014, 2015) that the experimental data of the temperature dependence of viscosities η of mixtures of molecular solvents containing different concentrations x_2 of ILs usually follow the VFT relation, Eq. (5.14). However, during the analysis of the $\eta(T)$ data of different binary IL mixtures, determination of the ideal glass transition temperature T_0 is found to be a critical step (Domańska and Królikowska, 2012; Domańska and Laskowska, 2009). The constants η_0, B^* and T_0 obtained from an analysis of the $\eta(T)$ data for solvent–IL systems of different IL concentration x_2 according to Eq. (5.14) show that their values usually increase with increasing x_2. Figure 5.24 shows an example of the dependence of B^* parameter and T_0 for GBL–[bmim][NTf$_2$] and GBL–[bmpyr][NTf$_2$] systems on IL concentration x_2. Here the abbreviation GBL denotes the solvent γ-butyrolactone. From the figure the following features may be noted:

(1) The value of T_0 for the two systems increases linearly with x_2 in the entire x_2 range

of GBL–[bmim][NTf$_2$] and GBL–[bmpyr][NTf$_2$] systems, following the relation initially proposed in the literature for electrolyte solutions (Angell and Bressel, 1972; Mohiuddin and Ismail, 1982, 1996)

$$y(x_2) = y_0 - Q_1(x_0 - x_2) = y_0^* - Q_1 x_2 , \tag{5.67}$$

where x_2 is expressed in mole fraction, y denotes T_0, T_0^* is the extrapolated temperature T_0 for the IL-free solution, and Q_1 is a constant characteristic of the solution–IL system. The intercept and the slope, of the $T_0(x_2)$ plots, denoted by T_0^* and Q_1, respectively, are listed in Table 5.11.

(2) The $B^*(x_2)$ data for the above system also follow relation (5.67), with the intercept and the slope of the plots denoted by B_0^* and Q_2, respectively. However, there are two x_2 regions below and above $x_2 \approx 0.5$ mole fraction for this linear relationship. With an increase in x_2, the B^* parameter initially increases linearly for $x_2 < 0.55$ and then remains practically constant for $0.55 < x_2 < 1$. These values of the intercept B_0^* and the slope Q_2 of the $B^*(x_2)$ plots for $x_2 < 0.55$ are listed in Table 5.11, where the corresponding values of B_0^* and Q_2 for $x_2 > 0.55$ are given in the parentheses.

(3) The increasing trends of T_0 and B^* with x_2 for the two systems are opposite to each other. While the values of T_0 for the GBL–[bmim][NTf$_2$] mixture are lower than those for the GBL–[bmpyr][NTf$_2$] system in the entire x_2 range, the values of B_0^* for the former are higher than those for the latter.

Table 5.11. Best-fits constants of Eq. (5.67) for different systems

System	Data	y_0^* (K)	Q_1 [K·(mole faction) $^{-1}$]	R^2
GBL–[bmim][NTf$_2$]	$T_0(x_2)$	132.8±1.0	34.2±1.7	0.9760
GBL–[bmpyr][NTf$_2$]		149.7±0.9	34.5±1.4	0.9829
GBL–[bmim][NTf$_2$]	$B^*(x_2)$	410 (720)	575 (0)	--
GBL–[bmpyr][NTf$_2$]		330 (595)	490 (0)	--

Data from: [a] Vraneš et al. (2014); [b] Vraneš et al. (2015).

The lower values of T_0 for the GBL–[bmim][NTf$_2$] system than those for the GBL–[bmpyr][NTf$_2$] system are directly related to the difference in their viscosities. This is associated with the fact that the value of T_0 for a liquid refers to the temperature of the liquid when the movement of its constituents is entirely frozen. However, the opposite trend of the values of the B^* parameter than that of T_0 for the above systems is due to the difference in the nature of this parameter, which is related to the free energy of a system. It may be seen from Figure 5.24 and Table 5.11 that this free energy change and the increase in B^* with an increase in the concentration x_2 of an IL essentialy occur only up to $x_2 \approx 0.55$ mole fraction and the maximum increase in B^* of the solvent GBL with the addition of x_2 for the GBL–[bmim][NTf$_2$] system is about 15% higher than that for the GBL–[bmpyr][NTf$_2$] system. This feature of these systems is related to differences in the miscibility of these ILs with the solvent due to the ion−dipole interactions and/or hydrogen bonding between the alkyl groups of the cation of an IL containing the same anion and the solvent molecules.

From the above dependences of T_0 and B^* on x_2 it may be seen that the strength parameter $\Psi = B^*/T_0$ for both systems increases practically linearly with x_2 up to $x_2 = 0.55$ but the value of Ψ thereafter shows slight decrease with an increase with x_2. It may also be seen that for both systems the B^* parameter increases with x_2 and then slowly decreases with x_2. The latter trend is similar to that described by Eq. (5.19) in the case of electrolyte solutions (Mohiuddin and Ismail, 1982). Here it should be mentioned that the B^* parameter of electrolyte solutions shows a trend to increase as well as decrease with an increase in solute concentration x_2 (Mohiuddin and Ismail, 1996). This behavior of electrolyte solutions is different from the above trends of variation of the B^* parameter with x_2 of ILs. However, this opposite behavior of B^* depends on the solvent used for the solution but, irrespective of the solvent, T_0 increases with an increase in the solute concentration x_2 (Mohiuddin and Ismail, 1996).

During the last two decades various models and correlative/predictive methods have been developed to describe the effect of composition and temperature of mixtures of ILs on the their viscosity. Correlative methods employ various empirical as well as theoretical equations (Section 5.3.1) whereas predictive approaches for the viscosity are usually based on quantitative structure−property relationship (QSPR) and group contribution methods (GCMs). It is outside the scope of this chapter to describe these methods. The reader is referred to the recent literature on the subject (for example, see: Rooney et al., 2009; Zhao and Jacquemin, 2017; Zhao et al., 2016a,b; and the references cited therein).

5.4. Viscosities of homogeneous solute−solvent mixtures

Binary homogeneous solute−solvent mixtures are solutions composed of a solute dissolved in a suitable solvent at a particular temperature. The most popular solvent used in these solutions is water but some organic solvents such as simple alcohols have also been used. Studies of viscosities of solutions up to nineteen eighties were mainly focused on aqueous solutions of electrolytes (like simple alkali halides, nitrates and sulfates) and simple nonelectrolytes (for example, sucrose). These studies have been reviewed by Stokes and Mills (1965) and Horvath (1985). Later studies have also been devoted to aqueous solutions of complex organic compounds such as drugs (for example, see: Abu-Daabes and Awwad, 2008; Dhondge et al., 2012).

The viscosities of binary homogeneous solute−solvent mixtures also change nonlinearly with solute content and follow temperature dependence similar to that observed for binary liquid mixtures discussed above. The similar trends suggest that the basic concepts of the dependences of viscosities of binary liquid mixtures on their composition and temperature described above may also be applied to understand the behavior of viscosities of solute−solvent systems in relation to their composition and temperature.

5.4.1. General features of viscosities of solutions

Figure 5.25 shows typical examples of the dependence of viscosities η of aqueous sucrose and sodium nitrate solutions at three selected temperatures on their concentration *m*. In accordance with the general trend of the temperature dependence of the viscosity η of solutions of different compounds of fixed concentrations, the viscosity η of the solution of a given concentration decreases with increasing temperature *T*. However, at a given temperature the viscosity η of a solution initially increases practically linearly with concentration up to about 1.5 m for sucrose solutions and about 3 m for sodium nitrate solutions and then increases relatively rapidly. Since the viscosity of a system is determined by the particles present in it, one may argue that, in addition to solvent molecules, solvated entities participate in the viscous flow of solutions and both the composition of a solution in a solvent and the temperature of the solution determine its viscosity. However, depending on whether the solute is a nonelectrolyte or an electrolyte, the solvated entities are likely to be their molecules or ions resulting from their dissociation by the solvent.

In the concentration region between 0.l and 10 m of aqueous nonelectrolyte and electrolyte solutions, several features of the viscosity of electrolyte solutions are known. For some compounds, a plot of viscosity η against molality *m* at a fixed temperature gives a roughly exponential function as seen from Figures 5.25 and 5.26a. For other compounds such as electrolytes however, pronounced minima occur in the plots as shown in Figure 5.26b. As seen from the experimental data of the viscosities of aqueous solutions of electrolytes reported by Goldsack and Franchetto (1978), the nature of exponential and nonexponential curves is related to the dimensions of cations and anions of an electrolyte in the solution as well as the solution temperature. The compounds that result in the appearance of minima in the $\eta(m)$ plots fall into the category of structure breakers, while those resulting in the exponential dependence fall into the category of structure makers; see below.

Experimental data of the viscosities η of aqueous solutions of different electrolytes, reported by Goldsack and Franchetto (1978), reveal that the viscosity of aqueous solutions of electrolytes, such as NaF, KF, NaBr and NaI, composed of significantly differing dimensions of cations and anions shows exponential dependence on solution concentration *m* irrespective of the solution temperature between 5 and 55 °C, but that of electrolytes like NH_4Cl, KBr, KI and KI, initially decreases and then, after attaining a minimum value, increases with increasing solution concentration *m* at all temperatures. In contrast, the viscosity η of aqueous NH_4Br solutions decreases practically exponentially with solution concentration *m* at 5 °C, but it shows minima at higher temperatures such that the solution concentration m_{min} corresponding to the minima in the $\eta(m)$ plots decreases with increasing solution temperature such that $\eta(m)$ plot at 55 °C is practically exponential. These observations are associated with the solvation behavior of ions of the electrolytes.

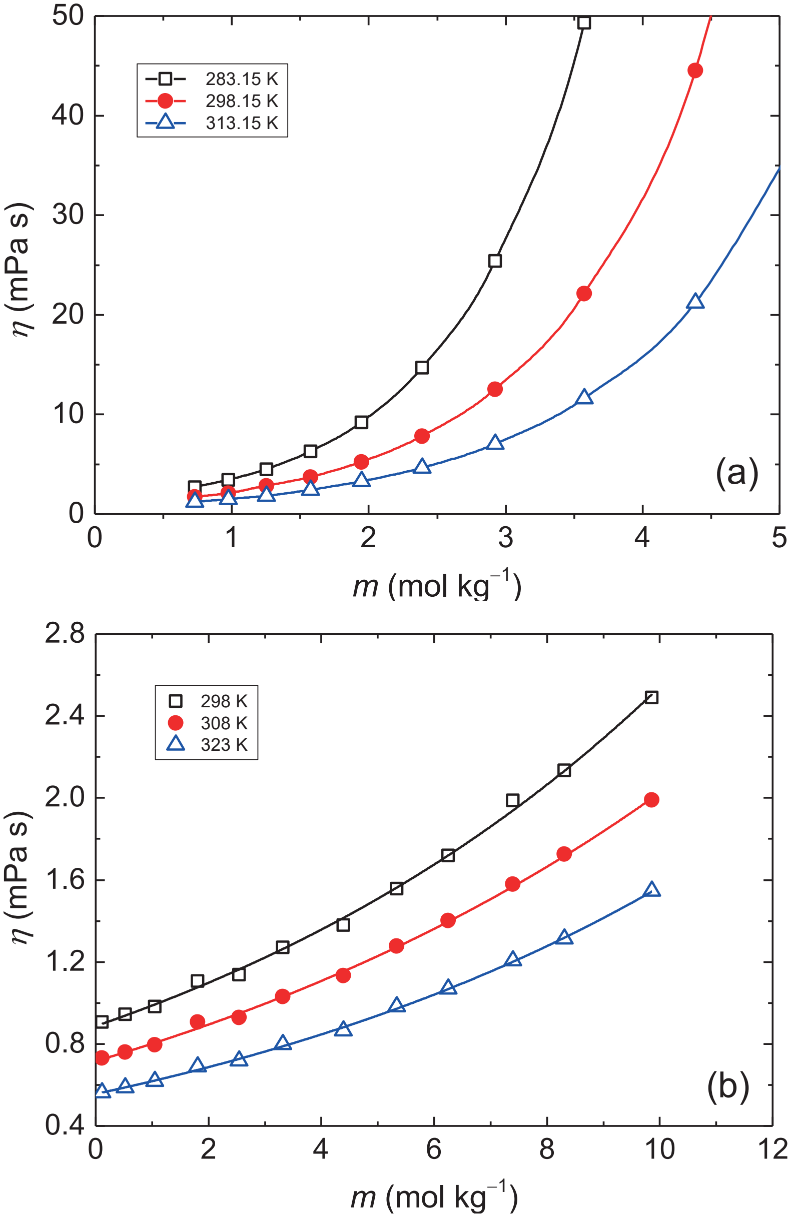

Figure 5.25. Examples of the dependence of viscosity η of aqueous solutions of (a) sucrose and (b) sodium nitrate on their concentration *m* at three selected temperatures. Temperature is given in the insets. Original data from: (a) Asadi (2006), and (b) Mahiuddin and Ismail (1996).

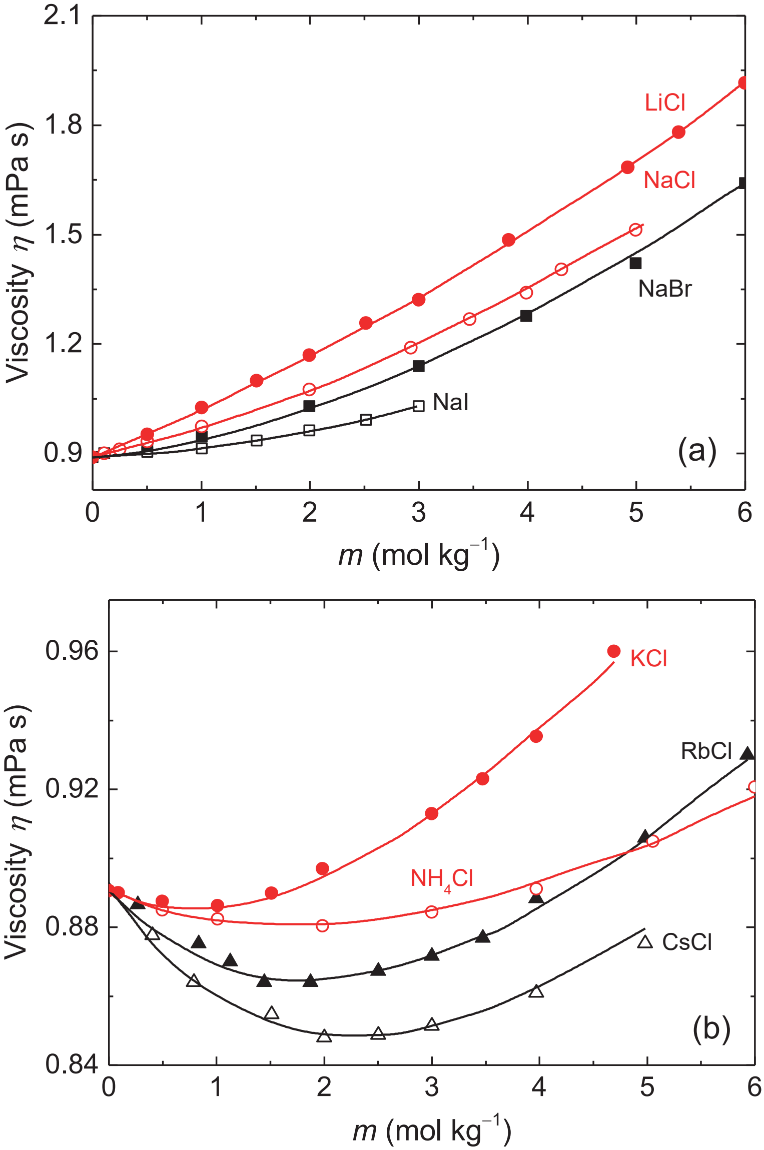

Figure 5.26. Plots of viscosity η against molality m of aqueous solutions of some salts: (a) exponential dependence and (b) minima in the $\eta(m)$ curves. Solid curves are calculated with Eq. (5.44). After Goldsack and Franchetto (1977).

As in the case of individual liquids and their mixtures, where the temperature dependence of viscosity is often described by an empirical Arrhenius-type equation, Eq. (5.4), fixed composition nonelectrolyte and electrolyte solutions and melts of high concentration are also found to follow this equation. However, in many cases the $\eta(1/T)$ curves markedly deviate from linearity with an increase in solute concentration, as shown in Figure 5.27.

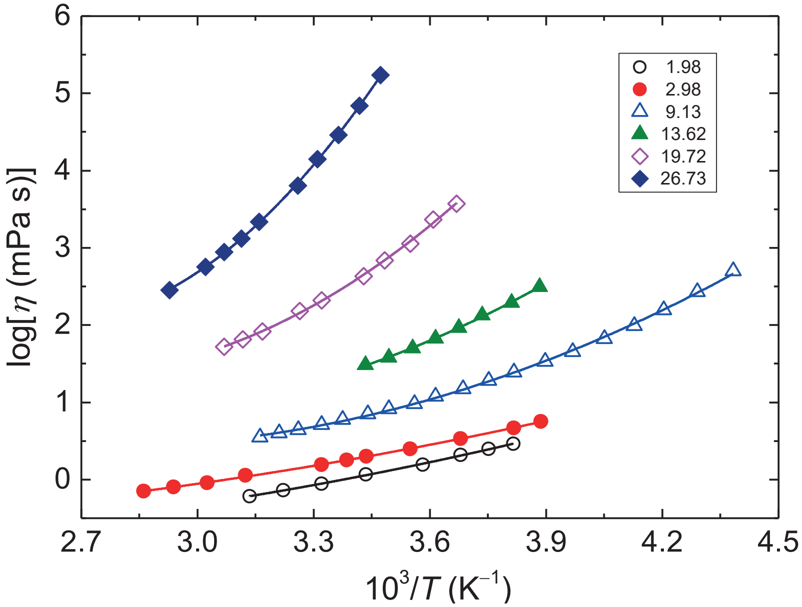

Figure 5.27. Examples of nonlinear Arrhenius plots of viscosity η for aqueous calcium nitrate solutions. Compositions are indicated in mol%. Original data from Angell (1966).

The activation energy E_η for viscous flow of many molten electrolytes remains constant (Bockris and Reddy, 1970), but there are cases, such as $ZnCl_2$ near its melting point, where the activation energy for viscous flow does not remain constant. These deviations are associated with structural changes, involving the formation of ionic aggregates, in the solution with increasing temperature.

5.4.2. Basic concepts and equations

5.4.2.1. Some frequently-used relations

The viscosity of a liquid is the result of relative motion of its particles. Therefore, it is expected that a solution containing solute particles larger than the solvent molecules will have a viscosity higher than that of the solvent. Assuming that the solute particles behave as rigid, uncharged spherical obstructions suspended in a solvent considered as a continuum, the relative viscosity $\eta_{\rm rel}$ of the suspension in the solvent of viscosity η_1 at a given temperature may be given by the Einstein relation (Robinson and Stokes, 1959; Stokes and Mills, 1965)

$$\frac{\eta}{\eta_1} = \eta_{\rm rel} = 1 + 2.5\theta\,, \qquad (5.68)$$

where η is the viscosity of the solution, and θ is the volume fraction of the particle in it. This relation holds for solution of small θ. To deal with higher concentrations of particles, Vand proposed the relation (Robinson and Stokes, 1959; Stokes and Mills, 1965)

$$\ln \eta_{\mathrm{rel}} = \frac{2.5\theta}{1 - Q\theta}, \tag{5.69}$$

where Q is a parameter characterizing the mutual interaction between the liquid surface layers. When $Q\theta << 1$, this equation may be written as

$$\ln \eta_{\mathrm{rel}} = 2.5\theta + 2.5Q\theta^2 . \tag{5.70}$$

For small volume fractions θ, this equation reduces to Eq. (5.68).

For small values of θ, the particle volume fraction $\theta = cV_{\mathrm{M}}$, where c is the solute concentration in moles·L^{-1} (i.e. molarity) and V_{M} is the molar volume in L·mole^{-1}. Then Eqs. (5.69) and (5.70) take the form

$$\ln \eta_{\mathrm{rel}} = \frac{B_2 c}{1 - Q' c}, \tag{5.71}$$

and

$$\eta = \eta_1 \exp(B_2 c + B_3 c^2), \tag{5.72}$$

respectively, where $B_2 = 2.5V_{\mathrm{M}}$, $B_3 = 2.5QV_{\mathrm{M}}^2$, and $Q' = QV_{\mathrm{M}}$. When $\ln(\eta/\eta_1) \approx (\eta/\eta_1) - 1$, Eq. (5.70) may also be expressed in the form

$$\eta = \eta_1 + B_2^* c + B_3^* c^2, \tag{5.73}$$

where $B_2^* = B_2 \eta_1$ and $B_3^* = B_3 \eta_1$.

The dependence of concentration c of an electrolyte in the solution at a given temperature on its viscosity is expressed by the Jones–Dole empirical equation (Desnoyers and Perron, 1972; Horvath, 1985; Robinson and Stokes, 1959; Stokes and Mills, 1965)

$$\eta_{\mathrm{rel}} = 1 + Ac^{1/2} + Bc, \tag{5.74}$$

where A and B are constants, which depend on solution temperature and are characteristic for an electrolyte. Eq. (5.74) describes the viscosity data for relatively dilute electrolyte solutions, but to describe concentrated solutions an additional c^2 term is added to the above relation (Desnoyers and Perron, 1972; Horvath, 1985; Stokes and Mills, 1965), i.e.

$$\eta_{\mathrm{rel}} = 1 + Ac^{1/2} + Bc + Cc^2, \tag{5.75}$$

where C is an empirical constant.

In Eqs. (5.74) and (5.75) the second term, with the constant A, accounts for long-range Coulomb forces between the ions considered as point charges. Therefore, this constant A is expected to be a positive quantity. Its value for various aqueous alkali and tetraalkylammonium halide solutions at 25 °C lies between $4.8 \cdot 10^{-3}$ and

$8.2 \cdot 10^{-3}$ (Desnoyers and Perron, 1972). Therefore, the contribution from ion–ion interaction to the viscosity of electrolyte solutions is very small and is important in the experimental $\eta(c)$ data only in very dilute solutions. At concentrations above about 0.002 M, a linear increase in viscosity with solute concentration is observed in strong electrolytes extending up to 0.1 M and higher in aqueous solutions and to somewhat lower concentrations in some nonaqueous systems. The linear concentration dependence of viscosity is associated with dominating solute–solvent interactions involving individual molecules/ions over ion–ion interactions. When the experimental $\eta(c)$ data begin to deviate from the linear dependence at still higher solute concentrations, interaction between individual molecules/ions results in the formation of larger aggregates of molecules/ions due to solvent deficiency in the solution. In this case, the empirical Cc^2 term accounts for the deviation from the linearity and the constant C is always a positive quantity (Desnoyers and Perron, 1972).

In the concentration range of linear increase in viscosity, the constant B, usually referred to as the viscosity B coefficient, of electrolyte solutions can be positive as well as negative, depending on the solute, the solvent and the solution temperature. The origin of this B coefficient in electrolyte solutions lies in ion–solvent interactions. Negative B coefficients are found for electrolytes composed of large ions in associated solvents such as water at relatively low temperatures. For example, at 25 °C, KCl and KI in aqueous solutions have negative B coefficients but NaCl in aqueous solutions has a positive B coefficient. However, KCl and KBr in methanol solutions have positive B coefficients. Large ions resulting in negative B coefficient are known as structure breakers, while small ones resulting in positive B coefficient are known as structure makers. Typical examples of the dependence of viscosity η of aqueous solutions of some alkali halides on the concentration m, expressed in molality m, at 25 °C are shown in Figure 5.26. The plots of Figure 5.26a follow an exponential dependence but those of Figure 5.26b show minima characteristic of the salt. As pointed out above, these trends of the concentration dependence of viscosities of electrolyte solutions are associated with the solvation characteristics of the ions of the electrolytes in their solutions.

The concentration dependence of viscosities η of electrolyte solutions is a result of overall effect of various contributions to the viscosity η_1 of the solvent, written in the form (Stokes and Mills, 1965)

$$\eta = \eta_1 + \eta^* + \eta^E + \eta^A + \eta^D , \tag{5.76}$$

where η^* is the positive contribution of Coulombian interaction between ions to viscosity, η^E is the positive contribution, closely related to the Einstein effect, caused by the size and shape of ions, η^A is the contribution due to the alignment or orientation of polar solvent molecules by the ionic field, and η^D is the contribution resulting from distortion of the solvent structure by the ions leading to hindrance in their movement. We note that the alignment of polar molecules by the ion stiffens the solution structure around it and restricts the movement of solvent molecules. Therefore, the contribution of η^A associated with the alignment of polar molecules by the ions is also positive. However, the contribution η^D associated with the distortion of the solvent structure results from the competing forces from ionic field and oriented or aligned solvent molecules with the ion and from the solvent structure in the bulk. Since this distortion hinders the movement of kinetic entities, the η^D contribution is negative.

Comparison of Eq. (5.76) with the Jones–Doles relation, Eq. (5.74), gives

$$\eta_1 Bc = \eta^E + \eta^A + \eta^D . \tag{5.77}$$

At a given concentration the *B* coefficient can be understood from this relation in terms of competetion between the three contributions at room temperature and as a function of solution temperature (Stokes and Mills, 1965). Another approach of summation of different contributions to the *B* coefficient is based on the size of kinetic entities participating in viscous flow (Mandal et al., 1973):

$$\eta_1 Bc = \eta^I + \eta^{ES} + \eta^V . \tag{5.78}$$

where η^I is the contrinution due to the intrinsic volume of the entitity ($\eta^I = A_1 r^3$), η^{ES} is the contribution due to electrostriction effect ($\eta^{ES} = A_2 z_{\mathrm{eff}}^2/r$), and η^V is the contribution of increase in the void volume ($\eta^V = A_3 r^2$), with A_1, A_2 and A_3 as constants, r as the crystal radius of the entitity, and z_{eff} as the effective charge on the kinetic entity. Like the contribution η^D of (5.77), in Eq. (5.78) η^V is negative while both η^I and η^{ES} are positive.

In general, the contribution η^E of molecules resulting in poor alignment of solvent molecules in their immediate neighborhood due to their shape and size is much greater than the sum of contributions η^A and η^D in Eq. (5.77). Similarly, η^I is greater than ($\eta^{ES}+\eta^V$). Therefore, the *B* coeffecient is expected to increase with increasing size of solute molecules. Consequently, the larger the viscosity η of a solution due to the size of solute particles, the higher is the value of the *B* coefficient. This aspect is pursued later in Section 5.5 during the discussion of ionic *B* coeffecients of electrolyte solutions.

It should be mentioned that the contribution of the square-root term to viscosity is zero in the case of solutions of nonelectrolyte and is negligible in not too-dilute electrolyte solutions. Then Eq. (5.75) takes the forms of Eq. (5.73) and the concept of the viscosity *B* coefficient and the structure-making and structure-breaking behavior of molecules/ions holds both for solutions of nonelectrolytes and electrolytes. Note that the value of the *B* coefficient is a result of interactions between solute and solvent molecules in nonelectrolyte solutions and between solute ions and solvent molecules in electrolyte solutions. Therefore, it is a very useful parameter for the investigation of these interactions (see Section 5.4.3). However, during the analysis of the concentration dependence of viscosities η of nonelectrolyte and electrolyte solutions, the solute concentration c in the above equations may also be replaced by some other unit of solute concentration such as molality m and mole fraction x.

5.4.2.2. Some other relations

In Section 5.2 it was pointed out that the temperature dependence of the viscosity η of individual liquids, including melts, and concentrated solutions in a wide range of temperature frequently shows nonlinearity in their Arrhenius plots and may be described by the VTF relation, Eq. (5.14). Typical examples of the nonlinear dependence of $\ln\eta$ against T^{-1} for aqueous calcium nitrate solutions of different concentrations in relatively large temperature intervals are shown in Figure 5.27. Concentrations of calcium nitrate in the solutions of the plots are indicated in the inset in mol%. A general feature of the plots of Figure 5.27 is that the nonlinearity in the plots increases with increasing calcium nitrate concentration. It is well known that the nonlinear behavior of the Arrhenius plots of $\ln\eta$ against T^{-1} is associated with the temperature T_0 of the liquid (i.e. melt, solvent or solution), when the movement of their molecules or ions is frozen (Angell and Bressel, 1972).

Eq. (5.14) can also be used to describe the relationship between viscosity and solute concentration contained in the solution by taking into account the composition dependent of the variables η_0, B^* and T_0, where the parameter $B^* = \Psi T_0$. As mentioned in Section 5.3.3, the concentration dependence of $T_0(x)$ is observed to follow relation (5.67), where T_0^* denotes the temperature T_0 for solute-free solution, and Q_1 is a constant characteristic of the solute–solvent system (Angell and Bressel, 1972; Mohiuddin and Ismail, 1982, 1996). Figure 5.28 shows examples of the plots of T_0 against the concentration x_2 of aqueous magnesium nitrate, sodium nitrate and sodium thiosulfate solutions and of aqueous and methanolic sodium thiocynanate solutions according to relation (5.67). Best-fits constants of the linear plots are given in Table 5.12.

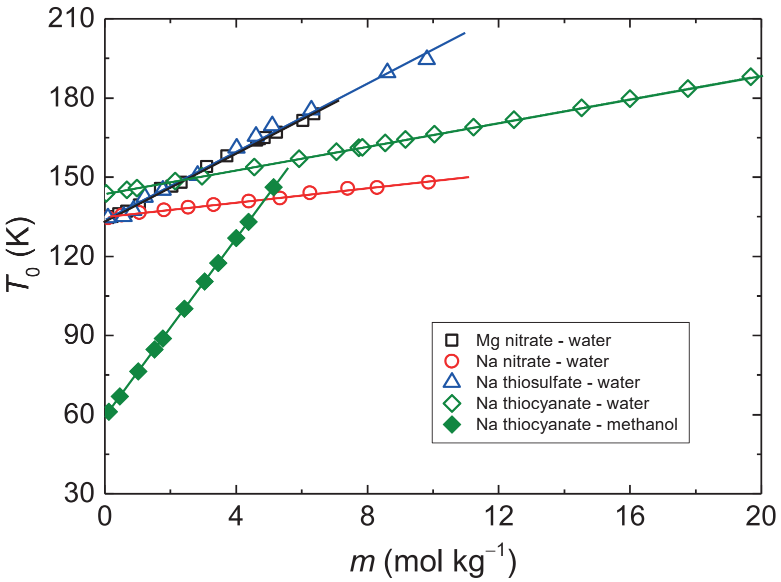

Figure 5.28. Linear dependence of freezing temperature T_0 on concentration m of different solutes in aqueous and methanolic solutions according to Eq. (5.67). Best-fit constants are given in Table 5.12. Original data for magnesium nitrate from Mahiuddin and Ismail (1982), for sodium nitrate and sodium thiosulfate from Mahiuddin and Ismail (1996), and for solutions of sodium thiocyanate in water and methanol from Rohman et al. (2001).

Table 5.12. Best-fits constants of Eq. (5.67) for different systems

System	T_0^* (K)	Q_1 [(mole faction) $^{-1}$]	R^2	Data
$Mg(NO_3)_2$–water	133.48	6.444	0.9977	a
$NaNO_3$–water	134.88	1.374	0.9933	b
$Na_2S_2O_7$–water	133.54	6.503	0.9924	b
NaSCN–water	143.69	2.248	0.9999	c
NaSCN–methanol	59.07	16.935	1	c

Data from: [a] Mahiuddin and Ismail (1982); [b] Mahiuddin and Ismail (1996); [c] Rohman et al. (2001).

From Table 5.12 the following features may be noted:

(1) The values of T_0^* depend on the solute as well as the solvent. Its value is higher for water than for methanol.
(2) The value of Q_1 depends on the type of solute and solvent. In aqueous solutions, its value is lowest for the 1:1 solutes and is about one-fifth of the value for the 1:2 and 2:1 solutes.
(3) The value of Q_1 for NaSCN in water is about one-eighth of the value for methanol solvent.

The above features are associated with the solvation characteristics of the ions present in the solutions. The higher values of T_0^* for different solutes in water in comparison with that for NaSCN in methanol appear to be related to the dielectric constant of the solvent and is directly associated with the molecular interactions in the two solvents. In contrast to the above trend, the values of Q_1 are associated with the nature of desolvation of solute ions/molecules with increasing solute concentration x_2. Solutes which result into more solvated ions in water, such as bivalent Mg^{2+} and $S_2O_7^{2-}$, are characterized by high Q_1 values than solutes resulting into monovalent ions alone. This behavior may be understood from consideration of relatively strong capability of these more solvated ions to shed off their solvent molecules with increasing solute concentration x_2. Similarly, solute ions/molecules poorly solvated in a solvent, such as methanol, of low dielectric constant also readily shed off their solvent molecules with increasing solute concentration x_2.

Considering that the strength parameter $\Psi = B^*/T_0$ is independent of solute composition and disregarding changes in η_0, substitution for T_0 from (5.67) in Eq. (5.15) gives

$$\eta(x) = \eta_0^* \exp\left(\frac{\Psi T}{Q_1(x_0 - x)} - \Psi \right), \tag{5.79}$$

which, under isothermal conditions, may be rewritten as

$$\eta(x) = \eta_0^* \exp\left(\frac{\Psi_1}{(x_0 - x)} \right), \tag{5.80}$$

where η_0^*, Ψ_1 and x_0 are constants at a particular temperature.

Upon replacing mole per cent x in Eq. (5.80) with the molar concentration c according to the relation

$$x = \frac{1800\,c}{[1000\,d - (M_2 - 18)c]}, \tag{5.81}$$

where d is the solution density and M_2 is the molecular mass of the solute, one obtains

$$\eta(x) = \eta_0^* \exp\left(\frac{D_1 + D_2 c}{D_3 - c}\right), \tag{5.82}$$

where D_1, D_2 and D_3 are new constants. This equation is very similar to Eq. (5.69) due to Vand.

During the derivation of Eq. (5.80) from Eq. (5.14) the dependence of solution concentration on η_0 was entirely neglected and the parameter B^* was assumed to follow the linear decreasing dependence given by Eq. (5.19). When the relation between η_0 and T_0 is of the form (Mahiuddin and Ismail, 1982)

$$\eta_0 = \eta_0^{\mathrm{o}} \exp\left(\frac{B_2}{T_0}\right), \tag{5.83}$$

where η_0^{o} and B_2 are constant parameters related to the system, then using Eqs. (5.19), (5.67) and (5.83) one obtains

$$\eta_0 = \eta_0^{\mathrm{o}} \exp\left(\frac{B_2[1 - Q_2(T_0^* + Q_1 m)]}{T - (T_0^* + Q_1 m)} - \frac{B_2}{T_0^* + Q_1 m}\right), \tag{5.84}$$

where $T_0^* = T - Q_1 m_0$, the solution concentation is taken in molality m, and m_0 is the solution concentration at temperature $T_0(0)$. When the following approximations hold:

$$\frac{1}{T - (T_0^* + Q_1 m)} \approx \left(1 + \frac{Q_1 m}{T - T_0^*}\right)\frac{1}{(T - T_0^*)}, \tag{5.85}$$

$$\frac{1}{T_0^* + Q_1 m} \approx \left(1 - \frac{Q_1 m}{T_0^*}\right)\frac{1}{T_0^*}, \tag{5.86}$$

under isothermal conditions Eq. (5.83) takes the simplified form

$$\eta = \eta_0^{\mathrm{o}} \exp(B_2^* m + B_3^* m^2)\,. \tag{5.87}$$

This is similar to Eq. (5.72), which was obtained from Vand's relation (5.69). Eq. (5.87) has been successfully used to describe the concentration dependence of viscosities of aqueous electrolyte solutions in high concentration range even up to 20 m (for example, see: Mahiuddin and Ismail, 1982, 1983, 1996; Rohman et al., 2001).

Eyring's transition-state theory has been used extensively to explain the dependence of solution viscosity η of electrolytes on solute concentration c and solution temperature T (for example, see: Feakins et al., 1974, 1993; Goldsack and Franchetto, 1977, 1978; Horvath, 1985). The basic ideas of this approach in the case of solutions are similar to those described in Section 5.3.1 dealing with binary solvent mixtures. According to this approach (Goldsack and Franchetto, 1977, 1978), the viscosity η of a solution composed of solvent 1 containing solute 2 of concentration x_2, expressed in mole fraction, is described by Eq. (5.44), where the dimensionless free energy E of activation for the viscous flow of the solution, dimensionless molar volume V of the holes in the solution and the solvent viscosity η_1 are given by Eqs. (5.45), (5.46) and (5.47), respectively. The values of V and E are constant for different types of salts and depend on the solution temperature.

Depending on the values of V and E, Eq. (5.44) can explain minima in the curves of viscosity η of solutions as a function of solute concentration x_2 as well as a steady increase with increasing x_2. Minima in the $\eta(x_2)$ curves are expected when $V > 0$ and $E > 0$, but maxima are expected when $V < 0$ and $E < 0$. However, for $x_2V << 1$, the viscosity η is expected to increase and decrease exponentially with increasing x when $E > 0$ and $E < 0$, respectively. The values of the E and V parameters may be obtained from the data of the experimental viscosities at fixed temperatures of solutions as a function of solute concentration x_2 using Eq. (5.44) rewritten in the linear form as Eq. (5.50). According to this relation, a correctly chosen value of V enables to obtain linear dependence of $[(\eta/\eta_1)(1+x_2V)]$ on x_2 with zero intercept and slope E. This value of E for the solution of solute concentration x_2 is related to the activation energy E_η for viscous flow by Eq. (5.49).

Figure 5.29 illustrates an example of the linear dependence according to Eq. (5.50) for aqueous solutions of some alkali chlorides at 25 ^{o}C. Note that the slope E of the linear plots decreases in the order: NaCl, LiF, KCl and NH_4Cl. This trend is associated with the dimensions of the kinetic entities participating in viscous flow and is related to their solvation characteristics in the solutions.

Figure 5.30a and b shows the data of the viscosity η of aqueous sucrose and sodium nitrate solutions as a function of their concentration x_2 at three selected temperatures, shown in Figure 5.25, in the form of plots of $\ln[(\eta/\eta_1)(1+x_2V)]$ against the concentration x_2 of the solutions, respectively, according to Eq. (5.50).

The values of η_1 and V selected to obtain the fit of the data are given in Table 5.13. The values of the intercept Δ of the fit with the selected values of η_1 and V for the two systems are also included in the table. The best-fit values of η_1 used to obtain zero intercept Δ are given, as an example, in the parentheses for the $NaNO_3$–water system.

It may be noted that the selected values of η_1 are mainly responsible for the nonzero values of the intercept Δ and, as shown for the $NaNO_3$–water system, a somewhat higher value of η_1 than that used in the plots leads to zero intercept Δ. The reason of these higher values of η_1 estimated from the best fit of the plots is associated with possible large scatter in the measurement of viscosities of solutions at low solute concentrations and somewhat lower values of η_1 at different temperatures reported in the literature. For example, for the $NaNO_3$–water solutions the deviation in the estimated values of η_1 from those reported in the literature is about 2 and 3.3% at 308 and 323 K, respectively.

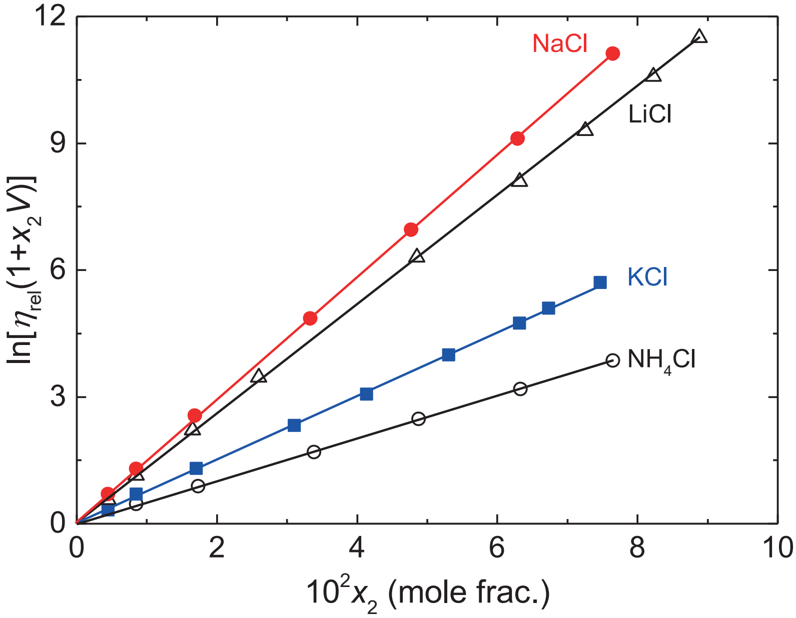

Figure 5.29. Plots of ln[(η/η_1)(1+x_2V)] against solute concentration x_2 of aqueous solutions containing different monovalent chlorides according to Eq. (5.50). Note that the behavior of structure-making LiCl and NaCl and structure-breaking KCl and NH_4Cl is the same. After Goldsack and Franchetto (1977).

The main conclusion following from Table 5.13 is that the values of both V and E parameters strongly depend on the nature of the solute dissolved in the solvent water and is intimately related to the concentration dependence of the viscosity η of the system. The higher the variation in the viscosity η of the solution caused by the solute in a solvent, the higher are the values of V and E for the system. In comparison with the values of these parameters for the $NaNO_3$–water system, their values are relatively high for the sucrose–water system. For the sucrose–water system, the values of both V and E parameters decrease significantly with increasing temperatures T. In the case of the $NaNO_3$–water system, one also observes a decrease in the value of V with increasing temperature, but the change in E with temperature is unrecognizable especially due to small variation in the viscosity of this system by the solute.

Another procedure of the determination of the dimensionless V and E parameters is based on the determination of η_0 and E_η from the temperature dependence of viscosity η of solutions of different concentrations x_2 using Eq. (5.4) and then from the plots of of η_0 and E_η as linear functions of x_2 determine V and E using Eqs. (5.48) and (5.49) for the solute-solvent system. A example of this procedure is described in Section 5.4.5.

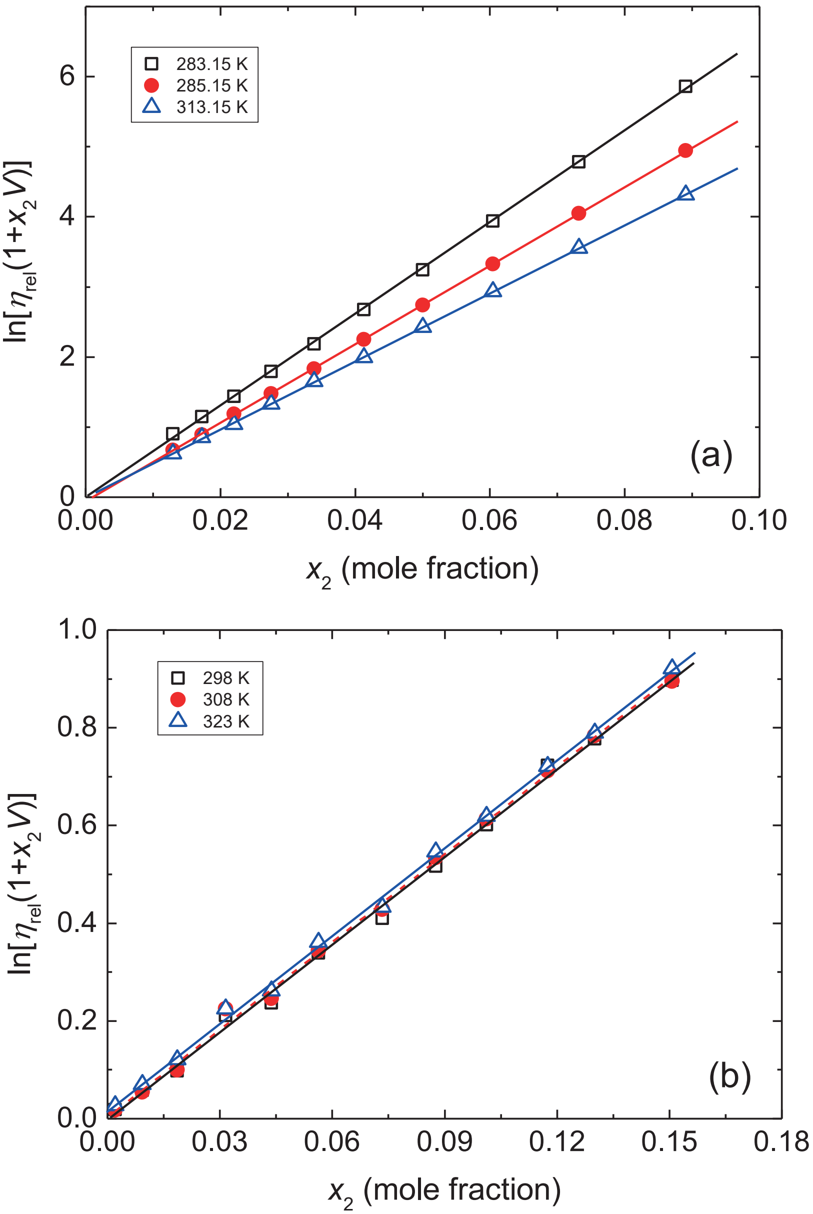

Figure 5.30. Plots of $\ln[(\eta/\eta_1)(1+x_2V)]$ against concentration x_2 of aqueous solutions of (a) sucrose and (b) sodium nitrate at three temperatures according to Eq. (5.50). Selected values of η_1 and V and best-fit values of E are listed in Table 5.13. Original data in (b) from Mahiuddin and Ismail (1996).

Finally, it should be mentioned that Eq. (5.50) based on the transition state theory of viscosity for fluids quantitatively accounts for the viscosity of concentrated solutions of alkali and ammonium halides and successfully links the B parameters of the Jones–Dole equation with the E and V parameters (Goldsack and Franchetto, 1977). Moreover, the temperature dependence of the E and V parameters of this equation, which are related to individual ionic parameters, also accounts for the temperature dependence of the viscosity of concentrated solutions (Goldsack and Franchetto, 1978). Some of these aspects are discussed below.

Table 5.13. Values of V and E for aqueous sucrose and sodium nitrate solutions

System	T (K)	η_1 (mPa·s)	V (–)	$10^2\Delta$	E (–)	R^2
Sucrose–water	283.15	1.138	3.0	0.11±1.93	65.36	0.9996
	298.15	0.8903	2.0	−6.74±0.58	56.21	0.9999
	313.15	0.6531	1.0	−0.80±0.89	48.58	0.9998
$NaNO_3$–water	298	0.890 (0.89016)	0.85	−0.29±0.82	5.984	0.9970
	308	0.710 (0.7245)	0.80	−0.28±0.73	5.987	0.9976
	323	0.540 (0.5580)	0.75	0.14±0.58	6.006	0.9985

5.4.3. Confrontation of experimental viscosity data with theoretical expressions

It was mentioned above that the square-root term in Eqs. (5.74) and (5.75) has its origin in electrostatic interactions and is always a positive quantity. In the concentration interval where the Jones–Dole equation, Eq. (5.74), applies, the A and B parameters are usually determined from the relation

$$\frac{\eta_{\text{rel}} - 1}{m^{1/2}} = A + Bm^{1/2}\,, \tag{5.88}$$

where we have denoted the solute concentration in molality m. According to this relation, the plot of $(\eta_{\text{rel}}-1)/m^{1/2}$ against $m^{1/2}$ gives a linear dependence of intercept A and slope B. Earlier publications on the study of viscosity of electrolytes have been concentrated on the determination of these parameters and covered relatively low concentrations (for example, see: Horvath, 1985; Stokes and Mills, 1965). However, omission of the contribution of the cC^2 term of Eq. (5.75) in the above equation casts doubts whether the values of B are determined correctly from the experimental $\eta(m)$ data for different systems.

If the contribution of the square-root term in Eqs. (5.74) and (5.75) can be assessed independently for an electrolyte system, the viscosity B coefficient can be determined from the experimental data of the concentration dependence of the viscosity of the system from the extended version of Jones–Dole equation, Eq. (5.75), written as

$$\frac{\eta_{\text{rel}} - 1 - Am^{1/2}}{m} = B + Cm\,. \tag{5.89}$$

According to this relation, a plot of $(\eta_{\text{rel}}-1-Am^{1/2})/m$ against m predicts a linear dependence of intercept B and slope C. However, the square-root term is zero for nonelectrolyte solutions and is present only at very low concentrations of electrolytes.

In general, in the case of electrolyte concentrations exceeding 0.01 m, the viscosity η increases linearly with solute concentration m. Therefore, the data of concentration dependence of viscosity η of nonelectrolytes and electrolytes may be analyzed using Eq. (5.75) rewritten in the form

$$\frac{\eta_{\text{rel}} - 1}{m} = B + Cm\,. \tag{5.90}$$

This relation predicts a linear dependence of $(\eta_{\text{rel}}-1)/m$ on m with intercept B and slope C. The intercept represents the value of the viscosity B coefficient whereas the slope C is a measure of deviation of viscosity η from the linear dependence on m.

According to Eqs. (5.89) and (5.90), accuracy in the determination of the value of the parameter B strongly depends on the accuracy in the viscosity measurements, the interval of solution concentration for the viscosity data and on the accuracy in the value of the viscosity η_1 of the solvent. In the range of very low concentrations of electrolytes, the square-root term is likely to result in a lower value of B than that obtained at high concentrations. At low concentrations when the solution viscosity η shows relatively small increase in its relative viscosity η_{rel}, even small measurement errors in η may result in large errors in the determined value of the B coefficient. Similarly, a lower value of solvent viscosity η_1 used in the calculations of the relative viscosity η_{rel} results in a higher value of B than the one obtained with a higher η_1. However, irrespective of high or low value of the B coefficient for a system due to measurement errors, the concentration interval used for viscosity measurements or the chosen value of solvent viscosity η_1 used to calculate η_{rel}, the value of the B coefficient for a system does not depend on solution concentration when $C = 0$.

The Jones–Dole equation, Eq. (5.74), and its extended version, Eq. (5.75), are essentially empirical and usually hold in a narrow concentration interval. Therefore, it is always tempting to look for other mathematical equations which are not only capable of describing experimental data of concentration dependence of viscosity η in a wide concentration interval but also provide some scientific basis. In this connection, Eq. (5.72), is of particular interest because its constants have physical interpretation and it transforms to Eq. (5.73) at low solute concentrations when the exponential term is expanded and the higher terms of the expansion are neglected.

There are two ways of analyzing the experimental viscosity data as a function of solute concentration according to Eq. (5.72). Taking logarithm on both sides, Eq. (5.72) may be written as

$$\ln \eta = \ln \eta_1^* + B_2 m\,, \tag{5.91}$$

$$\frac{\ln \eta_{\text{rel}}}{m} = B_2 + C_3 m\,, \tag{5.92}$$

where $\ln\eta_1^* = \ln\eta_1 + B_3 m^2 \geq \ln\eta_1$, depending on whether $B_3 m^2 = 0$ or $B_3 m^2 > 0$, and is practically a constant quantity in the investigated concentration interval.

Enormous research work has been devoted to determine values of different constants of the Jones–Dole equation for electrolyte solutions and to assign physical meaning to them (Desnoyers and Perron, 1972; Horvath, 1985; Stokes and Mills, 1965). For example, Desnoyers and Perron (1972) used Eq. (5.88) to determine the B and C parameters for aqueous alkali and tetraalkylammonium halide solutions from their viscosity measurements up to 1 M. These authors found that C is always a positive quantity, and its value depends on the size of ions (mainly cations) and structural solute–solute interactions. In this section the experimental data of concentration dependence of viscosity of aqueous sucrose and sodium nitrate solutions at different temperature, presented in Figure 5.25, are analyzed as examples of nonelectrolyte and electrolyte solutions.

Figure 2.31a, b and c shows the dependence of $(\eta_{\mathrm{rel}}-1)/m$, $\ln\eta$ and $\ln\eta_{\mathrm{rel}}/m$ on m of aqueous sucrose solutions according to Eqs. (5.90), (5.91) and (5.92), respectively. While analyzing the data according to Eqs. (5.90) and (5.92), the values of η_1 listed in Table 5.14 were used. It may be seen that in Figure 5.31a the viscosity data of sucrose solutions follow Eq. (5.88) only in a narrow concentration region below 1.25 m, but in Figure 5.31c the values of $\ln\eta_{\mathrm{rel}}/m$ attains constant values of B_2 only for solute concentration $m > 4$ m. The values of the solvent viscosity η_1 to calculate η_{rel} in the plots of Figure 5.31a and the calculated values of B and C from the first three points of the plots are given in Table 5.14. In Figure 5.31c the plots of $\ln\eta_{\mathrm{rel}}/m$ against m in the concentration region $m < 4$ m follow an empirical exponential dependence. In contrast to the above plots, the $\ln\eta(m)$ data for the three temperatures follow Eq. (5.91) in the entire concentration interval, with best-fit values of the constants $\ln\eta_1^*$ and B_2 given in Table 5.15. Thus, it may be concluded that Eq. (5.91) is more useful than Eq. (5.90) for the analysis of the experimental $\eta(m)$ data. An additional advantage of Eq. (5.91) is that it eliminates the choice of solvent viscosity η_1 and enables to evaluate the effect of other possible parameters on the viscosity.

Figure 5.32a and b shows the dependence of $(\eta_{\mathrm{rel}}-1)/m$ and $\ln\eta$ on m of aqueous sodium nitrate solutions at three selected temperatures according to Eqs. (5.90) and (5.91). As seen from Figure 5.32a, if the data for $m < 0.1$ mol·kg^{-1} are neglected, the data follow the linear dependence with the values of the parameters B and C listed in Table 5.14. In contrast to the plots of Figure 5.32b, the $\ln\eta(m)$ data for the three temperatures follows Eq. (5.90) satisfactorily in the entire concentration interval. The best-fit values of the constants $\ln\eta_1^*$ and B_2 of Eq. (5.91) for the data are given in Table 5.15.

From Figures 5.31a and 5.32a it may be noted that, although Eq. (5.90) also describes the data, it covers a narrow concentration range for aqueous sucrose solutions in comparison with practically the entire concentration range for aqueous sodium nitrate solutions. This difference in the applicability of Eq. (5.90) is related to the nature of the solute involved in viscous flow. For example, at 298 K the viscosity of 3.5 m sucrose solution is ten times higher than the viscosity of 3.5 m sodium nitrate solution (see Figure 5.25). This means that larger the changes caused by a solute in the viscosity of its solution, the smaller is the concentration range of the applicability of Eq. (5.90).

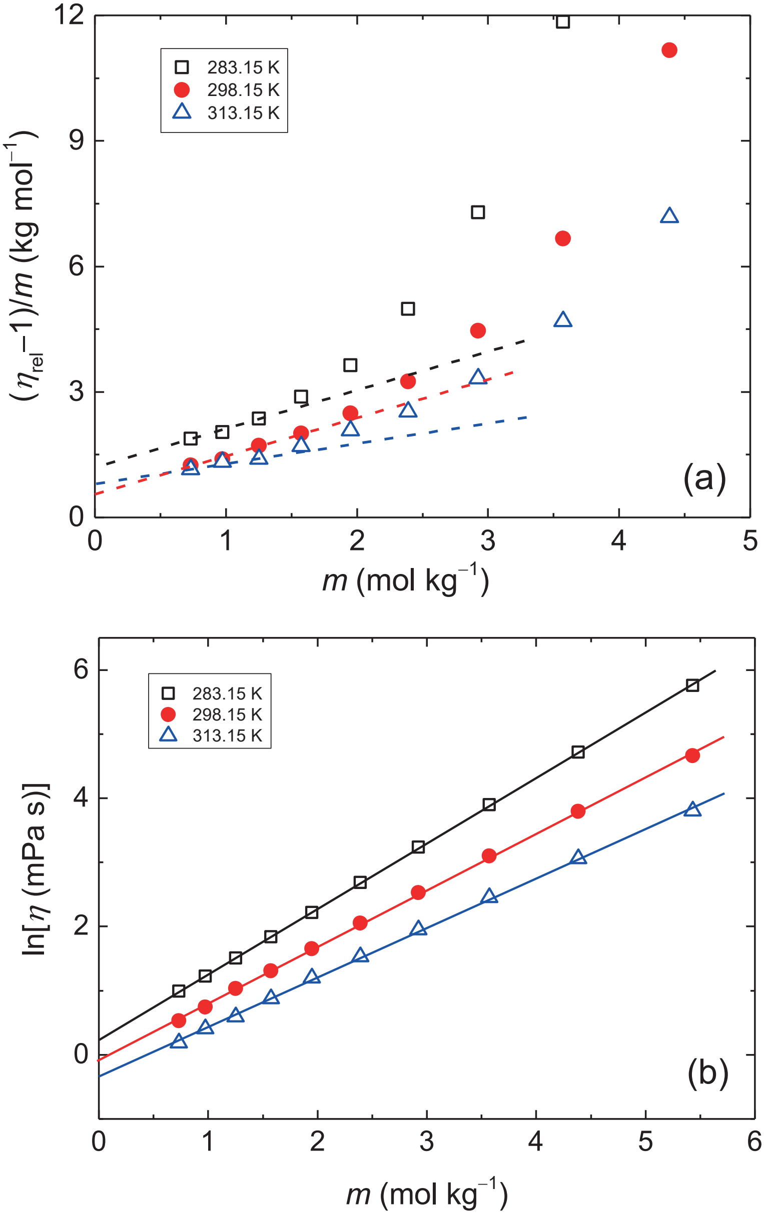
12
9
6
3
0
$(\eta_{rel}-1)/m$ (kg mol^{-1})
283.15 K
298.15 K
313.15 K
(a)
0
1
2
3
4
5
m (mol kg^{-1})
6
4
2
0
ln[η (mPa s)]
283.15 K
298.15 K
313.15 K
(b)
0
1
2
3
4
5
6
m (mol kg^{-1})

(Continued)

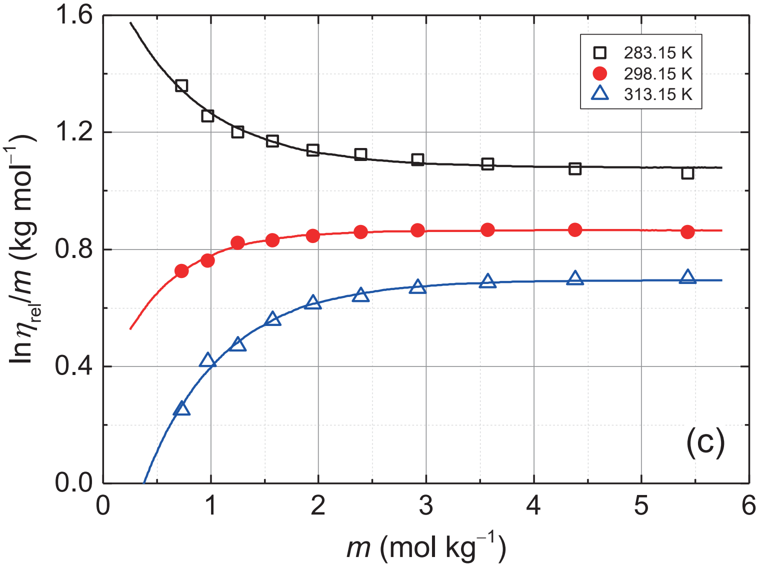

Figure 5.31. Dependence of (a) ($\eta_{rel}-1)/m$, (b) $\ln\eta$ and (c) $\ln\eta_{rel}/m$ on m of aqueous sucrose solutions according to Eqs. (5.90)), (5.91) and (5.92), respectively. Temperature of the data is given in the inset. Original data from Asadi (2006).

Table 5.14. Constants B and C of Eq. (5.90) for the two system

System	T (K)	η_1 (mPa)	B (kg mol^{-1})	10^3C [(kg mol^{-1})^2]	R^2
Sucrose–water	283.15	1.138^a	0.1046	7.55	--
	298.15	0.9186^a	0.1046	7.55	--
	313.15	0.7080^a	0.1046	7.55	--
$NaNO_3$–water	298	0.890^b	0.0969	8.59	0.8715
	308	0.719^b	0.1046	7.55	0.8122
	323	0.547^b	0.1153	6.42	0.8383

Data from: ^{a} Asadi (2006); ^{b} Lide (1996/1997)

In Figure 5.32a one observes large positive deviations of the experimental data of aqueous sodium nitrate solutions from the linear dependence of Eq. (5.90) in the concentration range below 1 m. Similar positive deviations have been observed before during the analysis of the viscosity data for aqueous solutions of tetramethylammonum bromide and tetrabutylammonium bromide at 298.15 K (Desnoyers and Perron, 1972). These positive deviations are mainly associated with the use of low values of the viscosity η_1 of the solvent in the calculation of η_{rel} of the solution but they may also result from measurement errors in the viscosities of the solutions.

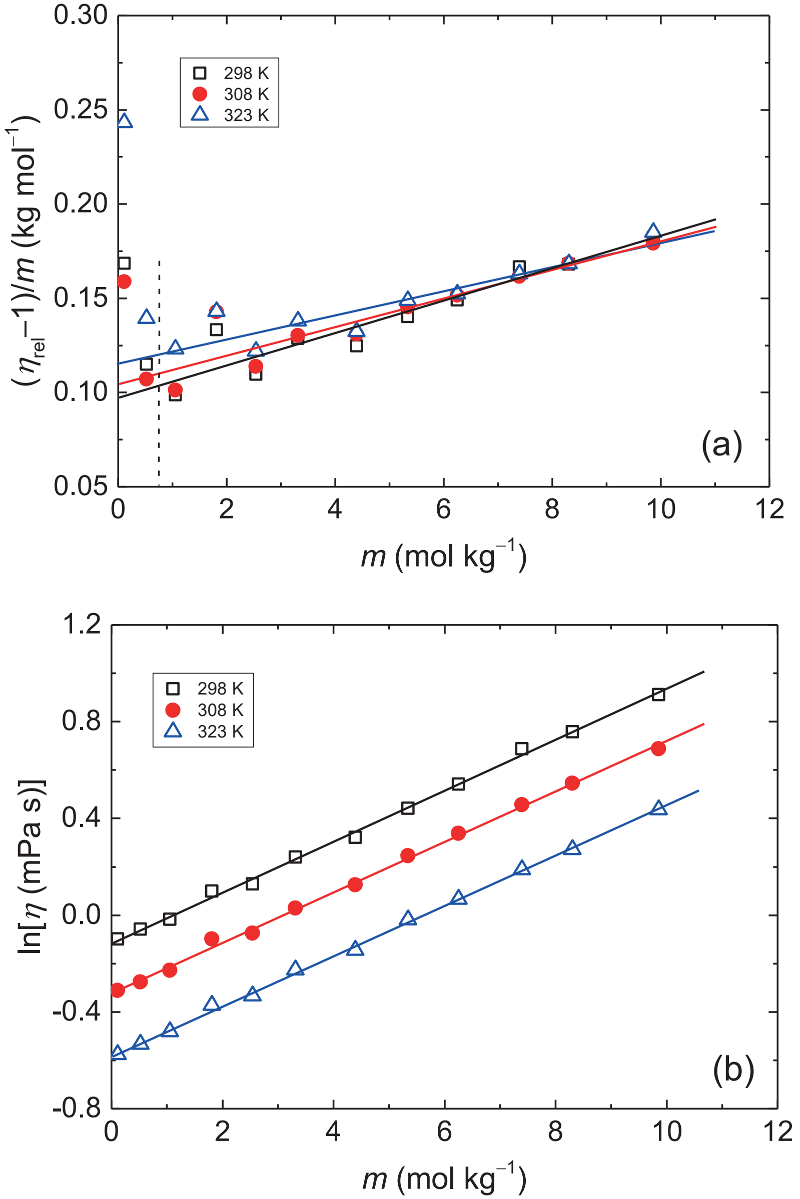

Figure 5.32. Dependence of (a) $(\eta_{\rm rel}-1)/m$ and (b) $\ln\eta$ on m of aqueous sodium nitrate solutions at three selected temperatures according to Eqs. (5.90) and (5.91). Temperature of the data is given in the inset. Original data from Mahiuddin and Ismail (1996).

Figures 5.31b and 5.32b show that in the entire concentration interval Eq. (5.91) represents the $\eta(m)$ data for both systems with a very high value of the goodness-of-the-fit parameter R^2 (Table 5.15). As seen from Figure 5.31a, although the $\eta(m)$ data for sodium nitrate solutions may also be described by Eq. (5.90) practically in the entire concentration interval, the value of the R^2 parameter is relatively low in comparison with that according to Eq. (5.91). One also notes that the value of B of Eq. (5.90) for sodium nitrate solutions is comparable with the value of B_2 of Eq. (5.91) and differs from each other no more than 12%; see Tables 5.14 and 5.15. However, in contrast to the possible erratic trend of the B coefficient of Eq. (5.90) with increasing temperature from Table 5.14, the B_2 parameter of Eq. (5.91) decreases with an increase in solution temperature. The important obsevation here is that the value of η_1^* obtained from the plots of $\ln\eta$ against m is always higher than the value of η_1 available from reference source. These values of η_1^* of Table 5.15 are in excellent agreement with the values of η_1, listed in the parentheses in Table 5.13 for the aqueous $NaNO_3$ solutions, obtained from analysis of the experimental $\eta(x_2)$ data according to Eq. (5.47) based on Eyring's formalism when the predicted linear dependence is observed with the correctly chosen values of the dimensionless parameters V and E.

Table 5.15. Constants $\ln\eta_1^*$ and B_2 of Eq. (5.90) for the two systems

System	T (K)	$\ln\eta_1^*$	η_1^* (mPa)	η_1 (mPa)	η_1^*/η_1	B_2 (kg mol^{-1})	R^2
Sucrose–water	283.15	0.2404	1.2717	1.138[a]	1.175	1.0190	0.9999
	298.15	−0.0849	0.9186	0.8903[a]	1.0318	0.8831	0.9995
	313.15	−0.3454	0.7080	0.6531[a]	1.0840	0.7732	0.9992
$NaNO_3$–water	298	−0.1164	0.89016	0.890[b]	1.0002	0.1051	0.9976
	308	−0.3221	0.7246	0.719[b]	1.0078	0.1041	0.9978
	323	−0.5835	0.5579	0.547[b]	1.0200	0.1036	0.9987

Data from: [a] Asadi (2006); [b] Lide (1996/1997).

As seen from Table 5.15, the value of η_1^* is higher up to 17.5% and 2.0% than η_1 for aqueous sucrose and sodium nitrate solutions, respectively. The value of η_1^* lies in the range of errors involved in the measurement of viscosity but the effect of trace amounts of impurities contained in the solute cannot be excluded. Irrespective of the effect of these impurities in the solution, large differences between η_1^* and η_1 suggest that a constant term m_0, characteristic of the system, should be added to the $\ln\eta_1$ term in place of B_3m^2. Then one has

$$\eta = \eta_1 \exp(m_0 + B_2 m)\,, \tag{5.93}$$

where the dimensionless quantity $m_0 = [(\eta_1^*/\eta_1) - 1] \geq 0$.

From the above discussion the following conclusions may be drawn:

(1) Logarithmic function (5.91) is better than the linear function (5.90) for the determination of the viscosity B coefficient for a solute–solvent system.
(2) The value of the B coefficient is related to the nature of the solute dissolved in a solvent. In general, the higher the viscosity of a solution at a particular solute concentration, the higher is the value of the B coefficient.
(3) The value of the B coefficient for a solute–solvent system decreases with an

increase in solution temperature.

The physical basis of these trends is discussed below.

5.4.4. Physical interpretation of the viscosity *B* coefficient

The *B* coefficient of Jones–Dole equation, Eq. (5.74), and the B_2 parameter of Eq. (5.72) are related to the parameters *V* and *E* of Eyring's formalism (see Eq. (5.44)) and to the molar volume $V_{\mathrm{M}2}^{\mathrm{s}}$ of the solute particles in the solution of Einstein's relation (5.68). These relationships are discussed below.

Upon expanding Eq. (5.44) and neglecting terms higher than x_2 when $x_2 \ll 1$, one obtains

$$\frac{\eta}{\eta_1} = 1 + (E - V)x_2 = 1 + \frac{(E - V)M_1 m}{1000}, \tag{5.94}$$

since $x_2 = m/(1000/M_1)$, where M_1 is the molar mass of the solvent. Eq. (5.93) is equivalent to Jones–Dole equation, Eq. (5.74), if the square-root is ignored. Thus, the *B*-coefficient becomes

$$B = \frac{M_1(E - V)}{1000}. \tag{5.95}$$

For aqueous electrolyte solutions, where the molar mass M_1 of water is 18, the above equation reduces to the form

$$B = \frac{E - V}{55.51}, \tag{5.96}$$

where *V* and *E* are given by Eqs. (5.46) and (5.45), respectively.

Comparison of Jones–Dole equation, Eq. (5.74), with Einstein's equation, Eqs. (5.68), gives the viscosity *B* coefficient

$$B = 2.5V_{\mathrm{M}2}^{\mathrm{s}}, \tag{5.97}$$

where $V_{\mathrm{M}2}^{\mathrm{s}}$ is the hydrodynamic molar volume (L·mole^{-1}) of solute particles dispersed in an ideal (dimensionless and structureless) solvent. In this case, the dispersed solute particles are unsolvated and the hydrodynamic molar volume $V_{\mathrm{M}2}^{\mathrm{s}}$ is equal to the partial molal volume V° of the solute. Therefore, with unsolvated solute molecules in an ideal solvent, one would expect a linear increase in the *B* coefficient with increasing partial molal volume V° of the solutes with a slope equal to 2.5. Thus, the ratio B/V° for a solute in its solution may be considered as measure of the structure breaking and structure making ability of its molecules. Solutes for which $B/V^{\circ} < 2.5$ are classified as structure breakers while those for which $B/V^{\circ} > 2.5$ are classified as structure makers. In general, solute molecules of larger and smaller sizes than those of the solvent are structure breakers and stucture makers, respectively.

The B coefficient reflects the degree of solvation of the molecule responsible for viscous flow. Therefore, the average number n_s of solvent molecules surrounding the molecule can be calculated from the hydrodynamic molar volume V_{M2}^{s} of solvated solute 2 using the relation

$$n_s = \frac{V_{M2}^{s} - V_{M2}}{V_{M1}}, \tag{5.98}$$

where V_{M2} (= V^{o}) and V_{M1} represent the molar volumes of the molecules of unsolvated solute 2 and solvent 1, respectively. Since V_{M2} may be calculated from the crystal structure, V_{M1} from the radius of a solvent molecule, while V_{M2}^{s} from the value of B, the average solvation number n_s of the solvent molecules attached to a solute molecule may be calculated.

Eq. (5.98) can be applied to calculate the solvation number n_s of the solvent molecules attached not only to a solute molecule (for example see: Zhao et al., 2005) but also to individual cation and anion of an electrolyte in the solution (for example, see: Millero, 1970, 1972); see below. This equation can also be used to explore the relationship between the viscosity B coefficient and the empirical deviation parameter b_v of Eqs. (3.11) and (3.12) relating apparent molar volume Φ_v to solute concentration c. Marcus (2006) examined this possible relationship for aqueous and nonaqueous electrolyte solutions and concluded that positive correlations occur in some cases but such correlations fail in others where increasing solute concentration leads to the crowding of solvation shells of molecules and ions.

5.4.5. Relationship between E_η and $\ln\eta_0$ of Arrhenius-type dependence

Analysis of the temperature dependence of the viscosity of solutions is equally useful in understanding the effect of solute concentration and obtaining the size of entities involved in viscous flow and crystallization of the solute. As an illustration of this approach, we consider the experimental data of the temperature dependence of viscosity of aqueous ammonium oxalate solutions of different concentrations, reported by Frej et al. (2000). Figure 5.33 shows examples of the dependence of $\ln\eta$ of aqueous ammonium oxalate solutions of four selected concentrations and solvent water on T^{-1} according to Eq. (5.4). In the figure the plot for water represents the temperature interval between 15 and 50 °C. As seen from the figure, the plots of $\ln\eta$ against T^{-1} follow linear dependence with intercept $\ln\eta_0$ and slope E_η/R_G for different solute concentrations x_2 (expressed in mole fraction) such that the linear plots of $\ln\eta$ against T^{-1} for the solutions are shifted upward relative to the plot for water and the shift increases with the solute concentration x_2 in the solution. Similar trends may be noted from the plots of $\ln\eta$ against T^{-1} for aqueous calcium nitrate solutions of different concentrations (see Figure 5.27).

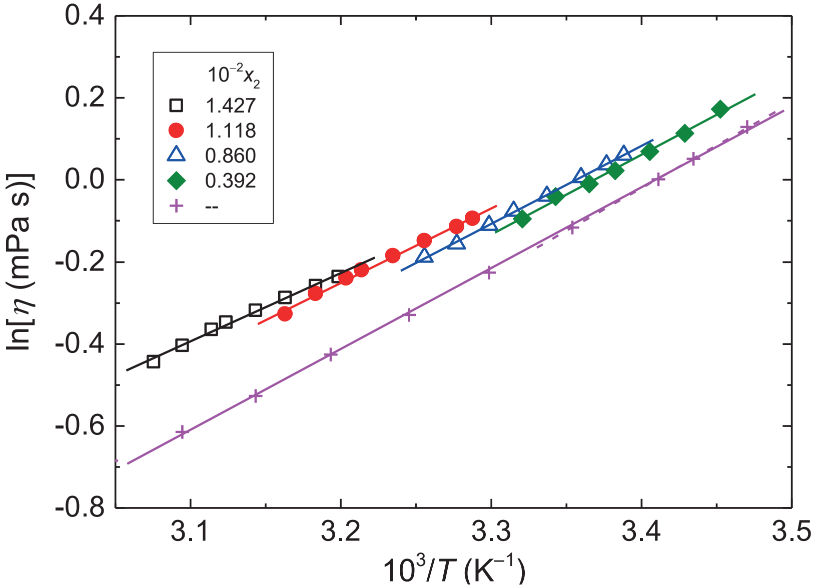

Figure 5.33. Dependence of ln η of aqueous ammonium oxalate solutions of four selected concentrations and water on T^{-1} according to Eq. (5.4). Solute concentration x_2 shown in the inset is given in mole fraction. Original data for ammonium oxalate solutions and water are from Frej et al. (2000) and Lide (1996/1997), respectively.

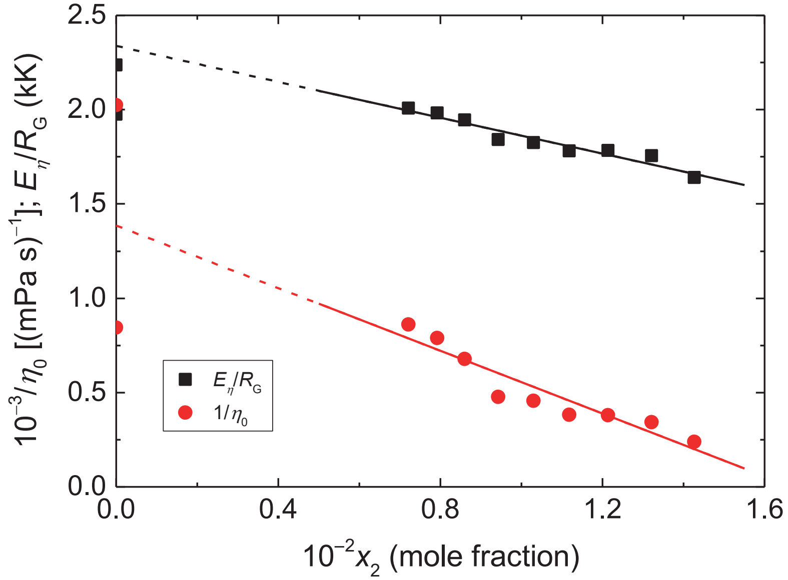

Figure 5.34. Relationship between $1/\eta_0$ and E_η/R_G on the concentration x_2 of aqueous ammonium oxalate solutions according to Eqs. (5.48) and (6.49). Data from Sangwal et al. (2004).

The various values of the intercept $\ln\eta_0$ and the slope E_η/R_G obtained by Sangwal et al. (2004) for different aqueous ammonium oxalate solutions from the $\eta(T)$ data reported of Frej et al. (2000) are shown in Figure 5.34 as plots of η_0^{-1} and E_η/R_G as a function of concentration x_2 according to Eqs. (5.48) and (5.49), respectively. In Figure 5.34 two values of η_0^{-1} and E_η/R_G are shown for water. These two values were obtained from the plots of $\ln\eta$ against T^{-1} in the temperature intervals of the experimental $\eta(T)$ data for water between 15 and 40 °C and between 15 and 60 °C. In the figure these two values are presented to show that, depending on the temperature interval of the data considered as a reference, the extrapolated values of E_η/R_G and η_0 for $x_2 = 0$, denoted hereafter as $\Delta G_1^*/R_G$ and η_0^*, can differ substantially from the values obtained from the experimental $\eta(T)$ data for water.

From the values of the intercept and the slope of the linear plots of Figure 5.34, the values of η_0^* and ΔG_1^* for $x_2 = 0$, and V and E parameters may be calculated. These values are: $\eta_0^* = 0.722$ mPa·s, $\Delta G_1^o = 19.4\pm0.5$ kJ/mol, $V = -60\pm8$, and $E = -20\pm2$. The value of ΔG_1^o agrees well with the value of 18.6 kJ/mol for viscous flow of water at high temperatures.

Both E_η and η_0 of solutions not only show linear dependence on solute concentration x_2, but they are also mutually related (Sangwal, 2018; Sangwal et al., 2004) and follow Eq. (5.22). A similar behavior is observed in the case of homologues of alcohols (Figure 5.11). In the case of aqueous ammonium oxalate solutions, the constants of Eq. (5.22) are: $b_0 = 97.5\pm23.7$ K and $b_1 = 282.9\pm3.8$ K. Corresponding to $E_\eta/R_G = 0$, from Eq. (5.4) one finds a temperature $T^{\lim} = b_1 = 282.9\pm3.8$ K and a new preexponential factor $b_0/b_1 = \ln\eta_0^* = 0.344\pm0.08$ or $\eta_0^* = 1.406$ mPa·s, which gives the corresponding molar volume $V^* = h_P N_A/\eta_0^* = 0.284$ cm^3·mol^{-1}, which is much lower than the molar volume $V_{M1} = 6.63$ cm^3·mol^{-1} of water. This is expected because the calculated molar volume V^* represents the effective volume for viscous flow. From V^* one obtains the critical radius $r^* = 0.048$ nm. This critical radius r^* is about one-third of the average radius $r_{H2O} = 0.138$ nm of water molecules and probably corresponds to the maximum displacement of thermal vibrations of water molecules about their equilibrium positions in the liquid state. Thus, it may be concluded that the values of the critical volume V^* and the critical radius r^* are associated with the structure of the solvent water, whereas the value of $T^{\lim}$ is close to the melting point T_m of water.

Finally, it should be emphasized that the values of the activation energies ΔH^o and E_η for viscous flow of solvents and solutions decrease with increasing temperature. This is due to the fact that water and aqueous solutions behave as associated liquids with network structure. In associated liquids the activation energy E_η for viscous flow is determined by the energy required to break the bonds of the network whereas the fraction of the broken bonds increases with temperature (O'Bockris and Reddy, 1970).

5.5. Viscosity *B* coefficients of ions

In the case of electrolyte solutions, the viscosity *B* coefficient is an additive parameter with contributions from anions and cations. The *B* parameters for anions and cations are usually analyzed by arbitrarily assuming that the contributions of the potassium and chloride ions in aqueous solutions are equal at all temperatures (Desnoyers and Perron, 1972; Horvath, 1985; Stokes and Mills, 1965), but based on nearly the same mobilitities of aqueous rubidium and bromide ions over a wide temperature range, the ionic *B* coefficients are also calculated taking equal contributions of rubidium and bromide ions (Marcus, 1994). Consideration of the RbBr pair instead of the popular KCl pair results in minor differences of –0.002 L·mol^{-1} for cations (Marcus, 1994). The ionic *B* coefficients are negative for structure-making ions and positive for structure breaking ions.

Since the *B* parameter for electrolytes is an additive parameter, both the *E* and *V* parameters are also analyzed on the assumption of equal contributions of potassium and chloride ions at all temperatures (Goldsack and Franchetto, 1978). The concentrations x_c and x_a of cations and anions for different types of salts and their contributions to the *E* and *V* parameters are listed in Table 5.16. In the table, ΔG_a^o denotes the free energy of activation for viscous flow per mole of anions, ΔG_c^o the free energy of activation for viscous flow per mole of cations, V_a the molar volume of the anion hole, and V_c the molar volume of the cation hole.

Table 5.16. Values of parameters of viscosity equation, Eq. (5.44), for single salt solutions[a]

Salt type	x	E	V
1:1	x_c	$\Delta G_c^o + \Delta G_a^o - 2\Delta G_1^o$	$\dfrac{V_c + V_a}{V_1} - 2$
1:2	x_c	$\Delta G_c^o + 2\Delta G_a^o - 3\Delta G_1^o$	$\dfrac{V_c + 2V_a}{V_1} - 3$
2:1	x_a	$2\Delta G_c^o + \Delta G_a^o - 3\Delta G_1^o$	$\dfrac{2V_c + V_a}{V_1} - 3$
1:3	x_c	$\Delta G_c^o + 3\Delta G_a^o - 4\Delta G_1^o$	$\dfrac{V_c + 3V_a}{V_1} - 4$
3:1	x_a	$3\Delta G_c^o + \Delta G_a^o - 2\Delta G_1^o$	$\dfrac{3V_c + V_a}{V_1} - 4$

[a] After Goldsack and Franchetto (1977).

Individual V_{ion} parameters of ions, calculated from the total salt *V* parameters on the assumption of equality of contributions of K$^+$ and Cl$^-$ ions and the value of V_1 for the solvent (cf. Table 5.16), correspond to their volumes and reflect the extent of hydration of each ion. By substracting out the volume V_{bare} of the bare ion, including a dead space correction (Conway et al., 1965), one obtains the volume V_{hydr} of the hydration sphere. Then dividing this volume V_{hydr} by the volume V_1 of the solvent, one obtains the hydration number n_h, i.e.

$$n_h = \frac{V_{\text{ion}} - V_{\text{bare}}}{V_1} = \frac{V_{\text{hydr}}}{V_1} . \tag{5.99}$$

Goldsack and Franchetto (1978) observed that the ionic radii scale of Gourary and Adrian (1960) ensures more consistent values of hydration number for the alkali halide and ammonium halide salts at different temperatures for the calculation of V_{bare} than the Pauling ionic radii scale. These authors also found that the hydration numbers of structure-making ions like Li^+, Na^+ and F^- are not much affected by an increase in temperature, while those of structure-breaking ions such as K^+, Rb^+, Cs^+, Cl^-, Br^- and I^- decrease markedly with an increase in temperature. As discussed below, the differences in the effect of temperature on the hydration number of ions and their classification into structure breakers and structure makers are associated with the process of viscous flow.

Viscous flow in solutions occurs as a result of movement of kinetic entities from their initial "equilibrium" positions to their "neighboring" positions occupied by solvent molecules. This process involves two stages: (1) creation of a hole or cavity at the position occupied previously by a solvent molecule, and (2) jumping of the kinetic entity into the hole created in its neighborhood. Therefore, to fit into this hole formerly occupied by a water molecule in electrolyte solutions, the radius r_{ion} of the moving ion must not exceed the radius r_{H2O} of a water molecule (0.138 nm). Using these ideas and the equality defined by Eq. (5.77), the behavior of different ions in the determination of the values of their B coefficients can be interpreted.

Small and highly charged cations like Li^+, Na^+ and Mg^{2+} of their radii smaller than the radius of a water molecule strongly orient water molecules and are solvated by firmly attached water molecules in their primary sheath. These solvated ions, having firmly attached water molecules in their primary sheath, of dimensions much greater than the corresponding bare ions, move as kinetic entities during viscous flow. These ions easily fit into the hole without disrupting its primary and secondary hydration shells consisting of 4 and 8 water molecules. This implies that the size-related contribution η^E of Eq. (5.77) is large for these solvated ions because of the firmly attached primary solvent sheath. At room temperature the ions are also likely to orient water molecules in the bulk water, implying that contribution η^A to the viscosity η due to the orientation of solvent molecules by the ionic field is positive (i.e. $\eta^A > 0$). Since water molecules are strongly bound to the surface of these ions than the water molecules among themselves and have hydrogen atoms of their firmly attached water molecules pointing outward, the solvated ions replacing the holes fit into the bulk water structure without causing distortion in it. This means that the contribution η^D related to the distortion of the solvent structure is small. Therefore, replacement of the hole by this class of ions, called structure-making ions, $\eta^E+\eta^A >> \eta^D$ and B is large and positive.

Cations like Rb^+, Cs^+ and NH_4^+ and most of the anions of radii larger than the radius of the water molecule have small surface charge densities and poorly orient water molecules in their first solvation sheath. Therefore, replacement of the hole by these ions is expected to result in poor disruption of their primary and secondary hydration shells. Consequently, the size-related contribution η^E will not differ much from that for these bare ions and will be small. Similarly, because of poor alignment of water molecules by their ionic fields, the contribution η^A related to the alignment of solvent molecules is also small. However, there is large distortion in the vicinity of the ion due to competition between the ionic field and the bulk structure. This distortion will lead to a weakening of the bonds holding these water molecules in the hydration shells, and the contribution η^D is quite large. Consequently, for this class of ions, referred to as structure-breaking ions, $\eta^E+\eta^A < \eta^D$ and B is negative.

Ions of intermediate size like K^+ and Cl^- (as well as Rb^+ and Br^-) between the above two extremes correspond to the situation when the sum of the former two positive contributions η^E and η^A is comparable with the small negative η^D due to a good fit of these ions in the water structure. Then $\eta^E+\eta^A \approx \eta^D$ and $B \approx 0$.

The temperature dependence of the ionic B coefficients is mainly associated with the weakening of the bonds holding the water molecules in the solvation shells of the ions. This results in the effect of temperature on all the three contributions of Eq. (5.77). For structure making ions, the water molecules are firmly bound in the primary solvation shells and their hydration numbers are temperature independent. An increase in temperature is expected to weaken the effect of secondary solvation shell of these ions, thereby decreasing the contribution η^A related to the alignment or orientation of solvent molecules by the ionic field, with poor effect on the contribution η^D. Consequently, the sum $\eta^E+\eta^A+\eta^D > 0$ and decreases with an increase in temperature. However, for structure-breaking ions where water molecules are weakly bound to the ions, the contribution η^E will remain constant independent of temperature, the contribution η^A related to the alignment or orientation of solvent molecules by the ionic field will decrease with an increase in temperature, and the contribution η^D related to the disruption of the solvent structure with decrease with an increase in temperature because of less competition between the ionic field and the reduced solvent structure in the bulk due to increased thermal vibrations of the molecules. Therefore, depending on the relative changes in the contribution η^A and η^D with temperature, one has not only $\eta^E+\eta^A+\eta^D > 0$ (i.e. $B > 0$) and $\eta^E+\eta^A+\eta^D < 0$ (i.e. $B < 0$), but also small increase and decrease in the ionic B coefficient with an increase in temperature. The variation of the ionic B coefficient with the temperature is an indication of the magnitude of the order or disorder in the structure of the solution.

It follows from the above discussion that the structure-making and structure-breaking behavior of ions is related to the strength or weakness of the bond between the ion and the solvent molecules in the primary solvation sheath. Because of higher charge density, ions having small size and high valency such as Li^+, Mg^{2+} and La^{3+}, bind the water molecules strongly and are structure makers, while ions having relatively large size and low valency behave as structure breakers.

Here it should be mentioned that large molecular ions such as tetraalkylammonium ions are expected to have large η^E because of their large size. The contributions η^A and η^D, related to the alignment or orientation of solvent molecules by the ionic field and to the disruption of the solvent structure, respectively, are small. Therefore, for these ions $\eta^E+\eta^A >> \eta^D$ and B is positive and large.

Ammonium oxalate is a 1:2 salt, and the crystallographic radii r_c and r_a of its cation NH_4^+ and bivalent anion $C_2O_4^{2-}$ are 0.148 nm and about 0.20 nm, respectively. Therefore, if it is assumed that the salt is completely dissociated into NH_4^+ and $C_2O_4^{2-}$

ions in aqueous solutions with the crystallographic radius r_{H2O} of the H_2O molecules of the solvent equal to 0.138 nm, one expects that both V and E are positive (cf. Table 5.16), i.e.

$$2V_{\mathrm{c}} + V_{\mathrm{a}} > 3V_1 , \tag{5.100}$$

$$(2\Delta G_{\mathrm{c}} + \Delta G_{\mathrm{a}}) > 3\Delta G_1^0 , \tag{5.101}$$

and the dissociated NH_4^+ and $C_2O_4^{2-}$ ions are structure breakers. However, as noted above, for aqueous ammonium oxalate solutions both V and E are negative. This obvious discrepancy between the experimental and the theoretically expected values of V and E indicates that the contributions of possible ions resulting directly from the complete dissociation of the salt in aqueous solutions do not account for the experimental values of V and E. This discrepancy may be associated with the partial dissociation of the salt into NH_4^+ and $HC_2O_4^-$ ions in the aqueous solution and subsequently the hydrolysis of $HC_2O_4^-$ ions to form $H_2C_2O_4$ and OH^- ions. As described in Section 6.7.2, this type of reactions have been suggested to explain the electrical conductivity of sodium and potassium formates (Bončina et al., 2010).

5.6. Ionic *B* coefficients and structure of electrolyte solutions

Addition of an electrolyte to a solvent like water leads to the dissociation of its molecules into cations and anions in the solution so that their total charge remains zero. The process of transfer of solid electrolyte molecules into ions involves three types of interactions between the ions and the solvent molecules: ion–solvent, ion–ion and solvent–solvent interactions. In dilute solutions an ion firmly holds with it a certain number of solvent molecules (first solvation sheath) and disrupts the solvent structure in its vicinity. Consequently, the presence of ions in the solution may be considered to induce order in their immediate neighborhood and a general disorder in the solvent structure. These changes in the solvent structure are manifested by macroscopic as well as microscopic properties of the solutions. The macroscopic properties involve changes in the thermodynamic properties such as the molar entropy of solutions, whereas among the microscopic properties are characteristics associated with the solvation of ions such as volume of solvated ions, number of firmly trapped solvent molecules and partial molar entropy of solvation (Horvath, 1985; Stokes and Mills, 1965; Robinson and Stokes, 1959).

The *B* coefficients for various electrolytes both in aqueous and nonaqueous solutions show a general tendency to decrease with the increasing molar entropy ΔS^{o} of their solutions (Stokes and Mills, 1965). The solution molar entropy ΔS^{o} is defined as the difference between the molar entropy S_{c} of the crystal and the partial molar entropy S_{s} in a hypothetical ideal 1 M solution, i.e. $\Delta S^{\mathrm{o}} = S_{\mathrm{s}} - S_{\mathrm{c}}$. The *B* coefficients for the salts in aqueous and nonaqueous solutions follow linear dependence with the corrected solution molar entropy $\Delta S^{\mathrm{o}} - S^*$, where S^* is the so-called cratic contribution of the solvent entropy. This contribution is nonspecific and is related to the concentration of ions in the solutions. Therefore, the part of entropy change of interest is the one that is related to the interactions between ions and solvent molecules.

Entropy of ions in a solution is a measure of the ordering of its structure. The higher the entropy of an ion in the solution, the higher is the disordering in the system. Since the viscosity *B* coefficient of a solute–solvent system is related to the state of ions, the *B* coefficients of different electrolyte solutions are usually considered as the sum of contributions made by the solute cations and anions (Horvath, 1985; Marcus, 1994; Stokes and Mills, 1965). Therefore, the B_i coefficients of ions have been related to their other properties. For example, the ionic B_i coefficients for both monoatomic and polyatomic ions decrease with increasing partial molar entropies of hydration at 25 °C, and the ionic B_i coefficients increase with increasing volumes V_H of hydrated ions. Similarly, the B_i coefficient and the ionic entropy $S°$, and the B_i coefficient and the entropy of hydration, S_h^o, of ions are related. However, most of these correlations are confined to a small number of simple ions.

Marcus (1994) reported that the ionic *B* coefficients are related to average number n_{HB} of hydrogen bonds in water structure and to the structural entropy S_{str} of ions. For the calculation of the S_{str} of ions he used a model based on consideration of translation immobilization of water molecules in the first hydration shell of the ions and a residual entropy due to the effect of the ion on the structure of water. The structure of water is defined in terms of the average number n_{HB} of hydrogen bonds in which a water molecule participates. Marcus tabulated for over 120 ions values of viscosity *B* coefficients, structural entropies S_{str} and heat capacities of hydration of ions and the average number n_{HB} of hydrogen bonds per water molecules in the firmly-held hydration sheath of ions, and reported correlations between S_{str} and *B* and between n_{HB} and *B* of ions of different charges.

Here relationships between *B* coefficients, structural entropies S_{str} and average number n_{HB} of hydrogen bonds are analyzed for various cations and anions of known *B* coefficients using the values of S_{str} and n_{HB} tabulated by Marcus. In the case of ions with more than one value of *B*, the first value was taken.

Figure 5.35 shows plots of *B* coefficients of mono-, bi- and trivalent (a) cations and (b) anions against their structural entropies S_{str}. As seen from the plots, good linear correlations between *B* and S_{str} are observed in the case of mono- and bivalent cations and bivalent anions (with SiF_6^{2-} as an outlier). Among monovalent ions, tetraalkylammonium ions, represented by filled squares (1A), follow a completely different linear dependence. With the exception of Cr^{3+} and several other trivalent cations with $S_{str} < 100$ J·mol^{-1}·K^{-1}, the data also follow a linear dependence of slope comparable with that for bivalent cations. In general, the data for monovalent anions show large scatter. However, except for tetraalkyl- ammonium ions, solid lines represent data taking best-fit parameters of the data for bivalent ions. As seen from the plots, the *B* coefficient decreases linearly with S_{str} such that they form a family of straight lines for ions of different charges. These data may be represented by the single empirical relation (Marcus, 1994)

$$B = 0.033(z^2 + |z|) - 1.65 \cdot 10^{-3} S_{str} , \tag{5.102}$$

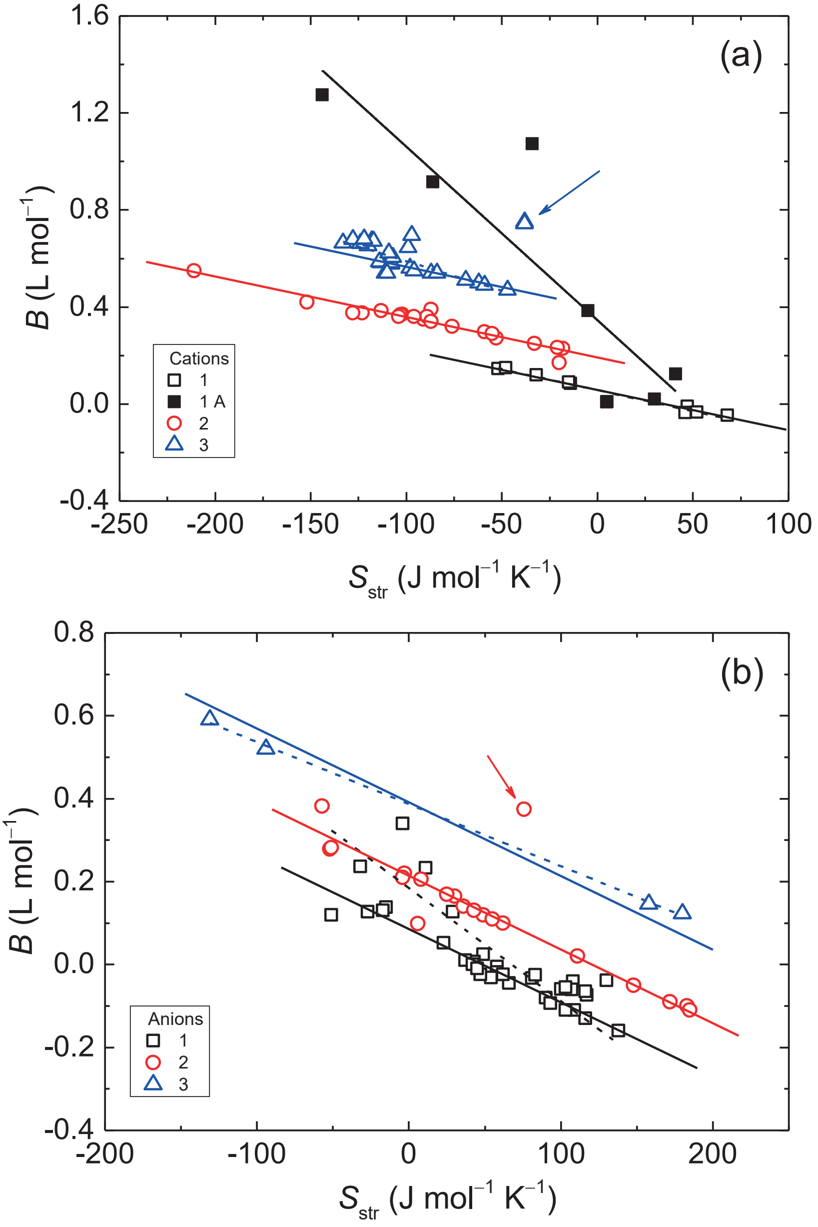

Figure 5.35. Relationship between B coefficients and structural entropies S_{str} of (a) cations and (b) anions of different charges given in insets. Family of straight solid lines for ions of different charges are drawn taking best-fit of data for bivalent ions. Noticeable outliers Cr^{3+} and SiF_6^{2-} are indicated by arrows. In (b) dashed lines represent best-fit plots. Data from Marcus (1994).

where z is the valency of an ion and $|z| \approx 1$ denotes possible error. If the data for NH_4^+, $CH_3NH_3^+$ and $(CH_3)_4N^+$ ions are included in tetraalkylammonium ions (filled squares), they follow the relation

$$B = 0.346 - 7.16 \cdot 10^{-3} S_{\mathrm{str}} . \tag{5.103}$$

The former two ions lie on the linear plot of other monovalent cations. The above values of the intercept and slope are comparable with the values of 0.371 $\mathrm{L \cdot mol^{-1}}$ and $6.29 \cdot 10^{-3}$ L·K reported by Marcus.

From Figure 5.35a one notes that the monovalent cations K^+, Rb^+, Cs^+, Tl^+, NH_4^+, $CH_3NH_3^+$ and $(CH_3)_4N^+$ ions are structure breakers ($S_{\mathrm{str}} > 0$), while the remaining monovalent cations and all bi- and trivalent cations are structure makers ($S_{\mathrm{str}} < 0$). The structure making behavior of cations is mainly due to the high charge density on their unhydrated surfaces, which is related both to the dimensions of bare ions and their valency. High values of the intercept and the slope of the plot of B against S_{str} for tetraalkylammonium ions are due to the combined effect of their relatively large dimensions and hydrophobic nature of these groups of ions.

Figure 5.36 illustrates plots of B coefficient of mono-, bi- and trivalent (a) cations and (b) anions against the average number n_{HB} of hydrogen bonds. The trends of these plots are similar to those of the $B(S_{\mathrm{str}})$ plots of Figure 5.35. With the exception of large tetraalkylammonium ions, once again one may discern a family of straight lines for the ions of different charges (solid lines). These data may be described by the relation

$$B = 0.044(z^2 + |z|) + 0.21 n_{\mathrm{HB}} . \tag{5.104}$$

Once again one may classify the ions taking $n_{\mathrm{HB}} = 0$ as a reference. Ions with $n_{\mathrm{HB}} < 0$ are structure breakers, while those with $n_{\mathrm{HB}} > 0$ are structure makers. As discussed above, the abnormal behavior of alkylammonium ions is due to the combined effect of their relatively large dimensions and hydrophobic nature of these groups of ions.

Marcus (1994) pointed out that assumptions used in the estimation of S_{str} and n_{HB} from the model of immobilized water in the neighborhood of ions are likely to result errors in their values. He suggested that ions have little or no effect on the structure of water in the borderline region of S_{str} values of width of ± 20 $\mathrm{J \cdot mol^{-1} \cdot K^{-1}}$. Therefore, he argued that ions with $S_{\mathrm{str}} > 20$ $\mathrm{J \cdot mol^{-1} \cdot K^{-1}}$ are definitely structure breakers and those with $S_{\mathrm{str}} < -20$ $\mathrm{J \cdot mol^{-1} \cdot K^{-1}}$ are structure makers. He also suggested a borderline region of n_{HB} width of ± 0.1 so that ions with $n_{\mathrm{HB}} < -0.1$ are structure breakers whereas those with $n_{\mathrm{HB}} > 0.1$ are structure makers.

Finally, it should be mentioned that a single linear relationship between ionic B coefficients and partial molar entropies of hydration, S_h^o, of both monovalent and polyatomic cations and anions, similar to that of relation (5.103), has been reported before (see Stokes and Mills, 1965).

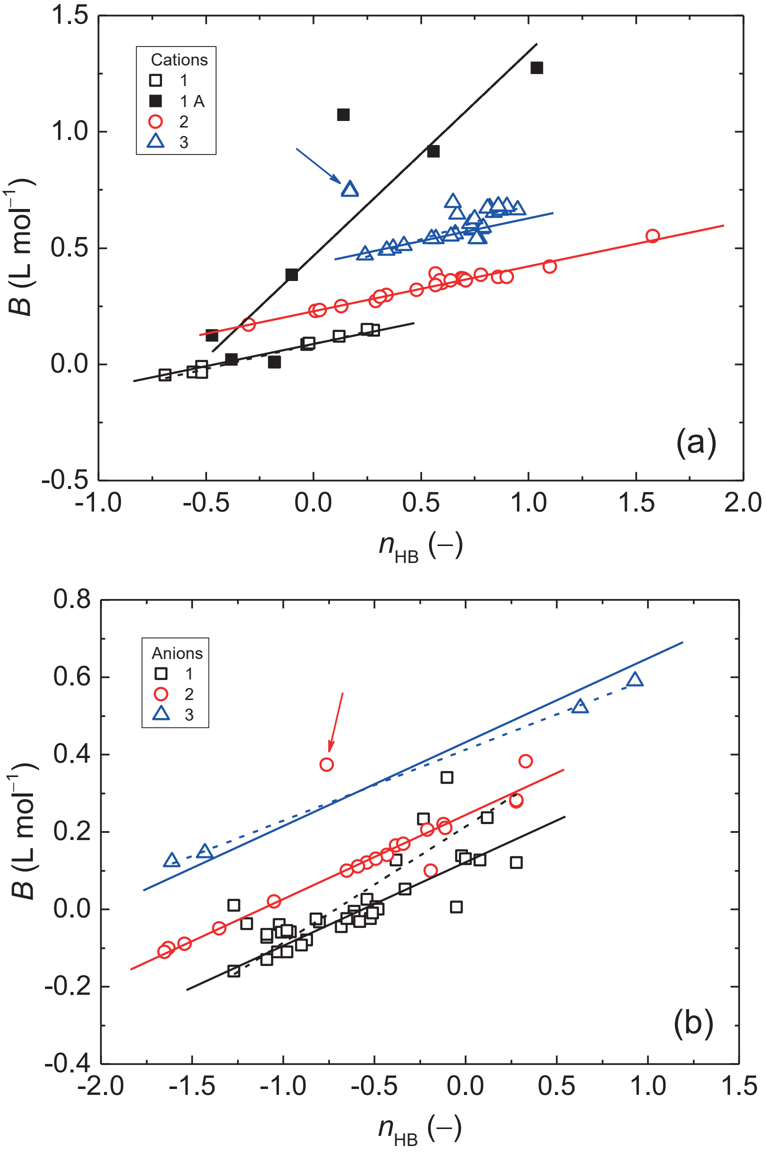

Figure 5.36. Relationships between B coefficient and average number n_{HB} of hydrogen bonds for (a) cations and (b) anions of different charges given in insets. Family of straight solid lines for ions of different charges are drawn taking best-fit of data for bivalent ions. Noticeable outliers Cr^{3+} and SiF_6^{2-} are indicated by arrows. In (b) dashed lines represent best-fit plots. Data from Marcus (1994).

5.7. Viscosity of saturated solutions

Viscosities η_s of saturated solutions of nonelectrolytes and electrolytes as a function of saturation temperature T_s differ from the temperature dependence of the viscosities η

of their solutions of constant concentrations x_2 because of the additional effect of changing solute concentration x_2 with solution temperature. Figure 5.37a and b shows typical examples of general trends of the dependence of the viscosity η_s of aqueous saturated solutions of three disaccharides and three salts, i.e. potassium bichromate and sodium and ammonium oxalates, on their saturation temperature T_s, respectively. As seen from these plots of viscosity η_s against T_s, the viscosities η_s of the three salts and sucrose decrease with increasing saturation temperature T_s of the solution but an opposite trend of an increase in the viscosities η_s of the saturated solutions with increasing temperature of two other disaccharides (i.e. trehalose and maltitol) is observed. These different trends of the temperature dependence of viscosity of saturation solutions are associated with the opposite effects of solution temperature and solute concentration (Gharsallaoui et al., 2008):

(1) At a particular temperature the viscosity increases with increasing solute concentration.
(2) For the solution of a given solute concentration the viscosity decreases with increasing solution temperature.

When factor (2) of the effect of temperature dominates factor (1) of solute concen tration, the viscosity η_s of the saturated solutions decreases with increasing saturation temperature T_s. This is the situation in the case of aqueous saturated solutions of potassium bichromate, sodium oxalate, ammonium oxalate and sucrose. Here solute–solute interactions are stronger than solute–solvent interactions. However, when factor (1) of solute concentration dominates factor (2) of solution temperature, the saturated solution viscosity increases with increasing temperature. This is the situation for aqueous saturated solutions of maltitol and trehalose. In this case, solute–solvent interactions are stronger than solute–solute interactions.

The additional effect of changing solute concentration x with temperature on the temperature dependence of viscosities η_s of nonelectrolytes and electrolyte solutions of saturation concentrations x_s in their solvents depends on the temperature coefficient of their solubilities. When the solubility x_s of a compound increases insignificantly, remains practically constant or decreases with increasing temperature T_s in the temperature range of interest, its viscosity η_s decreases with an increase in the saturation temperature T_s. However, when the solubility x_s of the compound increases rapidly with increasing temperature T_s (i.e. the temperature coefficient of its solubility is high), its viscosity η_s is expected to increase with an increase in the saturation temperature T_s. Different trends of the dependence of the viscosity η_s on the dissolved solute concentration x_s are illustrated in Figure 5.38 with aqueous saturated solutions of potassium bichromate and sodium sulfate as typical examples.

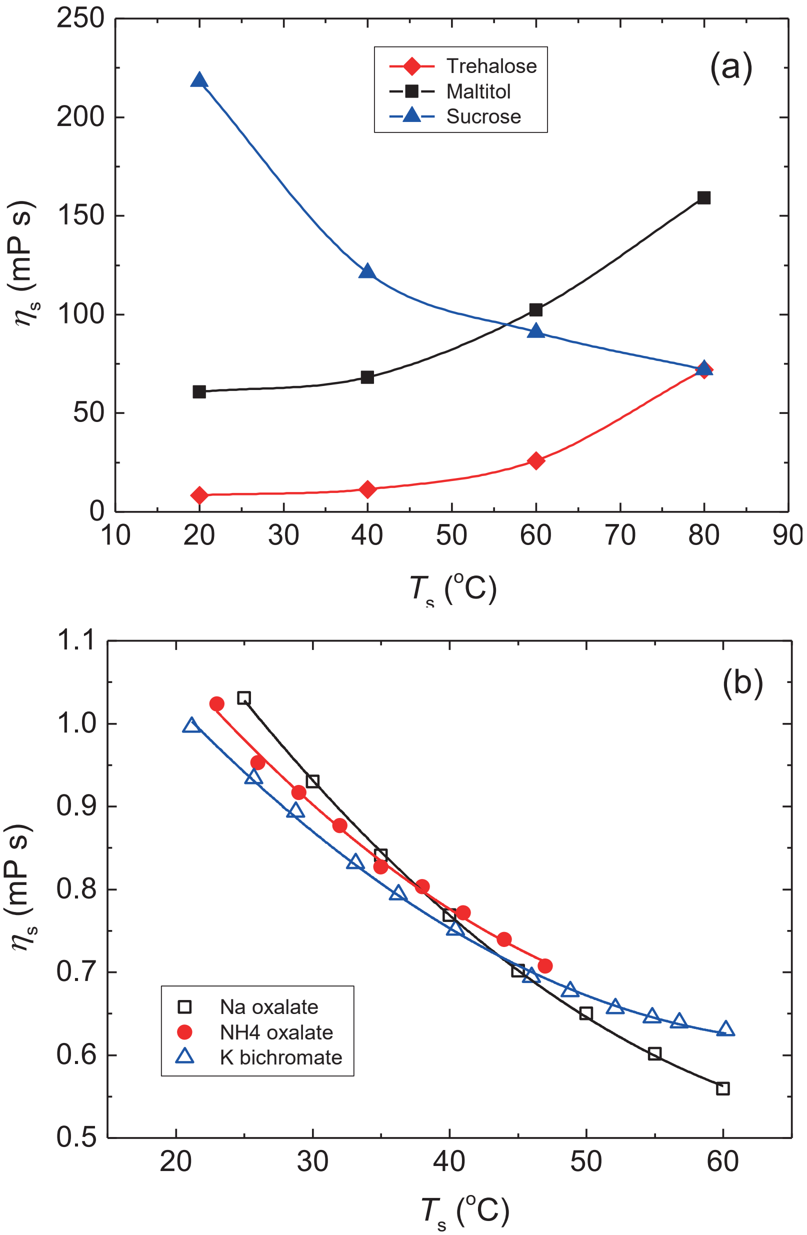

Figure 5.37. Dependence of viscosity η_s of aqueous saturated solutions of (a) three disaccharides and (b) sodium oxalate, ammonium oxalates and potassium bichromate on solute solubility x_s. Original data in (a) for disaccharides from Gharsallaoui et al. (2008), and in (a) for sodium oxalate, ammonium oxalate and potassium bichromate solutions from Misztal (2004), Frej et al. (2000) and Szewczyk et al. (1985), respectively.

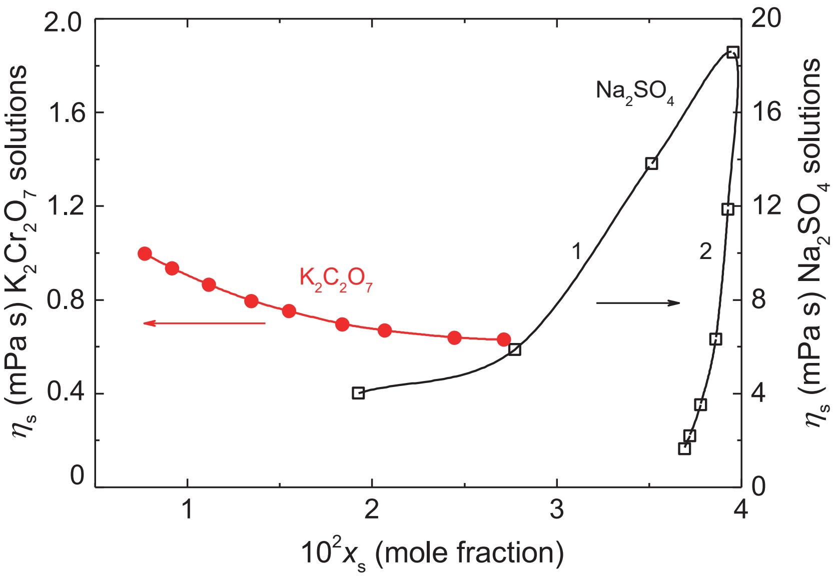

Figure 5.38. Relationship between viscosity η_s and dissolved solute concentration x_s of aqueous saturated solutions of potassium bichromate and sodium sulfate. Original data of viscosity η_s of potassium bichromate and sodium sulfate solutions are from Szewczyk et al. (1985) and T. Sokolowski (1981), respectively. Values of solubility x_s of potassium bichromate and sodium sulfate were estimated from solubility data published by W. Sokolowski and Sangwal (1983) and Söhnel and Novotny (1985), respectively.

In Figure 5.38 one observes two independent segments of increase in the viscosity η_s of saturated sodium sulfate solutions with x_s intersecting at the maximum value of sodium sulfate solubility x_s (about 0.04 mole fraction) corresponding to the highest viscosity η_s (about 19 mPa·s). Segment 1 represents a practically exponential increase in η_s with increasing x_s at low temperatures up to 305.5 K when the solubility x_s increases with an increase in saturation temperature T_s, but segment 2 corresponds to a rapid decrease in η_s with decreasing x_s at temperatures above 305.5 K when the solubility x_s increases with increasing temperature T_s. The two independent curves indicate the presence of two different types of kinetic entities participating in these two segments of the $\eta_s(x_s)$ plot of sodium sulfate solutions. The chemical constitution of these two different kinetic entities is likely to be related to the crystallization of sodium sulfate decahydrate and anhydrous sodium sulfate phases below and above 305.5 K (see Section 2.2). In contrast to the trend of the $\eta_s(x_s)$ plot of sodium sulfate solutions, the viscosity η_s of saturated potassium bichromate solutions decreases with its increasing solution concentration x_s.

The $\eta_s(T_s)$ data for the saturated solutions of different salts and disaccharides may be described reasonably well by a quadratic equation but the values of the parameters of the quadratic equation are not informative. Therefore, the $\eta_s(T_s)$ data for the saturated solutions of different solutes were analyzed using Eq. (5.4). Figure 5.39a and b shows the experimental $\eta_s(T_s)$ data as plots of $\ln \eta_s$ of aqueous saturated solutions of three disaccharides and of potassium bichromate, sodium oxalate and ammonium oxalate, respectively, as a function of T_s^{-1}.

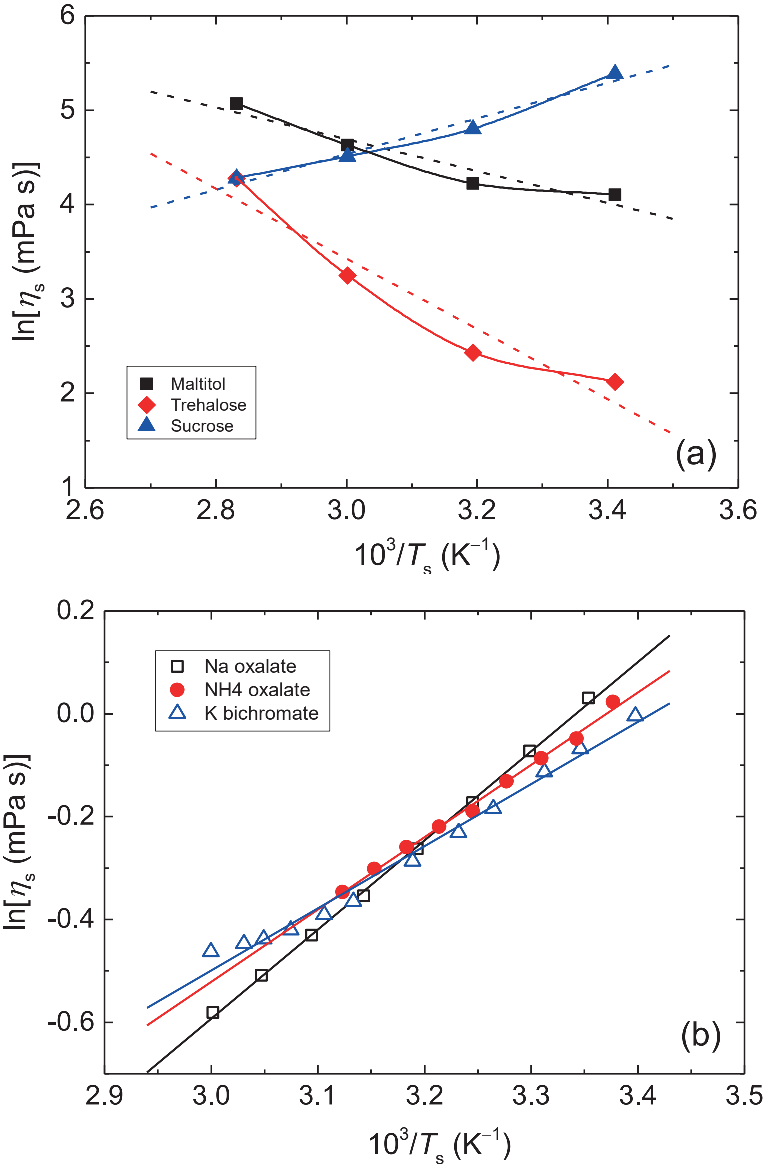

Figure 5.39. Plots of lnη_s of aqueous saturated solutions of (a) three disaccharides and (b) potassium bichromate, sodium oxalate and ammonium oxalate against T_s^{-1}. Data from Figure 5.37. Best-fit parameters of plots are listed in Table 5.16.

It may be seen in Figure 5.39 that the plots of $\ln\eta_s$ against T_s^{-1} for the solutions of sodium and ammonium oxalates and sucrose may be represented reasonably well according to Eq. (5.4) practically in the entire temperature range with positive values of their slopes E_η/R_G. In the case of potassium bichromate solutions the slope E_η/R_G somewhat decreases with increasing temperature. However, in contrast to the above cases, the slopes E_η/R_G of the plots for maltitol and trehalose solutions are not only negative but slowly attain increasingly more negative values with increasing temperature, the increase being more pronounced for trehalose solutions. Assuming the validity of the linear dependence according to Eq. (5.4), The best-fit parameters for the plots and the calculated values of E_η and η_0 are listed in Table 5.17.

Table 5.17. Values of constants of Eq. (5.4) for saturated solutions

Solvent	T_m (K)	$-\ln\eta_0$	E_η/R_G (kK)	E_η (kJ·mol^{-1})	η_0 (mPa·s)	V_M (cm^3·mol^{-1})
Water	273.15	6.3108	1.8608	15.47	$1.817 \cdot 10^{-3}$	220
$K_2Cr_2O_7$	671.15	4.1253	1.2086	10.04	$1.616 \cdot 10^{-2}$	25
$Na_2C_2O_4$	523.15	5.7986	1.7352	14.43	$3.032 \cdot 10^{-3}$	132
$(NH_4)_2C_2O_4$	406.15	4.7458	1.4081	11.71	$8.688 \cdot 10^{-3}$	46
Sucrose	459.15	1.1342	1.8898	15.71	0.322	1.2
Maltitol	419.15	−9.7409	−1.6836	−14.0	$1.70 \cdot 10^{4}$	$2 \cdot 10^{-5}$
Trehalose	488.15	−14.575	−3.7159	−30.90	$2.14 \cdot 10^{6}$	$1 \cdot 10^{-7}$

* Values in parentheses refer to concentrated solutions.

Figure 5.40 compares the behavior of plots of $\ln\eta_s$ against T_s^{-1} for aqueous saturated solutions of potassium bichromate and sodium sulfate. As pointed out above, the slope E_η/R_G of the plot somewhat increases with decreasing temperature in the temperature interval of viscosity measurements of potassium bichromate solutions. The dependence of viscosity η_s of saturated solutions of sodium sulfate on temperature T_s also follows an Arrhenius-type equation with constant slopes E_η/R_G not only in relatively narrow temperature ranges but also shows temperature regions with positive and negative values of the slopes E_η/R_G above and below $T_s \approx 305$ K ($T_s^{-1} \approx 3.28 \cdot 10^{-3}$ K^{-1}). In the temperature range above 305 K, the trend of the slope E_η/R_G of the plot of $\ln\eta_s$ against T_s^{-1} of sodium sulfate solutions is similar to that of potassium bichromate solutions. However, the slope of the plot of $\ln\eta_s$ against T_s^{-1} of sodium sulfate solutions in this temperature internal does not remain constant but shows a break at about 323 K ($T_s^{-1} \approx 3.096 \cdot 10^{-3}$ K^{-1}). The linear parts of the plot of $\ln\eta_s$ against T_s^{-1} of potassium bichromate solutions also show a break at about 320 K ($T_s^{-1} \approx 3.13 \cdot 10^{-3}$ K^{-1}). The breaks in the plots of $\ln\eta_s$ against T_s^{-1} for various solution systems have been attributed to structural changes of water network (T. Sokolowski, 1981; Szewczyk et al., 1985) as well as at the temperature of phase transition (T. Sokolowski, 1981).

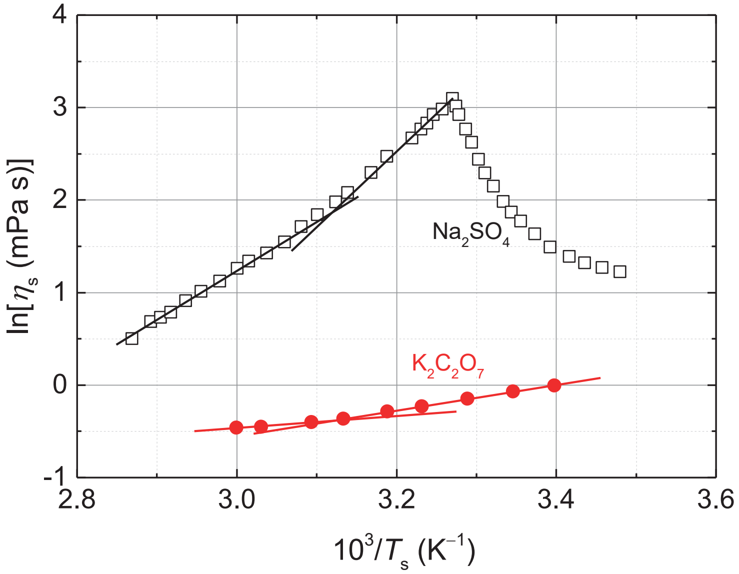

Figure 5.40. Plots of lnη_s of aqueous saturated solutions of potassium bichromate and sodium sulfate against T_s^{-1}. Data from Figure 5.35.

Breaks in the plots of lnη against T^{-1} have also been reported for undersaturated solutions of fixed concentrations (T. Sokolowski, 1981; W. Sokolowski and Sangwal, 1983). The value of the slope E_η/R_G and the activation energy E_η for viscous flow is lower in the higher temperature range, but the difference in the energies at low and high temperature range decreases with solution dilution (Figure 5.31). It has been suggested (T. Sokolowski, 1981; W. Sokolowski and Sangwal, 1983; Szewczyk et al., 1985) that the change in the slope of lnη versus T^{-1} curves at 40 or 50°C corresponds to structural changes of water network in solution.

Finally, it should be mentioned that the temperature dependence of viscosity of saturated and undersaturated solutions has been investigated in a relatively narrow range of temperature (from 25 to 60 °C). Therefore, any conclusion on structural changes in the solution from breaks in the data of lnη versus T^{-1} should be taken with caution.

References

Abu-Daabes, M.A., and A.M. Awwad (2008). Volumetric and viscometric properties of aqueous solutions of *N*-(2-hydroxyethyl)morpholine at T = (293.15, 303.15, 313.15, 323.15, and 333.15) K. *J. Chem. Thermodyn.* **40**, 874-878.

Adam, G., and J. Gibbs (1965). On the temperature dependence of cooperative relaxation properties in glass-forming liquids. *J. Chem. Phys.* **43**, 139-146.

Angell, C.A. (1966). Free volume–entropy interpretation of the electrical conductance of aqueous electrolyte solutions in the concentration range 2–20 N. *J. Phys. Chem.* **70**, 3988-3998.

Angell, C.A. (1991). Relaxation in liquids, polymers and plastic crystals: Strong/fragile patterns and problems. *J. Non-Cryst. Solids* **131-133**, 13-31.

Angell, C.A. (1995). Formation of glasses from liquids and biopolymers. *Science* **267**, 1924-1935.

Angell, C.A., and R.D. Bressel (1972). Fluidity and conductance in aqueous electrolyte solutions. An approach from the glassy state and high-concentration limit. I. $Ca(NO_3)_2$ solutions. *J. Phys. Chem.* **76**, 3244-3253.

Asadi, M. (2006). *Beet-Sugar Handbook*. Wiley, Hoboken, Table A12.

Assael, M.J., and S.K. Polimatidou (1994). Measurements of the viscosity of alcohols in the temperature range 290-340 K at pressures up to 30 MPa. *Intern. J. Thermophys.* **15**, 95-107.

Auslander, G. (1964). Predictions of the McAllister model parameters from pure component properties for liquid binary n-alkane systems. *Brit. Chem. Eng*. **9**, 610-618.

Bockris, J.O'M., and A.K.N. Reddy (1970). *Modern Electrochemistry*, Vol. 1, Plenum Press, New York.

Bončina, M., A. Apelblat, M. Bešter-Rogač (2010). Dilute aqueous solutions with formate ions: A conductometric study. *J. Chem. Eng. Data* **55**, 1951-1957.

Ciocirlan, O., O. Croitouru, and O. Iulian (2016). Viscosity of binary mixtures of 1-ethyl-3-methyllimidazolium tetrafluoborate ionic liquid with four organic solvents. *J. Chem. Thermodyn.* **101**, 285-292.

Convey, B.E., R.E. Verral, and J.E. Desnoyers (1965). Specificity in Ionic Hydration and the Evaluation of Individual Ionic Properties. *Z. Phys. Chem. Leipzig* **230**, 157-178.

Das, D., A. Messaâdi, N. Dhouibi, N. Ouerfelli, and A.H. Hamzaoui (2013). Viscosity Arrhenius activation energy and derived molar properties in N,N-dimethylacetamide + water binary mixtures at temperatures from 298.15 to 318.15 K. *Phys. Chem. Liq.* **51**, 677-685.

Das, D., H. Salhi, M. Dallel, Z. Trabelsi, A.A. Al-Arfaj, and N. Ouerfelli (2015). Viscosity Arrhenius activation energy and derived molar properties in isobutyric acid +water bunary mixtures near and far away from the critical temperature, 302.15 to 313.15 K. *J. Solution Chem.* **44**, 54-66.

D'Aprano, A., I.D., Donato, E. Caponetti, and V. Agrigento (1979). Viscosity studies of solutions of water in *n*-alphatic alcohols at various temperatures. *J. Solution Chem.* **8**, 793-800.

Desnoyers, J.E., and G. Perron (1972). The viscosity of aqueous solutions of alkali and tetraalkylammonium halides at 25^{o}C. *J. Solution Chem.* **1**, 199-212.

Dhondge, S.S., S.P. Zodape, and D.V. Parwate (2012). Volumetric and viscometric studies of some drugs in aqueous solutions at different temperatures. *J. Chem. Thermodyn.* **48**, 207-212.

Dikio, E.D., S.M. Nelana, D.A. Isabirye, and E.E. Ebenso (2012). Density, dynamic viscosity and derived properties of binary mixtures of methanol, ethanol, *n*-propanol, and *n*-butanol with pyridine at T = (293.15, 303.15, 313.15 and 323.15) K. *Int. J. Electrochem. Sci.* **7**, 11101-111022.

Domańska, U., and M. Królikowska (2012). Density and viscosity of binary mixtures of thiocyanate ionic liquids + water as a function of temperature. *J. Solution Chem.* **41**, 1422-1445.

Domańska, U., and M. Laskowska (2009). Effect of temperature and composition on the density and viscosity of binary mixtures of ionic liquids with alcohols. *J. Solution Chem.* **38**, 779-779.

Feakins, D. F.M. Bates, W.E. Waghorne, and K.G. Lawrence (1993). Relative viscosities and quasi-thermodynamics of solutions of tert-butyl alcohol in the methanol-water system: A different view of the alkyl-water interaction**.** *J. Chem. Soc. Faraday Trans.* **89**, 3381-3389.

Feakins, D., D.J. Freemantle, and K.G. Lawrence (1974). Transition state treatment of the relative viscosity of electrolytic solutions. Applications to aqueous, non-aqueous and methanol + water systems. *J. Chem. Soc. Faraday Trans.* **70**, 795-806.

Frej, H., A. Balińska, and M. Jakubczyk (2000). Density and viscosity of undersaturated, saturated, and supersaturated aqueous ammonium oxalate solutions from 287 K to 325 K. *J. Chem. Eng. Data* **45**, 415-418.

Gharsallaoui, A., B. Rogé, and M. Mathlouthi (2008). Water-disaccharides interactions in saturated solution and the crystallisation conditions, *Food Chem.* **106**, 1329-1339.

Glasstone, S., K.J. Laidler, and H. Eyring (1941). *The Theory of Rate Processes*. McGraw Hill, New York.

Goldsack, D.E., and R.C. Franchetto (1977). The viscosity of concentrated electrolyte solutions. I. Concentration dependence at fixed temperature. *Can. J. Chem.* **55**, 1062-1072.

Goldsack, D.E. and R.G. Francnetto (1978). The viscosity of concentrated electrolyte solutions. II. Temperature dependence. *Can. J. Chem.* **56**, 1442-1450.

Goldsack, D.E., R. Franchetto, and A. Franchetto (1976). Solvation effects on the conductivity of concentrated electrolyte solutions. *Can. J. Chem.* **54**, 2953-2966.

González, B., N. Calvar, E. Gómez, and A. Domínguez (2007). Density, dynamic viscosity, and derived properties of binary mixtures of methanol or ethanol with water, ethyl acetate, and methyl acetate at T = (293.15, 298.15, and 303.15) K. *J. Chem. Thermodyn.* **30**, 1578-1588.

Gourary, B.S., and F.J. Adrian (1960). Wave functions for electron-excess color centers in alkali halide crystals. *Solid State Physcs: Advances in Research and Applications* **10**, 127-247.

Grunberg, L., and A.H. Nissan (1949). Mixture law for viscosity. Nature **164**, 799-800.

Gupta, S.V. (2014). *Viscometry for Liquids: Calibration of Viscometers*. Springer, Cham (Switzerland).

Heintz, A., D. Klasen, and J.K. Lehmann (2002). Excess molar volumes and viscosities of binary mixtures of methanol and the ionic liquid 4-methyl-*N*-butylpyridinium tetrafluoborate at 25, 40, and 50°C. *J. Solution Chem.* **31**, 467-475.

Heric, E.L., and J.C. Brewer (1967). Viscosity of some binary liquid nonelectrolyte mixtures. *J. Chem. Eng. Dat*a **12**, 574-583.

Herráez, J.V., and R. Belda (2004). Viscous synergy of pure monoalcohol mixtures in water and its relation to concentration. *J. Solution Chem.* **33**, 117-129.

Herráez, J.V., R. Belda, Diez, O., and M. Herráez (2008). An equation for the correlation of viscosities of binary mixtures. *J. Solution Chem.* **37**, 233-248.

Hildebrand, J.H. (1971). Motions of molecules in liquids: Viscosity and diffusivity. *Science* **174**, issue 4008, 490-493.

Hildebrand, J.H. (1977). *Viscosity and Diffusivity: A Predictive Treatment*. Wiley-Interscience, New York.

Hind, R.H., E. McLaughlin, A.R. Ubbelohde (1960). Structure and viscosity of liquids – camphor and pyrene mixture. *Trans. Faraday Soc.* **56**, 328-334.

Horvath, A.L. (1985). *Handbook of Aqueous Electrolyte Solutions: Physical Properties, Estimation and Correlation Methods*. Ellis Horwood, Chichester, Chap. 2.14.

Jimenez, E., C. Franjo, L. Segade, J.L. Legido, and M.I. Paz Andrade (1998). Viscosities and densities for the 1-propanol + *n*-heptane system at several temperatures. *J. Solution Chem.*

27, 569-579.

Katti, P.K., and M.M. Chaudhri (1960). Viscosities of binary mixtures of benzyl acetate with diaoxane, aniline and m-cresol. *J. Chem. Eng. Data* **9**, 442-443.

Seddon, K.R., A. Stark, and M.-J. Torres (2000). Influence of chloride, water, and organic solvents on the physical properties of ionic liquids. *Pure Appl. Chem.* **72**, 2275–2287.

Koohyar, F., F. Kiani, S. Sharifi, M. Sharifirad, and S.H. Rahmanpour (2012). Study of the change of refractive index on mixing, excess molar volume and viscosity deviation for aqueous solution of methanol, ethanol, ethylene glycol, 1-propanol and 1,2,3-propantriol at T = 292.15 K and atmospheric pressure. *Res. J. Appl. Sci. Eng. Technol*. **4**, 3095-3101.

Lide, D.R. (1996/1997). *Handbook of Chemistry and Physics*, 77th edition. CRC Press, Boca Raton, FL.

Liew, K.Y., C.E. Seng, and B.H. Ng (1993). Viscosities of long chain *n*-alcohols from 15 to 80°C. *J. Solution Chem*. **22**, 1033-1040.

Mahajan, A.R., and S.R. Mirgane (2013). Excess molar volumes and viscosities for the binary mixtures of n-octane, n-decane, n-dodecane, and n-tetradecane with octan-2-ol at 298.15 K. *J. Thermodyn.* Article ID 371918, 11 pages.

Mahiuddin, S., and K. Ismail (1982). Temperature and concentration dependence of viscosity of $Mg(NO_3)_2$–H_2O systems. *Can. J. Chem.* **60**, 2883-2888.

Mahiuddin, S., and K. Ismail (1983). Concentration dependence of viscosity of aqueous electrolytes> A probe into the higher concentration. *J. Phys. Chem.* **87**, 5241-5244.

Mahiuddin, S., and K. Ismail (1996). Temperature and concentration dependence of the viscosity of aqueous sodium nitrate and sodium thiosulphate electrolyte systems. *Fluid Phase Equilibria* **123**, 231-243.

Mandal, P.K., B.K. Seal, and A.S. Basu (1973). Structural aspects of ionic viscosity *B*-coefficients in relation to ion-solvent interaction in aqueous solution (I). *Z. Phys. Chem. N.F.* **87**, 295-307.

Manfredini, M., A. Marchett, S. Sighinolfi, L. Tassi, A. Ulrici, M. Vignali, and C. Zucchi (2002). Kinematic viscosities of binary liquid mixtures of 2-butanone with 1,2-propanediol. *J. Solution Chem*. **31**, 235-252.

Marcus, Y. (1994). Viscosity *B*-coefficients, structural entropies snd heat capacities, and the effects of ions on the structure of ions. *J. Solution Chem.* **23**, 831-848.

Marcus, Y. (2006). On the molecular volumes and viscosities of electrolytes. *J. Solution Chem.* **35**, 1271-1286.

McAllister, R.A. (1960). The viscosities of liquid mixtures. *Am. Inst. Chem. Eng.* **6**, 427-431.

Messaâdi, A., N. Dhouibi, H. Hadma, F.B.M. Belgacem, Y.H. Abdelkader, N. Ouerfelli, and A.H. Hamzaoui (2015). A new equation relating the viscosity Arrhenius temperature and the activation energy for some newtonian classical solvents. *J. Chem.* Article ID 163262, pp. 1-12.

Messaâdi, A., N. Ouerfelli, D. Das, H. Hamada, and A.H. Hamzaoui (2012). Correspondence between Grunberg–Nissan, Arrhenius and Jouyban–Acree parameters for viscosity of isobutyric acid +water bunary mixtures from 302.15 to 313.15 K. *J. Solution Chem.* **41**, 2186-2208.

Millero, F.J. (1970). The apparent and partial molar volume of aqueous sodium chloride solutions at various temperatures. *J. Phys. Chem.* **74**, 356-362.

Millero, F.J. (1972). Partial molar volumes of electrolytes in aqueous solutions. In: *Water and Aqueous Solutions: Structure, Thermodynamics and Transport Propertie*s, R.N. Horne (Ed). Wiley, New York. Chapter 13, pp. 519-595.

Misztal, R. (2004). Badanie własności fizykochemicznych roztworów wodnych szczawianu sodu w obecności domieszek (Study of physico-chemical properties of aqueous sodium oxalate solutions in the presence of impurities), *PhD thesis*, Jagiellonian University, Kraków.

Mohammad, A.A., K.H.A.E. Alkhaldi, M.S. AlTuwaim, and A.S. Al-Jimaz (2014). Effect of temperature and chain length on the viscosity and surface tension of binary systems of N,N-dimethylformamide with 1-octanol, 1-nonanol and 1-decanol. *J. Chem. Thermodyn.* **74**, 7-15.

Mokhtarani, B., A. Sharifi, H.M. Mortahev, M. Mirzaei, M. Mafi, and F. Sadeghian (2009). Density and viscosity of pyridinium-based ionic liquids and their binary mixtures with water at several temperatures. *J. Chem. Thermodyn.* **41**, 323-329.

Ortega, J. (1982). Densities and refractive indices of pure alcohols as a function of temperature. *J. Chem. Eng. Data.* **27**, 312-317.

Ouerfelli, N., Z. Barhoumi, and O. Iulian (2012). Viscosity Arrhenius activation energy and derived molar properties in 1,4-dioxane + water binary mixtures from 293.15 to 323.15 K. *J. Sol. Chem.* **41**, 458-478.

Pang, F.-M., C.-E. Seng, T.-W. Teng, and M.H. Ibrahim (2007). Densities and viscosities of aqueous solutions of 1-propanol and 2-propanol at temperatures from 293 K to 333.15 K. *J. Mol. Liq.* **136**, 71-78.

Ranjith Kumar, B., B. Satyanarayana, A. Asra Banu, K. Amara Jyothi, T. Savitha Jyostna, and N. Satyanarayana (2009). Volumetric and transport properties of binary liquid mixtures of aromatic hydrocarbons with N-methylacetamide at 308.15 K. *Indian J. Pure Appl. Phys.* **47**, 511-516.

Redlich, O., and A.T. Kister (1948). Algebraic representation of thermodynamic properties and the classification of solutions. *Ind. Eng. Chem.* **40**, 345-348.

Robinson, R.A., and R.H. Stokes (1959). *Electrolyte Solutions*, 2nd edition, Butterworths, London.

Rohman, N., A. Wahab, N.A. Dass, and S. Mahiuddin (2001). Viscosity, electrical conductivity, shear relaxation time and Raman spectra of aqueous and methanolic sodium thiocyanate. *Fluid Phase Equilbria* **178**, 277-297.

Sangwal, K. (2018). *Nucleation and Crystal Growth: Metastability of Solutions and Melts*. Wiley, Hoboken. Chapter 1.

Sangwal, K., H. Frej, and R. Misztal (2004). On the dimensions of species participating in the growth of ammonium oxalate monohydrate crystals from viscosity data of concentrated aqueous solutions. *Cryst. Res. Technol*. **39**, 705-711.

Söhnel, O., and P. Novotny (1985). *Densities of Aqueous Solutions of Inorganic Substances.* Akademia, Prague.

Sokołowski, T. (1981). Physical properties of aqueous solutions of sodium sulphate. *J. Cryst. Growth* **52**, 329-831.

Sokolowski, W., and K. Sangwal (1983). Some physical properties of dilute and concentrated aqueous solutions of potassium bichromate. *Z. Phys. Chem. N.F.* **138**, 157-165.

Stokes, R.H., and R. Mills (1965). *Viscosity of Electrolytes and Related Properies*. Pergamon Press, Oxford.

Szewczyk, J., W. Sokołowski, and K. Sangwal (1985). Some physical properties of saturated, supersaturated, and undersaturated aqueous potassium bichromate solutions. *J. Chem. Eng. Data* **30**, 243-246.

Viswanath, D.S., T.K. Ghosh, D.H.L. Prasad, N.V.K. Dutt, and K.Y. Rani (2007). *Viscosity of Liquids: Theory, Estimation, Experiment, and Data*. Springer, Dordrecht (The Netherlands).

Vraneš, M., S. Papović, A. Tot, N. Zec, and S. Cadžurić (2015). Density, excess properties, electrical conductivity and viscosity of {1-butyl-1-methylimidazolium bis(trifluoromethylsulfonyl)imide + γ-butyrolactone} binary mixtures. *J. Chem. Thermodyn.* **76**, 161-171.

Vraneš, M., A. Tot, S. Papović, N. Zec, S. Dožić, and S. Cadžurić (2015). Ideal and non-ideal behaviour of {1-butyl-1-methylpyrrolydinium bis(trifluoromethyl- sulfonyl)imide + γ-butyrolactone} binary mixtures. *J. Chem. Thermodyn.* **81**, 66-76.

Zhao, C., P. Ma, and J. Li (2005). Partial molar volumes and viscosity B-coefficients of arginine in aqueous glucose, sucrose and L-ascorbic acid solutions at T = 298.15 K. *J. Chem. Thermodyn.* **37**, 37-42.

Zhao, N., and J. Jacquemin (2017). New method based on the UNIFAC-VISCO model for the estimation of dynamic viscosity of (ionic liquid + molecular solvent) binary mixtures. *Fluid Phase Equilibria* **449**, 41-51.

Zhao, N., J. Jacquemin, R. Oozeerally, and V. Degirmenci (2016a). New method for the estimation of viscosity of pure and mixtures of ionic liquids based on the UNIFAC-VISCO model. *J. Chem. Eng. Data* **61**, 2160-2169.

Zhao, N., R. Oozeerally, V. Degirmenci, Z. Wagner, M. Bendová, and J. Jacquemin (2016b). New method based on the UNIFAC-VISCO model for the estimation of ionic liquids viscosity using the experimental data recommended by mathematical gnostics. *J. Chem. Eng. Data* **61**, 3908-3921.

Živković, E.M., M.Lj. Kijevčanin, I.R. Radović, and S.P. Šerbanović (2014). Viscosities and refractive indices of binary systems acetone +1-propanol, acetone +1,2-propanediol and acetone +1,3-propanediol. *Chem. Ind. Chem. Eng. Q.* **20**, 441-455.

6

ELECTRICAL CONDUCTIVITY OF SOLVENTS AND SOLUTIONS

Solids, liquids and gases are usually conductors of electric current under certain conditions. The essential requirement for these substances to conduct electric current is the presence of free charge carriers (i.e. electrons or ions) which begin to flow in a particular direction under the influence of an applied electric field. Conductivity in gases arises only in the case of ionizing agents, for example electric or spark discharge, which ionize uncharged gas molecules into cations and electrons. Solid ionic salts dissolved in several solvents under normal temperature conditions as well as on melting are dissociated into free cations and anions which conduct electricity by their directed movement in the presence of an applied field.

Dismantling of an ionic solid into ions is a consequence of overcoming the coulombic cohesive forces holding the ions in the regular arrangement of the ionic lattice either by strong attraction of solvent molecules or by thermal agitation leading to the melting of the salts (see Section 6.3). Conducting melts of inorganic salts such as molten sodium chloride are usually known as *pure liquid electrolytes* or *ionic liquids*, which are obtained at temperatures much above the room temperature. However, various 1:1 ionic liquids composed of cations of large, complex organic groups and simple as well as complex anions are known, which melt at temperatures below the room temperature. These conducting liquids are frequently referred to as *low-temperature ionic liquids*. The liquid electrolytes, irrespective of whether they are formed at high- or low-temperature, have a conductivity many orders higher than that in their solid state. Although cations and anions participate in the electric conduction in solutions and melts of ionic solids, the mechanism of conduction in the two is entirely different.

The ionic conductivity of the most conductive electrolytes, for example strong acids, at 298.15 K is of the order of 100 $S{\cdot}m^{-1}$ (i.e. 1 $S{\cdot}cm^{-1}$), and chemically pure water $25{\cdot}10^{-6}$ $S{\cdot}m^{-1}$. In the case of molten electrolytes however, the conductivity remains high over a wide temperature range. An example is sodium chloride which has an ionic conductivity of the order of 100 $S{\cdot}m^{-1}$ in the temperature range between 1074 and 1738 K.

Conductivity of electrolyte solutions has received a great deal of attention both theoretically and experimentally. The subject has been competently dealt with by Robinson and Stokes (1959), and Bockris and Reddy (1970), whereas various correlations of specific and equivalent conductivities of electrolytes with electrolyte concentrations and solution temperatures are surveyed by Horvath (1985). Investigation of conductivities of electrolyte solutions at high temperature and pressure conditions has also drawn considerable interest recently (for example, see:

Zimmerman and Wood, 2002; Zimmerman et al., 2012).

The present chapter describes different problems related to conductivities of electrolyte solutions and low-temperature ionic liquids at usual temperatures. Measurement techniques (Section 6.1), basic concepts of conductivity (Section 6.2), types of electrolytes (Section 6.3), general trends of conductivity of solutions (Section 6.4), and the conductivity of water (Section 6.5) are briefly described first. Then, general features of the specific conductivity of electrolytes in relation to the electrolyte concentration and solution temperature, and the molar and equivalent conductivities of electrolytes are described and discussed against their theoretical background in Sections 6.6 and 6.7, respectively. Finally, some aspects related to Walden's rule, the behavior of conductivity of saturated solutions with temperature, and applications of conductivity measurements are presented in Sections 6.8, 6.9 and 6.10, respectively.

6.1. Measurement of conductivity of solutions

The electrical conductivity measurements of electrolyte solutions are carried out by direct current and alternating current methods. The direct current method is simple in principle requiring the passage of a steady current through the solution contained in a conductivity cell and through a standard resistance in series, and the comparison of the potential developed between two fixed points in the solution with that across the standard resistance. Figure 6.1a shows the schematic illustration of a simple Wheatstone bridge used for direct current resistance measurements, with resistances R_1, R_2, R_3 and the conductivity cell resistance R_4 and a galvanometer G to detect potential difference between the points A and B. When the potentials at these points are equal, the galvanometer shows no deflection, and $R_1/R_2 = R_3/R_4$, which enables to determine the cell resistance $R_4 = R_3(R_2 /R_1)$. The solution for measurement is contained in a suitably designed cell in which two flat electrodes, each of surface area A, separated by a fixed distance l are positioned opposite each another (Figure 6.1b). The cell is constructed in such a way that the electric field is prevented from spreading throughout the entire measuring vessel. Flow of direct current between the electrodes results in the deterioration of the interface between metal and solution, an effect known as polarization, that can severely affect the measurement. Therefore, the suitability of a conductivity cell for conductivity measurement depends on the occurrence of polarization on the surface of the electrode as well as on the cell constant. These effects are decreased with increasing measuring frequency and electrode surface in the alternating current method.

In the alternating current method, impedance Z of a condenser of capacitance C is measured instead of resistance R in the direct current method. The impedance is a complex quantity composed of a real part $Z' = R$, and an imaginary part $Z'' = j\omega C$, where ω is the angular frequence equal to $f/2\pi$ (with f as the linear frequency in Hz) and $j = (-1)^{1/2}$. The components Z' and Z'' of the impedance Z correspond to current and potential, respectively. These components are presented as plots of Z'' against Z' for a solution (known as Nyquist plots), having the form of semicircles with centers placed on the real impedance axis and following the relation (see: Robinson and Stokes, 1959; Świergiel et al., 2015a,b)

$$Z(\omega,T)=\frac{R(T)}{1+j\omega C(T)}, \tag{6.1}$$

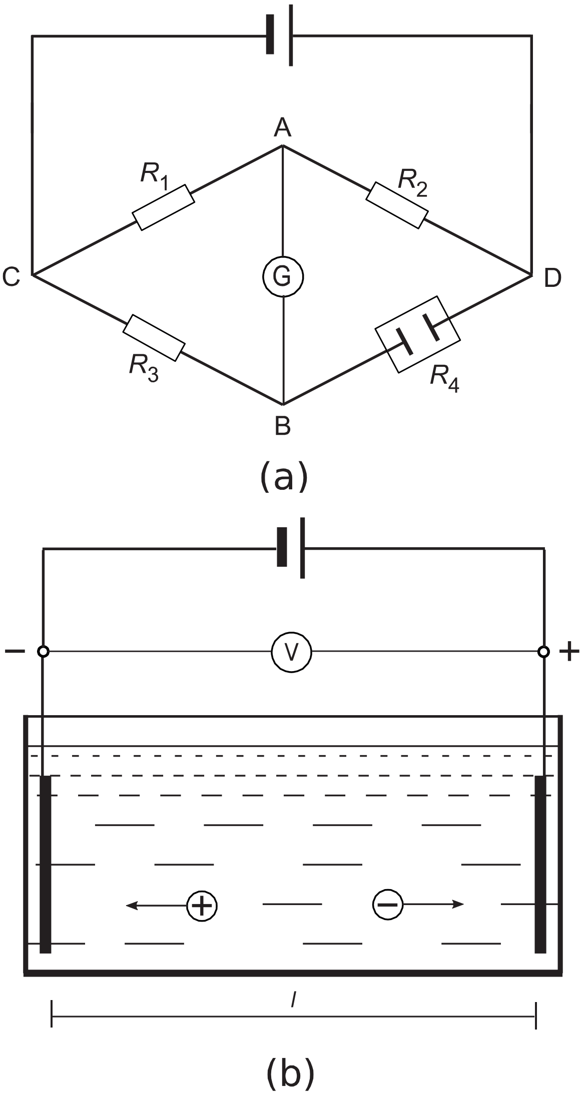

Figure 6.1. (a) Basic circuit of a simple Wheatstone bridge used for direct current resistance measurements; R_4 denotes the solution cell resistance. (b) Simplified illustration of an electric field of intensity E applied across two plane-parallel electrodes of surface area A each, mutually separated at a distance l, introduced into an electrolyte solution. Drift directions of cation and anion are shown.

where R is the direct-current resistance of the sample, which is related to the direct-current specific conductivity σ by: $\sigma = 1/kR$, with k as the cell constant; see Eq. (6.4) below. The dependence of conductivity σ on the frequency f is usually small, but itbecomes appreciable at very high frequencies. Typical frequencies used are in the range 1–3 kHz.

Evaluation of electrolyte conductivity requires high accuracy measurements in a sufficiently wide temperature range. Temperatures of conductometric measurements of solutions must be accurate within 0.001 and 0.005 K to obtain the required data reproducibility, just as their concentrations should be precisely determined with accuracy of 0.0001 $\mathrm{mol \cdot L^{-1}}$. A historical narration of principle of conductivity measurement methods, design of measurement cells, temperature control, and accuracy in conductivity measurements is easily accessible (Robinson and Stokes, 1959).

Conductivity measuring devices are usually known as conductometers. There is a wide variety of conductometers which are commercially available.

6.2. Basic concepts and definitions

The movement of ions of an electrolyte in solution is similar to the movement of gas molecules in its volume. The ions in a solution are in ceaseless motion, colliding with each other elastically, changing their directions between the collisions, and jumping from site to site with time. Since the movement of an ion between successive collisions is random in three dimensions, the mean distance traversed by the ion from its original position after a sufficiently long time in a particular direction is zero. In other words, the ions do not displace with any average preferred velocity in a specific direction in the solution due to their randomly-directed movement. However, when two plane-parallel electrodes of surface area A each, mutually separated at a distance l, are introduced into the solution and an electric field of intensity E is applied across the electrodes (see below), the random movement of the ions is biased in the direction of the applied field (see Figure 6.1b). The biasing of this motion of all the ions of one kind, say cations, with equal velocities v_1 in one direction and all the ions of the other kind, say anions, moving with velocities v_2 in the other direction results in the flow of electric current in electrolytes. In the solution cations and anions resulting from the dissociation of an electrolyte by the solvent are carriers of electric current.

The oriented movement of cations and anions of an electrolyte in the solution in opposite directions is always accompanied by a resistance by the electric fields of other ions and solvent molecules. This resistance of the solution in the oriented movement of ions is determined by the solvation characteristics of the ions and the viscosity of the solution, which are affected by the solution temperature.

A measure of flow of electric current in an electrolytic solution is its specific conductivity (or conductance) σ, which is the inverse of the specific resistance ρ. The device used to measure the conductivity of an electrolyte solution is an electrolytic cell.

Let us consider that n_1 and n_2 are the concentrations (number per unit volume) of cations 1 and anions 2, respectively, moving in opposite directions with drift velocities v_1 and v_a perpendicular to the electrodes of surface area A, and z_1e and z_2e are the corresponding charges on them. Here z_1 and z_2 are the valencies of cations and anions, respectively, and e is the elementary charge. Then the current intensity I resulting from the drift of cations and anions in the solution by the applied electric field is given by

$$I = A(n_1 z_1 e v_1 + n_2 q_2 e v_2)\,, \tag{6.2}$$

and is proportional to the applied potential difference U between the electrodes according to Ohm's law:

$$I = \frac{U}{R}\,, \tag{6.3}$$

where R is the resistance of the electrolyte contained in the cell of length l and cross-sectional area A, and the potential difference $U = El$. The resistance R of an electrolytic cell is given by

$$R = \frac{\rho l}{A} = k\rho\,, \tag{6.4}$$

where ρ is the specific resistance of the electrolyte and $k = l/A$ is known as the cell constant. The reciprocal of the specific resistance is the specific conductivity σ, which may be defined by rearranging Eq. (6.4) in the form

$$\sigma = \frac{1}{\rho} = \frac{l}{A}\frac{1}{R} = k\Lambda\,, \tag{6.5}$$

where $\Lambda = 1/R$ is the conductivity of the solution. The specific conductivity σ is the conductivity $1/R$ of a cube of electrolytic solution 1 cm long and 1 cm^2 in area. Since resistance R is measured in ohms, Ω (1 Ω = 1 volt divided by 1 ampere), conductivity $\Lambda = 1/R$ has the unit ohm^{-1} or mho, denoted by Ω^{-1} or Siemens ($1\ \Omega^{-1} = 1$ S). Therefore, σ has the units: $\text{S}\cdot\text{cm}^{-1}$ or $\text{S}\cdot\text{m}^{-1}$ ($1\ \text{S}\cdot\text{cm}^{-1} = 100\ \text{S}\cdot\text{m}^{-1}$).

Since the specific conductivity σ of a solution is related to the number of charge carriers, its value depends on the solution concentration c. Therefore, the specific conductivities of solutions of different electrolytes can be compared only when they have the same number of ions and the same measurement cell of known dimensions is used. In order to compare the conductivity of electrolytic solutions, it is customary to normalize both the cell geometry and the concentration of ions.

Normalization of the cell geometry, taking electrodes of 1 cm^2 area and placed 1 cm apart to define specific conductivity σ, defines a new conductivity, the molar conductivity, in the form

$$\Lambda_\text{m} = \frac{\sigma}{c} = \sigma V\,, \tag{6.6}$$

where V is the volume of the solution containing 1 mole of solute. The molar conductivity of solutions is measured in $S\cdot cm^2\cdot mol^{-1}$ or $S\cdot m^2\cdot mol^{-1}$ ($1\ S\cdot cm^2\cdot mol^{-1} = 0.1\ mS\cdot m^2\cdot mol^{-1}$). Obviously, the molar conductivity is the specific conductivity σ times the solution volume V containing 1 mole of solute. Since 1 mole of different solute dissolved in the same volume contains particles equal to the Avogadro number N_A ($N_A = 6\cdot 10^{23}$ particles per mole), the molar conductivity refers to conductivity per particle.

Charges borne by ions in solutions of the same concentration of different solutes are not the same and are related to their chemical constitution. For example, the same concentration of two solutions of singly-charged ions in a 1:1 electrolyte like NaCl and KCl and doubly-charged ions in a 2:2 electrolyte like $ZnSO_4$ contain different amounts of charge. Therefore, comparison of molar conductivities of two electrolytes is informative and useful only when the charges on the charge carriers in the two solutions are the same. In such cases, the specific conductivities of the two solutions is compared when they contain equivalent amount of charge. This is done by taking 1 mole of charge of each solute, i.e. 1 mole of ions divided by the valency z of the ions, or 1 eq-mole of the solute charge. Thus, the equivalent conductivity Λ_{eq} of a solution is defined as the specific conductivity σ of the solution times the volume V of that solution containing 1 eq-mole of solute dissolved in it. Therefore, the equivalent conductivity of a solution is given by (cf. Eq. (6.6))

$$\Lambda_{eq} = \frac{\sigma}{cz} = \frac{\Lambda_m}{z}, \tag{6.7}$$

where cz is the number of eq-mole per cm^3 of the electrolytic solution. The units of Λ_{eq} are: $S\cdot cm^2\cdot eq\text{-}mol^{-1}$ or $S\cdot m^2\cdot eq\text{-}mol^{-1}$. Since the observed values of Λ_{eq} of aqueous solutions of various electrolytes of different concentrations are usually lower than $50\ mS\cdot m^2\cdot eq\text{-}mol^{-1}$, it is convenient to use $mS\cdot m^2\cdot eq\text{-}mol^{-1}$, where it is understood that these units refer to equivalent conductivity. Obviously, for a 1:1 electrolyte only the molar conductivity Λ_m of its solution is equal to its equivalent conductivity Λ_{eq}.

The equivalent conductivity Λ_{eq} of an electrolytic solution is related to the current density I, which is determined by the concentration n of ions, their charge ze and drift velocity v (see Eq. (6.2)). Therefore, the value of Λ_{eq} for the electrolyte decreases with an increase in solution concentration c but increases with temperature T. These trends are observed for different types of electrolytes, but the dependences of Λ_{eq} on c and T are not so simple as Eq. (6.7) implies because of mutual interactions occurring between oppositely-charged ions moving in opposite directions in the solution. These ion–ion interactions are increased when the number N of ions per unit volume (i.e. concentration $n = N/V$) in the solution is increased but are decreased when their drift velocity v decreases with an increased in temperature. Stronger the ion–ion interactions occurring in the solution, the lower is the value of Λ_{eq}, and vice versa.

Using Eqs. (6.2) and (6.3) one may define equivalent conductivity Λ ($\Lambda_{eq} = \Lambda$) of an electrolytic solution as the sum of cationic and anionic equivalent conductivities λ_1 and λ_2 in the form

$$\Lambda = \frac{l}{A}\frac{I}{U} = \frac{N_A z_1 e v_1}{E} + \frac{N_A z_2 e v_2}{E} = \lambda_1 + \lambda_2 \,, \tag{6.8}$$

where N_A is the Avogadro number, v_1 and v_2 are the mean drift velocities of the cations and anions in the presence of the electric field of intensity E applied to a 1 cm cell, and the ratio v/E defines the ionic mobility u (i.e. $u = v/E$). The mobility u of an ion in the solution depends on its size and charge, the solvation sheath surrounding it, and the occurrence of interactions with other ions and solvent molecules. Consequently, cations and anions have different conductivities λ_1 and λ_2.

Extrapolated value of the equivalent conductivity Λ of an electrolytic solution diluted to concentration $c \to 0$ is called the limiting equivalent conductivity, and is usually denoted by Λ^0. Physically, its value for an electrolytic solution refers to the situation when the ions are infinitely distant from each other and the motion of an ion is limited entirely by its interactions with the surrounding solvent molecules. Thus, for an electrolyte

$$\Lambda^0 = \lambda_1^0 + \lambda_2^0 \,, \tag{6.9}$$

where λ_1^0 and λ_2^0 are the limiting equivalent conductivity of a cation and an anion, respectively. The values of λ_1^0 and λ_2^0 of individual ions depend on their size, charge and the properties of the medium. In aqueous solutions at 25 °C the values of λ_1^0 for various simple cations lie between 3.8 and 7.8 $\text{mS}\cdot\text{m}^2\cdot\text{eq-mol}^{-1}$, but those of λ_2^0 for various anions are somewhat higher and usually lie between 4.0 and 8.0 $\text{mS}\cdot\text{m}^2\cdot\text{eq-mol}^{-1}$. However, the values of λ_1^0 are as low as about 1.7 $\text{mS}\cdot\text{m}^2\cdot\text{eq-mol}^{-1}$ in the case of some large complex cations and those of λ_2^0 are between 10 and 11 $\text{mS}\cdot\text{m}^2\cdot\text{eq-mol}^{-1}$ for some polyvalent anions. Exceptions to these trends are the relatively high value of λ_1^0 of 34.98 $\text{mS}\cdot\text{m}^2\cdot\text{eq-mol}^{-1}$ for hydrogen ion (usually written as H_3O^+) and λ_2^0 of 19.83 $\text{mS}\cdot\text{m}^2\cdot\text{eq-mol}^{-1}$ for hydroxyl ion (OH^-).

In this chapter we are mainly concerned with solutions of electrolytes containing ions formed as a result of electrolytic dissociation and surrounded by solvation sheaths of solvent molecules.

6.3. True and potential electrolytes

Elements and their chemical compounds occurring as solids and liquids usually contain their building entities (i.e. atoms, molecules or ions) lying between 10^{28} and 10^{29} per m^3 corresponding to a distance of a few tenths of a nm and have comparable densities in the two states of aggregation. In the solid state, the building entities of the substance are held together at their equilibrium positions by long-range cohesive forces in a three-dimensional periodic structure. When heat energy is supplied to a crystalline solid, the cohesive forces holding its building entities are weakened because of increased amplitudes of their vibrations in the solid. In the heating process, a stage is reached when thermal forces become dominant and the long-range order of the crystalline arrangement is wiped out and the vibrating particles acquire the freedom of translational motion. In other words, the solid transforms to the liquid state.

The process of transformation of a solid substance into its liquid essentially involves the weakening of bonds between the entities building the solid. For example, in ionic solids these bonds are ionic, whereas in molecular solids weak van der Waals bonds are involved. Consequently, melting of ionic solids yields *ionic liquids* (also known as *ionic melts* or *liquid electrolytes*) composed of cations and anions, and melting of molecular solids gives *molecular liquids* composed of neutral molecules which are essentially nonionic. The molten ionic and molecular materials have much more empty space than that in the solid form and have somewhat lower density than their solid form. The ions of ionic liquids and the molecules of molecular liquids are in perpetual random motion, but an electric field applied to ionic liquids alone induces directional flow of ions resulting in electric current.

Another way of dismantling the three-dimensional periodic arrangement of ionic solids and producing mobile ions is to place the solid in a solvent like water. Since ionic solids consist of ions even before they come in contact with a solvent, the role of the solvent is to entice the ions out of the solid so that they move into the solution. This process of dissolution of an ionic solid is associated with ion–solvent forces which overcome the ion–ion forces holding them together in the solid. In the case of a polar solvent such as water, solvent molecules in contact with the ions of the solid result in ion–dipole forces which disengage the ions from the lattice site, solvate them, and disperse them in the solution. Ionic solids dissolved in a solvent like water are known as *ionic solutions* or *electrolytic solutions*. All ionic salts, whether as a melt or in its solution, are ionic conductors, and are known as *true* (i.e. *intrinsic* or *genuine*) electrolytes.

A salt that melts without decomposing or vaporizing usually is an ionic liquid. For example, NaCl melts at 801 °C into a liquid consisting of cations (Na^+) and anions (Cl^-). Since the ionic bond in ionic salts is stronger than the van der Waals forces between the molecules of molecular compounds, ionic salts usually melt at higher temperatures than other solids. However, during the last three decades a new class of ionic solids has emerged, which have their melting point below 100 °C and some salts are liquid at or below room temperature. Ionic melts below 100 °C are usually known as *low-temperature ionic liquids*, abbreviated hereafter as ILs (see below).

The main requirement of an electrolyte is that it should give rise to a conducting solution. Thus, one would anticipate that acetic acid, which is composed of nonionic molecules, will never behave as an electrolyte. However, when acetic acid is dissolved in water, ions are produced and its solution conducts electricity. Thus, acetic acid is also a type of electrolyte, but it is not a true electrolyte. Instead, when acetic acid is dissolved in water, it becomes an electrolyte. Substances like acetic acid are known as *potential electrolytes*. In contrast with true electrolytes, these electrolytes do not have their own ions but produce them in the presence of the solvent water. The ions are produced as a result of reaction between neutral acetic acid molecule and water molecule, and involves the transfer of a proton from the acetic acid molecule to the oxygen atom of the water molecule, i.e.

$$\mathrm{CH_3COOH+H_2O \Longleftrightarrow CH_3COO^-+H_3O^+}\,. \tag{6.10}$$

The proton transfer results in the production of two ions: (1) CH_3COO^-, and (2) H_3O^+. Similarly, the reaction of a molecule of a base like NH_3 with a water molecule involves the removal of a proton by it from water molecule, i.e.

$$\mathrm{NH_3+H_2O \Longleftrightarrow NH_4^+ + OH^-}\,. \tag{6.11}$$

The two reactions differ from each other whether the molecule of an ionizing substance donates a proton to the water molecule or accepts a proton from the water molecule. Thus, a weak acid like CH_3COOH is proton donor but a base is proton acceptor. Two substances such as CH_3COOH and NH_3 related by the difference of one proton are known as conjugate acid and base. In the above reactions, CH_3COO^- is the base conjugate of the acid CH_3COOH, and NH_4^+ is the acid conjugate of the base NH_3. In electrolyte solutions free H_3O^+ and OH^- ions do not exist, and an acid can donate a proton to an acceptor base by processes described by the above reactions, such that the presence of water results in the reaction between them giving the electrolyte NH_4CH_3COO (usually denoted as CH_3COONH_4):

$$\mathrm{CH_3COOH+NH_3 \Longleftrightarrow CH_3COO^-+NH_4{}^+}\,. \tag{6.12}$$

It should be mentioned that the salt NH_4CH_3COO behaves as a true electrolyte like various ionic salts such as NaCl and mineral acids like HCl and H_2SO_4, but the aqueous components CH_3COOH (frequently abbreviated as HAc) and NH_3 involved in its formation are potential electrolytes.

The ionization of an electrolyte in a solvent at a given temperature is an equilibrium process of equilibrium constant K_eq which is determined by the concentrations of reactants and products of the dissociation reaction according to the law of mass action. In the case of dissociation of a true a:b electrolyte A_aB_b of concentration c into solvated ions A^{z_1+} and B^{z_2-} in water:

$$\mathrm{A}_a\mathrm{B}_b \rightarrow a\,\mathrm{A}^{z_1+} + b\,\mathrm{B}^{z_2-}\,, \tag{6.13}$$

the equilibrium constant

$$K_\mathrm{eq} = \frac{[\mathrm{A}^{z_1+}]^a[\mathrm{B}^{z_2-}]^b}{[\mathrm{A}_a\mathrm{B}_b]}\,, \tag{6.14}$$

where a and b are the number of cations and anions, respectively, resulting from the dissociation of an A_aB_b molecule, and z_1 and z_2 are their valencies. If α is the degree of dissociation of the electrolyte A_aB_b of concentration c, the equilibrium concentrations $[A_aB_b]$ of A_aB_b, $[A^{z_1+}]$ of cations A^{z_1+} and $[B^{z_2-}]$ of anions B^{z_2-} are:

$c(1-\alpha)$, $a(c\alpha)$ and $b(c\alpha)$, respectively. Therefore, Eq. (6.14) may be written as

$$K_{\text{eq}} = \frac{a^a b^b c^{a+b} \alpha^{a+b}}{c(1-\alpha)} = \frac{a^a b^b c^{a+b-1} \alpha^{a+b}}{(1-\alpha)} . \tag{6.15}$$

This general relationship between K_{eq} and c describes the dissociation behavior of various types of electrolytes. For a 1:1 electrolyte like NaCl, Eq. (6.15) reduces to the form

$$K_{\text{eq}} = \frac{c\alpha^2}{(1-\alpha)} . \tag{6.16}$$

Eq. (6.15) enables to calculate the values of K_{eq} for A_aB_b electrolyte of any concentration c, provided that the value of its α is known.

The degree of dissociation α of an electrolyte of concentration c is described by

$$\alpha = \frac{\Lambda}{\Lambda^0} , \tag{6.17}$$

where Λ and Λ^0 are the equivalent conductivities of the electrolyte of concentration c and infinite dilution $c \to 0$, respectively. Since all true electrolytes are completely dissociated into ions in solutions of infinite dilution, α approaches unity in such solutions. Therefore, the values of the equivalent conductivities Λ^0 of different electrolytes are obtained directly from the extrapolation of the concentration dependence of Λ to infinite dilution using Onsager's limiting law (see Eq. 6.58)). Thus, from the measured value of Λ for a true electrolyte of known concentration c and the extrapolated value of Λ^0 for the electrolyte of infinite dilution, the value of the degree of their dissociation α of an electrolyte is calculated using Eq. (6.17).

In contrast to the dissociation of true electrolytes, the extent of generation of ions in potential electrolytes is determined by various processes of proton donation to the solvent by an acid and proton acceptance from the solvent by a base. Since the equivalent conductivities Λ of an electrolyte is associated with the concentration of ions present in it and the degree of dissociation α of an electrolyte increases with dilution, one may anticipate that potential electrolytes are also completely dissociated at infinite dilution and show Λ^0 comparable with that of true electrolytes. However, in view of limitations in the experimental values of Λ in dilute solutions, the procedure of extrapolation of the concentration dependence of Λ does not enable to determine Λ^0 of the potential electrolytes. Therefore, in the case of potential electrolytes, Λ^0 is calculated from a knowledge of the values of limiting equivalent conductivities λ_1^0 and λ_2^0 of individual ions of true electrolytes using Eq. (6.9). The measured values of Λ of potential electrolytes and the estimated values of Λ^0 from λ_1^0 and λ_2^0 of their individual ions show that the degree of dissociation α of these electrolytes is very low ($\alpha << 1$). This implies that the these electrolytes are partially dissociated in dilute solutions, and the dissociation (equilibrium) constant $K_{\text{eq}} \approx c\alpha^2$ (cf. Eq. (6.16)).

At 25 °C values of equivalent conductivities Λ^0 of ionic salts at infinite dilution in water usually lie between 9.0 and 15.0 mS·m^2, but those of mineral acids HCl and H_2SO_4 are 42.616 and 42.96 mS·m^2, acid HAc is 39.07 mS·m^2, and bases NaOH and NH_4OH are 24.78 and 27.14 mS·m^2, respectively. The higher values of Λ^0 of acids and bases than those of their salts are associated with the higher values of $\lambda_1{}^0$ of H^+ (or rather H_3O^+) and $\lambda_2{}^0$ of OH^- ions than those of cations and anions of their salts. These differences in the values of $\lambda_1{}^0$ and $\lambda_2{}^0$ of the ions are due to differences in their mobilities in the solution. The high mobilities of H^+ and OH^- ions are due to the fact that the proton is exchanged very quickly between neighboring water molecules and the OH^- ion is transmitted very quickly between two molecules of water (see Reactions (6.10) and (6.11)).

Ionic liquids of commonly available salts differ from their solutions not only by solvation of the ions present in the liquid state but also by the temperature interval of their formation. However, low-temperature ionic liquids consist of unsolvated ions, and are usually moderate to poor conductors of electricity, non-ionizing, and highly viscous. They are also good solvents and their miscibility with water and various organic solvents changes with the side chain lengths on the cation and with the choice of the anion. Low-temperature ionic liquids consist of bulky and asymmetric organic cations such as 1-alkyl-3-methylimidazolium, 1-alkylpyridinium, and *N*-methyl-*N*-alkylpyr-rolidinium ions and a wide range of anions ranging from simple halides to inorganic anions such as tetrafluoro-borate and hexafluorophosphate, and to large organic anions like bis(trifluo-romethane)sul-fonimide (denoted as bistriflimide), trifluoromethane-sulfonate (triflate), or para-toluenosulfonyl group (tosylate). Depending on their chemical structure, they may be classified into aprotic and protic ionic liquids. Aprotic ionic liquids consist of inherent cations and anions like true electrolytes but protic ionic liquids result by proton transfer reaction from acid conjugate HA to the base B according to the general reaction (see Eq. (6.12)):

$$\mathrm{HA}+\mathrm{B}\rightarrow \mathrm{HB}^{+}+\mathrm{A}^{-} \quad . \tag{6.18}$$

Since this proton transfer process in such a liquid does not always take place completely, the liquid is essentially a mixture of ions and neutral molecules because of low degree of its ionization. Consequently, most protic ionic liquids behave as potential electrolytes exhibiting low ionic conductivity.

Following Bockris and Reddy (1970), the terms true and potential electrolytes were used in the above discussion. This classification of electrolytes is based on relatively high and low conductivities of their aqueous solutions. Such electrolytes are traditionally known as *strong* and *weak* electrolytes, respectively. However, this classification of strong and weak electrolytes has no sense when some other solvent is used for the conductivity measurements of an electrolyte. For example, the behavior of conductivity of an otherwise strong electrolyte like sodium chloride in a nonaqueous solvent is similar to that of acetic acid in water, and that of a weak electrolyte like acetic acid in a solvent like liquid ammonia is similar to that of sodium chloride in water. This justifies the classification of different electrolytes into true and potential electrolytes, which does not depend on the solvent. Instead, according to this classification of electrolytes, the conductivity of an electrolyte is governed by the capability of the solvent to dissociate into ions and the concentration of the dissociated ions in the solution.

6.4. General trends of conductivity of solutions

The specific conductivity σ of an electrolyte is related to the concentration n_1 and n_2 of solvated cations and anions (i.e. number of ions per unit volume) and their mobility u_1 and u_2 in the solution (see Eqs. (6.2) and (6.8)). Its value in a solvent of dielectric constant ε is related to the coulombian force F of attraction between cations and anions of charges z_1e and z_2e at a separation r by

$$F = -\frac{z_1 z_2 e^2}{4\pi\varepsilon_0(\varepsilon/\varepsilon_0)r^2}, \tag{6.19}$$

where ε_0 is the dielectric constant of vacuum, and $(\varepsilon/\varepsilon_0)$ is the relative dielectric constant of the solution. In dilute solutions when the ions are far apart from each other and there is poor coulombian interaction between the ions, the conductivity σ of the electrolyte solution at a particular temperature is determined entirely by the viscous drag of the solvated ions in the solvent. With an increase in the concentration c of the electrolyte, its conductivity σ increases because of increase in the concentration n_1 and n_2 of ions. Further increase in the electrolyte concentration results not only an increase in n_1 and n_2 of ions, but also in the following effects: (1) a decrease in the distance r between dissociated cations and anions, (2) an increase in the tendency of formation of ion associates such as ion pairs, and (3) a decrease in the dielectric constant ε of the solution. In contrast to the initial increase in the conductivity σ with electrolyte concentration c, these three effects lead to a steady reduction in σ with c. Consequently, with an increase in concentration c, conductivity σ first increases and then, after attaining a maximum value $\sigma_{\max}$ of σ at a certain concentration $c_{\max}$, it decreases and acquires a finite positive value at the saturation concentration. Figure 6.2 shows examples of the dependence of the specific conductivity σ of some true and potential electrolytes on their concentration c.

A phenomenological interpretation of the relationship between σ and c of electrolytes may be given from the differential form of Eq. (6.6) for equivalent conductivity Λ written as (cf. Vila et al., 2005)

$$\mathrm{d}\sigma = c\,\mathrm{d}\Lambda + \Lambda\,\mathrm{d}c, \tag{6.20}$$

where the first term, $c\mathrm{d}\Lambda$, represents the effect of an increase in the concentration on the ionic mobility and the second term, $\Lambda\mathrm{d}c$, accounts for the effect of a decrease in the concentration of charge carriers on the variation of solution conductivity. At low concentrations the contribution of concentration of charge carriers dominates over the decrease in the ionic mobility, whereas at higher electrolyte concentrations the contribution of the decrease in the ionic mobility dominates over the concentration of charge carriers. This opposite behavior of the two contributions results in a maximum in the conductivity at a particular concentration.

The specific conductivity σ of electrolytes also increases with an increase in temperature as a consequence of the mobility u_1 and u_2 of the ions in the solution (see Eq. (6.2)). This effect is associated with a reduction in the viscous drag of the ions due to weakened interionic interactions. Irrespective of whether neutral entities such as ion pairs are present as in true electrolytes or are formed in the solution of a potential electrolyte, the above trend of the concentration dependence of the conductivity σ of different electrolytes is of general nature. Its value is determined by the movement of these cations and anions by their viscous drag in the solvent. Differences in the electrolytic conduction in solvents of high and low ε (for example, at 25 °C water and an organic solvent with $\varepsilon \approx 80$ and 10, respectively) and in a particular solvent containing varying electrolyte concentation may be explained in this way.

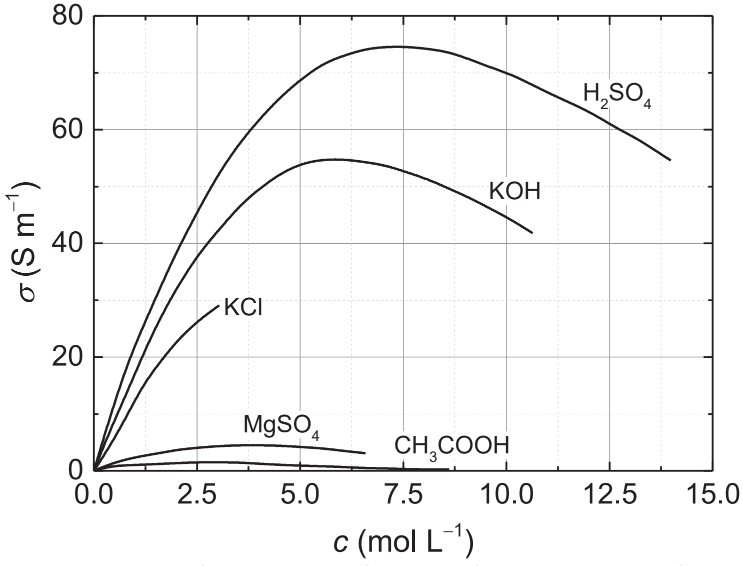

Figure 6.2. Examples of dependence of the specific conductivity σ of some true and potential electrolytes on their concentration c at 298.15 K.

Although the concentration of ions increases with increasing electrolyte concentration c, its molar conductivity Λ_m or equivalent conductivity Λ_{eq} decreases with an increase c. However, the observed dependence of equivalent conductivities Λ_{eq} of true and potential electrolytes on their concentration differs substantially from each other. Figure 6.3 illustrates examples of plots of measured Λ_{eq} of some true electrolytes and one potential electrolyte against $c^{1/2}$, where the concentration c is in molarity and $c^{1/2}$ is taken along the horizontal axis to facilitate extrapolation of the plots to infinitely dilute solutions and determine Λ^0 (see Section 6.7).

From Figure 6.3 one observes that the equivalent conductivities Λ of true electrolytes lie above about 9.0 $\mathrm{mS \cdot m^2 \cdot eq\text{-}mol^{-1}}$ in solutions of moderate concentrations. In these solutions Λ increases slowly with increasing dilution. Since these electrolytes are dissociated completely into ions in the concentration interval considered here, the observed behavior cannot be attributed to increasing dissociation. Instead, the increase in Λ with dilution can be attributed to the decreasing mutual interaction between the ions, which retards their mobility in the electric field. The value of Λ^0 is a measure of the conductivity of the ions determined only by their viscous drag in the solvent.

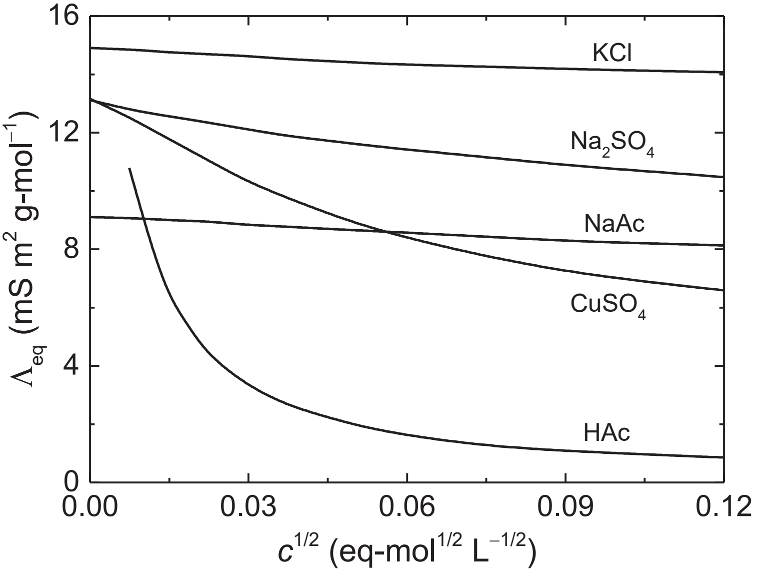

Figure 6.3. Plots of measured equivalent conductivity Λ_{eq} of some true electrolytes and one potential electrolyte against $c^{1/2}$ at 298.15 K.

In contrast to the behavior of true electrolytes, the value of Λ of potential electrolytes is very low in solutions of moderate concentrations and increases enormously with increasing dilution (see Figure 6.3 for HAc). Since conductivity is a measure of the number of ions present in the solution, it may be supposed that one eq-mole of these electrolytes gives comparatively few ions. This means that their degree of dissociation α is small, and the value of concentration of ions increases with dilution following the relation: $\alpha \propto c^{-1}$ (cf. Eq. (6.16)). Consequently, the equivalent conductivity Λ of these electrolytes increases with dilution, and at infinite dilution they would be completely dissociated (see Eq. (6.13)) and show conductivity Λ^0 comparable with that of true electrolytes but this is beyond the range of measurement or extrapolation.

6.5. Conductivity of water and its purity

Water even in its pure form always has a conductivity different from zero. The specific conductivity σ of the purest water at 25 °C is 5.5 μS·m^{-1} (5.5·10^{-6} S·m^{-1}). This value of the conductivity of water is associated with its self-hydrolysis (dissociation) involving both the donation of a proton by one of the water molecules and the acceptance of the donated proton by another water molecule. Consequently, water may be considered as a solution composed of cations and anions. Formally, the above equilibrium process is given by the acid–base reaction (see Eq. (6.12))

$$2\mathrm{H_2O} \Longleftrightarrow \mathrm{H_3O^+} + \mathrm{OH^-}\,, \tag{6.21}$$

with the equilibrium constant K_w given by

$$K_\mathrm{w} = \frac{[\mathrm{H_3O^+}][\mathrm{OH^-}]}{[\mathrm{H_2O}]^2} = [\mathrm{H_3O^+}][\mathrm{OH^-}]\,, \tag{6.22}$$

where $[H_3O^+]$ and $[OH^-]$ are the concentrations of H_3O^+ and OH^- ions, and the concentration of H_2O, $[H_2O]$, is unity. These concentrations refer to mole fraction.

The equilibrium constant K_w of water and the concentrations $[H_3O^+]$ and $[OH^-]$ of dissociated ions may be calculated from the values of molar concentation c of pure water from its density d at 25 °C and molar mass M, measured equivalent conductivity Λ of water, and the equivalent conductivity Λ^0 of completely dissociated water into H_3O^+ and OH^- ions. The density d of water at 25 °C is 0.997 g·cm^{-3}, its molar mass M = 18.02 g·mol^{-1}, the equivalent conductivities $\lambda_1{}^0$ and $\lambda_2{}^0$ of H_3O^+ and OH^- ions at 25 °C are: 34.98 and 19.83 mS·m^{-2}, respectively.

The concentation c of pure water from its density d at 25 °C may be given by

$$c = \frac{1000d}{M} = 55.3\ \mathrm{mol\cdot L^{-1}}\,, \tag{6.23}$$

the equivalent conductivity Λ of water:

$$\Lambda = \frac{10^{-3}\sigma}{c} = 9.946\cdot 10^{-11}\ \mathrm{S\cdot m^2}\,, \tag{6.24}$$

$$\Lambda_0 = \lambda_1^0 + \lambda_2^0 = 54.81\ \mathrm{mS\cdot m^2}\,, \tag{6.25}$$

its degree of dissociation at 25 °C is

$$\alpha = \frac{\Lambda}{\Lambda_0} = 1.8146\cdot 10^{-9}\,, \tag{6.26}$$

and the concentration of ions

$$[\mathrm{H_3O^+}] = [\mathrm{OH^-}] = \alpha c = 1.0\cdot 10^{-7}\,. \tag{6.27}$$

Using these concentrations of ions one finds from Eq. (6.22) the equilibrium constant

$K_w = 1.0 \cdot 10^{-14}$. Taking $[H_3O^+] \equiv [H^+]$ and defining $pH = -\log[H^+]$, one finds pH = 7 for pure water.

Freshly distilled water has its specific conductivity between 50–200 $\mu S \cdot m^{-1}$. When distilled water is stored, its electrolytic conductivity increases as a result of leaching glass ions from glass vessels, dissociation of trace amounts of unknown impurities present in them as well as dissolution of gases from the atmosphere, which subsequently undergo partial dissociation.

The specific conductivity of various natural waters (mineral waters) usually varies between 20 and 60 $mS \cdot m^{-1}$. The presence of H_3O^+ and OH^- ions in natural water is caused by leaching them from the bedrock and soils and dissolution of gases from the atmosphere. The permissible electrolytic conductivity of drinking water is about 250 $mS \cdot m^{-1}$ in comparison with the value between 50 and 200 $\mu S \cdot m^{-1}$ for freshly distilled water.

Conductivity measurements are commonly used to monitor feedwater purity and control the quality of drinking and process water. However, the presence of all undissociating substances such as many organic compounds and solid substances of very low solubility product remains undetected in these measurements.

6.6. Specific conductivity of electrolytes

Electrical conductivities of a variety of ionic salts in solutions and several low-temperature ionic liquids (ILs) mixed with water and different organic solvents have been reported. The ionic liquids are: 1-alkyl-3-methylimidazolium-based (for example, see: Li et al., 2010; Nishida et al., 2003; Hekaari and Mousavi, 2009; Vila et al., 2006a, b; Wang et al., 2007), and 1-alkyl-1-methylpyrroly-dinium-based (e.g. see: Vraneš et al., 2014, 2015). The cations of 1-alkyl-3-methylimidazolium-based ionic liquids are usually denoted as $[C_n\text{mim}]^+$ or $[C_n\text{mim}]^+$, with the number n of carbon atoms of the alkyl group exceeding 1, and the anions are halides, usually bromide $[Br]^-$ and sometimes chloride $[Cl]^-$, but tetrafluoroborate $[BF_4]^-$ and ethylsulfate $[C_2H_5SO_4]^-$ have also been used. However, in the case of methyl, ethyl and 1-butyl groups (i.e. with n = 1, 2 and 3), the cations are also denoted as $[\text{mmim}]^+$, $[\text{emim}]^+$ and $[\text{bmim}]^+$, respectively. The cations of 1-methylpyrrolydinium-based ionic liquids are denoted as $[C_n\text{mpyr}]^+$, with C_n replaced by “m”, “e” and “b” for methyl, ethyl and 1-butyl group, respectively.

As mentioned above, the specific conductivity σ of an electrolyte depend on its concentration and temperature. These effects are discussed above.

6.6.1. Concentration dependence of specific conductivity of electrolytes

6.6.1.1. General features of concentration dependence of specific conductivity

With an increase in concentration c, the conductivity σ of an electrolyte first increases and then, after attaining a maximum value $\sigma_{\max}$ of σ at a certain concentration $c_{\max}$, it decreases and acquires a finite positive value at the saturation concentration. No theoretical equation has been proposed to describe the above behavior of the dependence of σ on electrolyte concentration c. Casteel and Amis (1972) proposed the following empirical equation

$$\sigma = \sigma_{\max}\left(\frac{c}{c_{\max}}\right)^{a_1}\exp\left[b_1(c-c_{\max})^2 - a_1\left(\frac{c-c_{\max}}{c_{\max}}\right)\right], \tag{6.28}$$

where a_1 and b_1 are empirical constants, and $c_{\max}$ is the concentration when maximum conductivity $\sigma_{\max}$ is reached. This equation has been employed successfully to describe the experimental data of the concentration dependence of the specific conductivity of widely different electrolytes in various solvents: magnesium salts in water–ethanol system (Casteel and Amis, 1972), sodium thiocyanate in water and methanol solvents (Rohman et al., 2001), potassium iodide and ammonium nitrate in dimethyl sulfoxide (DMSO) (Płowaś et al., 2014; Świergiel et al., 2013), 1-butyl-1-methylpyrrolydinium bis(trifluoromethyl-sulfonyl)imide, [bmpyr][NTf$_2$], and 1-butyl-3-methylimidazolium bis(trifluoro-methylsulfonyl)imide, [bmim][NTf$_2$]), in γ-butyrolactone (GBL) (Vraneš et al., 2014, 2015).

The values of the parameters a_1, b_1, $\sigma_{\max}$ and $c_{\max}$ for a system depend on its composition and temperature. In general, the values of $\sigma_{\max}$ and $c_{\max}$ for a system increase with temperature, but the trends of variation of a_1 and b_1 with temperature are frequently erratic. However, irrespective of somewhat erratic trends of a_1 and b_1 for a system, the values of both maximum conductivity $\sigma_{\max}$ and its corresponding electrolyte concentration $c_{\max}$ for a system increase with increasing temperature and a change in the value of $\sigma_{\max}$ is accompanied by a similar change in the temperature of the system. Physically, this behavior of increases in both $\sigma_{\max}$ and $c_{\max}$ implies that the dimensionless relative concentration $c_{\text{rel}} = c/c_{\max}$ corresponding to the dimensionless relative conductivity $\sigma_{\text{rel}} = \sigma/\sigma_{\max}$ when $\sigma = \sigma_{\max}$ and $c = c_{\max}$ are practically the same and are independent of the temperature and composition of the system. Casteel and Amis (1972) first observed this behavior during the study of the specific conductivities σ of concentrated solutions of magnesium salts in water–ethanol system and later reported for other systems such as NH_4NO_3–DMSO system (Świergiel et al., 2013). When the values of the two fitting parameters $\sigma_{\max}$ and $c_{\max}$ are known for a system at different experimental conditions, Eq. (6.28) takes the form

$$\sigma_{\text{rel}} = c_{\text{rel}}^{a_1}\exp\left[\frac{b_1}{c_{\max}^2}(c_{\text{rel}}-1)^2 - a_1(c_{\text{rel}}-1)\right]. \tag{6.29}$$

Casteel and Amis (1972) demostrated that Eq. (6.29) enables to construct a universal, normalized plot, independent of the effects of temperature and solvent composition, of dimensionless relative conductivity σ_{rel} against dimensionless relative concentration c_{rel} for a system.

Using the above description of the concentration dependence of specific conductivity σ of electrolytes, the conductivity behavior of different electrolyte–solvent systems is discussed below. It should be mentioned here that, instead of molar concentration c used in the above discussion, expressed in molarity (mole·L^{-1}), molal m (mol·kg^{-1}) and mole fraction x have also been used during the analysis of the experimental data in different publications. However, the choice of the different concentration units does not affect the general inferences following from the analysis.

Figure 6.4 shows a typical example of the dependence of specific conductivity σ of aqueous sodium thiocyanate solutions on their concentration m at three temperatures (Rohman et al., 2001). Curves represent the best-fit of the data shown by open points according to Eq. (6.28). As seen from the figure, σ increases nonlinearly initially with the value of $a_1 \approx 0.93$ but, beyond the maximum value $\sigma_{\max}$ which increases with temperature from 16.32 S·m^{-1} at 298.15 K to 22.58 S·m^{-1} at 323.15 K at $m_{\max} \approx 6.3$ mol·kg^{-1} for concentration $m$exceeding about 8 mol·kg^{-1}, it increases practically linearly with m. A similar behavior of the concentration dependence of the conductivity σ of the salt was observed in methanol solutions at different temperatures, with the difference that the values of $\sigma_{\max}$, $m_{\max}$ and a_1 are much lower than those in aqueous solutions.

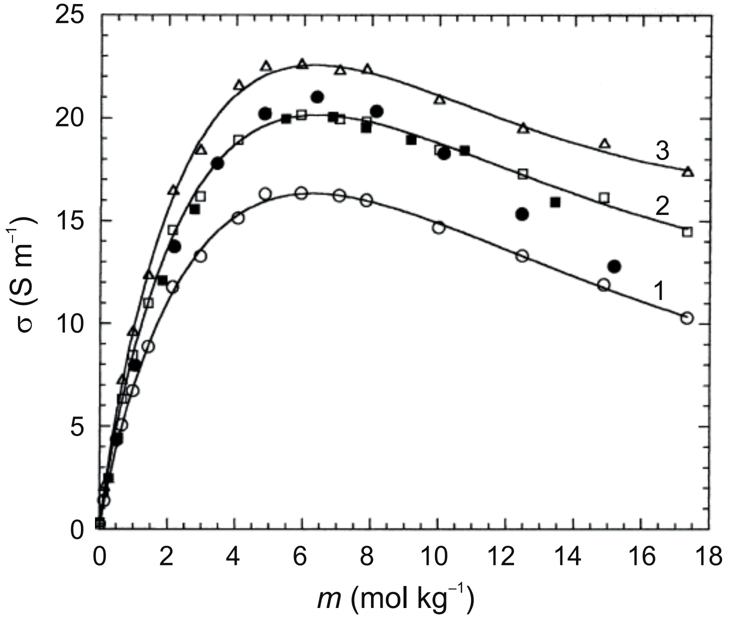

Figure 6.4. Dependence of specific conductivity σ of aqueous sodium thiocyanate solutions on their concentration m at three temperatures: (1) 298.15 K, (2) 313.15 and 323.15 K. Curves represent data shown by open points according to Eq. (6.28). Filled circles and squares represent data from other sources. Adapted from Rohman et al. (2001).

The initial increase in the conductivity σ with electrolyte concentration m in the solution is due to the increasing concentration of solvated ions involving ion–solvent interactions and reaches a maximum value of $\sigma_{\max}$ at $m_{\max} \approx 6.3$ mol·kg^{-1} when ion–ion interactions begin to dominate over the ion–solvent interactions. This results in the shedding off of the solvent molecules from the outer solvation sheaths of the ions as well as in increasing ion–ion interactions due to increasing solute concentration in the solution. The latter process results in the formation of cation–anion pairs, the concentration of which increases with increasing electrolyte concentration m such that the concentration of conducting cations and anions no longer increases with m. Consequently, both the reduced mobility u of solvated ions and the decreasing concentration of ions in the solution due to the formation of cation–anion pairs lead to a practically linear decrease in σ with increasing electrolyte concentration m.

The effect of a solvent is associated with its ability to dissociate the electrolyte into ions by solvation processes with its concentration m in the solvent and is intimately connected with the dielectric constant ε of the solvent and the structure of its molecule. In contast to the effect of dielectric constant of a solvent, the effect of an increase in its temperature on the electrolytic conductivity σ is associated with an increased mobility u of ions as well as a suppresion in the formation of ion pairs due to enhanced vibrations of ions in the solution.

Figure 6.5 illustrates another example of the dependence of specific conductivity σ of another true electrolyte NH_4NO_3 in strongly polar solvent DMSO on salt concentration x at different temperatures (Świergiel et al., 2013). Dashed line in the figure shows the dependence of maxima $\sigma_{\max}$ of conductivity on salt concentration $x < 0.404$ mole fraction and temperature T between 293.15 and 333.15 K. As in the case of the aqueous and methanolic sodium thiocyanate solutions described above, it was observed that in this system both $\sigma_{\max}$ and $x_{\max}$ increase with T, but the value of a_1 slowly decreases from 0.858 at 293.15 K down to 0.779 at 333.15 K. The explanation of the concentration and temperature dependence of σ of this system given above also holds here.

The trend of the concentration dependence of specific conductivity σ of ionic salts in different solvents described above is also encountered in low-temperature ionic liquids contained in their solvents. Figure 6.6 shows an example of the dependence of specific conductivity σ of [bmim][NTf$_2$] in γ-butyrolactone (GBL) binary mixture on IL concentration x at different temperatures between 293.15 and 323.15 K (Vraneš et al., 2014). Curves represent the data according to Eq. (6.28) with the constants listed in Table 6.1.

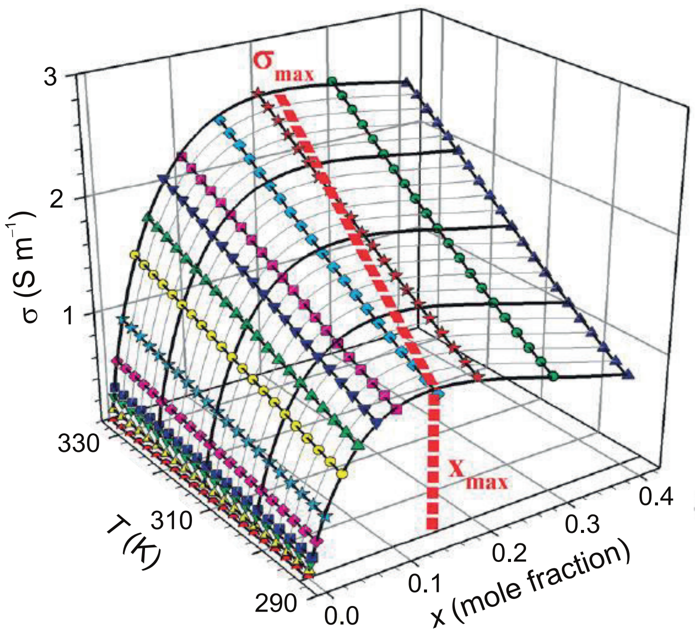

Figure 6.5. Dependence of specific conductivity σ of NH_4NO_3 in DMSO on its concentra-tion x_2 at different temperatures. Dashed line runs through maxima of conductivity. Reproduced from Świergiel et al. (2013).

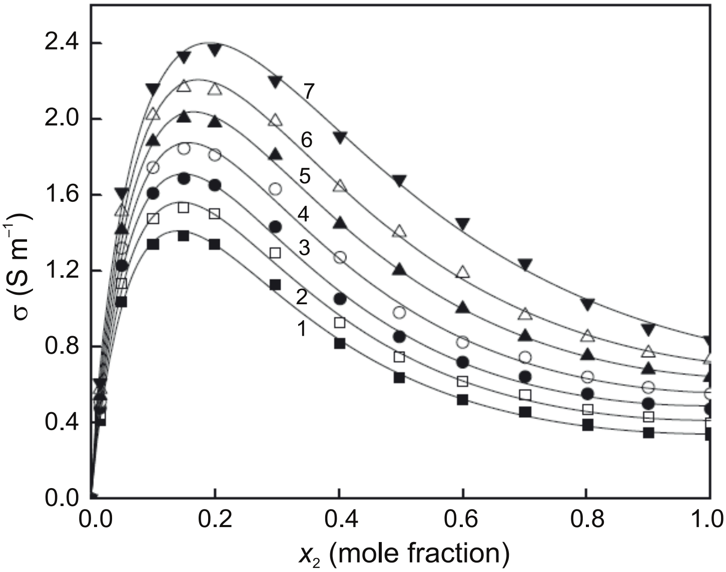

Figure 6.6. Dependence of specific conductivity σ of [bmim][NTf_2]) in γ-butyrolactone (GBL) binary mixture on its concentration x at different temperatures: (1) 293.15, (2) 298.15, (3) 303.15, (4) 308.15, (5) 313.15, (6) 318.15 and (7) 323.15 K. Curves represent data according to Eq. (6.28) with the constants listed in Table 6.1. From Vraneš et al. (2014).

Table 6.1. Values of parameters of Eq. (6.28) for [bmim][NTf$_2$]–GBL binary mixture*

T (K)	σ_{max} (S·m^{-1})	x_{max} (mole fraction)	a_1 (–)	$10^3 b_1$ (kg^2·mol^{-2})
293.15	14.25	0.141	0.928	3.285
298.15	15.45	0.145	0.924	3.175
303.15	17.02	0.149	0.919	3.105
308.15	18.99	0.157	0.906	2.793
313.15	20.49	0.165	0.872	2.410
318.15	22.26	0.174	0.846	2.083
323.15	23.88	0.191	0.789	1.507

* Data from Vraneš et al. (2014).

From Figure 6.6 it may be observed that addition of [bmim][NTf$_2$] to the solvent GBL leads to a rapid increase in σ of the mixture and its value approaches a maximum σ_{max} at $x_{max} \approx 0.2$ mole fraction. This is due to dissociation of ion–ion interactions of the IL molecules by the solvent to result in the formation of isolated solvated [bmim]$^+$ cations and [NTf$_2$]$^-$ anions in the solution by ion–dipole interaction between [bmim]$^+$ cations and [NTf$_2$]$^-$ anions of undissociated IL molecules. Beyond x_{max} the conductivity decreases essentially exponentially with concentration x and approaches a constant value due to the decreasing mobility of the ions and increasing ion–ion interactions.

Apart from the temperature of an electrolyte solution, the concentration of the solute contained in it and the solvent used to prepare the solution discussed above, the conductivity σ of electrolyte solutions strongly depends on the chemical constitution of cations and anions because of the difference in their mobility and degree of dissociation of the solute. Examples illustrating the effect of chemical constitution of cations and anions on the conductivity σ of aqueous solutions of six ILs at 25 °C as a function of their molar concentration c are shown in Figure 6.7 (Vila et al., 2006a). The ILs are of two different kinds (Vila et al., 2006a,b):

(1) Tailered ILs obtained by mixing an inorganic salt with an ionic liquid with melting point above 298.15 K, i.e. 0.35 and 0.60 mole fraction of $AlBr_3$ mixed with 1-ethyl-3-methylimidazolium bromide (denoted as [emim][Br]-$AlBr_3$ with $x_a(AlBr_3) = 0.35$ and 0.60), $AlBr_3$ mixed with 1-ethyl-3-methylpyrridinium bromide (denoted as [empyr][Br]-$AlBr_3$), and $AlCl_3$ mixed with 1-ethyl-3-methylimidazolium chloride (denoted as [emim][Cl]-$AlCl_3$) with $x_a(AlCl_3) = 0.33$; all these mixtures are liquids at 25 °C.
(2) Directly purchased commercially in the liquid state are: 1-ethyl-3-methylimidazolium tetrafluoroborate, [emim][BF$_4$], and 1-ethyl-3-methylimidazolium ethylsulfate, [emim][ESO$_4$].

From Figure 6.7 it may be observed that the conductivity σ of an IL is changed enormously in aqueous mixtures and this increase in σ to the maximum value from its water-free value varies between 5 times for [emim][ESO$_4$] and 30 times for [empyr][Br]-$AlBr_3$. The general behavior of these curves is similar to that observed for various electrolyte systems, including different aqueous solutions of ionic salts and low-temperature ILs, as seen in Figures 6.4-6.6 above. The maximum values of σ_{max} of different systems and the corresponding value of c of the IL are listed in Table 6.2.

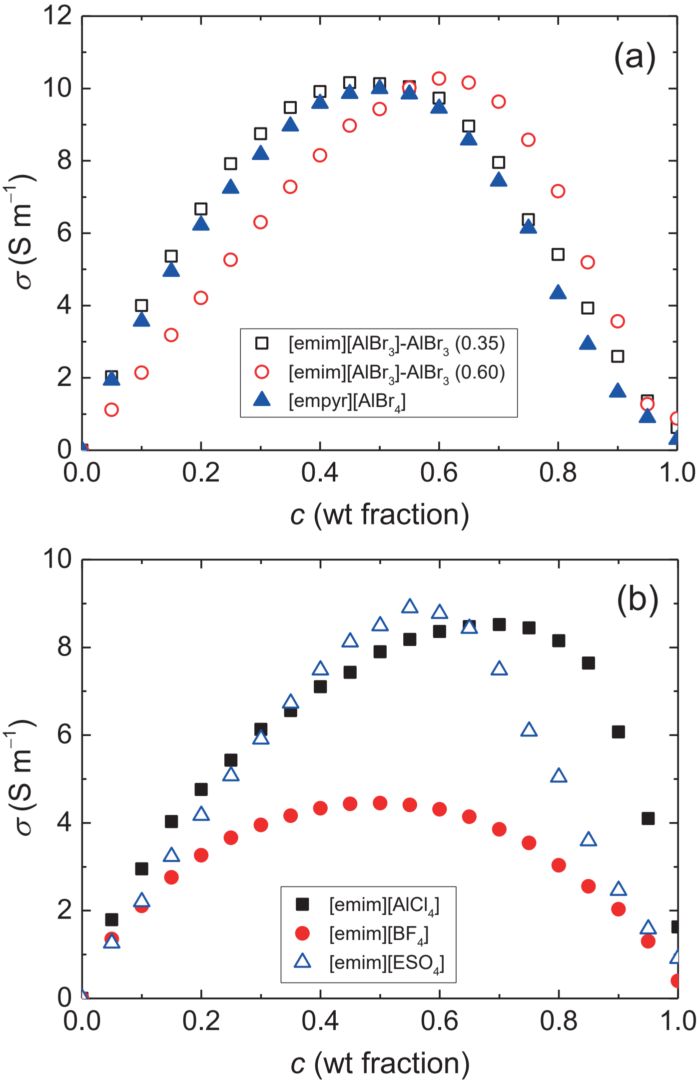

Figure 6.7. Conductivity σ of aqueous solutions of six ILs at 25 °C as a function of their molar concentration *c*: (a) (□) [emim][Br]-$AlBr_3$ with $x_a(AlBr_3)$ = 0.35, (○) [emim][Br]-$AlBr_3$ with $x_a(AlBr_3)$ = 0.60, and (▲) [empyr][$AlBr_4$], and (b) (■) [emim][$AlCl_4$], (●) [emim][BF_4], and (Δ) [emim][ESO_4]. Original data from Vila et al. (2006a).

Table 6.2. Values of σ_{max} and c_{max} for aqueous ILs of Figure 6.7 at 298.15 K

IL	x_a (mole fraction)	σ_{max} (S·m^{-1})	c_{max} (mol·L^{-1})
[emim][Br]-$AlBr_3$	0.35	10.16	0.45
	0.60	10.27	0.60
[empyr][Br]-$AlBr_3$	0.35	9.99	0.50
[emim][Cl]-$AlCl_3$	0.33	8.90	0.55
[emim][BF_4]		8.52	0.70
[emim][ESO_4]		4.45	0.50

* Data from Vila et al. (2006a).

It may be noted from Table 6.2 that the maximum value of conductivity σ_{max} of the aqueous [emim][Br]-$AlBr_3$ system is essentially the same for the ILs containing two different concentrations x_a of $AlBr_3$, and a lower $AlBr_3$ content in the IL sample is accompanied by a lower value c_{max} of its content in the solution. Physically, this observation means that the maximum concentration of cations and anions (i.e. [emim]$^+$ and [$AlBr_4$]$^-$) formed by the dissociation of the IL determines the value of σ_{max}, and that the differences in σ_{max} of aqueous solutions of ILs differing in their cations or anions are due to the differences in their mobilities. Examples of the former observation are [emim][Br]-$AlBr_3$ containing anionic content x_a equal to 0.35 and 0.60 mole fraction, and those of the latter are [emim][Br]-$AlBr_3$ and [empyr][Br]-$AlBr_3$ with x_a = 0.35 mole fraction containing different cations and [emim][Br]-$AlBr_3$ and [emim][Cl]-$AlCl_3$ with comparable $x_a \approx 0.35$ mole fraction and commercial [emim][BF_4] and [emim][ESO_4] containing different anions. The high values of σ_{max} for [emim][$AlBr_4$] , and [emim][$AlCl_4$] and [emim][BF_4] are probably due to the high charge on Al^{3+} and B^{3+} ions of their cations in contrast to the charge on $C_2H_5^+$ ion of [ESO_4]$^-$ anion (cf. Vila et al., 2006b).

The value of the concentation c_{max} of an electrolyte when σ_{max} is attained in its solution is characteristic of a system. If one assumes that the maximum conductivity σ_{max} of the electrolyte is related to the degree of its dissociation, α, in the solvent, the concentration c_{max} may be attributed to the dissociation constant K_{eq} of the electrolyte (see Eq. (6.17)). In the case of 1:1 electrolytes of comparable α, Eq. (6.16) predicts that the lower the dissociation constant K_{eq} for an electrolyte, the lower is the value of c_{max}.

Li et al. (2010) studied the concentration dependence of specific conductivity σ of aqueous solutions of [C_6mim][Br] and [C_8mim][Br] at three temperatures (293.15, 298.15 and 303.15 K) in a wide range of molal concentrations m up to about 140 and 200 mol·kg^{-1}. Figure 6.8 illustrates, as an example, plots of σ of aqueous [C_6mim][Br] solutions on m at the three temperatures. As observed in other electrolyte systems, a steep increase in σ appears in a narrow molality range up to 3 mol·kg^{-1}. Then σ rapidly decreases with an increase in m up to about 50 mol·kg^{-1} beyond which there is an insignificant decrease in σ with increasing m. The maximum conductivity σ_{max} occurs for m_{max} lying between 3 and 4.6 mol·kg^{-1}, and, as with other systems, the value of σ_{max} increases with an increase in temperature T.

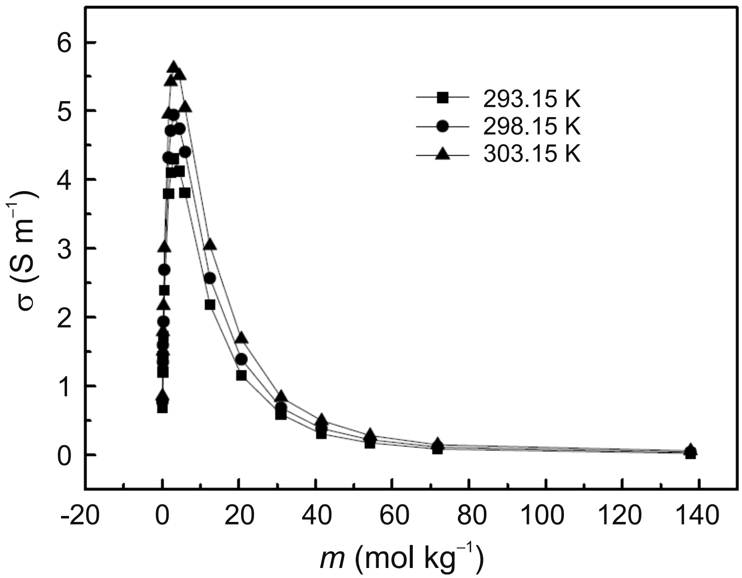

Figure 6.8. Plots of specific conductivity σ of [C$_6$mim][Br]) in water–IL mixture on IL molal concentration *m* at three temperatures. After Li et al. (2010).

In order to explain the above observations, Li et al. (2010) argued that nanodomains (i.e. aggregates) composed of anions and cations are formed in liquid [C$_n$mim][Cl], [C$_n$mim][BF$_4$], [C$_n$mim][PF$_6$] and [C$_n$mim][NTf$_3$] ionic liquids. In these nanodomains the anion and imidazolium ring are subjected to strong long-range interactions, thereby organizing in 3D ionic network whereas alkyl tails interacting mainly through weak short-range interactions tend to segregate into nonpolar domains that are imbedded into the charged ionic network. Therefore, the nanodomains of 3D ionic networks of anions and cations held together by hydrogen bonds may be considered to construct the ionic networks of [C$_n$mim][Cl]-like ionic liquids. Thus, the electrical conductivity of aqueous solutions of [C$_n$mim][Cl]-like ILs is determined by: (1) the compactness of these nonpolar nanodomains held together by hydrogen bonds, and (2) the number and mobility of charge carriers.

According to the above concept, at low concentration addition of IL to water results in rapid disruption of hydrogen-bonded water network whereby not only the structure of solvent water is changed but also the concentration of charge carriers increases with the concentration of the electrolyte (Li et al., 2010). These processes involve a decrease in the energy of formation of holes in the solvent water as well as in the energy barrier involved in the dissociation of the IL aggregates of different dimensions held together by weak short-range interactions between them. With an increase in the IL concentration in the solution, it is expected that the size of the aggregates increases and their mobility decreases due to decreasing diffusion coefficient *D* of these aggregates given by the Stokes–Einstein relation (Bockris and Reddy, 1970; Robinson and Stokes, 1959)

$$D = \frac{k_B T}{6\pi\eta r}, \tag{6.30}$$

where η is the viscosity of the solution at temperature T, k_B is the Boltzmann constant, and r is the radius of the moving aggregate considered to be spherical. Consequently, both increasing dynamic viscosity η solvent and the average size r of the charged aggregates at a particular temperature T lead to a reduction in the mobility. However, at very high IL concentration the conductivity is mainly determined by the disruption of the hydrogen-bonded network structure of water.

6.6.1.2. Other interpretations of concentration dependence of specific conductivity of solutions

Figure 6.9 shows the measured specific conductivity σ of aqueous AlI_3, $AlBr_3$, $AlCl_3$, and $Al(NO_3)_3$ solutions at 298.15 K as functions of their equivalent molar concentration c in the concentration range up to their saturations. Note that here the equivalent molar concentration c is equal to the molar concentration of a salt divided by 3. Following Vila et al. (2005), the above data are described below.

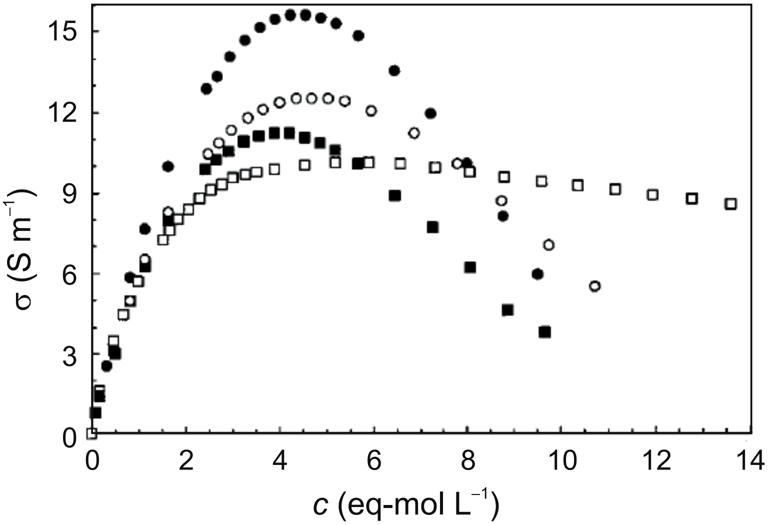

Figure 6.9. Specific conductivity σ of aqueous solutions of some aluminium salts at 298.15 K as functions of their equivalent molar concentration c; (●) AlI_3, (○) $AlBr_3$, (■) $AlCl_3$, and (□) $Al(NO_3)_3$. After Vila et al. (2005).

From Figure 6.9 it may be seen that the peaks in the plots of AlI_3, $AlBr_3$ and $AlCl_3$ solutions appear at the same $c \approx 4.5$ eq-mol·L^{-1}, but it is present at somewhat higher $c \approx 6$ eq-mol·L^{-1} for $Al(NO_3)_3$ solution. The initial increase in σ with concentration is insignificantly changed by the anion size due to their low hydration but, except in the case of $Al(NO_3)_3$ with the biggest anion, the value of σ_{max} increases with the size r_i of bare halide anions. This trend is in contradiction with the predictions of the Stokes formula where the ionic conductivity $\lambda \propto r_i$ (see Eq. (6.30)). This behavior of the halide ions is due to the difference in the electronegativity of these ions, which decreases in the sequence: Cl^-, Br^- and I^-. Consequently, chloride ions are more hydrated and have lower mobility than bromide and iodide ions.

As seen from Figure 6.9, in the vicinity of their saturated solutions, the value of σ of the nitrate is the highest but that of the above halides appears to be reversed in contrast to the trend corresponding to their maximum value of σ_{max}. This behavior is due to the dominant influence of interionic interactions at these high concentrations, where the mobility of the conducting species (ions) is significantly reduced. Under these conditions of high solute concentrations, due to their large size hydrated iodide ions are less mobile than hydrated bromide or chloride ions. The unusual behavior of the nitrate ions in comparison with that of halide ions at saturation may also be attributed to the hydrolysis of the salts. Aluminium halides violently react with water but the nitrate does not react. Consequently, the concentration of free ions in the aluminium nitrate solution is higher than that that in the halide solution.

Bešter-Rogač (2008) studied the dependence of specific conductivity σ of aqueous solutions of seven bivalent sulfates ($CoSO_4$, $CuSO_4$, $NiSO_4$, $MgSO_4$, $MnSO_4$, $CdSO_4$, and $ZnSO_4$) as a function their concentration m between 0.005 and 2.5 $mol{\cdot}kg^{-1}$ at temperatures between 278.15 and 308.15 K, and reported a behavior somewhat similar to that described above. This author observed the appearance of maxima in the $\sigma(m)$ plots at $m_{max} = (1.9\pm0.2)$ $mol{\cdot}kg^{-1}$ with maximum values σ_{max} of conductivity lying between (5.5 ± 0.5) $S{\cdot}m^{-1}$ at 298.15 K, and analyzed the data using Casteel–Amis equation (6.26), but both these parameters were observed to increase with temperature. The relationship between σ_{max} and c_{max} (or m_{max}) obtained at different temperatures is described later in Section 6.6.1.4.

Despite its great success in analyzing the concentration dependence of the specific conductance σ of different systems, the main disadvantage of the Casteel–Amis equation is that it contains empirical parameters. Moreover, since it is an empirical equation, in the literature simple polynomials (Gilliam et al., 2007) as well as semi-theoretical equations (Apelblat, 2017; Varela et al., 2010) have also been proposed.

To describe the specific conductivities σ of aqueous potassium hydroxide solutions in a wide concentration range up to 12 $mol{\cdot}L^{-1}$ and temperature between 0 and 100 °C, Gilliam et al. (2007) used the empirical relation

$$\sigma(c,T) = A(c) + B(c^2) + C(c \cdot T) + D(c/T) + E(c^3) + F(c^2 \cdot T^2)\,, \tag{6.31}$$

where A to F are fitting parameters and T is the temperature in Kelvin. Obviously, this relation represents a simple third-order polynomial for $\sigma(c)$ at constant T, i.e.

$$\sigma(c) = A_1(c) + B_1(c^2) + C_1(c^3)\,, \tag{6.32}$$

with A_1 to C_1 as constants and $\sigma(c) = 0$ when $c = 0$. However, it simplifies to the following temperature dependence at constant c:

$$\sigma(T) = A_2 + \frac{B_2}{T} + C_2 T + D_2 T^2 , \tag{6.33}$$

where A_2 to D_2 are new fitting parameters. In the case when the term $(A_2 + B_2/T)$ remains constant in the temperature range of measurements, Eq. (6.33) reduces to the form of a third-order polynomial, which may behave as a linear dependence in a narrow temperature interval. One may attempt to trace the theoretical basis of Eqs. (6.32) and (6.33) from conductivity equation (6.64) and equations of temperature dependence of molar conductivity (see Section 6.7.5).

Using the VFT equation, Eq. (6.41), and assuming that the constants A and B are independent of electrolyte composition and the glass-transition temperature T_0 depends on concentration, expressed in mass fraction w, following a binomial equation, Apelblat (2017) derived the relation

$$\sigma(w,T) = A_3 w \exp(B_3 w + C_3 w^2) , \tag{6.34}$$

where A_3 to C_3 are adjustable parameters, which can be obtained by employing its logarithmic form. According to this equation, the maximum conductivity σ_{max} occurs at the maximum mass fraction w_{max} given by

$$w_{\mathrm{max}}(T) = -\frac{B_3 + (B_3^2 + 8C_3)^{1/2}}{4C_3} . \tag{6.35}$$

Note that Eq. (6.34) contains three fitting parameters instead of four parameters in the Casteel–Amis equation. This author applied the above approach to describe the concentration dependence of conductivity σ of aqueous solutions of some 1:2 electrolytes.

Varela et al. (2010) reported a statistical mechanical framework for charge transport in solvent–IL mixtures based on the assumption of the existence of a statistical lattice structure (pseudolattice) throughout the whole range of the IL concentation. Ionic motion is assumed to occur through jumps between cells of two different types separated by different energy barriers of different heights. Assuming non-correlated ion transport, it was shown that the electrical conductivity has a maximum, resulting from transition from low-concentration region of high-mobility cells to the high-concentration region where low-mobility cells become dominant.

In the framework of the charge transport, taking ϕ_1 and ϕ_2 as volume fractions of species in a solution composed of cells of 1 and 2 types, respectively, Varela et al. (2010) derived the relation

$$\sigma = \frac{e^2 a^2}{V_2 k_{\mathrm{B}} T} [\phi_2^2 p_2 + (1 - \phi_2)\phi_2 p_1] . \tag{6.36}$$

where a is the lattice constant, e is the ionic charge, V_2 is the ionic volume in cells of the 2 type, and p_1 and p_2 are the net probabilities that an ion jumps barriers in the direction of the applied electric field in cells of 1 and 2 types, respectively, per unit time. Using the defintion of current density and taking the same ionic volumes for both types of cells, Eq. (6.36) may be written as

$$\sigma = (1-\phi_2)\phi_2\sigma_1 + \phi_2^2\sigma_2 \,. \tag{6.37}$$

where σ_1 and σ_2 are the specific conductivities of solvent and IL, respectively. As expected from the assumptions used in the derivation of this equation, the experimental conductivity of IL–solvent mixtures usually deviates significantly from its predictions at low as well as high IL concentrations (Vraneš et al., 2015).

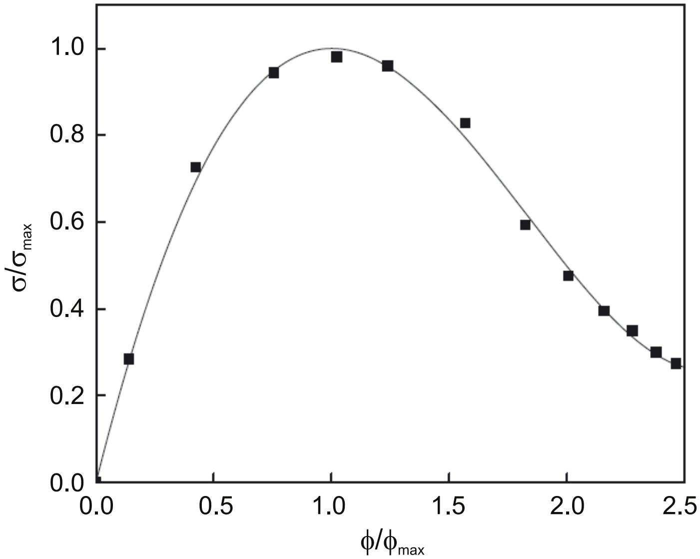

Figure 6.10. Dependence of normalized conductivity σ/σ_{max} of [bmpyr][NTf$_2$]–GBL mixture at 298.15 K on scaled ϕ_1/ϕ_{max}. Line represents the fit according to Eq. (6.38). From Vraneš et al. (2015).

Asuming that p_1 and p_2 in Eq. (6.36) are independent of IL concentration, the authors also gave explicit equations of the concentration ϕ_{max} of the maximum conductivity σ_{max} as well as a universal equation relating scaled or normalized conductivity σ/σ_{max} with normalized ionic concentration $\xi_2 = \phi_2/\phi_{max}$ of the IL in the form (Varela et al., 2010)

$$\frac{\sigma}{\sigma_{max}} = 2\xi_2\left(1-\frac{\xi_2}{2}\right). \tag{6.38}$$

This equation predicts a symmetrical curve with $\sigma/\sigma_{max} = 1$ appearing at $\xi_2 = 1$ (i.e. $\phi_{max} = 0.5$). Varela et al. (2010) examined the experimental conductivity data for some IL–water and IL–ethanol mixtures according to the above equation and observed deviation from it, especially at high IL concentrations. The authors attributed these deviations to ion–ion and ion–solvent interactions, and noted that the deviation from $\phi_1/\phi_{\max} = 2$ is equal to ($\exp\beta\varepsilon$–1), with ε as the dielectric constant of the mixture and β as a constant.

Eq. (6.38) has been employed to describe variations of normalized conductivity $\sigma/\sigma_{\max}$ of mixtures of [bmpyr][NTf$_2$] and [bmim][DCA] with GBL solvent at 298.15 K with scaled $\phi_2/\phi_{\max}$, where ϕ_2 is the IL volume fraction (Vraneš et al., 2015; Zec et al., 2016), and observed that this theoretical equation satisfactorily represents the data in the entire concentration range. Figure 6.10 presents an example of such dependence for [bmpyr][NTf$_2$]–GBL mixture where the line represents the fit according to Eq. (6.38).

6.6.1.3. Relationship between specific conductivity and solute concentration in dilute solutions

In order to analyze the relationship between specific conductivity and solute concentration in dilute solutions it is convenient to use Eq. (6.28) expressed in the logarithmic form

$$\ln\sigma = \left\{(\ln\sigma_{\max} - a_1\ln c_{\max}) + \left[b_1(c-c_{\max})^2 - a_1\left(\frac{c-c_{\max}}{c_{\max}}\right)\right]\right\} + a_1\ln c\,, \tag{6.39}$$

for a particular system of constant $\sigma_{\max}$ and $c_{\max}$, one expects a linear dependence of $\ln\sigma$ on $\ln c$ in a narrow range of c, when the term in the square brackets is much lower than 1, with intercept S equal to $\ln\sigma_0 = (\ln\sigma_{\max} - a_1\ln c_{\max})$ and slope a_1. When the concentration c is taken in mole fraction, the term $(\ln\sigma_{\max} - a_1\ln c_{\max}) > \ln\sigma_{\max}$, and $\sigma_0 > \sigma_{\max}$.

Figure 6.11 compares the solute concentration dependence of specific conductivity σ of NH_4NO_3 and KI in DMSO solvent for two temperatures 293.15 and 323.15 K reported by Świergiel et al. (2013) and Płowaś et al. (2014), respectively, and that of six low-temperature ILs in water at 298.15 K reported by Vila et al. (2006a) in the form of plots of $\ln\sigma$ against $\ln x$ according to Eq. (6.39). As expected from Eq. (6.39), $\ln\sigma$ increases linearly with $\ln x$ in the range of low x. Linear plots show best-fit of the data for KI below $\ln x = -4.5$ ($x = 0.01$ mole fraction) in Figure 6.11a and for ILs below $\ln x = -1.6$ ($x = 0.2$ weight fraction) in Figure 6.11b, with values of the intercept S and slope a_1 of the plots listed in Table 6.3. The calculated values of the extrapolated value of σ_0 from the intercepts $S = \ln\sigma_0$ of the plots when $\ln c \to 0$, and the values of $\sigma_{\max}$ for the KI–DMSO system, taken to be equal to that for the NH_4NO_3–DMSO system reported by Świergiel et al. (2013) and that for the ILs from Vila et al. (2006a) are also given in the table.

It may be seen from Figure 6.11a that the concentration dependence of the conductivities of the two electrolytes KI and NH_4NO_3 in dilute DMSO solutions of $\ln x$ below about –4.5 (i.e. $x \approx 0.01$ mole fraction) is practically independent of the nature of the solute and the solution temperature. This behavior of these two electrolytes is associated with the fact that being 1:1 electrolytes both are dissociated equally in this concentration range and probably their solvated ions have the same mobility u (see Eq. (6.2)). In contrast to the above electrolytes, although aqueous IL solutions also follow linear relationship between $\ln\sigma$ and $\ln x$ at low x, their intercepts S and slopes a_1 have completely different values (see Table 6.3).

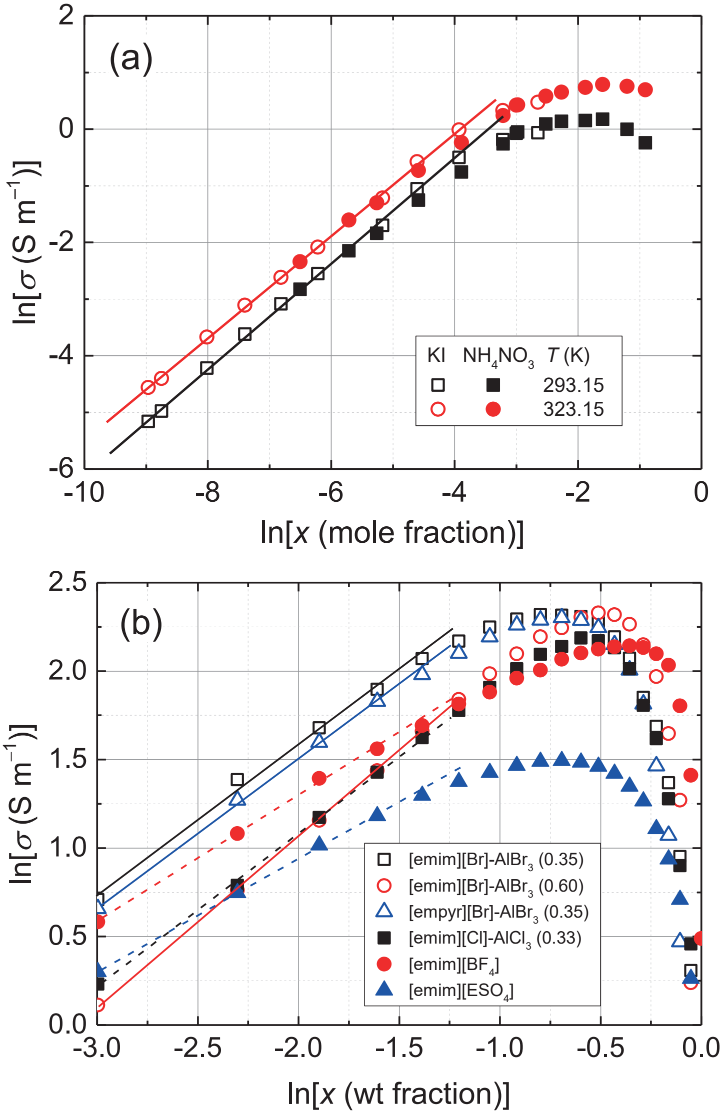

Figure 6.11. Dependence of specific conductivity σ of: (a) KI and NH_4NO_3 in DMSO at 293.15 and 323.15 K, and (b) six low-temperature ILs in water at 298.15 K on their concentration x shown as plots of $\ln\sigma$ against $\ln x$. Filled and open points refer to data. Data in (a) for NH_4NO_3 from Płowaś et al. (2014) and for KI from Świergiel et al. (2013), and (b) for ILs from Vila et al. (2006a).

Table 6.3. Values of intercept *S* and slope a_1 for KI–DMSO and aqueous ILs solutions

Solute	Solvent	*T* (K)	*S*	a_1	R^2	$\sigma_{\max}$ ($S \cdot m^{-1}$)	σ_0 ($S \cdot m^{-1}$)	Data*
KI	DMSO	293.15	3.202	0.930	0.9985	1.2	24.6	a
NH_4NO_3	DMSO	323.15	3.527	0.902	0.9989	2.1	34.0	a
[emim][Br]-$AlBr_3$ ($x_a = 0.35$)	H_2O	298.15	3.307	0.858	0.9913	10.16	27.3	b
[emim][Br]-$AlBr_3$ ($x_a = 0.60$)	H_2O	298.15	2.969	0.955	0.9907	10.27	19.5	b
[empyr][Br]-$AlBr_3$ ($x_a = 0.35$)	H_2O	298.15	3.198	0.845	0.9990	9.99	24.5	b
[emim][Cl]-$AlCl_3$ ($x_a = 0.33$)	H_2O	298.15	2.809	0.865	0.9979	8.90	16.6	b
[emim][BF_4]	H_2O	298.15	2.728	0.715	0.9978	8.52	15.3	b
[emim][ESO_4]	H_2O	298.15	2.220	0.640	0.9994	4.45	9.2	b

* Original data from: [a] Płowaś et al. (2014), [b] Vila et al. (2006a).

It may be noted from Table 6.3 that, at the lowest IL concentration $x = 0.05$ wt fraction investigated in the study, the conductivity σ decreases in the sequence: [emim][Br]-$AlBr_3$ ($x_a = 0.35$), [empyr][Br]-$AlBr_3$ ($x_a = 0.35$), [emim][BF_4], [emim][ESO_4], [emim][Cl]-$AlCl_3$ ($x_a = 0.33$), and [emim][Br]-$AlBr_3$ ($x_a = 0.60$). Mixing of x_a of 0.33 and 0.35 mole fraction of $AlCl_3$ and $AlBr_3$ with [emim][Cl], [emim][Br] and [empyr][Br] ensures stoichiometric composition of [emim][$AlCl_4$], [emim][$AlBr_4$] and [empyr][$AlBr_4$] ionic liquids whereas the commercial [emim][BF_4] and [emim][ESO_4] are stoichiometric in their composition. Therefore, the initial conductivity of these ILs may be attributed to the nature of the mobilities of dissociated cations and anions parti-cipating in electrical conduction. Similarly, in comparison with [emim][Br]-$AlBr_3$ ($x_a = 0.35$), [emim][Br]-$AlBr_3$ ($x_a = 0.60$) shows low conductivity σ because the dissociation of this nonstoichiometric IL in water does not ensure high concentration of $[emim]^+$ cations and $[AlBr_4]^-$. The comparable value, lying between 0.845 and 0.865, of the slope a_1 of the plots of $\ln\sigma$ against $\ln x$ of [emim][Br]-$AlBr_3$ ($x_a = 0.35$), [emim][Cl]-$AlCl_3$ ($x_a = 0.33$), and [empyr][Br]-$AlBr_3$ ($x_a = 0.35$) may also be attributed to the stoichometric composition of these ionic liquids.

The conductivity σ of KI–DMSO system is much lower than that of aqueous IL solutions. The maximum conductivity $\sigma_{\max}$ of KI–DMSO system is about one-tenth of that of aqueous IL solutions. Similarly, the ratio ($\sigma_0/\sigma_{\max}$) is about 20 for KI–DMSO system and between 2 and 2.7 for aqueous IL solutions. These observations are associated with the difference in the degree of dissociation of KI in DMSO and ILs in water. DMSO has a lower dielectric constant ε ($\varepsilon = 47$ at 293.15 K) and a higher viscosity η than water which has $\varepsilon = 80$ at 293.15 K and a lower η.

6.6.1.4. Relationship between maximum conductivity σ_{max} and corresponding concentration x_{max}, and the curvature of $\sigma(x)$ plots beyond x_{max}

As mentioned above, values of the maximum conductivity $\sigma_{\max}$ and the corresponding concentration $x_{\max}$ for different electrolyte systems obtained at different temperatures are mutually related. Figure 6.12 shows the relationship between maximum conductivity $\sigma_{\max}$ and the corresponding concentration $x_{\max}$ for NH_4NO_3–DMSO, [bmpyr][NTf$_2$]–GBL and [bmim][NTf$_2$]–GBL systems. One observes that $\sigma_{\max}$ increases practically linearly with $x_{\max}$ for different systems. Linear dependence of $\sigma_{\max}$ on the corresponding $x_{\max}$ have also been reported in other systems such as aqueous solutions of various bivalent metal sulfate solutions (Bešter-Rogač, 2008). These sulfates are strongly hydrated salts and exhibit similar properties in dilute aqueous solution, but they mainly differ in their solubility in water. This difference in the solubility is likely to affect their ability to form ion pairs and higher aggregates in concentrated solutions.

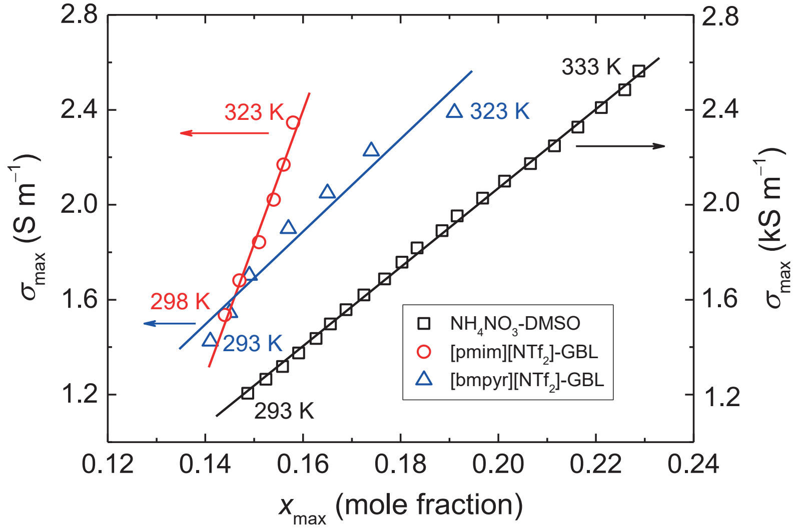

Figure 6.12. Relationship between maximum conductivity $\sigma_{\max}$ and the corresponding concentration $x_{\max}$ of NH_4NO_3–DMSO, [bmim][NTf$_2$]–GBL and [bmim][NTf$_2$]–GBL systems. Data for NH_4NO_3–DMSO system from Świergiel et al. (2013), for [bmim][NTf$_2$]–GBL from Vraneš et al. (2014), and for [bmpyr][NTf$_2$]–GBL from Vraneš et al. (2015).

It has been found (Barthel et al., 1994) that $\sigma_{\max}$ and $x_{\max}$ are linearly related for solutions where ion-pair association is small. This suggests an energy barrier to the conductivity of an electrolyte, which depend on the solvent properties such as their viscosity η. At the concentration $x_{\max}$ the electrolyte has an activation barrier of transport, which indicates the energy height of the barrier.

The linear dependence between $\sigma_{\max}$ and $x_{\max}$ may be described by the relation

$$\sigma_{\max} = \sigma^0_{\max} + \Lambda_0 x_{\max} , \tag{6.40}$$

where $\sigma_{\max}{}^0$ and Λ_0 are empirical constants characteristic of a system and $\sigma_{\max}{}^0$ corresponds to the value of $\sigma_{\max}$ when $x_{\max} = 0$. If one defines $\Lambda_{\max}$ as the molar conductivity corresponding to $\sigma_{\max}$, the linear dependence follows from Eq. (6.6), with $\Lambda_{max} = \Lambda_0+\sigma_{max}{}^0/x_{max}$. This suggests that Λ_0 and $\sigma_{max}{}^0/x_{max}$ are mutually related.

A general feature of the $\sigma(x)$ plots for different system described above is that the values of σ_{max} of aqueous ionic salt solutions (Figure 6.4) is about two and three times higher than those of aqueous solutions of low-temperature ILs [emim][$AlCl_4$] and [C_6mim][Br], respectively (see Figures 6.7 and 6.8). These differences are associated with the mobility of dissociated ions of these electrolytes, which is intimately connected with the chemical constitution of the cations and anions composing them. For example, bulkier [C_6mim]$^+$ cations have lower contribution to conductivity than lighter [emim]$^+$ cations.

It is a general tendency of the $\sigma(x)$ plots of the low-temperature ILs that their curvature in the x region beyond x_{max} reduces with increasing temperature (Li et al., 2010; Vraneš et al., 2014, 2015); see Figures 6.6 and 6.8. Pronounced curvatures in the $\sigma(x)$ plots have been reported for [bmpyr][NTf_2]–GBL (Vraneš et al., 2015), and [C_6mim][Br]–H_2O and [C_8mim][Br]–H_2O systems (Li et al., 2010). However, in the case of the [bmim][NTf_2]–GBL system (Vraneš et al., 2014), the nature of the $\sigma(x)$ plot at the highest temperature of 323.15 K does not differ substantially from that of the plots of aqueous sodium thiocyanate solutions of different temperatures shown in Figure 6.4. Once again one finds that higher curvatures in the $\sigma(x)$ plots appear in systems, such as [C_6mim][Br]–H_2O and [C_8mim][Br]–H_2O, containing relatively bulky [C_6mim]$^+$ and [C_8mim]$^+$ cations (see Figure 6.8). While Li et al. (2010) explained the trend of decreasing σ with increasing IL concentration in the solution in the $\sigma(x)$ plots in these systems from consideration of an increase in the size of the aggregates and a decrease in their mobility, Vraneš et al. (2015) suggested that the $\sigma(x)$ plots are composed of two linear parts: (1) an initial linear decrease in σ up to a certain concentration x^*, and (2) in the region beyond x^*, a relatively slow linear decrease in σ due to the formation of increasing concentration of [bmim]$^+$ and [bmpyr]$^+$ micellar structures with increasing x. This process involves an increase in ion–ion interactions with increasing x, which results in a reduction in the mobility of charge carriers and hence the conductivity of the solution.

6.6.2. Temperature dependence of specific conductivity of electrolytes

The specific conductivity σ of electrolytes increases with an increase in temperature as a consequence of the mobility u_1 and u_2 of the ions in the solution (cf. Eq. (6.2)). This effect is associated with a reduction in the viscous drag of the ions due to suppression of interionic interactions.

6.6.2.1. Basic equations and concepts

The specific conductivity σ of different systems on temperature T shows an exponential dependence. According to the hole theory of transport in molten salts, this exponential dependence is usually described by an Arrhenius-type relation (Bockris and Reddy, 1970):

$$\sigma = \sigma_\infty \exp\left(- \frac{E_A}{R_G T} \right), \tag{6.41}$$

where σ_∞ is the value of maximum conductivity at infinite T, R_G is the gas constant, and E_A is the so-called Arrhenius activation energy for ionic conductivity, which is the energy required for an ion to jump into a hole in the liquid. This relation predicts a linear dependence of $\ln\sigma$ on T^{-1} with intercept $\ln\sigma_\infty$ and slope E_A/R_G in the entire range of temperature. However, it is frequently observed that the plots of $\ln\sigma$ against T^{-1} reveal steadily increasing value of the slope with an increase in T^{-1}. This deviation in the behavior of the $\sigma(T)$ data from the Arrhenius-type relation is explained by the Vogel–Tamman–Fulcher (VTF) relation written in the form (cf. Angell, 1966, 1991, 1995; Angell and Bressel, 1972)

$$\sigma = A \exp\left(- \frac{B}{T - T_0} \right), \tag{6.42}$$

where A, B and T_0 are parameters of the VTF relation. When $T_0 = 0$, $A = \sigma_\infty$ and $B = E_A/R_G$. Then this equation takes the form of Eq. (6.41). All of the parameters σ_∞, E_A, and T_0 are electrolyte-concentration dependent, and T_0 is the so-called ideal glass transition or Vogel temperature.

From a consideration of the sensitivity of the liquid structure to temperature changes, Angell (1991, 1995) classified liquids into *strong* and *fragile* liquids. According to this classification, strong liquids are characterized by strong directional (covalent) bonds and have a built-in resistance to structural changes with temperature changes. Fragile liquids, on the other hand, are characterized by simple nondirectional Coulomb interactions or weak van der Waals interactions in substances with many π electrons (usually aromatic substances), and form glassy-state structure that easily collapses with little provocation from thermal excitation. Strong liquids follow Arrhenius relation (6.41), but fragile liquids show strongly non-Arrhenius manner and follow Eq. (6.42). This means that the observation of a glass-transition temperature T_0 is a characteristic feature of fragile liquids and the parameter B provides a connection between the glass-transition theory and the hole theory of ionic liquids.

According to the concepts of the glass-transition theory, ideal glass transition temperature T_0 is the temperature when the movement of liquid constituents is totally frozen. This temperature T_0 is lower than the scaled glass temperature T_g when the liquid viscosity η_g is 10^{13} P (with P for Poise; 1 P = 0.1 Pa·s). The temperatures T_g and T_0 are related to the B parameter of Eq. (6.42) as

$$\frac{T_g}{T_0} = 1 + \frac{\Psi}{\ln(\eta_g/\eta_0)}, \tag{6.43}$$

where $\ln(\eta_g/\eta_0) \approx 39$ with the lowest viscosity η_0 equal to 10^{-2} P, and a new parameter $\Psi = B/T_0$. The temperature ratio T_g/T_0 has values between 0 and 1 when the new parameter Ψ is equal to ∞ and 1, respectively. Therefore, the ratio T_g/T_0 may be considered as a measure of fragility of a system. $\Psi = \infty$ represents a system (i.e. strong liquid) following Arrhenius relation (6.41) whereas $\Psi = 1$ represents a maximum fragile system. Obviously, an increasing value of Ψ indicates decreasing fragility of system(s).

Some typical examples presenting the general behavior of temperature dependence of conductivity of solutions of common electrolytes and low-temperature ILs in solvents and of some neat ILs are presented below. Since in most cases VTF equation is followed satisfactorily, the concentration dependence of the preexponential factor A and the fragility parameter Ψ of the systems considered here are also described and discussed.

6.6.2.2. Experimental results and their interpretation

Figure 6.13 illustrates the specific conductivity σ of aqueous $Ca(NO_3)_2$ and $Mg(NO_3)_2$ solutions on salt concentrations x in the form of plots of $\ln\sigma$ against T^{-1} according to Arrhenius relation (6.41). It may be seen that the temperature dependence of conductivity of these systems is not described by the Arrhenius equation in the entire investigated temperature interval. The Arrhenius coefficients σ_∞ and E_A of Eq. (6.41) may be calculated from these plots only in a narrow temperature range where a linear dependence may be observed. However, these coefficients increase rapidly with decreasing temperature such that they exhibit similar trends for different solutions at low temperatures.

The above behavior of temperature dependence of conductivity is usually encountered in aqueous solutions of salts of polyvalent cations of sufficiently high concentrations, which can be cooled down to low temperatures when they lose their liquid character and become glassy at temperature T_0 without crystallization of the salt. In contrast to aqueous solutions of polyvalent-cationic salts, concentrated solutions of most univalent salts usually crystallize without showing the glassy behavior regardless of the initial salt concentration, implying that the glass-transition temperature of these solutions lies below the room temperature (Angell, 1966). This general inference is indeed corroborated from the study of the electrical conductivity of aqueous and methanolic sodium thiocyanate solutions (Rohman et al., 2001), as mentioned below.

Figure 6.14 shows the above data of aqueous $Ca(NO_3)_2$ and $Mg(NO_3)_2$ solutions of various concentrations x, expressed in mole fraction, in the form of plots of $\ln\sigma$ against $(T-T_0)^{-1}$ with appropriately chosen T_0 to obtain linear dependence according to VTF relation (6.42). The values of T_0 chosen to draw the plots are from Angell (1966) and are given in the inset. It may be seen that the value of T_0 increases with the salt concentration x.

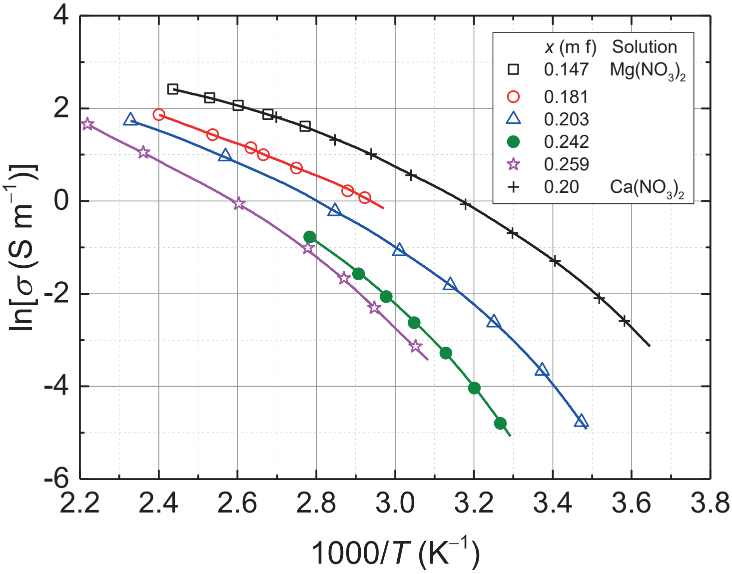

Figure 6.13. Dependence of specific conductivity σ of aqueous $Ca(NO_3)_2$ and $Mg(NO_3)_2$ solutions of various concentrations x according to Arrhenius relation (6.41). Original data from Angell (1966).

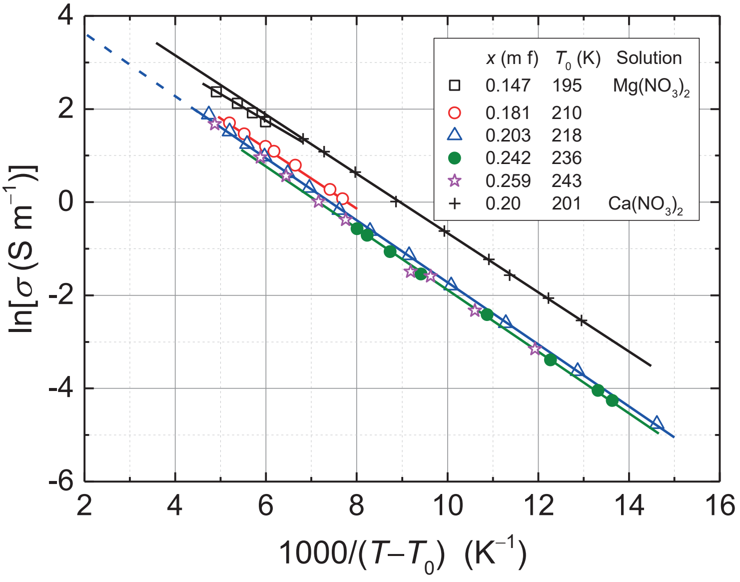

Figure 6.14. Dependence of specific conductivity σ of aqueous $Ca(NO_3)_2$ and $Mg(NO_3)_2$ solutions of various concentrations x according to VTF relation (6.42). Original data from Angell (1966).

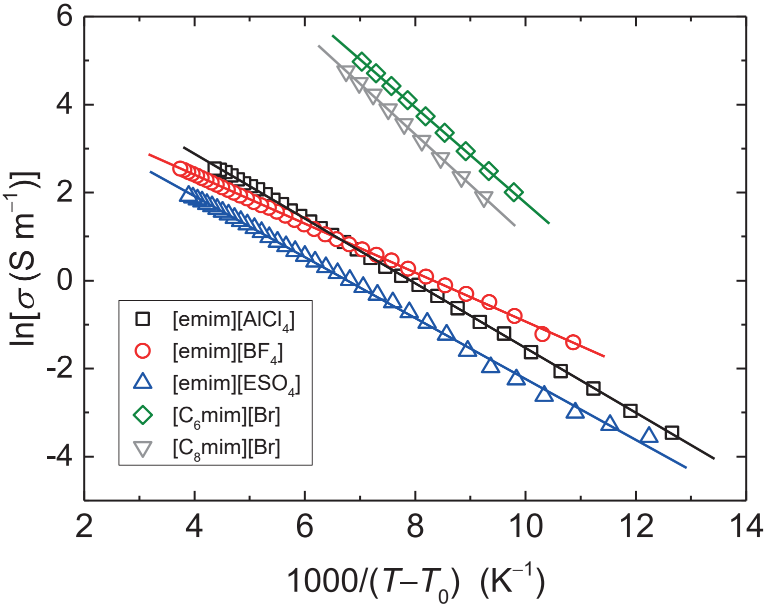

Figure 6.15. Dependence of specific conductivity σ of some low-temperature ionic liquids: (□) [emim][AlCl$_4$], (○) [emim][BF$_4$], (Δ) [emim][ESO$_4$], (◊) [C$_6$mim][Br], and (∇) [C$_8$mim][Br] according to VTF relation (6.42), with parameters listed in Table 6.4. Data of first three ILs from Vila et al. (2006b), and last two from Li et al. (2010).

Neat low-temperature ILs also follow VTF relation (6.42). Figure 6.15 shows, as an example, plots of lnσ against $(T–T_0)^{-1}$ for five ILs with appropriately chosen T_0 to obtain linear dependence according to VTF. The parameters of the plots are given in Table 6.4. From the values of B and T_0 the calculated values of the fragility parameter Ψ for these ILs are also listed in the table. These values of Ψ indicate that they are fairly fragile and [AlCl$_4$]$^-$ anion of the common [emim]$^+$ cation renders them less fragile, and that the fragility of [Br]$^-$-containing ILs decreases with increasing number n of CH$_2$– group.

The parameters A, T_0 and B of the VTF relation for different systems strongly depend on the electrolyte concentration in the solution, but the concentration dependence of these three parameters show different trends for different systems. For example, for aqueous and methanolic sodium thiocyanate solutions, the value of T_0 increases and that of B decreases with increasing electrolyte concentration m, whereas the preexponential shows an initial increase to a maximum value and then decreases with increasing m (Rohman et al., 2001). The concentration dependence of T_0 and B for other systems also shows similar trends. Examples are NH$_4$NO$_3$–DMSO solutions (Świergiel et al., 2013), and [bmim][NTf$_2$]–GBL and [bmpyr][NTf$_2$]–GBL solutions (Vraneš et al., 2014, 2015). Using the values of these VTF parameters the concentration dependence of the fragility parameter Ψ for these chemically different systems may be examined.

Table 6.4. Constants of VTF relations for selected ILs

IL	T_0 (K)	ln[A (S·m^{-1})]	A (S·m^{-1})	B (K)	Ψ (–)	R^2	Data*
[emim][AlCl$_4$]	174.1	5.826	3.38·10^2	736	4.23	0.9998	a
[emim][BF$_4$]	166.1	4.614	1.01·10^2	555	3.34	0.9993	a
[emim][ESO$_4$]	176.4	4.692	1.08·10^2	693	3.92	0.9979	a
[C$_6$mim][Br]	191.0	12.618	3.02·10^5	1084	5.68	0.9999	b
[C$_8$mim][Br]	185.0	12.550	2.82·10^5	1153	6.23	0.9998	b

[a] Vila et al. (2006b), [b] Li et al. (2010).

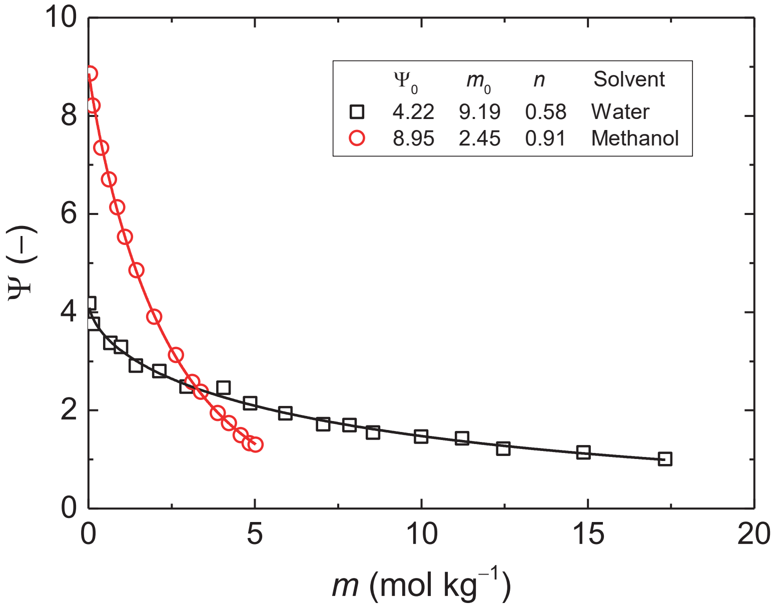

Figure 6.16. Dependence of dimensionless fragility parameter Ψ of aqueous and methanolic sodium thiocyanate solutions on their concentration m. Plots are drawn according to Eq. (6.44). Original data from Rohman et al. (2001).

Figure 6.16 shows the dependence of dimensionless fragility parameter Ψ of aqueous and methanolic sodium thiocyanate solutions on their concentration m. The values of Ψ were calculated from the values of T_0 and B for solutions of difference concentrations m reported by Rohman et al. (2001). It may be seen that the Ψ parameter decreases exponentially with increasing m following the empirical relation

$$\Psi = \Psi_0 \exp\left[-\left(\frac{m}{m_0}\right)^n\right], \tag{6.44}$$

where Ψ_0 is the maximum value of the fragility parameter Ψ at infinite dilution (i.e. when $m \to 0$) and m_0 and n are empirical fitting parameters. The values of these parameters for the two types of solutions are listed in the inset of Figure 6.16. Note that low solubility of the salt in a solvent is characterized by high values of Ψ_0 and n, and that the exponent n is a measure of reduction in the fragility of a system with increasing electrolyte concentration. The higher the value of the exponent n, the higher is the reduction in fragility parameter Ψ with electrolyte concentration m in the solution.

From Figure 6.16 one may conclude that: (1) an electrolyte solution becomes more fragile with an increase in the solute concentration m and approaches the maximum fragility of unity in the vicinity of saturation of a solution, and (2) the lowest fragility of an electrolyte solution is directly related to the solubility of the solute in a solution and the higher the solubility of the solute in a solvent, the lower is the fragility. This behavior of the fragility parameter Ψ of aqueous and methanolic sodium thiocyanate solutions on their concentration m is associated with the competition between solvent–solvent and solute–solvent interactions, where the latter interactions replace the former at the highest m.

Figure 6.17 shows the dependence of dimensionless fragility parameter Ψ of NH_4NO_3–DMSO, [bmim][NTf_2]–GBL and [bmpyr][NTf_2]–GBL solutions on electrolyte concentration x. The data of T_0 and B used to calculate Ψ of NH_4NO_3–DMSO system are taken from Świergiel et al. (2013), whereas those for [bmim][NTf_2]–GBL and [bmpyr][NTf_2]–GBL systems are taken from Vraneš et al. (2014, 2015). In the figure the values of Ψ equal to 11 and 16 for $x = 0$ and 0.0015 mole fraction, respectively, of NH_4NO_3–DMSO system are not shown.

It may be observed from Figure 6.17 that, if the values of Ψ for $x < 0.0205$ mole fraction in the case of the NH_4NO_3–DMSO system are considered erratic in view of a sudden decrease in Ψ from its highest value Ψ_0, lying between 11 and 16 for the neat solvent, down to the lowest value of about 0.3 at $x = 0.005$ mole fraction, the value of Ψ initially increases approaching a maximum value of about 2.8 at $x_{\max} = 0.18$ mole fraction and then slowly decreases attaining ultimately a value of about 1 at $x = 0.4$. The trend of the dependence of Ψ on electrolyte concentration x of the [bmim][NTf_2]–GBL and [bmpyr][NTf_2]–GBL is also similar to that of the NH_4NO_3–DMSO system. With an increase in x, the value of Ψ of these systems increases from an initial value of Ψ_0 equal to about 3.2 and then, after attaining a maximum value of about 5.2 at $x_{\max} \approx 0.6$ mole fraction, decreases to the value for the neat IL. Obviously, in Figure 6.17 not only the changes in Ψ caused by the addition of the solute NH_4NO_3 to DMSO and by [bmim][NTf_2] and [bmpyr][NTf_2] to GBL are much lower than those caused by sodium thiocyanate in water and methanol, but the $\Psi(x)$ dependence here is composed of two parts. The value of the fragility parameter Ψ increases with x in the concentration range $x < x_{\max}$, but later it decreases with an increase in x for $x > x_{\max}$.

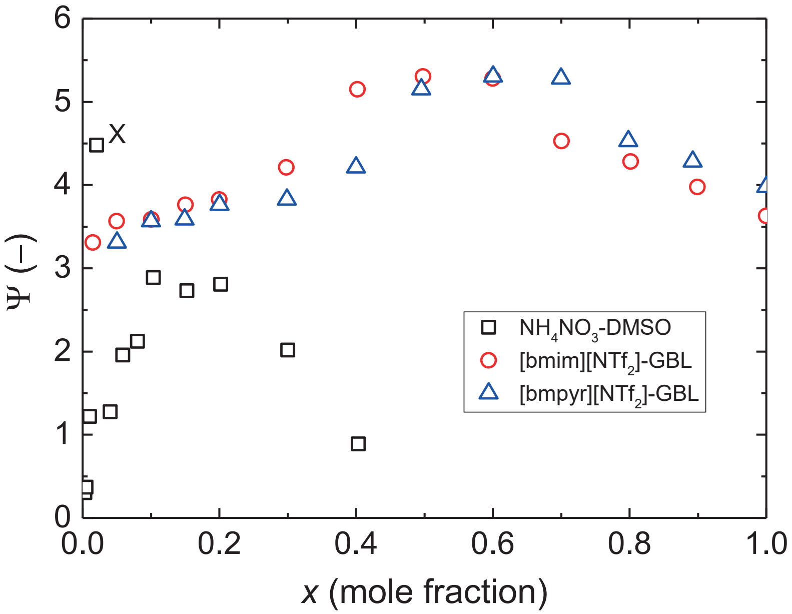

Figure 6.17. Dependence of dimensionless fragility parameter Ψ of NH_4NO_3–DMSO, [bmim][NTf_2]–GBL and [bmpyr][NTf_2]–GBL solutions on electrolyte concentration *x*. Original data of *B* and T_0 to calculate Ψ for NH_4NO_3–DMSO system from Świergiel et al. (2013), for [bmim][NTf_2]–GBL from Vraneš et al. (2014), and for [bmpyr][NTf_2]–GBL from Vraneš et al. (2015). Values of Ψ equal to 11 and 16 for $x = 0$ and 0.0015 mole fraction, respectively, of NH_4NO_3–DMSO system are not shown. Highly deviating point X for the NH_4NO_3–DMSO system corresponding to $\Psi \approx 4.5$ is omitted in the disussion.

The decrease in Ψ with an increase in x for $x > x_{\max}$ in Figure 6.17 is similar to that observed in Figure 6.16 for aqueous and methanolic sodium thiocyanate solutions, but the trend of the $\Psi(x)$ dependence for $x < x_{\max}$ is opposite to the behavior observed for $x > x_{\max}$. While the decrease in Ψ with an increase in solute concentration m of aqueous and methanolic sodium thiocyanate solutions in Figure 6.16 was attributed to stronger solute–solvent interaction than solvent–solvent interaction, a plausible explanation of the opposite trends is somewhat different types of interactions. In the solute concentration range $x < x_{\max}$, the increase in Ψ with x may be explained from a consideration of increasing dominance of solvent–solute interaction over solvent–solvent interaction. However, for $x < x_{\max}$, the decrease in Ψ with an increase in x is due to increasing dominance of solute–solute interaction over solvent–solute interaction.

Figure 6.18a and b shows plots of dimensionless fragility parameter Ψ of aqueous and methanolic sodium thiocyanate solutions, and NH_4NO_3–DMSO, [bmim][NTf_2]–GBL and [bmpyr][NTf_2]–GBL solutions against $\ln\sigma_\infty$ obtained from VTF plots of different concentrations. The direction of increasing solute concentration is indicated by arrows in the figures. The original data for sodium thiocyanate solutions are from Rohman et al. (2001), whereas those for

NH_4NO_3–DMSO system are from Świergiel et al. (2013), [bmim][NTf$_2$]–GBL from Vraneš et al. (2014), and [bmpyr][NTf$_2$]–GBL from Vraneš et al. (2015). As in Figure 6.17, the values of Ψ equal to 11 and 16 for $x = 0$ and 0.0015 mole fraction, respectively, of NH_4NO_3–DMSO system are not shown in Figure 6.18b.

From Figure 6.18a one observes that the value of Ψ of both aqueous and methanolic sodium thiocyanate solutions slowly decreases with increasing $\ln\sigma_\infty$ in a wide range, and then, after attaining a particular value at a maximum value of $\ln\sigma_\infty$, it decreases with decreasing $\ln\sigma_\infty$ in a relatively narrow $\ln\sigma_\infty$ interval. For example, in the methanolic sodium thiocyanate solutions, Ψ decreases slowly with increasing $\ln\sigma_\infty$ in the interval $0.8 < \ln\sigma_\infty < 3.9$ from the initial value of 8.95 at $\ln\sigma_\infty \approx 0.8$ down to 3.0 at the maximum $\ln\sigma_\infty \approx 3.9$ and then the decrease in Ψ occurs with decreasing $\ln\sigma_\infty$ in a relatively narrow interval between 3.9 and 3.6. However, in aqueous sodium thiocyanate solutions, Ψ decreases with increasing $\ln\sigma_\infty$ from the initial value of 4.2 down to 2.5 at the maximum value of $\ln\sigma_\infty \approx 5.2$. The maximum value of $\ln\sigma_\infty$ in these systems corresponds to concentrations comparable with m_0 estimated from the $\Psi(m)$ plots of Figure 6.16. This suggests that the maximum value of $\ln\sigma_\infty$ for an electrolyte system is related to the curvature in the plot of Ψ against m.

The trends of plots of the systems of Figure 6.18b are entirely different from the trends of sodium thiocyanate solutions of Figure 6.18a. If we omit the initial $\Psi(x)$ data for the NH_4NO_3–DMSO system, one observes that Ψ increases with increasing $\ln\sigma_\infty$ up to $\ln\sigma_\infty \approx 1.2$ when Ψ attains the maximum value of about 2.8 and then Ψ decreases with decreasing $\ln\sigma_\infty$. However, in the [bmim][NTf$_2$]–GBL and [bmpyr][NTf$_2$]–GBL systems, the variation of Ψ with $\ln\sigma_\infty$ is relatively complex and takes place in two stages as reflected from the dependence of Ψ on x (see Figure 6.17): (1) an initial increase in Ψ up to a maximum value, and (2) a decrease in Ψ from the maximum value. Consequently, in the first stage, the value of Ψ initially increases with a decrease in $\ln\sigma_\infty$ up to a minimum value of $\ln\sigma_\infty$ and then this increase in Ψ is accompanied with an increase in $\ln\sigma_\infty$ up to maximum Ψ. In the second stage, the value of Ψ decreases from its maximum value following a trend similar to that in the first stage.

The trends of $\Psi(\ln\sigma_\infty)$ plots of Figure 6.18 are also intimately connected with the nature of $\Psi(x)$ plots of Figures 6.16 and 6.17. Single $\Psi(x)$ curves like those in Figure 6.16 give single $\Psi(\ln\sigma_\infty)$ plots like Figure 6.18a, while $\Psi(x)$ plots like those of Figure 6.17, composed of two parts, give $\Psi(\ln\sigma_\infty)$ plots like those of Figure 6.18b composed of two parts. If it is assumed that, as in the case of Arrhenius plots, the value of $\ln\sigma_\infty$ for a system is an indicator of its entropy changes, the $\Psi(\ln\sigma_\infty)$ plots represent relationship between fragility parameter Ψ of a system and its entropy changes as indicated by the value of $\ln\sigma_\infty$.

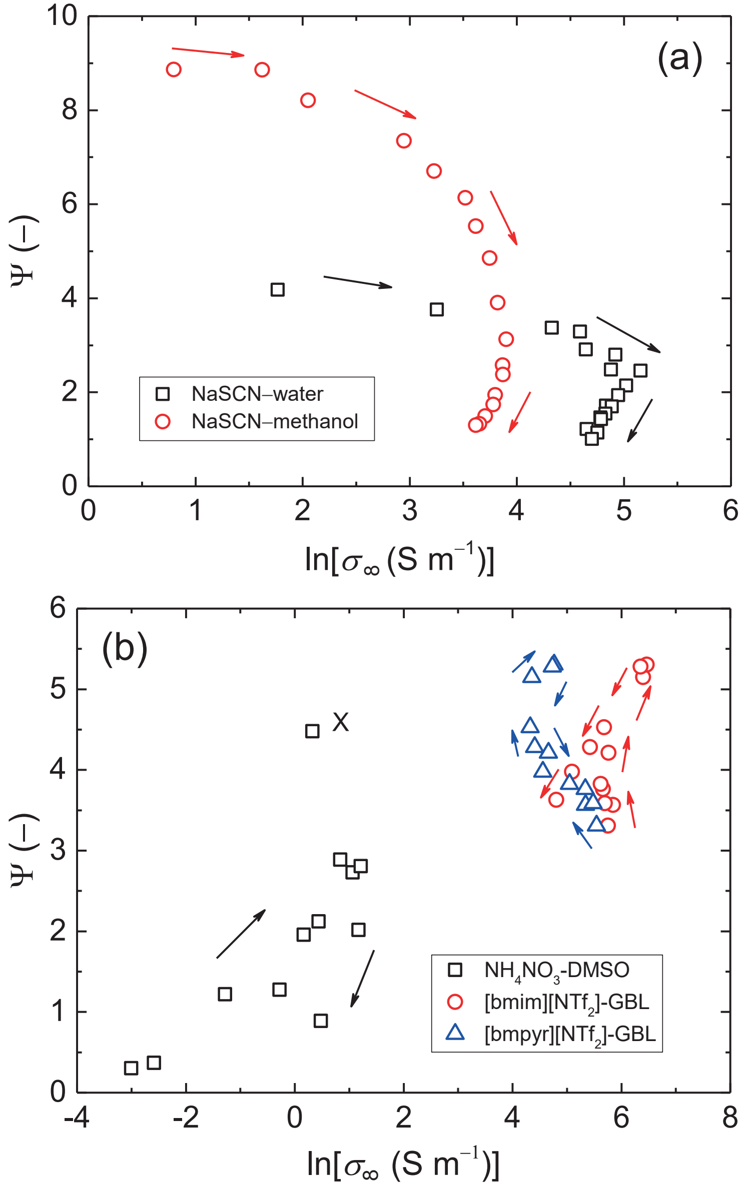

Figure 6.18. Plots of dimensionless fragility parameter Ψ of (a) aqueous and methanolic sodium thiocyanate solutions, and (b) NH_4NO_3–DMSO, [bmim][NTf_2]–GBL and [bmpyr][NTf_2]–GBL solutions against $\ln\sigma_\infty$ obtained from VTF plots of different concentrations. Original data for: (a) sodium thiocyanate solutions from Rohman et al. (2001), and (b) NH_4NO_3–DMSO system from Świergiel et al. (2013), [bmim][NTf_2]–GBL from Vraneš et al. (2014), and [bmpyr][NTf_2]–GBL from Vraneš et al. (2015). In (b) values of Ψ equal to 11 and 16 for $x = 0$ and 0.0015 mole fraction, respectively, of NH_4NO_3–DMSO system are not shown. Direction of increasing Ψ with x for the systems is indicated by arrows. In (b) highly deviating point for the NH_4NO_3–DMSO system corresponding to $\Psi \approx 4.5$ is omitted in the disussion.

6.7. Molar and equivalent conductivities of electrolytes

In the preceding section the behavior of specific conductivity σ of different types of electrolytes as a function of their concentration/composition and temperature was interpreted from consideration of mobility of "free ions" available in the liquid volume. Since the number of these conducting entities per unit volume in the liquid, usually referred to as concentration of charge carriers, changes with the liquid composition and temperature, experimental investigation of concentration and temperature dependence of equivalent conductivity Λ of electrolytes, defined by Eq. (6.7), instead of the specific conductivity σ, and their theoretical interpretation has a long history (for example, see: Horvath, 1985; Robinson and Stokes, 1959).

The equivalent conductivity Λ of true electrolytes at low concentrations c is observed to follow Kohlrausch's law of independent migration of ions, represented by

$$\Lambda = \Lambda^0 - A_1 c^{1/2} \,, \tag{6.45}$$

where Λ^0 is the limiting equivalent conductivity given by Eq. (6.9), and A_1 is a constant. The value of Λ^0 is related to the motion of an ion which is determined only by its interaction with the surrounding solvent molecules because other ions are at infinite distance from it. The moving ion drags along with it some of the surrounding solvent molecules. When more ions are present in the solution, they drag with them solvent molecules in the same direction or in the opposite direction as the reference ion. Since ions have electric fields surrounding them, this process of movement of the ions depends on electrolyte concentration and approaches zero at infinite dilution. The value of the parameter A_1 is associated with this effect of mutual interaction of moving ions in the dilute solution. Eq. (6.45) of the electrical conductivity of electrolyte solutions is similar in form to the Onsager limiting law (see below).

Derivation of equations of concentration dependence of electrical conductivity of electrolyte solutions is based on description of the velocity of ions from their distribution in the solution from electrostatic hydrodynamic considerations (see Robinson and Stokes, 1959). Since the Onsager limiting law holds only in very dilute solutions, experimental conductivity data of concentrated electrolyte solutions have been interpreted by introducing various modifications in the existing electrostatic hydrodynamic theories for dilute solutions. In the case of very high concentrations Angell and coworkers (1966, 1972) applied an expression based on the free-volume theory. These theoretical approaches of interpretation of the molar/equilvalent conductivity data of solutions are described below.

6.7.1. Concentration dependence of conductivity

6.7.1.1. Electrostatic hydrodynamic approaches

The starting point of interpretation of molar/equilivalent conductivities of electrolytes is consideration of infinite dilute solutions when the ions are far from one another to affect their motion. The motion of an ion is determined by the interaction between the electric charges of the moving ions in the solution and involves (for example, see Robinson and Stokes, 1959): (1) disturbance in their symmetrical distribution due to applied electric field (i.e. electrophortic effect), and (2) rearrangement of solvent molecules surrounding the moving ion (relaxation effect). With these effects the conductivity equation may be written in the form (Robinson and Stokes, 1959)

$$\Lambda = \left(\Lambda^0 - \frac{F^2}{6\pi\eta N_\mathrm{A}} (|z_1| + |z_2|) \frac{\kappa}{1+\kappa a} \right) \left(1 + \frac{\Delta X}{X} \right), \tag{6.46}$$

where Λ is the sum of cationic and anionic equivalent conductivities λ_1 and λ_2 (see Eq. (6.8), F is the Faraday constant, $\Delta X/X$ is the contribution due to the relaxation effect, a is the distance of closest approach between two ions in the solution, and the quantity

$$\kappa = \left(\frac{4\pi e^2}{\varepsilon k_\mathrm{B} T} \sum_i n_i z_i^2 \right)^{1/2} . \tag{6.47}$$

The quantity κ is a function of ionic charge $z_i e$, solute concentration (through n_i), solution temperature T and dielectric constant ε of the solvent, and has the dimensions of reciprocal length. Several expressions have been proposed to account for the relaxation term. The expression due to Falkenhagen et al. (1952) is given by

$$\frac{\Delta X}{X} = -\frac{z_1 z_2 e^2}{3\varepsilon k_\mathrm{B} T} \cdot \frac{q}{1+q^{1/2}} \cdot \frac{\kappa}{(1+\kappa a)\kappa a} \{\exp[\kappa a(1-q^{1/2})] - 1\} , \tag{6.48}$$

with the dimensionless parameter

$$q = \frac{|z_1 z_2|}{|z_1| + |z_2|} \cdot \frac{\lambda_1^0 + \lambda_2^0}{|z_1|\lambda_1^0 + |z_2|\lambda_2^0} . \tag{6.49}$$

The parameter q depends on the ionic valency z_i. Substitution of the contribution $\Delta X/X$ of relaxation from Eq. (6.48) in Eq. (6.46) gives the Falkenhagen–Leist–Kelbg equation:

$$\Lambda = \left(\Lambda^0 - \frac{F^2}{6\pi\eta N_\mathrm{A}} (|z_1| + |z_2|) \frac{\kappa}{1+\kappa a} \right) \left(1 - \frac{z_1 z_2 e^2}{3\varepsilon k_\mathrm{B} T} \cdot \frac{q}{1+q^{1/2}} \cdot \frac{\kappa}{1+\kappa a} \zeta \right), \tag{6.50}$$

where

$$\zeta = \frac{\exp[\kappa a(1-q^{1/2}) - 1}{\kappa a}, \tag{6.51}$$

with the approximation $\exp[\kappa a(1-q^{1/2})]-1 \approx \kappa a$ such that $\zeta \approx 1$.

Writing Eq. (6.47) in the form

$$\kappa = \left(\frac{8\pi N_\mathrm{A} e^2}{1000\varepsilon k_\mathrm{B} T} \right)^{1/2} I^{1/2} , \tag{6.52}$$

and the approximation $\zeta \approx 1$, from Eq. (6.50) one obtains the Falkenhagen–Leist–Kelbg equation in the simplied form

$$\Lambda = \left(\Lambda^0 - \frac{B_1 I^{1/2}}{1 + B_3 a I^{1/2}} \right) \left(1 - \frac{B_2 I^{1/2}}{1 + B_3 a I^{1/2}} \right), \tag{6.53}$$

where B_1, B_2 and B_3 are constants given by

$$B_1 = \frac{41.25\,(|\,z_1\,| + |\,z_2\,|)}{\eta(\varepsilon T)^{1/2}} , \tag{6.54}$$

$$B_2 = \frac{2.801 \cdot 10^6\,|\,z_1 z_2\,|\,q}{(\varepsilon T)^{3/2}(1 + q^{1/2})} , \tag{6.55}$$

$$B_3 = 50.29(\varepsilon T)^{-1/2} , \tag{6.56}$$

and the ionic strength

$$I = \frac{c}{2}\left(\nu_1 z_1^2 + \nu_2 z_2^2 \right), \tag{6.57}$$

where ν_1 and ν_2 are the numbers of moles of cations and anions, respectively, formed from 1 mole of the electrolyte, c is the molar concentration (mole·L^{-1}) of the solution, and η is its viscosity in Poise.

If the cross-product of the electrophoretic and relaxation terms is neglected and approximation $\kappa a << 1$ holds in Eq. (6.50), one obtains the Onsager limiting law (cf. Eq. (6.53) when $B_3 a I^2 << 1$):

$$\Lambda = \Lambda^0 - (B_1 \Lambda^0 + B_2) I^{1/2} , \tag{6.58}$$

where the constants B_1 and B_2 are defined above. This limiting law (6.58) describes the conductivity data of very dilute aqueous 1:1 electrolyte solutions of concentrations below 0.001 mole·L^{-1}. Without the approximation $\kappa a << 1$, Eq. (6.53) represents the Robinson–Stokes equation (Robinson and Stokes, 1954):

$$\Lambda = \Lambda^0 - \frac{B_1 \Lambda^0 + B_2}{1 + B_3 a I^{1/2}} I^{1/2} . \tag{6.59}$$

Eq. (6.59) has two variable parameters, the Debye–Hückel distance a and the limiting conductivity Λ^0 at infinite dilution. The applicability of this equation for the conductivity data of various salts may be tested when values of a and Λ^0 are appropriately chosen. A sensible value of a lies between 0.3 and 0.5 nm for different solutions. Inclusion of the $(1+\kappa a)$ term to the Onsager limiting law (6.58) accounts for the finite ionic size and enables to explain the conductivity of 1:1 electrolytes up to 0.01 mole·L^{-1}.

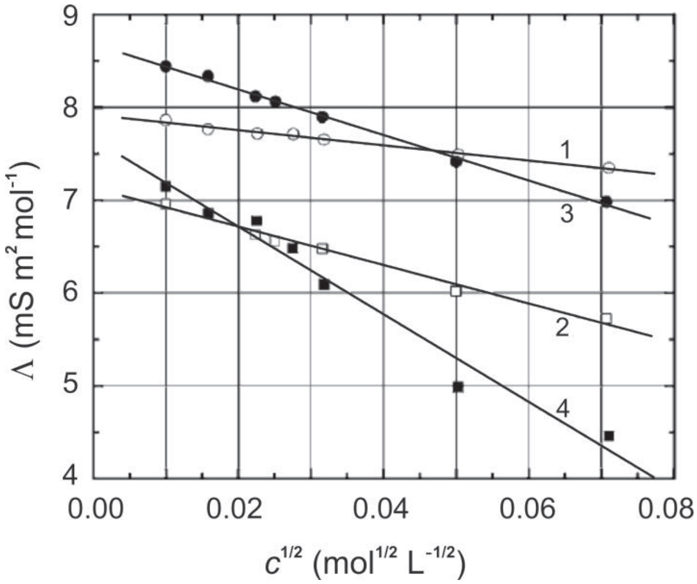

Figure 6.19. Examples of linear dependence of equivalent conductivities Λ of aqueous solutions of different ascorbates at 298.15 K on $c^{1/2}$ according to Onsager limiting law (6.58): (1) sodium ascorbate, (2) calcium ascorbate, (3) magnesium ascorbate, and (4) ferrous ascorbate. After Apelblat et al. (2006).

Figure 6.19 illustrates examples of the dependence of equivalent conductivites Λ of aqueous solutions of sodium ascorbate considered as 1:1 electrolyte and some 2:1 electrolytes at 298.15 K on $c^{1/2}$ according to Eq. (6.58) with the values of viscosity η and dielectric constant ε of water taken from the literature and Λ^0 calculated for the MeAn electrolyte from the relation (Apelblat et al., 2006)

$$\Lambda^0 = \lambda_1^0\left(\frac{1}{z_1}\right)+\lambda_2^0\left(\frac{1}{z_2}\right), \tag{6.60}$$

where z_1 and z_2 are the valencies of cation Me^{z_1+} and anion An^{z_1-}, respectively, and the limiting conductivity λ_2^0 of ascorbate anion is calculated by substracting the values of λ_1^0 of individual cations of the electrolytes from their corresponding Λ^0. In the calculations it was assumed that all these salts are completely dissociated into ions in dilute solutions.

In order to explain the conductivity data for 1:1 electrolytes at higher concentrations, where the ionic strength I equals the molarity c, Wishaw and Stokes (1954) extended Falkenhagen–Leist–Kelbg equation (6.50) in the form:

$$\Lambda_c = \frac{\eta_0}{\eta}\left(\Lambda^0 - \frac{B_1 c^{1/2}}{1+B_3 a c^{1/2}}\right)\left(1 - \frac{B_2 c^{1/2}}{1+B_3 a c^{1/2}}\zeta\right), \tag{6.61}$$

where η_0 and η are the viscosities of the solvent and the solution, respectively, and the constant B_3 and the parameter ζ are given by Eqs. (6.56) and (6.51), respectively. The Stokes–Wishaw relation (6.61) successfully describes the conductivity data of concentrated solutions, but the introduction of the relative viscosity factor is entirely empirical.

In deriving the above equations from Eq. (6.46) of the conductivity equation involving electrophoretic and relaxation effects, it is assumed that complete ionization of the solute takes place, interionic forces in the solution is based on the Debye–Hückel theory, and the dielectric constant ε of the solution is equal to that of the solvent. In practice, only a small number of true electrolytes in water, and perhaps in some other solvents of high dielectric constant ε, are completely ionized. It is likely that the distance a of closest approach of ions implies some degree of ion-association because it assumes that some ions do approach to mutual contacts. However, despite different assumptions the final expressions satisfactorily describe the data in the relatively high concentration region.

The fact that Wishaw–Stokes equation adequately represents the data at higher concentrations indicates that there is some correlation between viscosity and solvation effects. Solvent effects are included in the Debye–Hückel expression for the concentration dependence of activity coefficients of electrolytes (for example, see Bockris and Reddy, 1970), but the distance a between the ions in the solution does not include the shell formed by solvent molecules around the bare ions. Since higher electrolyte concentration leads to higher viscosity of the solution and lesser solvent molecules for the solvation of the salt, Goldsack et al. (1976) extended the Falkenhagen–Leist–Kelbg equation (6.50) to include the effect of solvation on the concentration of electrolyte solutions. To account for the effect of solvation due to solution concentration these authors introduced the concept of apparent molality m_s related to the total molality m of the salt by

$$m_s = \frac{1000\, m / M_h}{1000 - n_h m / M_h}, \tag{6.62}$$

where M_h is the molar mass of the solvent and n_h is a total solvation number parameter of solvation of the salt. Then, considering n_h to be a constant and independent of concentration (fixed-solvation parameter equation) and n_h of a salt to decrease with increasing concentration (variable-solvation parameter equation), from Eq. (6.50) they derived expressions for molal conductivity Λ_m as a function of the apparent molality m_s in terms of two adjustable parameters: (1) the Debye–Hückel distance a of closest approach of ions, and (2) the solvation number n_h of the salt.

The above authors found that the conductance data for aqueous solutions of alkali halides in the 0.5 to 10 m concentration range and 0 to 60°C temperature range are adequately reproduced by both fixed- and variable-solvation parameter equations, but in the case of more solvated salts the variable-solvation parameter equation yields better fits to the data. It was also found that the values of solvation number n_h obtained from the fixed-solvation parameter equation are similar to those obtained by other methods and correspond to primary hydration numbers. The variable-solvation parameter gives much higher values of hydration number, which corresponds to secondary and tertiary solvation numbers as well. In both cases the values of hydration number, especially for salts of large cations, were observed to increase with temperature.

Finally, it should be mentioned that in the early years of the development of the theoretical interpretation of electrolyte conductivity attempts were made to extend the concentration range of applicability of Eq. (6.58) with added terms in c, $c^{3/2}$, $c\ln c$, etc. However, to test the validity of these extended equations precisely determined value of Λ^0 by employing Eq. (6.58) from the intercept of plots of Λ against $c^{1/2}$ is required. For this purpose, Eq. (6.58) rewritten in the following form is used (Shedlovsky, 1932):

$$\Lambda^{0\prime} = \frac{\Lambda + B_2 c^{1/2}}{1 - B_1 c^{1/2}}, \qquad (6.63)$$

where the value of Λ^0 of Eq. (6.58) is now replaced by $\Lambda^{0\prime}$. According to this relation, the quantity on the right should be a constant equal to $\Lambda^0 \equiv \Lambda^{0\prime}$, as expected from Eq. (6.58); instead it varies with c up to about 0.1 mole·L^{-1}. The dependence of this $\Lambda^{0\prime}$ on c, $c^{3/2}$ or $c\ln c$ gives on extrapolation to $c \to 0$ the true value of Λ^0 (Fernandez-Prini and Prue, 1963; Shedlovsky, 1932). Instead of $\Lambda^{0\prime}$, the difference $\Delta\Lambda = (\Lambda^{0\prime} - \Lambda^0)$, determined as the deviation in calculated conductivity Λ(cal) from the measured conductivity Λ(exp), has also been analyzed as a function of concentration c (for example, see: Bianchi et al., 2000; Miyoshi, 1973).

6.7.1.2. Extended hydrodynamic conductivity theories

In the above conductivity equations, the relaxation effect was represented by Eq. (6.48) due to Falkenhagen et al. (1952). However, other treatments give not only different expressions for ζ in Eq. (6.48) but include higher order terms (Pitts, 1953; Fuoss and Onsager, 1957; Fuoss and Hsia, 1967; Lee and Wheaton, 1978a,b, 1979; Quint and Viallard, 1978). Regardless of symmetrical or asymmetrical nature of the electrolyte, the conductivity equation based on Fuoss–Onsager, Fuoss–Hsia and Pitts models is of the polynomial form (Bianchi et al., 2000; Miyoshi, 1973; Quint and Viallard, 1978c)

$$\Lambda = \Lambda^0 - SI^{1/2} + EI\ln I + J_1 I - J_2 I^{3/2}, \qquad (6.64)$$

where Λ^0 is the sum of conductivities λ_1^0 and λ_2^0 of cations and anions at infinite dilution, and the coefficients S, E, J_1 and J_2 depend on the properties of the solvent, Λ^0 and the charges of different ions. The coefficient S is the limiting slope of the concentration dependence of conductivity Λ. Analytical expressions for the coefficients of Eq. (6.64) for mixed as well as pure symmetrical and asymmetrical electrolytes based on different models are given in the literature (Fernandez-Prini, 1969; Fernandez-Prini and Prue, 1963; Miyoshi, 1973; Quint and Viallard, 1978). Starting from the same continuity and hydrodynamic equations used in the classical treatments, mean spherical approximation (MSA) version of conductivity equations has also been developed (Bernard et al., 1992; Durand-Vidal et al., 1996; Turq et al., 1995). The MSA equation contains ionic diameters instead of mean distance of closest approach between cation and anion.

Comparison of different conductivity equations with precisely determined experimental data of unassociated and associated electrolyte solutions has drawn constant interest. For example, Stokes (1961) compared Fuoss–Onsager and Pitts equations using the conductivity data of aqueous HCl solution at 25 °C, and observed that the former reproduces the data up to 0.004 mole·L^{-1} whereas the latter up to 0.02 mole·L^{-1}. Following a procedure similar to that used by Shedlovsky (1932), as decribed above, Fernandez-Prini and Prue (1963) compared these equations using data of inorganic salts composed of monoatomic ions in water, methanol and dimethyl formamide, which are hydrogen-bonded solvents and strongly solvate the dissociated ions. These authors found that the Pitts equation reproduces the data satisfactorily and the obtained parameters are reasonable except in methanol, in which the Pitts equation gave a much lower value of the distance a of closest approach between two ions than the Fuoss–Onsager equation. However, from the values of a given by these equations it remained unclear whether they correspond to ion pairs formed in the solution by bare or solvated ions.

Fuoss and Hsia (1967) pointed out that application of the linear form of Eq. (6.64) for unassociated salts, i.e. with $J_2c^{3/2}$ omitted, at concentrations above 0.01 mole·L^{-1} the parameters Λ^0 and J_1 begin to depend on the concentration range over which they are determined. To understand the origin of this deviation in the experimental conductivity from the calculated one, these authors tested the applicability of Eq. (6.64) by plotting the quantity Y_1, defined as

$$Y_1 = [\Lambda - (\Lambda^0 - Sc^{1/2} + Ec\ln c)]/c\,, \tag{6.65}$$

as a function of $c^{1/2}$ for the published conductivity data of KCl, CsI, NaCl and CsBr solutions in dioxane–water mixtures. The authors found that the $Y_1(c^{1/2})$ plots were linear with values of their slope different from the J_2 of Eq. (6.65), implying that the deviation between experimental and calculated conductivities cannot be explained by the $J_2c^{3/2}$ term. Therefore, they considered the effect of association of ions at high concentrations and proposed the following linearized conductivity equation for associated electrolytes:

$$\Lambda = \Lambda^0 - S\alpha^{1/2}c^{1/2} + E\alpha c\ln(\alpha c) + J_1\alpha c - K_\mathrm{A}\alpha^2 c\gamma^2\Lambda\,, \tag{6.66}$$

with the concentration range restricted to an upper limit such that $\kappa a < 0.1$, the ratio α of free ion concentration to stochiometric composition (i.e. degree of dissociation) defined by (cf. Eq. (6.46))

$$\alpha = \frac{\Lambda}{(\Lambda^0 - \Delta\Lambda)(1 + \Delta X / X)}, \tag{6.67}$$

and, according to the law of mass action, α is related to the association constant K_A by

$$K_A = \frac{1-\alpha}{\alpha^2 c} Y, \tag{6.68}$$

with the parameter

$$Y = \frac{\gamma_{\text{salt}}}{\gamma_+ \gamma_-} = \frac{1}{\gamma^2}, \tag{6.69}$$

where γ_+ and γ_- are the activity coeffcients of individual cation A^+ and anion B^-, respectively, γ_{salt} of the 1:1 salt AB in the solution is assumed to be unity, and, according to the Debye–Hückel limiting law, the mean activity coefficient γ, defined as $\gamma = (\gamma_+\gamma_-)^{1/2}$, is given by

$$\ln \gamma = -\frac{e^2}{2\varepsilon k_B T} \frac{\kappa}{1 + \kappa a}, \tag{6.70}$$

with κ related to solute concentration c by Eq. (6.52). Since, at a given temperature, α and γ are concentration dependent, K_A also depends on c.

The above authors observed that Eq. (6.66) explains the conductivity of the electrolytes over a large range of dielectric constant ε from that of water down to about 12, and that neglect of ion association at higher dielectric constants results in a variation in the value of contact distance a. It was found that the linear dependence of $\ln K_A$ on ε^{-1} for CsI, KCl and NaCl solutions in diaoxane–water mixtures over large ε^{-1} range with slopes calculated from the values of a for water, as predicted by the theory (cf. Eqs. (6.68) to (6.70)), with a value of a larger than the sum of the crystallographic radii of the ions, but for water-rich mixtures the authors also observed curvatures for KCl and NaCl solutions at high ε. The authors argued that the linear relationship between $\ln K_A$ and ε^{-1} is a convincing evidence of ion association in solutions even in true electrolyte solutions and that the deviation of the expected linear dependence of $\ln K_A$ on ε^{-1} in water-rich mixtures is due to difference in the water structure around free ions and around ion pairs.

In the calculation of association constant K_A the values of mean activity coefficient γ obtained by Eq. (6.70) based on the Debye–Hückel theory were used. Since the Debye–Hückel theory applies in dilute solutions, the values of γ and K_A estimated by Eqs. (6.68) and (6.70) do not take into account the effect of ion–solvent interactions associated with water available around free ions and around ion pairs in aqueous electrolyte solutions with increasing solute concentration. The relevant equation that includes this effect is given as (Bockris and Reddy, 1970)

$$\ln\gamma = -\frac{B_2}{1+B_3ac^{1/2}} - \frac{n_\mathrm{h}}{n}\ln a_\mathrm{w} + \ln\frac{n_\mathrm{w}+n}{n_\mathrm{w}+n-n_\mathrm{h}}, \tag{6.71}$$

where B_2 and B_3 are given by Eqs. (6.55) and (6.56), respectively, a_w is the activity of water, n is the number of moles of the electrolyte present in n_w moles of water, and n_h is sum of the moles of water in the primary solvation sheath per liter of solution for both ions of the 1:1 electrolyte. Note that n_h is the hydration number and refers to 1 molar solution. In Eq. (6.71) the first correction term is due to change in the free energy caused by the introduction of solute to the solvent whereas the second correction is due to change in the free energy by the removal of water molecules from the sheath of ions. These correction terms multiplied by $R_\mathrm{G}T$ give the corresponding energy changes. Since $a_\mathrm{w} \leq 1$ and $n_\mathrm{h} \geq n$, contribution of the correction terms in Eq. (6.71) due to ion–solvent interactions becomes important in solutions of electrolytes in which their concentration is sufficiently high. Thus, the value of γ increases and K_A decreases with an increase in electrolyte concentration for systems in which $a_\mathrm{w} < 1$ and $n_\mathrm{h} > n$.

It should be noted that Eq. (6.68) refers to an electrolyte solution in which some of its ions form nonconducting cation–anion pairs when the electrolyte concentration in the solution is increased or the dielectric constant ε of the solvent is decreased. Basically, this is another form of Eq. (6.15) based on the dissociation of the electrolyte $\mathrm{A}_a\mathrm{B}_b$, where the equilibrium constant $K_\mathrm{eq} = 1/K_\mathrm{A}$ and the activity coefficient γ is taken as unity. In contrast to the reaction scheme of dissociation, formation of ion pairs involves reverse reaction in which isolated ions are associated with the association constant K_A. In reaction (6.15), if the concentrations $[\mathrm{A}^+]$ and $[\mathrm{B}^-]$ of A^+ cations and B^- anions in the solution are denoted by $c\alpha\gamma_+$ and $c\alpha\gamma_-$, respectively, one obtains Eq. (6.68) with the mean activity coefficient $\gamma = (\gamma_+\gamma_-)^{1/2}$. Quantities $c\gamma_+$ and $c\gamma_-$ are the activities of cations and anions, respectively, but for the associated nonconducting molecules their activity coeficient is always unity and their concentration is $c(1-\alpha)$. Obviously, at infinite dilution, the activity coefficient is unity. It should be remembered here that positive and negative ions forming ion-pairs in true electrolytes retain their ionic identity as ions and are held together by short-range coulombian interactions. This process of formation of ion-pairs is different from neutral ionogenic molecules in potential electrolytes like acetic acid consisting of aggregates of atoms held together by covalent bonds (Bockris and Reddy, 1970).

Miyoshi (1973) compared the conductivity equations of Fuoss–Onsager, Fuoss–Hsia and Pitts using conductivity data of bis(2,9-dimethyl-1,10-phenanthroline)Cu(I) perchlorate in acetonitrile, nitrobenzene and nitromethane solvents at 25° C. Since these solvents have a relatively high dielectric constant, this chelate salt is completely dissociated into chelate and perchlorate ions. However, both dissociated perchlorate anions and large chelate cation may be assumed to be poorly solvated because large anions are least solvated and the positive charge on the chelate cation is screened by bulky aromatc ligands. Consequently, the a value in this system may be considered to correspond to the contact distance between anion–cation pair of bare ions.

It was found that the Pitts equation represents the conductivity data most satisfactorily in the three solvents than the Fuoss–Onsager and Fuoss–Hsia equations. For this complex composite salt, the *a* values obtained from the Pitts equation in these solvents are unrealistically small and are lower by about 0.08 and 0.12 nm than those from the Fuoss–Onsager and Fuoss–Hsia equations, respectively. It was concluded that the Fuoss–Hsia equation is preferable for the analysis of conductivity data for associated and unassociated electrolytes.

Bianchi et al. (2000) compared the performance of mean spherical approximation (MSA), Fuoss–Hsia and Lee–Wheaton conductivity equations at the level of experimental uncertainty in the conductivity data reported in the literature for some typical symmetrical and asymmetrical electrolyte solutions at 25 °C. The systems selected for the analysis were: a simple symmetrical electrolyte with no ionic association (aqueous NaCl solutions), two symmetrical electrolytes with partial association (aqueous $MgSO_4$ solutions and $LaFe(CN)_6$ in formamide), and two unsymmetrical electrolytes with partial association (aqueous $MgCl_2$ and $LaCl_3$ solutions). For the analysis the authors considered the concentration dependence of the difference $\Delta\Lambda$ between the experimental and calculated conductivities in the dilute concentration range of experimental uncertainty. These authors observed that all equations reproduce well the conductivity data within experimental uncertainty in the case of aqueous NaCl solutions over the traditionally accepted concentration range for the classical conductivity equations (i.e. $\kappa a < 0.1$) but beyond the traditional concentration limit over a wider concentration range the differences in the extrapolated value of Λ^0 are higher than those found in the dilute solutions and the *a* parameter becomes closer to the sum of crystallographic radii of the ions. A similar situation is encountered in the case of multiple charged symmetrical electrolytes, but the situation is not clear for unsymmetrical electrolytes. However, MSA equation gives too low *a* values for both symmetrical and unsymmetrical electrolytes.

Finally, it should be mentioned that the differences in the predictions of these theories lie in the assumptions used to derive the final equations.

6.7.1.3. Concentration dependence of molar conductivity

It was mentioned in Section 6.6.2 that the temperature dependence of specific conductivity of a variety of electrolytes follows VTF relation (6.42). However, it is observed that the VTF relation also describes the temperature dependence of molar and equivalent conductivities. Assuming that the parameter B and the preexponential factor A of the VTF relation (6.42) are independent of electrolyte concentration, Angell (1966) proposed a simple relation between equivalent conductivity Λ_{eq} and charge concentration represented by equivalent concentration N. To derive the final expression, he considered a linear dependence of the ideal glass transition temperature T_0 on N according to the relation

$$T_{0(N)} = T_0^0 + QN\,, \tag{6.72}$$

where T_0^0 is the value of T_0 at infinite dilution (i.e. for the solvent), and the proportionality constant Q is characteristic of the system under consideration. Examples of the validity of Eq. (6.72) are shown in Figure 6.20 for aqueous and methanolic sodium thiocyanate solutions at 25 °C. Since under isothermal composition conditions, the temperature T in Eq. (6.42) is constant, one may define a limiting concentration N_0 when T_0 is equal to the isothermal temperature T and $T = T_0^0 + QN_0$. Then for isothermal conditions Eq. (6.42) may be expressed as

$$\Lambda_{\mathrm{eq}} = A_\Lambda \exp\left(-\frac{B}{Q(N_0 - N)}\right), \tag{6.73}$$

where A_Λ is a concentration independent preexponential factor. According to this relation a plot of $\ln\Lambda_{\mathrm{eq}}$ against $(N_0 - N)^{-1}$ is expected to give linear dependence.

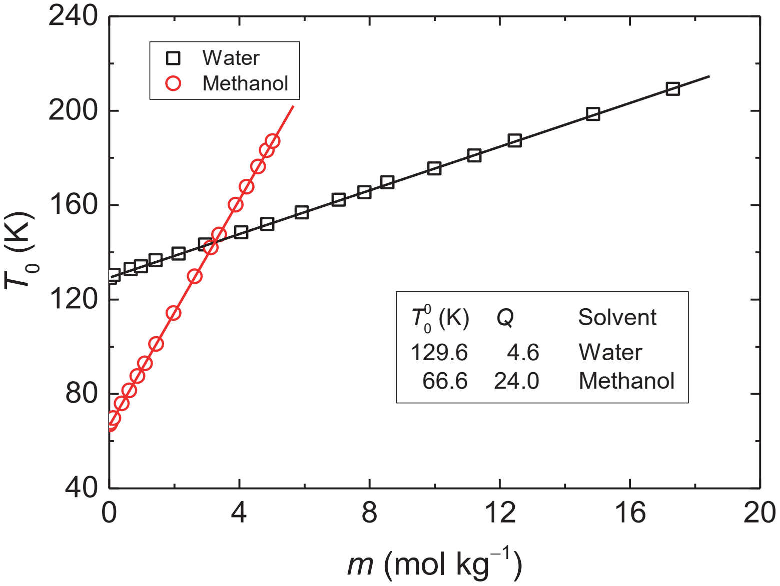

Figure 6.20. Linear dependence of the ideal glass transition temperature T_0 on m for aqueous and methanolic sodium thiocyanate solutions at 25 °C according to Eq. (6.72). Original data from Rohman et al. (2001).

Angell (1966) tested the validity of Eq. (6.73) by analyzing the experimental data of the dependence of equivalent conductivity Λ_{eq} of aqueous $Ca(NO_3)_2$ solutions on $(N_0 - N)^{-1}$ at 0.35 and 18.1 °C. He found that: (1) the linear relation is indeed followed by the conductivity of this system extending over about three orders of magnitude in the concentration range between about 2 and 15 N, (2) the slope and the intercept of the plots lead to realistic values of B, Q and N_0, and (3) if a lower value of Q than that obtained for the above concentration range is used, the conductivity data at lower concentrations can also be reproduced. The main criticism of this interpretation is that the concentration independence of the parameters *B*, *A* and *Q* is not entirely correct.

6.7.2. Interpretation of conductivity of true electrolytes

6.7.2.1. Role of cation–anion association in conductivity of electrolytes

In the preceding section various approaches devoted to the concentration dependence of equivalent conductivity of true electrolytes capable of dissociating into free ions in very dilute solutions were described. When the electrolyte concentration in the solution increases, cations and anions come into contact forming nonconducting ion pairs for all types of symmetrical electrolytes. This leads to a decrease in the conductivity of the electrolyte with an increase in its concentration *c* in the solution. In fact, Fuoss and Hsia (1967) used the concept of formation of ion pairs by the association of cations and anions of different alkali halides in dioxane–water mixtures to explain the observed linear dependence of $\ln K_A$ on ε^{-1} for them. The values of K_A and α were evaluated from the conductivity data using linearized conductivity equation (6.66).

Ion association is not confined to simple symmetrical 1:1 electrolytes but is expected in various symmetrical as well as asymmetrical electrolytes. However, it has been argued (Apelblat, 2011a,b) that, with the exception of the Lee–Wheaton and Quint–Viallard conductivity equations, other equations applied in the literature are suitable only for symmetrical electrolytes. Lee–Wheaton equation has been used to study aqueous solutions of 1:1 electrolytes (Sokol et al., 2006) and 2:2 electrolytes (Pethybridge and Taba, 1980, 1982), whereas Quint–Viallard equation has been widely used to study various symmetrical 1:1 electrolytes (Apelblat et al., 2006, 2008; Bončina et al., 2010), 2:2 electrolytes (Apelblat, 2011a, c) and 3:3 electrolytes (Apelblat, 2011c) as well as a variety of asymmetrial polyvalent electrolytes (Apelblat, 2011b,c, 2017; Bešter-Rogač et al., 2002). Following Apelblat (2011a-c), a generalized representation of the molar conductivity of an electrolyte as a function of solute concentration *c*, solution temperature *T* and composition of solvent mixtures is given below.

The molar conductivity Λ of a z_1:z_2 electrolyte AB of concentration *c* in a solvent at a given temperature *T* is the sum of ionic conductivities λ_i and is given by

$$\Lambda(c,T) = \frac{1000\sigma}{c} = \sum_i \frac{|z_i| c_i \lambda_i(c,T)}{c}, \tag{6.74}$$

where *i* denotes cation A^{z_1+} and anion B^{z_2-}, σ is the specific conductivity, z_1 and z_2 are the valencies of cations and anions, and c_i is their molar concentrations. The ionic conductivities λ_i are represented by the relation (see Eq. (6.64))

$$\lambda_i(c,T) = \lambda_i^0(T) - S_i(T) I^{1/2} + E_i(T) I \ln I + J_{1i}(T) I + J_{2i}(T) I^{3/2}, \tag{6.75}$$

where I is the ionic strength given by Eq. (6.57), the parameters S_i, E_i, J_{1i} and J_{2i} are complex functions of the limiting equivalent ionic conductivities λ_i^0, the distance parameters a_i, and the dielectric constant ε and the viscosity η of the solvent. The parameters S_i, E_i, J_{1i} and J_{2i} are available from the Quint–Viallard theory (Quint and Viallard, 1978a-c). In the case of a partially associated electrolyte of concentration c, if α is the fraction of free ions at a given temperature T, the concentrations of free and associated ions are $c\alpha$ and $c(1-\alpha)$, respectively. Since the process of association of ions is in equilibrium with the dissociated ions in the system at the temperature T, according to the law of mass action the association constant $K_{\mathrm{A}}(T)$ is given by (see Eq. (6.68))

$$K_{\mathrm{A}}(T) = \frac{1-\alpha(c,T)}{\nu_1\nu_2 c\alpha^2(c,T)} Y(c,T)\,, \tag{6.76}$$

where the fraction α and the parameter Y depend both on c and T, ν_1 and ν_2 are the number of cations and anions of a dissociated molecule of the electrolyte AB and the parameter Y is given by (see Eq. (6.69))

$$Y(c,T) = \frac{\gamma_{\mathrm{AB}}(c,T)}{\gamma_{\mathrm{A}^{z_1+}}(c,T)\gamma_{\mathrm{B}^{z_2-}}(c,T)}\,, \tag{6.77}$$

where it is assumed that γ_{AB} is unity, and γ_i is the activity coefficient of individual ion i and is given by the Debye–Hückel equation

$$\ln[\gamma_i(c,T)] = -\frac{z_i^2 B_2(T) I^{1/2}}{1 + B_3(T) a_i I^{1/2}}\,, \tag{6.78}$$

with B_2 and B_3 given by Eqs. (6.55) and (6.56), respectively, and the ion size a_i is assumed to be temperature independent. In conductivity equation the distance parameters a_i are taken to be half of the cation and anion sizes. If the solvent used for conductivity measurements is a binary solvent mixture of added solvent composition x, the values of the association constant K_{A}, the ionic fraction α, the parameter Y, and the ionic activity coefficient γ_i also become dependent on x.

At each temperature T and solvent mixture composition x, the experimental conductivity data become: $(\Lambda, c) = f(K_{\mathrm{A}}, \Lambda^0, a_i, \varepsilon, \eta, c)$ and is solved by an optimization procedure to obtain K_{A} and Λ^0 values that ensure the best fit between the experimental and calculated conductivities. Using Eqs. (6.76)-(6.78), (6.55) and (6.56) the iteration process is started with the fraction $\alpha = 1$ and fixed values of a_i to evaluate $K_{\mathrm{A}}(T)$ for a given c by solving the quadratic equation:

$$\alpha(c)] = \frac{1}{2}\left\{ -\frac{Y(c)}{\nu_1\nu_2 K_{\mathrm{A}} c} + \left[\left(\frac{Y(c)}{\nu_1\nu_2 K_{\mathrm{A}} c} \right)^2 + \frac{4Y(c)}{\nu_1\nu_2 K_{\mathrm{A}} c} \right]^{1/2} \right\}. \tag{6.79}$$

Iteration is stopped when the average standard deviation $s(\Lambda)$ is minimal:

$$s(\Lambda) = \left(\frac{\sum_{n=1}^{N} (\Lambda_{n,\mathrm{exp}} - \Lambda_{n,\mathrm{cal}})^2}{N-1} \right)^{1/2}, \tag{6.80}$$

where N denotes the number of experimental points.

The above procedure enables to determine for different systems the values of Λ^0 which are comparable with those reported in the literature (Apelblat, 2011a-c; 2017) and represents the association of ions by the association constant K_A according to law of mass action. The constant K_A is an indirect indication of the existence of association of ions in electrolyte solutions but in the analysis of the experimental conductivity data K_A is an adjustable parameter.

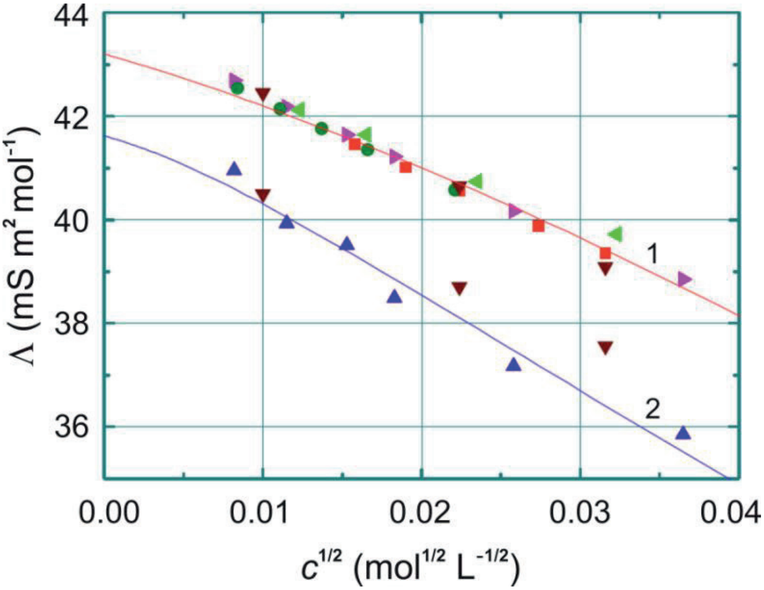

Figure 6.21. Dependence of experimental data of molar conductivity Λ of aqueous solutions of (1) lanthanum chloride and (2) lanthanum nitrate at 298.15 K on $c^{1/2}$. Continuous lines represent the data according to the Quint–Viallard equation. Different symbols of the electrolytes denote data from various sources. Adapted from Apelblat (2011b).

Quint–Viallard equation has been employed to interpret the experimental data of molar conductivity Λ of various symmetrical and asymmetrical electrolytes as functions of electrolyte concentration, solution temperature and solvent composition. Figure 6.21 shows the dependence of experimental data of molar conductivity $\Lambda(c,x)$ of aqueous solutions of two 3:1 electrolytes, lanthanum chloride and lanthanum nitrate, at 298.15 K on $c^{1/2}$, whereas continuous lines represent the data according to the Quint–Viallard equation. As seen from the figure, the Quint–Viallard equation represents the experimental data satisfactorily in the entire concentration range. Figure 6.22 shows another example of satisfactory description of the experimental data of the concentration dependence of molar conductivity $\Lambda(c,x)$ of magnesium sulfate, a 2:2 electrolyte, in water–1,4-dioxane mixtures containing different 1,4-dioxane content x at 298.15 K. The figure presents plots of the experimental $\Lambda(c,x)$ data obtained in solvent mixtures of different compositions x on $c^{1/2}$ and the best fit of the data by continuous lines according to the Quint–Viallard equation. Adequate description of the experimental data for this 2:2 electrolyte in different compositions of the solvent mixtures by the Quint–Viallard equation is evident.

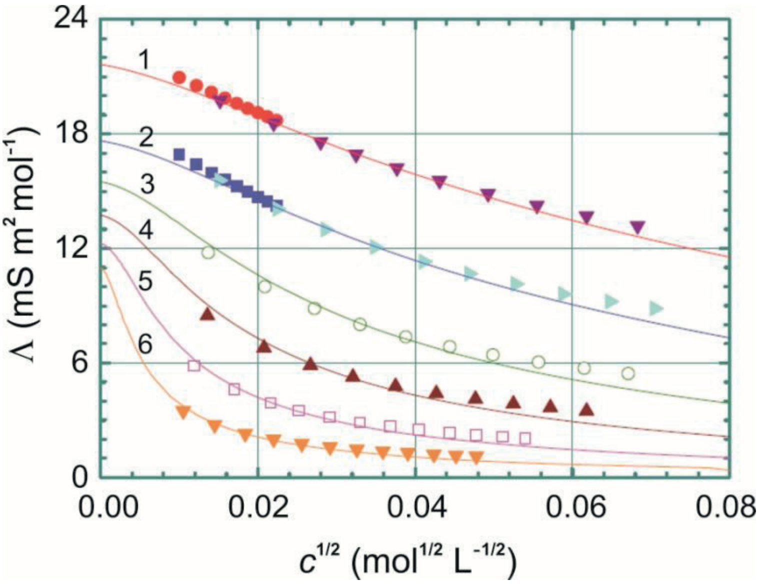

Figure 6.22. Plots of experimental molar conductivity Λ of magnesium sulfate in different water–1,4-dioxane mixtures containing different 1,4-dioxane content x in wt% as a function of $c^{1/2}$ and the best fit of the data by continuous lines according to the Quint–Viallard equation. 1,4-dioxane content x: (1) 0.0222, (2) 0.0486, (3) 0.0806, (4) 0.1072, (5) 0.1384, and (6) 0.1698. Different symbols denote data from various sources. Adapted from Apelblat (2011c).

Although Quint–Viallard model provides adequate description of the molar conductivity of various electrolytes in individual solvents and different solvent mixtures, for some systems the agreement between the measured and predicted conductivities in the plots of Λ against $c^{1/2}$ is observed only at low concentrations c. Examples of this behavior are aqueous solutions of sodium and potassium formates at different temperatures (Bončina et al., 2010), aqueous solutions of various alkali metal sulfates at different temperatures (Apelblat, 2017), strontium chloride solutions in water–ethanol mixtures containing increasing ethanol content x (Apelblat, 2011c), and aqueous solutions, *inter alia*, of various polyvalent electrolytes like potassium hexacyanoferrate (II) ($K_4[Fe(CN)_6]$), sodium tripolyphosphate ($Na_5P_3O_{10}$), sodium tetrametaphosphate ($Na_4P_4O_{12}$) and tris-triethylenetetramine-cobalt(III) chloride (Apelblat, 2011b). At higher concentrations the experimental conductivities in these cases are always higher than those predicted by the Quint–Viallard model and the deviation increases with increasing electrolyte concentration *c*. This means that experimental molar conductivities in these systems do not follow the behavior of true electrolytes.

In the case of formates, the disagreement between experimental and theoretically predicted conductivities is enormous at 278.15 K but vanishes at higher temperatures. In the $SrCl_3$ solutions, the Quint–Viallard model satisfactorily represents the experimental conductivity data in water–ethanol mixture with ethanol content $x = 0.02$ mole fraction for *c* below about 0.02 mol·L^{-1} but the concentration range of the applicability of the model decreases with increasing ethanol content *x* and is merely about 0.0025 mol·L^{-1} in the mixture of $x = 0.7789$ mole fraction. These observations mean that experimental molar conductivities in these systems do not follow the behavior of true electrolytes.

Ion association is already included in the Quint–Viallard equation used above for the analysis of the experimental conductivity data considering the salts in their solutions as true electrolytes. However, the experimental conductivity data at not sufficiently dilute solutions used in the analysis of concentration dependence of molar conductivities by the Quint–Viallard model are the limitation here. This limitation of the data leads to imprecise assessment of the role of ion association in the solution by this model. Apart from this limitation, the deviation in the experimental conductivity from the predictions of the Quint–Viallard model at high concentrations may also be due to some other reason. One of the explanations to account for the deviation in the measured and calculated conductivities in the entire concentration range is based on the hydrolysis of cations and anions resulting from the dissociation of salts dissolved in water and its mixtures with other solvents such as alcohols and dioxane of lower dielectric constant. In the case of aqueous sodium and potassium formate solutions, Bončina et al. (2010) considered the hydrolysis of dissociated $HCOO^-$ ions to form HCOOH and OH^-, which enables to rewrite the Quint–Viallard equation for the 1:1 electrolyte (AB) in the form

$$\Lambda = \alpha\Lambda_1 + (1-\alpha)\Lambda_2 + \beta\Lambda_3, \tag{6.81}$$

where the three contributions are:

$$\Lambda_1 = \lambda_1(\mathrm{Me}^+) + \lambda_2(\mathrm{An}^-), \tag{6.82}$$

$$\Lambda_2 = \lambda_1(\mathrm{Me}^+) + \lambda_2(\mathrm{OH}^-), \tag{6.83}$$

$$\Lambda_3 = \lambda_1(\mathrm{H}^+) + \lambda_2(\mathrm{OH}^-). \tag{6.84}$$

and the individual ionic contributions are given by

$$\lambda_i = \lambda_i^0 - S_i[c(1+\beta)]^{1/2} + E_i c(1+\beta)\ln[c(1+\beta)] + J_{1i}c(1+\beta) + J_{2i}[c(1+\beta)]^{3/2}, \tag{6.85}$$

with β as the fraction of H^+ ions. In Eq. (6.81) the first two terms come from ion-pair formation and the third term from the hydrolysis process. From an analysis of their conductivity data of aqueous HCOONa and HCOOK solutions, the authors concluded that ion pairs mainly contribute to the conductivity in HCOOK solutions but the relative contributions of the two processes remain unsettled.

6.7.2.2. Dependence of association constant K_A on temperature and solvent-mixture composition

The association constant K_A, or the dissociation constant $K_\mathrm{eq} = K_\mathrm{A}^{-1}$, in the above approach is considered as a fitting parameter because its value used in the analysis is usually not compared with that expected directly from chemical equilibria. However, it is observed that, with an increase in solution temperature T, the value of K_A determined by analysis of the conductivity data by the Quint−Viallard model increases for some electrolyte−solvent systems and decreases for others. Examples of the former are: aqueous solutions of formic acid (Bončina et al., 2010), oxalic acid (Bešter-Rogač et al., 2002), 1:2 electrolytes like lithium, rubidium and cesium sulfates (Apelblat, 2017), 2:2 electrolytes like alkaline-earth and transition metal sulfates (Apelblat, 2011a), and 3:2 electrolytes like hexaaminecobalt and tris-ethylenediaminecobalt sulfates (Apelblat, 2011b), whereas that of the latter are: aqueous solutions of ascorbic acid (Apelblat et al., 2006) and 3:1-type electrolytes like hexaaminecobalt and tris-ethylenediaminecobalt halides, perchlorides, nitrates and sulfates (Apelblat, 2011b). Analysis of the conductivity data of dilute solutions of KBr in water−2-butanol mixtures of fixed alcohol content by the Lee−Wheaton model also revealed that the values of K_A increases with increasing temperature for this 1:1 electrolyte (Sokol et al., 2006).

Analysis of the conductivity data of different symmetrical and asymmetrical electrolytes in water−ethanol, water−2-butanol and water−dioxane mixtures containing different content of the second solvent of low dielectric constant ε using the Quint−Viallard model shows that the value of the association constant K_A at a given temperature increases and that of limiting conductivity Λ^0 decreases with an increase in the content x of the second solvent in the mixture (Apelblat et al., 2011c). Since the dielectric constant ε of the above solvent mixtures decreases with increasing content of the second solvent, the above observations may be attributed to the effect of ε of the solvent mixture. Analysis of the conductivity data of dilute solutions of KBr in water−2-butanol mixtures containing different alcohol content by the Lee−Wheaton model also revealed a similar behavior of the values of K_A and Λ^0 for this 1:1 electrolyte at different fixed temperatures (Sokol et al., 2006).

In the theory of electrolyte solutions, the value of association constant K_A is a measure of ion-pair formation. The higher the value of K_A, the more extensive is the ion-pair formation. If it is assumed that the values of K_A obtained from the conductivity data for different systems indeed represent ion-pair formation anticipated from the theory of electrolyte solutions, its relationship with experimental parameters and thermodynamic processes may be discussed.

Depending on the assumption whether the contact distance r between free ions is less than q or equal to a, for ion-pair formation there are two approaches due to Bjerrum and Fuoss (see Bockris and Reddy, 1970). According to the Bjerrum theory, the ion-association constant is given by

$$K_A = \frac{Z_1}{Z_2} \varepsilon T \exp\left(\frac{Z_2}{\varepsilon T}\right), \tag{6.86}$$

whereas the Fuoss approach gives

$$K_A = \frac{Z_1}{3} \exp\left(\frac{Z_2}{\varepsilon T}\right), \tag{6.87}$$

where $Z_1 = 4\pi N_A a^3/1000$, and $Z_2 = |z_1 z_2 e^2|/a k_B$. When $Z_2/\varepsilon T << 1$, Eq. (6.86) reduces to

$$K_A = \frac{Z_1}{Z_2} \varepsilon T + Z_1 . \tag{6.88}$$

The above equations predict that K_A is a function of both ε and T, but they predict different trends. Eq. (6.86) predicts an initial increase in K_A followed by a rapid decrease with increasing ε and T when the exponential term dominates the εT term. According to this relation, a linear decrease in K_A with increasing ε and T is expected when $Z_2/\varepsilon T << 1$ (see Eq. (6.88)). However, Eq. (6.87) predicts that a linear decrease in $\ln K_A$ with increasing ε^{-1} and T^{-1} (i.e. with decreasing ε and T, respectively). The observed dependences of K_A on ε and T may be understood along the above lines.

The association constant K_A of ions in an electrolyte–solvent system is associated with cation–anion interactions in the medium. The main physical quantity that determines the strength of ion–solvent interactions is the polarizability μ of solvent molecules. Therefore, one may argue that an increase in the strength of ion–ion interaction and a decrease in the strength of ion–solvent interactions are a result of decreasing polarizability μ of the solvent molecules and their dipolar polarizability μ^2. It was indeed reported (Płowaś et al., 2014) that the association constant K_A of K^+ and I^- ions in solvents of different dipolar polarizabilities decreases with an increase in μ_i^2 and follows the relation: $K_A \propto \exp(-\mu_i^2)$, where μ_i is the dipole moment of the ith solvent.

If ion-pair formation is considered as a thermodynamic process involving standard enthalpy ΔH^o, Eq. (6.87) may be written as

$$\ln K_A = -\frac{\Delta H^o}{R_G T} + C , \tag{6.89}$$

where ΔH^o is assumed to be independent of temperature, and C is a constant. Since the Gibbs energy of the reaction

$$\Delta G^o = R_G T \ln K_A , \tag{6.90}$$

the standard entropy of ion-pair formation, ΔS^{o}, may be estimated as

$$\Delta S^{\text{o}} = \frac{\Delta H^{\text{o}} - \Delta G^{\text{o}}}{T} \,. \tag{6.91}$$

It has been reported (Sokol et al., 2006) that the value of ΔS^{o} increases with an increase in the content of the second solvent.

Analysis of the conductivity data of dilute aqueous solutions of small as well as large quaternary amonium iodides, with cyclic and straight-chain cations, at 298.15 K with the Fuss–Hsia and Pitts equations shows that these salts form ion pairs and that the limiting molar conductivities of the salts depend primarily on the size rather than the shape of the cation (Lowe and Rendall, 1972; Lowe et al., 1973). It was also found that the product $\lambda_1^0(\Phi_1^0)^{2/3}$, with Φ_1^0 as the limiting apparent molar volume, for the cations of different salts is practically constant. Since Φ_1^0 is related to the density d_0 of the solvent, one may also anticipate a similar relationship between λ_1^0 and d_0.

Since a change in solution temperature during the movement of ions involves thermal expansion of the solvent, the Eyring theory of transition state is usually applied to describe the temperature dependence of limiting conductivities in the form (Brummer and Hills, 1961)

$$\frac{\partial \ln[\lambda^0(T) d_0^{2/3}(T)]}{\partial T} = \frac{\Delta H^{\#}}{R_{\text{G}} T^2} \,, \tag{6.92}$$

where d_0 is the density of the solvent and $\Delta H^{\#}$ is the partial molar enthalpy of activation associated with ionic transport. When $\Delta H^{\#}$ is temperature independent, integration of (6.92) gives

$$\ln[\lambda^0(T) d_0^{2/3}(T)] = -\frac{\Delta H^{\#}}{R_{\text{G}} T} + C' \,, \tag{6.93}$$

where C' is an integration constant. The values of limiting conductivities of ions are obtained by applying the Onsager equation together with the Kohlrausch law of independent migration of ions at infinite dilution. The validity of Eq. (6.93) has been reported in various studies (Apelblat et al., 2006, 2008; Bončina et al., 2010; Bešter-Rogač et al., 2002). The value of $\Delta H^{\#}$ for the movement of anions like formate, acetate, oxalate, ascorbate and aspartate has been found to lie between 14.4 and 16. 9 kJ·mol^{-1}.

6.7.2.3. Universal curves of limiting conductivities of electrolytes in solvent mixtures

A discussed above, investigations of electrical conductivities of various electrolytes in mixed solvent mixtures provide important information about ion–ion and ion–solvent interactions in solutions when changes in composition of the mixture result in changes in its dielectric constant ε and viscosity $\eta(x,T)$. The mixture composition is usually expressed by the mole fraction x or the weight fraction w of one of its components. Analysis of the experimental data of conductivity $\Lambda(c,T)$ of an electrolyte at a given composition x of the mixture using the Onsager limiting equation involves four parameters: the limiting conductivity $\Lambda^0(x,T)$, the association constant $K_\mathrm{A}(x,T)$, the ion-size parameter $a(x,T)$, and the Walden product $\Lambda^0(x,T)\eta(x,T)$. Therefore, difference in the behavior of various electrolytes in solvent mixtures involving changes is due to changes in the physical properties of solvents and the nature of ions composing electrolyte molecules.

Electrical conductivities of various symmetrical and unsymmetrical electrolytes of different types in a variety of solvent mixtures have been analyzed using different conductivity equations and values of limiting conductivities $\Lambda^0(x,T)$ of the electrolytes have been reported. Using the correctly determined values of $\Lambda^0(x)$ for different electrolytes at 298.15 K, Apelblat (2008,2009,2011c) found that there exists one universal curve of the dependence of Λ^0 of different electrolytes, irrespective of their type, on the composition x of a particular solvent–cosolvent mixture in the solvent-rich region for any type of electrolyte.

The existence of a unique universal $\Lambda^0(x)$ curves for different electrolytes in a solvent mixture is based on the following concepts (Apelblat, 2008,2009,2011c):

(1) In the solvent-rich region with $x = 0$ and 1, the limiting conductivities $\Lambda_i^0(x,T)$ of different electrolytes, where the subscript i denotes a particular electrolyte i, follows the relations

$$\frac{\Lambda_i^0(x,T)}{\Lambda_j^0(x,T)} = \frac{\Lambda_i^0(0,T)}{\Lambda_j^0(0,T)} = \text{constant} , \tag{6.94}$$

and

$$\frac{\Lambda_i^0(x,T)}{\Lambda_j^0(x,T)} = \frac{\Lambda_i^0(1,T)}{\Lambda_j^0(1,T)} = \text{constant} , \tag{6.95}$$

where j denotes another electrolyte. Since $\Lambda_i^0(0,T) \neq \Lambda_i^0(1,T)$ and $\Lambda_j^0(0,T) \neq \Lambda_j^0(1,T)$, the constants are not equal in the above relations. In the case where one solvent has a very low ε, one of the above relations covers the entire mixture composition range. Thus, for the solvent-rich regions of a particular solvent mixture, it is sufficient to determine the limiting conductivities of only one electrolyte because the conductivities of other electrolytes can be calculated from the above equations. The choice of this reference electrolyte, referred to as *the standard electrolyte*, is arbitrary but an electrolyte with many accurate conductivity measurements over a wide concentration range is selected as standard. If $\Lambda_j^0(x,T)$ denotes the limiting conductivities of the standard electrolyte, the curve $\Lambda_j^0(x,T) = f(x,T)$ represents the *universal curve of limiting conductivities* of electrolytes in the mixed-solvent system.

(2) As in the case of the universal curve of limiting conductivities of electrolytes, the above procedure can be extended to obtain *the universal curve of limiting*

conductivities λ_i *of ions* where Λ_i and Λ_j are replaced by λ_i and λ_i, respectively. The accuracy of the universal curve here also depends on factors, such as measurement uncertainties, solvent purity, and conductivity equation chosen for data analysis, associated with the accuracy in the values of limiting conductivities of different electrolytes.

(3) The mathematical equation used to represent the conductivity data of electrolytes in a mixed-solvent system should be simple and with a small number of parameters. One equation representing the limiting conductivity data of the standard electrolyte AB with reasonable accuracy is the following two-parameter equation

$$\Lambda^0_{\mathrm{AB}}(x,T) = \Lambda^0_{\mathrm{AB}}(0,T) + Zx^{\delta}(1-x^{\delta})\,, \tag{6.96}$$

where Z and δ are the parameters characteristic of a system, and $0 \le x \le 1$. Similar equations are used for ionic conductivities λ^0_{A} and λ^0_{B}.

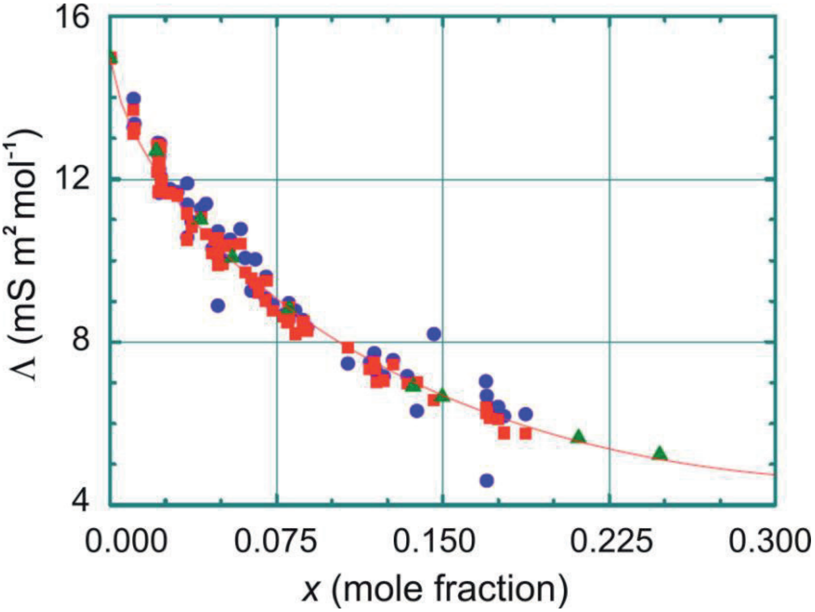

Figure 6.23. Example of plot of limiting molar conductivities $\Lambda^0(x)$ at 298.15 K of various symmetrical and unsymmetrical electrolytes as a function of mole fraction x of 1,4-dioxane in water–1,4-dioxane mixtures. Values of $\Lambda^0(x)$ for other electrolytes are shifted according Eq. (6.94). Universal curve is drawn for KCl as the standard electrolyte with using Eq. (6.96). Electrolytes are: KCl, $MgSO_4$, $MnSO_4$, $CuSO_4$, $ZnSO_4$, La[Fe(CN)$_6$], La[Co(CN)$_6$], MnBDS, [Co(NH$_3$)$_5$NO$_2$]SO$_4$, [Cu(en)$_2$]X$_2$ and [Ni(en)$_2$]X$_2$, with X = Cl, Br, I. Adapted from Apelblat (2011c).

Using the above approach, simple 1:1 as well as various symmetrical and unsymmetrical electrolytes in different solvent mixtures have been analyzed

(Apelblat, 2008, 2009, 2011c). Figure 6.23 shows an example of plot of limiting molar conductivities $\Lambda^0(x)$ at 298.15 K of various symmetrical and unsymmetrical electrolytes as a function of mole fraction x of 1,4-dioxane in water–1,4-dioxane mixtures and the universal curve is drawn for KCl as the standard electrolyte using Eq. (6.96) with the parameters: Λ^0_{AB} = 14.974 mS·m^2·mol^{-1}, Z = 41.50 mS·m^2·mol^{-1} and δ = 0.6798 (Apelblat, 2011c). The values of $\Lambda^0(x)$ for other electrolytes are shifted according Eq. (6.94). The data represent the electrolytes: KCl, $MgSO_4$, $MnSO_4$, $CuSO_4$, $ZnSO_4$, La[Fe(CN)$_6$], La[Co(CN)$_6$], MnBDS, [Co(NH$_3$)$_5$NO$_2$]SO$_4$, [Cu(en)$_2$]X$_2$ and [Ni(en)$_2$]X$_2$, with X = Cl, Br, I. Obviously, one universal curve of limiting conductivities exists for these mixed solvent systems.

In the above water–1,4-dioxane mixtures their dielectric constant has a wide range but the change in their viscosity is not large. Water–ethanol and water–methanol mixtures also show a similar behavior. However, there are solvent mixtures which are characterized by a large change in viscosity (0.543 mPa·s ≤ η ≤ 17 mPa·s) and a narrow change in their dielectric constant ($32.62 \le \varepsilon \le 40.8$). An example is methanol–ethylene glycol mixtures. These systems also follow universal curves of limiting conductivities, but the values of the parameters of Eq. (6.96) are much higher than those for water–1,4-dioxane and water–ethanol mixtures. For the standard electrolyte Ni(ClO$_4$)$_2$ in the methanol–ethylene glycol (1,2-ethanediol) mixtures at 285.15 K for example, Λ^0_{AB} = 26.3 mS·m^2·mol^{-1}, Z = 78.9 mS·m^2·mol^{-1} and δ = 1.035 (Apelblat, 2011c).

Universal curves of limiting conductivities of ions are established by taking into account the values of $\lambda^0(\mathrm{Cl}^-,x)$ and $\lambda^0(\mathrm{K}^+, x)$ and the Kohlrausch law (see Eqs. (6.9) and (6.45))

$$\Lambda^0_{\mathrm{eq}}(\mathrm{A}^{z_1+},\mathrm{B}^{z_2-},x) = \lambda^0(1/z_{1+},\mathrm{A}^{z_1+},x) + \lambda^0(1/z_{2-},\mathrm{B}^{z_2-},x)\,. \tag{6.97}$$

This procedure enables to estimate the values of limiting conductivities of ions of polyvalent electrolytes. The importance of this approach lies in the fact that it is difficult to know the values of conductivities of ions of these polyvalent electrolytes due to lack of information of their transference numbers.

Finally, it should be mentioned that the values of the parameters Z and δ of various electrolytes in different binary solvent mixture are intimately connected with changes in the viscosity of the mixture. High values of Z and δ for the electrolytes are observed solvent mixtures involving high changes in their viscosities. This behavior of binary solvent mixtures is related to the nature of interactions in the mixtures and is reflected by variations in the Walden product. This aspect is discussed in Section 6.8.

6.7.3. Conductivities and dissociation constants of potential electrolytes

Various simple and complex organic acids, which find many applications in industrial, geological, biological and bichemical systems, behave as potential (or weak) electrolytes and are characterized by a steep decrease in molar conductivity Λ

with increasing $c^{1/2}$ in extremely dilute aqueous solutions. Some examples of these electrolytes are: formic acid (Bončina et al., 2010), acetic acid (MacInnes and Shedlovsky, 1932; Zimmerman and Wood, 2002), oxalic acid (Bešter-Rogač et al., 2002), ascorbic acid (Apelblat et al., 2006) and aspartic acid (Apelblat et al., 2008). Figure 6.24 shows, as an example, the dependence of molar conductivities Λ of aqueous formic acid solutions at 298.15 K as a function of $c^{1/2}$. Solid line in the figure represents the best fit of the Quint–Viallard model.

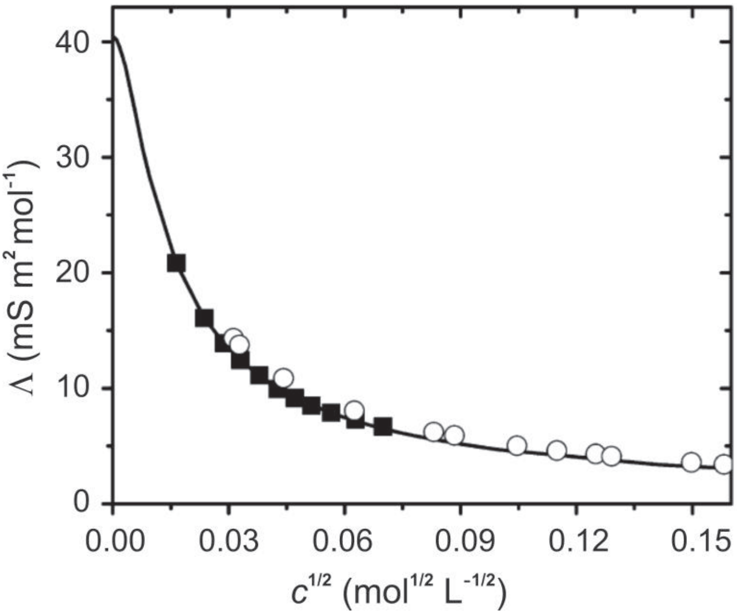

Figure 6.24. Molar conductivities of aqueous formic acid solutions as a function of $c^{1/2}$ at 298.15 K. Data are from two different sources. Solid line represents the best fit of the Quint–Viallard model using Eqs. (6.74) to (6.78), and (6.98) to (6.100). Adapted from Bončina et al. (2010).

In the analysis the following dissociation reaction was considered (also see: Sections 6.3 and 6.7.2):

$$\mathrm{AB} \rightarrow \mathrm{A}^+ + \mathrm{B}^-, \tag{6.98}$$

with A^+ and B^- as the dissociated cation H^+ and anion HCOO^- involving the dissociation constant

$$K = \frac{[\mathrm{A}^+][\mathrm{B}^-]}{[\mathrm{AB}]}Y = \frac{c^2\alpha^2}{c(1-\alpha)}Y, \tag{6.99}$$

where α is the degree of dissociation of the electrolyte AB of concentration c and the quotient Y of the activity coefficients of the ions in dilute solution is approximated by the Debye–Hückel equation (see Eq. (6.77)) and the molar conductivity Λ is given by Eq. (6.75) with the values of conductivities λ_1 and λ_2 of H^+ and $HCOO^-$ determined independently. The degree of dissociation α is evaluated in an iteration process using the quadratic equation (Bončina et al., 2010)

$$\alpha = \frac{1}{2}\left\{ -\frac{K}{cY} + \left[\left(\frac{K}{cY} \right)^2 + \frac{4K}{cY} \right]^{1/2} \right\}. \tag{6.100}$$

The iteration process is started by setting the dissociation constant K as a variable. Since accurately determined value of λ_2^0 of the anion at infinite dilution is required in the iteration process, this value is obtained independently from analysis of conductivity data of its salts at infinite dilution.

As in the case of association constant K_A of ion-pair formation (see Section 6.7.2.2), the dissociation constant K is also temperature dependent and is described by thermodynamic functions similar to those represented by Eqs. (6.89) to (6.91). It was observed (Bončina et al., 2010) that the value of their Gibbs energy for dissociation, $\Delta G^o(T) = -R_G T \ln K(T)$, of simple carboxylic acids involving a single dissociation constant increases linearly with temperature and that $T\Delta S^o(T) >> \Delta H^o(T)$, implying that $\Delta G^o(T) \approx -T\Delta S^o(T)$. This indicates that the dissociation process in these potential electrolytes is mainly controlled by the entropy term.

Finally, it should be mentioned that in the case of di- and tribasic acids one has to take into consideration two and three dissociation constants. Conseqently, the iteration process involves expressions containing succesive partial degrees of dissociation of the acid representing primary, secondary and tertiary steps of dissociations (for example, see Bešter-Rogač et al., 2002, and the literature cited therein).

6.7.4. Low-temperature ionic liquids mixed with water and other solvents

The behavior of conductivities of mixtures of low-temperature ILs with water and other organic solvents has features somewhat different from those of mixtures of common true electrolytes with various solvents. One of the distinct differences lies in the much wider composition range, $0 < x < 1$, of the ILs in their mixtures than those of the common electrolytes, usually restricted up to their solubility limit, in the mixtures of the same solvents. Moreover, as shown by Weingartner et al. (2000), in associating ionic liquids the minimum degree of their dissociation results in molar conductivity which can be treated as the measurement of the ionic density of a liquid.

Figure 6.25 shows typical examples of the dependence of molar conductivity Λ of aqueous solutions of six ILs at 298.15 K on their molar concentration c. The original data are taken from Vila et al. (2006a). The three ILs in Figure 6.25a, i.e. [emim][$AlBr_4$], [empyr][$AlBr_4$] and [emim][ESO_4], are of stochiometric composition in their cation–anion ratio, and the curves represent the best fit of the data according to the exponential relation

$$\Lambda = C + \Lambda^0 \exp\left[-\left(\frac{c}{c^*} \right)^n \right], \tag{6.101}$$

where C, Λ^0, c^* and n are empirical constants listed in Table 6.5. However, in Figure 6.25b [emim][AlCl$_4$] and [emim][BF$_4$] are of stoichiometric composition and [emim][Br]-AlBr$_3$ mixed with x_a(AlBr$_3$) = 0.60 is of nonstoichiometric composition. It may be seen that the $\Lambda(c)$ data for the stoichiometric ILs of Figure 6.25a follow Eq. (6.101) practically in the entire composition range, but the data for both stoichiometric [emim][BF$_4$] and [emim][AlCl$_4$] in Figure 6.25b appear to follow this relation only up to about 3 mol·L^{-1}. In contrast to the above stoichiometric ILs, the $\Lambda(c)$ data for the only nonstochiometric IL appears to follow in a very low composition range ($c < 1.5$ mol·L^{-1}).

Figure 6.26 shows some more examples of the experimental data of molar conductivity Λ of solutions of three ILs in GBL at 298.15 K as functions of their mole fraction x. The original data for [bmim][DCA] are from Zec et al. (2016), from [bmim][NTf$_2$] from Vraneš et al. (2014), and for [bmpyr][NTf$_2$] from Vraneš et al. (2015). As in Figure 6.25a, these $\Lambda(x)$ data may also be represented by Eq. (6.101), with the values of the constants included in Table 6.5.

It may be noted that stoichiometric composition of an IL results in the concentration dependence of its molar conductivity Λ in a solvent according to Eq. (6.101) practically in its entire composition range (Figures 6.25a and 6.26) but this exponential decrease in the entire composition range is not observed in ILs of nonstoichiometric chemical composition as well as in ILs containing some of the anions in its chemical constitution (Figures 6.25b). The value of Λ^0 of an IL corresponding to infinite dilution depends on the chemical nature of the cation as well as the anion of the IL. For example, in GBL the value of Λ^0 of [bmim][DCA] is higher than that of [bmim][NTf$_2$], and that of [bmpyr][NTf$_2$] is higher than that of [bmim][NTf$_2$]. Similarly, in water the value of Λ^0 of [empyr][AlBr$_4$] is higher than that of [emim][AlBr$_4$], but that of [emim][ESO$_4$] is higher than that of [emim][AlBr$_4$]. In fact, the conductivity behavior of [emim][ESO$_4$] in water at low concentrations c is somewhat similar to that potential electrolytes. Generally, the values of Λ^0 of [emim]-based ILs are higher than those of [bmim]-based ILs. These observations are associated with the ionic conductivities of the cations and anions composing the ILs. However, as seen from the estimated values of Λ^0 for [emim][ESO$_4$], these values should be taken with caution because of the empirical nature of Eq. (6.101) and the interdependence of its parameters.

Using Walden's rule (i.e. $\Lambda\eta = K$, with constant K) and the dependence of the viscosity η of water–IL mixture on IL content x_IL, following Vila et al. (2006a), we may write

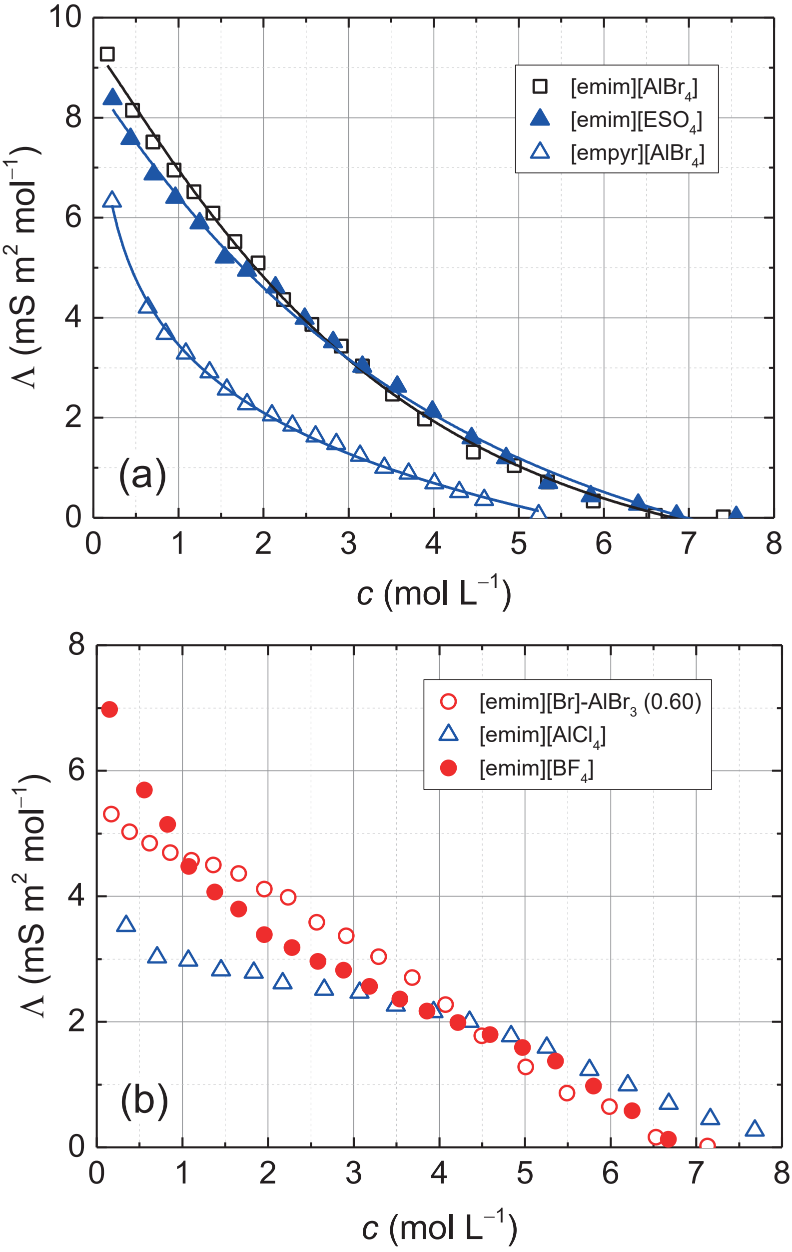

Figure 6.25. Dependence of molar conductivity Λ □of aqueous solutions of six ILs at 298.15 K on their molar concentration *c*: (a) [emim][AlBr$_4$], [empyr][AlBr$_4$] and [emim][ESO$_4$], and (b) [emim][Br]-AlBr$_3$ with x_a(AlBr$_3$) = 0.60, [emim][AlCl$_4$] and [emim][BF$_4$]. Original data from Vila et al. (2006a).

Table 6.5. Constants of Eq. (6.101) for different IL–solvent systems

System	Data	Figure	$-C$ ($\mathrm{mS \cdot m^2 \cdot mol^{-1}}$)	Λ_0 ($\mathrm{mS \cdot m^2 \cdot mol^{-1}}$)	c^*, x^*	n	R^2
[emim][$AlBr_4$]–water	$\Lambda(c)$	6.25a	1.124	10.542	3.299 $\mathrm{mol \cdot L^{-1}}$	1.110	0.9977
[empyr][$AlBr_4$]–water	$\Lambda(c)$	6.25a	1.889	10.628	4.043 $\mathrm{mol \cdot L^{-1}}$	1.003	0.9982
[emim][ESO_4]–water	$\Lambda(c)$	6.25a	27.64	53.14	221.7 $\mathrm{mol \cdot L^{-1}}$	0.116	0.9965
[bmim][DCA]–GBL	$\Lambda(x)$	6.26	–	10.886	0.0832 mol frac.	0.634	0.9999
[bmim][NTf_2]–GBL	$\Lambda(x)$	6.26	–	2.782	0.1744 mole frac.	0.789	0.9962
[bmpyr][NTf_2]–GBL	$\Lambda(x)$	6.26	–	3.273	0.1332 mole frac.	0.684	0.9996

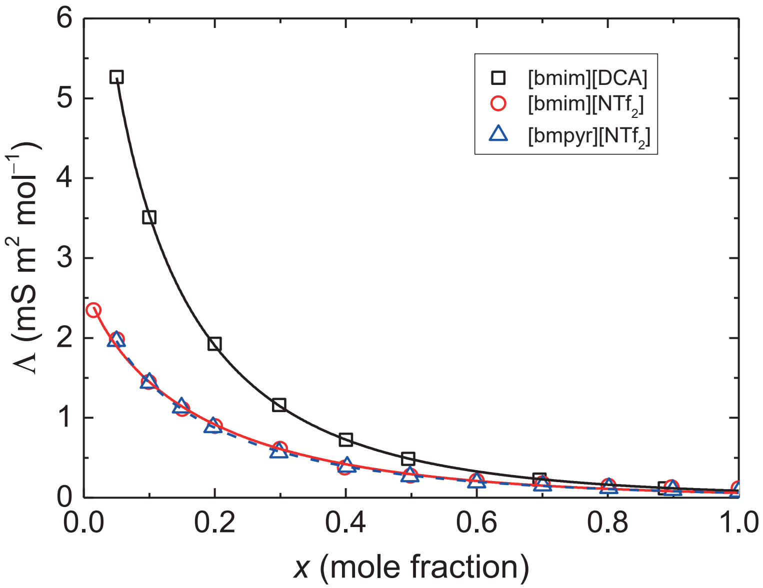

Figure 6.26. Dependence of molar conductivity Λ of solutions of three ILs in GBL at 298.15 K on their molar concentration c. Original data for [bmim][DCA] from Zec et al. (2016), [bmim][NTf_2] from Vraneš et al. (2014), and [bmpyr][NTf_2] from Vraneš et al. (2015).

$$\Lambda = \frac{K}{\eta} = K^* \exp\left[-\left(\frac{x_{\mathrm{IL}}}{x^*}\right)\right], \tag{6.102}$$

where K^* and x^* are constants. The form of this equation is similar to that of Eq. (6.101). Taking water content x_{CS} in the mixture instead of $-x_{\mathrm{IL}}$, Vila et al. (2006a) analyzed the data for aqueous [emim][$AlBr_4$] and [emim][ESO_4] solutions using Eq. (6.102) and observed a poor fit. The authors attributed this behavior due to nonvalidity of Walden's rule for these systems. However, they made an attempt to interpret their data of the dependence of specific conductivity σ on x_{CS} of selected water–IL mixtures in the framework of the conventional hole theory and derived the relation

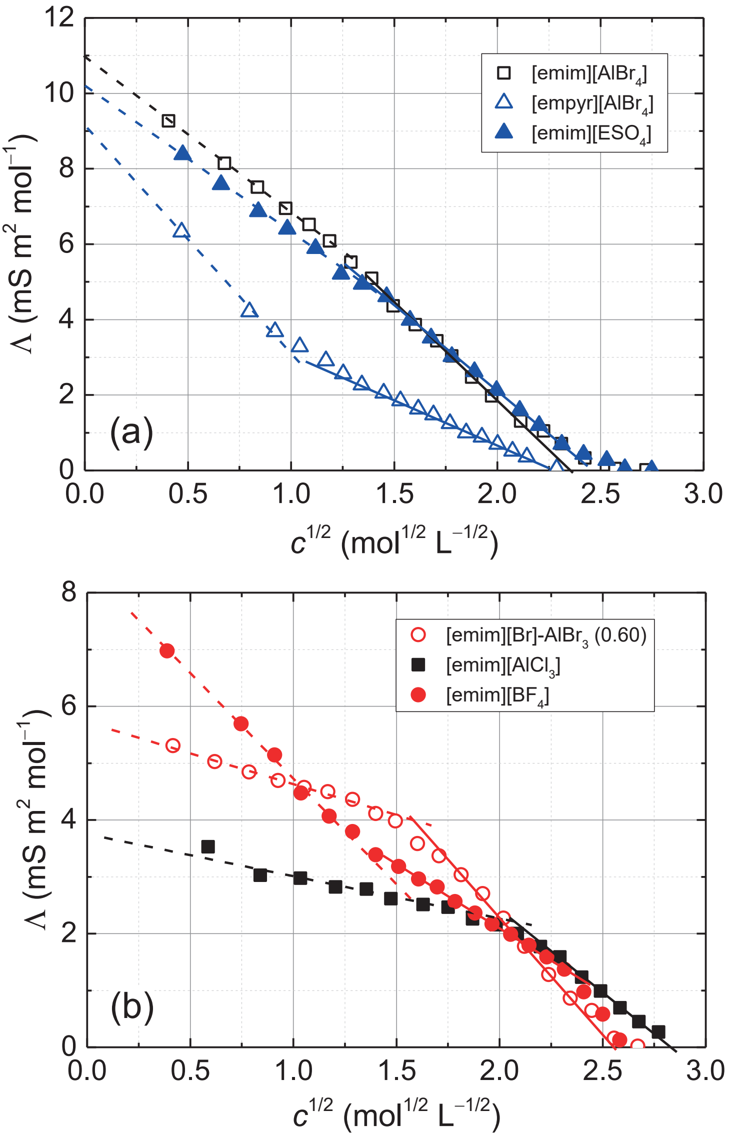

Figure 6.27. Dependence of Λ of aqueous solutions of six ILs at 298.15 K on $c^{1/2}$: (a) [emim][AlBr$_4$], [empyr][AlBr$_4$] and [emim][ESO$_4$], and (b) [emim][Br]-AlBr$_3$ with x_a(AlBr$_3$) = 0.60, [emim][AlCl$_4$] and [emim][BF$_4$]. Original data from Vila et al. (2006a).

$$\sigma = \frac{\sigma_{\mathrm{IL}}}{(1 - K^{**} x_{\mathrm{CS}})^{1/2}}, \tag{6.103}$$

where K^{**} is a fitting parameter and σ_{IL} is the conductivity of the pure IL. It was observed that Eq. (6.103) explains the data for very low water content alone.

The experimental $\Lambda(c)$ data for the aqueous solutions of six ILs at 298.15 K, shown in Figure 6.25, were analyzed using the limiting law (6.45) in the entire concentration range. Figure 6.27 presents these data in the form of dependence of Λ on $c^{1/2}$, while straight lines represent the data in different concentration regions. From these figures the following features may be noted:

(1) The $\Lambda(c^{1/2})$ data for [emim][$AlBr_4$], [empyr][$AlBr_4$] and [emim][ESO_4] up to 6 mol·L^{-1} in Figure 6.27a, and for [emim][$AlCl_4$] up to 8 mol·L^{-1} and [emim][Br]-$AlBr_3$ with $x_a(AlBr_3) = 0.60$, [emim][BF_4] up to 6.5 mol·L^{-1} in Figure 6.27b may be represented by the linear dependence in two distinct concentration regions of different slope A_1.

(2) The values of the slopes A_1 of the linear dependences of the $\Lambda(c^{1/2})$ data for [emim][$AlBr_4$], [emim][ESO_4], [emim][$AlCl_4$] and [emim][Br]-$AlBr_3$ with $x_a(AlBr_3) = 0.60$ in the low c region are lower than those in the higher c region.

(3) The slopes A_1 of the $\Lambda(c^{1/2})$ data for [empyr][$AlBr_4$] in low and high c regions show an opposite trend. For this IL, the slope A_1 of the $\Lambda(c^{1/2})$ data for [empyr][$AlBr_4$] in the low c region is higher than those in the higher c region. The trend of the value of the slopes A_1 for [emim][BF_4] is somewhat similar to that for [empyr][$AlBr_4$] up to $c \approx 5$ mol·L^{-1}, but this IL shows an additional third, lower, slope A_1 in concentration region between 5 and 6.7 mol·L^{-1}.

Eq. (6.45) of the limiting law predicting a linear dependence of Λ on $c^{1/2}$ applies only in a narrow range of solute concentration (< 0.001 mol·L^{-1}). Therefore, one cannot attach too much importance to the above concentration regions of linear dependence. However, it is interesting to note that in the region of low IL concentrations the slopes of the $\Lambda(c^{1/2})$ plots are practically the same equal to about 4 for [emim][$AlBr_4$], [emim][ESO_4] and [emim][BF_4] solutions, and about 1.0 for [emim][Br]-$AlBr_3$ with $x_a(AlBr_3) = 0.60$ and [emim][$AlCl_4$] solutions. In the region of high IL concentrations, the slope A_1 is about 4.5 for [emim][$AlBr_4$], [emim][ESO_4], and [emim][Br]-$AlBr_3$ with $x_a(AlBr_3) = 0.60$ whereas it is about 2 for [empyr][$AlBr_4$] and [emim][$AlCl_4$] solutions. These trends suggest that nonstochiometry of an IL results in a slow change in Λ with IL concentration in low IL concentration region, but anions alone have insignificant effect on the value of slope A_1 in high IL concentration region.

Finally, it should be mentioned that two different $c^{1/2}$ regions of linear dependence of Λ on $c^{1/2}$ are not confined to the above IL systems. For example, in their study of the molar conductivity Λ of KI in DMSO for four temperatures between 293 and 323 K up to 1 mol·L^{-1} (i.e. $x = 0.0707$ mole fraction), Płowaś et al. (2014) reported two regions of high and low slopes in the plots of Λ against $c^{1/2}$ below and above $c^{1/2} = 0.16$ mol$^{1/2}$·L$^{-1/2}$ (i.e. $c \approx 0.025$ mol·L^{-1}). Using Fuoss–Onsager equation in conjunction with ionic association, the authors determined the limiting conductivities Λ^0 of the electrolyte and $\lambda_{1,2}{}^0$ of ions, and the association constant K_A of the electrolyte in the low concentration range at different temperatures. Vila et al. (2005) reported approximate linear dependence of equivalent conductivity Λ_{eq} of aqueous $AlCl_3$, $AlBr_3$, AlI_3 and $Al(NO_3)_3$ solutions at 298.15 K on $c^{1/2}$ at concentrations between 2 and 8 eq-mol·L^{-1} covering the concentration region where their specific conductivities σ show maxima. However, no explanation of the linear dependence of Λ on $c^{1/2}$ in high concentration interval was given in these works.

6.7.5. Temperature dependence of molar conductivity

The VTF relation (6.42) based on the free-volume theory equation, as applied by Angell and coworkers, is frequently used to explain the temperature dependence of molar or equivalent conductivity, assuming that $\sigma/\sigma_0 = \Lambda/\Lambda^0$. This relation has three parameters A, B and T_0, which are not related to intrinsic properties of the electrolyte itself, but to the configurational entropy content of the solvent in the solution and a glass transition temperature T_0 for the solution.

In contrast to the above approach, for $1 \ll \kappa a$ we write Eq. (6.53) as

$$\Lambda = \Lambda^0\left(1-\frac{B_1}{B_3 a\Lambda^0}\right)\left(1-\frac{B_2}{B_3 a}\right) \approx \Lambda^0 \exp\left[-\left(\frac{B_1+B_2\Lambda^0}{B_3 a\Lambda^0}\right)\right], \tag{6.104}$$

where the term in the square brackets may be written as (cf. Eqs. (6.54), (6.55) and (6.56))

$$\frac{B_1+B_2\Lambda^0}{B_3 a\Lambda^0} = \frac{0.8(|z_1|+|z_2|)}{\Lambda^0\eta a} + \frac{5\cdot 10^4\,|z_1 z_2|\,q}{(1+q^{1/2})a\varepsilon T}\,. \tag{6.105}$$

When $B_1 \ll B_2\Lambda^0$, Eq. (6.104) transforms to the Arrhenius-type equation

$$\Lambda = \Lambda^0 \exp\left(-\frac{E_\Lambda}{R_G T}\right), \tag{6.106}$$

with the activation energy E_Λ for conductivity given by

$$E_\Lambda = \frac{5\cdot 10^4\,|z_1 z_2|\,q}{(1+q^{1/2})a\varepsilon}\,. \tag{6.107}$$

Thus, Λ^0 and E_Λ depend on the intrinsic properties of the electrolyte and the solvent.

6.8. The Walden rule and its applicability

The temperature dependence of specific conductivity σ of true electrolytes is large involving a five- to six-fold increase from 0 to 100 °C. Since the specific conductivity σ and the molar conductivity Λ of an electrolyte are determined by the mobility u of ions in the solution (cf. Eq. (6.8)), the increasing mobility u of ions is intimately related to the increasing fluidity Φ, i.e decreasing viscosity η, of the solvent. It is found that the product $\Lambda^0\eta$ (where η is the viscosity of solvent) is either practically independent of temperature or the variation is only of the order of 30% over the temperature range 0 to 100 °C. The ions for which the product $\Lambda^0\eta$ is constant are those of large size, which may be due to their being polyatomic (acetic or substituted ammonium ions) or to extensive solvation (e.g. small ions). The monoatomic ions, such as K^+, Rb^+, Cl^-, Br^-, I^-, or polyatomic as ClO_4^- and NO_3^-, show a decreasing trend of $\Lambda^0\eta$ with increasing temperature.

It is often observed that for salts containing large-sized ions in various solvents the value of the product $\Lambda^0\eta$ = constant. The constancy of the product $\Lambda^0\eta$ is known as the Walden rule. Assuming that the ions of an electrolyte in the solution follow the Stokes formula (6.30), and using the relation between diffusion constant D_i and the conductivity λ_i of the ith ion according to the Nernst–Einstein law (for example, see: Bockris and Reddy, 1970; Robinson and Stokes, 1959)

$$\lambda_i = \frac{|z_i|eF}{k_B T} D_i , \tag{6.108}$$

one obtains

$$\Lambda T = \frac{eF}{6\pi}\left(\frac{T}{\eta}\right)^p \left(\frac{|z_1|}{r_1} + \frac{|z_2|}{r_2}\right). \tag{6.109}$$

where $\lambda_1+\lambda_2 = \Lambda$, F is the Faraday constant, the exponent p represents the general case, and r_i is the hydrodynamic radius of an ion of charge z_i and depends on the degree of solvation of the ion. When $p = 1$ and T is constant, from Eq. (6.109) one obtains the Walden rule. Depending on the solvation characteristics of the moving ions, the product $\Lambda\eta$ in the solution as well as the product $\Lambda^0\eta^0$ for the infinite dilution in a pure solvent may increase, decrease or remain constant.

The validity of the Walden rule is justified on the assumption that the radii r_1 and r_2 of ions of an electrolyte do not change with temperature. It is also assumed that the dielectric constant ε of the medium is equal to that of the pure solvent, and that there is no association of ions. The deviation of experiments data from the Walden rule is due to these factors.

Addition of a nonelectrolyte to an aqueous solution of an electrolyte leads to a reduction in the limiting mobility of ions as well as to an increase in the viscosity η of the solvent mixture. The effects of addition of different nonelectrolytes on the mobility of a given ion in the solvent mixture and its viscosity are not the same. Therefore, the extent of reduction in the ionic mobility usually does not occur in proportion with the extent of increase in the viscosity η of the solvent mixture. This behavior approximates to the relation (see Robinson and Stokes, 1959)

$$\Lambda^0 \eta^p = K , \tag{6.110}$$

where K is a constant and the lowest observed value of the exponent $p \approx 0.8$. The index *p* varies with both the ion and the solvent mixture. For a given ion, *p* is approximately a linear function of the molar volume *V* of the nonelectrolyte, decreasing as *V* increases, while for a given electrolyte *p* increases with the size of the ions, approaching unity for large ions.

In order to explain the effect of temperature on the Walden product a model, due to Smolyakov, involving migration of ions and molecules through the solution by a series of jumps from one equilibrium position requiring characteristic activation energies E_η and E_λ for viscous flow and ionic conductivity, respectively, has also been proposed in the form (see Horvath, 1985)

$$\lambda_i^0 \eta = A \exp\left(\frac{E_\eta - E_{\lambda_i}}{R_\mathrm{G} T} \right), \tag{6.111}$$

where A is a constant. It was found that in aqueous solutions the temperature coefficient of $\lambda_i^0 \eta$ is negative for structure-breaking ions like K^+, Rb^+, Cs^+, NH_4^+, Cl^-, Br^-, I^-, and ClO_4^-, but $\lambda_i^0 \eta$ is practically temperature independent for structure-making ions such as Li^+, Ba^{2+}, Ca^{2+}, Mg^{2+} and SO_4^{2-}.

In pure solvents the Walden product corresponds to the situation where ion–ion interactions do not play any role but interactions between ions and water molecules in its neighborhood are important. However, in binary mixtures, interactions between the molecules of the two solvents are present apart from interactions between two different solvent molecules. To account for this situation in a binary solvent mixture composed of second solvent of composition x a modified Walden rule has been proposed (Apelblat, 2008, 2011c):

$$\Lambda^0(x,T)\eta^\#(x,T) = \Lambda^0(x,T)[x\eta_2(T) + (1-x)\eta_1(T)], \tag{6.112}$$

where $\eta_1(T)$ and $\eta_2(T)$ are the viscosities of the pure solvents 1 and 2, respectively, at the temperature T, and the viscosity $\eta(x,T)$ of the mixture is taken as its ideal viscosity $\eta^\#(x,T)$, which is the sum of additive contributions of the viscosities of the pure solvents and is represented by the term in the square brackets. At a given temperature, $\eta(x,T)$ is a function of composition x of the cosolvent 2, and has curvatures either convex upward or concave downward. The so-called excess viscosity, defined by the difference $\eta^\mathrm{E}(x,T) = \eta(x,T) - \eta^\#(x,T)$, is a measure of solvent–solvent interactions due to replacement of molecules of solvent 1 by those of cosolvent in the mixture. Then from Eq. (6.112), the excess Walden product is defined as

$$\begin{aligned}\Lambda^0(x,T)\eta^\mathrm{E}(x,T) &= \Lambda^0(x,T)[\eta(x,T) - \eta\#(x,T)] \\ &= \Lambda^0(x,T)\{\eta(x,T) - [x\eta_2(T) + (1-x)\eta_1(T)]\}\,.\end{aligned} \tag{6.113}$$

The sign of the excess Walden product is the same as the sign of the excess viscosity $\eta^\mathrm{E}(x,T)$. Positive values of $\eta^\mathrm{E}(x,T)$ are associated with attractive interactions between the mixture components (structure-making effects) but negative values of $\eta^\mathrm{E}(x,T)$ result from repulsive interactions (structure-breaking effects).

Using the above approach, Apelblat (2011c) concluded that for polyvalent electrolytes in water-rich mixtures with ethanol or with 1,4-dioxane the excess Walden product $\Lambda^0(x)\eta^E(x) > 0$, which implies that attractive interactions dominate in these solvent mixtures. However, in methanol-rich mixtures with 1,2-ethanediol the excess Walden product $\Lambda^0(x)\eta^E(x) < 0$, implying that repulsive interactions prevail in this system.

The physical interpretation of the exponent p in the Walden relation between molar conductivity Λ of electrolytes with different solvents and the viscosity of the mixtures, as described by Eq. (6.110) with Λ^0 replaced by Λ, has been discussed (Couadou et al., 2013, Xu et al., 2003). It has been argued (Xu et al., 2003) that the value of the exponent is associated with the decoupling of mobile ion relaxation modes from matrix modes in superionic conductors.

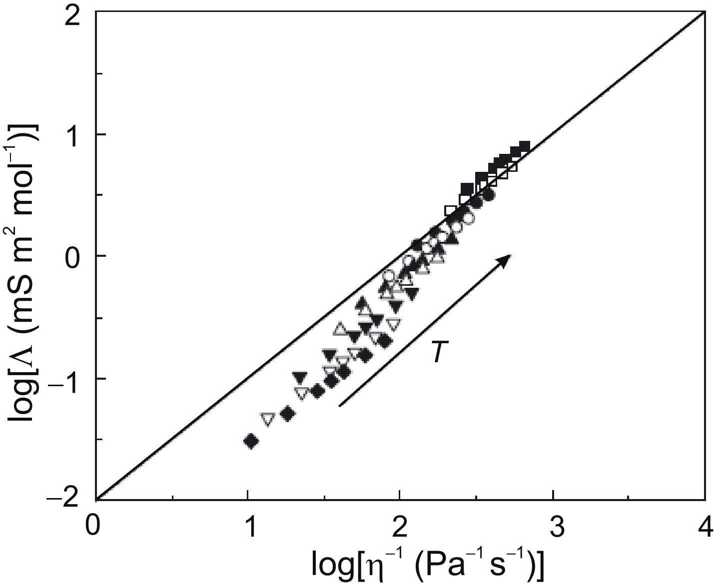

Figure 6.28. Walden plots for [bmim][DCA]–GBL mixtures at temperatures from 273.15 to 323.15 K for different x_{IL}: (■) 0.0504, (□) 0.1002, (●) 0.2002, (○) 0.2984, (▲) 0.4005, (△) 0.4954, (▼) 0.6957, (▽) 0.8871, and (♦) 1.00 mole fraction. Arrow indicates the direction of increasing *T*. Adapted from Zec et al. (2016).

In various studies devoted to ILs mixed with different solvents (for example, see: Makino et al., 2014; Vraneš et al, 2014, 2015; Zec et al., 2016), the Walden relation has been used in the linearized form

$$\log\Lambda = \log K + p\log(\eta^{-1})\,. \tag{6.114}$$

Figure 6.28 shows Walden plots for [bmim][DCA]–GBL mixtures at temperatures from 273.15 to 323.15 K for different x_{IL}. The solid line, usually referred to as the so-called ideal Walden line, represents 0.01 mol·L^{-1} aqueous KCl solution which is known to be fully dissociated and have ions of equal mobility (Xu et al., 2003). From these plots it may be seen that the most favorable conditions for the high conductivity of the pure IL and its mixtures are high temperatures when they have low viscosity. The data are close to the ideal line for dilute IL mixtures but they are increasingly shifted away from the ideal line with increasing IL content x_{IL} in the mixtures and that the slope p of the data decreases with increasing IL content. In other words, both K and p for a mixture decrease with increasing IL content x_{IL} in the mixtures and the decrease in their values is associated with increasing ionicity of an IL with increasing addition of the solvent GBL in the mixture. Increased ionicity of an IL implies the existence of strongly-bonded ion pairs in the solution, which do not contribute to the electric current.

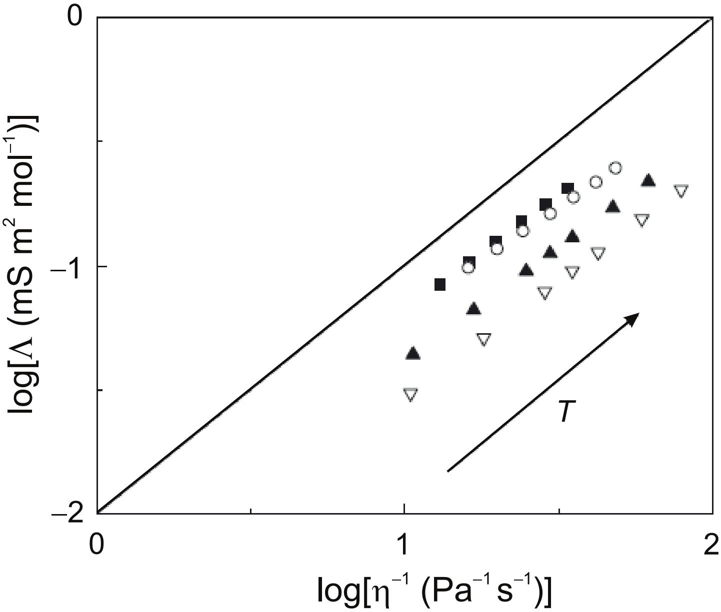

Figure 6.29. Walden plots for different neat ILs with increasing temperatures: (▽) [bmim][DCA], (▲) [bmpyr][DCA], (○) [bmim][TFSI] and (■) [bmpyr][TFSI]. Arrow indicates the direction of increasing *T*. Adapted from Zec et al. (2016).

Figure 6.29 illustrates Walden plots for four neat ILs composed of two different cations (i.e. [bmim]$^+$ and [bmpyr]$^+$) and anions (i.e. [DCA]$^-$ and [TFSI]$^-$). It may be noted that [DCA]$^-$–based ILs are shifted far away from their [TFSI]$^-$–based counterparts, and [bmim]$^+$–based ILs are farther away from their [bmpyr]$^+$–based counterparts. This means that the two [DCA]$^-$–based ILs and the two [bmim]$^+$–based ILs involve more ion pairs or ion aggregates than their corresponding counterparts.

In a study on the conductivity σ of dilute electrolyte solutions of lithium perchlorate (c = 1.94 mmol·L^{-1}) in polyethylene glycols of [CH_2–CH_2–O] units of 4.2, 6.4, 9.1

and 12.8 (PEG-200, PEG-300, PEG-400 and PEG-600) in the temperature range between 298.15 and 333.15 K, Świergiel et al. (2015a) used the linearized form of Eq. (6.109) and observed that the exponent $p < 1$ for all glycols and somewhat decreases with the number of the units composing them. The authors attributed this behavior of these glycols to a decrease in the ionic mobility in the polymer matrix due to increased flexibility of longer polyethylene glycols.

6.9. Conductivity of saturated, undersaturated and supersaturated solutions

As discussed in Section 6.6.2, Arrhenius and VTF relations provide the theoretical basis of the dependence of specific conductivity σ of the solution of a true electrolyte of a given concentration c on T. However, as mentioned in Section 6.6.1, the dependence of conductivity σ of electrolyte solutions on concentration c and solution temperature T may also be described by empirical polynomial relations, and the dependence of σ of an electrolyte solution of a given c on T is linear in a narrow temperature range.

A continuous increase in σ of the electrolyte solution of a given concentration with temperature is a result of two factors: (1) a steady increase in the mobility of current carriers (ions), and (2) if the electrolyte contains associated ion-pairs, increasing temperature contributes to increasing concentration of ions. Temperature dependence of the conductivity σ of saturated solutions of an electrolyte differs from that of a solution of a given concentration in a change in the concentration of current carriers with the temperature dependence of the solubility of the electrolyte, and a change in the mobility of current carriers due to change in the viscosity of the electrolyte. Since both of these factors are associated with the solubility of the electrolyte with an increase in temperature, it is difficult to predict the temperature dependence of the conductivity σ of their saturated solutions.

As in the case of aqueous solutions of electrolytes of fixed concentrations, the specific conductivity σ of an electrolyte saturated at a temperature T_s changes with temperature T both below and above T_s following a second-order polynomial relation (Figure 6.30)

$$\sigma = A_4 + B_4 T + C_4 T^2 \,, \tag{6.115}$$

where A_4, B_4 and C_4 are fitting parameters, and the temperature intervals $T > T_\mathrm{s}$ and $T < T_\mathrm{s}$ correspond to undersaturated and supersaturated regions of electrolyte concentation, respectively. Examples of this behavior are aqueous solutions of aqueous solutions of sodium sulfate (Sokolowski, 1981) and lithium formate (Karniewicz et al., 1982). In the latter case, it was found that the $\sigma(T)$ data follow a linear dependence with the values of the constants A_4 and B_4 increasing with increasing saturation temperature T_s.

The dependence of conductivity σ of aqueous saturated solutions of true electrolytes at different temperature T_s is also linear (Sokolowski, 1981; Karniewicz et al., 1982). However, as shown in Figure 6.30, two different linear $\sigma(T)$ plots of different slopes B_4, accompanied with a break in the vicinity of temperature of phase change, appear in the case of aqueous electrolyte solutions. In the temperature range of phase change the conductivity increases insignificantly with increasing temperature.

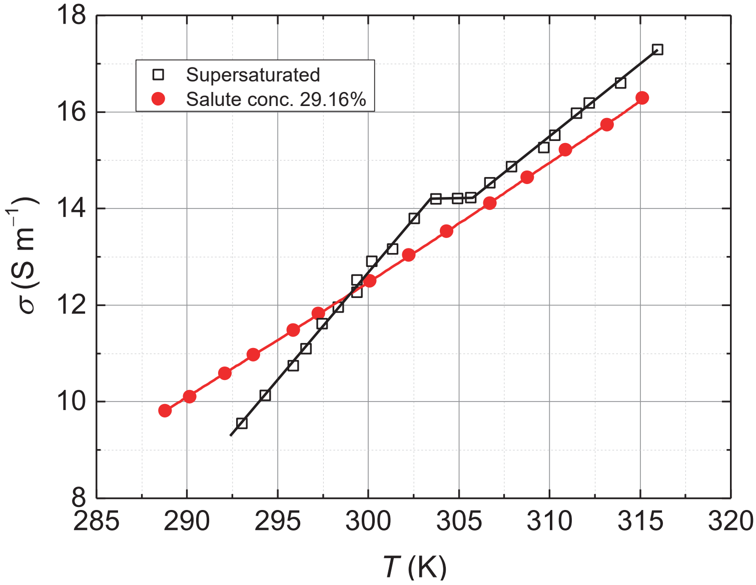

Figure 6.30. Temperature dependence of specific conductivity σ of aqueous solutions of Na_2SO_4: (●) constant concentration 29.16% and (□) saturated solutions. Data from Sokołowski (1981).

6.10. Some applications of conductivity measurements

The conductivity of a solution depends, inter alia, on the size and charge of ionic species present in it. This fact has made conductivity measurement useful in various applications. Some applications are described below.

One of the main applications of conductivity measurements is checking the quality of water in public water supplies, in hospitals, in boiler water and industries. The conductivity of water depends, among others, on the pH, the temperature, and the amount of atmospheric carbon dioxide dissolved in it to form ions. This type of conductivity of water is its intrinsic conductivity. However, conductivity also depends on Cl^-, SO_4^{2-}, Na^+, NH_4^+, Ca^{2+} and Mg^{2+} ions contained in water as its impurities (extraneous conductivity). The total conductivity, intrinsic *plus* extraneous, of water is considered to evaluate its suitability for use in laboratories, pharmaceutics and drinking. However, if the composition of the solution and its conductivity behavior are known independently from analytical tests, conductivity measurements determine the amount of total dissolved solids.

The CO_2–H_2O system with free carbon dioxide concentration, varying from that close to the saturation one to the equilibrium one under environmental conditions, has drawn interest to determine the dependence of ionic concentrations on the pH of the solutions by simultaneous measurements of specific conductivity and pH of the solution as functions of time (Gajevskiy, 2015). It was found that HCO_3^- ions resulting from the absorption of CO_2 in water mainly contribute to the conductivity of this system.

The conductivity of electrolyte solutions prepared from heavy water molecules as a solvent has been investigated (Biswas and Bagchi, 1997). It was found that the value of the limiting ionic conductivity λ^0 of monovalent ions (e.g. tetraalkylammonium cations or alkali metal cations) shows a strong temperature dependence and that its value shows a significant isotopic effect of the solvent. The experimental results indicated a significant (almost 20%) reduction in the value of λ^0 of a given ion in D_2O in relation to H_2O. This reduction in mobility was observed for all monovalent cations, regardless of their size.

Conductivity measurements are widely used in the dairy industry for controlling milk quality, analyzing fermentation processes for production of cheese starters, and to monitor the start-up and prerinsing phases of the milk pasteurization process. Start-up and prerinsing processes involve raw material waste. Therefore, measurements of the electrical conductivity of milk at various dilutions and at different temperatures and the development of mathematical models to predict milk conductivity in terms of model parameters have been a topic of interest (Henningsson et al., 2005).

Paraffin chain salts such as sodium *n*-alkyl sulfates (with *n*-alkyl group usually being octyl, decyl and dodecyl groups) are widely used as synthetic chemical surfactants in various applications. In aqueous solution they dissociate into sodium cation and alkylsulfate anion where the anion is active. Due to dissociation of these salts in aqueous solution, their conductivity σ at a given temperature increases with an increase in the concentration of their aqueous solutions. Therefore, conductivity measurements of aqueous solutions of sodium *n*-alkyl sulfates provide a simple method for the study of critical micelle concentration (CMC) from a change in the slope of the conductivity–concentration curves in a wide range of temperature (Bhattarai et al., 2014; Goddard and Benson, 1957; Miura and Kodama, 1972). These measurements for the aqueous solutions of the three sodium *n*-akyl sulfates mentioned above revealed (Goddard and Benson, 1957) that variation in the CMC with temperature in these systems has a minimum at about 298.15 K whereas the value of the CMC for a system increases with temperature as well as the length of the carbon chain of the *n*-akyl group.

Investigation of the conductivity σ of aqueous sodium dodecylsulfate (SDS) solutions at 298.15 K over a wide range of concentation up to 0.12 $\text{mol}\cdot\text{L}^{-1}$ without and with inorganic salt NaCl and three organic substances (i.e. dodecanol, *n*-hexane and benzene), with their highest content of 0.2 molar ratio in the solution, has revealed (Miura and Kodama, 1972) that there exists a second CMC at 0.065 $\text{mol}\cdot\text{L}^{-1}$ in addition to the first CMC at 0.0083 $\text{mol}\cdot\text{L}^{-1}$, and that the second CMC is significantly affected by electrolyte and nonelectrolyte additives but the effect depends on the nature of the additives. The experimental data of the dependence of change $\Delta\sigma$ in the conductivity σ of aqueous SDS solutions containing different concentrations of the three additives on SDS concentration also showed that the second CMC is not formed due to stabilization of the micelle in the regions of low SDS concentration when an appropriate amount of the nonelectrolyte additive is present in the solution.

References

Angell, C.A. (1966). Free volume–entropy interpretation of the electrical conductance of aqueous electrolyte solutions in concentration range 2–20 N. *J. Phys. Chem*. **70**, 3988-3998.

Angell, C.A. (1991). Relaxation in liquids, polymers and plastic crystals: Strong/fragile patterns and problems. *J. Non-Cryst. Solids* **131-133,** 13-31.

Angell, C.A. (1995). Formation of glasses from liquids and biopolymers. *Science* **267**, 1924-1935.

Angell, C.A., and R.D. Bressel (1972). Fluidity and conductance in aqueous electrolyte solutions. An approprach from the glassy state and high-concentration limit. I. $Ca(NO_3)_2$ solutions. *J. Phys. Chem.* **76**, 3244-3252.

Apelblat, A. (2008). Limiting conductances of electrolytes and the Walden product in mixed solvents in a phenomenological approach. *J. Phys. Chem. B* **112,** 7032-7044.

Apelblat, A. (2011a). Representation of electrical conductances for polyvalent electrolytes by the Quint–Viallard conductivity equation. Part 1. Symmetrical 2:2 type electrolytes. Dilute aqueous solutions of alkaline earth metal sulfates and transition metal sulfates. *J. Solution Chem.* **40**, 1209-1233.

Apelblat, A. (2011b). The representation of electrical conductances for polyvalent electrolytes by the Quint–Viallard conductivity equation. Part 3. Unsymmetrical 3:1, 1:3, 3:2, 4:1, 1:4, 4:2, 2:4, 1:5, 1:6 and 6:1 type electrolytes. Dilute aqueous solutions of rare earth salts, various cyanides and other salts. *J. Solution Chem*. **40,** 1291-1316.

Apelblat, A. (2011c). Representation of electrical conductances for polyvalent electrolytes by the Quint–Viallard conductivity equation. Universal curves at limiting conductances and Walden products of electrolytes in mixed solvents. Part 5. Symmetrical 2:2, 3:3 and unsymmetrical 1:2, 2:1 and 1:3 type electrolytes. *J. Solution Chem*. **40**, 1544-1562.

Apelblat, A. (2017). The representation of electrical conductances for polyvalent electrolytes by the Quint–Viallard conductivity equation. Part 7. Unsymmetrical 1:2 type electrolytes. Alkali metal (Li, Na, K, Rb and Cs) sulfates and ammonium sulfate. *J. Solution Chem*. **46,** 103-123.

Apelblat, A., E. Manzurola, and Z. Orekhova (2006). Electrical conductance studies in aqueous solutions with ascorbate ions. *J. Solution Chem*. **35,** 879-888.

Apelblat, A., E. Manzurola, and Z. Orekhova (2008). Electrical conductance studies in aqueous solutions with aspartic ions. *J. Solution Chem*. **37,** 97-105.

Bernard, O., W. Kunz, P. Turq, and L. Blum (1992). Conductance in electrolyte solutions using the mean spherical approximation. *J. Phys. Chem*. **96,** 3833-3840.

Bešter-Rogač, M. (2008). Electrical conductivity of concentrated aqueous solutions of divalent metal sulfates. *J. Chem. Eng. Data* **53,** 1355-1359.

Bešter-Rogač, M., M. Tomšič, J. Barthel, R. Neueder, and A. Apelblat (2002). Conductivity studies of dilute aqueous solutions of oxalic acid and netral oxalates of sodium, potassium, cesium, and ammonium from 5 to 35 °C. *J. Solution Chem*. **31,** 1-17.

Bartel, J., H. Graml, R. Neueder, P. Turq, and O. Bernard (1994). Electrolyte conductivity from infinite dilution to saturation. *Curr. Top. Solution Chem*. **1**, 223-239.

Bhattarai, A., S.K. Shah, and K. Limbu (2014). Conductance of sodium dodecylsulfate in presence and absence of $NaSO_4$ and $ZnSO_4$ in aqueous media at room temperature. *Scientific World* **12,** 41-43.

Bianchi, H.L., I. Dujovne, and R. Fernández-Prini (2000). Comparison of electrolytic conductivity theories: Performance of classical and new theories. *J. Solution Chem*. **29**, 237-253.

Biswas, R., and B. Bagchi (1997). The presence of hydrogen isotopes in solutions. *J. Am. Chem. Soc*. **119**, 5946-5953.

Bockris, J.O'M., and A.K.N. Reddy (1970). *Modern Electrochemistry*, Vol. 1, Plenum Press, New York.

Bončina, M., A. Apelblat, M. Bešter-Rogač (2010). Dilute aqueous solutions with formate ions: A conductometric study. *J. Chem. Eng. Data* **55**, 1951-1957.

Brummer, S.B., and G.J. Hills (1961). Kinetics of ionic conductance. *Trans. Faraday Soc.* **57**, 1816–822.

Casteel, J.F., and E.S. Amis (1972). Specific conductance of concentrated solutions of magnesium salts in water–ethanol system. *J. Chem. Eng. Data* **17**, 55-59.

Couadou, E., J. Jacquemin, H. Galiano, C. Hardacre, and M. Anouti (2013). A comparative study on the thermophysical properties for two bis[(trifluoromethyl)-sulfonyl]imide-based ionic liquids containing the trimethyl-sulfonium or the trimethyl-ammonium cation in molecular solvents. *J. Phys. Chem*. B. **117,** 1389-1402.

Durand-Vidal, S., P. Turq, and O. Bernard (1996). Model for the conductivity of ionic mixtures within the mean spherical approximation. 1. Three simple ionic species. *J. Phys. Chem*. **100,** 17345-17350.

Falkenhagen, H., M. Leist, and G. Kelbg (1952). Zur theorie der leitfahigkeit starker nicht assoziierender elektrolyte bei hoheren konzentrationen. *Ann. Phys. (Leipzig)* **11**, 51-59.

Fernández-Prini, R. (1969). Conductance of electrolyte solutions. A modified expression for its concentration dependence. *Trans. Faraday Soc.* **65**, 3311-3315.

Fernández-Prini, R., J.E. Prue (1965). A comparison of conductance equations for unassociated electrolytes. *Z. Phys. Chem. Leipzig*, **228**, 373-379.

Fuoss, R., and L.-L. Hsia (1967). Association of 1-1 salts in water. *Proc. Natl. Acad. Soc*. **57**, 1550-1557.

Fuoss, R., and L. Onsager (1957). Conductance of unassociated Electrolytes. *J. Phys. Chem.* 61, 668-682.

Gajevskiy, V.R. (2015). Electrical conductivity of carbon dioxide aqueous solutions. *Ukr. J. Phys*. **60**, 258-262.

Gilliam, R.J., J.W. Graydon, D.W. Kirk, and S.J. Thorpe (2007). A review of specific conductivities of potassium hydroxide solutions for various concentrations and temperature. *Intern. J. Hydrogen Energy* **32**, 359-364.

Goddard, E.D., and G.C. Benson (1957). Conductivity of aqueous solutions of some paraffin chain salts. *Can. J. Chem.* **54,** 986-991.

Goldsack, D.E., R. Franchetto, and A. Franchetto (1976). Solution effects on the conductivity of concencentrated electrolyte solutions. *Can. J. Chem*. **54,** 2953-2966.

Henningsson, M., K. Östergren, and P. Dejmek (2005). The electrical conductivity of milk – The effect of dilution and temperature. *Intern. J. Food Properties* **8,** 15-22.

Horvath, A.L. (1985). *Handbook of Aqueous Electrolyte Solutions: Physical Properties,* *Estimation and Correlation Methods*. Ellis Horwood, Chichester, Chap. 2.11.

Karniewicz, J., W. Kolasiński, and J. Szewczyk (1982). Some properties of lithium formate solutions near the saturation temperature. *J. Cryst. Growth* **57**, 462-465.

Kielland, J. (1937). Individual activity coefficients of ions in aqueous solutions. *J. Am. Chem. Soc.* **59,** 1675–1678.

Lee, W.H., and R.J. Wheaton (1978a). Conductance of symmetrical, unsymmetrical and mixed electrolytes. Part 1. Relaxation terms, *J. Chem. Soc., Farad. Trans. II* **74,** 743–766.

Lee, W.H., and R.J. Wheaton (1978b). Conductance of symmetrical, unsymmetrical and mixed electrolytes. Part 2. Hydrodynamic terms and complete conductance equation, *J. Chem. Soc., Farad. Trans. II* **74,** 1456–482.

Lee, W., and R. Wheaton (1979). Conductance of symmetrical, unsymmetrical and mixed electrolytes. Part 3. Examination of new model and analysis of data for symmetrical electrolytes. J. *Chem. Soc. Faraday Trans. II* **75**, 1128-1145.

Li, J.-G., Y.-F. Hu, C-W. Jin, H.-D. Chu, X.-M. Peng, and Y.-G. Liang (2010). Study of the conductivities of pure and aqueous bromide-based ionic liquids at different temperatures. *J. Solution Chem*. **39**, 1877-1887.

Lowe, B.M., and H.M. Rendall (1972). Dilute aqueous solutions of unsymmetrical quaternary ammonium iodides. Part 2. Conductance measurements. *J. Chem. Soc. Faraday 1*, **68**, 2191-2202.

Lowe, B.M., N.A. MacGlip, and J.M. Prichard (1973). Conductivities and densities of aqueous solutions of quaternary ammonium iodides containing pentyl and ethoxyethyl groups. *J. Chem. Eng. Data* **18**, 220-223.

MacInnes, D.A., and T. Shedlovsky (1932). The determination of the ionization constant of acetic acid, at 25°, from conductance measurements. *J. Am. Chem Soc*. **54**, 1429-1438.

Makino, T., M. Kanakubo, Y. Masuda, T. Umecky, and A. Suzuki (2014). CO_2 absorption properies, densities, viscosities, and electrical conductivities of ethylimidazolium and 1-alkyl-3-methylimidazolium ionic liquids. *Fluid Phase Equilibria* **362,** 300-306.

Miura, M., and M. Kodama (1972). The second CMC of the aqueous solution of sodium dodecyl sulfate. I. Conductivity. *Bull. Chem. Soc. Japan* **45,** 428-431.

Miyoshi, K. (1973). Comparison of the conductance equations of Fuoss–Onsager, Fuoss–Hsia and Pitts with the data of bis(2,9-dimethyl-1,10-phenanthroline)Cu(I) perchlorate, *Bull. Chem. Soc. Japan* **46**, 426-430.

Nishida, T., Y. Tashiro, and M. Yamamoto (2003). Physical and electochemical properties of 1-alkyl-3-methylimidazolium tetrafluoroborate for electrolyte. *J. Fluorine Chem*. **120**, 135-141.

Pitts, E. (1953). An extension of the theory of the conductivity and viscosity of electrolyte solutions. *Proc. Roy. Soc*. **217A**, 43-70.

Płowaś, I., J. Świergiel, and J. Jadżyn (2014). Electrical conductivity in dimethyl sulfoxide + potassium iodide solutions at different concentrations and temperatures. *J. Chem. Eng. Data* **59,** 2360-2366.

Płowaś, I., J. Świergiel, and J. Jadżyn (2015). Frequency dependence of the ionic conductivity in water + ammonium nitrate electrolyte solutions. *Electrochim. Acta* **178**, 511-516.

Quint, J., and A. Viallard (1978a). Relaxation field for the general case of electrolyte mixtures. *J. Solution Chem*. **7,** 137-153.

Quint, J., and A. Viallard (1978b). The electrophoretic effect for the case of electrolyte mixtures. *J. Solution Chem*. **7,** 525-531.

Quint, J., and A. Viallard (1978c). Electrical conductance of electrolyte mixtures of any type.

J. Solution Chem. **7**, 533-548.

Robinson, R.A., and R.H. Stokes (1954). The Variation of equivalent conductance with concentration and temperature. *J. Am. Chem. Soc*. **76,** 1991-1994.

Robinson, R.A., and R.H. Stokes (1959). *Electrolyte Solutions*, 2nd edition, Butterworths, London.

Rohman, N., A. Wahab, N.N. Dass, S. Mahiuddin (2001). Viscosity, electrical conductivity, shear relaxation time and Raman spectra of aqueous and methanolic sodium thiocyanate solutions. *Fluid Phase Equilibria* **178,** 277-297.

Shedlovsky, T. (1932). An equation for electrolytic conductance. *J. Am. Chem. Soc*. **54,** 1405-1411.

Shekaari, H., and M.S. Mousavi (2009). Conductometric studies of aqueous ionic liquids, 1-alkyl-3-methylimidazolium halide, solutions at T = 298.15–328.15 K. *Fluid Phase Equilibria* **286,** 120-126.

Sokolowski, T. (1981). Physical properties of aqueous solution of sodium sulphate. *J. Cryst. Growth* **52,** 829-831.

Świergiel, J., I. Płowaś, and J. Jadżyn (2014). Temperature and concentration dependence of the electrical conductivity of dimethyl sulfoxide + ammonium nitrate electrolytes. *J. Chem. Eng. Data* **58,** 2302-2306.

Świergiel, J., I. Płowaś, J. Grembowski, and J. Jadżyn (2015a). Stokes–Einstein–Nernst relation in dilute electrolyte solutions of lithium perchlorate in polyethylene glycols (200, 300, 400, and 600). *J. Chem. Eng. Data* **60,** 3588-3393.

Świergiel, J., I. Płowaś, and J. Jadżyn (2015b). Charge relaxation and Stokes–Einstein relation in diluted electrolyte solution of propylene carbonate and lithium perchlorate. *Ind. Eng. Chem. Res*. **54,** 2108-2113.

Turq, P., L. Blum, O. Bernard, and W. Kunz (1995). Conductance in associated electrolytes using the mean spherical approximation. *J. Phys. Chem.* **99**, 822-827.

Varela, L.M., J. Carrete, M. Garcia, L.J. Gallego, M. Turmine, E. Rilo, and O. Cabeza (2010). Pseudolattice theory of charge transport in ionic solutions: corresponding states law for the electric conductivity. *Fluid Phase Equilibria* **298,** 280-286.

Vila, J., P. Ginés, J.M. Pico, C. Franjo, E. Jiménez, L.M. Varela, and O. Cabeza (2006a). Great increase of the electrical conductivity of ionic liquids in aqueous solutions. *Fluid Phase Equilibria* **247**, 32-39.

Vila, J., P. Ginés, E. Rilo, O. Cabeza, and L.M. Varela (2006b). Temperature dependence of the electrical conductivity in EMIM-based ionic liquids: Evidence of Vogel–Tamman–Fulcher behavior. *Fluid Phase Equilibria* **242**, 141-146.

Vila, J., E. Rilo, L. Segade, O. Cabeza, and L. M. Varela (2005). Electrical conductivity of aqueous solutions of aluminum salts. *Phys. Rev. E* **71,** 031201(1-8).

Vraneš, M., S. Popović, A. Tot, N. Zec, and S. Gadžurić (2014). Density, excess properties, electrical conductivity of 1-butyl-1-methylimidazolium bis(trifluoromethylsulfonyl)-imide + γ-butylrolactone binary mixtures. *J. Chem. Thermodyn.* **76**, 161-171.

Vraneš, M., A. Tot, S. Popović, N. Zec, S. Dožić, and S. Gadžurić (2015). Ideal and non-ideal behaviour of {1-butyl-1-methylpyrrolydinium bis(trifluoromethylsulfonyl)imide + γ-butylrolactone} binary mixtures. *J. Chem. Thermodyn*. **81**, 66-76.

Wang, J.J., H.Y. Wang, S.L. Zhang, H.C. Zhang, and Y. Zhao (2007). Conductivities, volumes, fluorescence, and aggregation behavior of ionic liquids [C_4mim][BF4] and [$C_n$mim][Br] (n = 4, 6, 8, 10, 12) in aqueous solutions. *J. Phys. Chem. B* **111**, 6181-6188.

Weingartner, H., V.C. Weiss, and W. Schroer (2000). Ion association and electrical conductance minimum in Debye–Hückel-based theories of the hard sphere ionic fluid, *J. Chem. Phys*. **113**, 762-770.

Wishaw, B.F., and R.H. Stokes (1954). The Diffusion coefficients and conductances of some concentrated electrolyte solutions at 25°. *J. Am. Chem. Soc*. **76**, 2065-2071.

Xu, W., E.J. Cooper, and C.A. Angell (2003). Ionic liquids: ionic mobilities, glass temperatures, and fragilities. *J. Phys. Chem. B* **107**, 6170-6178.

Zimmerman, G.H., and R.H. Wood (2002). Conductance of dilute sodium acetate solutions to 469 K and of acetic acid and sodium acetate/acetic acid mixtures to 548 K and 20 MPa. *J. Solution Chem*. **31**, 995-1017.

Zimmerman, G.H., H. Arcis, and P.R. Trmaine (2012). Limiting conductivities and ion association of aqueous NaCl under hydrothermal conditions: Experimental data and correlations. *J. Chem. Eng. Data* **57**, 2415-2429.

Zec, N., M. Bešter-Rogač, G. Marolt, M., Vraneš, and S. Gadžurić (2015). Electrical and electrochemical behavior of [bmim][DCA] + γ-butylrolactone electrolyte. *J. Chem. Thermodyn*. **101**, 293-299.

7

ISOBARIC EXPANSIVITY OF SOLVENTS, SOLUTIONS AND SOLUTES

Physical properties of liquids depend on external conditions such as pressure and temperature of their measurements as well as on internal conditions like the composition of the liquid. Under isobaric conditions, these properties essentialy depend on their temperature and composition.

Physical properties of liquids are different from those of solids due to differences in the nature of interactions between atoms/molecules in the two states. It is the long-range interactions between the atoms/molecules in the solid state, and the short-range interactions in the liquids. Consequently, although the average distance between the atoms/molecules in the both phases increases with temperature, the temperature dependence of decrease in the density d of liquids is higher than that of solids and the volume thermal expansion coefficient α_V of liquids is usually one-order higher than that in the solids state.

Addition of a solid to a solvent in which it is soluble at a particular temperature leads to a reduction in its volume due to attractive interaction of its molecules/ions with the surrounding solvent molecules. This reduction in the solution volume increases with the solute concentration. Therefore, in contrast to the effect of temperature, the density d of the solution increases with an increase in the concentration of the solute. This effect of concentration of solute to the solvent is opposite to that of temperature.

The present chapter deals with general trends of the expansivity of solvents and solutions in relation to the nature of solvents and solutions. Since expansivity is not an experimentally measured quantity, after presenting basic concepts of expansivity and its temperature dependence in the next section, procedures of calculations of expansivity from density data of solvents as a function of temperature and of solvent mixtures and solutions as functions of temperature and cosolvent and solute content are described in Section 7.2. General features of thermal expansivity of solvents and solvent mixtures, and of solutions and solutes are described and discussed from consideration of their concentration and temperature in Sections 7.3 and 7.4, respectively. Finally, some features of saturated solutions are presented in Section 7.5.

7.1. Basic concepts

7.1.1. Expansivity and its temperature dependence

At a given pressure p the densities d of the solid and liquid phases decrease with increasing temperature T according to the relation

$$d(T) = d_{\mathrm{m}} - k(T - T_{\mathrm{m}})\,, \tag{7.1}$$

where T_{m} is the melting point of the material, d_{m} is the density of the solid and the liquid at the melting temperature T_{m} and k is a constant characteristic of the phase and the material. Note that the value of the density d_{m} of a solid at T_{m} is always different from the density d_{m} of the molten liquid at T_{m} due to the restricted translational motion of the entities in the solid state than in the liquid state.

From Eq. (7.1) one obtains the expression for the thermal expansivity (also called volumetric thermal expansion coefficient) of a liquid in the form

$$\alpha_{\mathrm{V}} = \frac{k}{d_{\mathrm{m}}} = -\frac{d - d_{\mathrm{m}}}{d_{\mathrm{m}}(T - T_{\mathrm{m}})} = -\frac{1}{d_{\mathrm{m}}}\left(\frac{\Delta d}{\Delta T}\right), \tag{7.2}$$

where the density difference $\Delta d = (d - d_{\mathrm{m}})$ and the temperature difference $\Delta T = (T - T_{\mathrm{m}})$. Elemental transformation of Eq. (7.2) under isobaric and composition conditions gives

$$\alpha_{\mathrm{V}} = -\frac{1}{d}\left(\frac{\mathrm{d}d}{\mathrm{d}T}\right)_{p,x} = -\left(\frac{\mathrm{d}\ln d}{\mathrm{d}T}\right)_{p,x} = \left(\frac{\mathrm{d}\ln \phi_{\mathrm{V}}}{\mathrm{d}T}\right)_{p,x}, \tag{7.3}$$

where ϕ_{V} ($\mathrm{cm}^3\cdot\mathrm{g}^{-1}$) is the specific volume of the liquid. If M is the molar mass of the liquid of molar volume V_{M}, using the definition of density $d = M/V_{\mathrm{M}}$, $\mathrm{d}d/\mathrm{d}V_{\mathrm{M}} = -M/V_{\mathrm{M}}^2$, the differential form of Eq. (7.3) may be expressed in the form

$$\alpha_{\mathrm{V}} = -\frac{1}{d}\left(\frac{\mathrm{d}d}{\mathrm{d}V_{\mathrm{M}}}\right)_{p,x}\left(\frac{\mathrm{d}V_{\mathrm{M}}}{\mathrm{d}T}\right)_{p,x} = -\frac{V_{\mathrm{M}}}{M}\left(-\frac{M}{V_{\mathrm{M}}^2}\right)\left(\frac{\mathrm{d}V_{\mathrm{M}}}{\mathrm{d}T}\right)_{p,x} =$$

$$= \frac{1}{V_{\mathrm{M}}}\left(\frac{\mathrm{d}V_{\mathrm{M}}}{\mathrm{d}T}\right)_{p,x} = \left(\frac{\mathrm{d}\ln V_{\mathrm{M}}}{\mathrm{d}T}\right)_{p,x}, \tag{7.4}$$

where V_{M} and $\mathrm{d}V_{\mathrm{M}}$ are the molar volume and the change in the molar volume, respectively, of the liquid. This relation predicts a decrease in the density d and an increase in the specific volume ϕ_{V} and the molar volume V_{M} of the liquid with increasing T.

Eq. (7.4) gives

$$V_{\mathrm{M}} = V_{\mathrm{M}}^{\mathrm{o}} \exp[\alpha_{\mathrm{V}}(T - T_0)]\,, \tag{7.5}$$

or

$$\frac{V_{\mathrm{M}}}{V_{\mathrm{M}}^{\mathrm{o}}} \approx 1 + \alpha_{\mathrm{V}}(T - T_0) + \frac{\alpha_{\mathrm{V}}^2}{2}(T - T_0)^2, \tag{7.6}$$

where the isobaric expansion coefficient α_{V} depends on liquid composition. From Eq. (7.4) one may also obtain

$$\frac{\Delta V_{\mathrm{M}}}{V_{\mathrm{M}}^{\mathrm{o}}} = \alpha_{\mathrm{V}} \Delta T, \tag{7.7}$$

where $\Delta V_{\mathrm{M}} = (V_{\mathrm{M}} - V_{\mathrm{M}}^{\mathrm{o}})$ with reference to a constant molar volume $V_{\mathrm{M}}^{\mathrm{o}}$ of a liquid at a particular temperature T_0. According to Eq. (7.7), the change in the molar volume V_{M} of a liquid increases linearly with an increase in temperature T.

Assuming that the volumetric expansion coefficient α_{V} is temperature independent, integration of Eq. (7.3) for a liquid with densities d_0 and d in the temperature interval between T_0 and T, respectively, gives the expansion coefficient as

$$\alpha_{\mathrm{V}} = -\frac{\ln d - \ln d_0}{T - T_0} = -\frac{\Delta \ln d}{\Delta T}, \tag{7.8}$$

and

$$d = d_0 \exp[-\alpha_{\mathrm{V}}(T - T_0)], \tag{7.9}$$

or

$$\frac{d}{d_0} \approx 1 - \alpha_{\mathrm{V}}(T - T_0) - \frac{\alpha_{\mathrm{V}}^2}{2}(T - T_0)^2. \tag{7.10}$$

When the reference temperature T_0 for measurements of d and α_{V} is taken as 273.15 K, the temperature difference $(T - T_0)$ taken in K is equivalent to $^{\mathrm{o}}$C, and α_{V} is customarily given in $^{\mathrm{o}}\mathrm{C}^{-1}$. Eqs. (7.9) and (7.10) following from Eq. (7.1) are similar to those used to describe the temperature dependence of the density d of solvents and solutions.

Eqs. (7.3) and (7.4) based on elemental transformations predict linear dependence of $\ln d$, $\ln \phi_{\mathrm{V}}$ and $\ln V_{\mathrm{M}}$ for a liquid on its temperature T with constant slope equal to volumetric thermal expansion coefficient α_{V} of the liquid. It is a common observation that the thermal expansion coefficient α_{V} increases with temperature T. This means that Eq. (7.3) requires modification to account for the observed increase in α_{V} above the melting temperature T_{m} of the liquid up to its boiling point T_{b} when its density decreases from d_{m} to d_{b}. This suggests that the increase in α_{V} is associated with the effective density $d_{\mathrm{m}} - d_{\mathrm{b}}$ and the effective molar volume $V_{\mathrm{m}} - V_{\mathrm{b}}$.

7.1.2. Expansivity of solvent–solvent and solute–solvent mixtures

Solvent–solvent and solvent–solute mixtures are composed of a solvent in which another solvent or a solute is dissolved to form a homogeneous phase. If the composition of the second dissolved solvent or solute is taken in mole fraction x_2, and the density d of the mixture increases with increasing content x_2 of the added phase at a particular temperature according to the relation

$$\frac{d(x_2)-d_0}{d}=\alpha_x(x_2-x_0)\,, \tag{7.11}$$

where d_0 and $d(x_2)$ are the densities of the mixture in the presence of second phase of contents x_0 and x_2, respectively, and the second component-related coefficient α_x is similar to the temperature-related expansivity α_V of Eq. (7.2) and is determined by interactions between the mixture components. However, the effect of addition of the second component to the density d of the solvent at a particular temperature is opposite to that of increase in temperature of the liquid of a given composition. Addition of second component to the liquid leads to an increase in its density d in contrast to a decrease in the liquid density d with increasing temperature. Integration of Eq. (7.11) for a liquid mixture of densities d_0 and d in the interval of the second-phase content between x_0 and x_2 gives the coefficient as

$$\alpha_x=\frac{\ln d-\ln d_0}{x_2-x_0}\,, \tag{7.12}$$

and

$$d=d_0\exp[\alpha_x(x_2-x_0)]\,, \tag{7.13}$$

or

$$\frac{d}{d_0}\approx 1+\alpha_x(x_2-x_0)+\frac{\alpha_x^2}{2}(x_2-x_0)^2\,. \tag{7.14}$$

Since mole fraction $x_2 \approx m(M/1000)$, where m is the molality of the second component and M is the molar mass of the solvent, Eqs. (7.13) and (7.14) may also be expressed in simple forms:

$$d=d_0\exp(k_1m)\,, \tag{7.15}$$

or

$$d\approx d_0+k_1m+k_2m^2\,. \tag{7.16}$$

where $k_1 = 10^{-3}d_0\alpha_xM$ and $k_2 = 5\cdot10^{-5}d_0\alpha_x^2M^2$. Eqs. (7.15) and (7.16) are similar to those used to describe the dependence of solute concentration on the density of their solutions.

7.1.3. Temperature dependence of expansivity of liquids

From Eq. (7.3) one notes that a change Δd in the initial liquid density d_0 is proportional to the change ΔT in the liquid temperature, and the proportionality constant is the volumetric expansion coefficient α_V. Similarly, according to Eq. (7.7) a change ΔV in the initial liquid volume V_0 is proportional to the change ΔT in the liquid temperature, and the proportionality constant is the volumetric expansion coefficient α_V. Obviously, the coefficient α_V is a constant quantity for a liquid of initial density d_0 and molar volume V_0. However, for a given temperature change ΔT for different liquids the coefficient α_V decreases with a decrease in d_0 and an increase in V_0 of a liquid, since d_0 and V_0 are related to the average distance r_0 between nearest liquid atoms/molecules.

Physical interpretation of Eqs. (7.3) and (7.7) is based on the premise that atoms/molecules composing a liquid vibrate about their "temporary" equilibrium sites like harmonic oscillators and the displacement x of the vibrating entities from their equilibrium positions x_0 increases with an increase in temperature T due to increase in the internal energy E of the liquid. Here the use of symbols x and x_0 to denote positions of an oscillating atom/molecule is just a matter of tradition and is in no way related to the composition of a solution mixture. If one considers an analogy between the vibrating entities in lattice-like liquids with those in crystalline solids, the effect of temperature on the displacement involved in these oscillations about their equilibrium sites may be described in terms of deviations from their harmonic behavior. If r_0 is the distance of an atom/molecule from its neighbor at temperature $T = 0$, its displacement x follows an anharmonic behavior with the potential $E_p(x)$ given by (for example, see: Kittel, 1976)

$$E_{\mathrm{p}}(x) = ax^2 - bx^3 + cx^4 , \tag{7.17}$$

where the constants a, b and c are positive. The ax^2 term represents harmonic contribution whereas the second and third terms represent anharmonic contributions due to mutual repulsion of atoms/molecules and softening of vibration at large amplitudes, respectively. If $E(r_0)$ is the equilibrium energy of the crystal, corresponding to the distance $r = r_0+x$ its total energy $E(x)$ is

$$E(x) = E(r_0) + ax^2 - bx^3 + cx^4 . \tag{7.18}$$

Then the average displacement x_{av} of vibrating entities during heating of the liquid to the temperature T may be expressed in the form

$$x_{\mathrm{av}} = \frac{3bk_{\mathrm{B}}T}{4a^2}\left(1 - \frac{3ck_{\mathrm{B}}T}{4a^2}\right), \tag{7.19}$$

which gives the linear thermal expansion coefficient

$$\alpha_{\ell} = \frac{\mathrm{d}\,x_{\mathrm{av}}}{r_0\,\mathrm{d}T} = \frac{3bk_{\mathrm{B}}}{4r_0a^2}\left(1 - \frac{3ck_{\mathrm{B}}T}{2a^2}\right), \tag{7.20}$$

and the volumetric thermal expansion coefficient

$$\alpha_V = 3\alpha_\ell \approx \alpha_V^* - \alpha_1 T = \alpha_V^o - \alpha_1 (T - T_0) , \tag{7.21}$$

where

$$\alpha_V^* = \alpha_V^o + \alpha_1 T_0 = \frac{9bk_B}{4r_0 a^2}\left(1 - \frac{3ck_B T_0}{2a^2}\right), \tag{7.22}$$

$$\alpha_1 = \alpha_V^o \frac{3ck_B}{2a^2} = \frac{27bck_B^2}{8r_0 a^4} . \tag{7.23}$$

In Eq. (7.21) $\alpha_V{}^o$ is the value of α_V when $T = T_0$. This relation predicts a linear decrease in the thermal expansivity α_V of a liquid with increasing temperature T with an intercept $\alpha_V{}^o$ and slope α_1. The values of both $\alpha_V{}^o$ and α_1 decrease with an increase in the equilibrium distance r_0 between nearest neighbors, but the value of the slope α_1 for different liquids is related to the ratio bc/a^2. Consequently, when anharmonic contributions to thermal vibrations of the atoms/molecules of a liquid are weak in comparison with the harmonic contribution, its expansivity α_V shows poor dependence on temperature. In contrast to this, when harmonic contribution is weak, the expansivity α_V of the liquid shows pronounced dependence on temperature. Magnitudes of harmonic and anharmonic contributions of vibrations of entities composing a liquid are related to the strength of the bonds between them and the structure of the liquid molecules.

As in the case of crystalline solids, when a liquid is heated, the supplied heat leads to a change in its internal energy, which is composed of the kinetic energy E_k of thermal vibrations of atoms/molecules about their equilibrium sites and the potential energy E_p of their mutual interaction. This heating results not only an increase in the energy of the liquid but also an increase in the average distance between the equilibrium sites (linear and volumetric expansion). In this process the amplitude of anharmonic thermal vibrations of the atoms/molecules in the lattice-like liquid increases and the bonds between them become weak. Due to thermal fluctuations involving different amplitudes of vibrations some of the atoms/molecules in the liquid are also knocked out of their temporary equilibrium sites, thereby forming increasing number of holes or voids in it with increasing temperature. The maximum displacement $\Delta x_{\max}$ of a liquid molecule from its equilibrium position due to the thermal energy $k_B T$ is given by

$$\Delta x_{\max} = \left(\frac{2k_B T}{f}\right)^{1/2} , \tag{7.24}$$

where the force constant f (N/m) is related to the strength of bonds between neighboring atoms/molecules of the liquid. Obviously, the lower the force constant f for a liquid, the higher is the concentration of holes formed in it. The increase in the volume V of a liquid with an increase in its temperature may be explained in this way.

7.2. Calculation of thermal expansivity of liquids

As seen above, the expansivity α_V of solvents may be calculated from the data of their measured density d, or molar volume V_M calculated therefrom, as a function of temperature T (see Eqs. (7.3) and (7.4)). Since α_V is defined in terms of $-(\mathrm{d}d/\mathrm{d}T)/d$ and $-(\mathrm{d}\ln d/\mathrm{d}T)$, or alternatively as $(\mathrm{d}V_M/\mathrm{d}T)/V_M$ and $(\mathrm{d}\ln V_M/\mathrm{d}T)$, α_V may be calculated by fitting the $d(T)$ or $V_M(T)$ data for a solvent using some functions $F(T)$ and then taking its differentials $F'(T)$. For example, when the temperature dependence of the density d of a liquid follows the quadratic relation

$$d(\Delta T) = d_0 + a_1\Delta T + b_1(\Delta T)^2\,, \tag{7.25}$$

where $\Delta T = (T - T_0)$, d_0 is the value of density when $\Delta T = 0$, and a_1 and b_1 are constants, the expansivity

$$\alpha_V(T) = -\frac{1}{d}\left(\frac{\mathrm{d}d(T)}{\mathrm{d}T}\right) = -\frac{a_1 + 2b_1\Delta T}{d_0 + a_1\Delta T + b_1(\Delta T)^2} \approx$$
$$\approx -(a_1^* + b_1^*\Delta T) + A_1(\Delta T)^2 + A_2(\Delta T)^3\,, \tag{7.26}$$

where we have used the approximation: $[1+\{(a_1/d_0)\Delta T+(b_1/d_0)(\Delta T)^2\}]^{-1} \approx [1-\{(a_1/d_0)\Delta T+(b_1/d_0)(\Delta T)^2\}]$, and a_1^*, b_1^*, A_1 and A_2 are new constants embracing the constants of the approximation. It may be noted that here the approximation predicts the dependence of α_V on ΔT by a third-order polynomial and the initial value of α_V^{o} corresponding to $\Delta T = 0$ is equal to $-a_1/d_0$. Since the density d of a solvent is a positive quantity at all T, the sign of the slope $\mathrm{d}[\alpha_V(T)]/\mathrm{d}T$ of the plot of α_V against T is essentially determined by the value of $-2b_1$ (cf. Eq. (7.26)). The value of α_V increases with T when $2b_1 < 0$, and vice versa.

An alternative and relatively simple procedure is to consider the data of $\ln d$ as a function of ΔT. When the temperature dependence of $\ln d$ follows a similar quadratic relation, i.e.

$$\ln d(\Delta T) = \ln d_0 + a_2\Delta T + b_2(\Delta T)^2\,, \tag{7.27}$$

where a_2 and b_2 as new constants and $\ln d_0$ is the value of $\ln d$ when $\Delta T = 0$, one has

$$\alpha_V(T) = -\frac{\mathrm{d}\ln d(T)}{\mathrm{d}T} = -(a_2 + 2b_2\Delta T)\,, \tag{7.28}$$

which predicts a linear dependence of α_V on T, with intercept $-a_2 = -a_1/d_0$ and slope $\mathrm{d}\alpha_V/\mathrm{d}T = -2b_2$. The intercepts represents the initial thermal expansivity α_V^{o} corresponding to $\Delta T = 0$, whereas the slope is a measure of change in α_V with T. As in the case of Eq. (7.26), α_V increases with T when $2b_2 < 0$, and vice versa.

The density d (or ϕ_V and V_M) of mixtures of two solvents and solutions of a solute dissolved in its solvents is a function of two variables: the temperature T and the cosolvent or solute content x_2 in the mixture or solution. Therefore, their expansivity α_V is also a function of these two variables. The temperature dependence of d or ln$d$ in these systems also follows relations similar to those in the one-component liquids, but the best-fit parameters of these relations are now dependent on the cosolvent or solute content x_2. For example, when this type of system follows a quadratic relation, the constants a_2 and b_2 of Eq. (7.28) relating the expansivity α_V with ΔT are also functions of x_2. If these constants follow the relation

$$y = y_0 + y_1 x_2 + y_2 x_2^2 = \sum_{i=0}^{n} y_i x_2^i \ , \tag{7.29}$$

where i is an integer with its maximum value equal to n, and y denotes both a_2 and b_2, the expansivity α_V may be described by

$$\alpha_V(\Delta T, x) = A_0(\Delta T) + A_1(\Delta T)x_2 + A_2(\Delta T)x_2^2 = \sum_{j=0}^{m} A_j(\Delta T)x_2^j \ , \tag{7.30}$$

where j is an integer with its maximum value equal to m different from the integer n, and the ΔT-dependent constants are given by

$$A_0(\Delta T) = -(a_{20} + 2b_{20}\Delta T) \ , \tag{7.31}$$

$$A_1(\Delta T) = -(a_{21} + 2b_{21}\Delta T) \ , \tag{7.32}$$

$$A_2 = -(a_{22} + 2b_{22}\Delta T) \ , \tag{7.33}$$

with a's and b's as new constants.

Instead of analyzing the data of density d of solvent mixtures and homogeneous solutions as a function of temperature T to determine the values of constants of some equation and subsequently to establish the dependence of these constants on x_2, the data may equally be analyzed using the reverse order. An example of this procedure is presented in Section 7.3.3.

7.3. Thermal expansivity of solvents

Common solvents are various compounds existing in the liquid state under usual temperature and pressure conditions. Typical examples are: water, alcohols and many low melting-point aliphatic compounds (González et al., 2007; Holguin et al., 2011; Pang et al., 2007), ketones, aromatic hydrocarbons such as benzene and xylene (Vraneš et al., 2015; Zhang et al., 2013), and different types of ionic liquids (Domańska and Królikowska, 2012; Domańska and Laskowska, 2009; Mokhtarani et al., 2009; Vraneš et al., 2015). Water is a popular solvent because it has low toxity and low viscosity, it is cheap and easily available in the pure state, and is miscible with many organic solvents and ionic solvents. In contrast to water, organic solvents, in general, are volatile, toxic and inflammable. However, ionic liquids are a new class of solvents which have low vapor pressure, low flammability, good chemical stability, and excellent miscibility with water and organic and semiorganic solvents.

In this section, some characteristic features of the thermal expansivity α_V of individual solvents and solvent mixtures are presented and discussed from examination of the published data of the temperature and composition dependences of the density d of selected solvents and solvent mixtures.

7.3.1. General features of thermal expansivity of individual solvents

Here general trends of the temperature dependence of the thermal expansivity α_V of solvents are presented from an examination of the published data of density d or molar volume V_M of the *n*-alcohols up to 1-tetradecanol and for some randomly selected organic solvents and thiocyanate ionic liquids. Theoretical relations (7.5) and (7.6), rewritten in the form of Eq. (7.27), were used to analyze the data taking $T_0 = 273.15$ K as the reference temperature, with $\ln d_0$, a_2 and b_2 as best-fit constants ($a_2 < 0$ and $b_2 \leq 0$), and $\Delta T = (T-T_0) > 0$. However, when $V_M(\Delta T)$ data are analyzed according to a similar equation, $\ln V_M^o$ is the value of $\ln V_M$ when $\Delta T = 0$ and both best-fit constants $a_2 > 0$ and $b_2 \geq 0$. Note that $\ln d_0 = \ln M - \ln V_M^o$ where M is the molar mass of the solvent. In order to verify whether $\ln d(\Delta T)$ or $d(\Delta T)$ data for the liquids provide their better description, the temperature dependence of d for water covering the data in a wide temperature interval between 10 and 90 °C was considered for the analysis. The parameters a_2 and b_2 of Eq. (7.27) directly give values of the initial thermal expansivity α_V^o and its change, equal to $2b_2$ in α_V per °C, with an increase in ΔT of the liquid. These parameters a_2 and $2b_2$, which define the initial thermal expansivity α_V^o and its change $2b_2$, follow from the differentiation of Eq. (7.27).

Figure 7.1a and b shows the dependence of ln*d* of water, and methanol and ethanol, respectively, on their temperature T according to Eq. (7.27). The density data for these solvents are taken from different sources. It may be seen from Figure 7.1a that the data for water from the three sources are in excellent agreement with each other. However, the values of ln*d* for methanol and ethanol reported by González et al. (2007) in Figure 7.1b are somewhat higher than those by Ortega (1982), whereas those for ethanol are comparable with those reported by Holguin et al. (2011). Therefore, in view of relatively wide temperature intervals and reliability of measured density, the data of density d for water reported by Lide (1996/1997), for methanol by Ortega (1982) and for ethanol by Holguin et al. (2011) are considered for the analysis. Curves in Figure 7.1 represent the above data with the best-fit values of the constants listed in Table 7.1. The values of d_0, a_1 and b_1 obtained from the $d(\Delta T)$ data for water according to Eq. (7.25) are also given in the parenthesis in this table.

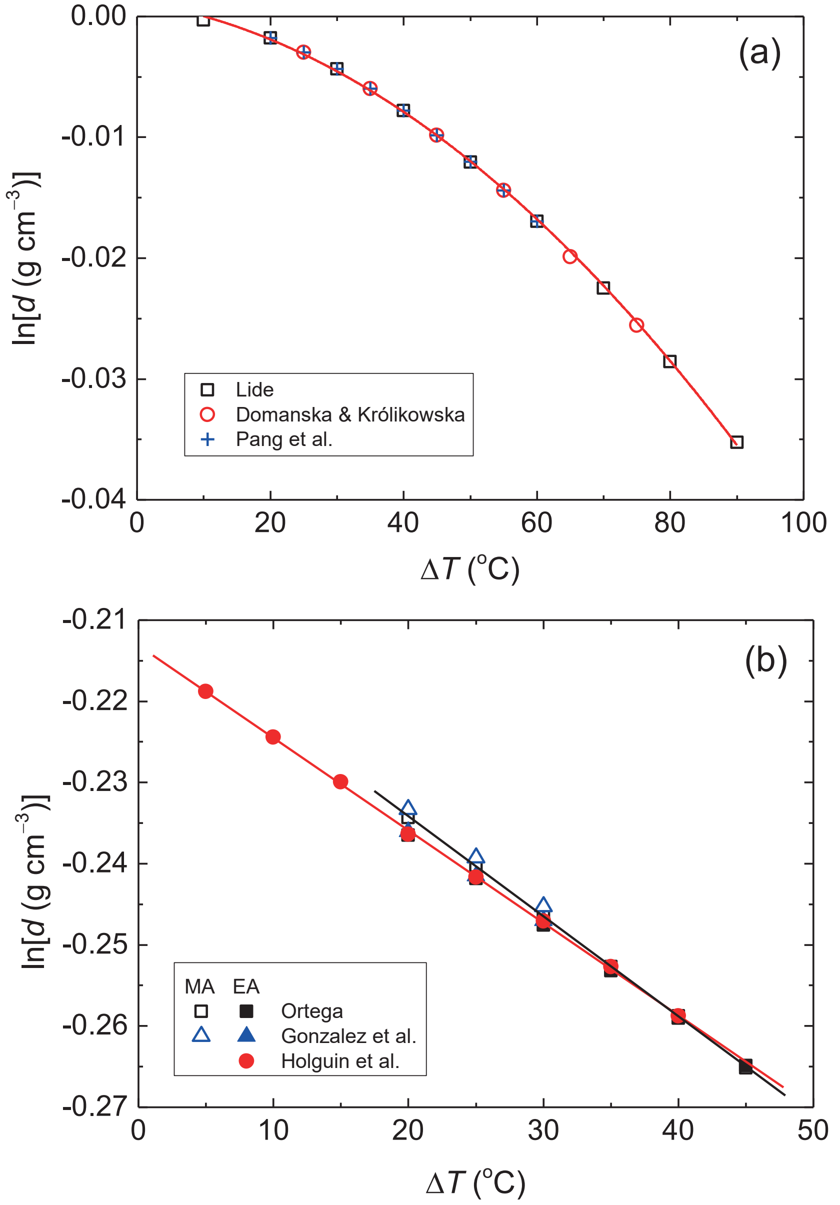

Figure 7.1. Dependence of ln*d* of (a) water and (b) methanol and ethanol on temperature difference ΔT. Data for water are from Lide (1996/1997), Domańska and Królikowska (2012) and Pang et al. (2007), for methanol (MA) from Ortega (1982) and González et al. (2007), and for ethanol (EA) from Ortega (1982), González et al. (2007) and Holguin et al. (2011). Plots are drawn with best-fit constants given in Table 7.1. See text for details.

Table 7.1. Values of the constants of Eq. (7.27)

Solvent	Notation	$\ln d_0$	$-a_2$ (°C^{-1})	$-b_2$ (°C^{-2})	R^2	Data
Water	C0	$1.23\cdot10^{-3}$	$8.42\cdot10^{-5}$	$3.60\cdot10^{-6}$	0.99971	a
		(1.0013)	($9.18\cdot10^{-5}$)	($3.45\cdot10^{-6}$)	(0.99964)	a*
Methanol	C1	−0.2108	$1.15\cdot10^{-3}$	$1.31\cdot10^{-6}$	0.99996	b
		−0.2095	$1.23\cdot10^{-3}$		0.99989	
Ethanol	C2	−0.2130	$1.15\cdot10^{-3}$	$2.84\cdot10^{-7}$	0.99955	c
		−0.2131	$1.14\cdot10^{-3}$		0.99962	
1-Propanol	1-C3	−0.1982	$9.80\cdot10^{-4}$	$1.75\cdot10^{-7}$	0.99963	d
		−0.1979	$9.95\cdot10^{-4}$		0.99968	
2-Propanol	2-C3	−0.2227	$8.91\cdot10^{-4}$	$3.09\cdot10^{-6}$	0.99984	d
		−0.2182	$1.14\cdot10^{-3}$		0.99878	
1-Butanol	C4	−0.1938	$8.41\cdot10^{-4}$	$1.88\cdot10^{-6}$	0.99999	e
		−0.1896	$1.03\cdot10^{-3}$		0.99911	
1-Pentanol	C5	−0.1882	$8.14\cdot10^{-4}$	$1.64\cdot10^{-6}$	0.99999	e
		−0.1846	$9.78\cdot10^{-4}$		0.99925	
1-Hexanol	C6	−0.1839	$7.94\cdot10^{-4}$	$1.49\cdot10^{-6}$	1	e
		−0.1806	$9.43\cdot10^{-4}$		0.99933	
		−0.1830	$8.44\cdot10^{-4}$	$9.54\cdot10^{-7}$	0.99968	f
		−0.1812	$9.35\cdot10^{-4}$		0.99946	
1-Octanol	C8	−0.1754	$8.11\cdot10^{-4}$	$7.94\cdot10^{-7}$	0.99968	f
		−0.1739	$8.86\cdot10^{-4}$		0.99943	
1-Decanol	C10	−0.1698	$7.89\cdot10^{-4}$	$8.86\cdot10^{-7}$	0.99989	f
		−0.1682	$8.73\cdot10^{-4}$		0.99954	
1-Dodecanol	C12	−0.1687	$7.39\cdot10^{-4}$	$1.06\cdot10^{-4}$	0.99903	f
		−0.1661	$8.51\cdot10^{-4}$		0.99873	
1-Tetradecanol	C14	−0.1671	$3.67\cdot10^{-4}$	$1.31\cdot10^{-6}$	0.99675	f
		−0.1626	$8.47\cdot10^{-4}$		0.99490	

[a] Lide (1996/1997); [b] Ortega (1982); [c] Holguin et al. (2011); [d] Pang et al. (2007); [e] Domańska and Laskowska (2009); [f] Liew et al. (1993). * From $d(\Delta T)$ data instead of $\ln d(\Delta T)$ data.

Figure 7.2a and b shows plots of $\ln d$ of *n*-alcohols from 1-propanol to 1-hexanol (open points) and 2-propanol (filled squares), and $\ln V_M$ of *n*-alcohols from 1-hexanol (open squares and plus signs) to 1-tetradecanol (open points) on their temperature T. The original data of the density d in Figure 7.2a for 1-propanol (1-C3) and 2-propanol (2-C3) and for 1-butanol, 1-pentanol and 1-hexanol are from Pang et al. (2007) and Domańska and Laskowska (2009), respectively, whereas the original data of molar volume V_M for 1-hexanol up to 1-tetradecanol in Figure 7.2b are from Liew et al. (1993). In Figure 7.2b the V_M data for 1-hexanol, calculated from density data reported by Domańska and Laskowska (2009), are shown by plus signs. It may be seen that the $V_M(\Delta T)$ data obtained from the density data reported by Domańska and Laskowska (2009) are in excellent agreement with those from Liew et al. (1993). Linear plots in Figure 7.2 are drawn according to Eq. (7.27) with the best-fit parameters listed in Table 7.1. For higher alcohols the values of $\ln d_0$ listed in this table were obtained from the best-fit values of $\ln V_M^{\circ}$ from the plots of Figure 7.2b and their molar masses M.

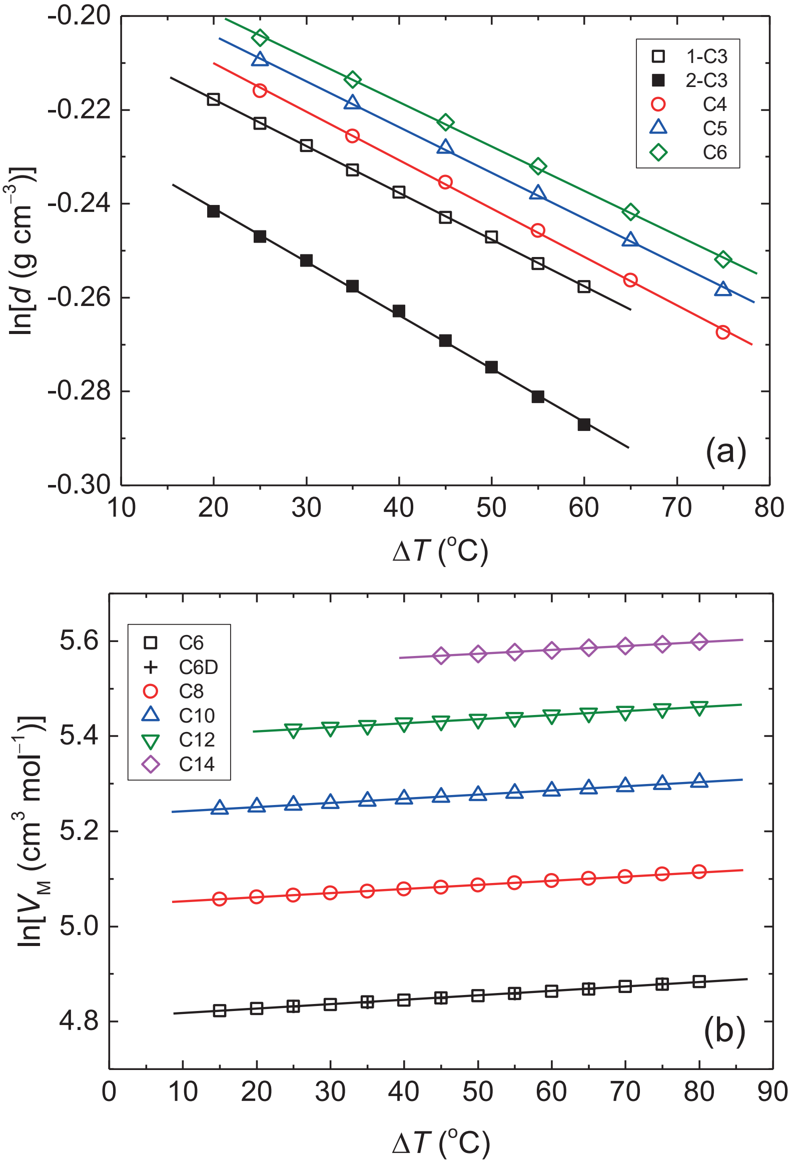

Figure 7.2. Dependence of (a) ln$d$ of n-alcohols from 1-propanol to 1-hexanol (open points) and 2-propanol (filled squares), and (b) lnV_M of n-alcohols from 1-hexanol (open squares and plus signs) to 1-tetradecanol (open points) on temperature difference ΔT. Original data of density d (a) for 1-propanol (1-C3) and 2-propanol (2-C3) from Pang et al. (2007), and for 1-butanol, 1-pentanol and 1-hexanol from Domańska and Laskowska (2009), and of molar volume V_M (b) for 1-hexanol up to 1-tetradecanol from Liew et al. (1993). Linear plots are drawn according to Eq. (7.27) with best-fit parameters listed in Table 7.3. In (b) data for 1-hexanol shown by plus signs (C6D) were calculated from density data reported by Domańska and Laskowska (2009). See text for details.

As seen from the goodness-of-the-fit parameter R^2 listed in Table 7.1, the $\ln d(\Delta T)$ data for different solvents are represented by the quadratic dependence better than the linear dependence. Similarly, as seen in the case of the temperature dependence of the density d of water which shows enormous decrease in its density d with increasing temperature, the quadratic dependence of $\ln d$ on ΔT represents the experimental data better than that of d on ΔT. A general feature of the differences in the values of $\ln d_0$ and $-a_2 = \alpha_V^o$ obtained from the analysis of the $d(\Delta T)$ data for various solvents, with the exception of 1-tetradecanol, is that the value of both $\ln d_0$ and α_V^o obtained by the quadratic function are lower up to about 2 and 20% than those obtained by the linear function. It may be seen from Table 7.1 that the value of $\ln d_0$ (and also d_0) increases and that of y_1 decreases with an increase in the number N of CH_2- groups in the chains of alcohol molecules. However, the general trends of the variation of $\ln d_0$ and $-a_2 = \alpha_V^o$ obtained by quadratic and linear functions as a function of N are essentially the same. One also notes that, despite large scatter in their values, the value of b_2 shows a general tendency to decrease with an increase in N.

In the quadratic function (7.27) the value of the constant $-a_2$ for a solvent represents the initial, lowest value of its expansivity α_V when $\Delta T \to 0$ °C and the corresponding value of d_0 is related to the average distance between the molecules of the liquid whereas the constant b_2 is a measure of loosening of attractive interaction between the molecules with increasing temperature. These observations are associated with decreasing interaction between the solvent molecules due to increasing distance between them with increasing temperature.

Figure 7.3 illustrates some examples of the dependence of the published data of the thermal expansivity α_V of solvents so diverse as some organic solvents, complex thiocyanate ionic liquids and water on temperature ΔT. Figure 7.3a and b shows the temperature dependence of α_V of a silicone intermediate (D4Vi), ethylbenzene and three xylene polymers, and of four thiocyanate ionic liquids and water, respectively. Plots are drawn according to Eq. (7.21), with the constants listed in Table 7.2. The constants α_V^o and α_1 are equal to a_2 and $2b_2$, respectively, of relation (7.28). The abbreviations of the solvents are: 2,4,6,8-tetramethyl-2,4,6,8-tetraethenylcyclotetrasiloxane (D4Vi), 1-butyl-3-methylimidazolium thiocyanate ([bmim][SCN]), 1-butyl-4-methylpyridinium thiocyanate ([bmpy][SCN]), 1-butyl-1-methylpyrrolidinium thiocyanate ([bmpyr][SCN]), and 1-butyl-1-methylpiperidinium thiocyanate ([bmpip][SCN]), with their molar masses M and densities d^{25} at 25 °C included in Table 7.2. The values of α_V^o and α_1 for another solvent γ-butyrolactone and two ionic liquids: 1-butyl-1-methylpyrrolydinium bis(trifluoromethylsulfonyl)imide ([bmpyr][NTf_2]) and 1-butyl-3-methylimadazolium hexafluorophosfate ([bmim][Pf_6]) calculated from the data of α_V as a function of ΔT published by Vraneš et al. (2015), and Marsh et al. (2004) are also listed in the table.

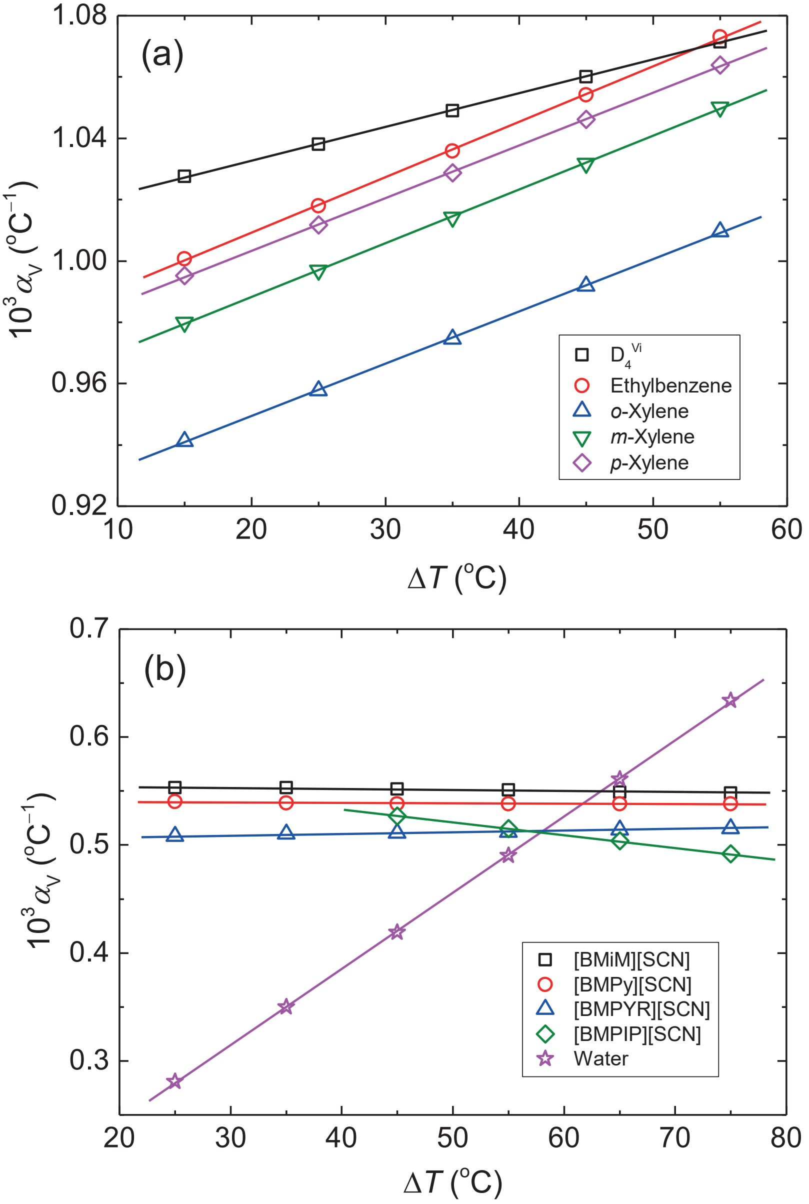

Figure 7.3. Dependence of thermal expansivity α_V of some organic solvents, thiocyanate ionic liquids and water on temperature difference ΔT: (a) a silicone intermediate (D4Vi), ethylbenzene and xylene polymers, and (b) four thiocyanate ionic liquids and water. Original α_V data from: (a) Zhang et al. (2013), and (b) Domańska and Królikowska (2012). Plots are drawn according to Eq. (7.28) with constants listed in Table 7.2.

Table 7.2. Values of constants of Eq. (7.21) for some liquids

Solvent	M	d^{25} (g·cm^{-3})	$10^3\alpha_V^o$ (^{o}C^{-1})	$10^6\alpha_1$ (^{o}C^{-2})	R^2	Data
D4Vi	344.66	0.98765	1.0107	1.01	0.9997	a
Ethylbenzene	106.17	0.86255	0.9730	1.81	0.9997	a
o-Xylene	106.17	0.87567	0.9152	1.71	0.9997	a
m-Xylene	106.17	0.85983	0.9533	1.75	0.9997	a
p-Xylene	106.17	0.85662	0.9691	1.72	0.9996	a
γ-butyrolactone	--	1.12426	0.8777	0.82	0.9996	c
[bmim][SCN]	197.3	1.06979	0.5564	−0.11	0.9221	b
[bmpy][SCN]	208.2	1.06127	0.5404	−0.04	0.6122	b
[bmpyr][SCN]	200.4	1.02477	0.5048	0.14	0.9843	b
[bmpip][SCN]	214.4	--	0.5791	−1.16	0.9998	b
[bmpyr][NTf$_2$]	--	1.39457	0.6206	0.40	0.9996	c
[bmim][Pf$_6$]	--	1.3850	0.6080	0.42	0.9998	d
Water	18.0	0.99704	0.1031	7.05	0.9998	b

[a] Zhang et al. (2013); [b] Domańska and Królikowska (2012); [c] Vraneš et al. (2015); [d] Marsh et al. (2004).

The values of the thermal expansivity α_V^o and the increment α_1 obtained for water from the plot of Figure 7.3b (see Table 7.2) are comparable with their values obtained from the plot of Figure 7.1b (Table 7.1). The values of α_V^o and α_1 for D4Vi, ethylbenzene, and three xylene polymers and γ-butyrolactone are comparable with those of alcohols mentioned above. With the exception of γ-butyrolactone, these characteristics are intimately connected with their densities d^{25}, which are also similar to those of the alcohols. In contrast to the above solvents, the values of α_V^o and α_1 for the six ionic liquids, with their densities d^{25} exceeding 1 g·cm^{-3} analyzed here, are not only relatively low but the value of the change α_1 for the three of them are even negative. Comparison of the values of α_V^o and α_1 for ionic liquid pairs, such as [bmim][SCN] and [bmim][Pf$_6$], as well as [bmpyr][SCN] and [bmpyr][NTf$_2$] composed of common cations and anions, shows that the contributions of anions [Pf$_6$]$^-$ and [NTf$_2$]$^-$ to the cations [bmim]$^+$ and [bmpyr]$^+$ are more than that of the anion [SCN]$^-$. This observation suggests that the contributions of anions and cations of ionic liquids to the values of α_V^o and α_1 are additive.

7.3.2. Relationship between expansivity and alcohol molecules

It was mentioned above that the extrapolated values of lnd_0 at $T \to 0$ °C increases and the corresponding expansivity α_V^o decreases with an increase in the number N of CH$_2$– groups in *n*-alcohol molecule chains (see Table 7.1). These trends are followed by both lnd_0 and α_V^o data of the alcohols, and may be described by different empirical functions, including the simple power-law relation: $y = y_0N^q$, expressed in the form

$$\ln y = \ln y_0 + q \ln N, \tag{7.34}$$

where y denotes both d_0 (g·cm^{-3}) and α_V^o (^{o}C^{-1}), lny_0 represents the values of lnd_0

and $\ln\alpha_V^o$ corresponding to $\ln N = 0$ (i.e. $N = 1$), and q is a constant. Figure 7.4 shows plots of $\ln d_0$ and $\ln\alpha_V^o$, obtained from linear (LR) and quadratic (QR) dependences of $\ln d$ on ΔT according to Eq. (7.27), against $\ln N$. With the exception of methanol, Eq. (7.34) represents the data for other alcohols reasonably well, with the best-fit constants given in Table 7.3.

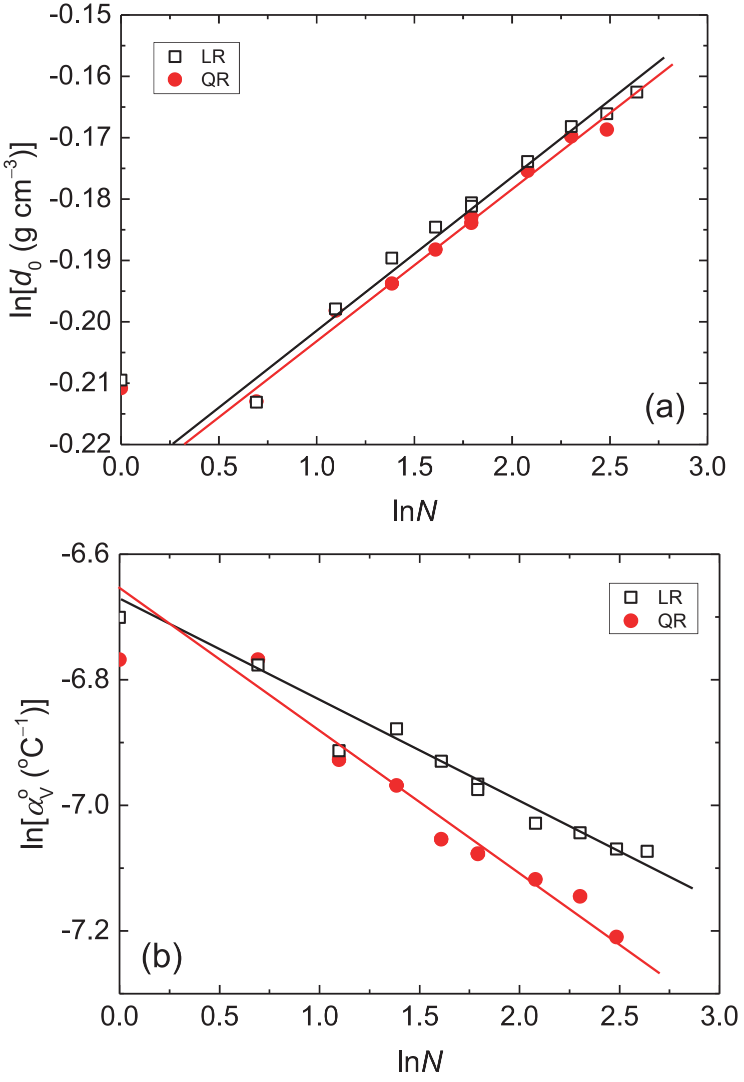

Figure 7.4. Dependence of (a) $\ln d_0$ and (b) $\ln\alpha_V^o$, corresponding to $\Delta T \to 0$ °C, obtained from $\ln d(\Delta T)$ data by linear (LR) and quadratic (QR) relations on $\ln N$ of CH_2– groups in *n*-alcohol molecule chains. Plots are drawn according to exponential function (7.34), excluding data for methanol, with constants listed in Table 7.3. LR data for 1-propanol in (b) was omitted during analysis. Original data from Table 7.1.

Table 7.3. Constants of Eq. (7.34) for $d_0(N)$ and $\alpha_V^o(N)$ data

Data	Source	$-\ln y_0$	q (–)	R^2
$d_0(N)$	LR	0.2280	0.0248	0.9863
	QR	0.2265	0.0250	0.9824
$\alpha_V^o(N)$	LR	6.671	−0.161	0.9759
	QR	6.654	−0.227	0.9567

It should be mentioned that, although Eq. (7.34) describes both $d_0(N)$ and $\alpha_V^o(N)$ data well, as seen from the R^2 parameter listed in Table 7.3, the LR data give a better fit than the QR data. This is associated with the fact that the expansivity α_V^o of these alcohols is practically independent of temperature in the range of temperature of density measurements used in the above analysis. The extrapolated values of $\ln d_0$ and $\ln\alpha_V^o$ corresponding to $\ln N = 0$ (i.e. methanol) practically do not depend on the source of their data for the analysis, but deviate significantly from the "experimental" values of $\ln d_0$ and $\ln\alpha_V^o$. In the case of methanol, one also observes that the value of $\ln d_0$ obtained from the experimental $d(T)$ data is higher than the extrapolated $\ln d_0$, and the "experimental" value of $\ln\alpha_V^o$ is lower than the extrapolated $\ln\alpha_V^o$. These observations are due to the fact methanol is an associated liquid which results in a weak dependence of $\ln\alpha_V^o$ on ΔT (see Figure 7.1b).

The opposite trends of the dependences of the data of d_0 and α_V^o on the number N of CH_2– groups in *n*-alcohol molecule chains seen in Figure 7.4 suggest that both d_0 (and V_M^o) and α_V^o are mutually related. However, instead of studying the relationship between d_0 and α_V^o for the alcohols, the data of α_V^o as a function of the molar volumes V_M^o of these alcohols are more informative because, with the exception of methanol, V_M^o of alcohols is directly related to their N. As an illustration of this type of relationship, Figure 7.5 shows the data of the molar volume V_M^o of different *n*-alcohols, calculated from $\ln d_0$ data of Table 7.1 for the linear (LR) and quadratic (QR) fits, the number N of CH_2– groups in their molecule chains according to relation (7.34) in the form of plot of $\ln V_M^o$ against $\ln N$. Since the two values of $\ln V_M^o$ for an alcohol differ insignificantly, the LR data were analyzed, as shown from the plot drawn the following best-fit values of the constants: $\ln y_0 = 3.468\pm0.032$ and $q = 0.761\pm0.018$, $R^2 = 0.9954$.

Figure 7.6a and b shows that the LR and QR data of $\ln\alpha_V^o$ of different alcohols as functions of $\ln d_0$ and $\ln V_M^o$, respectively, follow the linear relation:

$$\ln\alpha_V^o = \alpha_0 - \beta_0 \ln(d_0, V_M^o), \tag{7.35}$$

where the intercept α_0 represents the value of $\ln\alpha_V^o$ when $\ln d_0$ or $\ln V_M^o = 1$ and the intercept β_0 is a measure of increase in $\ln d_0$ or $\ln V_M^o$. These constants are listed in Table 7.4. The higher values of α_0 and the lower values of β_0 from the $\ln\alpha_V^o(\ln d_0)$ than those from the $\ln\alpha_V^o(V_M^o)$ are associated with the fact that $\ln V_M^o = \ln d_0 - \ln M$ and $\partial\ln V_M^o > \partial\ln d_0$. However, in view of deviation of some of the points of the

$\ln\alpha_V^o(\ln d_0)$ and $\ln\alpha_V^o(\ln V_M^o)$ data obtained by linear and quadratic relations according to Eq. (7.35), it is difficult to decide which data are superior.

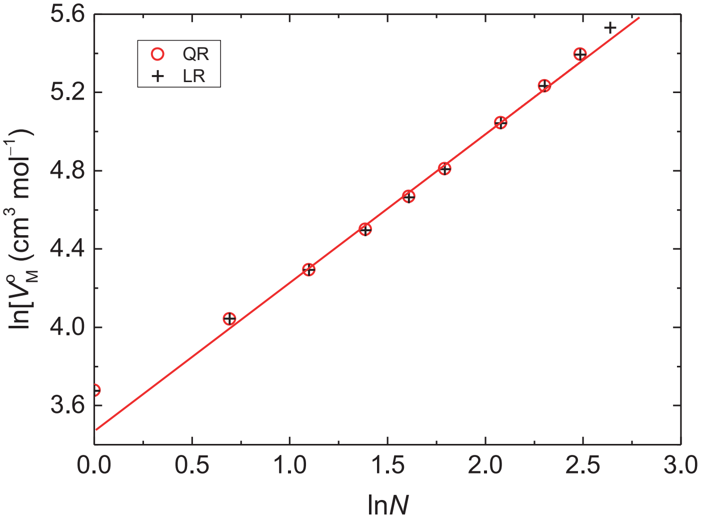

Figure 7.5. Dependence of $\ln V_M^o$ on $\ln N$ for different *n*-alcohols. Values of $\ln V_M^o$ were obtained from $\ln d_0$ data of Table 7.1. Methanol was excluded from analysis. See text for details.

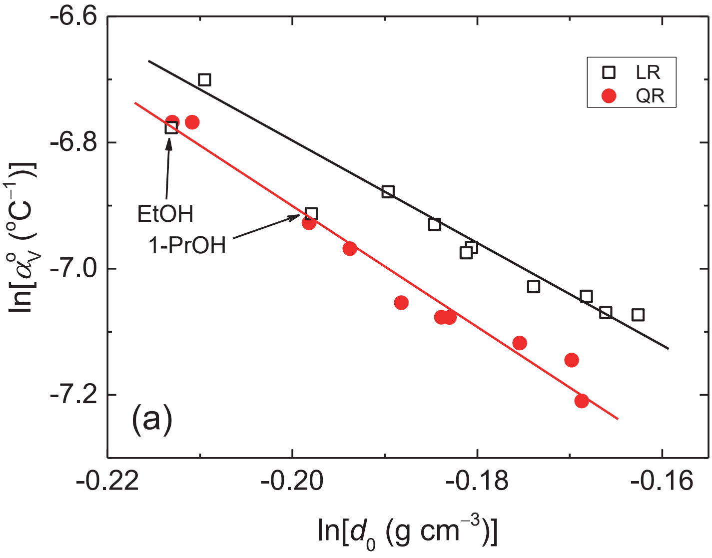

(Continued)

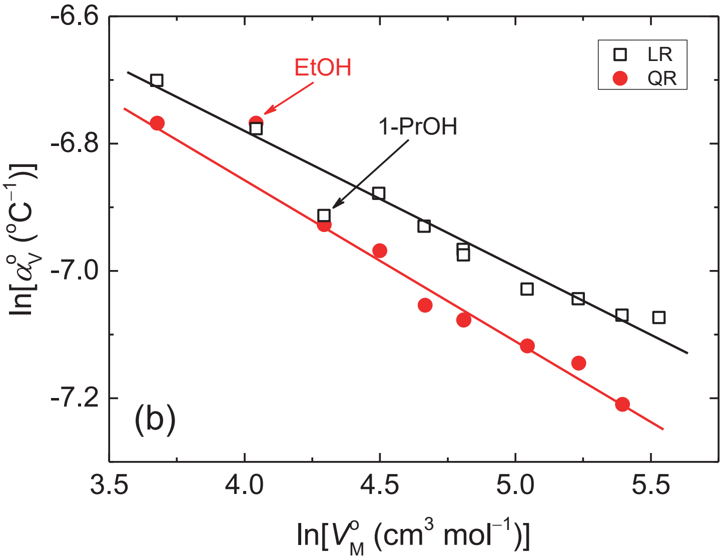

Figure 7.6. Linear dependence of data of lnα_V^o on (a) lnd_0 and (b) lnV_M^o for various *n*-alcohols. Best-fit constants for LR and QR data according to Eq. (7.35) are given in Table 7.4. Data indicated by arrows were omitted during analysis. Values of lnV_M^o were calculated from lnd_0 data of Table 7.1.

Table 7.4. Constants of Eq. (7.35) for lnα_V^o(lnd_0) and lnα_V^o(lnV_M^o) data

Data	Source	$-\alpha_0$	$-\beta_0$	R^2
lnα_V^o(lnd_0)	LR	8.420±0.084	8.11±0.46	0.9744
	QR	8.818±0.109	9.59±0.58	0.9684
lnα_V^o(lnV_M^o)	LR	5.926±0.053	0.213±0.011	0.9787
	QR	5.845±0.050	0.253±0.012	0.9825

Finally, it should be mentioned that Eq. (7.35) follows from Eq. (7.21), which predicts that $\alpha_V^o \propto V_M^{-1/3}$ since molar volume $V_M \propto r_0^3$. The value of β_0 from the lnα_V^o(lnV_M^o) data, although somewhat lower than the expected value, is consistent with the above prediction.

7.3.3. Thermal expansivity of mixtures of solvents

In this section examples of calculation of the expansivity α_V of solvent mixtures of different cosolvent content x_2 from the data of their density d in relation to mixture composition and temperature are presented. Two systems of mixtures composed of the popular solvent water and two cosolvents 1-propanol and [bmim][SCN], which are miscible with water in all proportions and have their densities higher than that of water at different temperatures, were selected for analysis.

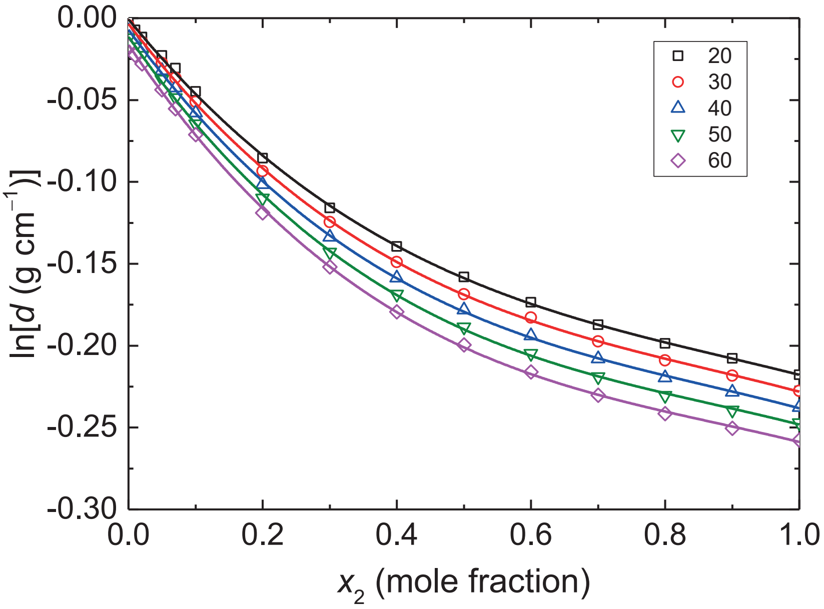

Figure 7.7. Plots of density *d* of water–1-propanol mixture against alcohol content x_2 for some selected temperatures *T*. Curves represent best fit of the data according to third-order polynomial, with the values of constants a_i shown in Figure 7.8. Original density data from Pang et al. (2007).

Figure 7.7 shows typical examples of the data of density *d* of water–1-propanol mixture as ln*d* against alcohol content x_2 for some selected temperatures *T*. Plots represent best fit of the data according to the polynomial

$$\ln d = \sum_{i=0}^{n} a_i x_2^i , \tag{7.36}$$

where *i* as an integer with its highest value of *n* equal to 3 for the above system.

The best-fit values of constants a_i from the plots of ln*d* against different temperatures ΔT of the mixtures are shown in Figure 7.8. These data may be represented by the relation

$$a_i = \sum_{j=0}^{m} a_{ij} (\Delta T)^j , \tag{7.37}$$

where *j* is an integer, with its highest value equal to *m*, and a_i's denote the parameters of Eq. (7.36). The $a_i(\Delta T)$ data were analyzed with $m = 1$ and 2, with the constants a_{ij} listed in Table 7.5.

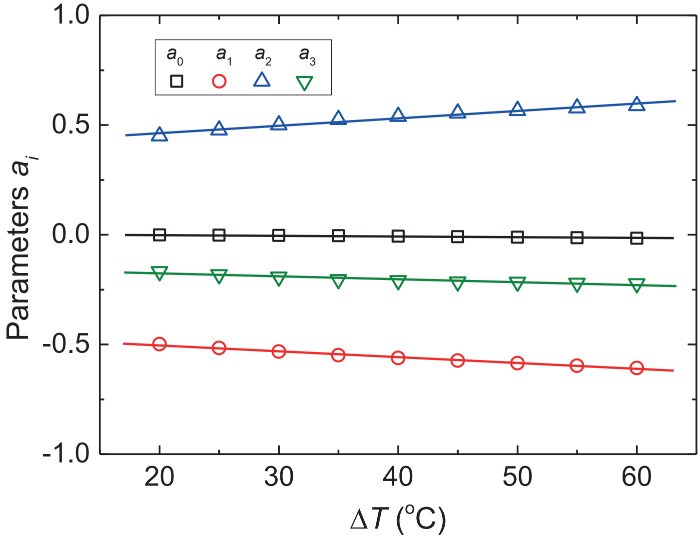

Figure 7.8. Constants a_i of third-order polynomial against mixture temperature difference ΔT of water–1-propanol mixture. Plots are drawn according to their linear dependence on ΔT, with best-fit values listed in Table 7.5.

Table 7.5. Values of best-fit constants a_{ij} of Eq. (7.37) for water–1-propanol mixture

Data	a_{i0}	a_{i1}	a_{i2}	R^2
$a_0(\Delta T)$	$7.95\cdot10^{-3}$	$-3.907\cdot10^{-4}$	--	0.9882
	$2.92\cdot10^{-3}$	$-1.102\cdot10^{-4}$	$-3.507\cdot10^{-6}$	0.9999
$a_1(\Delta T)$	−0.4504	$-2.70\cdot10^{-3}$	--	0.9901
	−0.4193	$-4.43\cdot10^{-3}$	$2.172\cdot10^{-5}$	0.9994
$a_2(\Delta T)$	0.3951	$3.38\cdot10^{-3}$	--	0.9644
	0.3206	$7.54\cdot10^{-3}$	$-5.197\cdot10^{-5}$	0.9976
$a_3(\Delta T)$	−0.1501	$-1.32\cdot10^{-3}$	--	0.9047
	−0.1015	$-4.03\cdot10^{-3}$	$3.388\cdot10^{-5}$	0.9047

Using the definition of α_V and the dependences of constants a_i on ΔT, one obtains (cf. Eq. (7.28))

$$\alpha_V = -\frac{d\ln d}{d\Delta T} = -d\left(\sum_{i=0}^{n} a_i x_2^n\right)\Big/ d\Delta T\,, \tag{7.38}$$

where $n = 3$ and $m = 1$ or 2. Note that the constants a_i change linearly with ΔT (linear relation; LR) when $m = 1$ and α_V is independent of ΔT. In this case, one obtains a single curve, independent of the temperature ΔT of the d data, of the dependence of α_V on x_2. However, the constants a_i change with ΔT following a quadratic relation (QR) when $m = 2$, and α_V depends both on ΔT and x_2.

It may be noted from Table 7.5 that, in comparison with the linear relation, the quadratic relation (7.37) with $m = 2$ used for their analysis significantly improves the fit of the $a_i(\Delta T)$ data. The values of the expansivity α_V of water–1-propanol mixture, calculated with the constants of Table 7.5 obtained for $m = 1$ (LR) and $m = 2$ (QR) for 20 and 60 °C, are shown against alcohol content x_2 in Figure 7.9. As expected, the quadratic relation alone explains the temperature dependnce of α_V.

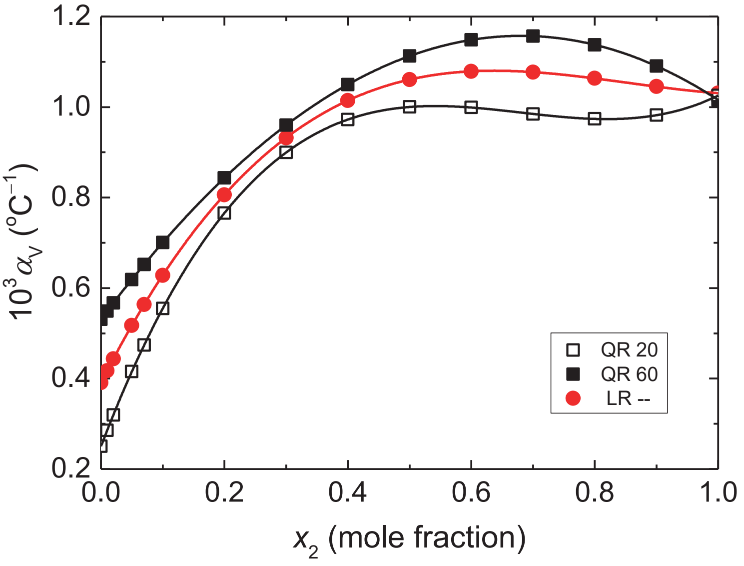

Figure 7.9. Values of expansivity α_V of water–1-propanol mixture against alcohol content x_2. Values of α_V were calculated according to Eq. (7.38) with the constants of Table 7.5 obtained for $m = 1$ (LR) and $m = 2$ (QR) for 20 and 60 °C. See text for details.

The above analysis of the dependence of α_V of solvent mixture on cosolvent content x_2 reveals that precise determination of the dependence of constants a_i's on ΔT is an important step using quadratic relation. However, the dependence of a_i's on ΔT for other systems may not be so simple as encountered in the above example. Systems of different ionic liquids mixed with water and different organic solvents in different proportions are typical examples of this behavior.\

Figure 7.10 presents plots of density d of water–[bmim][SCN] mixture against cosolvent content x_2 for selected temperatures T. In contrast to the above example of decrease in the density d of the mixture with increasing x_2 of 1-propanol in Figure 7.7, the values of the density d of the water–[bmim][SCN] mixture at different temperature increase with an increase in the [bmim][SCN] content x_2. These differences in the decreasing and increasing trends of the densities of the mixtures at various temperatures are associated with lower and higher densities of the cosolvents 1-propanol and [bmim][SCN] than those of the solvent water. In the figure the curves represent best fit of the data according to nineth-order polynomial (cf. Eq.

(7.36)), with the values of first four constants a_i, as examples, shown in Figure 7.11. The dependence of these constants a_i's on ΔT is not a simple polynomial as observed in the case of the water–1-propanol mixture discussed above but follows the exponential relation

$$a_i = a_{i0} + a_{i1} \exp\left(\frac{\Delta T}{\Delta T^*}\right), \tag{7.39}$$

where a_{i0}, a_{i1} and ΔT^* are empirical constants characteristic of the parameter a_i.

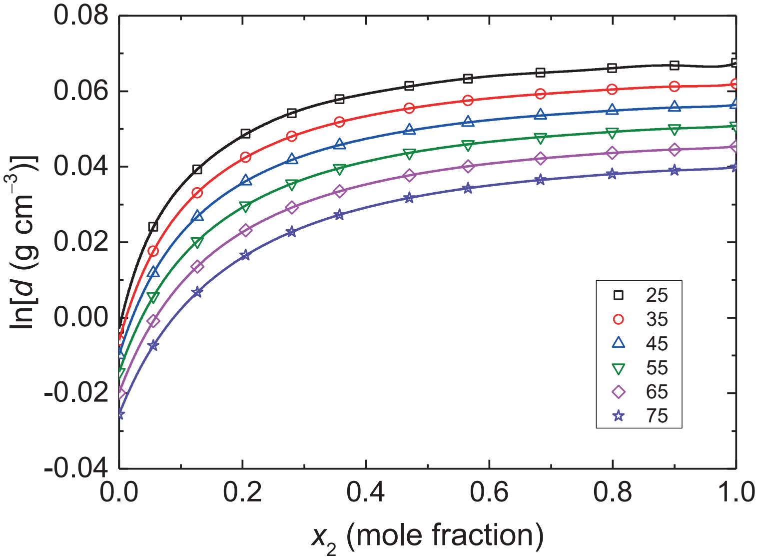

Figure 7.10. Plots of density *d* of water–[bmim][SCN] mixture against cosolvent content x_2 at different temperatures listed in the inset in °C. Curves represent best fit of the data according to nineth-order polynomial, with the values of first four constants a_i shown in Figure 7.8 as a function of ΔT. Original density data from Domańska and Królikowska (2012).

A general feature of the dependence of the expansivity α_V of solvent mixtures on their composition x_2 is that it shows a maximum value at a particular value of x_2 and that the value of x_2 is related to the nature of interactions between the molecules of the two solvents. This behavior may be observed in the case of the water–1-propanol mixture of Figure 7.9. Figure 7.12 illustrates other examples of this feature. This figure presents data of the expansivity α_V of water–[bmim][SCN] (squares) and water–[bmpy][SCN] mixtures (circles) against cosolvent content x_2 for two temperatures. Here ionic liquids [bmim][SCN] and [bmpy][SCN] are 1-butyl-3-methylimidazolium thiocyanate ($C_9H_{15}N_3S$; MW 197.3) and 1-butyl-4-methylpyridinium thiocyanate ($C_{10}H_{20}N_2S$; MW 200.3), respectively. The plots reveal not only higher values of α_V at higher temperature but the values of x_2 corresponding to the maximum value of α_V for the two solvent mixtures also are different and relatively low. In view of the low value of x_2 for the corresponding maximum value of α_V, the $\alpha_V(x_2)$ data for the two systems can be described only by high-order polynomial associated with strong interactions of cosolvent molecules with water molecules. The increase in the values of α_V with increasing temperature is associated with the nonlinear dependence of mixture density on temperature (see Eq. (7.27)).

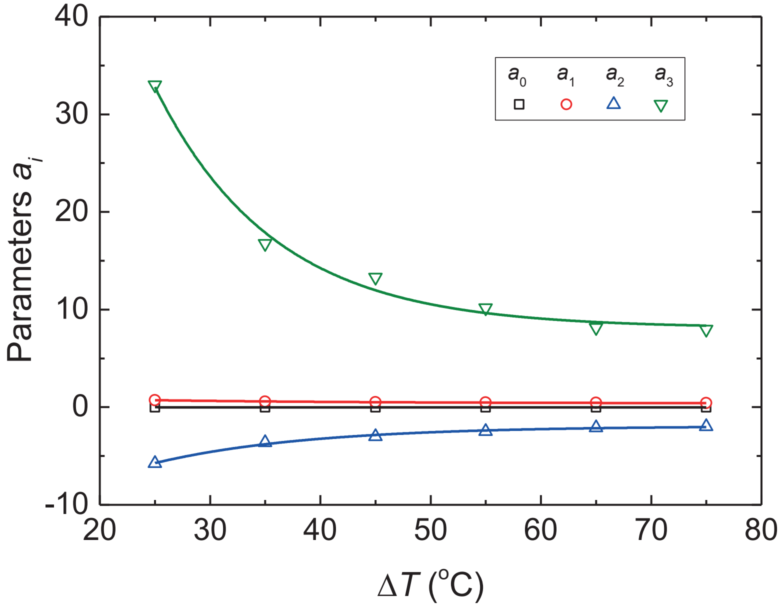

Figure 7.11. First four constants a_i of nineth-order polynomial against mixture temperature difference ΔT of water–[bmim][SCN] mixture. Plots are drawn according to Eq. (7.39).

Figure 7.13 shows plots of excess expansivity $\alpha_V{}^E$ of water–[bmim][SCN] (open points) and water–[bmpy][SCN] mixtures (filled points) against cosolvent content x_2 for two temperatures. The values of $\alpha_V{}^E$ were calculated according to the relation

$$\alpha_V^E = \alpha_V - (\alpha_{V1}x_1 + \alpha_{V2}x_2)\,, \tag{7.40}$$

where the term in the bracket represent the ideal expansivity of the mixture, α_{V1} and α_{V2} are the expansivities of solvent 1 and cosolvent 2, of contents x_1 and x_2, respectively, and $(x_1+x_2) = 1$. It may be seen that $\alpha_V{}^E$ is positive over the entire composition range at the two temperatures and the nature of the curves is asymmetrical, with a maximum $\alpha_V{}^E$ in the plots located at a low value of x_2 of the cosolvent and a decrease in $\alpha_V{}^E$ with an increase in temperature.

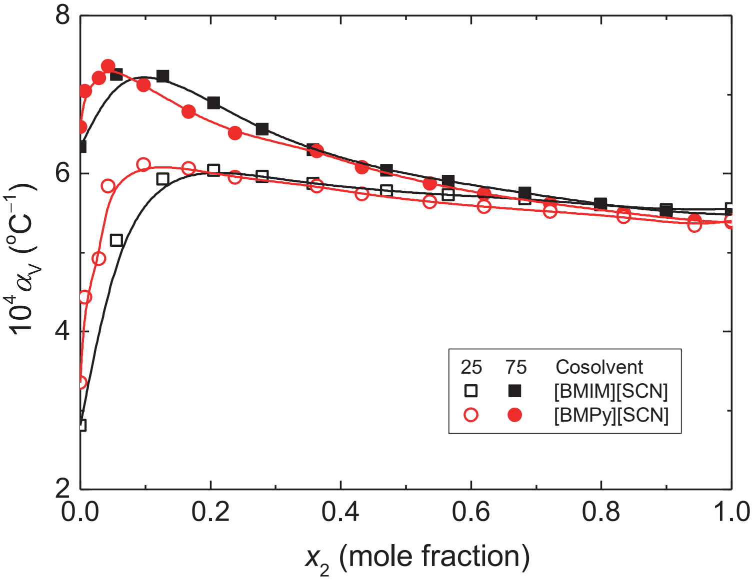

Figure 7.12. Plots of expansivity α_V of water–[bmim][SCN] (squares) and water–[bmpy][SCN] mixtures (circles) against cosolvent content x_2 for two temperatures. Temperatures given in the inset are in °C. Original data from Domańska and Królikowska (2012).

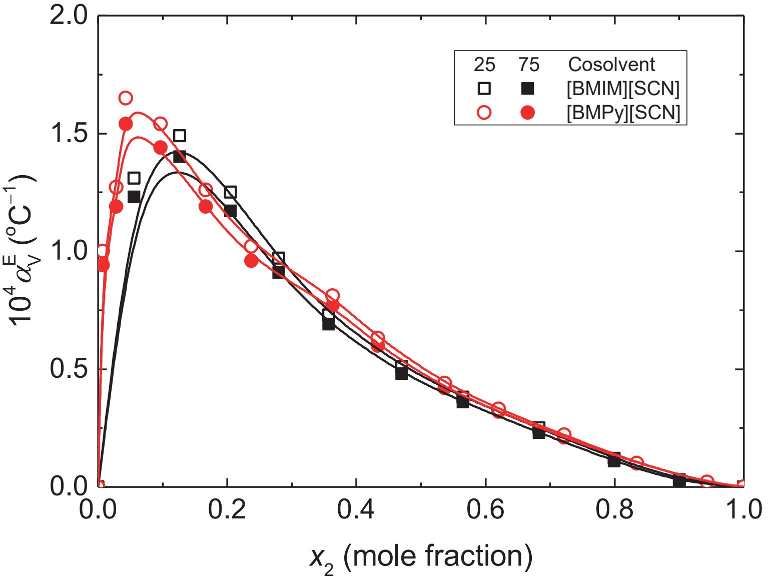

Figure 7.13. Plots of excess expansivity $\alpha_V{}^E$ of water–[bmim][SCN] (squares) and water–[bmpy][SCN] mixtures (circles) against cosolvent content x_2 for two temperatures. Temperatures given in the inset are in °C. Original data from Domańska and Królikowska (2012).

The above example is not an exception. For example, Vraneš et al. (2015) observed a similar behavior of variation of α_V^E of γ-butyrolactone–[bmpyr][NTf2] system as a function of x_2 of the cosolvent [bmpyr][NTf2] at different temperatures between 293.15 and 323.15 K. This system revealed two maxima: a small maximum at $x_2 \approx 0.1$ mole fraction and an abrupt, sharp maximum at $x_2 \approx 0.89$ mole fraction. As mentioned above, these features of the curves are associated with specific interactions between solvent and cosolvent molecules in different composition range. The sharp maximum at $x_2 \approx 0.89$ mole fraction of the solute indicates significant self-association of the ionic liquid. Positive values of α_V^E are typical for systems containing self-associating molecules (for example, see: Tamura et al., 1997; Vraneš et al., 2015). However, some systems, such as γ-butyro-lactone–[bmim]- [NTf2], show negative values of α_V^E, which indicates absence of self-association of the liquid in its entire composition range (Vraneš et al., 2014).

7.4. Expansivity of solutions

Solutions may be composed of nonelectrolytes such as different organic compounds and electrolytes like commonly available salts and different semiorganic compounds dissolved in suitable solvents. Examples of non-electrolytes are: sweeteners and drugs like sucrose and aspartame (Klofutar et al., 2006) and *N*-(2-hydroxyethyl)morpholine (Abu-Daabes and Awaad, 2008), whereas those of electrolytes are: simple salts (Lide, 1996/1997; Mohiuddin and Ismail, 1996) and complex salts such as sweeteners sodium saccharin and potassium acesulfame (Klofutar et al., 2006) and drugs like hydrochlorides of metformin, ranitidine and tramadol (Dhondge et al., 2012). Here it should be mentioned that mixtures of ionic liquids with other solvents are also examples of electrolyte solutions. The chemical consitution of the sweeteners considered below are (Klofutar et al., 2006): 2,3-dihydroxo-3-oxobenzisosulfonazole-Na (sodium saccharin) and 6-methyl-1,2,3-oxathiazine-4-(3H)-one-2,2-dioxide-K (potassium acesulfame) and *N*-L-α-asparyl-L-phenylalaline-1-methyl ester (aspartame).

In this section the trends of the expansivity α_V of solutions of selected salts in some solvent are described as functions of solute concentration x_2 and solution temperature T. The procedure of analysis of the $\alpha_V(x_2,T)$ data of solutions is similar to that used for solvent mixtures discussed above.

Figure 7.14 shows typical examples of plots of ln$d$ of aqueous sodium saccharin solutions at selected temperatures T against salt content m according to Eq. (7.36). The increasing trend of these ln$d$ plots as a function of solute concentration m is similar to that observed in the case of ln$d(x_2)$ plots of water–[bmim][SCN] mixture of Figure 7.10 and is associated with the higher solute density d than that of solvent water. The curves in Figure 7.14 represent the best fit of the data according to the second-order polynomial (cf. Eq. (7.36)), with the values of constants a_i presented in Figure 7.15. This figure shows the constants a_i against the solution temperature difference ΔT. It was observed that the $a_i(\Delta T)$ data may be described satisfactorily according to Eq. (7.37) in the form of quadratic dependence, with the best-fit values of the constants a_{ij} listed in Table 7.6.

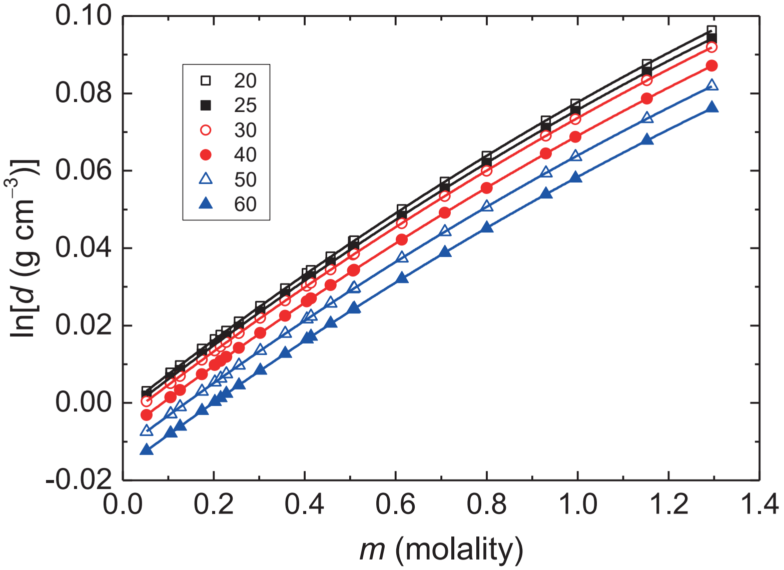

Figure 7.14. Plots of ln*d* of aqueous sodium saccharin solutions of different ΔT against solute concentration *m*. Curves represent best fit of the data according Eq. (7.36), with values of constants a_i shown in Figure 7.15. Original density data from Klofutar et al. (2006).

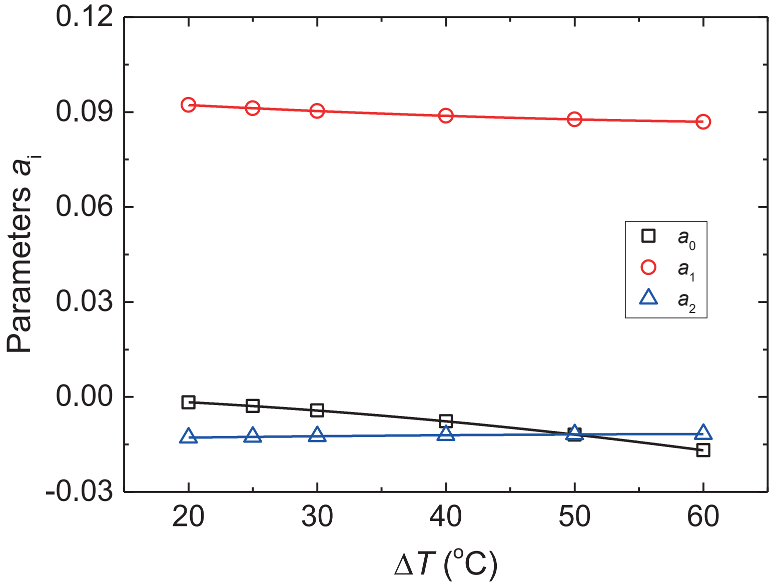

Figure 7.15. Constants a_i of Eq. (7.36) for aqueous sodium saccharin solutions against ΔT. Plots are drawn according to Eq. (7.37), with best-fit values listed in Table 7.6.

Table 7.6. Values of constants a_{ij} of Eq. (7.38) for aqueous sodium saccharin solutions

Data	$10^2 a_{i0}$	$10^4 a_{i1}$	$10^6 a_{i2}$	R^2
$a_0(\Delta T)$	0.125	−0.673	−3.905	0.9999
$a_1(\Delta T)$	9.714	−2.848	1.914	0.9998
$a_2(\Delta T)$	−1.397	0.6658	−0.476	0.9990

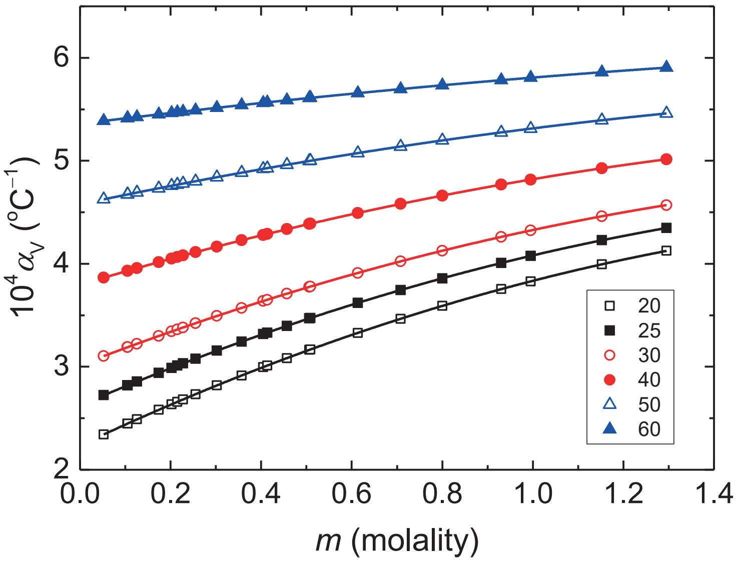

Figure 7.16. Values of expansivity α_V of aqueous sodium saccharin solutions against solute concentration m at different ΔT given in the inset. Plots are drawn according to Eq. (7.41). Values of α_V were calculated according to Eq. (7.38) with the constants of Table 7.6.

Figure 7.16 shows plots of the expansivity α_V of aqueous sodium saccharin solutions, calculated according to Eq. (7.38) with the constants of Table 7.6, as a function of solute concentration m. The concentration dependence of the solution expansivity α_V at a given temperature also follows the quadratic equation

$$\alpha_V = \alpha_{V0} + \alpha_3 m + \alpha_4 m^2 , \tag{7.41}$$

where α_{V0}, α_3 and α_4 are constants which depend on the solution temperature and characterize the nature of the solute–solvent interactions. The constant α_{V0} is the expansivity of the solvent at the temperature T_0 = 293.15 K. A general behavior of these $\alpha_V(m)$ curves is that their curvature decreases with an increase in temperature T. This behavior is due to the decreasing contribution of the $\alpha_4 m^2$ term in comparison with that of the $\alpha_3 m$ term with an increase in T, and there is an expected temperature when α_V increases practically linearly with x_2. At still higher temperatures, the order of these relative contributions is reversed, which leads to an opposite curvature in the

$\alpha_V(m)$ curves (see below). In the case of aqueous sodium saccharin solutions, this transition temperature of solute-concentration independent α_V seems to be about 70 °C when the value of α_V is about $6.2 \cdot 10^{-4}$ °C^{-1}.

Figure 7.17 shows another example of the dependence of volumetric thermal expansivity α_V of aqueous NaCl solutions on its concentration m at four selected temperatures. As seen from the $\alpha_V(m)$ plots, the curvature of the curves is different at the four temperatures, but the values of α_V at 60 °C, shown by the dashed line, is $5.2 \cdot 10^{-4}$ °C^{-1} and is independent of m. The dependence of α_V on the solute concentration m at the other three temperatures may be described well by Eq. (7.41), with the values of the constants given in Table 7.7. However, as shown by the dashed curve, the $\alpha_V(\Delta T)$ data at the highest temperature of 80 °C considered here may also be represented reasonably well by the linear relation.

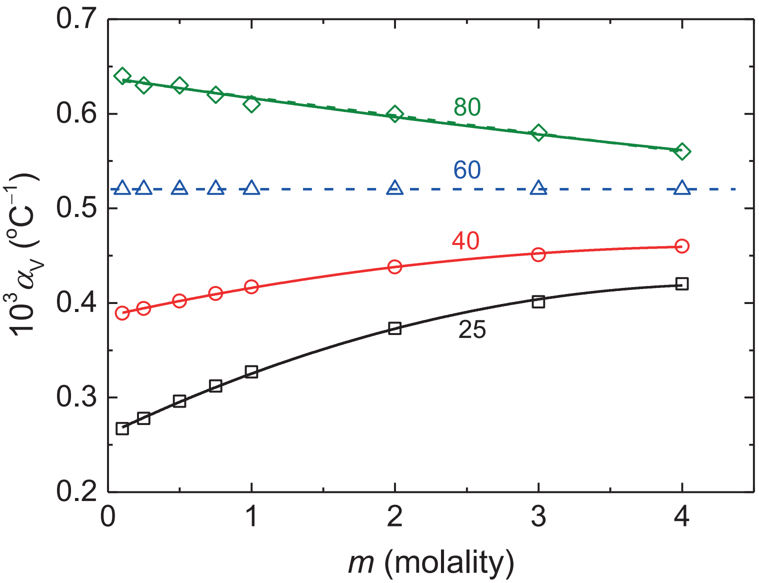

Figure 7.17. Dependence of expansivity α_V of aqueous NaCl solutions on solute concentration m at four selected ΔT. Plots are drawn according to Eq. (7.41), with constants listed in Table 7.7. Linear fit of data for 80 °C is shown by dashed line. Concentration-independent values of α_V at 60 °C are shown by dashed line. Original data of α_V of solutions from Lide (1996/1997).

Table 7.7. Constants of Eq. (7.41) for aqueous NaCl solutions

T (°C)	$10^3\alpha_{V0}$ (K^{-1})	$10^5\alpha_3$ (kg·mol^{-1}·K^{-1})	$10^6\alpha_4$ (kg^2·mol^{-2}·K^{-1})
25	0.261	7.22	−8.21
40	0.386	3.33	−3.80
60	0.520	0	0
80	0.628	−2.25	0.83

As seen from Table 7.7, and consistent with the inference made above from the $\alpha_V(m)$ data of aqueous sodium saccharin solutions, the signs of the constants α_3 and α_4 are changed as the temperature is increased, and the transition takes place at a temperature of about 60 °C. This type of behavior is also observed for other electrolytes dissolved in water (see Horvath, 1985) and is associated with the adiabatic compressibilities β_S of electrolyte solutions (see below), which go through minima between 50 and 70 °C for alkali metal chlorides.

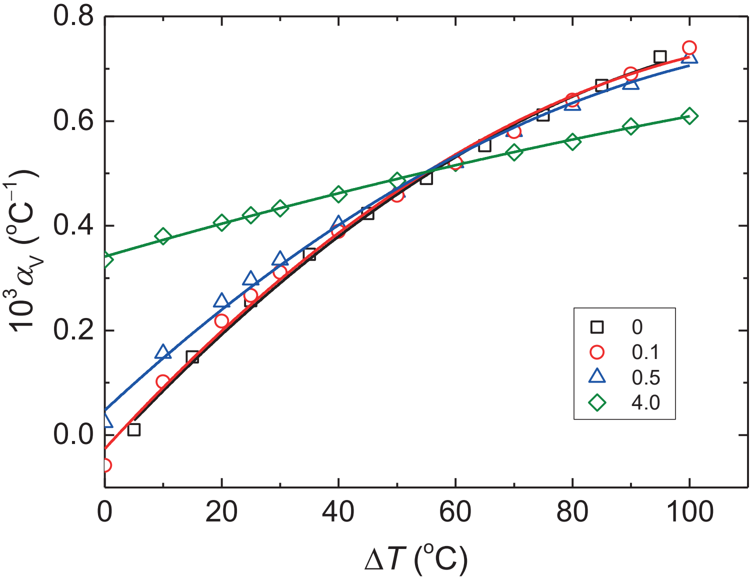

Figure 7.18. Dependence of expansivity α_V of water and aqueous NaCl solutions of three selected concentrations *m* on their temperature ΔT. Plots are drawn according to Eq. (7.42) with the best-fit constants listed in Table 7.8. Original data of α_V of solutions and *d* of water to calculate its α_V values from Lide (1996/1997).

The dependence of expansivity α_V of solutions of a given solute concentration *m* on their temperature ΔT follows the same relation as observed for solids and liquids (see Sections 7.2 and 7.3; Eq. (7.38)), i.e.

$$\alpha_V = \alpha_{V0} + \alpha_5 \Delta T + \alpha_6 (\Delta T)^2 , \tag{7.42}$$

where constants α_{V0}, α_5 and α_6 depend on solute concentration *m*. Figure 7.18 shows the experimental data of the volumetric thermal expansivity α_V of water and aqueous NaCl solutions of three selected concentrations *m* as a function of their temperature *T*, where the plots are drawn according to Eq. (7.42) with the best-fit constants listed in Table 7.8.

From Table 7.8 it may be noted that the values of constants α_{V0} and α_6 increase with increasing solute concentration *m*, but the increment in the expansivity α_V with temperature, as determined by the parameter α_5, is retarded by the addition of the solute to the solvent water. This results in the intersection of plots of α_V of solutions of various concentrations m against ΔT at the transition temperature of about 60 °C, when the value of α_V is temperature independent. In the case of aqueous NaCl solutions this value of α_V is $5.2\cdot10^{-4}$ °C^{-1}, which is somewhat lower than that noted above for aqueous sodium saccharin solutions.

Table 7.8. Constants of Eq. (7.42) for aqueous NaCl solutions

m (m)	$10^5\alpha_{V0}$ (°C^{-1})	$10^5\alpha_5$ (°C^{-2})	$-10^8\alpha_6$ (°C^{-3})
0	−3.13	1.207	4.49
0.1	−2.62	1.220	4.72
0.5	4.76	1.036	3.77
4.0	34.11	0.327	0.57

The dependence of α_V on m and ΔT and the observation of transition temperature when α_V of a solution is independent of solute concentration m may be understood from the relationship between α_V of solutions and their isothermal and adiabatic compressibilities β_T and β_S, given by (see Horvath, 1985)

$$\alpha_V^2 = \left(\frac{\beta_T - \beta_S}{T}\right)C_p\,, \tag{7.43}$$

where C_p is the heat capacity of solutions at constant pressure per unit volume, and isothermal and adiabatic compressibilities β_T and β_S of a solution of solute concentration x_2 are defined in terms of changes in its density d with respect to pressure p at constant temperature T and constant entropy S, respectively, by

$$\beta_T = \left(\frac{\mathrm{d}\ln d}{\mathrm{d}p}\right)_{T,x_2}, \tag{7.44}$$

$$\beta_S = \left(\frac{\mathrm{d}\ln d}{\mathrm{d}p}\right)_{S,x_2}. \tag{7.45}$$

According to Eq. (7.43), α_V decreases with decreasing heat capacity C_p of solutions for comparable values of $(\beta_T-\beta_S)/T$ for solutions of two solutes in a solvent. Similarity in the definitions of β_T and β_S of solutions with that of the thermal expansivity α_V of liquids under isobaric conditions may be noted.

It should be mentioned that precise measurements of density d of solutions of solutes of known concentrations m in a wide range of temperature interval are required to determine the above types of transitions. An example illustrating this point is the dependence of data of density d of aqueous sodium nitrate and sodium thiosulfate solutions on temperature T between about 15 and 55 °C, reported by

Mohiuddin and Ismail (1996). These authors found that the density d of these solutions decreases linearly with ΔT (see Eq. (7.25)), which implies that the expansivity α_V of these solutions follows Eq. (7.26) expressed in the form

$$\alpha_V = -\frac{a_1}{d_0 - a_1\Delta T} \approx \alpha_V^o + \alpha_V^{o2}\Delta T \, , \tag{7.46}$$

where $\alpha_V^o = (a_1/d_0)$ and the parameters d_0 and a_1 are functions of solute concentration m. Using the values of d_0 and a_1 given in the paper by Mohiuddin and Ismail (1996), one may calculate α_V of solutions of various concentrations m at selected values of ΔT.

The calculated values of α_V of solutions at different temperatures may be analyzed as a function of their concentration m. In fact, the data of $\alpha_V = a_1/d_0$ corresponding to $\Delta T = 0$ for aqueous $NaNO_3$ and $Na_2S_2O_7$ solutions as a function of m were considered before in Figure 3.21 (see Section 3.5.5). The main drawback of such plots is that the effect of the physicochemical properties of different solutes dissolved in the solutions is poorly revealed. In contrast to this, dependence of the data of α_V of different solvents on their concentration x_2 (mole fraction) is more informative.

Figure 7.19 shows the calculated values of α_V of aqueous $NaNO_3$ and $Na_2S_2O_7$ solutions of 20 and 50 ^oC as a function of solute concentration x_2. From the figure one observes that the value of α_V increases practically linearly with x_2 for both 20 and 50 ^oC, and the value of α_V increases with ΔT. These findings are consistent with the concepts of expansivity of liquids. However, the calculated values of α_V show large scatter from the linear dependence. This large scatter is mainly due to the errors involved in the estimated values of a_1 and, associated with it, d_0 from the original $d(\Delta T)$ data. When the highly deviating points for 0.05 and 0.452 mole fraction of $NaNO_3$ solutions and 0.08 and 0.448 mole fraction of $Na_2S_2O_7$ solutions are excluded from the analysis, the $d(\Delta T)$ data may be represented satisfactorily by the linear plots shown in the figure for 20 ^oC, with intercept $\alpha_V^o = 4.38\cdot10^{-4}$ $^oC^{-1}$ and slopes $\Delta\alpha_V/\Delta x_2 = 3.95\pm0.41$ and 1.24 ± 0.51 $^oC^{-1}$ for $NaNO_3$ and $Na_2S_2O_7$ solutions, respectively. One also notes that the values of the intercept α_V^o and the slopes $\Delta\alpha_V/\Delta x_2$ for the two solutions at 50 ^oC are somewhat higher than those at 20 ^oC.

The above value of α_V^o is comparable with the value of the expansion coefficient α_V of pure water at about 50 ^oC (see: Figs. 7.3b, 7.12, 7.16 and 7.18). The value of the slope $\Delta\alpha_V/\Delta x_2$ of $NaNO_3$ solutions is higher, by a factor of 3, than that of $Na_2S_2O_7$ solutions. This difference in the slope is associated with the mass of the solute molecules/ions (and the molar mass M of the solute) participating in thermal expansion of the solutions. Since the thermal expansion coefficient α_V of a solution is determined by thermal vibrations of molecules/ions in the solution, the above differences may be attributed to the ax^2 term in Eq. (7.17), the parameter a^2 in the denominator of Eq. (7.22), and the maximum displacement Δx_{max} of the vibrating entities in it (see Eq. (7.24)).

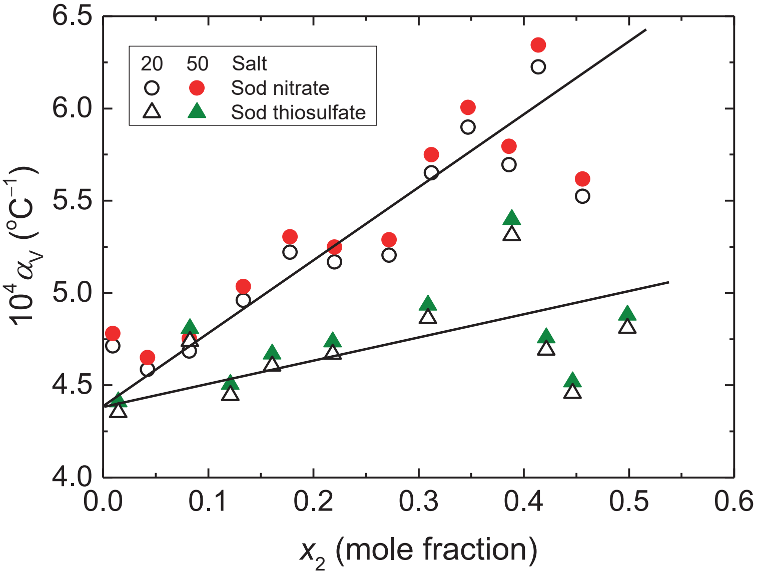

Figure 7.19. Expansivity α_V of aqueous $NaNO_3$ and $Na_2S_2O_7$ solutions of 20 and 50 °C as a function of their concentration x_2. Values of α_V were calculated from density relations reported by Mohiuddin and Ismail (1996). Linear plots represent $\alpha_V(x_2)$ data at 20 °C. Highly deviating points for 0.05 and 0.452 mole fraction of $NaNO_3$ solutions and 0.08 and 0.448 mole fraction of $Na_2S_2O_7$ solutions were excluded from analysis.

7.5. Thermal expansivities of solutes

The thermal exansivity α_V^* of a solute dissolved in a solvent is calculated from the dependence of the limiting apparent molar volume Φ_v^o of the solute, the values of which are obtained from an analysis of the apparent molar volume Φ_v at different temperatures T as a function of solute concentration c_2. The apparent molar volume Φ_v of the solute of molar mass M_2 is related to the solution density d by (see Eq. (3.6); Section 3.2.1)

$$\Phi_v = \frac{10^3(d_1 - d)}{d_1 c_2} + \frac{M_2}{d_1}, \tag{7.47}$$

where d_1 is the solute density (g·cm^{-3}) and c_2 is the solute concentration (moles of solute per liter of solution). The dependence of Φ_v on the concentration c_2 of a solute is given by the general relation (see Eq. (3.12); Section 3.2.1)

$$\Phi_v = \Phi_v^o + S_v c_2^{1/2} + b_{v1} c_2 + b_{v2} c_2^{3/2} + b_{v3} c_2^2, \tag{7.48}$$

where the limiting apparent molar volume Φ_v^o of the solute corresponds to the value of Φ_v at infinite dilution when $c_2 \to 0$, the constant S_v results from the Debye–Hückle theory of interionic interaction, and b_v's are empirical constants. This relation is typical of concentrated electrolyte solutions. In the case of nonelectrolyte solutions where interionic interactions are not present, the S_v, $c_2^{1/2}$ and $c_2^{3/2}$ terms are zero and, therefore, depending on the concentration range involved, Eq. (7.48) reduces to linear and quadratic relations. Since the partial molar volumes of components i are usually denoted by V_{Mi}, it is customary to denote Φ_v^o by V_{M2}^o.

The limiting apparent molar volume V_{M2}^o of solutes depends on temperature difference ΔT with reference to the temperature T_0 and usually follows the relation (Helper, 1969; Helgeson and Kirkham, 1976; Klofutar et al., 2006)

$$V_{M2}^o = A_0 + A_1 \Delta T + A_2 (\Delta T)^2 , \tag{7.49}$$

where A's are empirical constants with their values dependent on solute and solvent, and the reference temperature $T_0 = 273.15$ K. This quadratic relation implies that the volumes V_{M2}^o of solutes go through a maximum. This behavior is typical of most aqueous electrolye solutions. Eq. (7.49) is used to define the limiting apparent molar expansivity Φ_{2E}^o ($cm^3 \cdot mol^{-1} \cdot {}^oC^{-1}$) and the thermal expansivity α_V^* (${}^oC^{-1}$) of solutes as

$$\Phi_{2E}^o = \left(\frac{d V_{M2}^o}{d \Delta T} \right)_p = A_1 + 2 A_2 \Delta T , \tag{7.50}$$

$$\alpha_V^* = \frac{1}{V_{M2}^o} \left(\frac{d V_{M2}^o}{d \Delta T} \right)_p = \frac{A_1 + 2 A_2 \Delta T}{A_0 + A_1 \Delta T + A_2 (\Delta T)^2} . \tag{7.51}$$

According to Eq. (7.50), Φ_{2E}^o changes linearly with temperature T in the ΔT range. In contrast to this, according to Eq. (7.51), α_V^* is expected to follow a polynomial dependence on ΔT and, depending on the relative contribution of the $A_1\Delta T$ and $A_2(\Delta T)^2$ terms to A_0 in its denominator, α_V^* may show linear and quadratic dependences. When $A_0 >> [A_1\Delta T + A_2(\Delta T)^2]$, Eq. (7.51) reduces to the form

$$\alpha_V^* = A_0^* + A_1^* \Delta T - A_2^* (\Delta T)^2 - A_3^* (\Delta T)^3 , \tag{7.52}$$

where $A_0^* = (A_1/A_0)$, $A_1^* = [2A_2/A_0) - (A_1/A_0)^2]$, $A_2^* = (3A_1A_2/A_0^2)$, and $A_3^* = 2(A_2/A_0)^2$. Since in Eq. (7.49) the constants $A_0 > A_1 > A_2$, the third and fourth terms are insignificant, and, depending on their values for a solute in the solution, the parameter A_1^* may be positive as well as negative. Then Eq. (7.52) predicts a linear dependence of α_V^* on ΔT with intercept A_0^* and slope A_1^*. Since V_{M2}^o of different solutes is a positive quantity, the sign of the slope $A_1^* = \Delta\alpha_V^*/\Delta T$ of the plot of α_V^* on temperature T is related to the sign of $2A_2$ in Eq. (7.50). Note that the values of empirical constants A_0, A_1 and A_2 obtained from Eq. (7.49) of the temperature dependence of V_{M2}^o of solutes are required to determine the values of the limiting apparent molar expansivity Φ_{2E}^o and the thermal expansivity α_V^* of solutes at different temperatures.

Figure 7.20 shows examples of the dependence of limiting apparent molar expansivity Φ_{2E}^o of two electrolytes sodium saccharin and potassium acesulfame and nonelectrolyte aspartame in aqueous solutions on their temperature ΔT. As seen from the plots, Φ_{2E}^{o} for both electrolytes decreases whereas that for the nonelectrolyte aspartame increases with an increase in ΔT. This means that the coefficient $2A_2$ of Eq. (7.50) is negative for these electrolytes and positive for the nonelectrolytes. These negative and positive values of $2A_2$ are associated with the structure-breaking and structure-making behavior of solutes in aqueous solutions. The difference in the behavior of different solutes in solutions may be explained from thermodynamics of solutions using the thermodynamic equation of state

$$\left(\frac{\partial H}{\partial T}\right)_T = V - T\left(\frac{\partial V}{\partial T}\right)_p , \tag{7.53}$$

where H is the enthalpy of solution and V is its volume. Differentiation of this equation with respect to the number $n_2(p,T)$ of moles of solute in dilute solutions of constant number n_1 of moles of the solvent and then with respect to $T(n_1,n_2)$ at constant p gives (Helper, 1969)

$$T\left(\frac{\partial^2 V_{M2}^{o}}{\partial T^2}\right)_p = -\left(\frac{\partial C_p^{o}}{\partial p}\right)_T , \tag{7.54}$$

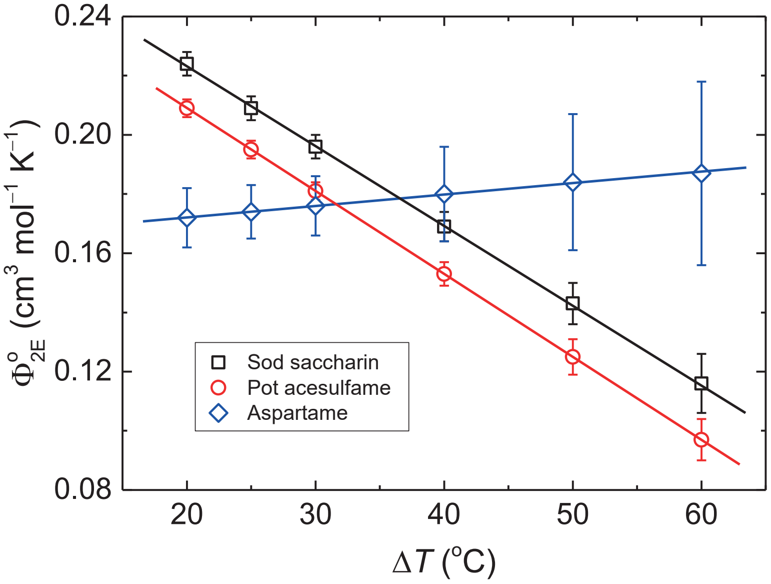

Figure 7.20. Examples of dependence of limiting apparent molar expansivity Φ_{2E}^{o} of aqueous solutions of two electrolytes sodium saccharin and potassium acesulfame and nonelectrolyte aspartame on their temperature ΔT. Note that Φ_{2E}^{o} for the two electrolytes decreases and that for the nonelectrolyte aspartame increases with an increase in ΔT. Original data from Klofutar et al. (2006).

where the superscript zero denotes partial molal properties of the solute at infinite dilution and the heat capacity of solute at infinite dilution: $C_p{}^{\circ} = (\partial H^{\circ}/\partial T)$. The sign of the parameter $(\partial C_p{}^{\circ}/\partial T)$ is an indicator of solute–solvent interactions. A positive value of $(\partial C_p{}^{\circ}/\partial T)$ for a solute–solvent system implies that the solute is structure breaking whereas a negative value implies that the solute is structure making. Alternatively, negative and positive values of $(\partial^2 V_{\mathrm{M2}}{}^{\circ}/\partial T^2)$ at a given temperature T are indicators of structure-breaking and structure-making solutes in solutions.

Figure 7.21 illustrates examples of the dependence of the thermal expansivity $\alpha_{\mathrm{V}}{}^{*}$ of three electrolytes sodium saccharin, potassium acesulfame and sodium cyclohexylsulfamate and nonelectrolyte aspartame in water on solution temperature ΔT. From the plots it may be noted that the values of $\alpha_{\mathrm{V}}{}^{*}$ of the electrolytes are higher than that of the nonelectrolyte aspartame, and that the values of $\alpha_{\mathrm{V}}{}^{*}$ of the electrolytes decrease linearly with increasing temperature T whereas those of the nonelectrolyte increase linearly with temperature T.

Figure 7.22 shows another example of the linear dependences of the thermal expansivity $\alpha_{\mathrm{V}}{}^{*}$ of ionic liquid [bmpyr][NTf2] and the thermal expansivity $\alpha_{\mathrm{V1}}{}^{*}$ of solvent γ-butyrolactone on ΔT of γ-butyrolactone–[bmpyr][NTf2] system. The values of $\alpha_{\mathrm{V}}{}^{*}$ and $\alpha_{\mathrm{V1}}{}^{*}$ were calculated by using Eq. (7.51) from the values of the limiting partial molar volumes $V_{\mathrm{M2}}{}^{\circ}$ and $V_{\mathrm{M1}}{}^{\circ}$ of the ionic liquid [bmpyr][NTf2] and the solvent γ-butyrolactone, respectively, at different temperatures between 293.15 and 323.15 K reported by Vraneš et al. (2015). The values of the intercept $A_0{}^{*}$ and the slope $A_1{}^{*}$ of the linear plots of Figures 7.21 and 7.22 are listed in Table 7.9.

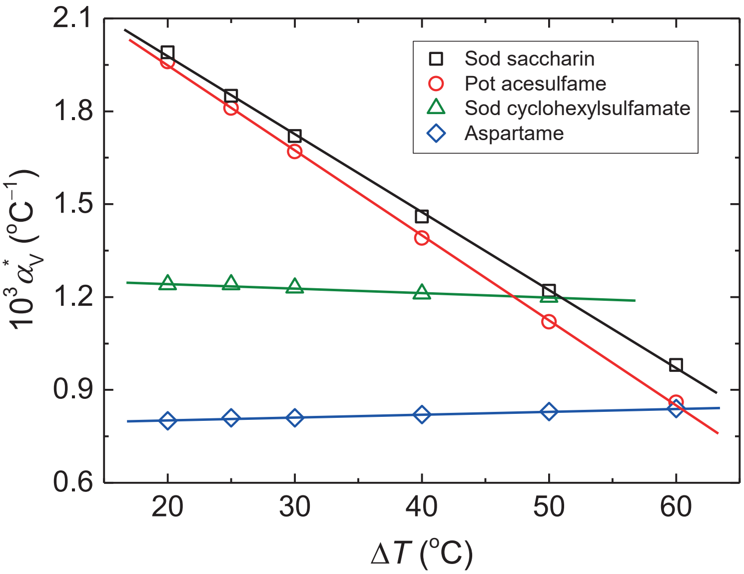

Figure 7.21. Examples of dependence of the thermal expansivity $\alpha_{\mathrm{V}}{}^{*}$ of three electrolytes sodium saccharin, potassium acesulfame and sodium cyclohexylsulfamate and non-electrolyte aspartame in water on solution temperature ΔT. Original data from Klofutar et al. (2006). See text for details.

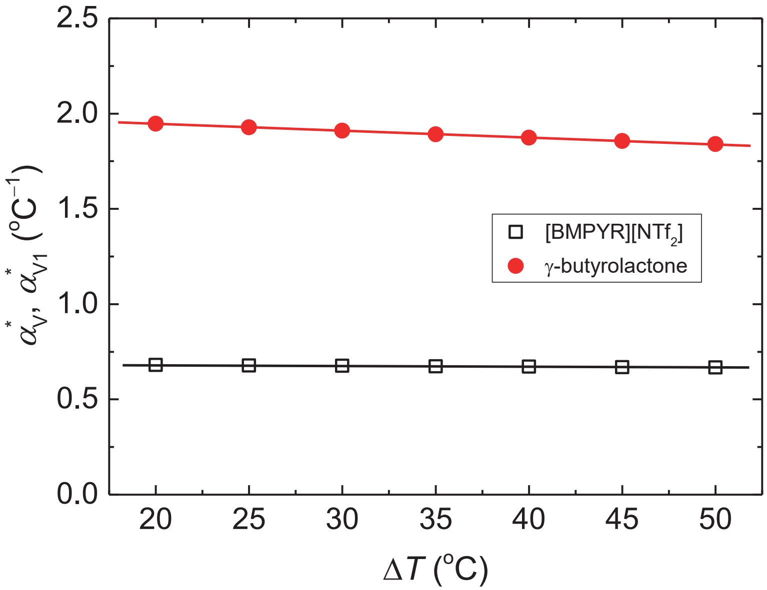

Figure 7.22. Another example of linear dependences of the thermal expansivity α_V^* of ionic liquid [bmpyr][NTf2] and the thermal expansivity α_{V1}^* of solvent γ-butyrolactone on ΔT of γ-butyrolactone–[bmpyr][NTf2] mixtures. Values of α_V^* and α_{V1}^* were calculated from data of their limiting partial molar volumes V_{M2}° and V_{M1}° reported by Vraneš et al. (2015). See text for details.

Table 7.9. Constants of Eq. (7.52) for some solutes

Solute	$10^3 A_0^*$ (°C^{-1})	$10^5 A_1^*$ (°C^{-2})	R^2	Source
Sodium saccharin	2.481	−2.518	0.9992	a
Potassium acesulfame	2.499	−2.747	0.9995	a
Sodium cyclohexylsulfamate	1.273	−0.148	0.9547	a
Aspartame	0.783	0.095	0.9797	a
[bmpyr][NTf2]	0.621	0.040	0.9996	b
γ-Butyrolactone	0.878	0.082	0.9996	b

[a] Klofutar et al. (2006); [b] Vraneš et al. (2015).

The above discussion of structure-making and structure-breaking behavior of solutes in solutions and cosolvents in solvent–cosolvent mixtures may also be analyzed from the sign of the slope A_1^* of plots of α_V^* on temperature T. The values of α_V^* of the ionic compounds listed in Table 7.9 are similar to those reported for aqueous solutions of several inorganic salts, and decrease with increasing temperature (Cabani et al., 1981; Klofutar et al., 2006). As mentioned above, the negative values of the slope A_1^* for these ionic salts of large-sized anions are due to their structure-breaking behavior but the positive value of this slope for aspartame is a result of its structure-making behavior. Dilute solutions of alcohols in water with positive slope are structure makers (Helper, 1969). Similarly, the solvent γ-butyrolactone and the cosolvent [bmpyr][NTf2] of the γ-butyroactone–[bmpyr]-[NTf2] system have positive values of A_1^* and are structure makers.

Finally, it should be mentioned that, as discussed in Section 3.5.3, the limiting apparent molar volumes V_{M2}^o of ionic salts are due to contributions from individual ions. Consequently, the limiting apparent molar expansivity Φ_{2E}^o and the thermal expansivity α_V^* of an ionic salt in the solvent also comprise contributions of its ions. In general, the values of Φ_{2E}^o and α_V^* for different types of solutes in solvents are associated with structural characteristics such as valency, size and type of ions of electrolytes and the relative proportions of hydrophobic or hydrophilic parts of molecules of nonelectrolytes. Discussion on this topic for sodium saccharin and potassium acesulfame salts may be found in the paper by Klofutar et al. (2006).

7.6. Expansivity of saturated solutions

Densities of homogeneous solutions of solids of particular concentrations dissolved in their solvents, as a rule, decrease with an increase in their temperature, but the densities of solutions at particular temperatures usually increase with an increase in solute concentration. However, depending on the nature of solute dissolved in a solvent, its solubility in the solvent frequently increases or decreases with the solution temperature in the entire temperature interval or shows both increase as well as decrease in different temperature intervals. Therefore, the temperature dependence of the densities of saturated solutions of various solutes shows trends different from that of solutions of fixed solute concentrations, and are determined by the temperature dependence of their solubility. In general, one expects that the temperature dependence of densities of saturated solutions of solutes of negative and small positive temperature coefficient of solubility decreases but that of solutes of positive temperature coefficient of solubility increases. Figure 7.23 shows typical examples of the experimental data of densities d^* of aqueous saturated solutions of some inorganic electrolytes as a function of temperature T in the form of plots of $\ln d^*$ against ΔT according to the polynomial (cf. Eq. (7.27)):

$$\ln d^*(\Delta T) = \sum_{i=0}^{n} a_i^*(\Delta T)^i \ , \tag{7.55}$$

where a_i^* is a constant corresponding to the integer i, and $n = 2$ and 3 represent second- and third-order polynomials, and we have used the symbols denoted as d^* and a_i^* to distinguish them from the densities d and constants a_i of unsaturated solutions. In the figure dashed and solid curves, respectively, are drawn with the best-fit constants listed in Table 7.10.

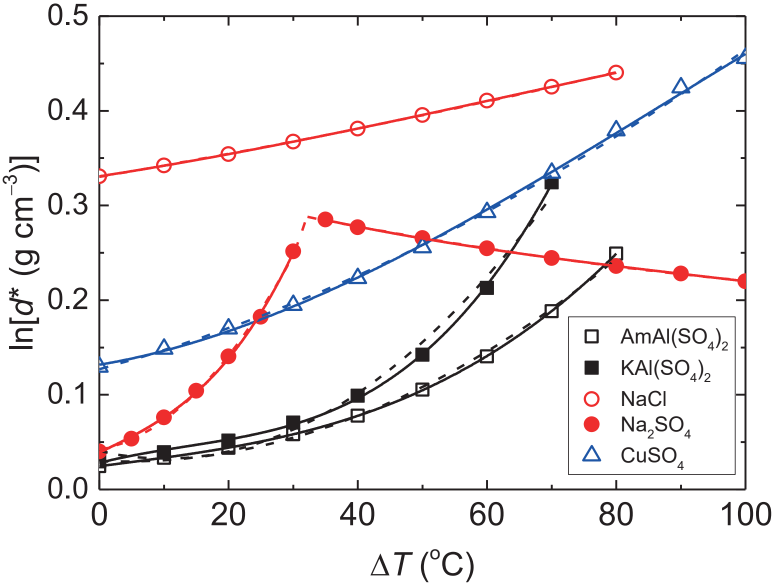

Figure 7.23. Plots of lnd^* of aqueous saturated solutions of some electrolytes a function of ΔT according to Eq. (7.55). Dashed and solid curves represents ln$d^*(\Delta T)$ data with best-fit constants listed in Table 7.10. Original data from Söhnel and Novotný (1985).

Table 7.10. Constants of polynomial (7.55) for aqueous saturated solutions of some electrolytes

Electrolyte	ΔT[a]	a_0^*	$10^3 a_1^*$ (K^{-1})	$10^5 a_2^*$ (K^{-2})	$10^7 a_3^*$ (K^{-3})	R^2	$10^3 \alpha_V^{25}$ (K^{-1})	$10^3 \alpha_V^{70}$ (K^{-1})
$NH_4Al(SO_4)_2$	E[b]	0.02996	−0.2776	3.6852	--	0.9958	−1.57	−3.98
		0.02457	0.8443	−0.1662	3.2095	0.9999	−1.40	−5.37
$KAl(SO_4)_2$	E	0.04067	−1.57	7.7356	--	0.9829	−2.30	−1.40
		0.02808	1.73	−4.8596	11.9954	0.9991	$1.12\cdot10^7$	$8.82\cdot10^7$
$CuSO_4$	E	0.12716	1.87	1.5039	--	0.9980	−2.62	−3.98
		0.13177	1.14	3.4261	−1.2815	0.9988	−2.61	−4.05
Na_2SO_4	L[c]	0.04206	1.24	18.6264	--	0.9961	−2.17	--
		0.03906	3.24	0.64881	39.9502	0.9978	−11.06	--
	H[d]	0.33622	−1.66	50.3477	--	0.9991	--	0.96
		0.35125	−2.43	1.7093	−0.5956	0.9995	--	0.91
NaCl	E	0.33031	1.17	0.2672	--	0.9998	−1.30	−1.54
		0.33084	1.05	0.6446	−0.3145	0.9999	−0.79	−1.49

[a] ΔT range; [b] E entire, [c] L < 30 °C; [d] H > 35 °C.

As in the case of the temperature dependence of the solubilities of the above electrolytes (see Section 2.2), the value of lnd^* of aqueous saturated $NH_4Al(SO_4)_2$, $KAl(SO_4)_2$, $CuSO_4$ and NaCl solutions continuously increases with ΔT in the entire range of their measured density d^*, but the value of lnd^* of Na_2SO_4 solutions initially increases up to about 33 °C and then steadily decreases up to 100 °C. The

$\ln d^*(\Delta T)$ data for solutions of NaCl, $CuSO_4$ and $NH_4Al(SO_4)_2$ in the entire temperature interval and for Na_2SO_4 solutions in the two ΔT regions appear to be described reasonably well by both second- and third-order polynomial relations, but the fit of the data somewhat improves by the third-order polynomial in comparison with that of the second-order polynomial. In contrast to the above salts, the fit of the $\ln d^*(\Delta T)$ data for $KAl(SO_4)_2$ solutions by the second-order polynomial is poor. Using the values of the a_i^* parameters obtained by the second- and third-order polynomials given in Table 7.10 and the definition of the expansivity $\alpha_V = -d(\ln d^*)/d\Delta T$, the values of α_V of different electrolytes solutions were calculated at 20 and 70 ^{o}C. These values of α_V are included as α_V^{25} and α_V^{70} in Table 7.10.

From Table 7.10 one notes that Na_2SO_4 solutions have negative value of α_V at 20 ^{o}C and positive one at 70 ^{o}C whereas solutions of the other electrolytes have negative α_V at both 20 and 70 ^{o}C. The positive and negative values of α_V of these solutions are due to the decreasing and increasing values of their densities, respectively, with increasing ΔT. With the exception of $KAl(SO_4)_2$ solutions which give erratic values of α_V, the absolute values of α_V predicated by the second- and third-order polynomials are comparable and the values of α_V of the solutions increase with temperature.

References

Abu-Daabes, M.A., and A.M. Awaad (2008). Volumetric and viscometric properties of aqueous solutions of *N*-(2-hysroxyethyl)morpholine at T = (293.15, 303.15, 323.15, 333.15) K. *J. Chem. Thermodyn*. **40,** 874-878.

Cabani, S., G. Conti, E. Matteoli, M.R. Tiné (1981). Volumetric properties of amphionic molecules in water. Part 2. Thermal expansibility and compressibility related to the formation of zwitterionic structures. *J. Chem. Soc. Farady Trans. 1*. **77,** 2385-2394.

Domańska, U., and M. Królikowska (2012). Density and viscosity of binary mixtures of thiocyanate ionic liquids + water as a function of temperature. *J. Solution Chem*. **41,** 1422-1445.

Domańska, U., and M. Laskowska (2009). Effect of temperature and composition on the density and viscosity of binary mixtures of ionic liquids with alcohols. *J. Solution Chem*. **38,** 779-779.

Dhondge, S.S., S.P. Zodape, and D.V. Parwate (2012). Volumetric and viscometric studies of some drugs in aqueous solutions at different temperatures. *J. Chem. Thermodyn*. **48,** 207-212.

González, B., N. Calvar, E. Gómez, and A. Domínguez (2007). Density, dynamic viscosity, and derived properties of binary mixtures of methanol or ethanol with water, ethyl acetate, and methyl acetate at T = (293.15, 298.15, and 303.15) K. *J. Chem. Thermodyn*. **30,** 1578-1588.

Helgeson, H.C., and D.H. Kirkham (1976). Theoretical prediction of the thermodynamic properties of aqueous electrolytes at high pressures and temperatures. III. Equation of state for aqueous species at infinite dilution. *Am. J. Sci*. **276,** 97-240.

Helper, L.G. (1969). Thermal expansion and structure in water and aqueous solutions. *Can. J. Chem*. **47,** 4613-4617.

Holguin, A.R., D.R. Delgado, F. Martinez, M. Khoubnasabjafari, and A. Jouyban (2011). Study of some volumetric properties of glycerol formal + ethanol mixtures and correlation with the Jouyban-Acree model. *Rev. Acad. Colomb. Cienc*. **35,** 315-328.

Horvath, A.L. (1985). *Handbook of Aqueous Electrolyte Solutions: Physical Properties, Estimation and Correlation Methods*. Ellis Horwood, Chichester.

Kittel, C. (1976). *Introduction to Solid State Physics*, 5th edition. Wiley, New York, Chapter 5.

Klofutar, C., J. Horvat, and D. Rudan-Tasic (2006). Apparent molar volumes and apparent molar expansibility of sodium saccharin, potassium acesulfame and aspatame. *Acta Chim. Slov.* **53,** 274-283.

Lide, D.R. (1996/1997). *Handbook of Chemistry and Physics*, 77th edition. CRC Press, Boca Raton, FL.

Liew, K.Y., C.E. Seng, and B.H. Ng (1993). Viscosities of long chain *n*-alcohols from 15 to 80°C. *J. Solution Chem.* **22,** 1033-1040.

Marsh, K.N., J.A. Boxall, and R. Lichtenthaler (2004). Room temperature ionic liquids and their mixtures. *Fluid Phase Equilibria* **219,** 93-98.

Millero, F.J., G.K. Ward, and P. Chetirkin (1976). Partial specific volume, expansibility, compressibility, and heat capacity of aqueous lysozyme solutions. *J. Biolog. Chem.* **251,** 4001-4004.

Mohiuddin, S., and K. Ismail (1996). Temperature and concentration dependence of the viscosity of aqueous sodium nitrate and sodium thiosulphate electrolyte systems. *Fluid Phase Equilibria* **123,** 231-243.

Mokhtarani, B., A. Sharifi, H.R. Mortaheb, M. Mirzaei, M. Mafi, and F. Sadeghian (2009). Density and viscosity of pyridinium-based ionic liquids and their binary mixtures with water at several temperatures. *J. Chem. Thermodyn*. **41,** 323-329.

Ortega, J. (1982). Densities and refractive indices of pure alcohols as a function of temperature. *J. Chem. Eng. Data* **27,** 312-317.

Pang, F.-M., C.-E. Seng, T.-W. Teng, and M.H. Ibrahim (2007). Densities and viscosities of aqueous solutions of 1-propanol and 2-propanol at temperatures from 293 K to 333.15 K. *J. Mol. Liq.* **136**, 71-78.

Söhnel, O., and P. Novotný (1985). *Densities of Aqueous Solutions of Inorganic Substances*. Academia, Prague.

Tamura, K., M. Nakamura, S. Murakami (1997). Excess volumes of water + acetonitrile and water + dimethylsulfoxide at 30°C and the effect of the excess thermal expansivity coefficients on derived thermodynamic properties. *J. Solution Chem*. **26,** 1199-1207.

Vraneš, M., S. Popović, A. Tot, N. Zec, and S. Gadžurić (2015). Density, excess properties, electrical conductivity and viscosity of 1-butyl-3-methylimidazolium bis(trifluoromethylsulfonyl)imide + γ-butyrolactone binary mixtures. *J. Chem. Thermodyn*. **76,** 161-171.

Vraneš, M., A. Tot, S. Popović, N. Zec, S. Dožić, and S. Gadžurić (2015). Ideal and non-ideal behaviour of {1-butyl-1-methylpyrrolydinium bis(trifluoromethylsulfonyl)-imide + γ-butyrolactone} binary mixtures. *J. Chem. Thermodyn*. **81,** 66-76.

Zhang, Y., H. Dong, Y. Yue, and C. Wu (2013). Effect of temperature and composition on the density, refractive index, and excess quantities of binary mixtures of 2,4,6,8-tetramethyl-2,4,6,8-tetraethenylcyclotetrasiloxane with aromatic hydrocarbons. *J. Chem. Thermodyn*. **57,** 114-130.

SUBJECT INDEX